

SIXTH INTERNATIONAL WORKSHOP

ON LASER RANGING INSTRUMENTATION

ANTIBES JUAN-LES-PINS



6^e COLLOQUE INTERNATIONAL
SUR L'INSTRUMENTATION
DE LA TELEMETRIE LASER

EDITED BY / EDITE PAR :

- JEAN GAIGNEBET
- FRANCOISE BAUMONT

WE WISH HEREBY TO EXPRESS OUR THANKS TO /
NOUS TENONS A REMERCIER ICI :

- MINISTERE DES AFFAIRES ETRANGERES
- ASSOCIATION INTERNATIONALE DE GEODESIE
- UNION GEODESIQUE ET GEOPHYSIQUE INTERNATIONALE
- INSTITUT NATIONAL DES SCIENCES DE L'UNIVERS
- CENTRE NATIONAL D'ETUDES SPATIALES
- AEROSPATIALE
- BRASSARD MICHELET INDUSTRIES
- QUANTEL
- SOCIETE D'ETUDES ET DE CONSTRUCTION D'INSTRUMENTS ASTRONOMIQUES

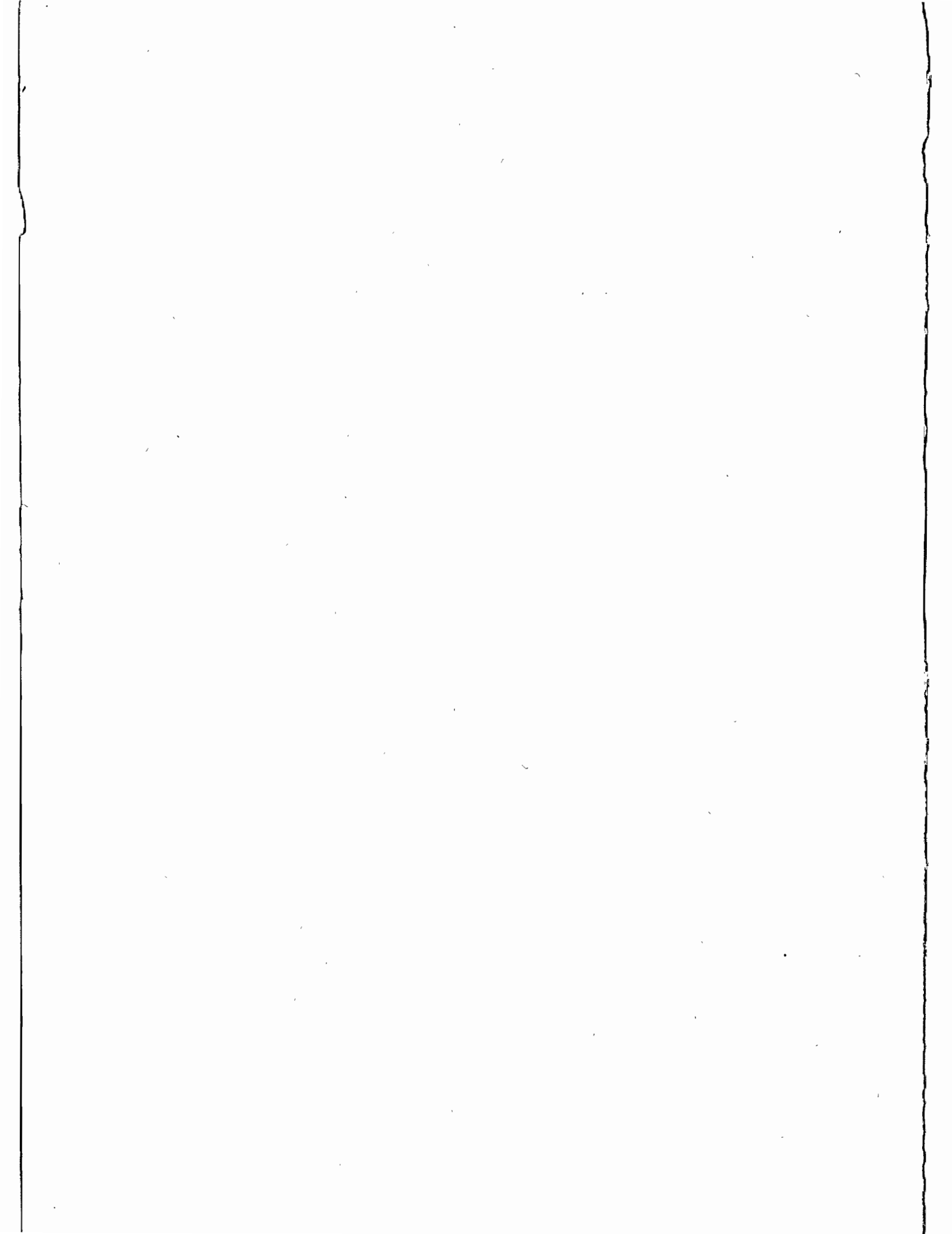


TABLE OF CONTENTS
=====

| | PAGE |
|--|------|
| WELCOMING ADDRESS J.P. Rozelot | V |
| PREFACE J. Gaignebet | VII |
| RESOLUTIONS | XI |
| LIST OF PARTICIPANTS | XVI |
| <u>SCIENTIFIC RESULTS AND FUTURE GOALS OF LASER RANGING</u> | |
| Chairman : F. Barlier (Invited Papers) | |
| I. Ciufolini | |
| New Relativistic Measurements With Laser Ranged Satellites | 1 |
| <u>NORMAL POINTS</u> Chairman : D. Leigeman | |
| R. Kolenkiewicz et al. | |
| Comparison Of Lageos Satellite Ranging Normal Points | 11 |
| <u>SATELLITE MOBILE STATIONS</u> Chairman : P. Wilson | |
| T. Varghese, M. Hernick | |
| Sub Cm Multiphotoelectron Satellite Laser Ranging | 21 |
| T. Varghese et al. | |
| TLRS-1 ; System Upgrade And Performance Results | 33 |
| N. Sasaki, Y. Suzuki | |
| Satellite Laser Ranging System At The Simosato Hydrographie Observatory And The Transportable system, HTLRS | 45 |
| Z. Wen-Yao, T. De Tong | |
| Progress In SLR At Shanghai Observatory | 59 |
| K. Hamal et al. | |
| Interkosmos Laser Radar, Version Mode Locked Train | 69 |
| F. Pierron et al. | |
| Upgrades And New Developments On Satellite Laser Ranging Station From Grasse | 73 |
| L. Grunwaldt et al. | |
| The SBG Laser Radar Stations Potsdam And Santiago De Cuba Status And Performance Report | 93 |
| K. Hamal et al. | |
| 3. Generation Laser Radar, Version Mode Locked Train Proposal | 109 |
| A. Banni, V. Capoccia | |
| The New Satellite Laser Ranging System At Cagliari Observatory | 113 |
| P. Kloeckler, Th. Schildknecht | |
| Zimmerwald Satellite Observation Station | 123 |

LUNAR AND COMBINED Chairman : K. Hamal

| | |
|---|-----|
| Ch. Veillet et al. The New CERGA LLR Station | 129 |
| M.L. White Recent Improvements And Future Plans At The University Of Hawaïi Lunar And Satellite Ranging Station | 135 |
| J.R. Wiant, P.J. Shelus The McDonald Observatory Laser Ranging Station : MLRS | 139 |

DETECTORS : SOLID STATE AND PMT Chairman : S.R. Bowman

| | |
|--|-----|
| I. Prochaska Start Detector For The Mode Locked Train Laser Radar | 145 |
| R. Neubert et al. Ambiguity And Resolution of A Mode Locked Pulse Train Laser Radar | 149 |
| I. Prochaska, J. Gaignebet Microchannel/Dynode Photomultipliers Comparison Experiment | 161 |
| Z. Neumann Detectors For III Generation Laser Ranging Systems | 165 |
| S.R. Bowman et al The Use Of Geiger Mode Avalanche Photodiodes For Precise Laser Ranging At Very Low Light Levels : An Experimental Evaluation | 173 |
| K. Hamal et al. Single Photon Solid State Detector For Ranging At Room Temperature | 185 |
| W.A. Kielek "Constant Fraction" Discriminators In Few And Multiphotoelectron Laser Ranging | 189 |

TIMING AND EPOCH Chairman : C.A. Steggerda

| | |
|--|-----|
| B.A. Greene Calibration Of Sub-Picosecond Timing Systems | 197 |
| P. Dachel et al. Recent Advances In The GLTN Timing And Frequency Instrumentation | 205 |
| C.A. Steggerda The Development Of A Dual Frequency Event Timer | 225 |

LASERS Chairmen : F. Moya, H. Jelinkova

| | |
|---|-----|
| K. Hamal, H. Jelinkova Saturable Dye For 1.06 μ m | 243 |
| H. Jelinkova et al. Spatial Structure Of The Doubled Nd:YAG Laser Transmitter Beam | 251 |
| L. Jiyu Some Special Requirements To Lasers For Satellite Laser Ranging | 261 |

OPTICS, TRACKING AND MOUNTS Chairman : M.L. White

| | |
|--|-----|
| S.R. Bowman et al. Analysis And Performance Of A Passive Polarization Telescope Coupling Switch For Lunar Laser Ranging | 273 |
| H. Feng et al. An Accurate Test Of The Azimuth Axis Of A 1.2M Alt-AZ Telescope Mount For The Lunar Laser Ranging And The Analysis Of The Results | 281 |
| M.L. White Double Peak Polarized Interference Filters | 289 |
| R. Korakitis Effects Of Telescope Design On Laser Beam Pointing Accuracy | 297 |

CALIBRATION Chairman : M. Pearlman

| | |
|---|-----|
| T. Varghese System Characterization Of Moblas-7 For Colocation With TLRS-1 & 2 | 311 |
| R. Appller Calibration Error Sources | 323 |
| B.A. Greene Calibration Of Sub-Millimeter Precision Satellite Laser Ranging Systems | 331 |
| P. Kloeckler, T. Schildknecht Measuring And Modelling Pulse Discriminator Amplitude Dependence | 343 |
| H. Junginger MTLRS Ground Tests | 357 |
| J.D. Rayner et al. Zero Range Realtime Calibration | 373 |
| K. Hamal, I. Prochaska System Stability Using Mode Locked Train | 377 |
| L. Jiyu Satellite Laser Ranging Errors | 379 |

SOFTWARE BENCHMARKING AND COLOCATION Chairman : E. Vermaat

| | |
|--|-----|
| M.R. Pearlman Some Current Issues On Laser Collocations | 399 |
| A. Cenci Management Of The Laser Ranging Systems Colocation | 409 |
| D.L.F. Van Loon Eccentricity Vectors For Colocation Purposes | 441 |
| V. Husson, D. Edge Polyquick Collocation Analysis | 453 |
| A. Caporali Colocation Data Analysis : Dynamical Approach | 467 |
| R. Kolenkiewicz Geodyn Collocation Analysis And Its Comparison With Polyquick | 481 |

RAPID ON SITE DETERMINATION OF THE EARTH ROTATION

Chairmen : D. Smith, Ch. Veillet

| | |
|--|-----|
| P.J. Shelus, R. Ricklefs Real Time, On Site Earth Orientation Parameter Generation At The MLRS Using Laser Ranging Data | 493 |
| G.M. Appleby, A.T. Sinclair A Note On The Use Of The CRS Lageos Ephemerides | 499 |
| Ch. Veillet et al. Real Time UTO Determination At CERGA LLR Station | 507 |
| P.J. Shelus A Simple Software Scheduling Tool For Efficient Observing Operations At A Lunar/Lageos Laser Ranging Station | 511 |

HIGHT AVERAGE POWER AND NEW LASERS, NEW SATELLITES

Chairman : C.O. Alley

| | |
|--|-----|
| S.R. Bowman et al. A Neodimium YAG Active Mirror For The Amplification Of Mode Locked Laser Pulses | 523 |
| M. Sasaki Japanese Geodetic Satellite "AJISAI" Launched In August 1986 | 527 |
| F.M. Yang The Proposal Of Strictly Simultaneous Satellite Laser Ranging | 549 |

TWO WAVELENGTH SYSTEMS AND STREAK CAMERA Chairman : B. Greene

| | |
|---|-----|
| I. Prochaska, K. Hamal Streak Camera Based Laser Radar Receiver. Its Performance and Limitations | 559 |
| J. Gaignebet et al., K. Hamal et al. Two Wavelength Ranging On Ground Target Using Nd:YAG 2HG and Raman 0.68 μm Pulses | 565 |
| I. Prochaska, K. Hamal Picosecond Laser Ranging Using Photodiode | 577 |
| B.A. Greene Multiple Wavelength Laser ranging | 581 |
| F. Guerin, G. Cerutti-Maori Problems Induced By Multicolor Telemetry On Laser Retroreflector Development | 593 |

SPECIAL STUDY GROUP ON LUNAR LASER RANGING

Report prepared by Ch. Veillet 623

LUNAR AND COMBINED (Additive)

| | |
|--|-----|
| C.O. Alley et al. First Lunar Ranging Results From The University Of Maryland Research Station At The 1.2M Telescope Of The GSFC | 625 |
|--|-----|

WELCOMING ADDRESS AT THE JUAN-LES-PINS
WORKSHOP ON LASER INSTRUMENTATION

J.P. ROZELOT
Directeur du CERGA
Avenue Copernic
06130 - Grasse - France -

First at all, on behalf of the local organizing committee, I would like to welcome you here in Juan-Les-Pins for this Sixth International Workshop on Laser Instrumentation.

The intent of the scientific committee is to summarize the advances in this technique in the broader context of current research in the physics of lasers, and I am not afraid to say that this symposium is almost unique in bringing together a large scientific community that includes not only physicists but also astrophysicists, atmospheric specialists, fluid mechanics specialists, and so on.

LASER : what a magic name nowadays ! Lasers in theaters, laser in night-club and cabarets, compact discs with lasers, medical therapy with laser, what else more ? Every one knows now this word, laser, but what a long way ! Remember. In July 1960, MAIMAN, working at the Hughes Aircraft Company was the first man to notice that a rubis, in special conditions of lightning, was able to flash in a monochromatic way. A few months later, JAVAN at the Bell Telephone laboratories was able to do the same thing with an Helium-neon blending. The Light Activation by Simulated Emission of Radiations, which was abbreviated in laser, was born. And noticing that the light in one picosecond cover 0.3 millimeter, the high accuracy telemetry was also born...

As Director of the CERGA, this well-known Agency for research in the field of Geodynamics and Astronomy, it is my pleasure to thank all the participants of this meeting for their enthusiasm and I am sure, for their generous cooperation. The brunt of responsibility during this meeting fall to the working group leaders, and especially to Mrs. Françoise BAUMONT, Dr. Jean GAIGNEBET, and Prof. C.O. Alley, Dr. B.A. Greene, Dr. K. Hamal. I would like to extend my warm congratulations to all experts who worked in the shadow to make this meeting a success.

An international technical meeting is one of the effective ways to propel the World's science forward. I believe that this exchange and discussion not only be beneficial to the academic researches carried out by every country's laser engineers, but also can promote the existing friendship between people, and further the mutual understanding and cooperation among the scientists of all countries.

Friends and colleagues from distant part of the World ! It is Apollo's rover that has brought you here from all different directions, from the States, from China, from Eastern Countries, from all Europe. The Rendez-Vous is not Olympia, but a city where we can have dialogue with Apollo for about 300 days in the year. A marvellous city, where flowers blossom in all four seasons. Every cloud has a silvery nimbused : take this one and don't forget to go back home with the last jasmine or a lot of carnations.

At last, I am impressed by the High quality of the program booklet : this guarantee that we may look forward to a highly inspiring and successful meeting.

Thank you for all that you have done so far !

I wish you all success in this workshop, and a pleasant stay on the French Riviera.

PREFACE

Le Sixième Colloque International sur l'Instrumentation en Télémétrie s'est déroulé du 22 au 26 Septembre 1986 à Antibes Juan-Les-Pins (France).

Comme lors des précédents colloques, un nombre important de présentations ont eu lieu. Les progrès accomplis depuis la dernière réunion (Herstmonceux) sont spectaculaires et extrêmement prometteurs. L'exactitude des stations a continué à s'améliorer grâce aux avancées technologiques et à une meilleure maîtrise des problèmes liés à la calibration. La mobilité et la fiabilité opérationnelle de quelques stations ouvrent la voie à des systèmes complètement automatisés. De nouveaux concepts (2 couleurs, haute cadence de répétition, logiciels de traitement, photodiodes en régime Geiger,...) ouvrent le champ à un nouveau progrès des performances (stations millimétriques) et à la possibilité de concevoir des équipements embarqués.

Ce tableau impressionnant des progrès réalisés et à venir, ne doit pas masquer quelques problèmes qui me semblent apparaître :

Le développement de systèmes de positionnement "Tout Temps" comme le système GPS Navstar (D.O.D), du V.L.B.I. va concurrencer sérieusement la télémétrie laser dans ses applications traditionnelles (Géodésie, Geodynamique) et l'application de notre technique à des domaines et objectifs moins additionnels (relativité, altimétrie spatiale laser sur les continents et les glaces, synchronisation horaire de très haute exactitude...) me semble nécessaire pour continuer à exister à moyen ou long terme. La part de plus en plus grande prise par les sessions non techniques (organisation de campagnes) au cours des derniers colloques me semble également dangereuse. Les discussions et les contacts personnels entre techniciens deviennent difficiles, donc rares, tant le programme est chargé. Par ailleurs les organisateurs de campagnes ont déjà à leur disposition un nombre annuel important de réunions spécialisées. Je pense que le temps dédié à l'instrumentation laser tous les deux ou trois ans doit être sauvegardé. Enfin la représentation de plus en plus fréquente de groupes par un seul exposé de "manager" exclu les rapports techniques détaillés qui me semblent le sang de ce type de colloque.

Ces remarques pour personnelles quelles soient et n'entraînant que ma responsabilité me semblent néanmoins refléter la sensibilité d'un nombre non négligeable de participants. Elles peuvent servir à ouvrir une réflexion générale, je serais heureux de connaître la réaction de notre Communauté.

Avant de terminer en souhaitant bonne chance au Nouveau Comité Scientifique d'Organisation, je tiens à remercier tous ceux qui ont aidé à faire de ce colloque une réussite. C'est à dire :

- Les participants sans lesquels nous n'existerions pas,
- les responsables de session dont la tâche ne s'arrête pas à la fin du colloque, puisqu'ils ont collecté les exposés pour les minutes,
- le Comité Local d'Organisation et en particulier Madame F. Baumont sans qui le colloque eut été assez "pagaille",
- le Comité Scientifique d'organisation :
C.O. Alley, son dynamisme inlassable a apporté beaucoup aux derniers colloques et à la télémétrie laser en général,
B.A. Greene dont les idées nouvelles et non conformistes ont dynamisées la discipline,
K. Hamal, pilier infatigable de la physique du laser et hôte à plusieurs reprises de comités d'organisation
- enfin, Madame M. Perrin pour la préparation du tirage des minutes.

Merci à tous et que vive la télémétrie laser.

J. GAIGNEBET

Membre du Comité Scientifique et Responsable du
Comité Local d'Organisation du VI I.W.L.R.I.

PREFACE

The Sixth International Workshop On Laser Ranging Instrumentation was held in Antibes Juan-Les-Pins (France) 22-26 September, 1986. A large number of presentations was given as in the previous workshops. The improvements accomplished since the last meeting (Herstmonceux) are spectacular and very promising. The accuracy of the station is still increasing thanks to the technological progress and to a better knowledge of the problems related to calibration. Completely automated systems are foreseen driven by the need for the mobility and operational efficiency of some stations.

We have to be aware of some approaching problems despite the impressive progress of our technique. Development of all weather and accurate positioning networks such as GPS/NAVSTAR (D.O.D.) or the VLBI will present competition to some traditional of laser ranging (Goedesy and Geodynamics). I feel that our technique has to aim towards less conservative goals (relativity, spaceborne altimetry to the ground and ice caps, time synchronization,..) to be able to grow in the medium and long term. I feel a dangerous trend in the increase of the time devoted to the technical sessions. The difficulties in holding adequate discussions and in managing personal contact among those participants interested in improving the experimental techniques of laser ranging have increased as the schedule has become really crowded. Campaign organizers have at their disposal a number of specialized meetings every years for that purpose. I do not think they need to take a substantial part of the time intended for laser ranging instrumentation during the only meeting every two or three years devoted to this topic. Last of all we see more and more managers representing their group with a single presentation. This tendency eliminates detailed technical reports wich are the life blood of such workshop. These personal remarks are on my own responsibility but I feel that they reflect the sensitivity of a non negligible part of the attendees. They may be a starting point for a general discussion and I would be happy to know the reaction of the community.

Prior to ending with my best wishes to the New Scientific Organizing Committee, I want to thank everyone who helped to make a success of this Workshop, that is to say :

- Participants,
- session chairmen and cochairmen for their task during and after the workshop,
- local organizing committee and particularly Mrs. F. Baumont whose work prevented the transformation of the workshop into a happy jumble,
- scientific organizing committee.:
- C.O. Alley whose permanent dynamism was a great support for the organization of the session and laser ranging in general,
- B.A. Greene whose bright new ideas and 'non conformism' have boosted the discipline,
- K. Hamal tireless pillar of the laser physics and host of many organizing committees
- at last but not the least, Mrs. M. Perrin for the preparation of the proceedings.

Thanks to everyone and hurrah for laser ranging.

J. GAIGNEBET
Member of the Scientific Organizing Committee
and Chairman of the Local Organizing Committee
of the 6th I.W.L.R.I.

The 6th International Workshop Laser Ranging Instrumentation
meeting at Antibes Juan-Les-Pins, France,

RECONGNISING the unique value and complementary nature of joint
lunar/artificial satellite tracking stations for the determination
of earth orientation parameters and recognising that new facilities
of this kind are under development, strongly recommends that due
attention be given to ensuring the continuation of these measurements
and their exploitation to the fullest extent.

The 6th International Workshop on Laser Ranging Instrumentation meeting at Antibes Juan-Les-Pins, France,

NOTING that since October 1983 the Royal Greenwich Observatory's laser ranging group has been one of the major contributors to international collaborative programmes related to the dynamics of earth satellites and the surface and body of the earth and

RECOGNISING that the quality and quantity of these observations are comparable with the best achieved elsewhere,

VIEWS with concern the uncertain future of the group and

REQUESTS that all feasible steps be taken to ensure its continued activity in a suitable environment.

The 6th International Workshop on Laser Ranging Instrumentation meeting at Antibes Juan-Les-Pins, France,

RECOGNISING that most institutions creating normal points are conforming now to the Herstmonceux recommendations and recognising the normal point comparison experiment initiated by NASA,

STRONGLY recommends that all institutes performing normal point calculations should create normal points for the October 1983 Lageos test data set and send the results to NASA for detailed intercomparisons which may lead to further refinements and definitions.

The 6th International Workshop on Laser Ranging Instrumentation,
meeting at Antibes Juan-Les-Pins, France,

· RECOGNIZING the important scientific results being obtained with
the LAGEOS spacecraft, and recognizing the remarkable improvements in
ground-based laser ranging technology that have occurred in the last
decade since the launch of LAGEOS,

strongly endorses

- (1) the plans to develop and launch a second LAGEOS (LAGEOS II)
in support in geodetic, geodynamics, and technology objectives
and urges its launch at the earliest possible opportunity.

In addition,

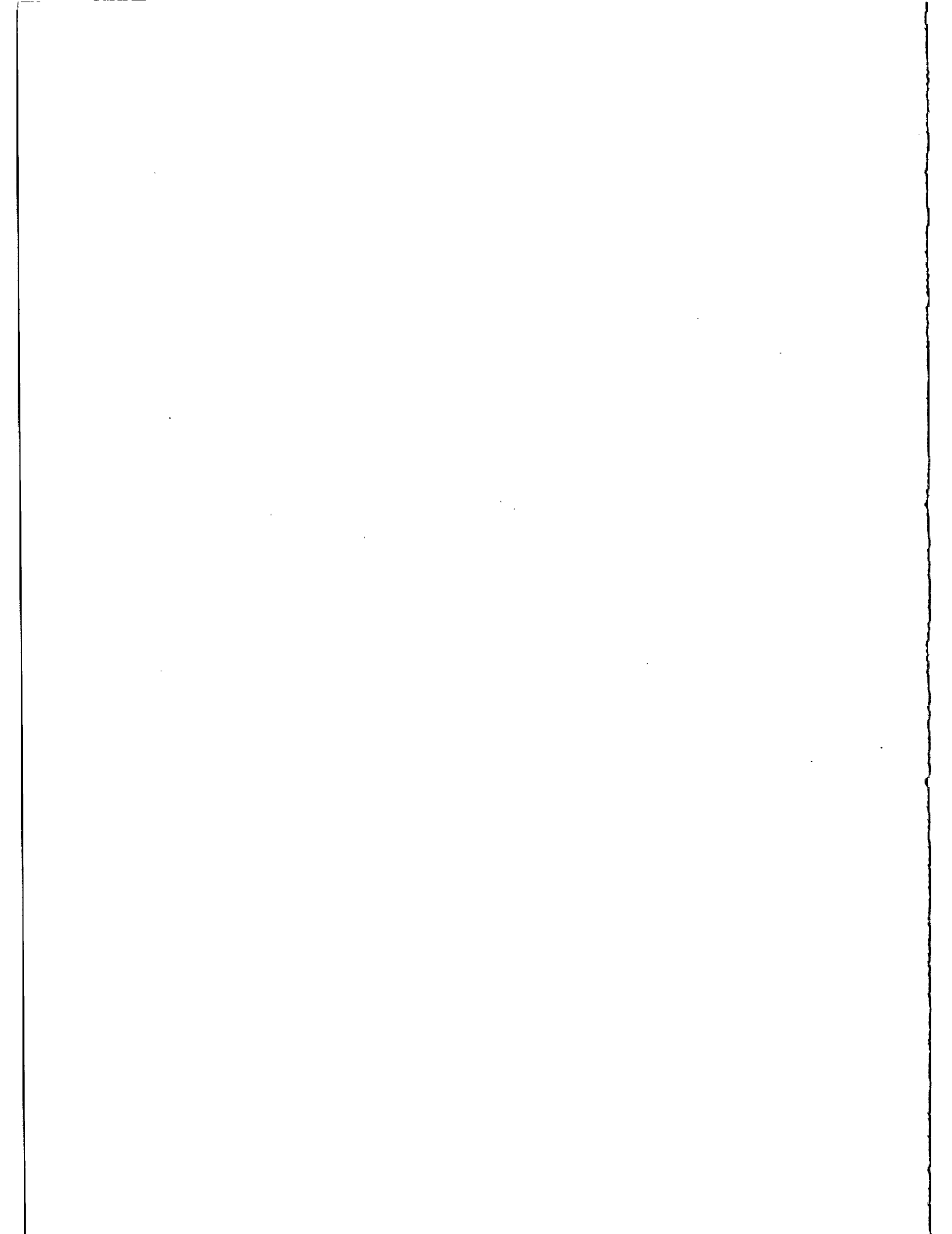
recognizing the unique value of precise laser ranging to satellites
in increasing our knowledge and understanding of fundamental forces
of nature , including the "gravito-magnetic force" predicted by
Einstein's theory of gravity,

urges strongly

- (2) that a third LAGEOS satellite (LAGEOS III) be constructed and
launched into an appropriate orbit allowing the detection and
measurement of the gravito-magnetic orbit precession produced
by the rotating Earth, as well as increasing our ability to
monitor Universal Time.

The 6th International Workshop on Laser Ranging Instrumentation
meeting at Antibes Juan-Les-Pins, France,

· RECOGNISING the significant contributions that Laser Ranging
systems are making to geodesy, geophysics, geodynamics and other
disciplines hereby GRATEFULLY ACKNOWLEDGES the dedicated efforts of
the crews operating these systems for the benefit of the scientific
community.



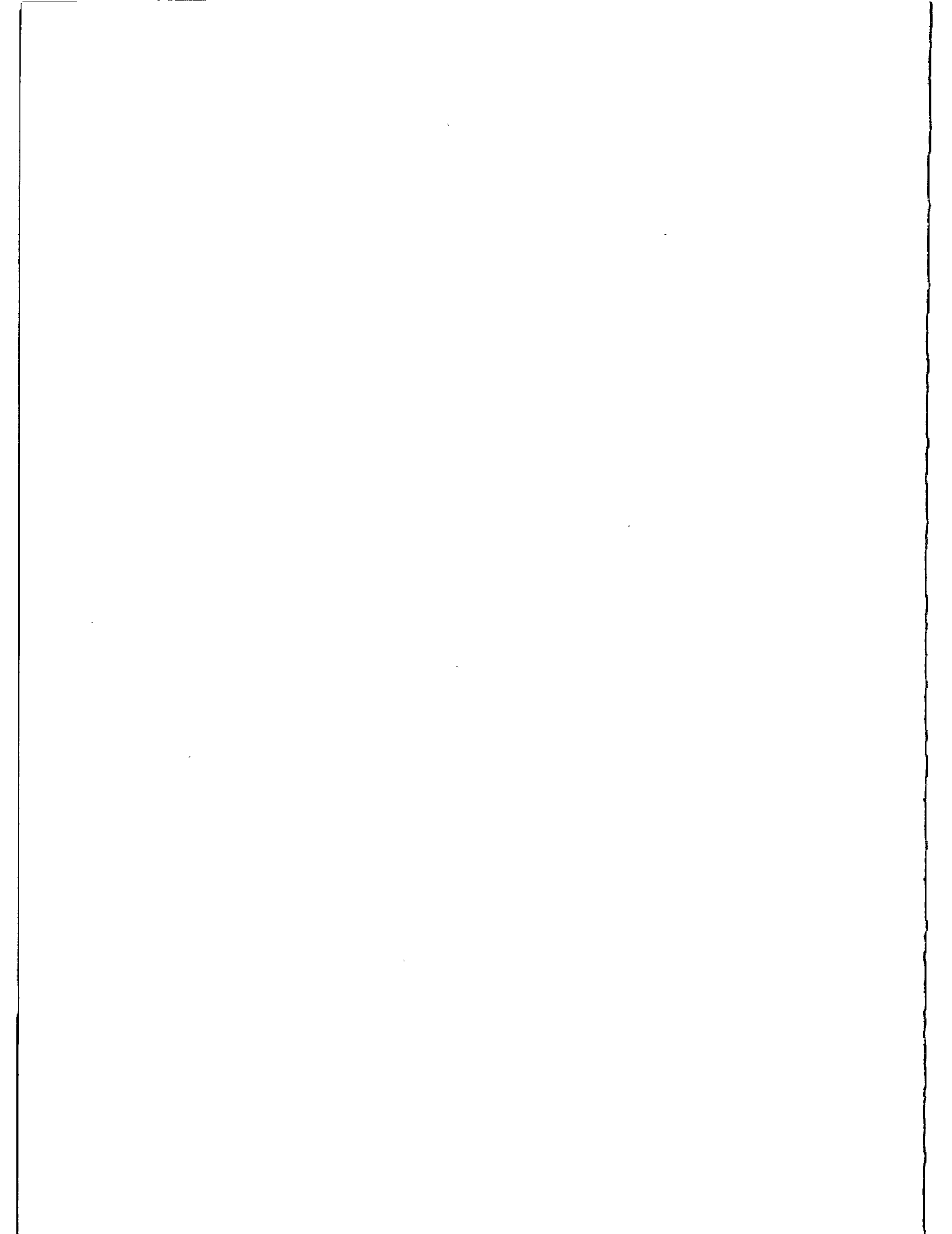
The 6th International Workshop on Laser Ranging Instrumentation meeting at Antibes, France,

NOTING that since October 1983 the Royal Greenwich Observatory's laser ranging group has been one of the major contributors to international collaborative programmes related to the dynamics of earth satellites and the surface and body of the earth and

RECOGNISING that the quality and quantity of these observations are comparable with the best achieved elsewhere,

VIEWS with concern the uncertain future of the group and

REQUESTS that all feasible steps be taken to ensure its continued activity in a suitable environment.



AT ANTIBES JUAN LES PINS ON 22 - 26 SEPTEMBER 1986
=====

LIST OF PARTICIPANTS

Prof. C.O. ALLEY
Dept of Physics & Astronomy
University of Maryland
Code def 3
College Park, MD 20742
U.S.A.

Tel : (301) 4543405
Telex : 908787 PHY UN MD CORK

Dr. R. APPLER
Code 601
G.S.F.C.
Greenbelt, MD 20771
U.S.A.

Tel : (301) 286 8119
Telex : 257559

Dr. S.G. ALBANESI
Piano Spatiale Nazionale
CNR
Via Regina Margherita, 202
00198 ROMA
ITALIE

Tel : 64 76 72 35
Telex : 616162 CNRTSN

F. BARLIER
CERGA / GRGS
Avenue Nicolas Copernic
06130 GRASSE
FRANCE

Tel : 93 36 58 49
Telex : 470865 F.

F. BAUMONT
CERGA/GRGS
Avenue Nicolas Copernic
06130 GRASSE
FRANCE

Tel : 93 36 58 49
Telex : 470865 F.

Dr. W. BEEK
Dept. of Geodesy
Delft University of Technology
Observatorium Kootwijk
Postbus 581
7300 AN APELDOORN
PAYS BAS

Tel : 057 69 341
Telex : 36 442 (SATKO UL)

Prof. B. BERTOTTI
University of Cambridge
Institute of Astronomy
CAMBRIDGE
ROYAUME UNI

Tel : 382 31 341
Telex : 817 297 (ASTRON G)

Dr. J. BIANCO
Piano Spatiale Nazionale
CNR
Via Regina Margherita, 202
00198 ROMA
ITALIE

Tel : 64 76 72 35
Telex : 616162 CNRTSN

Mr. BOKOBZA
QUANTEL
B.P. 23
91941 LES ULIS CEDEX
FRANCE

Tel : (1) 690 76 615
Telex : 691329

Dr. S.A. BOWMAN
Physics and Astronomy
University of Maryland
College Park, MD 20742
U.S.A.

Tel : 301 454 3405
Telex : 908797 PHY UN MD CORK

Dr. J. A. BUISSON
Naval Research Laboratory (NRL)
Code 7773
4555 Overlook Ave S.W
WASHINGTON, DC 20375
U.S.A.

Tel : (202) 767 2595
Telex :

Dr. A. CAPORALI
Dipartimento di Fisica G. Galilei
Universita di Padova
Via Marzolo N 8
I-35131 PADOVA
ITALIE

Tel : 49 844 278
Telex : 43330308 (DFGGPD-I)

Dr. G. CECCHET
I.N.F.N.
University of Pavia
V. Bassi 6
I-27100 PAVIA
ITALIE

Tel :
Telex :

Dr. A. CENCI
Telespazio, Via Bergaamini 50
ROMA
ITALIE

Tel : 64 987 254
Telex : 620424 (TSPZRO I)

Dr. I. CIUFOLINI
University of Texas
AUSTIN, TX 78712
U.S.A.

Tel : (512) 471 5573
TWX : 910 874 1351

Dr. R. J. COATES
Code 904
NASA/G. S. F. C.
GREENBELT, MD 20771
U.S.A.

Tel : 301 286 8809
Telex : 257559

E. CUOT
CERGA
Avenue Nicolas Copernic
06130 GRASSE
FRANCE

Tel : 93 36 58 49
Telex : 470 865 F

Dr. P. R. DACHEL
Bendix Field Engineering Corp.
1 Bendix Road
COLUMBIA, MD 21045
U.S.A.

Tel : 301 964 7189
Telex : 198120

Dr. P. J. DUNN
Analytical Services Center,
Inc. Lanham,
MARYLAND 20752
U.S.A.

Tel : 301 731 2044
Telex : 590613

Dr. R. J. EANES
Dept. of Aerospace Eng.
University of Texas
AUSTIN, TX 78712
U.S.A.

Tel : (512) 471 4273
Telex : 7044265 (CSRUTX UD)

Dr. D. R. EDGE
Bendix Aerospace
One Bendix Road
COLUMBIA, MD 21045
U.S.A.

Tel : (301) 344 5013
Telex : 197700 (GLTN)

P. EXERTIER
CERGA/GRGS
Avenue Nicolas Copernic
06130 GRASSE
FRANCE

Tel : 93 36 58 49
Telex : 470865 F

Dr. A.N. M.FADHL
Director
King Abdul Aziz City of Science
P.O. Box 6086
RIYADH
11442 ARABIE SAOUDITE

Tel : 478-8000:580
Telex : 401590 (KACST SJ)

Dr. FALCONER
Divison of National Mapping
P.O. Box 31
BELCONNEN A.C.T. 2616
AUSTRALIE

Tel : 61 52 50 95
Telex : 62 230 (NATMAP)

D. FERAUDY
CERGA/GRGS
Avenue Nicolas Copernic
06130 GRASSE
France

Tel : 93 36 58 49
Telex : 470 865 F.

Dr.M. FERMI
Telespazio SPA
via Bergamini, 50
00159 ROMA
ITALIE

Tel : 64 987 489
Telex : 620424(TSPZRO I)

Dr. T. FISCHETTI
2609 Village Lane
Silver Spring, Md 20906
U.S.A.

Tel : (301) 871 6272
Telex : 650 272 86 72 (MCI)

Dr. E. A. FLINN
Mail Code EEG
NASA Headquarters
WASHINGTON DC 20546
U.S.A.

Tel : (202) 453 1675
Telex : 89530 (NASA WSH)

Dr. H. FUNG
Yunnan Observatory
P.O. Box 110
KUNMING
Yunnan Province
R.P. CHINE

Tel : 72 946
Telex : 64040 (YUOBS.FN)

J. GAIGNEBET
CERGA/GRGS
Avenue Nicolas Copernic
06130 GRASSE
FRANCE

Tel : 93 36 58 49
Telex : 470 865 F.

Dr. B.A. GREENE
Division of National Mapping
P.O. Box 31
BELCONNEN A.C.T. 2616
AUSTRALIE

Tel : 61 52 5095
Telex : 62 230 (NATMAP)

P. GRUDLER
CERGA/GRGS
Avenue Nicolas Copernic
06130 GRASSE
FRANCE

Tel : 93 36 58 49
Telex : 470 865 F.

Dr. L. GRUNWALTD
Central Institute for
Physics of the Earth
Telegrafenberg A17
DDR 1500 POTSDAM
R.D.A

Tel :
Telex : 15305 (VDEPDM DD)

Mr. F. GUERIN
Aerospatiale
100. Boulevard du Midi
06322 CANNES LA BOCCA Cedex
FRANCE

Tel : 93 90 00
Telex : 470 902F (AECAN)

Dr. K. HAMAL
Faculty of Nuclear Science
Physical Engineering
BREHOVA 7
115 19 PRAGUE 1
TCHECOSLOVAQUIE

Tel : 284 8840
Telex : 121254 (FJFI)

J.L. HATAT
CERGA/GRGS
Avenue Nicolas Copernic
06130 GRASSE
FRANCE

Tel : 93 36 58 49
Telex : 470 865 F.

Prof. H. FENG
Deputy Director of Yunnan
Observatory
P.O. Box 110
KUNMING, YUNNAN Province
R.P. CHINE

Tel : 72 946
Telex : 64040 (YUOBS CN)

Dr. R. HOPFL
Satellitenbeobachtungsstation
Wettzell
8493 KOETZTING
R.F.A.

Tel : 09941 / 8643
Telex : 69 937 (WESAT D)

Dr. B. HYDE
Alpoptics
267, Rue du Chateau du Roi
38220 VIZILLE
FRANCE

Tel : 76 68 24 05
Telex :

Mr. P. JAQUET
Hamamatsu Photonics France
49-51 Rue de la Vanne
92120 MONTRouGE
FRANCE

Tel : 46 55 47 58
Telex : 631 895

Dr. H. JELINKOVA
Faculty of Nuclear Science
Physical Engineering
BREHOVA 7
115 19 PRAGUE 1
TCHECOSLOVAQUIE

Tel : 284 8840
Telex : 121254 (FJFI)

Dr. H. JUNGINGER
Satellitenbeobachtungsstation
Wettzell
8493 KOETZTING
R.F.A.

Tel : 09941/8643
Telex : 69937 (WESAT D)

Mr. M. KASSER
I.G.N.
2. Avenue Pasteur
94160 SAINT MANDE
FRANCE

Tel : 43 74 12 15
Telex : 210 551 F.

Dr. W. KIELEK
Warsaw Radiotechnical Institute
Faculty of Electronics
Institute of Radioelectronics
00-665 NOVOWIEJSKA STR. 15/19
VARSOVIE POLOGNE

Tel :
Telex : 813307 (PW PL)

Dr. D. KIRCHNER
Technische Universitat
Inffeldgasse 12
A-8010 GRAZ
AUTRICHE

Tel : 316 70 61
Telex : 311221 (TUGRZ A)

DR.G. KIRCHNER
Observatory of Graz Lustbuehel
Lustbuehelstrasse 46
A-8042 GRAZ
AUTRICHE

Tel : (316) 42 231
Telex : 311 078 (OBSLG A)

Dr. W. J. KLEPCZYNSKI
U.S. Naval Observatory
Washington, D.C.20390
U.S.A.

Tel : 19 1 (202) 653 15 21
Telex : 710 822 1970

Dr. P. KLOECKLER
Astronomisches Institut
Bern Universitat
Sidlerstrasse 5
CH-3012 BERNE
SUISSE

Tel : 31 65 85 91
Telex : 32 320 (PHYBE)

Dr. R. KOLENKIEWICZ
NASA/G. S. F. C.
Code 621
GREENBELT, MD 20771
U.S.A.

Tel : 301 286 5373
Telex : 710 828 9716

Dr. KORAKITIS
National Technical University
9 K. Zographou
ATHENES 624
GRECE

Tel : 18131961
Telex : 215032 (GEO GR)

Dr. S. LABINI
Piano Spatiale Nazionale
Via Regina Margherita, 202
OO198 ROMA
ITALIE

Tel : 64 76 72 75
Telex : 616162 (CNRTSN)

J.G. LANGLOIS
CERGA/GRGS
Avenue Nicolas Copernic
06130 GRASSE
FRANCE

Tel : 93 36 58 49
Telex : 470 865 F.

M. LAPLANCHE
CERGA/GRGS
Avenue Nicolas Copernic
06130 GRASSE
FRANCE

Tel : 93 36 58 49
Telex : 470 865 F.

Dr. J. LATKA
Space Research Center
UL Bartycka 18
00-716 WARSZAWA
POLOGNE

Tel : 41 00 41
Telex : 081 56 70 (CBK PL)

Dr. D. LELGEMAN
Technische Universitat
Schr. H. 12
Strasse Des 17 Juni, 135
1000 BERLIN 12
R.F.A.

Tel : 30 314 3205
Telex : 184 262 (TUBLN D)

Prof. S. LESCHIUTA
Dipartimento Electronica
Politecnico
Coso Duca Degli Abruzzi, 24
10123 TORINO
ITALIE

Tel : 11 55 67 235
Telex : 220 646

Dr. H.L. LINDER
Code 634
NASA/G.S.F.C.
GREENBELT MD 20771
U.S.A.

Tel : (301) 2865373
Telex : 710 828 9716

J.F. MANGIN
CERGA/GRGS
Avenue Nicolas Copernic
06130 GRASSE
FRANCE

Tel : 93 36 58 49
Telex : 470865 F

Mr. J.M. MARTEAU
QUANTEL
Avenue de l'Atlantique
Z.I. Courtaboeuf
91940 LES ULIS
FRANCE

Tel : 69 07 66 15
Telex :

Mr. F. H. MASSMANN
Deut. Geod. Forschlings Inst.
Marstallplatz 8
D8000 MUNCHEN 22
R.F.A.

Tel : (089) 230 31 217
Telex : 5213 550 (DGFI D)

Dr. W.E. MATTHEWS
Royal Greenwich Observatory
Herstmonceux Castle
HAILSHAM, EAST SUSSEX
ROYAUME UNI

Tel : 323 83 31 71
Telex : 87451

Dr. J.J. MILLER
Bendix Field Engin. Corp.
1 Bendix Road
COLUMBIA, MD 21045 1897
U.S.A.

Tel : (301) 344 75 30
Telex : 197700 (GLTN)

Mr. F. MOYA
B.M.I.
26 Rue du Petit Fief
Z.I. La croix blanche
91700 STE GENEVIEVE DES BOIS
FRANCE

Tel : 60 16 12 45
Telex :

O. MULHOLLAND-CALAME
CERGA/GRGS
Avenue Nicolas Copernic
06130 GRASSE
FRANCE

Tel : 93 36 58 49
Telex : 470865F

Dr. H. MULLER
Deut. Geod. Forschlings Inst.
Marstallplatz 8
D8000 MUNCHEN 22
R.F.A.

Tel : (089) 230 31 217
Telex : 5213 550 (DGFI D)

Dr. Z. NEUMANN
Observatory Ondrejov
25165 ONDREJOV
TCHECOSLOVAQUIE

Tel : 27 245 25
Telex : 121579 (ASTR C)

Dr. S. NEWHALL
JPL, 138.208
4800 Oak Grove DR.
PASADENA, CA 91109
U.S.A.

Tel : 818 354 4371
Telex : 675 429 (JPL COMM PSD)

Dr. A. NOVOTNY
Faculty of Nuclear Science
and Physical Engineering
Brehova 7
115 19 PRAGUE 1
TCHECOSLOVAQUIE

Tel : 2 84 88 40
Telex : 121254 (FJFI)

Dr. K.H. OTTEN
Delft University of Technology
P.O. BOX 581
7300 AN APELDOORN
PAYS-BAS

Tel :
Telex :

J. PARIS
CERGA/GRGS
Avenue Nicolas Copernic
06130 GRASSE
FRANCE

Tel : 93 36 58 49
Telex : 470865F

Dr. M. PAUNONEN
Finnish Geodetic Institute
Ilmalankatu 1A
00240 HELSINKI
FINLANDE

Tel : 358 0 26 4994
Telex : 12 2771 (ROKTA SF)

Dr. M.R. PEARLMAN
Smithsonian Astrophysical Obs.
60. Garden St.
CAMBRIDGE, MASS 02138
U.S.A.

Tel :
Telex : 921428 (SATELLITE CAM)

Dr. P. PETRONI
Lab. CISI
Via Reggio Emilia, 39
20090 SEGRATE
ITALIE

Tel :
Telex :

F. PIERRON
CERGA/GRGS
Avenue Nicolas Copernic
06130 GRASSE
FRANCE

Tel : 93 36 58 49
Telex : 470 865F.

Dr. J.D.H. PILKINGTON
Royal Greenwich Observatory
Herstmonceux Castle
HAILSHAM, EAST SUSSEX BN27 1RP
ROYAUME UNI

Tel : 323 83 3171
Telex : 87451

Dr. P. PIZZOLATI
Lab. CISI
Via Reggio Emilia, 39
20090 SEGRATE
ITALIE

Tel :
telex :

J. PHAM-VAN
CERGA/GRGS
Avenue Nicolas Copernic
06130 GRASSE
FRANCE

Tel : 93 36 58 49
Telex : 470 865 F.

Dr. I. PROCHAZKA
Faculty of Nuclear Science
Physical Engineering
BREHOVA 7
115 19 PRAGUE 1
TCHECOSLOVAQUIE

Tel : 284 88 40
Telex : 121254 (FJFI C)

Prof. S.A. RAMSDEN
Dept. of Applied Physics
University of Hull
HULL HU6 7RX
ROYAUME UNI

Tel : 482 46 51 24
Telex : 592530 (UNIHUL G)

Dr. J.D. RAYNER
Physics Dept.
University of Maryland
College Park, MD 20742
U.S.A.

Tel : 301 454 34 05
Telex : 908 787 (PHY UN MD CORK)

Dr. G. REICHERT
Geodetic Institute
University of Bonn
Nussallee 17
D 5300 BONN
R.F.A.

Tel : 223 33 77 33
Telex : 88 69693 (PHYBE D)

Dr. T. SCHILTKNECHT
Astronomisches Institut
Universitat Bern
Sidlerstrasse 5
CH-3012 BERNE
SUISSE

Tel : 41 65 85 91
Telex : 32320 (PHYBE)

Dr. W. SCHLUTER
Institut fur Angewandte Geod.
(ABT, II DGF I)
Richard Stauss Allee 11
D-6000 FRANKFURT AM MAIN 70
R.F.A.

Tel : 069 63 331
Telex : 413592

Dr. B.E. SCHUTZ
Center for Space Research
University of Texas
AUSTIN, TX 78712
U.S.A.

Tel : (512) 471 42 67
Telex : 704265 (CSRUTX UD)

Mr. B. SERENE
Centre Spatial de Toulouse
18. Avenue E. Belin
31055 TOULOUSE Cedex
France

Tel : 61 27 35 63
Telex : 520 862 (ESA TLS F)

Dr. P. SHELUS
Dept. of Astronomy
University of Texas
AUSTIN, TEXAS 787 12
U.S.A.

Tel : (512) 471 339
TWX : 910 874 1351

Dr. D. E. SMITH
Code 621
NASA/G.S.F.C.
GREENBELT, MD 20771
U.S.A.

Tel : (301) 286 85 55
TWX : 710 828 97 16

Dr. C. A. STEGGERDA
Physics & Astronomy
University of Mariland
College Park, MD 20742
U.S.A.

Tel : (301) 454 34 05
Telex : 90 87 87 (PHY UN MD CORK)

Dr. Y. SUZAKI
Defense Electronic Systeme Dpt.
Totsuka Works, Hitachi, LTD
216 Totsuka-Machi, Totsuka-Ku
YOKOYAMA 244
JAPAN

Tel :
Telex : 3823 503 (HITUKA J)

J.M. TORRE
CERGA/GRGS
Avenue Nicolas Copernic
06130 GRASSE
FRANCE

Tel : 93 36 58 49
Telex : 470 865 F.

Dr. M. TORRENCE
EG&G
5000 Philadelphia Way
Sweet J
LANHAM, MD 20706
U.S.A.

Tel : 301 731 20 44
Telex :

Dr. M.R. VAN DER KRAAN
C/O Technisch Physische
Dients Tno-Th
Postbus 155
Stieltjesweg 1
200 AD DELFT-NL
PAYS BAS

Tel : 15 78 71 49
Telex : 38091 (TPDDT NL)

Dr. D.L.F. VAN LOON
Observatory for Satellite
Geodesy Kootwijk
P.O. Box 581
7300 AN APELDOORN
PAYS-BAS

Tel : 57 69 341
Telex : 36442 (SATKO UL)

Dr. T. K. VARGHESE
Bendix Aerospace
1 Bendix Road
COLUMBIA, MD 21045
U.S.A.

Tel : (301) 345 56 40
Telex : 197 700 (GLTN GRNBLT UT)

C. VEILLET
CERGA/GRGS
Avenue Nicolas Copernic
06130 GRASSE
FRANCE

Tel : 93 36 58 49
Telex : 470 865 F.

Dr. E. VERMAAT
Delft University of Technology
P.O. Box 581
7300 AN APELDOORN
PAYS BAS

Tel : 57 69 341
Telex : 36 442 (SATKO NL)

Dr. H. VISSER
Technisch Physische Dienst Tno-th
Stielljesweg 1
Postbus 155
2600 AD DELFT
PAYS BAS

Tel : 15 78 72 10
Telex : 38091 (TPDDT NL)

Mr. P. VOLUER
Quantel
B.P. 23
91941 LES ULIS Cedex
FRANCE

Tel : (1) 690 76 615
Telex : 691329

Dr. B. C. WANG
P.O. Box 110
KUNMING Yunnan Province
R.P. CHINE

Tel : 72 946
Telex : 64 040 (YUOBS.FN)

Dr. M.L. WHITE
Institute for Astronomy
University of Hawaii
P.O. Box 209
KULA, HI 96790
U.S.A.

Tel :
Telex : 723 8459 (UH AST HR)

Dr. J. WIANZ
MacDonald Observatory
FT. Davis, TX 79734
U.S.A.

Tel : (915) 426 36 68
TWX : 910 874 1351

Dr. P. WILSON
Institute für Angewandte
Geodäsie
Richard Strausse Allee 11
D-6000 FRANKFURT M70
R.F.A.

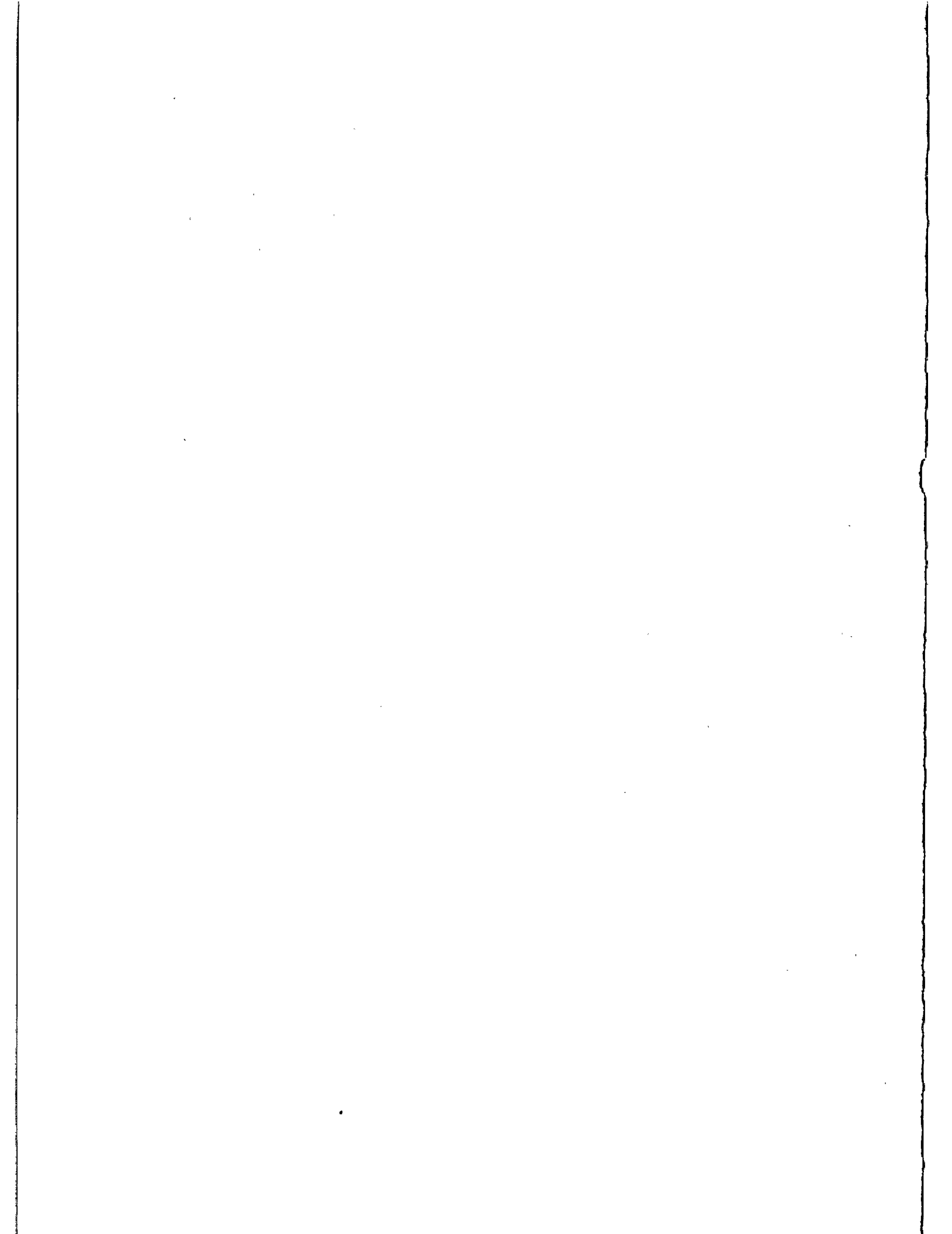
Tel :
Telex : 413592 (JPA D)

Dr. Z. W. YAO
Shanghai Observatory
Academia Sinica
SHANGHAI
R.P. CHINE

Tel : 386 191
Telex : 33164 (SHAO CN)

Dr. YANG
Shanghai Observatory
Academia Sinica
SHANGHAI
R.P. CHINE

Tel : 386 191
Telex : 33164 (SHAO CN)



NEW RELATIVISTIC MEASUREMENTS WITH LASER RANGED SATELLITES

I. Ciufolini
Center for Space Research
The University of Texas at Austin
Austin, Texas 78712 - USA -

Telephone (512) 471 5573
TWX 910874-1351

ABSTRACT

The accuracy of laser ranging associated with the use of a LAGEOS like satellite (inclination supplementary to the existing LAGEOS) allows the measurement of the gravitomagnetic field of the earth.

The proposal of a satellite for this determination is developed here.

NEW RELATIVISTIC MEASUREMENTS WITH LASER RANGED SATELLITES

Ignazio Ciufolini
 Center for Space Research
 The University of Texas at Austin
 Austin, Texas 78712*

Telephone (512) 471-5573

The importance of measuring the gravitomagnetic field is comparable to the importance of measuring gravitational waves.

In electrodynamics the wave equation describing electromagnetic waves in vacuum is, in the Lorentz gauge:

$$\square A^\alpha = 0 \quad (1)$$

where $\square = \eta^{\alpha\beta} \frac{\partial^2}{\partial x^\alpha \partial x^\beta}$ and A^α is the 4-vector potential.

Similarly in General Relativity ^{(1), (2), (3)} in the weak field limit, the wave equation describing gravitational waves in vacuum is:

$$\square h_{\alpha\beta} = 0 \quad (2)$$

where $\square = g^{\alpha\beta} \frac{\partial^2}{\partial x^\alpha \partial x^\beta}$ is the D'Alambertian operator in curved spacetime and in the weak field limit: $h_{\alpha\beta} \approx g_{\alpha\beta} - \eta_{\alpha\beta}$ ($g_{\alpha\beta}$ is the spacetime metric tensor and $\eta_{\alpha\beta}$ is the Minkowski metric tensor).

A similar analogy is valid for the gravitomagnetic field.

In electrodynamics the equation of motion of a particle with mass m and charge q subjected to an electric field \vec{E} and a magnetic field \vec{B} is the Lorentz equation:

$$m \frac{d^2 \vec{x}}{dt^2} = q (\vec{E} + \vec{v} \times \vec{B}) \quad (3)$$

The torque acting on a test magnet with magnetic dipole moment $\vec{\mu}$ is $\vec{\tau} = \vec{\mu} \times \vec{B}$ and the force on the magnetic dipole is $\vec{F} = (\vec{\mu} \cdot \nabla) \vec{B}$ where $\vec{B} = \nabla \times \vec{A}$ and for a source with magnetic moment \vec{m} : $\vec{B} = \frac{3\vec{n}(\vec{n} \cdot \vec{m}) - \vec{m}}{|\vec{x}|^3}$ and $\vec{A} = \frac{\vec{m} \times \vec{x}}{|\vec{x}|^3}$.

Similarly in General Relativity ^{(4), (5)} the equation of motion of a test particle in the field of a central body with mass M and angular momentum \vec{J} , can be written in the weak field and slow motion

* Supported by Grant NAS 5-28192

limit:

$$m \frac{d^2 \vec{x}}{dt^2} = m(\vec{g} + \frac{d\vec{x}}{dt} \times \vec{H}) \quad (4)$$

where $\vec{g} \equiv -\frac{M}{r^2} \hat{r}$ is the standard, radial Newtonian acceleration, \vec{H} is the gravitomagnetic field given in this limit by $\vec{H} \equiv \nabla \times \vec{\beta} \equiv 2 \left[\frac{\vec{J} - 3(\vec{J} \cdot \hat{r})\hat{r}}{r^3} \right]$ and $\vec{\beta}$ is the gravitomagnetic or Lense-Thirring potential $\vec{\beta} = (\beta^r, \beta^\theta, \beta^\phi) = \left[0, 0, -\frac{2J}{r^3} \right]$, in geometrized units: $G \equiv c \equiv 1$. Furthermore in General Relativity ^{(4), (5)} the torque acting on a gyroscope with spin angular momentum \vec{s} is in the weak field and slow motion approximation:

$$\vec{\tau} = \frac{d\vec{s}}{dt} = \frac{1}{2} \vec{s} \times \vec{H} \quad (5)$$

and therefore the gyroscope precesses with respect to an asymptotic inertial frame, defined by the distant stars, with angular velocity:

$$\vec{\Omega} = -\frac{1}{2} \vec{H} = \frac{-\vec{J} - 3(\vec{J} \cdot \hat{r})\hat{r}}{r^3} \quad (6)$$

This phenomenon is the "dragging of gyroscopes" or "dragging of inertial frames" of which the gyroscopes define the axes. The force exerted on the gyroscope by the gravitomagnetic field \vec{H} is

$$\vec{F} = \left(\frac{1}{2} \vec{s} \cdot \nabla \right) \vec{H} \quad (7)$$

Finally, due to the second term in the force (4), the orbital plane (and the orbital angular momentum) of a test particle - which can be thought as an enormous gyroscope - is dragged in the sense of rotation of the central body. This dragging of the whole orbital plane is described by the formula for the rate of change of the longitude of the node discovered by Lense and Thirring in 1918 ^{(6), (7)}:

$$\Omega^{\text{Lense-Thirring}} = \frac{2J}{a^3(1-e^2)^{3/2}} \quad (8)$$

where a is the satellite semimajor axis, e the eccentricity and J the angular momentum of the central body.

Many experiments have been proposed to measure the gravitomagnetic field: Everitt - 1974 and Lipa, Fairbank and Everitt - 1974; Van Patten and Everitt - 1976; Braginski, Caves and Thorne - 1977; Scully - 1979; Braginski and Polnarev - 1980; Braginski, Polnarev and Thorne - 1984. In particular the experiment of Lipa, Fairbank and Everitt ⁽⁸⁾ will try to measure the gravitomagnetic precession (6) of a gyroscope orbiting the Earth.

We propose here a different experiment based on the Lense-Thirring effect (8). The idea ^{(9), (10), (11), (12)} is to measure the gravitomagnetic nodal precession (8) due to the angular momentum of the Earth on laser ranged satellites like LAGEOS ^{(13), (14)}. The Lense-Thirring precession (8) is for LAGEOS $\Omega^{\text{Lense-Thirring}} \approx 31$ milliarcsec/year. The total nodal precession is ⁽¹⁴⁾ for LAGEOS $\Omega^{\text{total}} \approx 126^\circ$ and can be measured ⁽¹⁵⁾ with laser ranging with an accuracy of 1 or 2 milliarcsec/year. Therefore, if all the classical perturbations on LAGEOS were known, it would be possible to measure Ω^{LT} with a few percent accuracy. The deviations of the Earth gravity field from

spherical symmetry - quadrupole and higher mass moments of the Earth - are responsible for the most part of the total nodal precession⁽¹⁶⁾. Even though the Earth's multiple mass moments are very well known^{(17), (18)}, they are unfortunately not known at the level of accuracy to measure the Lense-Thirring precession. The uncertainty in the even zonal harmonic coefficients J_{2n} relative to J_2 is⁽¹⁷⁾,

⁽¹⁸⁾ of the order of $\frac{\delta J_{2n}}{J_2} \approx 10^{-6}$, which uncertainty corresponds for J_2 to an uncertainty in the nodal precession of ± 450 milliarcsec/year, much larger than the Lense-Thirring precession (8).

The idea^{(9), (10), (11), (12)} is to launch a tandem laser ranged satellite "LAGEOS-X" with the same orbital parameters of LAGEOS apart from a supplementary inclination i.e. $I_{\text{LAGEOS-X}} \approx 70^\circ$ ($I_{\text{LAGEOS}} \approx 110^\circ$). In such a way the classical precession will be equal and opposite for the two satellites; in fact this classical precession is proportional to the cosine of the inclination I and is a function of even trigonometric functions of I ⁽¹⁶⁾. On the contrary, the Lense-Thirring precession will be the same in both magnitude and sign, thus allowing^{(9), (10), (11), (12)} the extraction of the general relativistic drag.

In other words, the two tandem satellites define a "gyroscope".

The bisector of the angle between the nodal lines of the two satellites is not affected by the Earth's multipole mass moments but only by the Lense-Thirring drag and by other small calculable classical precessions⁽¹²⁾. Since the precession of the nodal lines of the two satellites, due to the Earth's multiple moments, is equal and opposite, the precession of the bisector between the two nodal lines is zero, apart for other small classical precessions⁽¹²⁾.

We studied⁽¹²⁾ several non-gravitational nodal perturbations.

The result⁽¹²⁾ is that the error in the calculated value of the secular nodal precession or the value of the secular nodal precession itself is for each perturbation less than 1% of the Lense-Thirring drag, we list some of the dominant perturbations.

Direct solar radiation pressure:

The rate of change of the nodal longitude Ω , due to an external force \vec{f} , can be written⁽¹⁶⁾:

$$\frac{d\Omega}{dt} = \frac{1}{na \sin I} (1-e^2)^{-1/2} f W \frac{r}{a} \sin(\nu + \omega) \quad (9)$$

where n is the mean motion, a the semimajor axis, I the inclination, e the eccentricity, r the radial coordinate, ω the argument of the pericenter, ν the mean anomaly, f is the magnitude of the external force per unit satellite mass and W is the direction cosine of the force \vec{f} along the normal to the orbital plane, which can be written^{(19), (20), (21)}:

$$W = \sin I \cos^2 \frac{\epsilon}{2} \sin(\lambda_0 - \Omega) - \sin I \sin^2 \frac{\epsilon}{2} \sin(\lambda_0 + \Omega) - \cos I \sin \epsilon \sin \lambda_0 \quad (10)$$

where ϵ is the obliquity of the ecliptic and λ_0 is the ecliptic longitude of the Sun.

The acceleration f_\odot due to direct solar radiation pressure on a spherical satellite like LAGEOS, can be written^{(20), (21)}:

$$f_\odot = s \frac{A}{m} P \left[\frac{a_0}{r_0} \right]^2 \quad (11)$$

where s is a number between 0 and 2, depending on the reflection properties of the satellite surface, $\frac{A}{m}$ is the satellite cross-sectional area to mass ratio and $P \equiv \frac{\phi}{c} = \frac{\text{solar constant}}{\text{speed of light}} \approx 4.65 \times 10^{-5} \text{ dyn} \times \text{cm}^{-2}$

is the solar radiation pressure at the Earth when the geocentric distance r_0 is equal to its mean distance a_0 .

Integrating equations (9) and (10) with the proper initial conditions ⁽¹⁵⁾, we found ⁽¹²⁾ that over one orbital period $P = 3.758h$:

$$\dot{\Omega}^{\text{Direct radiation pressure}}|_P \approx 10^{-1} \dot{\Omega}^{\text{Lense-Thirring}}|_P \quad (12)$$

Since ⁽¹⁵⁾ the uncertainty in the value of f_0 is for LAGEOS less than 1%, the error in the calculated nodal precession due to direct solar radiation pressure is over one orbital period P :

$$\text{Error} \left[\dot{\Omega}^{\text{Direct radiation pressure}}|_P \right] \lesssim 10^{-3} \dot{\Omega}^{\text{Lense-Thirring}}|_P \quad (13)$$

Earth's albedo:

On the basis of works of Lautmann ^{(22), (23)} and Bender ^{(24), (25)} and due to the periodicity in the sign of W , we found that the secular nodal precession due to the Earth's albedo is over one year:

$$\dot{\Omega}^{\text{Albedo}}|_{1y} \lesssim 10^{-1} \dot{\Omega}^{\text{Lense-Thirring}}|_{1y} \quad (14)$$

Assuming a 10% error in the model ^{(22), (23)} we have:

$$\text{Error} \left[\dot{\Omega}^{\text{Albedo}}|_{1y} \right] \lesssim 10^{-2} \dot{\Omega}^{\text{Lense-Thirring}}|_{1y} \quad (15)$$

Satellite eclipses by the Earth:

Because of the change of sign of W , when the Sun is in opposite regions with respect to the satellite orbital plane, we have that the secular nodal precession due to satellite's eclipses is small over one year ⁽¹²⁾:

$$\dot{\Omega}^{\text{Eclipses}}|_{1y} \lesssim 10^{-1} \dot{\Omega}^{\text{Lense-Thirring}}|_{1y} \quad (16)$$

Assuming ^{(15), (26)} an uncertainty of 10^{-2} radians in the determination of the boundary of the shadow's region and an uncertainty ⁽¹⁵⁾ in f_0 of less than 1%, we have that the error in the calculated secular nodal precession due to satellite's eclipses by the Earth, is over one year:

$$\text{Error} \left[\dot{\Omega}^{\text{Eclipses}}|_{1y} \right] \lesssim 10^{-3} \dot{\Omega}^{\text{Lense-Thirring}}|_{1y} \quad (17)$$

Neutral and charged particles drag:

The neutral particle drag force on a satellite can be written ^{(16), (27)}:

$$F = \frac{C_D}{2} A \rho v^2 \quad (18)$$

where C_D = drag coefficient, ρ is the density of the atmosphere and v is the velocity of the satellite relative to the atmosphere.

Even with the extreme hypothesis that the atmosphere is corotating with the Earth at the LAGEOS altitude - 12,270 km - and with the hypothesis that the total drag on LAGEOS - neutral plus charged particles - is ^{(26), (27)} of the order of $2.3 \times 10^{-10} \text{ cm/sec}^2$ (≈ 6 times the neutral drag (18)), we find ^{(12), (25)} that the secular nodal precession due to atmospheric drag is:

$$\dot{\Omega}^{\text{Total drag}} \lesssim 10^{-2} \dot{\Omega}^{\text{Lense-Thirring}} \quad (19)$$

Anisotropic thermal radiation:

Due to the finite heat conductivity of the body, there is an anisotropic distribution of temperature on the satellite⁽²⁶⁾ and therefore an anisotropic flux of radiation causing its acceleration. Over one period P , the corresponding secular nodal precession is⁽⁷⁾:

$$\dot{\Omega}^{\Delta T}_P \lesssim 1.3 \times 10^{-3} \dot{\Omega}^{\text{Lense-Thirring}}_P \quad (20)$$

Satellite albedo:

Due to the anisotropic temperature distribution on LAGEOS, there is an anisotropic flux of reflected radiant energy from the satellite. The corresponding secular nodal precession is⁽¹²⁾:

$$\dot{\Omega}^{\text{Albedo}}_P \lesssim 6.6 \times 10^{-4} \dot{\Omega}^{\text{Lense-Thirring}}_P \quad (21)$$

Poynting-Robertson effect:

Because of the relative velocity between LAGEOS and the Sun there are^{(28), (29)} small corrections, of the order of v , to the formula (11); over one period P , we have⁽¹²⁾:

$$\dot{\Omega}^{\text{Poynting-Robertson}}_P \lesssim 7.2 \times 10^{-7} \dot{\Omega}^{\text{Lense-Thirring}}_P \quad (22)$$

Infrared radiation:

The Earth's infrared radiation contribution to the nodal precession was studied by Sehnal-81⁽³⁰⁾. From his work we find that:

$$\dot{\Omega}^{\text{Infrared-radiation}}_{1 \text{ day}} \approx \dot{\Omega}^{\text{Lense-Thirring}}_{1 \text{ day}} \quad (23)$$

and assuming an error of less than 10% in the model we have:

$$\text{Error} \left[\dot{\Omega}^{\text{Infrared radiation}}_{1 \text{ day}} \right] \lesssim 10^{-1} \dot{\Omega}^{\text{Lense-Thirring}}_{1 \text{ day}} \quad (24)$$

However, the infrared radiation is mainly described by zonal terms of zero and second degree, that is the flux of infrared radiation has⁽³⁰⁾ a latitudinal dependence:

$$\sigma = A_0 + A_2 P_2(\sin\phi) \quad (25)$$

therefore, for the particular configuration LAGEOS plus LAGEOS X, we have:

$$\dot{\Omega}^{\text{Infrared radiation}}_{\text{LAGEOS}} \approx -\dot{\Omega}^{\text{Infrared radiation}}_{\text{LAGEOS X}} \quad (26)$$

and consequently a null contribution from the Earth's infrared radiation to the uncertainty in the measurement of the Lense-Thirring drag.

Solar wind:

With a calculation similar to the atmospheric drag, for the neutral and charged solar wind⁽³¹⁾ drag, we have⁽¹²⁾:

$$\dot{\Omega}^{\text{Solar wind}}_P \lesssim 2.1 \times 10^{-3} \dot{\Omega}^{\text{Lense-Thirring}}_P \quad (27)$$

Drag from interplanetary dust:

With a similar calculation, we have ⁽¹²⁾:

$$\dot{\Omega}^{\text{Cosmic dust}}|_P \lesssim 1.8 \times 10^{-3} \dot{\Omega}^{\text{Lense-Thirring}}|_P \quad (28)$$

Earth's magnetic field:

Assuming ⁽²⁷⁾ a LAGEOS total surface charge $q_L \approx 3.3 \times 10^{-11}$ C, we have:

$$\dot{\Omega}^{\text{B e}}|_P \lesssim 1.6 \times 10^{-4} \dot{\Omega}^{\text{Lense-Thirring}}|_P \quad (29)$$

In conclusion, formulae (13), (15), (17), (19), (20), (21), (22), (26), (27), (28), (29) show that each non-gravitational perturbation contributes to the secular rate of nodal precession of LAGEOS less than 1% of the Lense-Thirring drag, or can be calculated to an accuracy better than 1% of the Lense-Thirring precession.

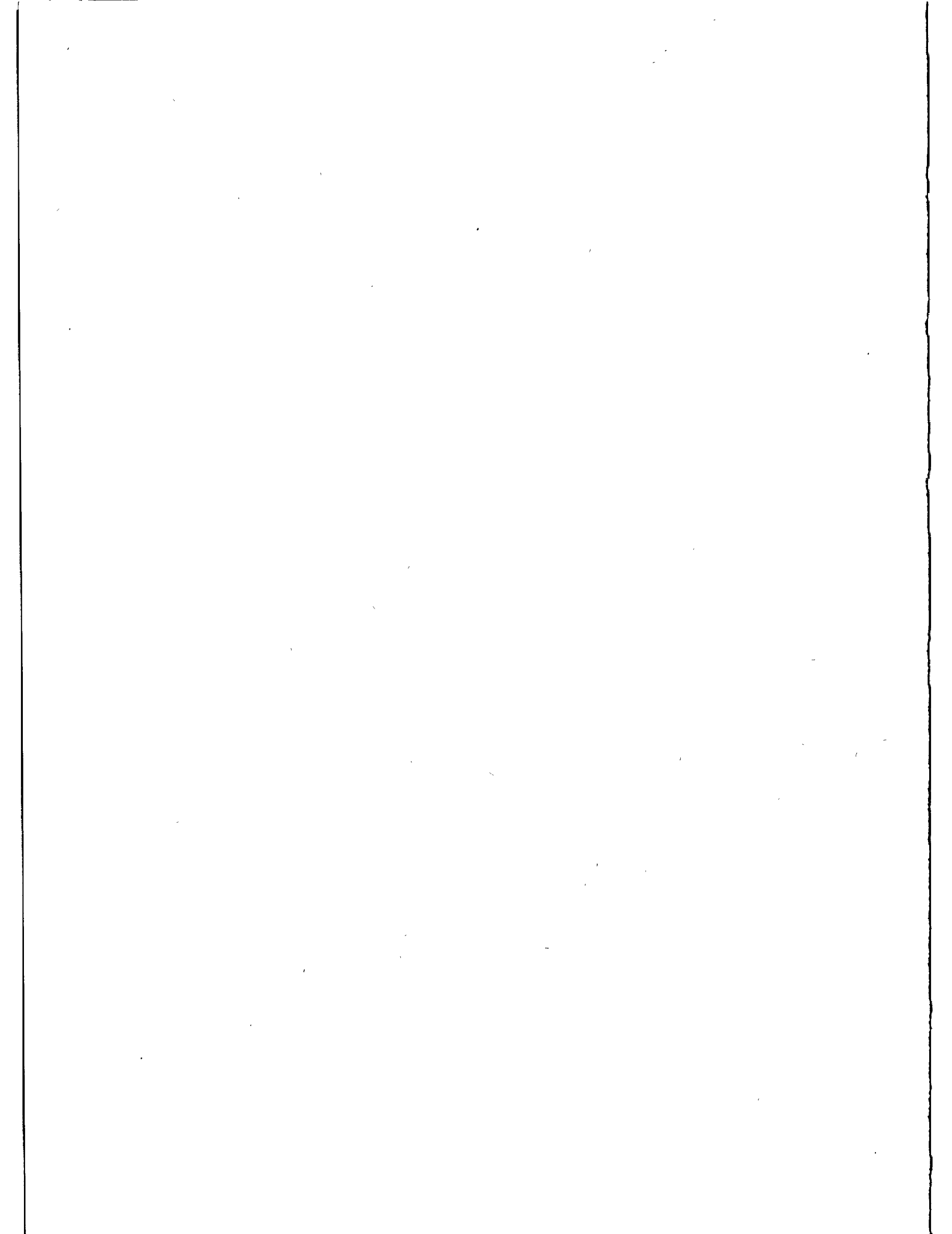
Concerning the earth's tides, due to the periodicity of the Earth's tides, the measurement of the total nodal precession should be taken over a period of a few years, over such a period of time the corresponding uncertainty should be of a few milliarcsec ^{(15), (32)}. We must also consider the accuracy of our knowledge of the orbital parameters. For the special configuration LAGEOS plus LAGEOS X with supplementary inclinations, the error in the measurement of Ω^{LT} due to errors in the determination of the inclination, including polar motion determination errors, should be ^{(15), (32)} of a few milliarcsec when averaged over a period of a few years. Finally we observe that to have less than 3% individual contribution to the experimental uncertainty - with the hypothesis of improvements in the uncertainties $\frac{\delta J_{2n}}{J_2}$ to 3×10^{-7} - the differences between the orbital parameters of two satellites should be: $a_e = (a_x - a_f) \lesssim \pm 16$ km, $I_e = (I_x - I_f) \lesssim \pm 0.13^\circ$, and $e_e = (e_x - e_f) \lesssim \pm 0.04$.

I thank C. Alley, P. Bender, B. Bertotti, R. Eanes, P. Farinella, R. Matzner, W. Miller, J. Ries, D. Rubincam, B. Schutz, D. Smith, B. Tapley, K. Thorne, H. Yilmaz and J. A. Wheeler for helpful discussions.

REFERENCES

1. C. W. Misner, K. S. Thorne and J. A. Wheeler, Gravitation (Freeman, San Francisco, 1973).
2. S. Weinberg, Gravitation and Cosmology: Principles and Applications of the General Theory of Relativity (Wiley, New York, 1972).
3. J. Weber, General Relativity and Gravitational Waves (Wiley-Interscience, New York, 1961).
4. K. S. Thorne, Rev. Mod. Phys. 52, 299 (1980).
5. K. S. Thorne, R. H. Price, and D. A. Macdonald, eds., Black Holes, the Membrane Paradigm (Yale University Press, New Haven and London, 1986), p. 72.
6. J. Lense and H. Thirring, Phys. Z. 19, 156 (1918), english translation by:
7. B. Mashhoon et al., Gen. Relativ. Gravit. 16, 711 (1984).
8. J. A. Lipa, W. M. Fairbank, and C. W. F. Everitt, in: Experimental Gravitation, B. Bertotti, ed. (Academic Press, New York, 1974), p. 361.
9. I. Ciufolini, Bull. Am. Phys. Soc., Cleveland, Ohio, October 1984, 6, 1169 (1985).
10. I. Ciufolini, Phys. Rev. Lett. 56, 278 (1986).
11. I. Ciufolini, Found. of Phys. 16, 259 (1986).
12. I. Ciufolini, to be published in Celestial Mechanics.
13. D. E. Smith and P. J. Dunn, J. Geophys. Res. Lett. 7, 437 (1980).
14. C. F. Yoder, J. G. Williams, J. O. Dickey, B. E. Schutz, R. J. Eanes, and B. D. Tapley, Nature 303, 757 (1983).
15. B. D. Tapley, B. E. Schutz and R. J. Eanes, private communication (1984).
16. W. M. Kaula, Theory of Satellite Geodesy (Blaisdell, Waltham, 1966).
17. F. J. Lerch et al., J. Geophys. Res., A84, 3879 (1979).
18. F. J. Lerch et al., J. Geophys. Res., 90, 9312 (1985).
19. Y. Kozai, Smithsonian Astrophys. Obs. Spec. Rep. No. 56.
20. K. Aksnes, Cel. Mech., 13, 89 (1976).
21. L. Anselmo, B. Bertotti et al., Cel. Mech., 29, 27 (1983).
22. D. A. Lautmann, Cel. Mech., 15, 387 (1977).
23. D. A. Lautmann, Cel. Mech., 16, 3 (1977).
24. P. Bender in The Use of Satellites for Geodesy and Geodynamics Volume II; Proceedings of the Second International Symposium on the use of Artificial Satellites for Geodesy and Geodynamics, G. Veisard and E. Livieratos editors, National Technical University of Athens (1979), p. 145.
25. P. Bender, private communication.
26. F. Barlier et al., to be published in Cel. Mech.
27. D. P. Rubincam, Cel. Mech., 26, 361 (1982).

28. H. P. Robertson, Mon. Not. Roy. Astron. Soc. 97, 423 (1937).
29. R. R. Allan, Planet. Space Sci. 15, 53 (1967).
30. L. Sehnal, Cel. Mech. 25, 169 (1981).
31. V. M. Blanco and S. W. McCuskey, Basic Physics of the Solar System, Addison-Wesley, Reading, Mass., USA (1961).
32. I. Ciufolini, paper in preparation.



COMPARISON OF LAGEOS SATELLITE LASER RANGING NORMAL POINTS

R. Kolenkiewicz
NASA Goddard Space Flight Center
Greenbelt, Maryland

P.J. Dunn
EG & G Washington Analytical Services Center, Inc.
Lanham, Maryland

R.J. Eanes
Center for Space Research
University of Texas at Austin

R. Johnson
Bendix Field Engineering Corp.
Columbia, Maryland

ABSTRACT

The high repetition rates of currently deployed satellite laser ranging instruments allow the data to be compressed into normal points which will contain the essential characteristics of the original data. The generation of normal points is desirable in that it reduces both the computer storage space and time necessary for the analyses of these data to obtain the final end product of geophysical parameters. Several groups have been generating the LASER GEODynamics Satellite (LAGEOS) normal points, and the resulting points can be evaluated by subjecting them, and the full rate data from which they come, to a common geodetic test. For this evaluation the raw full rate laser measurements were comprised of an edited set of LAGEOS observations taken by 20 laser stations, located worldwide, and collected in October 1983. The noise level of the 206,000 range measurement residuals varied between 1 and 20 cm, and when compressed yielded approximately 5800 two-minute normal points. The geodetic test consisted of a data reduction, using the GEODYN computer program, to obtain a simultaneous estimate of the orbit parameters and station positions. In particular, the laser site heights were compared among the four data sets used in each reduction. The overall fit of the normal point residuals to the finally adjusted satellite and station parameters was 8 cm, with individual stations fitting between 5 and 20 cm. The expected standard error in the estimated station heights varied between 1 and 3 cm, and in every case the difference in the estimated heights from each normal point data set fell within this expected range. The conclusion is that starting with the same set of LAGEOS edited data, the algorithms used by the various groups are adequate in producing normal points which are in agreement with each other.

Normal Point Generation

At the Fifth International Workshop on Laser Ranging Instrumentation at Herstmonceux, England in September 1984 a procedure for generating normal points from full-rate laser ranges was adopted. The steps in the procedure are listed in Table 1, which also indicates at which stage a choice of technique is necessary for its implementation. Even when a particular step is so rigorously defined that no choice is required, alternative algorithms are possible which can improve data concentration or computational efficiency.

The choices of technique at each stage are listed in Table 2, which shows, for example, in step 6 the possibility of starting a bin interval at the first point in the pass instead of at an even UTC time. This alternative allows more information to be concentrated in the first normal point in the pass, but could reduce the total number of points in each pass by one. The median epoch time within the bin interval is simpler to compute than the arithmetic mean suggested in the Herstmonceux standard and is therefore presented as an alternative in step 7.

Normal Point Test Date

Each of the groups represented by the co-authors of this paper applied their normal point generation technique to a test data set comprising of edited LAGEOS observations collected by the global laser ranging network during the month of October 1983. The quantity of data from each station in the reference set is shown in the second column of Table 3. When the first point acquired within each second was chosen to reduce the normal point computation time, the number of ranges in the third column were obtained. The fourth column of Table 3 gives the number of normal points obtained with the regular UTC bin intervals recommended at Herstmonceux, and the reduced number of observations given by starting the bin interval at the first point in the pass is shown in the last column.

The data set generated by the Bendix group (BEN HER) adheres most closely to the Herstmonceux standard, although the University of Texas normal points were adopted as the base in the tests described here. They differ from the strict convention by the occasional estimate of a linear trend within each two-minute bin interval (choice 7(c) in Table 2). The normal point generation at GSFC (GOD MED) was based on one second samples (choice 1(c) in Table 2) and the choice 7(b) of the median epoch time tag. Another reasonable option (GOD FIRST) employed choice 6(b) for the bin interval. A final coarse data set was generated by simply taking the actual range at the times of the GOD FIRST normal points with no bin correction at all (2 MIN.DATA).

Normal Point Testing Procedure

Each normal point data set was subjected to a common geodetic test, which corresponds to the standard dynamic technique used by the Goddard Space Flight Center's Geodynamics Branch for laser data analysis. To assess the quality of the observations from each station, the 30-day data arc was reduced adjusting six orbital elements, an along-track orbit

acceleration parameter, a solar radiation coefficient and all components of station position except for three. The latitude and longitude of the Greenbelt station and the latitude of the Hawaii laser were fixed at arbitrary values to stabilize the reference system for the adjustment of earth orientation parameters every 5 days. The characteristics of each of the test data sets were essentially the same and are given in Table 4.

To monitor the differences between the test data sets, all parameters of the orbit, force model and earth orientation were fixed at the same reasonable values and all components of each station were estimated. The differences in millimeters for the height components of each station are tabulated in Table 5. The formal standard deviation for data at the 10cm. noise level (20cm. for station 7181) is also given in Table 5. A key to the station numbers used throughout this analysis is presented in Table 6.

Test Results

Examination of Table 5 shows that necessary choices in normal point generation make insignificant differences to the results of a properly designed geodetic experiment. Some differences are detectible in the results from sparse, noisy data such as provided by stations 7181 and 7833. Possible choices of procedure such as sampling the original observations each second, taking the median epoch time and starting the bin interval at the first point in the pass, give acceptable differences in results, which are always within the expected uncertainties. Simply sampling the data every two minutes gave a data set which occasionally yielded results outside the allowable formal error. It should finally be pointed out that editing procedures, which are likely to cause the greatest differences in alternative normal point generation procedures, were not examined in the tests described here.

TABLE 1. NORMAL POINT GENERAL PROCEDURE

- ** 1. GENERATE RESIDUALS
- ** 2. COARSE EDIT
- ** 3. COMPUTE TREND FUNCTION
- ** 4. FINE EDIT
- 5. GO TO 3
- * 6. CHOOSE BIN INTERVAL
- * 7. COMPUTE MEAN RESIDUAL AND MEAN EPOCH WITHIN BIN
- ** 8. LOCATE CLOSEST RANGE TO MEAN EPOCH
- 9. APPLY RESIDUAL BIN CORRECTION
- 10. COMPUTE STATISTICS
- 11. REPORT STATISTICS
- 12. FOLLOW STANDARD FORMAT
- 13. QUICK LOOK CARRY OVER CHECK
- 14. REPORT SCREENED FULL-RATE DATA

**A CHOICE OF TECHNIQUE IS NECESSARY

* A CHOICE OF TECHNIQUE IS POSSIBLE

TABLE 2. CHOICES OF TECHNIQUE

**1. GENERATE RESIDUALS

- a. FIT or FIX 'PREDICTION'
- b. If FIX go to 2
- c. Sample data
- d. Fit ORBIT over arc
- e. Fit FORCE MODEL over some interval
- f. Fit EARTH ORIENTATION over some interval
- g. Fit STATIONS over arc
- h. Fit RB/TB over pass

**2. COARSE EDIT

- a. Sample data
- b. Choose RMS multiplier per arc
- c. Choose RMS Multiplier per pass

**3. COMPUTE RESIDUAL TREND FUNCTION

- a. Fit ORBIT over pass
- b. Fit POLYNOMIAL over pass
- c. Fit RB/TB over pass

**4. FINE EDIT

- a. Choose RMS multiplier per pass

*6. CHOOSE BIN INTERVAL

- a. Count from zero hours UTC
- b. Count from first point in pass

*7. COMPUTE MEAN RESIDUAL AND MEAN EPOCH

- a. Pick arithmetic MEAN TIME
- b. Pick MID.TIME (MEDIAN)
- c. Fit residual TB/RB as well as MEAN

**8. LOCATE CLOSEST RANGE

- a. Equidistant TIMES from MEAN (eg: 2 points)
- b. Even number of points for MEDIAN

TABLE 3. 8310 TEST DATA QUANTITY

| STATION | TOTAL OBS | SAMPLED ONE SEC. | NORMAL ZERO UTC | NORMAL FIRST POINT |
|---------|--------------|---------------------|--------------------|-----------------------|
| 7062 | 3,800 | 2,600 | 108 | 101 |
| 7086 | 1,800 | 1,400 | 66 | 61 |
| 7090 | 7,200 | 3,000 | 40 | 39 |
| 7105 | 91,500 | 36,800 | 507 | 492 |
| 7109 | 52,900 | 24,800 | 343 | 335 |
| 7110 | 71,600 | 32,000 | 521 | 508 |
| 7112 | 5,500 | 5,500 | 220 | 211 |
| 7121 | 4,500 | 4,500 | 175 | 176 |
| 7122 | 21,400 | 21,400 | 313 | 299 |
| 7181 | 100 | 100 | 43 | 40 |
| 7210 | 13,800 | 13,800 | 390 | 371 |
| 7220 | 51,900 | 19,800 | 504 | 489 |
| 7831 | 16 | 16 | 7 | 6 |
| 7833 | 229 | 229 | 79 | 77 |
| 7834 | 15,000 | 9,900 | 252 | 240 |
| 7838 | 5,100 | 4,100 | 204 | 186 |
| 7839 | 6,400 | 5,800 | 271 | 256 |
| 7840 | 1,600 | 1,500 | 241 | 231 |
| 7907 | 12,300 | 12,300 | 1122 | 1085 |
| 7939 | <u>6,400</u> | <u>6,400</u> | <u>437</u> | <u>430</u> |
| TOTAL | 373,300 | 206,100 | 5843 | 5633 |

TABLE 4. 8310 TEST DATA QUALITY

| STATION | NORMAL POINTS | BEST NOISE NORMAL PT. | FINAL 30 DAY FIT | BEST NOISE SINGLE SHOT |
|---------|---------------|-----------------------|------------------|------------------------|
| 7062 | 108 | 1 cm. | 6 cm. | 8 cm. |
| 7086 | 66 | 2 | 7 | 7 |
| 7090 | 40 | 1 | 2 | 2 |
| 7105 | 507 | 1 | 7 | 2 |
| 7109 | 343 | 1 | 6 | 2 |
| 7110 | 521 | 1 | 7 | 4 |
| 7112 | 220 | 3 | 9 | 12 |
| 7121 | 175 | 2 | 9 | 10 |
| 7122 | 313 | 1 | 7 | 7 |
| 7181 | 43 | 16 | 22 | 16 |
| 7210 | 390 | 1 | 5 | 4 |
| 7220 | 504 | 1 | 8 | 7 |
| 7831 | 7 | 21 | 21 | 23 |
| 7833 | 79 | 10 | 14 | 15 |
| 7834 | 252 | 1 | 7 | 7 |
| 7838 | 204 | 2 | 11 | 8 |
| 7839 | 271 | 1 | 8 | 4 |
| 7840 | 241 | 1 | 7 | 4 |
| 7907 | 1122 | 3 | 10 | 13 |
| 7939 | 437 | 3 | <u>13</u> | 12 |
| TOTAL | | | 9 cm. | |

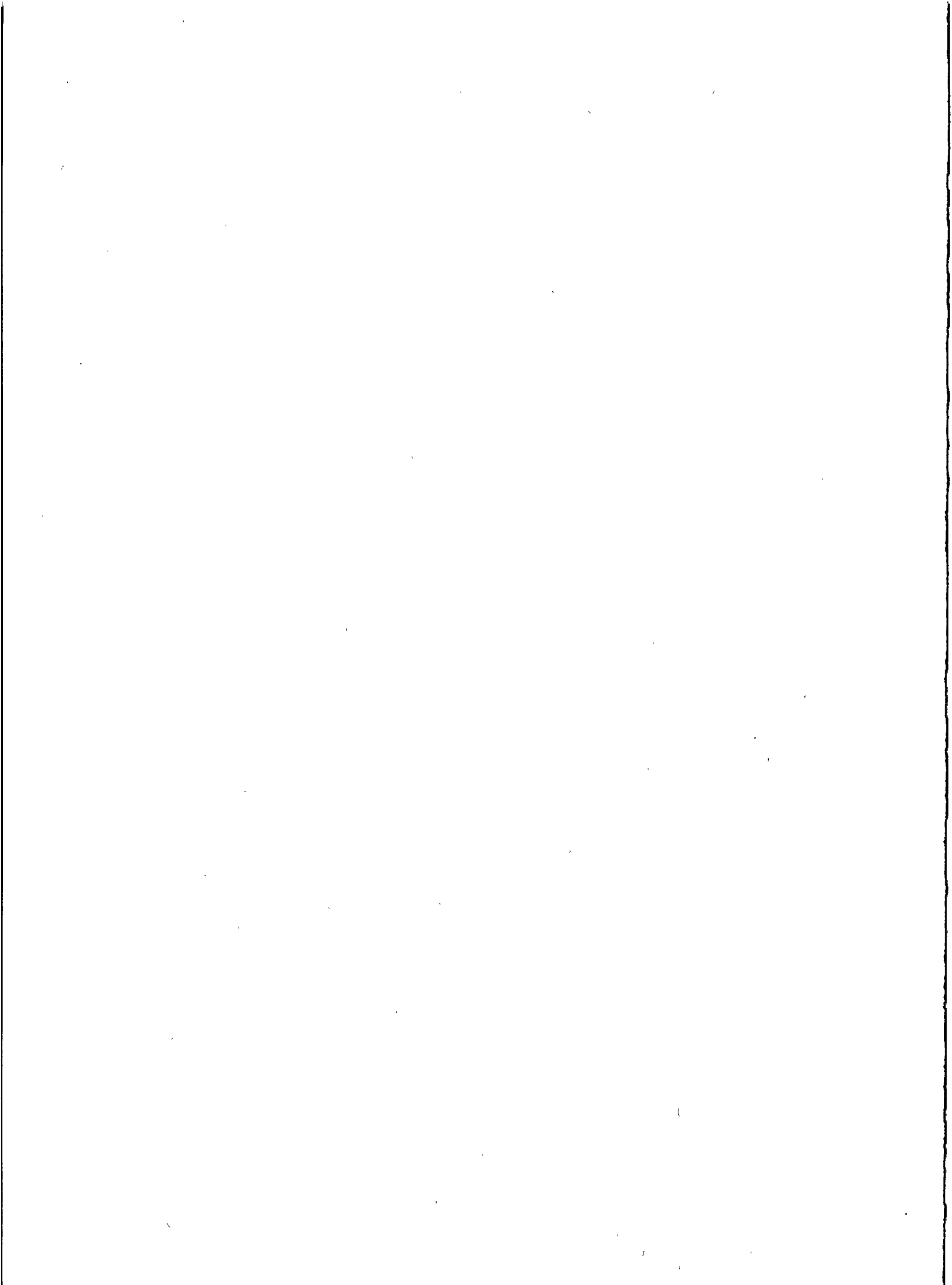
TABLE 5. DIFFERENCES OF HEIGHT ESTIMATES
FROM THOSE USING TEST DATA SET

| STATION | FORMAL SIGMA | BEN HER | GOD MED | GOD FIRST | 2 MIN. DATA | FORMAL SIGMA |
|---------|-----------------|------------|------------|--------------|----------------|-----------------|
| 7062 | 14 mm. | 0 mm. | 0 mm. | -3 mm. | - 6 mm. | 14 mm. |
| 7086 | 21 | - 1 | -1 | -1 | .23 | 21 |
| 7090 | 26 | - 1 | 1 | 4 | 6 | 26 |
| 7105 | 7 | - 1 | 0 | -3 | 1 | 7 |
| 7109 | 10 | 0 | 2 | 1 | - 1 | 10 |
| 7110 | 7 | 0 | -1 | 0 | 1 | 7 |
| 7112 | 10 | 1 | -1 | 8 | - 8 | 10 |
| 7121 | 11 | 0 | -1 | -9 | -11 | 11 |
| 7122 | 9 | - 1 | -1 | -2 | - 7 | 9 |
| 7181 | 42 | -37 | -2 | 21 | 54 | 42 |
| 7210 | 8 | 1 | 0 | 4 | 6 | 8 |
| 7220 | 7 | 0 | 2 | 7 | 10 | 7 |
| 7831 | ∞ | - | - | - | - | ∞ |
| 7833 | 30 | 5 | 7 | 4 | 27 | 30 |
| 7834 | 8 | 0 | -1 | 1 | -10 | 8 |
| 7838 | 11 | - 2 | -1 | 9 | 13 | 11 |
| 7839 | 9 | 0 | 0 | 3 | 1 | 9 |
| 7840 | 8 | 0 | 0 | 1 | 3 | 8 |
| 7907 | 5 | 1 | 0 | -2 | - 5 | 5 |

HER: STRICT HERSTMONCEUX
MED: MEDIAN EPOCH IN BIN
FIRST: BIN STARTS AT FIRST POINT

TABLE 6. KEY TO STATION NUMBERS

| STATION | NO. | OCC. | NAME | LOCATION |
|---------|-----|------|----------|----------------|
| 7062 | 12 | 05 | TLRS-2 | OTAY MOUNTAIN |
| 7086 | 24 | 03 | MLRS | MACDONALD OBS. |
| 7090 | 05 | 01 | MOBLAS-5 | YARRAGADEE |
| 7105 | 07 | 02 | MOBLAS-7 | GREENBELT |
| 7109 | 08 | 02 | MOBLAS-8 | QUINCY |
| 7110 | 04 | 02 | MOBLAS-4 | MONUMENT PEAK |
| 7112 | 02 | 01 | MOBLAS-2 | PLATTEVILLE |
| 7121 | 01 | 01 | MOBLAS-1 | HUAHINE |
| 7122 | 06 | 01 | MOBLAS-6 | MAZATLAN |
| 7181 | 39 | 01 | GRDLAS | POTSDAM |
| 7210 | 23 | 01 | HOLLAS | HALEAKALA |
| 7220 | 11 | 01 | TLRS-1 | MONUMENT PEAK |
| 7831 | 46 | 01 | HELLAS | EGYPT |
| 7833 | 32 | 01 | KOOLAS | KOOTWIJK |
| 7834 | 30 | 01 | WETLAS | WETZELL |
| 7838 | 36 | 01 | SHOLAS | SIMOSATO |
| 7839 | 34 | 01 | AUSLAS | GRAZ |
| 7840 | 35 | 01 | RGOLAS | RGO |
| 7907 | 40 | 01 | SAO201 | AREQUIPA |
| 7939 | 41 | 01 | SAO102 | MATERA |



SUB-CM MULTIPHOTOELECTRON SATELLITE LASER RANGING

T. Varghese, M. Heinick
Allied Bendix Aerospace
BFEC, GLTN
10210 Greenbelt Road Seabrook
Maryland 20706 - USA -

Telephone (301) 7318916
Telex 197700 GLTN

ABSTRACT

A satellite laser ranging receiver configuration has been developed and tested to generate sub-cm precision in laser ranging to earth-bound satellites. Multiphotoelectron data taken within the dynamic range of the receiver has shown a standard deviation of 5 mm on ground targets and 7-9 mm on Lageos satellite data residuals. The systematic error from this receive package is measured to be less than 3 mm and is a significant improvement over the previous configuration.

1. INTRODUCTION

The projected requirements of the NASA Crustal dynamics program for the 1990s include sub-cm observational accuracy in laser ranging to Lageos. This would be particularly relevant since Lageos-II is projected for deployment in the not so distant future and accuracy enhancement would significantly impact the high volume data period. The precision of Mobile Laser ranging systems (MOBLAS) of the NASA Goddard Laser Tracking Network (GLTN) has been receiver limited above 1cm. To meet the program requirements of increased accuracy and precision, Bendix designed a receiver system based on a Microchannel plate photomultiplier tube (MCP-PMT) and a Tennelec constant fraction discriminator. Prototype testing of this advanced receiver package in the laboratory yielded RMS around 3.5mm over a dynamic range ~ 15 , and during the field tests in November of 1984 the system produced calibration rms of 4.5mm and satellite data RMS of 9-10mm. Further improvements were made to the system which was installed for field operation in April of 1986. This paper describes briefly the device characteristics and performance features of the receiver package in the laboratory, and also sub-cm satellite data results from approximately 1 year operation from Moblas-7.

2.0 DEVICE CHARACTERISTICS

The desirable device features for precision opto-electronic detection of low photoelectron are high gain, low electron transit time (and jitter), and low pulse spread. Conventional photomultipliers have a fairly large electron transit time and have an impulse response time of several nanoseconds, and, hence, are not suitable for low photoelectron optical detection with sub-cm precision. The use of a proximity focussed microchannel plate in the pmt instead of conventional electron photomultipliers generates all of the above desirable features. Besides, it has low transit time, large dynamic range, and is well suited for precision laser ranging.

GLTN requirements for satellite ranging include daytime tracking. Although a 10 angstrom spectral filter is used for daytime tracking, the 30 inch telescope still produces a large mean background. The lifetime of the DC biased (normally-ON) device would be considerably reduced if used for daylight tracking due to increased charge accumulation at the anode from high continuous background noise. However, electronic gating of the device would alleviate this problem. We have performed qualitative and quantitative evaluation to examine spatial and temporal ON-voltage uniformity of the tube under gated conditions to determine problems in the mm domain.

Our receiver package consisted of ITT F4129f 3-stage MCP-PMT,

Tennelec TC 454 constant fraction discriminator, a gating module with output of -600 volts, and a delay unit for delayed proportional gating of the discriminator. In laboratory measurements, the system produces 3-4mm rms data over a dynamic range ~ 15 and hence covers 5-60 photoelectrons. This design also accomplishes electron isolation of ~ 500 . The gate is adjustable from 100ns-10us and the time walk is ~ 1 mm within this interval. The discriminator response also is adjusted to have variation of no more than 2mm.

3.0 MOBLAS 7 DATA AND DATA PROCESSING

Targets currently used by MOBLAS 7 are the satellites LAGEOS, Starlett, and Ajisai, corner cubes mounted as ground targets at ranges from 75 to 3500 meters, and an internal calibration target.

Raw ranging data from the station contain the round trip time of flight of the laser pulse, the epoch time at which the pulse is transmitted, meteorological data consisting of pressure, temperature, and humidity, and system measurements of transmit and receive energy.

Data processing takes place on two levels, operational data processing and engineering analysis processing. For operational data processing, the rigidly controlled and heavily benchmarked DSG Laser Processor is used to prepare satellite data for release to the scientific community and to provide basic information on data quality. During operational data processing, time of flight measurements are converted to ranges and corrected for system delays, atmospheric refraction, and satellite center of mass. The epoch times of the range measurements are corrected to the times the laser pulses are at the satellite. For MOBLAS 7, a single system delay is applied throughout each pass. A 15 degree polynomial is fit to the ranges in each pass for an analysis of data quality.

Engineering analysis processing utilizes several specialized routines to provide information beyond the scope of the DSG Laser Processor on tracking system characteristics. For the data presented here, a 20 degree polynomial was fit to the time of flight measurements of each pass without corrections. The least squares fitting procedure includes editing of data beyond 3 sigma (standard deviation) from the polynomial and refitting of the remaining data. Editing and refitting cycles are repeated until no improvement in the standard deviation is obtained, or a maximum of 10 iterations is reached. The residuals are then used in several types of analysis plots including those displayed in the text.

4.0 RESULTS

The plots which follow demonstrate the sub-centimeter precision of the MOBLAS-7 ranging system. Fig.1 displays the RMS value of every LAGEOS pass(day and night) and associated combined pre-post pass calibration tracked by MOBLAS-7 during the month of November, 1986. All rms values were taken from the DSG Laser Processor. Of the 30 LAGEOS passes tracked, only two passes have RMS values greater than or equal to 1.00 centimeter(cm). The mean RMS of all 30 passes is 0.866cm, and the mean RMS of the combined calibrations is 0.595cm. A corner cube mounted on a water tower at a range of 3482.547 meters from MOBLAS-7 was the operational calibration target during this time frame. Targets located at distances of 200 meters show data RMS of ~5mm. The larger RMS in calibration on the operational target is a consequence of the target distance, the meteorological variations and the dynamics of the target. Results from four individual passes are illustrated in Fig.2-4 where satellite residuals are displayed using 20 degree polynomial least squares fitting and editing (as described above). These passes include:

| DATE | TIME (GMT) | OBSERVATIONS | RMS (CM) |
|---------------|------------|--------------|----------|
| June 18, 1986 | 01:18 | 7537 | 0.79 |
| Nov. 17, 1986 | 07:19 | 8546 | 0.80 |
| Nov. 22, 1986 | 07:30 | 8995 | 0.88 |
| Nov. 25, 1986 | 06:57 | 10233 | 0.89 |

Satellite range residuals vs. time(minutes) into the pass are shown in Fig.2(a),3 and 4. Two of these plots have polynomial fit errors as can be seen in Fig.2(a) and 3(b) while fig.3(a) and Fig.4 show no such problems.

Two types of Receive Energy Dependence plots illustrate the response of the system over a wide range of receive energies. In Fig.2(a), a scatter plot of satellite residuals vs. relative receive energy is provided. The anomalous accumulation of long residuals just above the value of 1200 is due to a hardware/software limitation(bit error) which reduces the values above 1999 by 1000 units. These very high energy returns represent data around 80-100 photoelectrons and are present only in high elevation passes under very good tracking conditions. Typically, this constitutes less than 5% of the data within a pass and have little impact on overall data.

quality. Fig.2(c),3(c-d)& 4 display the mean and rms of all residuals within 20 standard deviations of the polynomial with a bin resolution of 20 units of relative receive energy. The slight increase in the variation of the mean and larger RMS values at the higher receive energies are due, in part, to the small number of data occurring within each receive energy interval.

5.0 SUMMARY

We have shown for the first time the possibility of obtaining consistent ranging precision of sub-cm on Lageos. The proven dynamic range in this design is particularly relevant considering the transmitted power level and the telescope aperture. The Goddard Laser Tracking Network is presently undergoing the necessary hardware upgrade to meet sub-cm satellite laser ranging goal of NASA Crustal Dynamics program.

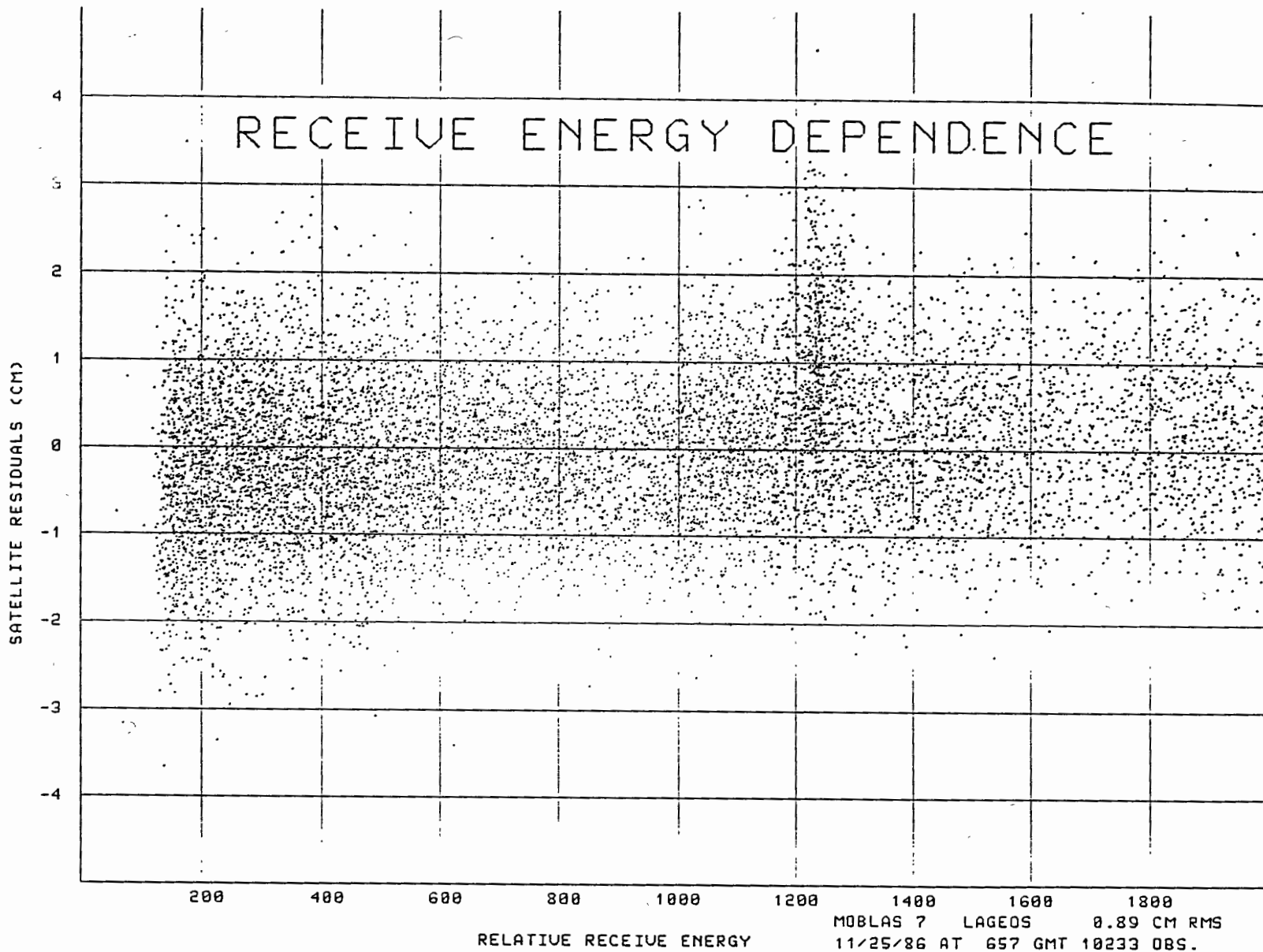


FIG. 2(B)

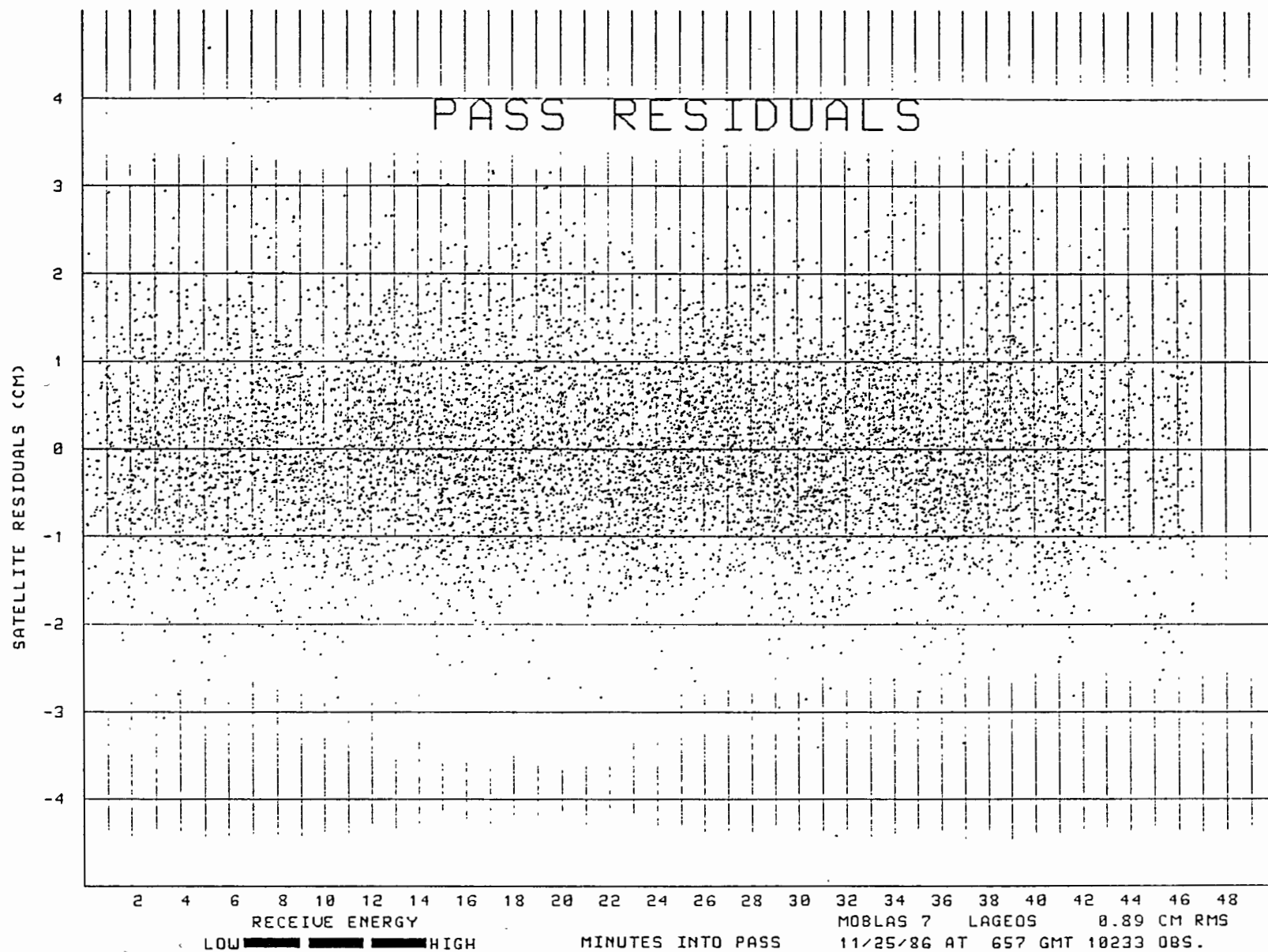


FIG. 2(A)

LAGEOS & CALIBRATION RMS

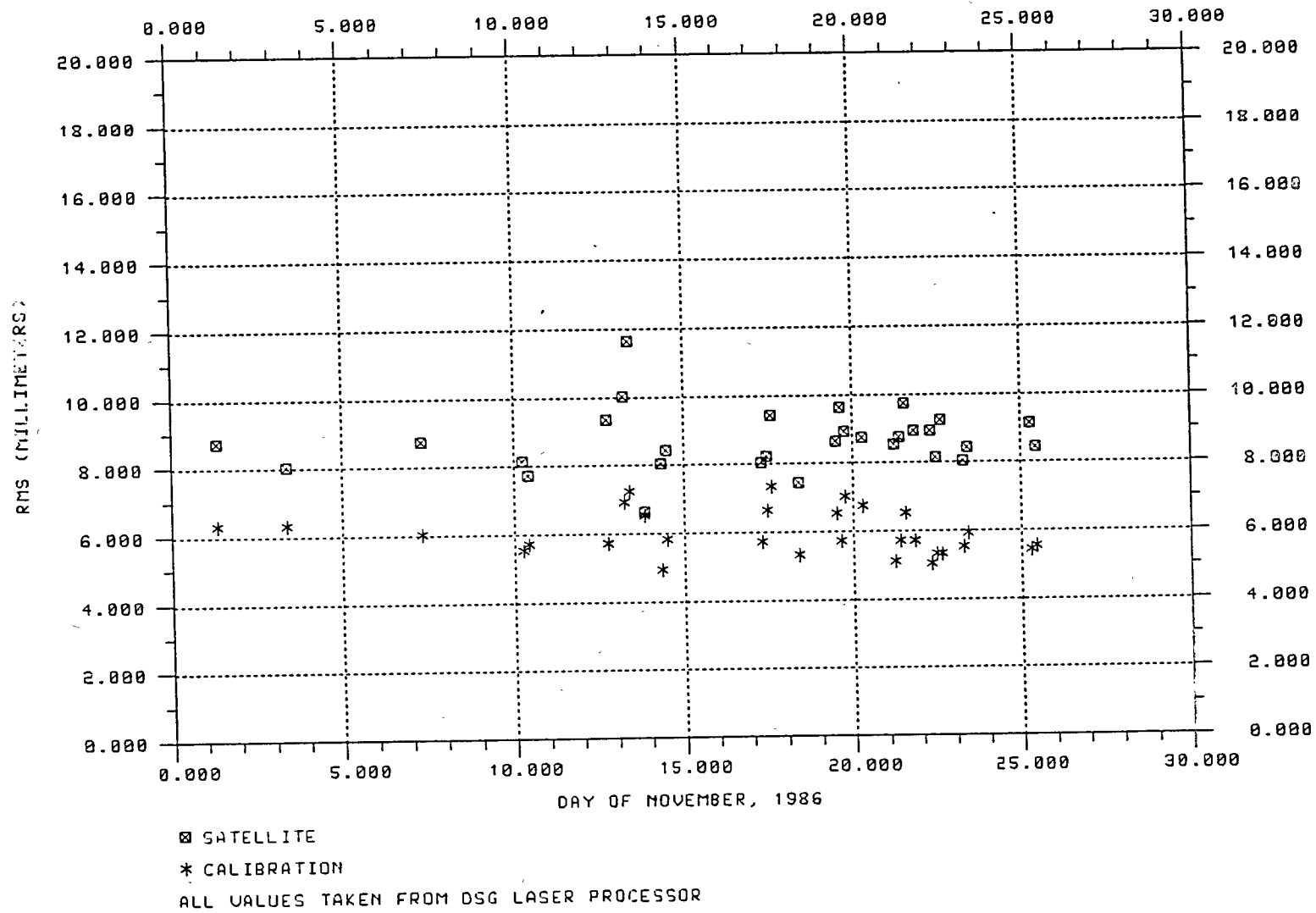


FIG. 1

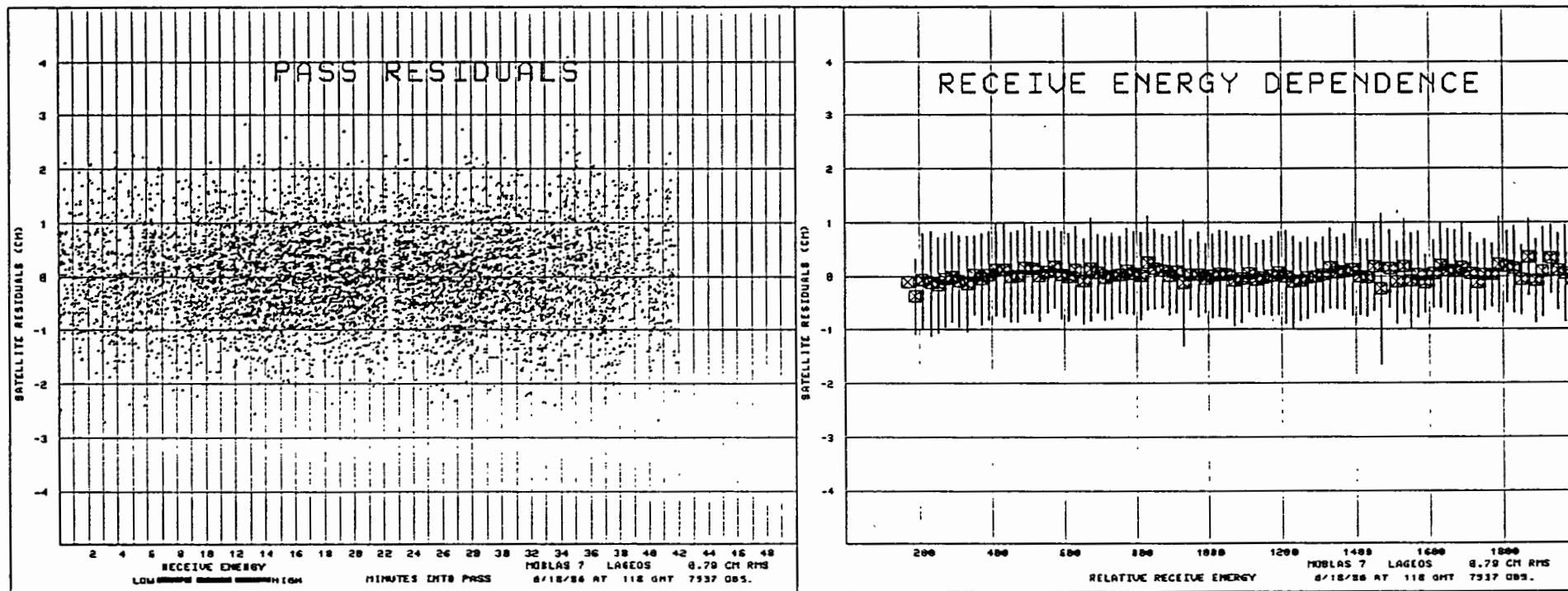


FIG. 4

FIG. 3(A)

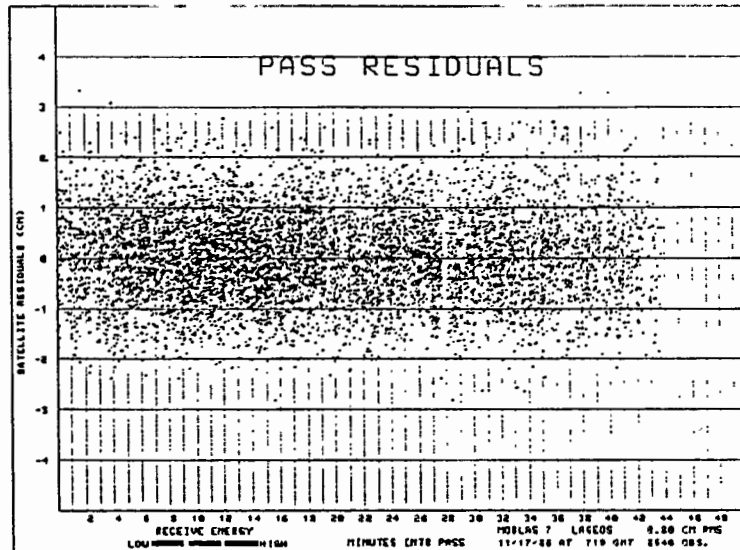


FIG. 3(C)

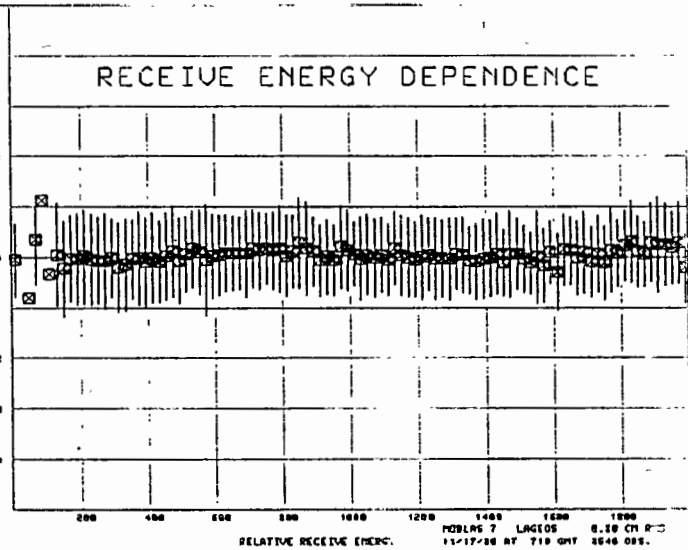


FIG. 3(B)

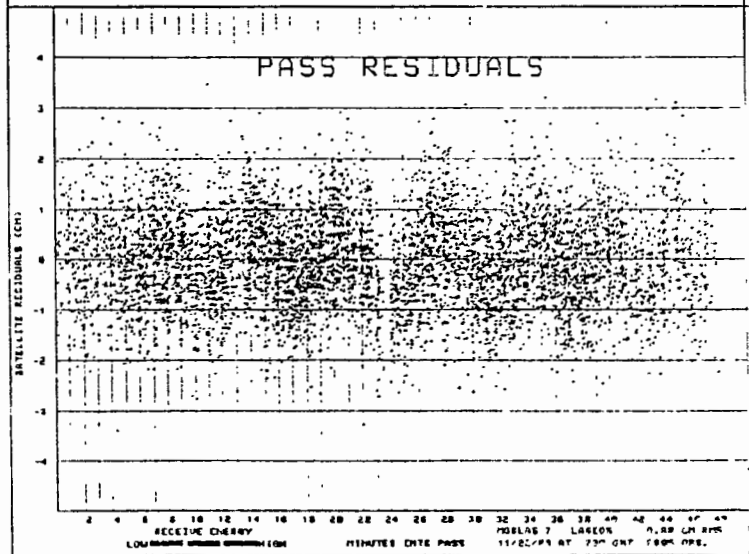
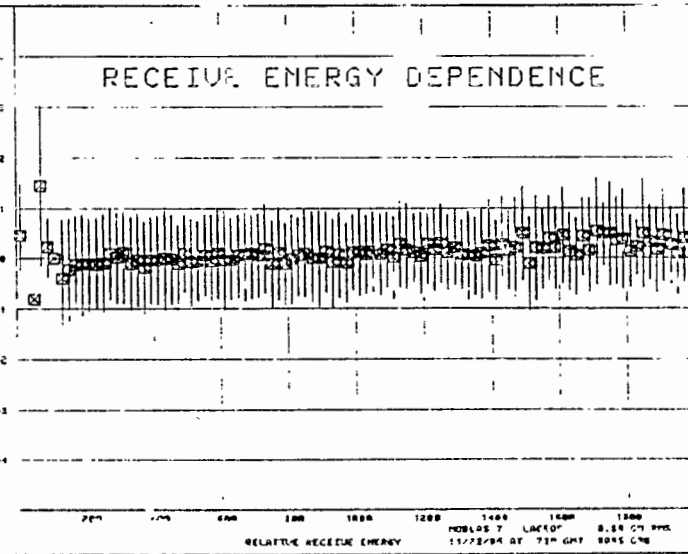


FIG. 3(D)



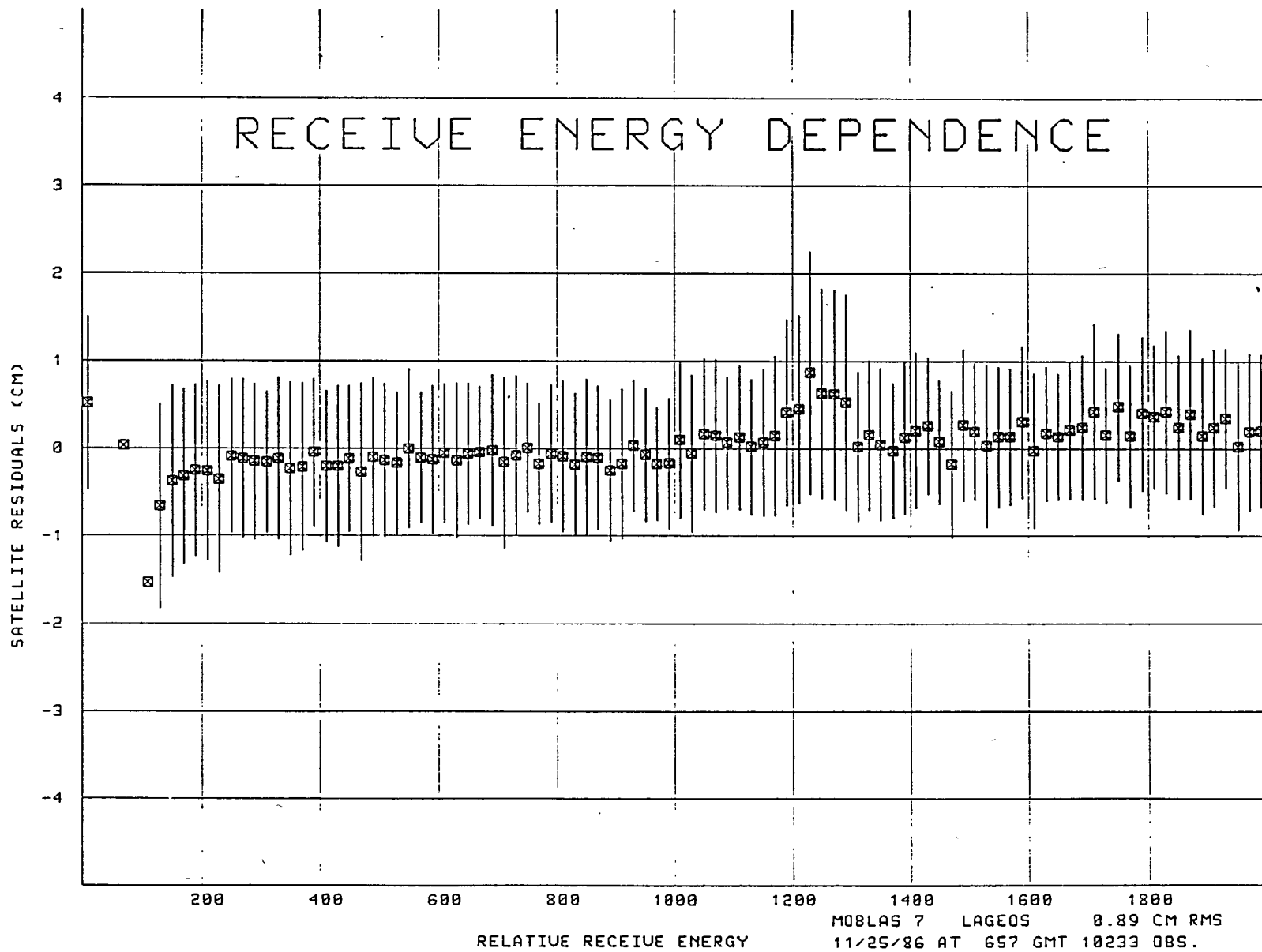
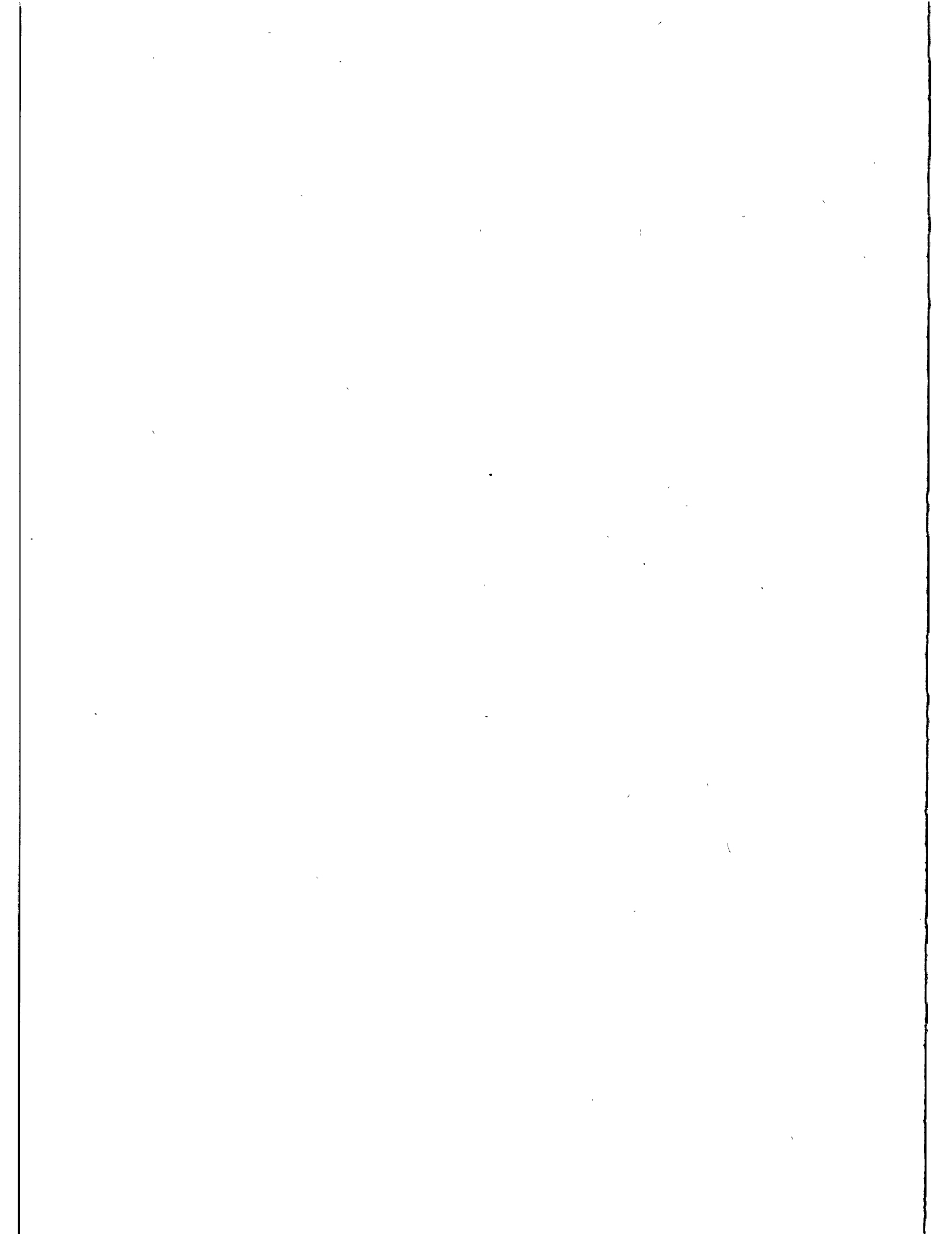


FIG. 2(c)



TLRS-1 ; SYSTEM UPGRADE AND PERFORMANCE RESULTS

T. Varghese, P. Seery, H. Donovan, Patterson,
K. Emenheiser, D. Gurovich, D. Yannuzzi
Allied Bendix Aerospace
BFEC, GLTN
Seabrook, MD 20706 - USA -

Telephone (301) 2867743
Telex 19770 GLTN

R. Appler
Code 601 NASA
Goddard Space Flight Center
Greenbelt MD 20770 - USA -

Telephone (301) 2868119
Telex 257559 CDPO UR

ABSTRACT

A major system upgrade was undertaken in TLRS-1 to improve the ranging accuracy as well as to eliminate the biases observed during collocation with Moblas-4 & -8. The goal is to obtain collocated Lageos passes with Moblas-7 at the sub-cm level with calibration and satellite data residual RMS values of ~ 1 cm and comparable ground calibration data. Recent operational results show satellite and ground data close to the projected performance. In this paper we overview past system bias characteristics, causes for the bias and engineering upgrades accomplished to meet the goals.

1.0 INTRODUCTION

The collocation of TLRS-1 (Transportable Laser Ranging System) with MOBLAS-4 in Monument Peak and MOBLAS-8 in Quincy, California, during Sept. 1984-July 1985, revealed an azimuth dependent bias of approximately 10cm. Extensive investigations were carried out by the crew in the field with external help to identify and correct the problem to no avail. Hence the NASA Crustal dynamics program decided to bring the system to Goddard Optical Research Facility for detailed engineering evaluation and analysis by Bendix Engineering group and to make appropriate modifications to the system so as to reduce the bias to the 1-cm level.

2.0 COLLOCATION RESULTS FROM QUINCY AND MONUMENT PEAK

Fig.1 illustrates the bias as a function of azimuth angle. It is evident that the data shows a transition to 1.0 cm bias in the azimuth angle range of 30 - 210 degrees ("frontside"), and is close to zero in the range of 211 - 29 degrees ("backside"). An important feature to recognize here is the difference in the nature of the bias when the mount is switching from "backside" to "frontside" mode.

3.0 ENGINEERING EVALUATION

The AZ-EL mount of TLRS-1 has a 2 feet lever-arm and this produces two equivalent orientations for the mount which are mutually realizable by azimuth rotation of 180 degrees and elevation rotation of twice the angle with respect to zenith. These two equivalent orientations are known as backside and frontside modes. The mount can exhibit few mm of optical path length difference depending on the orientation. The magnitude of the observed bias was too large to be a consequence of the mount orientation. However, if the optical alignment of the system is such that the beam shifts at the field of view of the telescope depending on the orientation, this can produce significant bias if the detector is sensitive to the spatial positioning of the beam.

For optoelectronic detection of the received signal from the satellite the system had a high quantum efficiency Varian photomultiplier tube as the detector. Laboratory experiments have shown that the tube can exhibit 6-8cm time-walk even for few mm of spatial displacement of the beam on the photocathode. The electron beam inside this tube has a cycloidal trajectory between dynodes due to the longitudinal electric field and hence the transit time is not space-invariant. The single largest contribution towards the bias could thus be attributed to the detector. The errors in calibration

path distances, discriminator calibration, nonlinearity in the TD811 time interval counter etc., may be considered as additional sources for the observed bias.

4.0 HARDWARE/SOFTWARE UPGRADES AND PERFORMANCE RESULTS

The need for hardware/software upgrade was imperative following the determination of the above problems. To verify that the data-loop hardware changes (Table-1) would accomplish the set objectives, horizontal ranging was performed on 8 targets. These targets were located to provide fairly uniform azimuth angle coverage and had ranges of 50-400 meters. Fig.2 illustrates the measured system delay as a function of azimuth angle for various targets. Each division on the horizontal axis is 15 degrees while that on the vertical axis is 50ps ($\sim 7.5\text{mm}$). Measurements were performed on the front and backside modes. As can be seen from the plot the azimuth dependence was not more than 6mm and is within the uncertainty of the hardware and survey measurement. The mean difference between the front and backside mode was less than 2mm and the upgraded hardware thus should meet the projected goals.

Table-1 illustrates the hardware configuration before and after the upgrade. Major software upgrade was also necessary for hardware interface, system diagnostics, shot-shot measurements of system parameters, and real-time computation/display of the statistics of ranging. A new analytical mount model was also developed to provide smoother alignment and tracking capability and is expected to become operational in the near future.

The system has been subjected to extensive ground testing prior to the commencement of collocation to meet collocation prerequisites. These tests included cube map, system stability as a function of time, range, signal amplitude, temperature and azimuth. These results are displayed in Fig.3-6 and it is clear that the system is capable of providing sub-cm collocation data.

Collocation is presently underway at Goddard Optical Research facility between TLRS 1 and MOBLAS 7 and the initial results are meeting the sub-cm criteria and look very encouraging. More collocated passes are to be taken and analyzed and the results will be published at a future time.

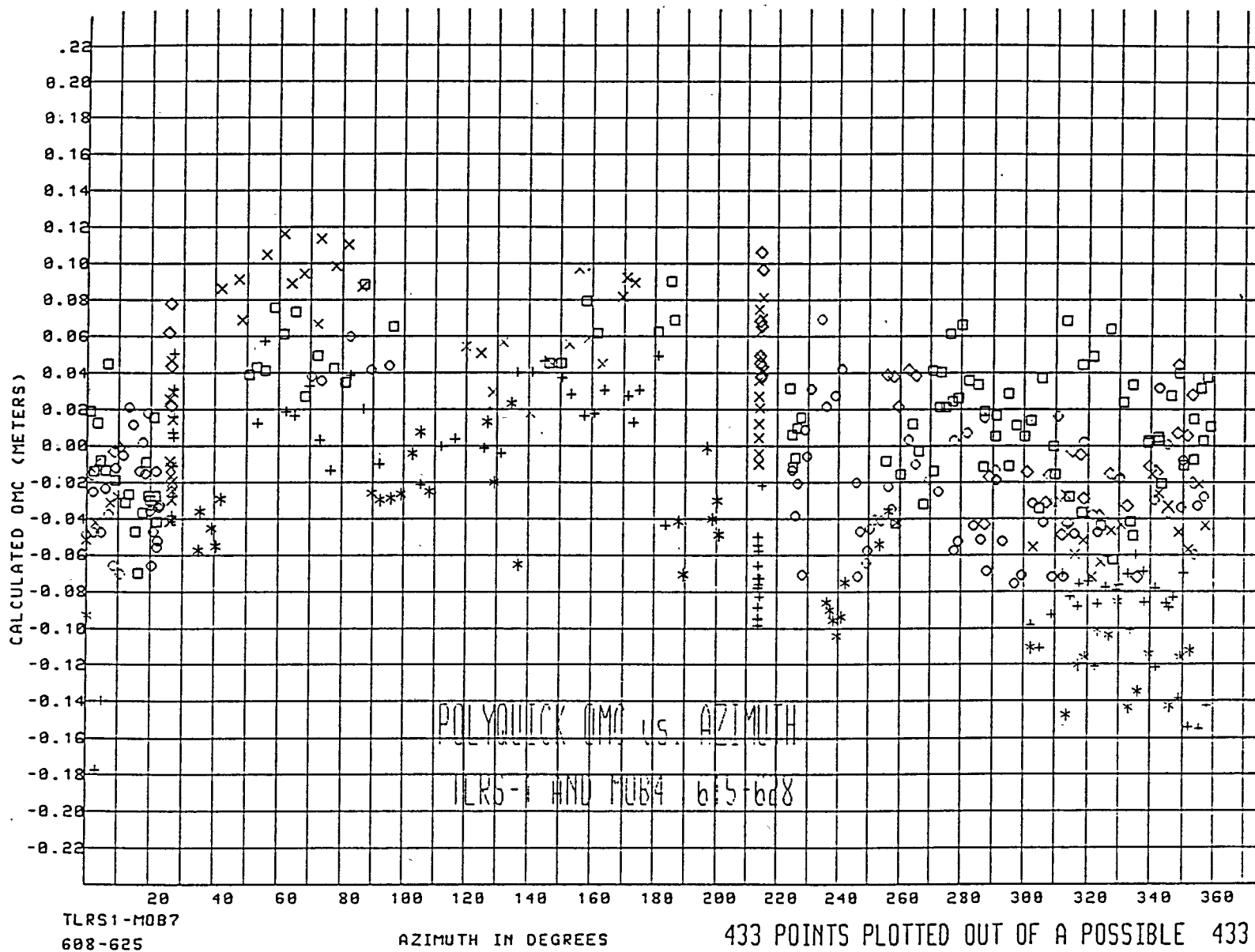


FIG. 1

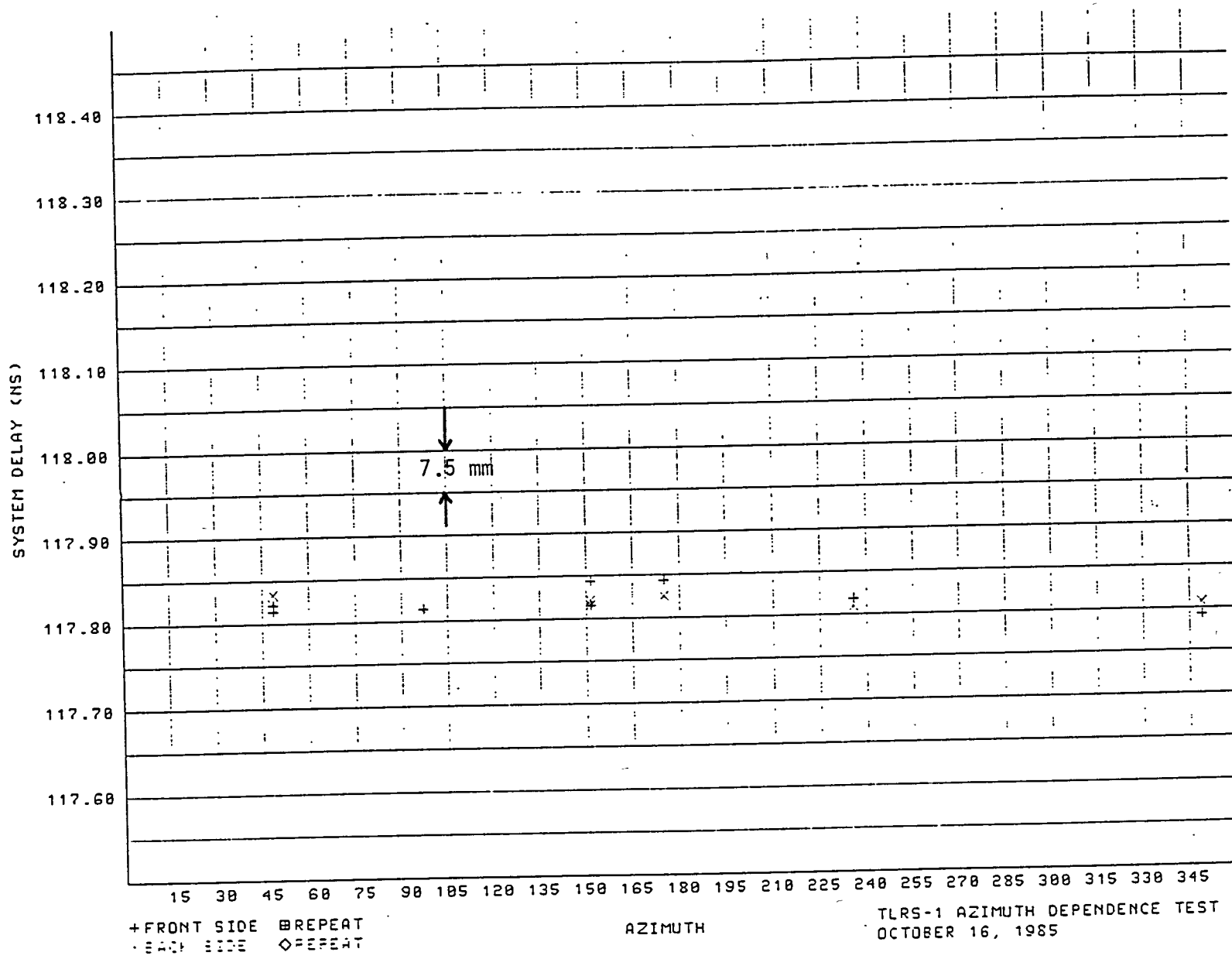


FIG. 2

TLRS-1 SYSTEM CONFIGURATION

| | <u>BEFORE UPGRADE</u> | <u>AFTER UPGRADE</u> |
|-----------------------------|---------------------------|---------------------------|
| o LASER | QUANTEL YG441ML | QUANTEL YG402DP |
| - OUTPUT ENERGY | 4 MJ | 100 MJ |
| - PULSE WIDTH | 200 PICOSECONDS (PS) | 200 PICOSECONDS (PS) |
| - PULSE RATE | 5 PULSES PER SECOND (PPS) | 5 PULSES PER SECOND (PPS) |
| o RECEIVE ELECTRONICS | | |
| - PHOTOMULTIPLIER TUBE | VARIAN | ITT MICROCHANNEL PLATE |
| - DISCRIMINATOR | ORTEC 934 | TENNELEC TC 454 |
| - TIME TO DIGITAL CONVERTOR | TD 811 | HP 5370B |
| - DETECTION | SINGLE PE | SINGLE PE |
| o OPTICAL SYSTEM | | |
| - TELESCOPE | 25 CM REFRACTIVE | SAME |

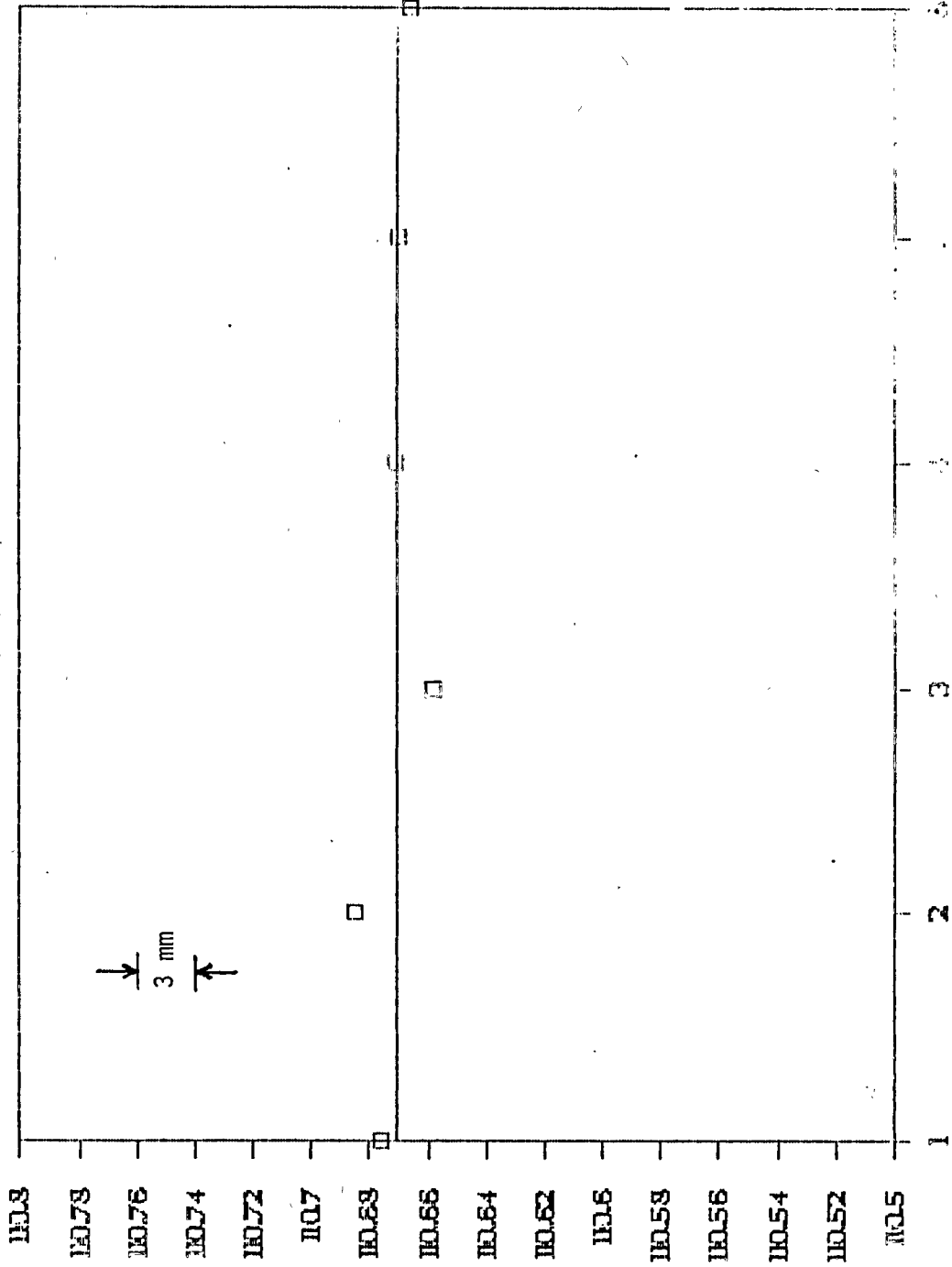
TABLE 1

| | | |
|-------------------------|---|----------------------------|
| ● TRACKING MOUNT | | |
| - TYPE | AZ-EL (U. OF TX DESIGN) | SAME |
| - ENCODER RESOLUTION | 2^{22} (.31 ARC SEC) | SAME |
| ● TIMING ELECTRONICS | | |
| - SHORT TERM STANDARD | CESIUM | SAME |
| - EPOCH STANDARD | LORAN RECEIVER | GPS RECEIVER (TRIMBLE) |
| ● COMPUTER | | |
| - HARDWARE | NOVA | SAME |
| - SOFTWARE | U. OF TEXAS | U. OF TEXAS + BFEC |
| ● CALIBRATION | INTERNAL CALIBRATION (INSENSITIVE TO POSSIBLE MOUNT BIASES) | EXTERNAL + INTERNAL |
| ● ENVIRONMENTAL CONTROL | | |
| - TEMPERATURE | CONTROLLED BUT | $70 \pm 5^{\circ}\text{F}$ |
| - HUMIDITY | RANGE UNKNOWN | $50\% \pm 10\%$ |

TABLE 1 (CONT'D.)

CUBE MAP ON TARGET #1 FROM TLRS 1

JULY 28, 1955



□ SYSTEM DELAYS

FIG. 3

STABILITY TEST OF TLRS 1 ON TARGET #1

JULY 28, 1955

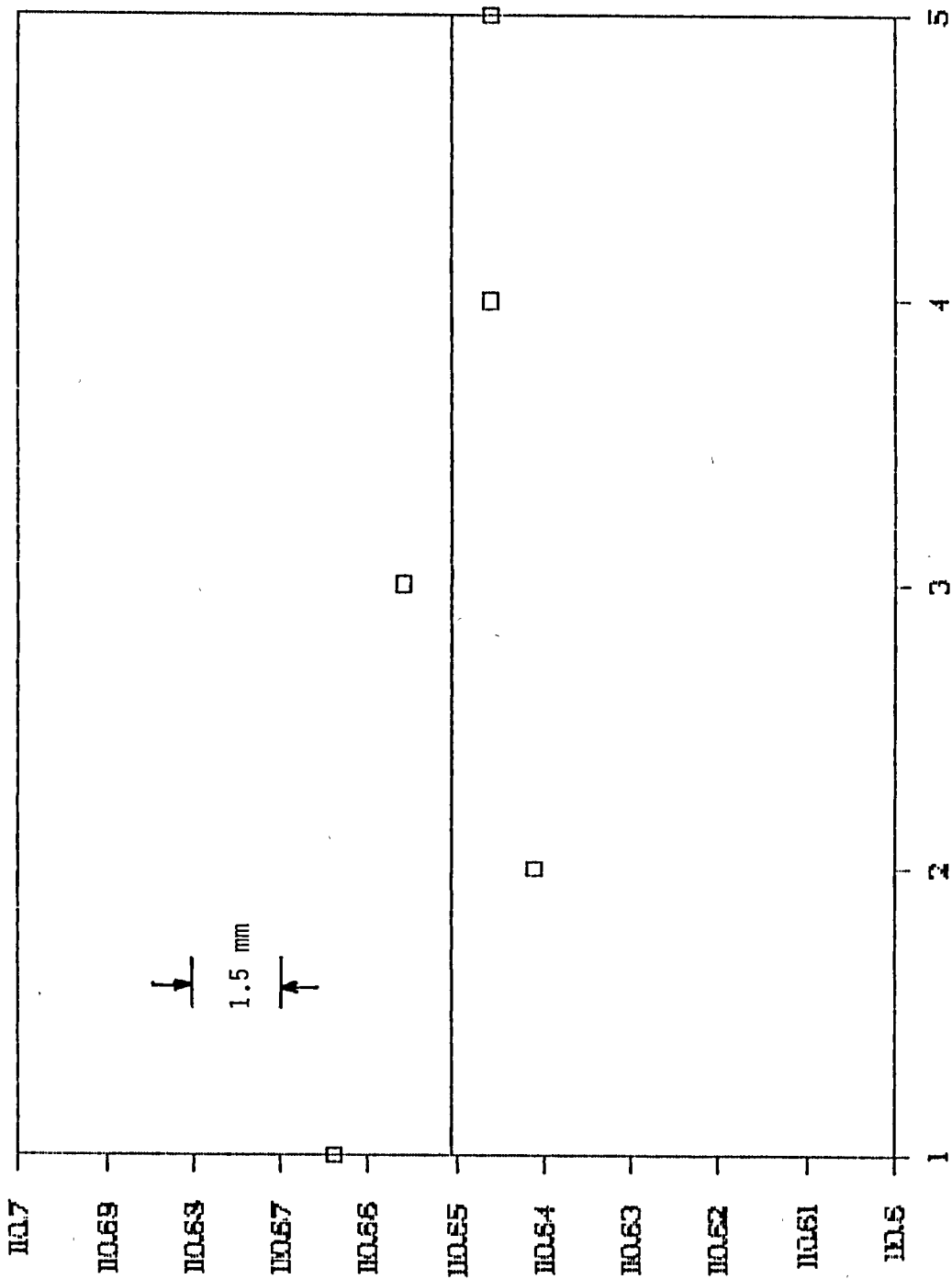


FIG. 4

MULTITARGET RANGE STABILITY

JULY 26 - 27, 1995

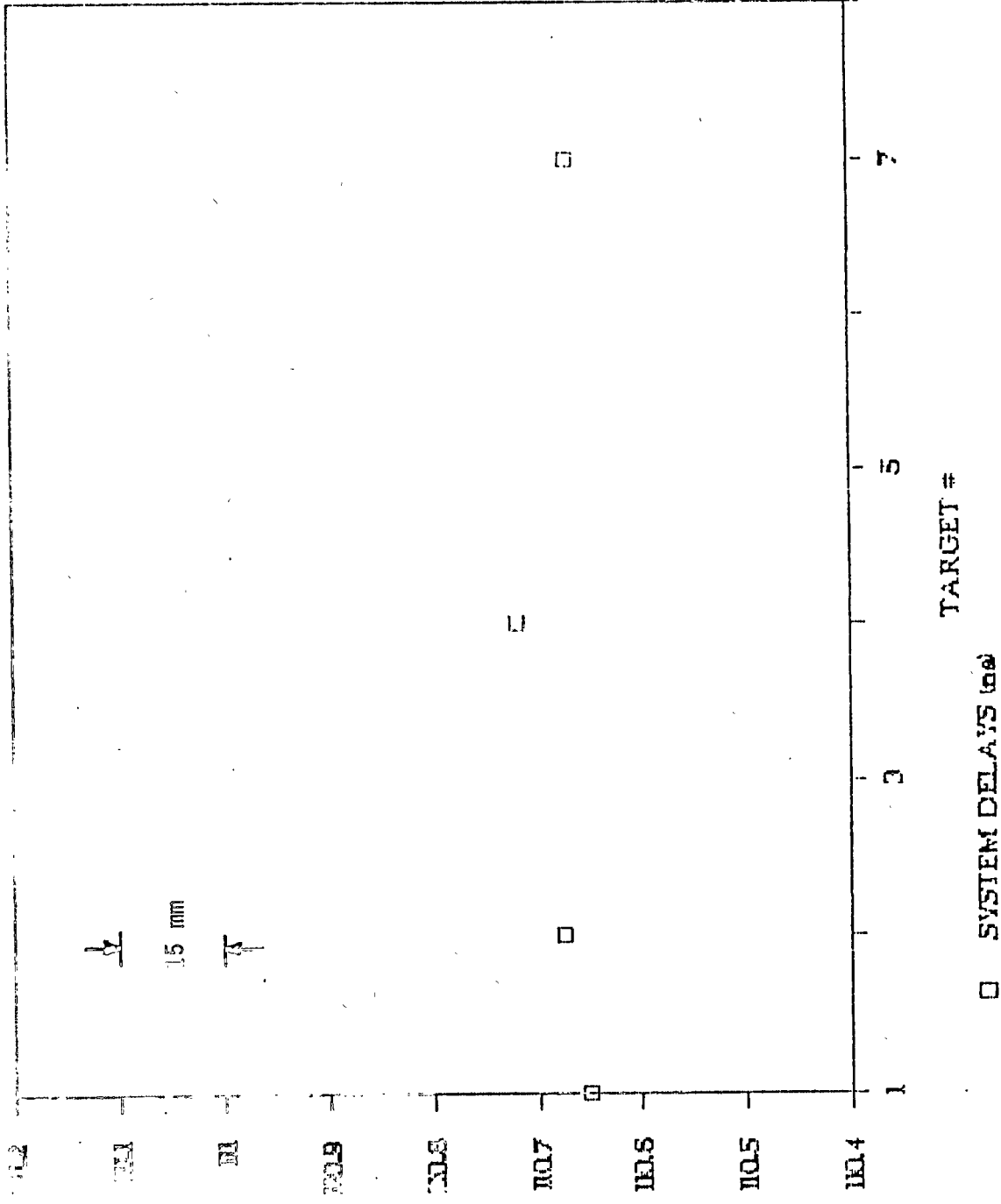


FIG. 5

AZIMUTH DEPENDENCE (FOUR TARGETS)

JULY 26 - 27, 1985

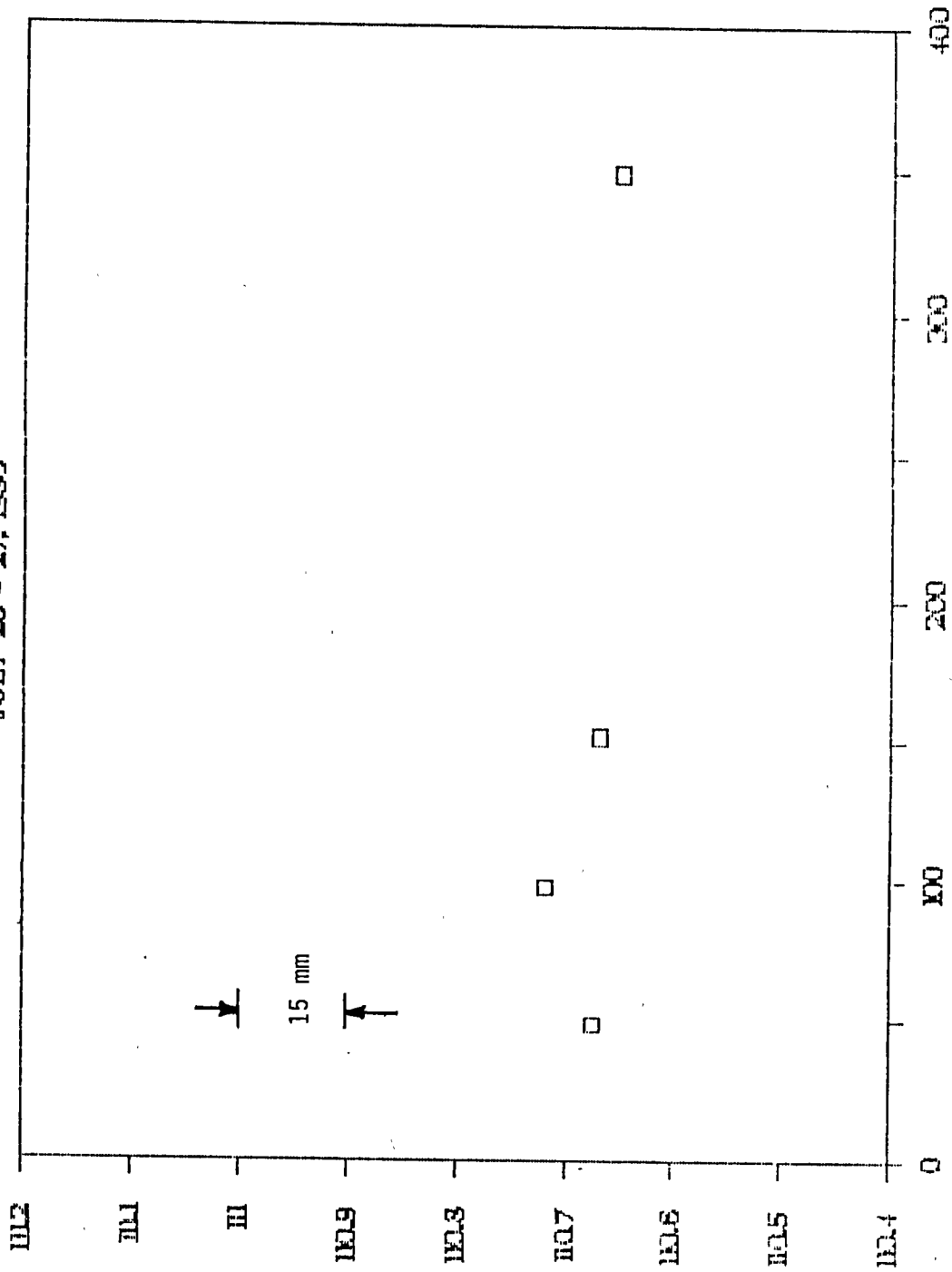
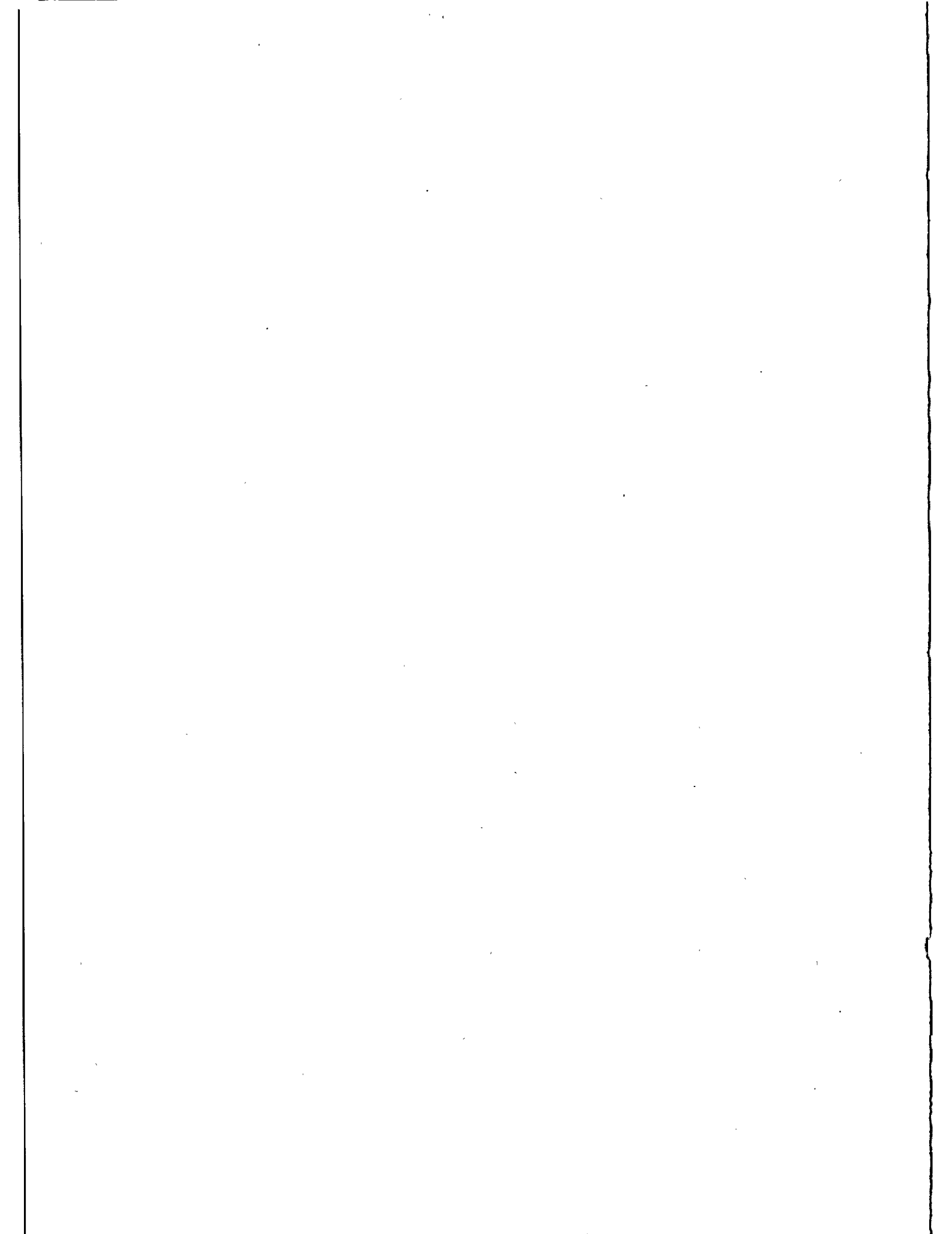


FIG. 6



SATELLITE LASER RANGING SYSTEM AT THE SIMOSATO HYDROGRAPHIC
OBSERVATORY AND THE TRANSPORTABLE SYSTEM ; HTLRS

M. Sasaki
Hydrographic Department,
Maritime Safety Agency
Tsukiji-5, Chuo-ku, Tokyo 104 - Japan -

Telephone (03) 541 3811
TWX 2522 452 HDJODC J

Y. Suzuki
Totsuka Works, Hitachi Ltd.
216 Totsuka-machi, Totsuka-ku
Yokohama 244 - Japan -

Telephone (045) 881 1221
TWX 3823 503

ABSTRACT

The paper outlines the history of laser ranging in Japan, and introduces the SLRS installed in the Simosato Hydrographic Observatory of Hydrographic Department, Maritime Safety Agency. It also describes the transportable system ; TLRS now under development for determining the locations of isolated islands around Japan.

INTRODUCTION

The work on laser ranging in Japan began with an experiment of ranging the GEOS and DIADEME satellites at the Dodaira Station of Tokyo Astronomical Observatory (TAO) in December 1968. A satellite laser ranging system (SLRS) using a receiving telescope with diameter of 60 cm, and a ruby laser with pulse width of 50 ns, output of 1 J, 1 pps, was manufactured for the experiment⁽¹⁾⁽²⁾.

A lunar ranging experiment was made at the Okayama Astrophysical Observatory in 1971 with the target of the retro-reflector installed by Apollo 11 on the surface of the moon. The experiment employed an astronomical telescope with diameter of 188 cm as the transmitting and receiving optics, and a ruby laser with output of 5 J, 12 ppm⁽³⁾⁽⁴⁾. Above two systems were developed by TAO and Hitachi.

The work of TAO has since been continued at the Dodaira Station, and the system was improved several times.

A test model of an SLRS for geodetic observation was built up jointly by the Hydrographic Department (JHD) of Maritime Safety Agency (MSA) and Geographical Survey Institute (GSI) and installed at the Kanozan Geodetic Observatory in 1976. The system employed a receiving optics with diameter of 40 cm, a ruby laser, and a three-axis mount⁽⁵⁾.

Upon reviewing the experiment results and the world's technological trends, the JHD decided to use an SLRS for marine geodetic control, and to determine the locations of isolated islands around Japan. The JHD introduced a fixed type SLRS for the base station into the Simosato Hydrographic Observatory (SHO)⁽⁶⁾.

The SLRS is of the same size with the system of the IFAG station in West Germany. It is provided with a receiving telescope, 60 cm in diameter, and an Nd-YAG laser having a pulse width of 200 ps, 4 pps.

Japan's first geodetic satellite "AJISAI" which means "HYDRANGER" of flower in Japanese was launched on an orbit on August 12, 1986(UT), by the first H-1 rocket which was developed by the National Space Development Agency (NASDA).

Following the introduction of the fixed type SLRS, the MSA has started developing a transportable SLRS:TLRS which is intended for determining the locations of isolated islands in combination with the satellite "AJISAI". The TLRS, now being manufactured by Hitachi Limited, is expected to be completed in October 1987.

THE SLRS AT SIMOSATO

The laser site of the Simosato Hydrographic Observatory is situated close to the point of Kii Peninsula of Honshu Island (135° 56 min. E, 33° 34 min.). The site, at an altitude of 60 meters above the sea level, faces the Sea of Kumano. With annual precipitation of more than 2,700 mm, the climate is not so suitable for satellite ranging.

The SLRS at Simosato was manufactured jointly by GTE of the U.S.A. and Hitachi of Japan under the supervision of JHD. GTE manufactured the laser, optics and mount, control and data-processing equipment subsystem, and main software. Hitachi took the roles of manufacturing the timing system, the system calibration equipment including the ground target, various types of support software for operation and data processing,

and of integrating, installing and adjusting the entire system.

The SLRS was brought into the Simosato site in February 1982. Regular observation was started in April after some adjustment and testing. Since then, the SLRS has been continuously operating for four years to date.

Figure 1 shows an external view of the entire Simosato station. The SLRS installation is housed in the building on the right side. Figure 2 shows the electronics including the control and data-processing equipment subsystem. Figure 3 shows the optics and mount.

Table 1 lists the main items of the system specification.

During the discussions on the proposed SLRS installation at Simosato, those who concerned with the project were afraid that satisfactory observation might not be performed at the low-altitude, seashore site, where the climatic conditions are not favorable for the purpose. Table 2 lists the results of the observation during the past four years, which indicate that the number of annual data acquisitions has been increasing. Ranging data of 297 passes and 243,800 ranges was acquired for the LAGEOS in 1985.

System operation and ranging of LAGEOS, STARLETTE and BEACON-C is conducted around-the-clock by five staff members headed by Mr. E. Nishimura. One of the ranging objects was changed from BEACON-C to AJISAI last August. Figure 4 shows the ranging data of AJISAI obtained immediately after its launching.

Hitachi has been contracting with JHD for the SLRS maintenance.

The coordinates of the base point at the SHO were estimated from the satellite ranging data obtained at the Simosato site, and were reported^{(7),(8)}.

In addition to the main work for marine geodetic control, the JHD participates in the efforts to detect plate motions and crustal movements in the SLRS observation project which will contribute to estimating the earth rotation and geophysical parameters.

The following additions and changes were made to the SLRS:

(1) Laser attenuator

The ground target is used to calibrate the system delay time. An attenuator of the construction shown in Fig. 5 is added to the system in order to assure safety against the laser beam and to match the signal intensity with the level of the signal reflected by the satellite. A high attenuation ratio is obtained from the diffractive effect of a pin hole aperture and a beam splitter with high reflection ratio.

(2) Photomultiplier tube (PMT)

The static crossed field type photomultiplier tube initially employed for the system caused deterioration of the dynode gain in about two years after the start of its use, and needed to be replaced. However, the PMT was then out of production. Its substitute selected was the Micro channel plate PMT with gate. At the same time, a wideband amplifier (DC to 3.15 GHz) was added to the back of the PMT in order to

prevent the output from being saturated by the strong background light in the daytime, and to improve the signal level detectable by the system.

Its employment resulted in the increase in the data acquisition rate and similar ranging accuracy to the initial PMT, helped by the additional amplifier.

(3) Software

Support software was developed and added to the main software. The major items of the support software include the satellite path charting feature for observation scheduling, the star position computing and tracking feature for correcting mount pointing errors, the ranging accuracy calculating feature, satellite position calculating feature using numerical integration method, and the joystick hold feature for facilitating satellite tracking with offset error.

Prior to the construction of the Simosato site, the one of authors visited the laser sites of CERGA in France, IFAG in West Germany, NASA Goddard, SAO Boston and Hawaii Haleakala in the U.S.A. The authors wish to thank the personnel of these organizations for their kind advice and useful suggestions.

TRANSPORTABLE SYSTEM; HTLRS

The transportable system: HTLRS the JHD plans to introduce is to be used for AJISAI satellite ranging to determine the locations of ten major isolated islands around Japan. Figure 6 shows these ten islands (marked with a double circle) where mobile observation is expected.

The observation is scheduled to be done on two islands a year. The SLRS will be transported by truck, by ship (cargo boat or ferry boat), or by aircraft.

To permit transportation by the above means, the entire system will be housed in two shelters as shown in Fig. 7 and designed to weigh less than five tons.

The optics/mount and the laser are assembled on the same bench. Upon arrival at the site, the bench is installed on a concrete pier constructed on the ground independently of the shelters. The electronics including the control and data processing equipment subsystem are housed in the other shelter.

Table 3 lists the major specifications of the system. Figure 8 is a block diagram showing the system configuration. The major target satellite of the HTLRS is the AJISAI. It is, however, designed to be capable of ranging the LAGEOS.

The ability of a ranging system is represented by the concept of system size⁽⁹⁾. The authors defined the system size parameter S for the SLRS as follows:

$$S = n \cdot E_o \cdot A_r \cdot \alpha \beta \gamma \cdot \eta \dots\dots\dots (1)$$

where,

Table 2 Data Acquisition at Simosato Hydrographic
Observatory and Its Mean Range Accuracy

| year | LAGEOS | | STARLETTE | | BEACON C | | AJISAI | |
|-----------|--------|---------|-----------|--------|----------|--------|--------|--------|
| | passes | ranges | passes | ranges | passes | ranges | passes | ranges |
| 1982 | 47 | 11,000 | 36 | 4,700 | 59 | 11,900 | - | - |
| 1983 | 137 | 30,000 | 116 | 29,400 | 199 | 92,200 | - | - |
| 1984 | 223 | 93,300 | 118 | 37,800 | 150 | 56,100 | - | - |
| 1985 | 297 | 243,800 | 108 | 38,800 | 154 | 67,500 | - | - |
| ~Aug 1986 | 156 | 103,900 | 53 | 11,700 | 56 | 15,400 | 27 | 25,300 |
| accuracy | 9.0 cm | | 9.8 cm | | 9.2 cm | | | |

n : Laser output repetitions
E₀ : Laser output energy
A_r : Area of receiving optics
αβγ: Efficiency of transmitting and receiving optics
η : Quantum efficiency of detector.

Figure 9 shows the system size of the transportable SLRS defined by the equation (1) above. The horizontal axis in Fig. 9 represents "S" in equation (1), while the vertical axis shows the beam divergence of the transmitting laser. The oblique lines in the diagram indicate the relationship between system size S to detect reflected signals from the LAGOS and the GS-1 at an output of rate of one photoelectron per second, and beam divergence θt.

System size S of the transportable SLRS is designed to be 3.5 to 17 w.sq.cm, which means that the detection of one photoelectron output per second can be obtained (detectable) by shooting at the LAGEOS with beam divergence of approximately 100 arc seconds.

The HTLRS is expected to be operated with beam divergence of 40 arc seconds. Then, the theoretical value of the signal level received from the LAGEOS will be 10 to 1 p.e. per shot. The system is designed to operate during the period of night to twilight time.

Figure 10 shows the calculated results of the detection probability of a few receiving systems based on the authors' studies on weak pulse light detection^{(10),(11),(12)}. The horizontal axis in the diagram shows the noise level per gate 10

microsec., while the vertical axis shows the detection probability. Parameter N_s indicates the average number of received photons. The curves of detection probability are, from left to right, the results of threshold detection at single p.e. level, multichannel (8 channel) detection, and coincidence detection using double pulses by two output branching, respectively.

One-channel threshold detection (single p.e. detection) will be conducted in the early days of the transportable system introduction, although the multichannel or coincidence system is more desirable for twilight operation. Possibility of day time ranging may be discussed by narrowing range gate from 10 μ s to 100 ns and the bandwidth of interference filter from 8 Å to 1 Å.

The HTLRS will employ the Nd-YAG laser. Its output is 50 mJ per pulse, pulse width is up to 200 ps, and repetition is 10 pps.

Hitachi's personal computer, Model B16/FX will be used to control the system and process data.

The Rb frequency standard with a time calibration by Loran will be employed for the timing subsystem.

The detector will be used for the micro channel PMT with gate, similarly to the Simosato system.

The optics/mount subsystem will be of a new configuration. Figure 11 illustrates a rough sketch of the optics/mount subsystem, while Fig. 12 shows its configuration. The receiving telescope is arranged so that the light axis will coincide with the elevation axis, and will be stationary for the elevation axis. The transmitting laser beam passes along the azimuth

axis, and is shot via the reflector mirror on the rear of the secondary mirror of the receiving telescope and the tracking mirror. Only the tracking mirror, installed at an angle of 45° to the elevation axis, revolves around the elevation axis. This arrangement has such advantages as that the receiving telescope can be stabilized because it is used in a nearly stationary state, that the load can be reduced because the elevation axis needs to drive only the tracking mirror, and that the transmitting optics can be simplified.

The two axes, elevation and azimuth, are driven by a direct drive torque motor.

The HTLRS is provided with an additional for detecting the flash light of the sun reflected by the AJISAI (star of magnitude 2 to 4, 2 pps, 5 ms width) and determining the flash times (rise and fall) besides the main feature for tracking and ranging the satellite. This additional feature is used to fix the time of photographic observation of the AJISAI with fixed stars in the background.

REFERENCES

- (1) T. Takenouchi, K. Tomita, S. Yamamoto and Y. Suzaki: Experimental Laser Ranging of Artificial Satellites, Nat'l. Conv. Record of I.E.C.E., Japan, 659 (1969)
- (2) T. Takenouchi, K. Tomita, S. Yamamoto, Y. Hasegawa, A. Tachibana, S. Yamamoto and M. Takatsuji: Satellite Ranging with a Laser, Hitachi Review (1972) Vol. 19, No. 4 pp 153-164

- (3) A. Tachibana, Y. Yamamoto, M. Takatsuji, K. Murasawa and Y. Kozai: A Preliminary System of Lunar Laser Ranging, Space Research XII-Akademie-Verlag, Berlin (1972) pp 179-195
- (4) Y. Kozai: Lunar Ranging Experiments in Japan, Space Research XII-Akademie-Verlag, Berlin (1972) pp 212-217
- (5) Research Coordination Bureau, Science and Technology Agency: Comprehensive Study on the Development of the Laser Ranging System; Performance Report, (1977)
- (6) M. Sasaki, Y. Ganeko, and Y. Harada: Satellite Ranging system at Simosato Hydrographic Observatory. Data Rep, Hydrogr. Obs. Series of Astronomy and Geodesy, JHD, No. 17 (1983), pp 49-60
- (7) M. Sasaki: Satellite Laser Ranging at the Simosato Hydrographic Observatory and its Preliminary Results., Journal of Geodetic Society of Japan, Vol. 30, No. 1 (1984) pp 29-40
- (8) M. Sasaki: Algorithm for Determination of a Satellite Orbit and Geodetic Parameters by Using Laser Ranging Data and Preliminary Results of its Application, Report of Hydrographic Researches, No. 19, March (1984) pp 107-132
- (9) E.C. Silverberg: Operation and Performance of a Lunar Laser Ranging Station Applied Optics, Vol. 13, No. 3, March (1974) pp 565-574
- (10) Y. Suzaki and A. Tachibana: Detection Probability of Laser Radars for Satellite Ranging, Trans. IECE Vol 55-B No. 10 '72/10 pp 569-576

- (11) Y. Suzaki and A. Tachibana: Influence of the Photo-electron Fluctuations on Accuracy of Ranging by Pulsed Laser Radar, Trans. IECE Vol. 56-c, No. 11 '73/11 pp 609-614
- (12) Y. Suzaki and A. Tachibana: Detection Times and Errors of Returned Optical Pulses for Satellite Ranging, Trans. IECE Vol. 63-c, No. 8, '80/8 pp 500-506

Table 1 Major Specifications of the SLRS at Simosato

| Subsystem | Specification |
|------------------------------|--|
| Mount | |
| Configuration | elevation over azimuth |
| Transmitter system | laser stationary – two axes Coudé path |
| Tracking rate | from sidereal to 1° per second |
| Orthogonality | ±5 arcsec |
| Wobble | ±2 arcsec in elevation, ±5 arcsec in azimuth |
| Angular resolution | 20 bits (1.2 arcsec) |
| Drive | DC direct drive torque motors |
| Transmitting optics | |
| Type | Galilean |
| Diameter | 17 cm |
| Beam divergence | 25 μrad – 2 mrad (computer controlled) |
| Start pulse detector | common with receiver electronics connected by fiber optics |
| Receiving optics | |
| Type | Cassegrain |
| Diameter | 60 cm |
| Field of view | 100 μrad – 2 mrad (computer controlled) |
| Sun shutter | automatic |
| Spectral filter | 0.8 nm bandpass (temperature controlled) |
| Optical attenuator | 0 – 40 dB (computer controlled) |
| Laser | |
| Type | Nd:YAG |
| Wave length | 532 nm |
| Output energy | 150 mJ (normal) |
| Pulse width | 200 ps |
| Repetition rate | 1 – 4 pps (4 pps normal) |
| Receiving electronics | |
| Detector type | PMT (static crossed-field) |
| Quantum efficiency | 29 % |
| Rise time | 120 ps |
| Gate position | 2 μs – 130 ms (computer controlled) |
| Gate width | 0.2 μs – 33 ms (computer controlled) |
| Flight time counter | 20 ps resolution |
| Control | |
| Mount control | DC servo amplifiers (45 A peak current) with torque motors, tachometers and encoders (manual, computer and computer aided) |
| Data flow rate | 30 Hz |
| Clock | |
| Frequency standard | a Rubidium (2×10^{-11}) oscillator |
| Comparison | multi-Loran C waves (NW Pacific Chain) |
| Computer | |
| CPU | PDP 11/60 (64 kw Mos- and 1 kw cache memory) |
| Peripherals | two 5.2 Mbyte disk drives, a magnetic tape unit, a paper tape reader/punch, a hardcopy terminal and a CRT display |

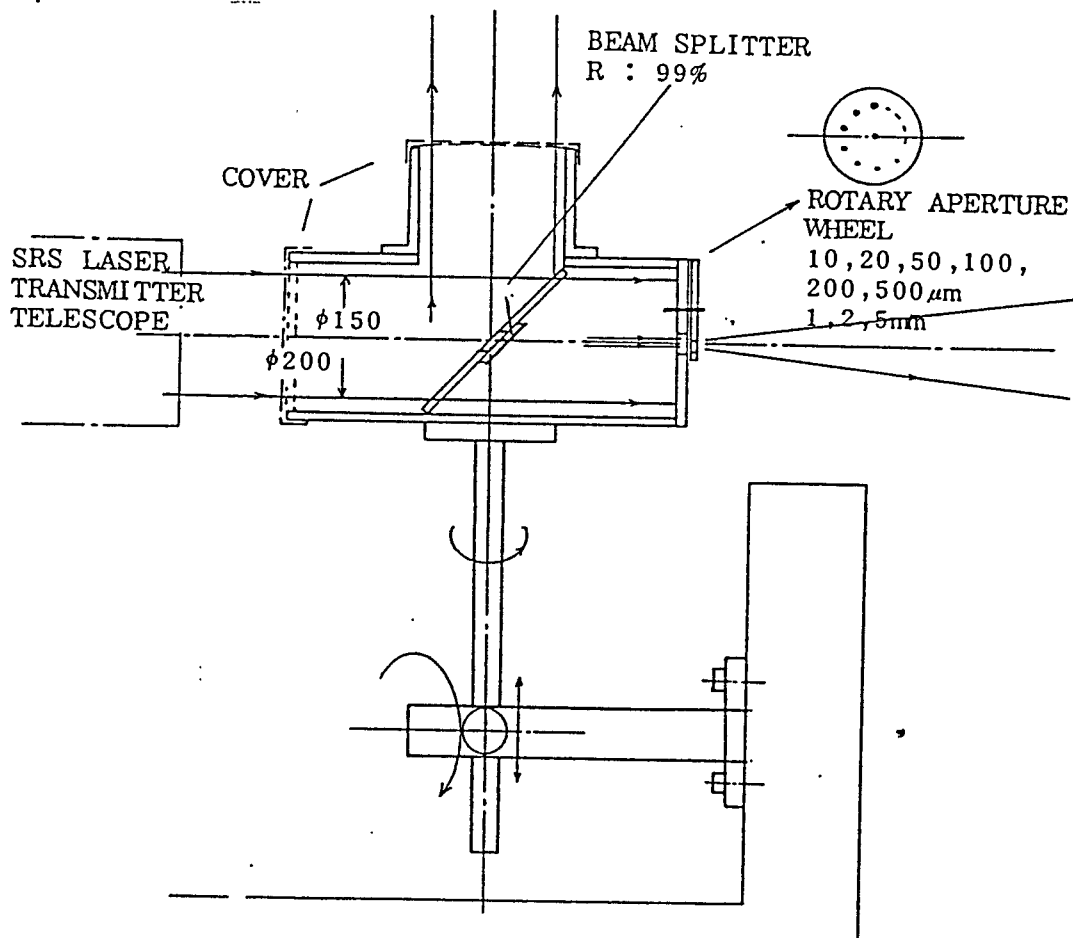
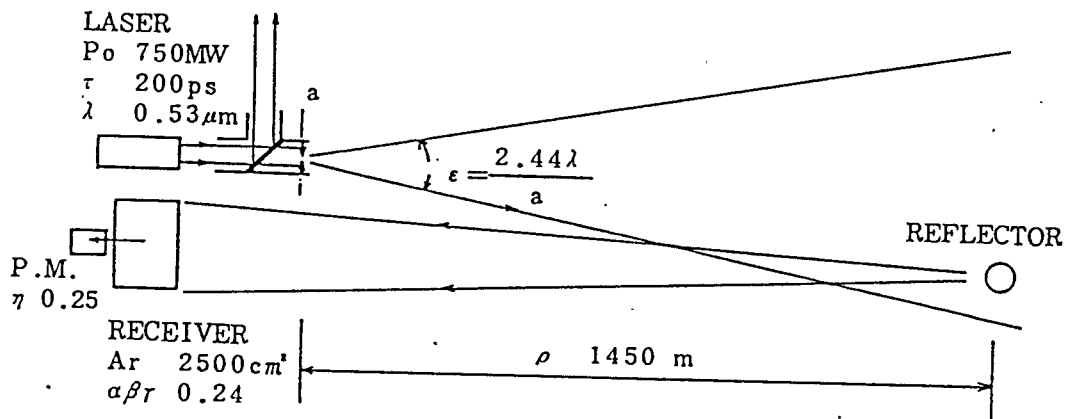


Fig. 5 Laser Attenuator for Ground Target Ranging

Marine Geodetic Controls around Japan

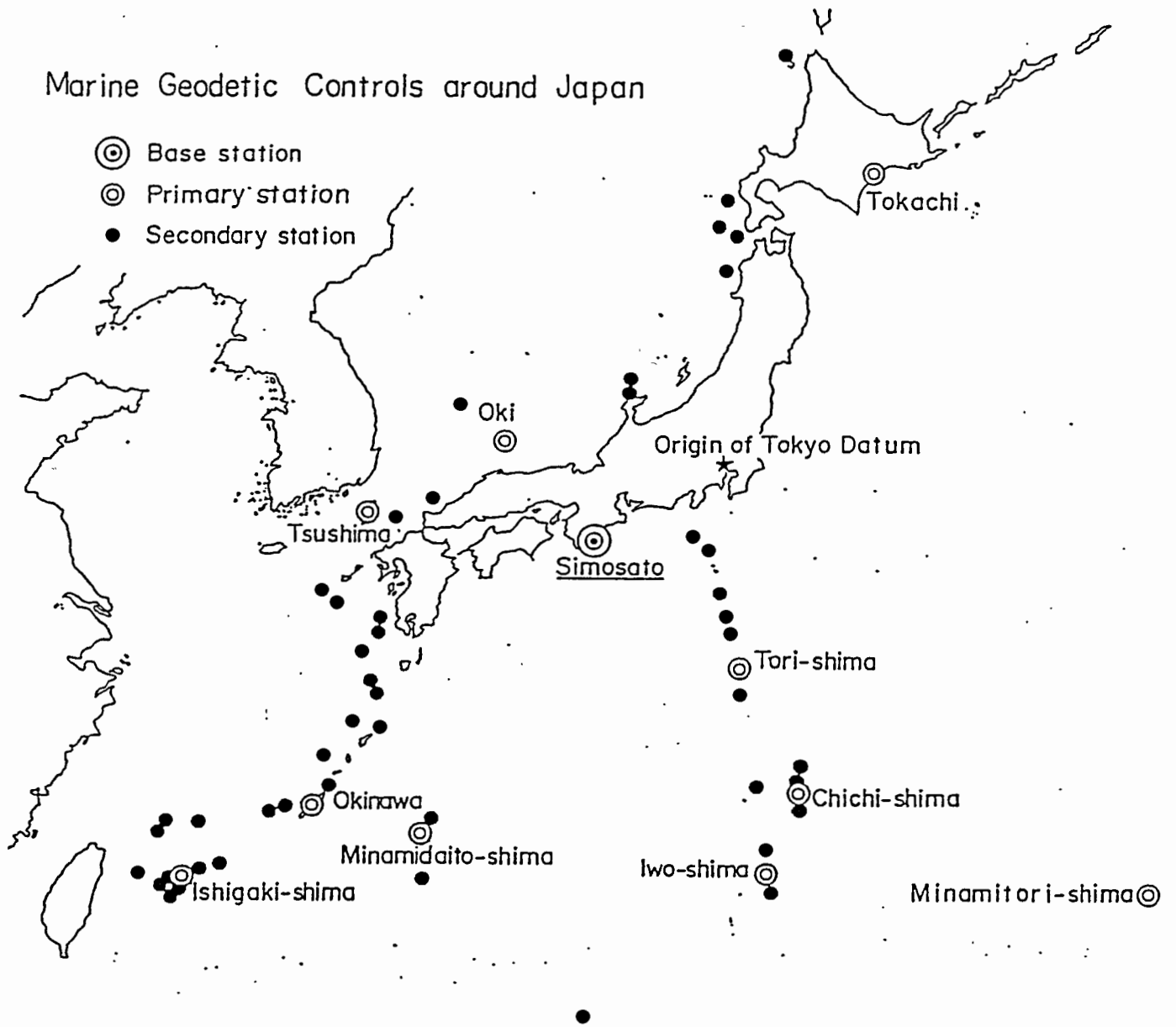


Fig. 6 Isolated Island where Observation by HTLRS is expected (with double circle)

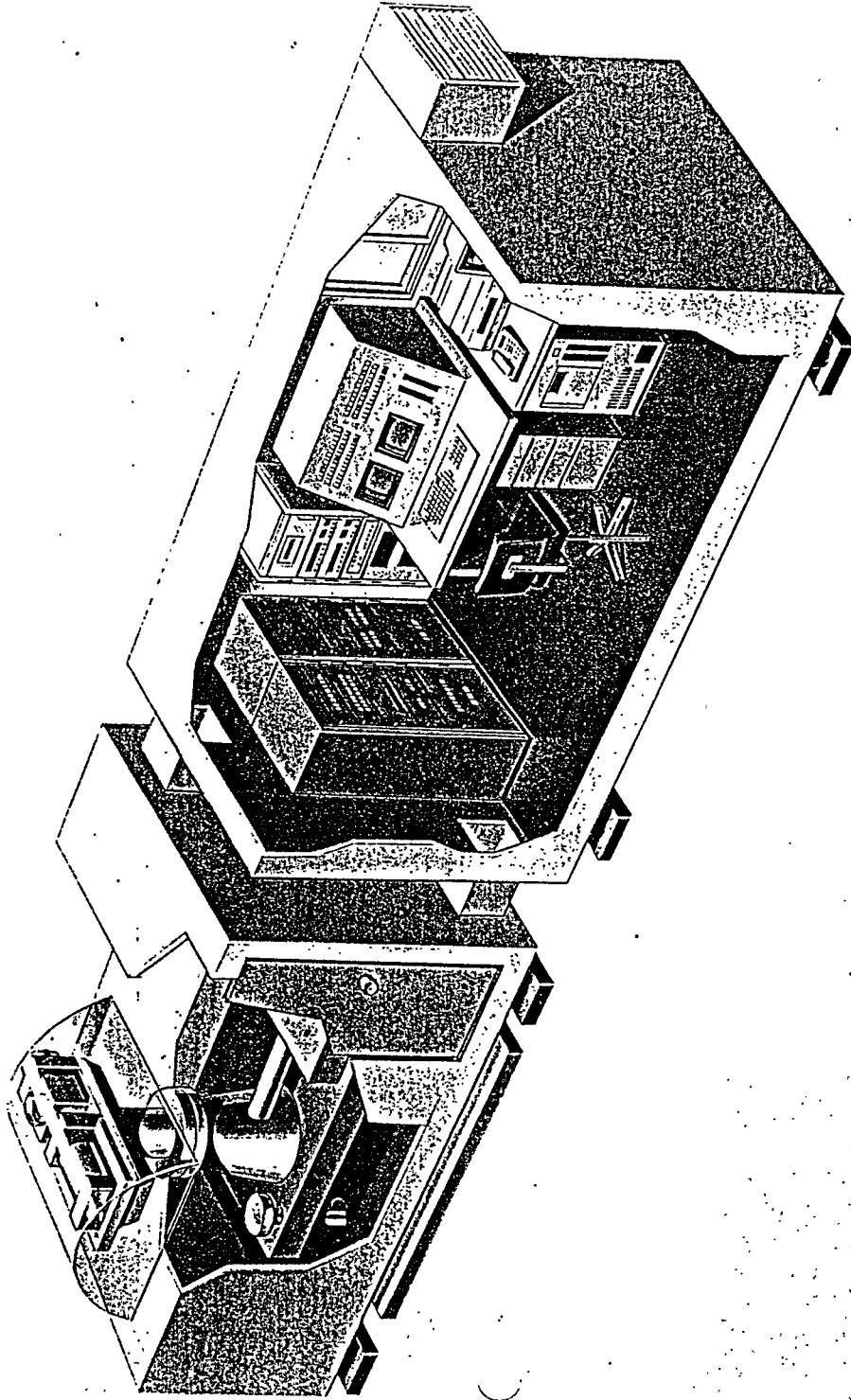


Fig. 7 HTLRS Housed in Shelters

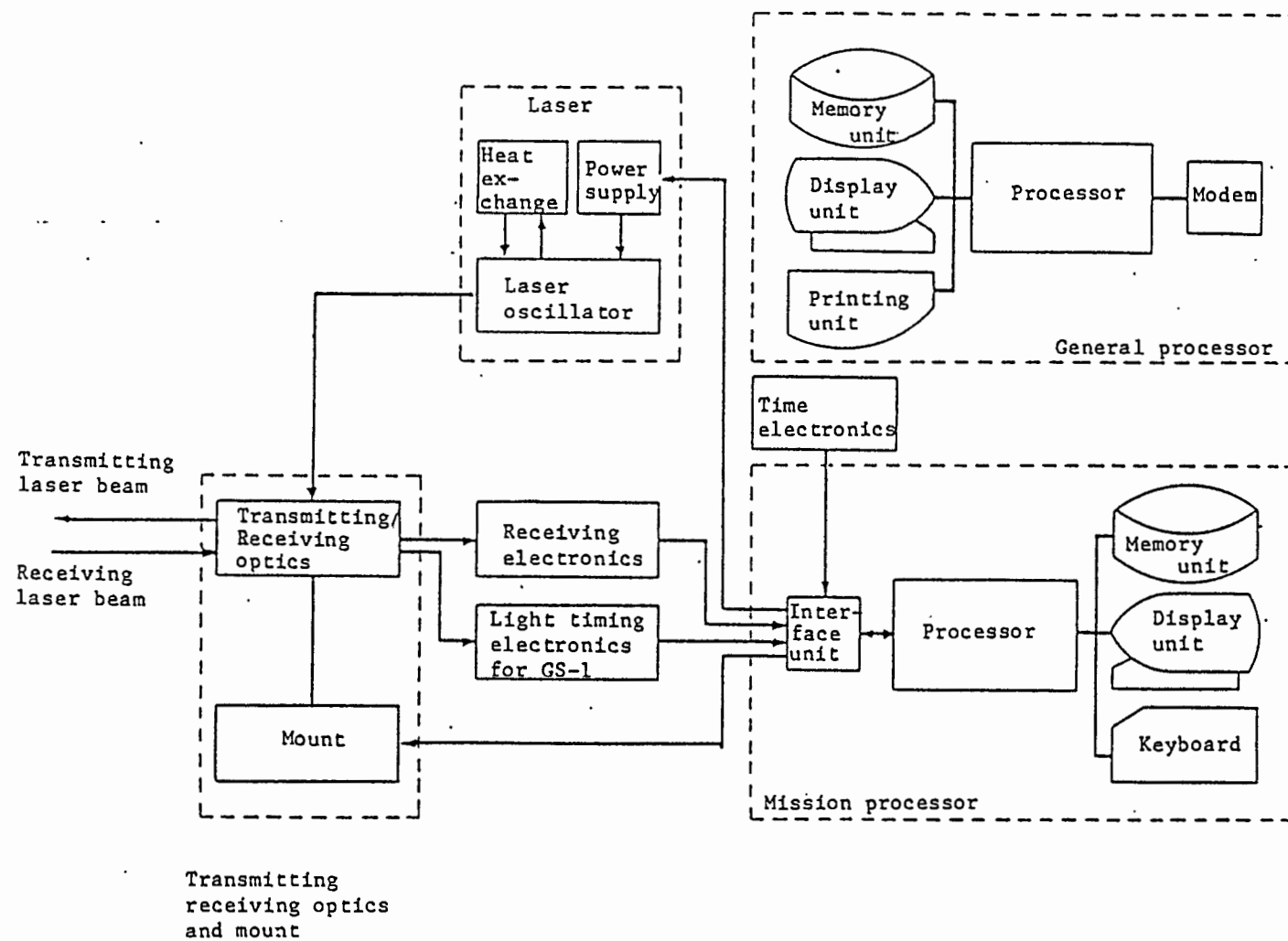


Fig. 8 System Cofiguration of the HTLRS

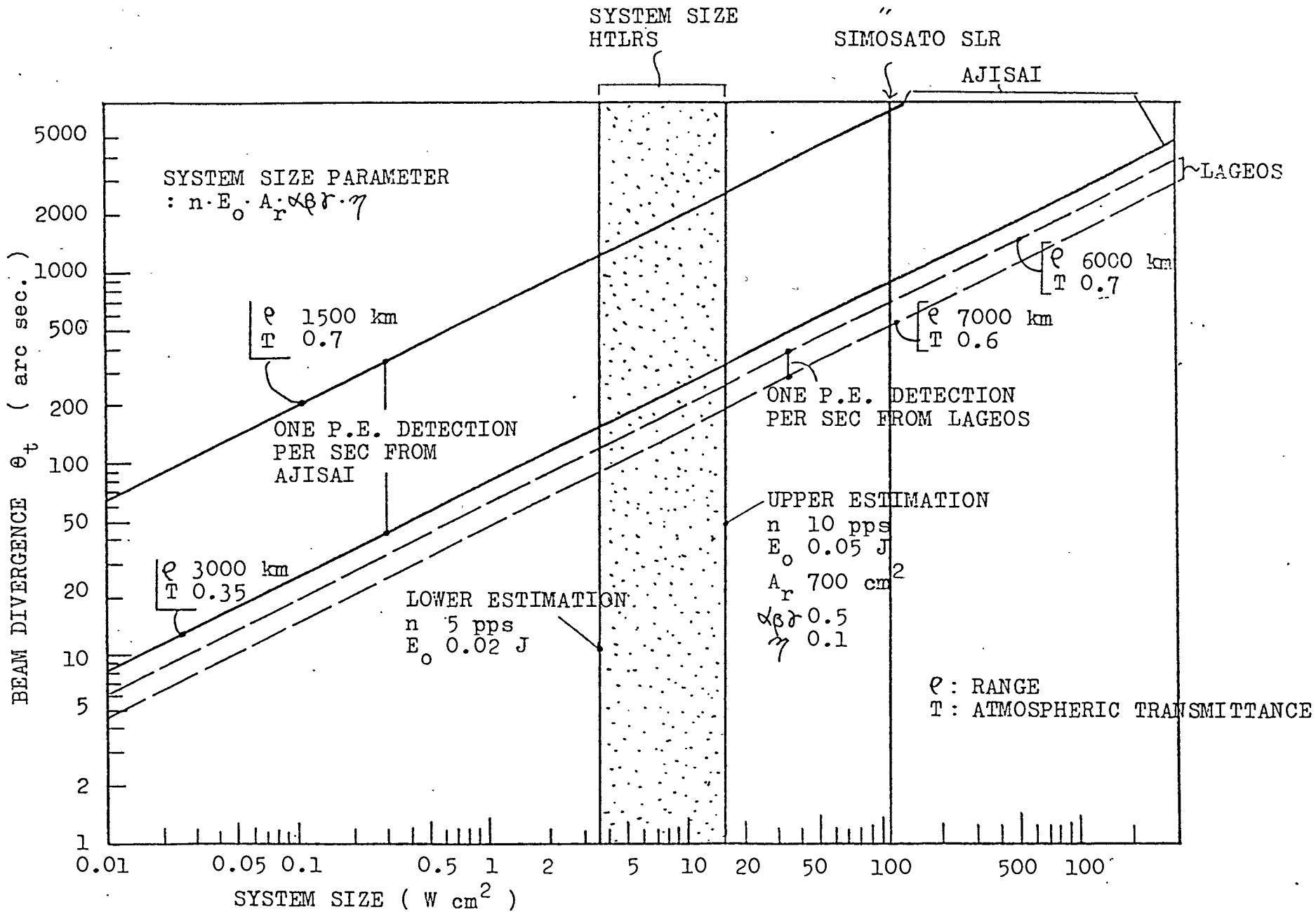


Fig. 9 System Size of the HTLRS

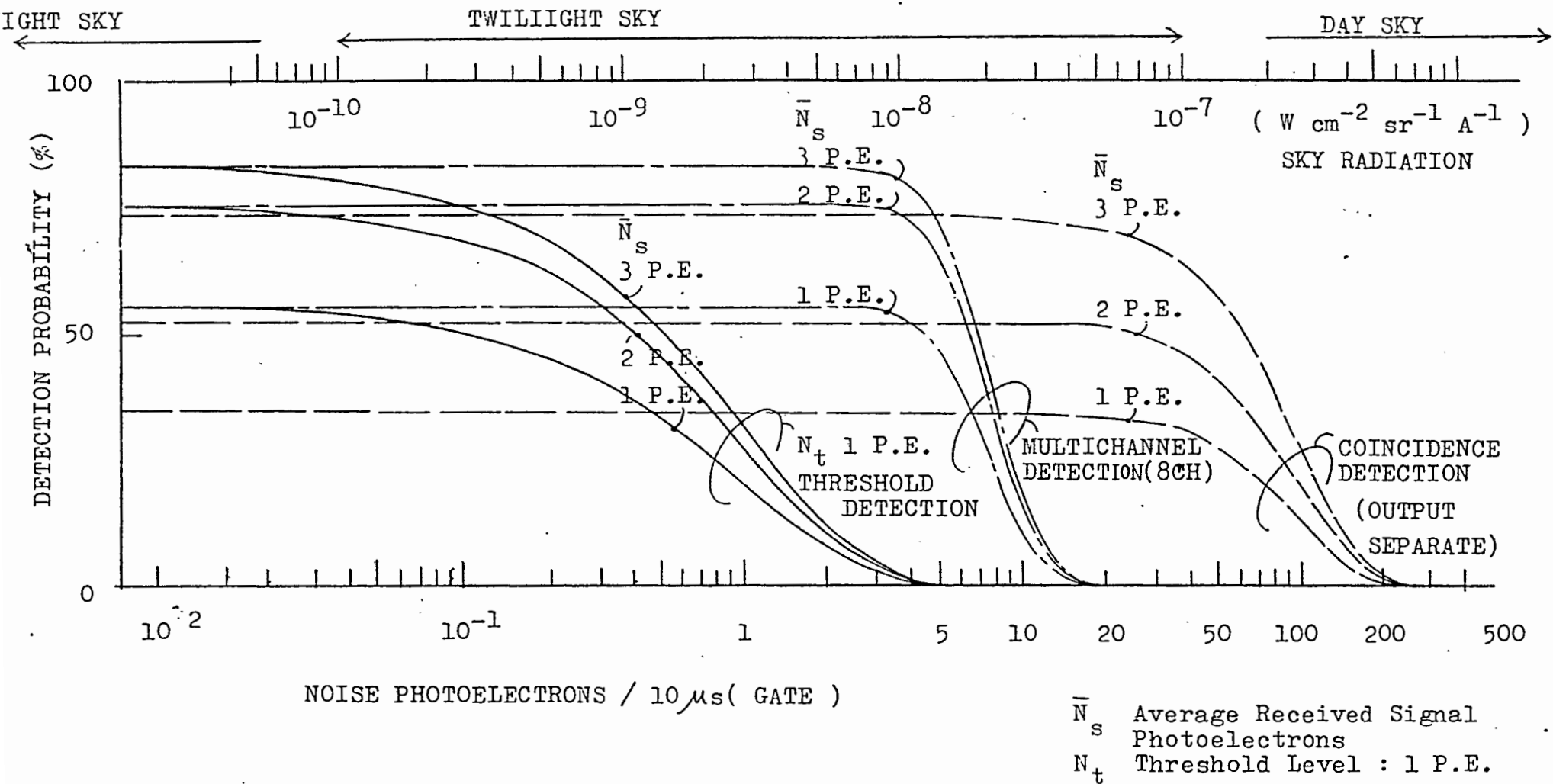


Fig. 10 Calculated Detection Probability of the HTLRS

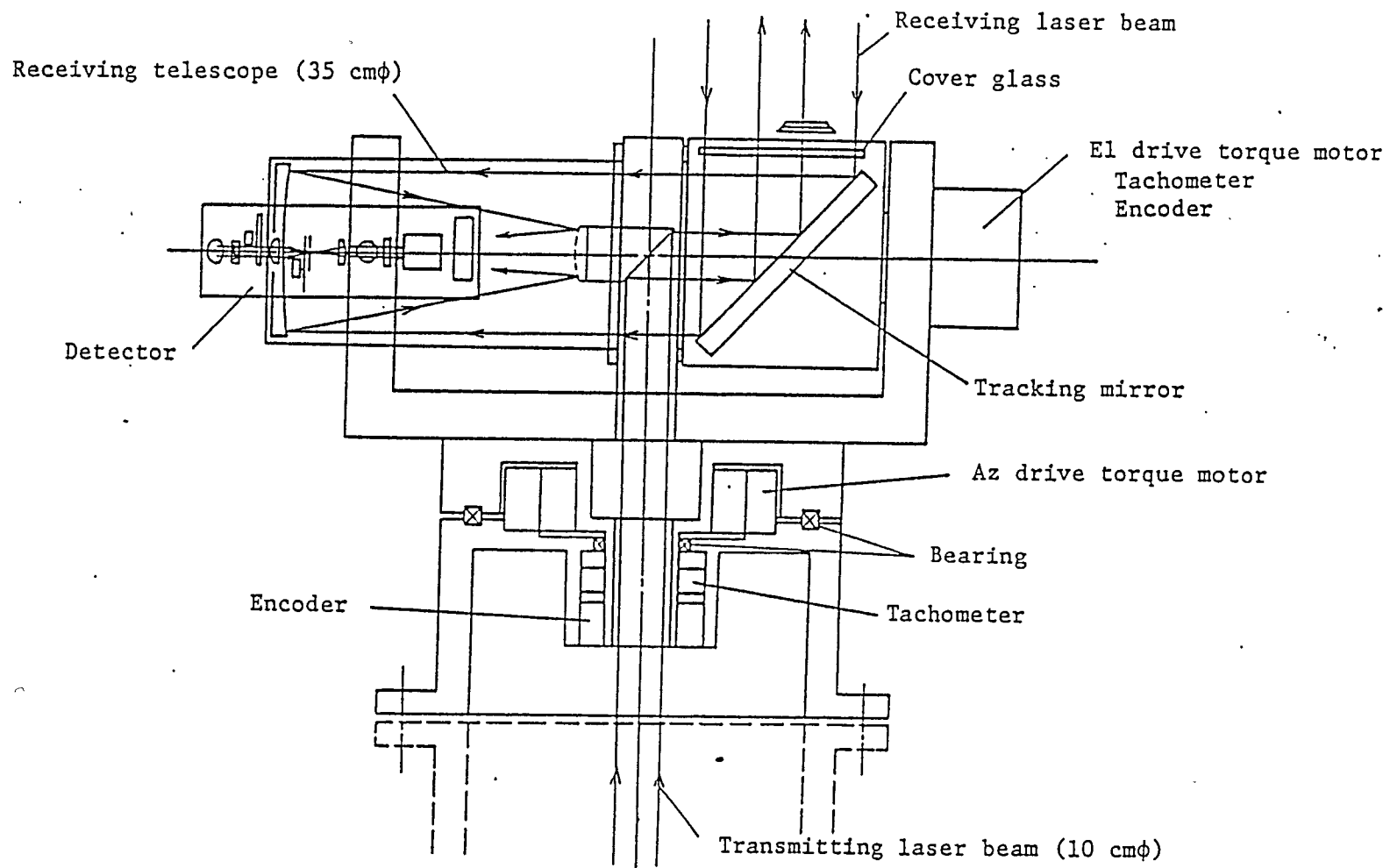


Fig. 11 Optics / Mount of the HTLRS

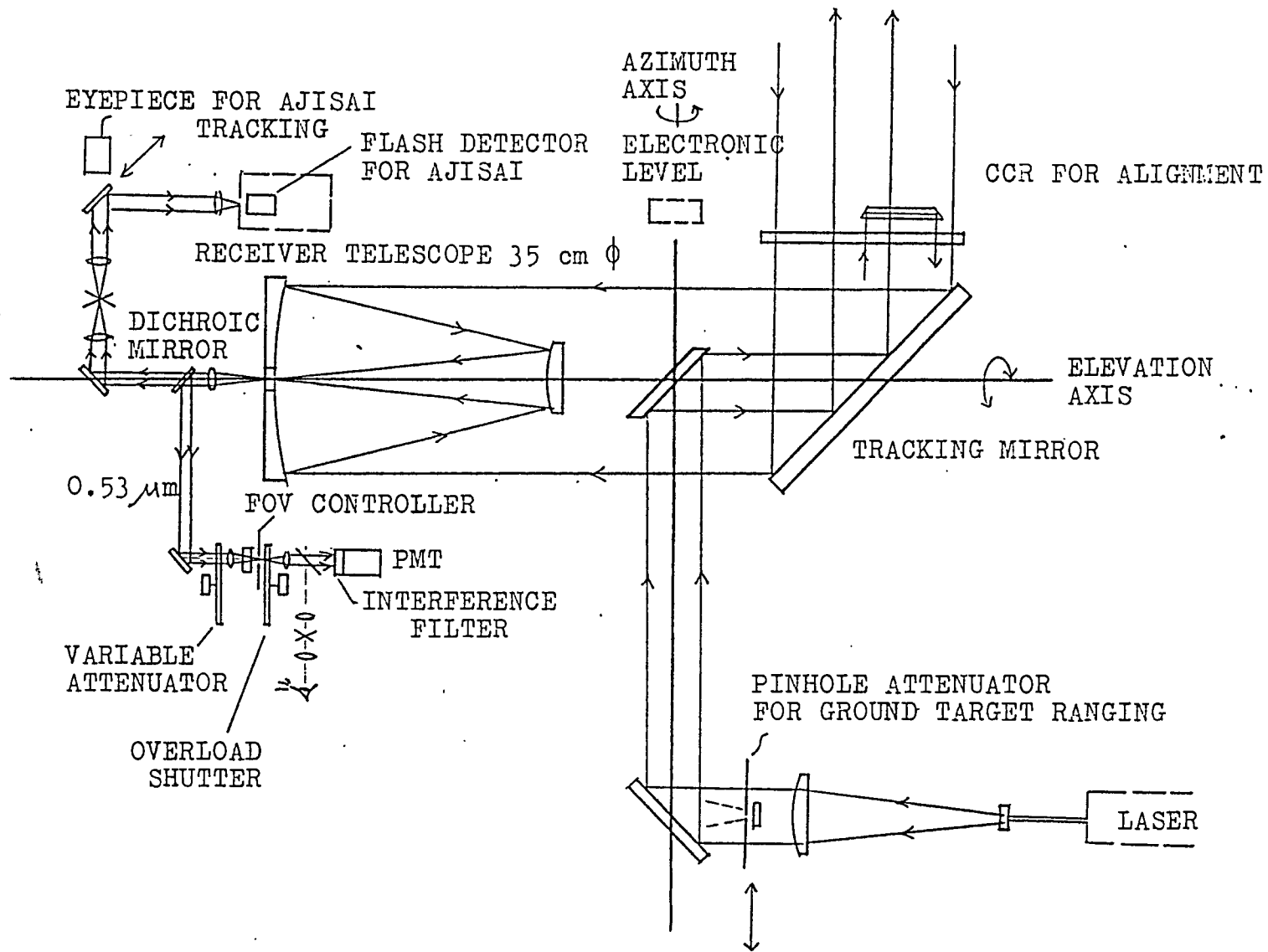


Fig. 12 Optical Configuration of the HTLRS

PROGRESS IN SLR AT SHANGHAI OBSERVATORY

Z. Wen-Yao, T. De-Tong
Shanghai Observatory
Academia Sinica
Shanghai - China -

Telephone 386191
Telex 33164 SHAO CN

ABSTRACT

SLR work at Shanghai Observatory was started in 1975, while development of the second-generation SLR system, with the aperture of the telescope 60 cm and the width of the Nd:YAG laser pulse 4-5 nsec, was begun in 1978. During the MERIT Main Campaign the Laser Geodynamic Satellite LAGEOS has been successfully observed with this laser system. According to the CSR analyses, the accuracy of our data for single shot is about 15 cm. In that period, the system has the capability of a maximum range of about 8542 km, the lowest elevation angle of 20 degrees for LAGEOS and the longest track arc of 45 minutes in a pass.

After MERIT Campaign we began to set up a new Nd/YAG frequency-doubled mode-locked laser ranging system in order to improve the accuracy of LAGEOS ranging.

PROGRESS IN SLR AT SHANGHAI OBSERVATORY

Contact: Zhu Wen-yao, Tan De-tong
Shanghai Observatory
Academia Sinica
Shanghai, China

Tel: 386191
Telex: 33164 SHAO CN

1. THE SLR EXPERIMENTAL SYSTEM WITH 5 CM ACCURACY AT SHANGHAI OBSERVATORY

SLR work at Shanghai Observatory was started in 1975, while development of the second-generation SLR system, with the aperture of the telescope 60 cm and the width of the Nd:YAG laser pulse 4-5 nsec, was begun in 1978. During the MERIT Main Campaign the Laser Geodynamic Satellite LAGEOS has been successfully observed with this laser system. According to the CSR analyses, the accuracy of our data for single shot is about 15 cm. In that period, the system has the capability of a maximum range of about 8542 km, the lowest elevation angle of 20 degrees for LAGEOS, and the longest track arc of 45 minutes in a pass.

After MERIT Campaign we began to set up a new Nd:YAG frequency-doubled mode-locked laser ranging system in order to improve the accuracy of LAGEOS ranging. This system consists of an oscillator, a pulse selector, two amplifiers and a frequency-doubler. The oscillator mode-locked by using both acousto-optic modulator and saturable dye produces a sequential laser pulse trains.

The width of each pulse with TEMOO mode is 32 picoseconds. The pulse selector extracts one single pulse out of the pulse train, then is amplified through the two amplifiers. The output energy from the amplifiers is about 100 mj per pulse at 1.06 μm . In order to match the pulse width with the rise time of receiving system, the pulse width are expanded to 120 ps by using two F-P mirrors. After frequency doubled with a KDP crystal, the output energy is now 30-50 mj at 0.53 μm . The block diagram of Nd:YAG mode-locked laser system is shown in Fig. 1. The width of output pulse has been measured with a streak camera, it is shown in Fig. 2.

A 8-bit microcomputer with 64k byte memory is used for real-time tracking control which is made in China. The accuracies of both predicting and tracking are about 10 arcseconds.

In Nov. 1985, the mode-locked laser system was set up at Zo-Se Station of the Shanghai Observatory. On Dec. 12, 1985, we received the first echo from LAGEOS by the new laser system. Five passes with 606 data were obtained

during the experimental stage. These data had been preprocessed with a residual analytic program of our Observatory. The result is shown in Table 1 and Fig. 3-6. Meanwhile we transmitted these quick-lock data to NASA/GITN. The GITN and CSR have analyzed these data, Table 2 lists their results.

From Table 1, 2, we can see that the accuracy of this new SLR system is about 5 cm for single shot.

In order to explore the stability of the experimental system, a ground target set on the top of a water tower separated by 675.6 meters away from the laser, is used for calibration of the laser system. apertures of different size representing different return signal strength have been used on both receiving and transmitting telescopes to simulate the return signal strength from the satellite. The results of the calibration for ground target indicate that the stability of mode-locked ranging system is about 0.11 ns (2 cm). See Table. 3.

It is expected that the third-generation SLR system at Shanghai Observatory will be in routine operation from Sept. 1986 onwards.

2. SLR DATA ANALYSIS

During the MERIT Main Campaign, as one of the Associated Analysis Center, the Shanghai Observatory had processed the global data of LAGEOS satellite, using the software named SHORDE, which stands for Shanghai Observatory Orbit Determination Processor. The results obtained are A series of ERP-ERP (SHA) 85L01. It lists the solutions for two components of polar motion for each 5-day arc since the beginning of Sept. 1983. The interval precision is approximately 2.1 mas for x_p , 2.2 mas for y_p and 0.13 ms for D_R . In addition, the ability to detect the rate of change of polar motion \dot{x}_p and \dot{y}_p , with 5-day arc solution has been estimated to be approximately 1 mas/day.

The accuracy of the determination of the orbit of LAGEOS satellite is about 14 cm for each 5-day arc from the overall weighted RMS fit of the laser observations to the orbits.

Using SHORDE software, we determined the length of the baseline between two Chinese SLR stations of Shanghai Observatory and Xian Institute of Geodesy and Cartography. All observational data are divided into two arcs: 5-day arc from 18 through 22, Oct. 1984 and 4-day arc during 23-26, Oct. 1984. They are processed respectively. The weighted mean value of two solutions is equal to 1192562.89 ± 0.11 m. The obtained result can be for checking the length survey of geodetic triangulated network. The researching work of the determination of global plate motion and deformation using LAGEOS tracking data is also underway.

Recently we have also completed a program for the transfer of the full-rate data to normal point data. This program includes: (1) pre-processing of full-rate data, (2) generating short-arc/long-arc trajectories for LAGEOS and removing some of the effects of the unmodeled perturbations, and (3) obtaining normal point data and identifying bad observations.

3. THE CHINESE SLR NETWORK

The Chinese SLR network is also being developed. At present, this network consist of seven stations located at Shanghai, Wuhan, Changchun, Kunming,

Xian, Guangzhou, and Zhengzhou. The ranging accuracy of these stations, except the Shanghai and Wuhan Stations, is about 2. cm for single shot. By 1988, two SLR systems of the third generation will be joined into this network. The Chinese SLR network is aimed at geodesy, astronomy and geodynamcis applications such as building of the zero order geodetic controlling network, monitoring of the regional crustal deformation and so on.

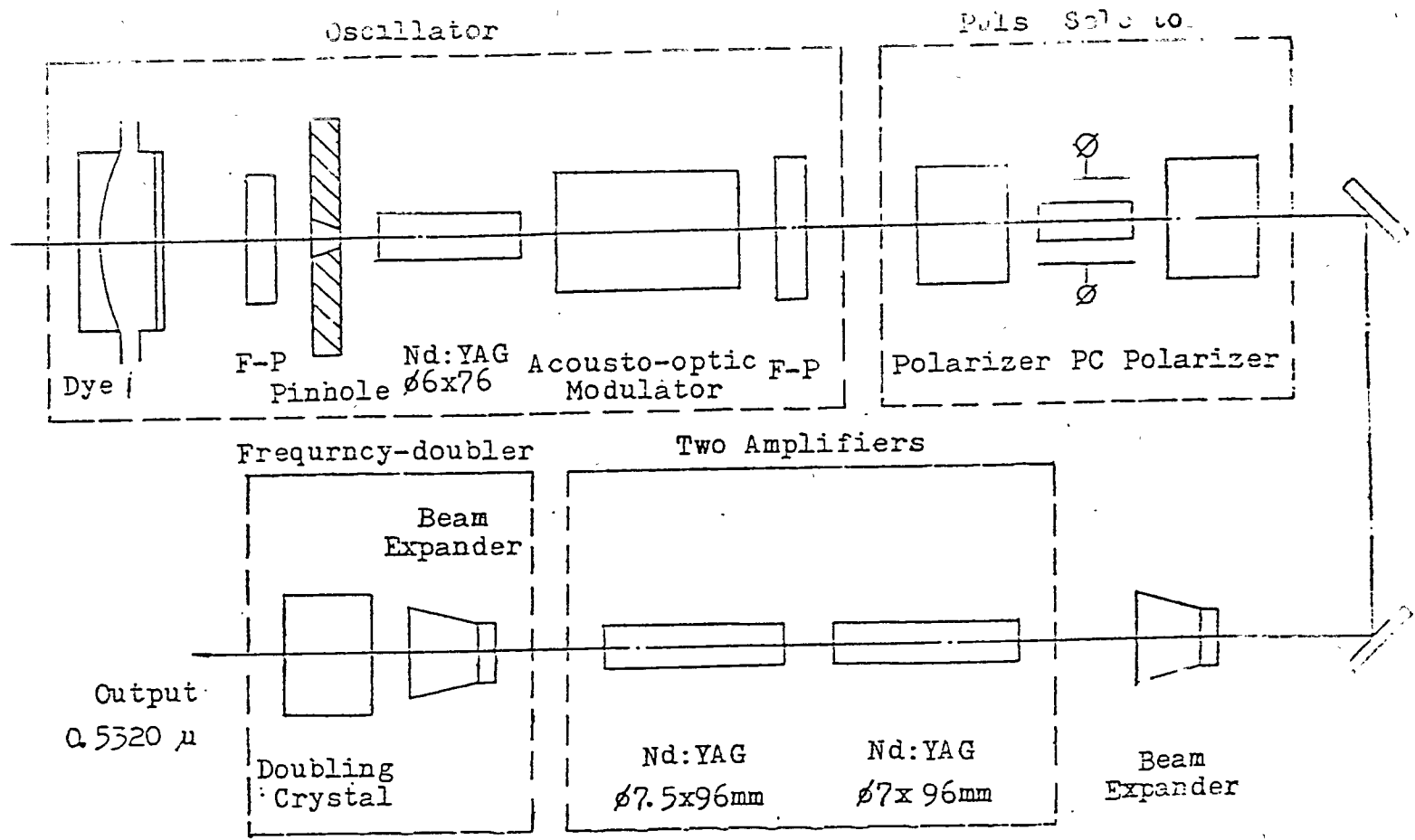


Fig.1 The Block Diagram of Nd:YAG Frequency-Doubled Mode-Locked Laser System

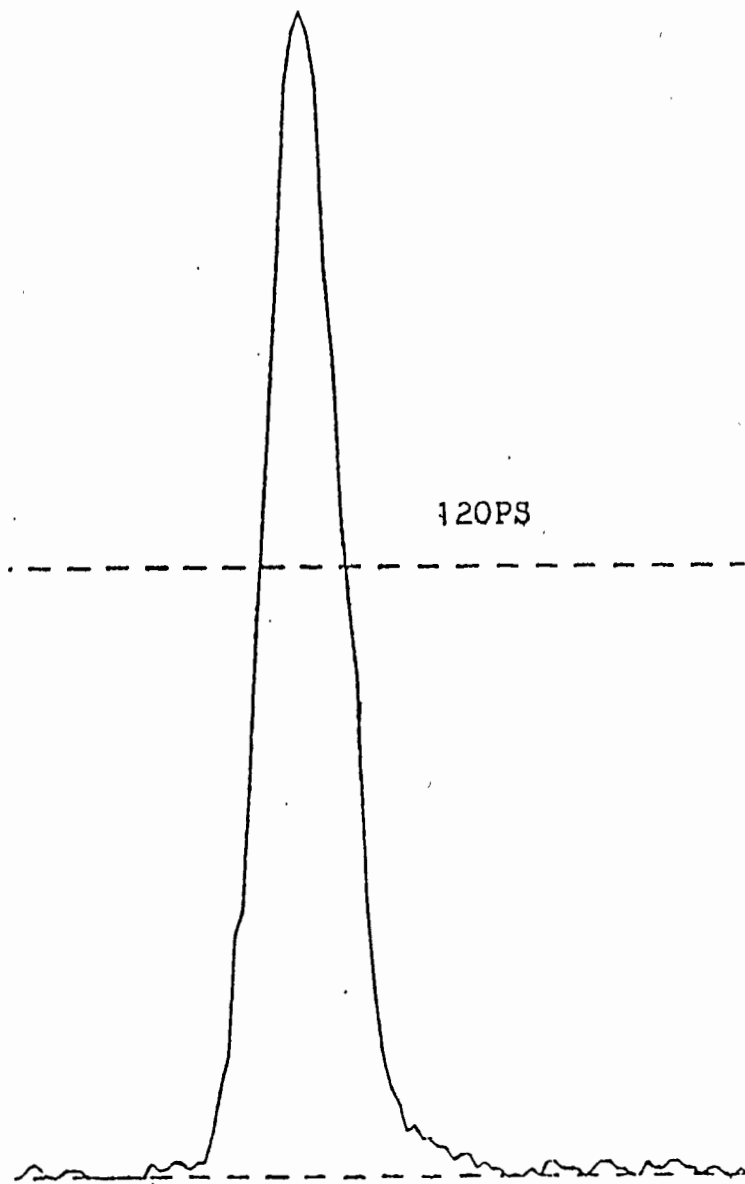


Fig.2 Pulse Width Measured with Streak Camera .

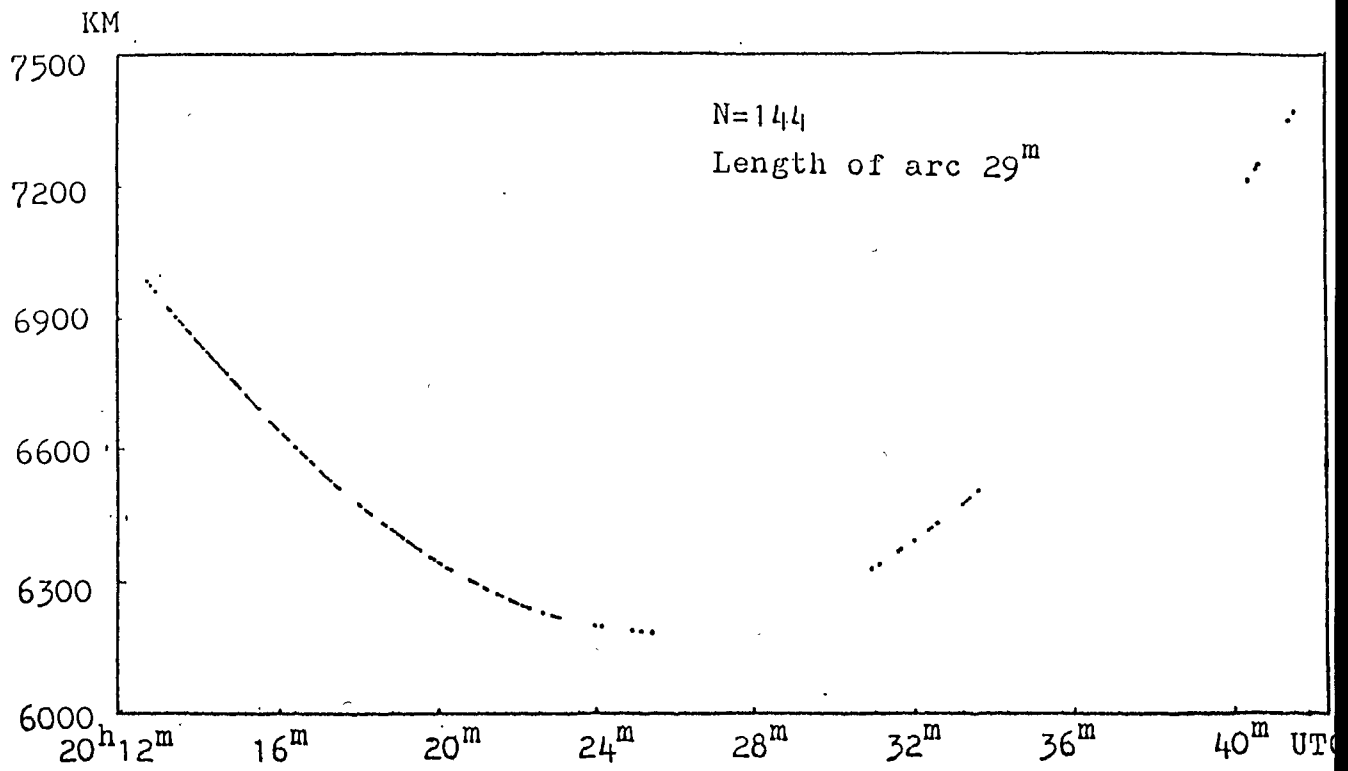


Fig.3 The Observing values for LAGEOS (Dec.16,1985)

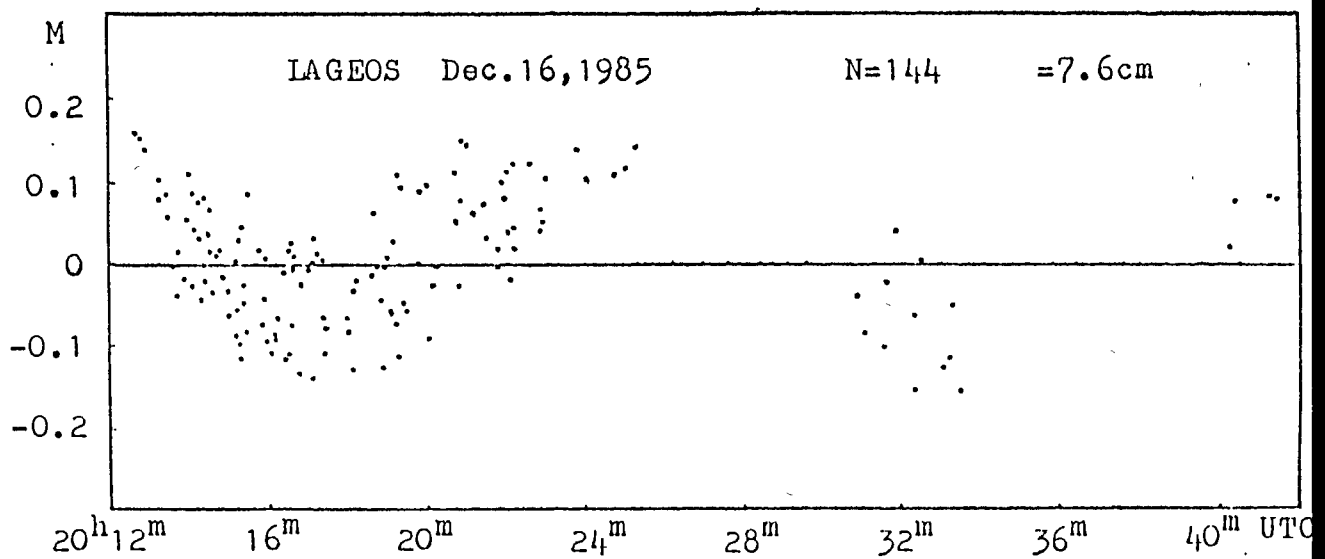


Fig.4 The residuals after polynomial fitting

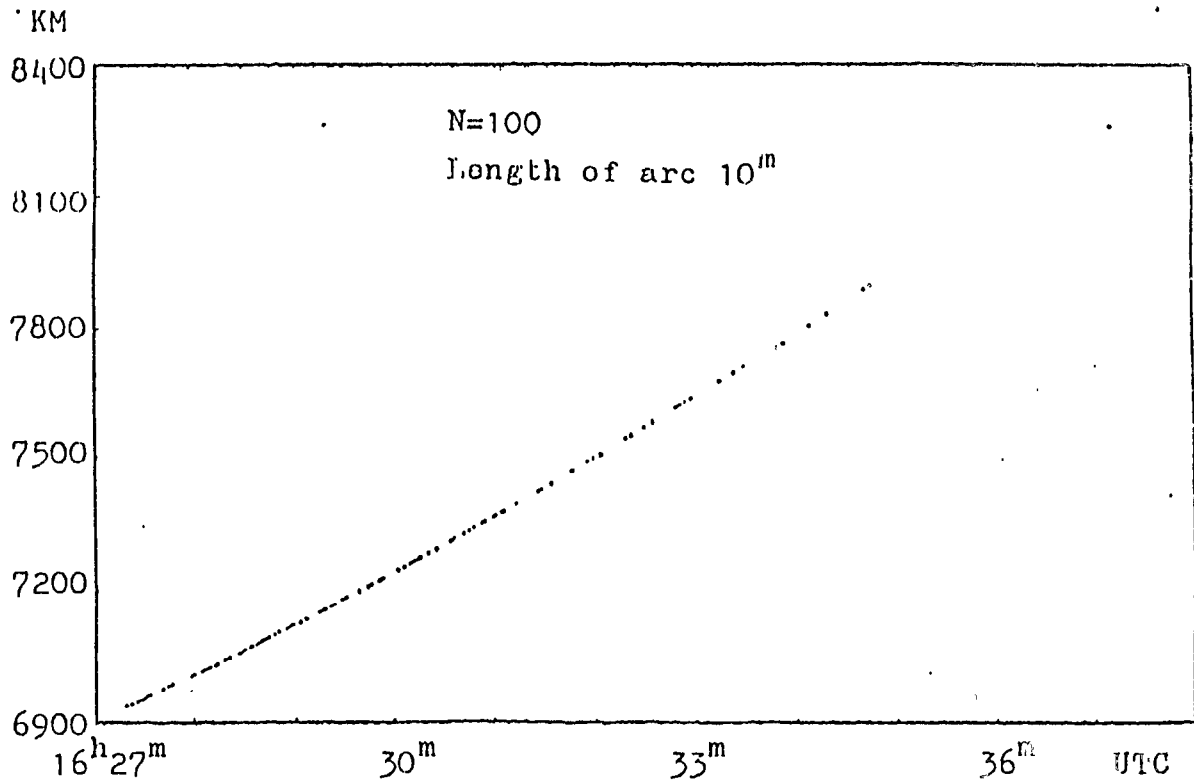


Fig.5 The Observing values for LAGEOS (Jan. 8, 1986)

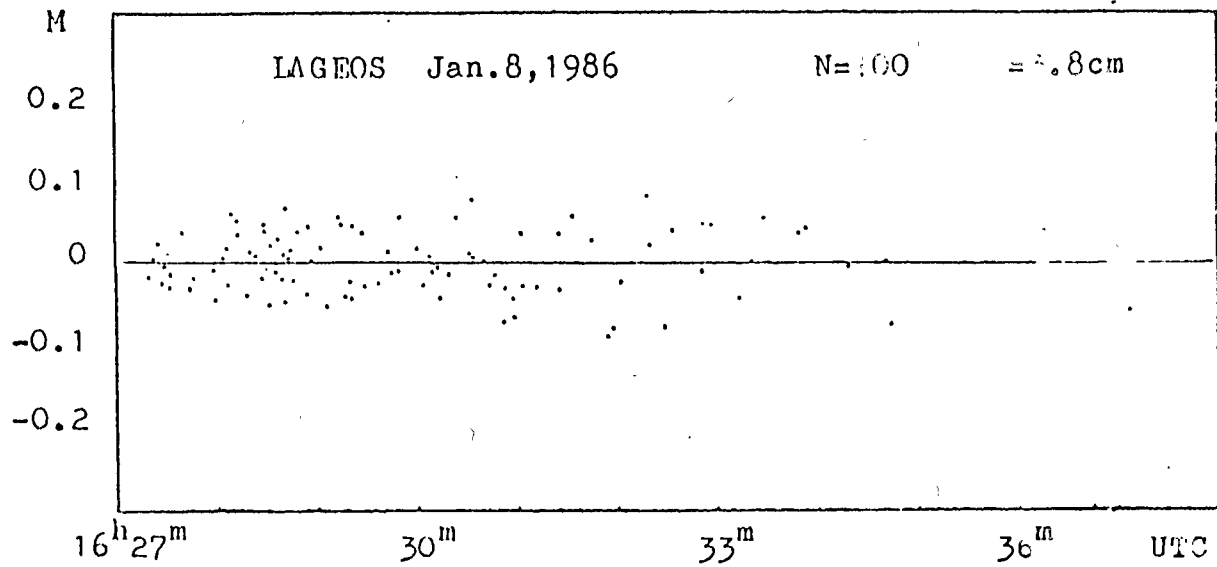


Fig.6 The residuals after polynomial fitting

Table 1 The Summary of Observation for IAGEOS with Mode-Locked Laser

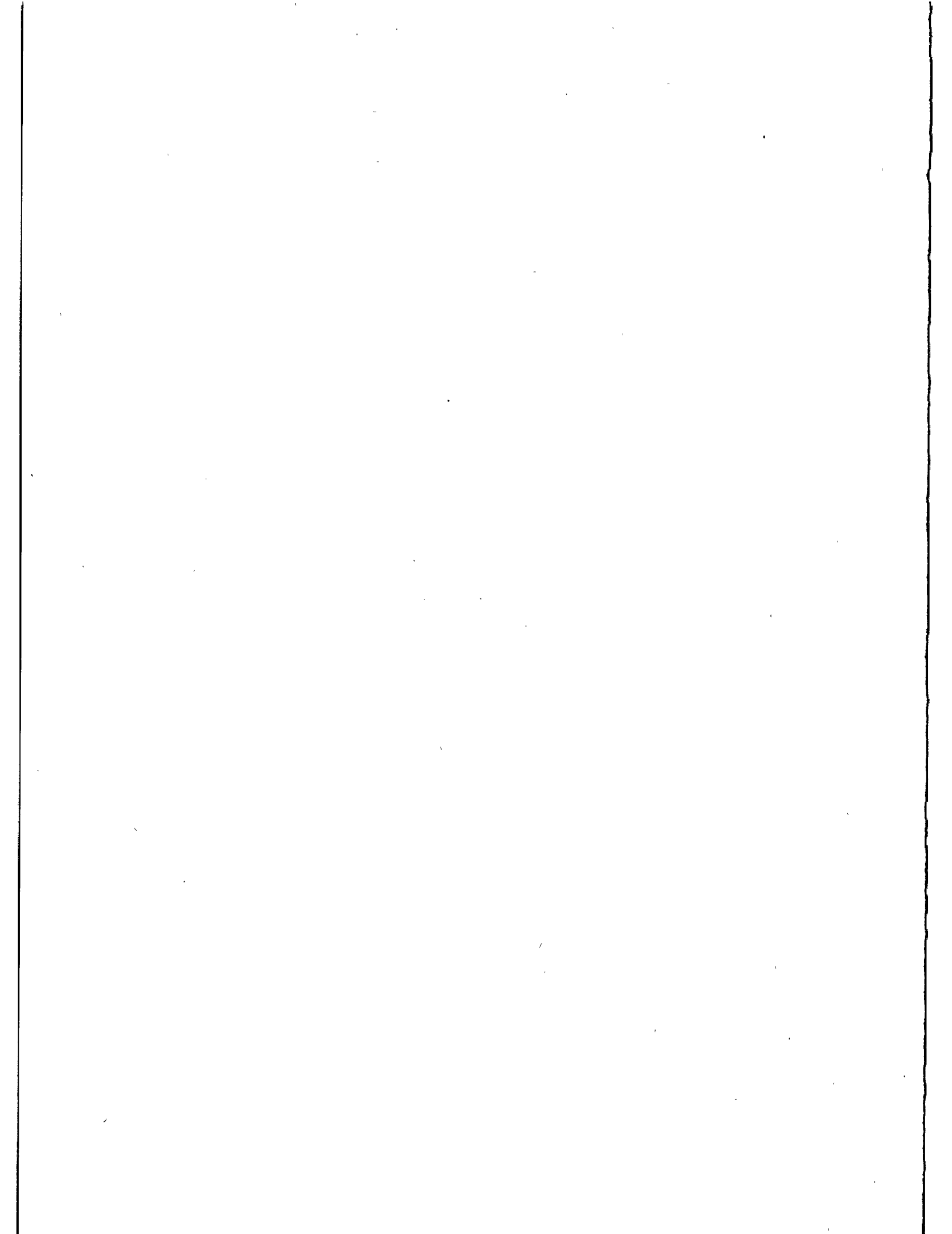
| Date | Time | Length of arc | Total Obs. | Accuracy (cm) |
|---------------|---|-----------------|------------|---------------|
| Dec. 12, 1985 | 18 ^h 48 ^m --18 ^h 59 ^m | 11 ^m | 182 | 6.3 |
| Dec. 16, 1985 | 20 ^h 12 ^m --20 ^h 41 ^m | 29 ^m | 144 | 7.6 |
| Jan. 5, 1986 | 17 ^h 43 ^m --17 ^h 56 ^m | 13 ^m | 133 | 6.1 |
| Jan. 8, 1986 | 17 ^h 21 ^m --17 ^h 37 ^m | 10 ^m | 131 | 6.9 |
| Jan. 9, 1986 | 19 ^h 16 ^m --19 ^h 23 ^m | 7 ^m | 16 | 5.0 |

Table 2 The Results of Analysis at GLTN and CSR

| Date | No. of the Obs. Sent | GLTN | | CSR | |
|---------------|----------------------|-----------|---------------|-----------|---------------|
| | | Good Obs. | Accuracy (cm) | Good Obs. | Accuracy (cm) |
| Dec. 12, 1985 | 80 | 61 | 7.2 | 75 | 6.4 |
| Dec. 16, 1985 | 50 | 49 | 4.9 | 49 | 5.9 |
| Jan. 5, 1986 | 100 | 97 | 4.5 | 97 | 4.4 |
| Jan. 8, 1986 | 100 | 100 | 3.5 | 100 | 3.8 |
| Jan. 9, 1986 | 15 | 14 | 6.0 | 14 | 5.2 |

Table 3 Calibrated Stability for Ground Target (Dec. 16, 1985)

| Transmitter Aperture(cm) | Receiver Aperture(mm) | No. of Measure | Value of Obs.(ns) |
|---------------------------|------------------------|----------------|-------------------|
| 1 x 4 | 2 | 51 | 4650.19 |
| 1 x 4 | 8 | 54 | 4650.15 |
| 1 x 4 | 2 | 97 | 4650.09 |
| 0.5 x 4 | 2 | 53 | 4649.97 |
| 1 x 4 | 2 | 69 | 4649.91 |
| 0.3 x 4 | 1 | 11 | 4650.16 |
| Average | | | 4650.08 ± 0.11 |



INTERKOSMOS LASER RADAR, VERSION MODE LOCKED TRAIN

K. Hamal, M. Cech, H. Jelinkova
A. Novotny, I. Prochazka
Czech Technical University
Faculty of Nuclear Science and Physical Eng.
Brehova 7, 115 19 Prague - Czechoslovakia -

Telephone 848840
TWX 121254 FJFI C

B.B. Baghos, M. Tawadros, Y. Helali
Helwan Institute of Astronomy and Geophysics
Academy of Scientific Research and Technology
Helwan, Cairo - Egypt -

TWX 93070 HIAG UN

ABSTRACT

The INTERKOSMOS 2.generation satellite laser station, built in 1980, located in Helwan, has been operating since 1982 in the mode locked train version. To improve the performance several upgradings have been made since 1984. To improve RMS, the new Start detector and HP5370B counter have been implemented. To improve the reliability the transmitter has been placed into the Coude. To study new detectors, the independent receiver chain No.2, consisting of Newtonian 32 cm telescope, detector and HP5360 counter has been implemented. This arrangement allows to apply different detectors including solid state silicon diode operating at room temperature on single/multi photon signal level.

INTERKOSMOS LASER RADAR, VERSION MODE-LOCKED TRAIN

K.Hamal, M.Čech, H.Jelínková, A.Novotný, I.Procházka
B.B.Baghos, M.Tawadros, Y.Helali

The INTERKOSMOS 2.generation laser radar, built in 1980 [1] located in Helwan, has been operating since 1982 in mode-locked train version [2]. To improve the performance several upgradings have been made since 1984.

To improve RMS, the new Start detector and HP5370B counter have been implemented. The Start Detector [3], using a transistor, contributed 50 psec to the RMS budget. The detector chain Nr.1 consists of PMT RCA31034A, two HP8447 amplifiers, ORTEC 473A discriminator and HP5370B counter.

To improve the reliability, the transmitter has been placed into Coude focus. A tremendous increase of the laser output stability was resulted. The laser transmitter itself was examined to identify the optical elements influencing the beam quality [4]. The saturable dye was tested under different conditions [5].

To study new detectors [6], the independent receiver chain Nr.2, consisting of the Newtonian 32cm telescope, detector and HP5360 counter has been implemented. This arrangement allows to apply different detectors (solid state diode [6]), while routine ranging has been provided using the original receiver chain Nr.1. To have a comparison, the MCP PMT Varian has been tested at the indoor calibration facilities [7].

To collect data from both chains, the computer software package has been modified. To simplify the calibration, ranging and data processing procedures, some other modifications have been implemented into the software package.

The calibration and system stability tests have been acomodated to the upgraded version [10].

The strong signal response from the photodiode was measured at the indoor calibration facilities [9].

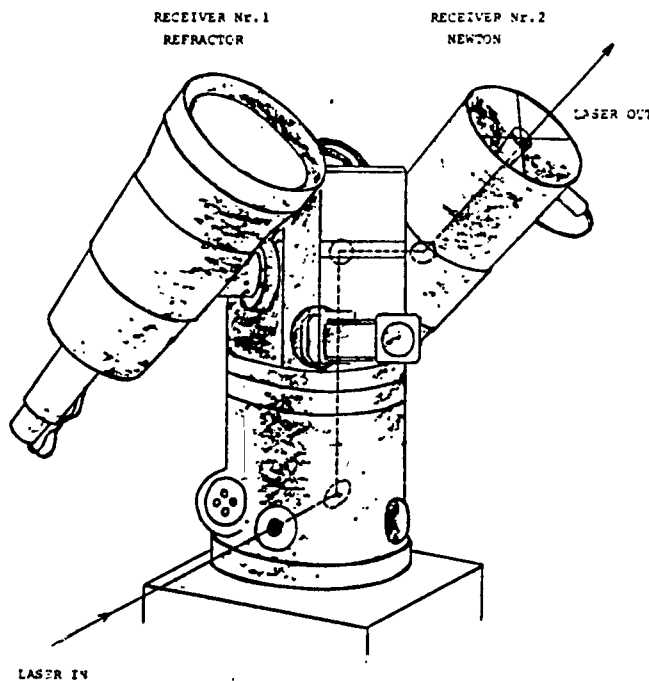
Summary.

| | before upgrading 1984 | after upgraging 1986 | | |
|-----------------------|--------------------------|-------------------------|---------|-------|
| | | PMT | MCP-PMT | diode |
| System stability (ps) | 150 | 110 | | 25 |
| System jitter (ps) | 520 | 300 | 100 | 100 |

Upgrading of the existing 2.generation laser station into 3.generation has been proposed [10].

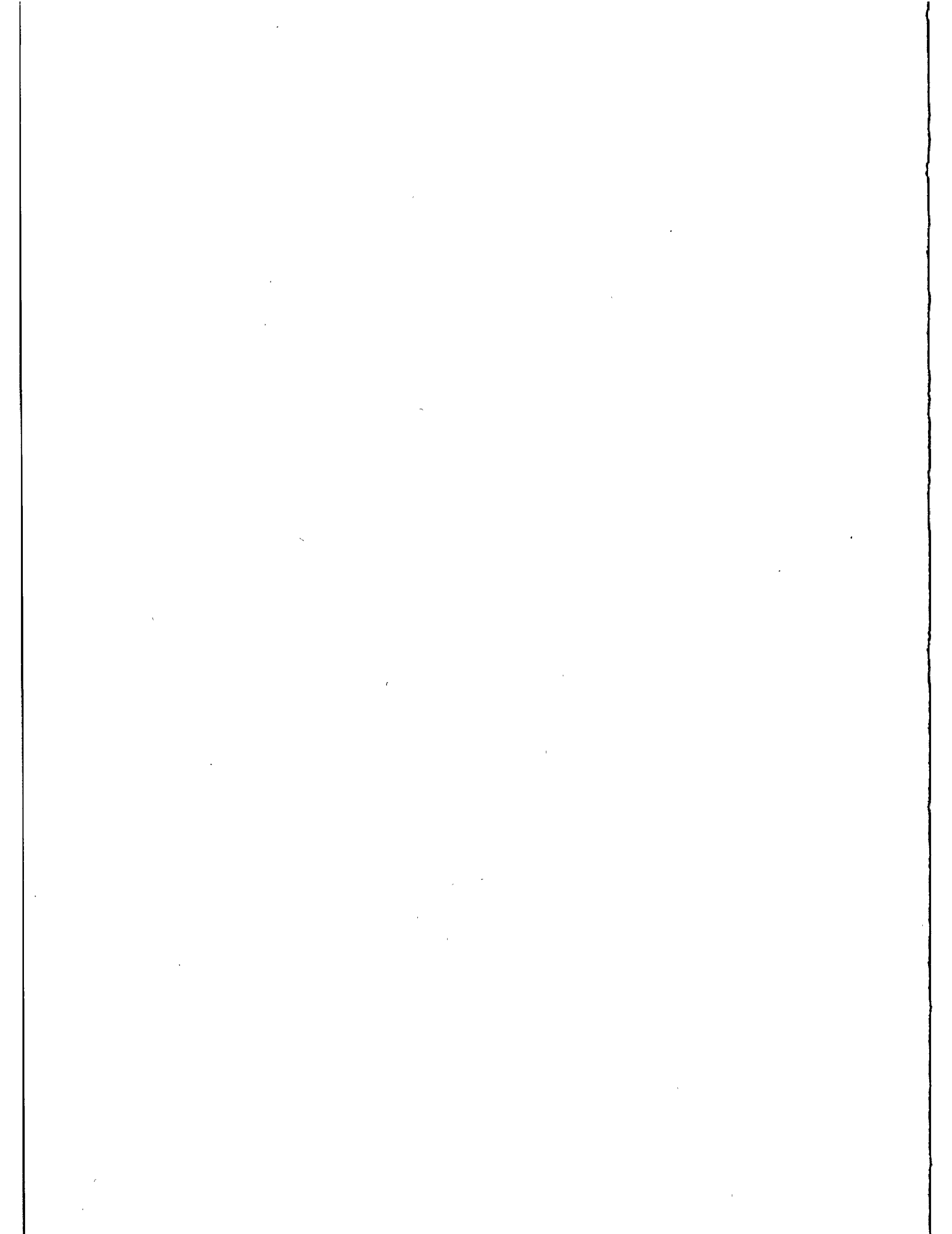
Abstracts:

- [1] K.Hamal, H.Jelinkova, A.Novotny, I.Prochazka, M.Cech
INTERKOSMOS SECOND GENERATION SATELLITE LASER RADAR
Proceedings of The Fourth International Workshop, Austin, 1983
- [2] K.Hamal, H.Jelinkova, A.Novotny, I.Prochazka
INTERKOSMOS LASER RADAR, VERSION MODE LOCKED TRAIN
Proceedings of The Fifth International Workshop, Greenwich, 1984
In this Proceedings:
- [3] I.Prochazka
START DETECTOR FOR MODE LOCKED TRAIN LASER RADAR
- [4] H.Jelinkova, J.del Pino, P.Valach
SPATIAL STRUCTURE OF THE DOUBLED ND:YAG LASER TRANSMITTER BEAM
- [5] K.Hamal, H.Jelinkova, STABLE SATURABLE DYE FOR 1.06UM
- [6] K.Hamal, H.Jelinkova, I.Prochazka, B.Sopko, SINGLE PHOTON
SOLID STATE DETECTOR FOR RANGING AT ROOM TEMPERATURE
- [7] I.Prochazka, K.Hamal, J.Caignebet, MICROCHANNEL/DYNODE PMT
COMPARISON EXPERIMENT
- [8] K.Hamal, I.Prochazka, SYSTEM STABILITY USING MODE LOCKED TRAIN
- [9] I.Prochazka, K.Hamal, H.Jelinkova, PICOSECOND LASER RANGING
USING PHOTODIODE
- [10] K.Hamal, I.Prochazka, 3.GENERATION/VERSION MODE LOCKED TRAIN



View of the mount. Refractor receiver Newton receiver.

| 2.Generation Mode Locked Train, Helwan 1986 | | | | |
|---|--|------|---------|-------|
| UPGRADINGS 1985 - 1986 | | | | |
| RMS | START DETECTOR <50ps COUNTER HP5370B | | | |
| LASER RELIABILITY | COUDE LASER SYSTEM BEAM STRUCTURE SATURABLE DYE | | | |
| EXPERIMENTAL RECEIVER No.2 | NEWTONIAN 32CM | | | |
| SOLID STATE DETECTOR | SINGLE MULTI PHOTON DETECTION | | | |
| SOFTWARE PACKAGE | MODIFICATION TO SIMPLIFY CALIBRATION RANGING, DATA PROCESSING PROCEDURE | | | |
| | 1984 | 1986 | | |
| | PMT | PMT | MCP PMT | DIODE |
| SYSTEM STABILITY ps | 150 | 110 | | 25 |
| SYSTEM JITTER ps | 528 | 308 | 100 | 100 |
| K. Hamal, M. Cech, H. Jelinkova, A. Novotny, I. Prochazka Interkosmos Laser Radar, Version Mode Locked Train | | | | 1 |



UPGRADES AND NEW DEVELOPMENTS
ON SATELLITE LASER RANGING
STATION FROM GRASSE

F. Pierron and the laser staff
Observatoire de Calern
Causols
06460 Saint Vallier de Thiey - France -

Telephone 93 42 62 70 - 93 36 58 49
Telex 470865 F

ABSTRACT

The Grasse Satellite Laser Station, operating since 1978, in a first step with a decimeter accuracy has successively been upgraded.

At first the ruby laser was replaced by an active mode locked Nd:YAG laser in 1984 and it puts the system at a centimeter level.

After that, in view to give to this station a total efficiency and autonomy the replacement of the computer was undertaken and this improvement should be ready before the end of 1986.

This paper describes the station today (hardware and software), its performances and its possibilities.

1.OVERVIEW OF THE SATELLITE LASER RANGING FROM GRASSE

=====

The Satellite Laser Ranging of GRASSE is, in fact, installed in the mountains just above Grasse where the astronomical Observatory of the CERGA has been built. (Annexe 1.)

The site is a plateau at a 1250 meter altitude at 20 Kilometers from Grasse and the weather is particularly favorable to Laser Ranging.

This S.L.R. Station developed in the Years 75-78 and entirely financed by the French Spatial Organisation (C.N.E.S.) obtained the first returns in 1978 and, since this time, in spite of some interruptions, it has provided to the Scientific community a lot of data of an increasing quality.

In order to minimize the interruptions of data, the modifications and upgrade have been carried out in stages.

In a first time the Ruby Laser System (3 Nanosecondes of PWHM) was replaced by an active Mode-locked ND:YAG in 1984 and in a second time (1985) the change of the computer and software was undertaken.

For this occasion, the software was totally refurbished in taking into account the new technology and the requirements for the data (great number of data, need of quick dispatching the results with the new link possibilities, ...)

This very important work is being terminated in a few weeks and so, the station will acquire all the possibilities of a modern station.

2.HARDWARE EQUIPMENTS

=====

Except the Mount,the Telescope and the computer,all the hardware equipments are installed in a shelter,where the operators stand during the ranging,close to the building.

The mount rests on a concrete pier at 3 meters from the ground and a floor independant from the mount allows to reach the equipment attached to the telescope.

2.1 MOUNT,TELESCOPE(Annexe 2)

The optical system consists of:

- The Telescope(Cassegrain)proper of a diameter of 1 meter and a focal length of 8 meters;it is especially dedicated receiving light from returns.

- The transmitting afocal optics made of lenses with a diameter of 20 Centimeters.

-A sighting Refracting Telescope to achieve some adjustments(particularly the alignment of the transmitting and receiving axes,the firing direction,and to observe the satellites when they are illuminated.

As the Telescope,the Mount was designed,drawn and built in FRANCE,it is an altazimuth system with an absolute accuracy of about 10 arcseconds.

The encoders(absolute)have a resolution of 1.2 arcseconds (20 bits).

The laser beam is going to the transmitting optic through a coude path with five coated mirrors.

2.2 ND:YAG LASER(Annexe 3)

This transmitter built by QUANTEL FRANCE currently provides a single 200 Picoseconde pulse at a repetition rate of 5 Hertz or 10 Hertz.

One of the distinctive features of this system is that it is possible to operate the oscillator either in passive (with dye) or in active(with pockel cells) mode;this active mode is generally used for an easier operating.

An active mode-locker(at 70 Megahertz)in the cavity increase the stability of the pulse train.

At the outgoing of the oscillator,the slicer(with avalanches transistors)selects one pulse and,after a double pass and the final amplifier,the single pulse energy is currently 100 Millijoules per shot in the green.

2.3 TIMING EQUIPMENTS.(Annexe 4)

The chronometry is achieved by a Thomson event-timer of for channels(1 start and 3 stop).The resolution of this equipment is of 100 Picosecondes.

The start time is triggerred by a photodiode on the Laser bench and through a TENNELEC discriminator.

The Photomultiplier tube(RTC 2233b)is going replaced in a few time by a Micro channel plate HAMAMATSU PMT in view to increase the RMS of the data and reduce systematic biases. A constant fraction discriminator TENNELEC is used for the stop channels.

With such a configuration,the RMS currently achieved is from 3 to 5 Centimeters on a satellite pass.

2.4 COMPUTER:

The Computer is a DIGITAL EQUIPMENT(DEC) PDP 11-73 with a memory size of one Mega-byte and an optional hardware to increase the speed of floating operations.

- Numerous specialized interfaces to control the Servo of mount, the encoders, the event-timer, electronic systems to elaborate the range gate,...

- * 3 parallel I/O 64 bits

- * 1 Real-time clock

- * 1 Digital/Analog converter

-A Track-ball (connected by an asynchronous link) in view:

- * To introduce corrections during the tracking

- * To process the data

Different mass storages are connected to this computer:

- Two removable disk systems of 10 Mega-bytes

- * One for the system.

- * One for the software developments.

- One Winchester disk of 160 Mega-bytes

- * Storage and editing the data.

One Magnetic Tape drive(one-half inch,1600 BPI)

* Disk backups

* Editing full rate data

* Different exchanges

This computer is connected(by the VAX in grasse) to the computing center of CNES in TOULOUSE.

3.SOFTWARE

=====

The computer is running under the Real-time Multitask, Multiusers RSX 11 M PLUS Operating System.

According to their functions,all the modules were written either in Assembly language(Driver modules,Process control, Interrupt services routine modules,...) or in Fortran 77 Language for all the scientific calculations and every time it was possible.

The programs are accessible to the operators through a system of Menu .

The different possibilities are:

-Computing the shedules of a given satellite.

-Tracking:

* Stars.

* Satellite(Ranging)

*Target(Calibration)

- Preprocessing Data
 - * Manual
 - * Automatic

- Editing
 - *Quick-Look
 - *Full rate Data

3.1 SCHEDULE COMPUTING(Annexe 5)

Once a Month the Operator computes the Schedule of LAGEOS, STARLETTE and AJISAI(Rise time, Set time ,Max Elevation) in view to establish work schedule for the crew.

These computations are achieved with the IRV for LAGEOS and Keplerian Elements for other satellites.

3.2 TRACKING(Annexe 6 et 7)

The capability to track the stars(direct and reverse) is needed to adjust the encoders and the parameters of the mount.

The tasks which control the tracking of a satellite are numerous.

-Preliminary computation of Site, Azimuth and range of the satellite every second of time.

In real time:

- Interpolating position(50 Hertz)
- * Servo control of the mount(activation every 20 Milliseconds by internal clock)
 - Reading Encoders
 - Reading Track-Ball for correction
 - elaborating speed orders for servo amplifier site and azimuth
- * Interpolating range and derived of range
- * Loading Range Gate(Activation by an interrupt on firing,5 Hertz)
- * Reading Start an Stop time on the event timer(Interrupt on the end of gate)
- * Computing of residuals for the exact firing time(With predicted range and his derived)for later processing and recording on a file.
- * Ploting on Graphic display residuals and informations for operator.
- * Reading operator commands.

3.3 TARGET CALIBRATION(Annexe 8)

After each pass,a calibration is achieved on a ground target erected at a distance of about 2.5 Kilometers.

Five hundred returns are recorded and processed.

The calibration is appended to the file of the preceding pass with the meteorological data.

3.4 PREPROCESSING DATA

The preprocessing of the data is entirely based on the residuals computed during the pass.

To avoid to spend a lot of time to read files and to give more flexibility to the software,all the data are loaded in the memory of the computer at the beginning with managment memory facilities.

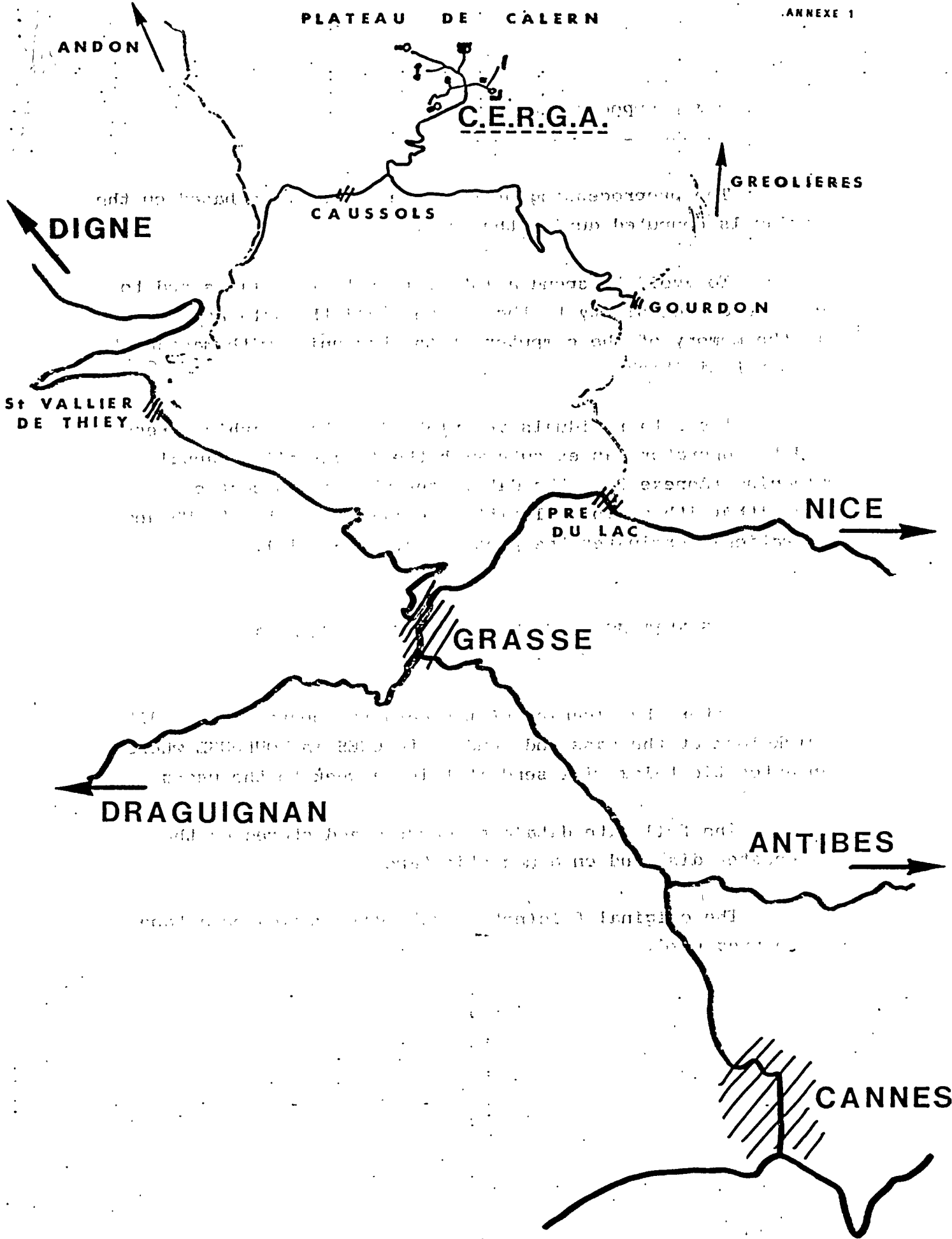
The data residuals are plotted on the graphic screen and the operator can execute with the Track-ball a manual cleaning (Annexe 9)of the data,after what an automatic algorithm(with polynomial fitting,elimination at 2.5 RMS and iteration) terminates the processing.(Annexe 10).

3.5 EDITING QUICK LOOK AND FULL RATE DATA:

After the cleaning of the data,the operator can edit quick-look of the pass and send it to CNES in TOULOUSE where an automatic telex will send it twice a week to the users.

The full rate data are computed and stored on the Winchester disk and on a magnetic tape.

The original file(not processed)is copied on a tape to be preserved.



ANDON

C.E.R.G.A.

GREOLIÈRES

DIGNE

CAUSSOLS

GOURDON

St VALLIER
DE THIEY

PRE
DU LAC

NICE

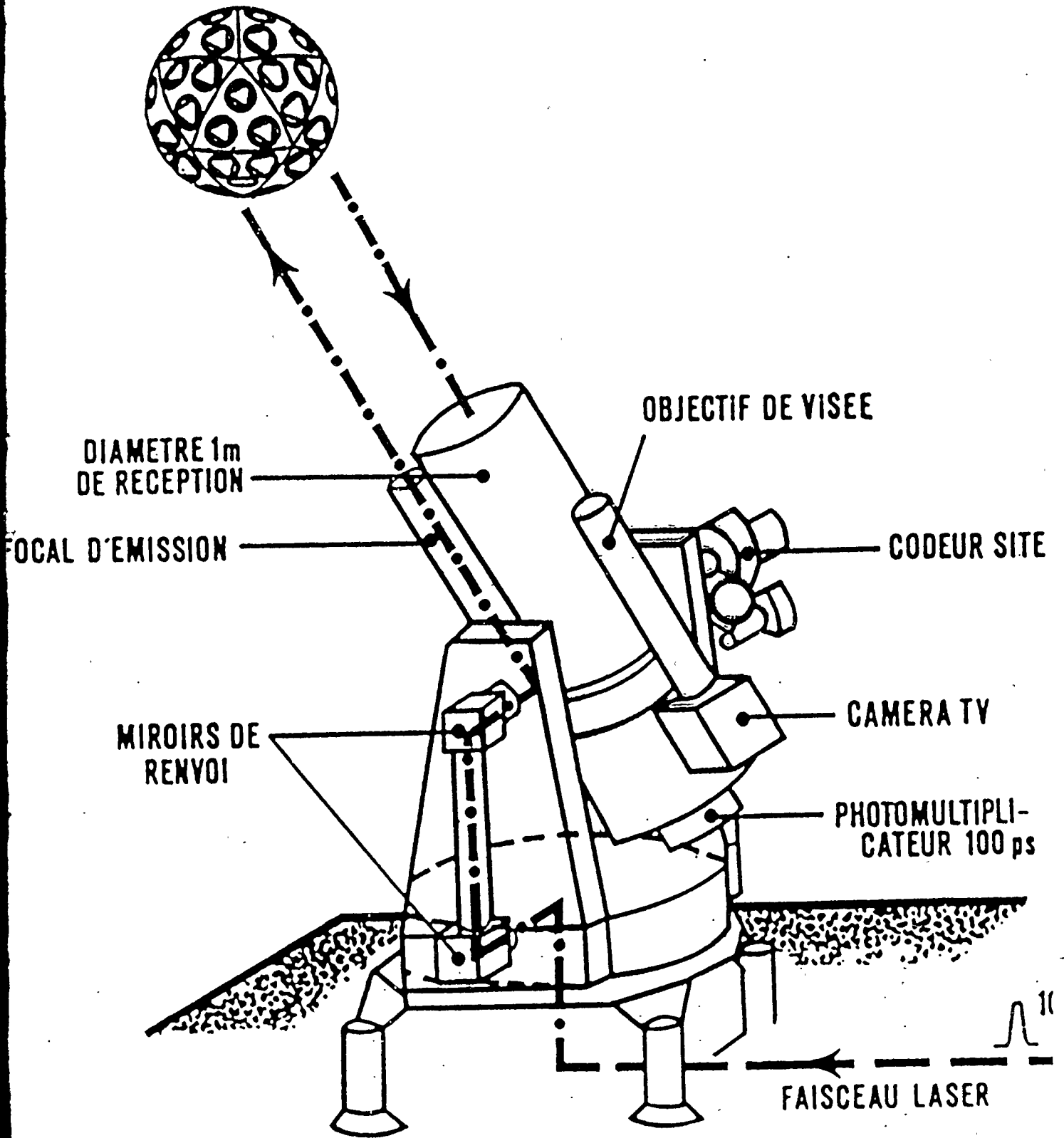
GRASSE

DRAGUIGNAN

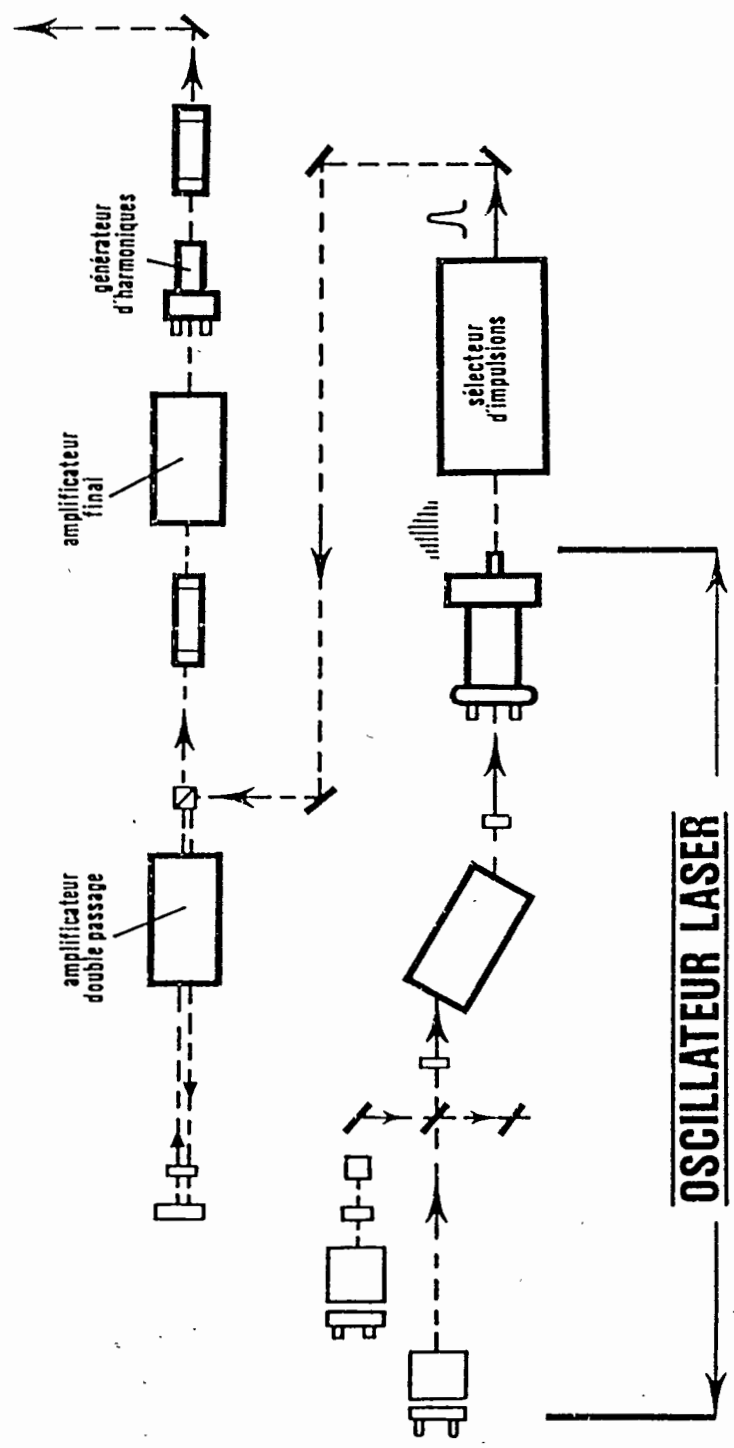
ANTIBES

CANNES

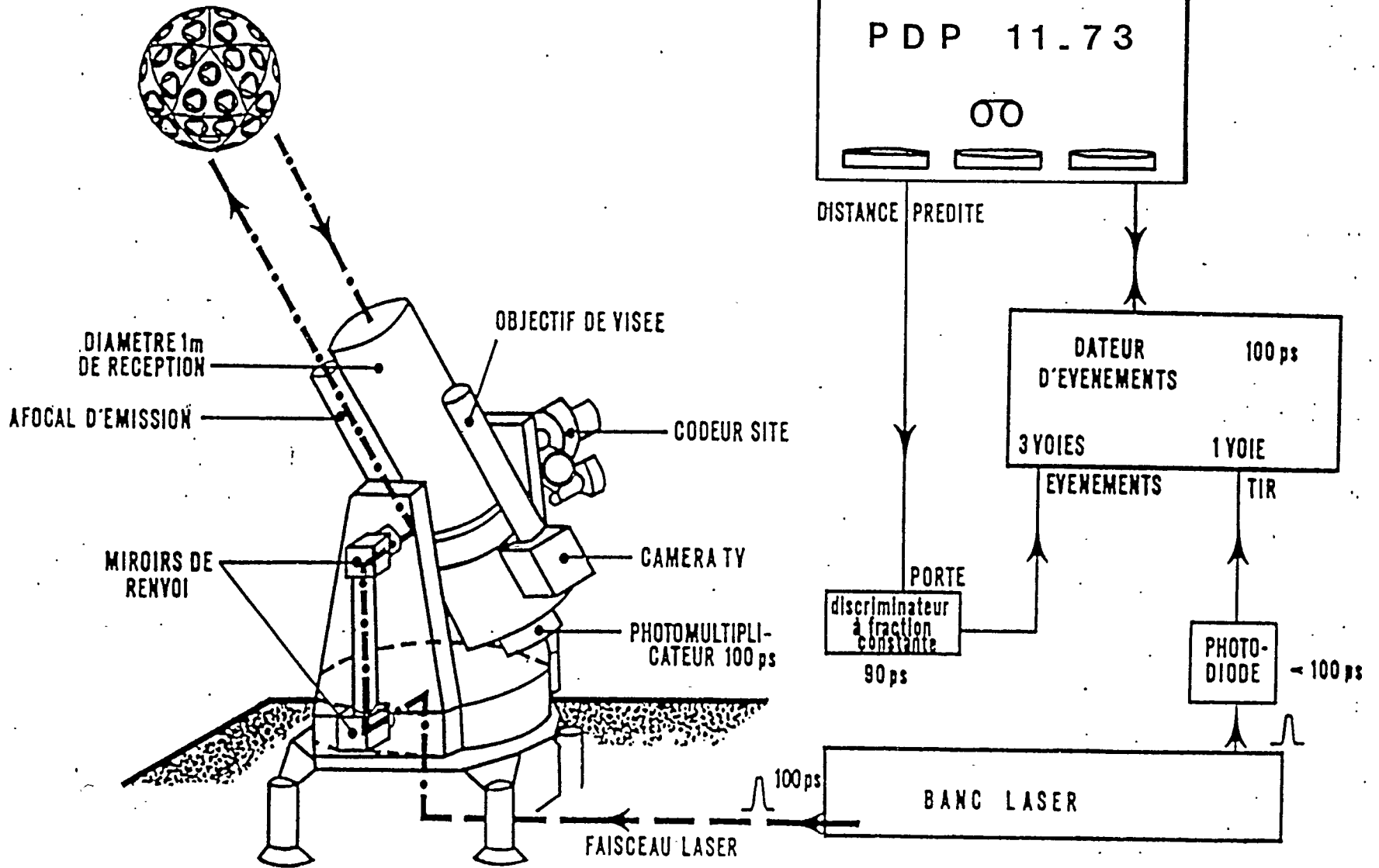
SATELLITE GEODESIQUE



LASER 406
100 ps



SATELLITE GEODESIQUE



ANNEXE DE LA BIBLIOTHEQUE

EGS DEBUT: MERCREDI 17 SEPTEMBRE 86

FIN: LUNDI 6 OCTOBRE 86

| | | | | | | | | | | |
|--------------------------|----------|----|---|-----|-----|-----|---|--------|--------|--------|
| MERCREDI 17 SEPTEMBRE 86 | 10H 40H | 21 | - | 164 | 116 | 77 | + | 390451 | 524031 | 643049 |
| MERCREDI 17 SEPTEMBRE 86 | 12H 14H | 68 | - | 223 | 106 | 62 | + | 218467 | 560735 | 689738 |
| MERCREDI 17 SEPTEMBRE 86 | 14H 20H | 65 | + | 264 | 15 | 69 | - | 100085 | 824278 | 688200 |
| MERCREDI 17 SEPTEMBRE 86 | 16H 04H | 62 | + | 290 | 40 | 93 | - | 23830 | 751231 | 597680 |
| MERCREDI 17 SEPTEMBRE 86 | 18H 94H | 74 | - | 296 | 175 | 131 | + | 5333 | 357961 | 487389 |
| MERCREDI 17 SEPTEMBRE 86 | 20H 114H | 25 | - | 284 | 223 | 183 | + | 41960 | 217866 | 336681 |
| JEUDI 18 SEPTEMBRE 86 | 9H 134H | 10 | - | 139 | 112 | 92 | + | 463852 | 542936 | 599109 |
| JEUDI 18 SEPTEMBRE 86 | 11H 84H | 52 | - | 207 | 119 | 64 | + | 264725 | 522064 | 681340 |
| JEUDI 18 SEPTEMBRE 86 | 13H 94H | 74 | + | 253 | 29 | 64 | - | 132543 | 783577 | 681815 |
| JEUDI 18 SEPTEMBRE 86 | 15H 124H | 59 | + | 284 | 37 | 83 | - | 39791 | 760764 | 626813 |
| JEUDI 18 SEPTEMBRE 86 | 17H 144H | 86 | + | 297 | 105 | 118 | - | 4402 | 563092 | 524984 |
| JEUDI 18 SEPTEMBRE 86 | 19H 174H | 37 | - | 288 | 220 | 153 | + | 28191 | 228312 | 392761 |
| VENREDI 19 SEPTEMBRE 86 | 10H 154H | 35 | - | 190 | 123 | 67 | + | 313778 | 509720 | 672569 |
| VENREDI 19 SEPTEMBRE 86 | 12H 154H | 83 | + | 240 | 59 | 62 | - | 169944 | 697595 | 687014 |
| VENREDI 19 SEPTEMBRE 86 | 14H 184H | 59 | + | 277 | 17 | 76 | - | 60790 | 819111 | 647626 |
| VENREDI 19 SEPTEMBRE 86 | 16H 204H | 73 | + | 295 | 63 | 106 | - | 9684 | 685685 | 559558 |
| VENREDI 19 SEPTEMBRE 86 | 18H 224H | 52 | - | 295 | 196 | 148 | + | 10216 | 298154 | 438019 |
| VENREDI 19 SEPTEMBRE 86 | 20H 274H | 13 | - | 266 | 232 | 212 | + | 94406 | 193534 | 250312 |
| SAHEDI 20 SEPTEMBRE 86 | 9H 234H | 2 | | | | | | | | |

LACCOC DEBUT: JEUDI 18 SEPTEMBRE 86

FIN: LUNDI 3 NOVEMBRE 86

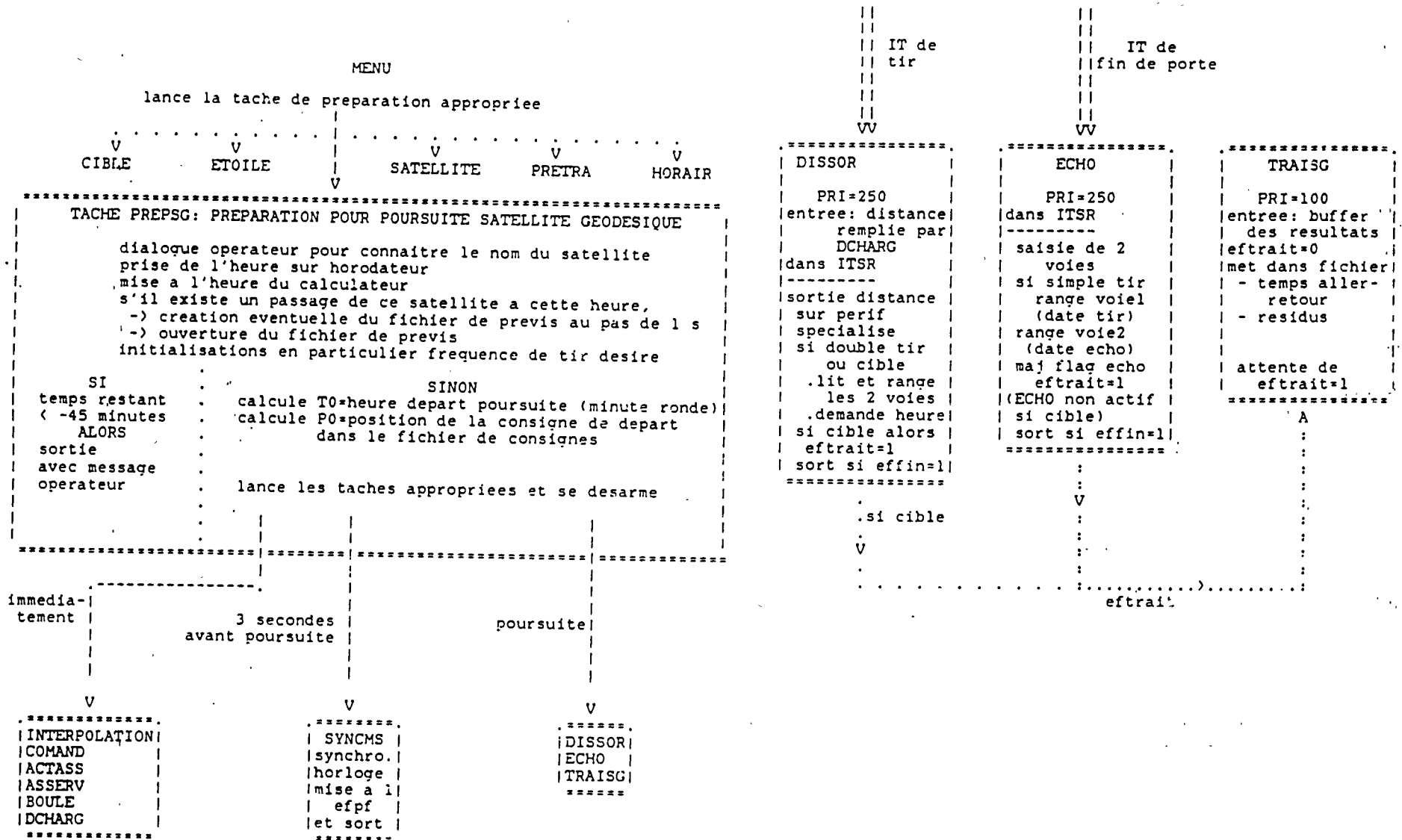
| | | | | | | | | | | |
|--------------------------|----------|----|---|-----|-----|-----|---|--------|---------|---------|
| JEUDI 18 SEPTEMBRE 86 | 4H 114H | 68 | + | 27 | 119 | 197 | - | 790217 | 521346 | 294565 |
| JEUDI 18 SEPTEMBRE 86 | 7H 344H | 51 | - | 35 | 327 | 263 | + | 766184 | 963706 | 102786 |
| JEUDI 18 SEPTEMBRE 86 | 10H 574H | 43 | - | 77 | 12 | 315 | + | 643355 | 834055 | 999516 |
| JEUDI 18 SEPTEMBRE 86 | 14H 204H | 83 | - | 142 | 329 | 333 | + | 454154 | 957670 | 948353 |
| JEUDI 18 SEPTEMBRE 86 | 18H 744H | 23 | + | 222 | 273 | 322 | - | 221659 | 73941 | 976419 |
| VENREDI 19 SEPTEMBRE 86 | 2H 384H | 42 | + | 29 | 104 | 170 | - | 784489 | 566399 | 322638 |
| VENREDI 19 SEPTEMBRE 86 | 6H 124H | 68 | - | 29 | 309 | 238 | + | 783501 | 1016040 | 174470 |
| VENREDI 19 SEPTEMBRE 86 | 9H 404H | 40 | - | 57 | 354 | 300 | + | 703682 | 886658 | 1044249 |
| VENREDI 19 SEPTEMBRE 86 | 13H 044H | 66 | - | 117 | 32 | 329 | + | 526756 | 775857 | 958746 |
| VENREDI 19 SEPTEMBRE 86 | 16H 344H | 45 | + | 186 | 260 | 332 | - | 327508 | 110665 | 950227 |
| SAHEDI 20 SEPTEMBRE 86 | 14 204H | 20 | + | 41 | 89 | 134 | - | 748108 | 608071 | 477919 |
| SAHEDI 20 SEPTEMBRE 86 | 4H 494H | 87 | + | 27 | 176 | 214 | - | 791088 | 356202 | 245577 |
| SAHEDI 20 SEPTEMBRE 86 | 8H 214H | 44 | - | 42 | 339 | 278 | + | 746615 | 930361 | 57418 |
| SAHEDI 20 SEPTEMBRE 86 | 11H 424H | 49 | - | 93 | 22 | 322 | + | 598605 | 805373 | 978554 |
| SAHEDI 20 SEPTEMBRE 86 | 15H 944H | 71 | + | 159 | 251 | 333 | - | 404351 | 136027 | 947105 |
| SAHEDI 20 SEPTEMBRE 86 | 19H 144H | 10 | + | 269 | 283 | 296 | - | 84491 | 45465 | 6575 |
| DIMANCHE 21 SEPTEMBRE 86 | 3H 264H | 59 | + | 27 | 116 | 188 | - | 790916 | 529219 | 319703 |
| DIMANCHE 21 SEPTEMBRE 86 | 7H 044H | 55 | - | 33 | 321 | 255 | + | 772935 | 982279 | 125335 |
| DIMANCHE 21 SEPTEMBRE 86 | 10H 254H | 41 | - | 70 | 7 | 310 | + | 665505 | 847815 | 1013104 |

STARLETTE DEBUT: MERCREDI 17 SEPTEMBRE 86

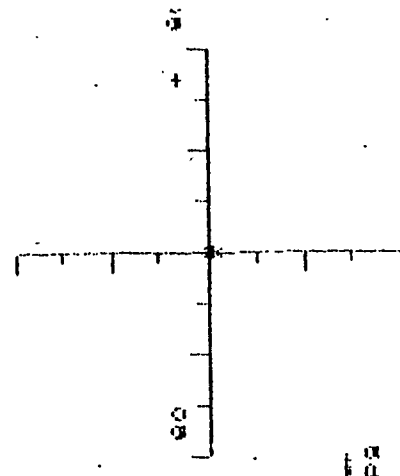
FIN: LUNDI 6 OCTOBRE 86

| | | | | | | | | | | |
|--------------------------|----------|----|---|-----|-----|-----|---|--------|--------|--------|
| MERCREDI 17 SEPTEMBRE 86 | 11H 344H | 16 | - | 160 | 114 | 96 | + | 401014 | 535892 | 618366 |
| MERCREDI 17 SEPTEMBRE 86 | 13H 204H | 68 | - | 226 | 98 | 63 | + | 209713 | 581577 | 683986 |
| MERCREDI 17 SEPTEMBRE 86 | 15H 944H | 54 | + | 270 | 32 | 65 | - | 82235 | 774941 | 678679 |
| MERCREDI 17 SEPTEMBRE 86 | 16H 594H | 52 | + | 294 | 51 | 89 | - | 10776 | 721191 | 612214 |
| MERCREDI 17 SEPTEMBRE 86 | 18H 404H | 82 | - | 296 | 139 | 123 | + | 5598 | 462472 | 589379 |
| MERCREDI 17 SEPTEMBRE 86 | 20H 384H | 27 | - | 278 | 212 | 171 | + | 59090 | 251288 | 370234 |
| JEUDI 18 SEPTEMBRE 86 | 11H 524H | 29 | - | 186 | 115 | 71 | + | 326746 | 533815 | 661335 |
| JEUDI 18 SEPTEMBRE 86 | 13H 394H | 77 | + | 244 | 54 | 62 | - | 158230 | 709720 | 687697 |
| JEUDI 18 SEPTEMBRE 86 | 15H 294H | 49 | + | 282 | 17 | 71 | - | 47553 | 819227 | 661568 |
| JEUDI 18 SEPTEMBRE 86 | 17H 184H | 61 | + | 296 | 49 | 99 | - | 5859 | 726373 | 578706 |
| JEUDI 18 SEPTEMBRE 86 | 19H 844H | 57 | - | 292 | 173 | 139 | + | 19092 | 365101 | 464923 |
| JEUDI 18 SEPTEMBRE 86 | 20H 584H | 16 | - | 268 | 222 | 191 | + | 87692 | 221607 | 312149 |
| VENREDI 19 SEPTEMBRE 86 | 12H 104H | 47 | - | 211 | 114 | 65 | + | 253079 | 536890 | 678437 |
| VENREDI 19 SEPTEMBRE 86 | 13H 544H | 64 | + | 260 | 20 | 63 | - | 111358 | 810820 | 684010 |
| VENREDI 19 SEPTEMBRE 86 | 15H 494H | 49 | + | 291 | 30 | 79 | - | 20417 | 782230 | 637767 |
| VENREDI 19 SEPTEMBRE 86 | 17H 384H | 78 | + | 298 | 91 | 112 | - | 1541 | 603698 | 543222 |
| VENREDI 19 SEPTEMBRE 86 | 19H 274H | 38 | - | 287 | 201 | 155 | + | 31353 | 282928 | 417681 |
| SAHEDI 20 SEPTEMBRE 86 | 10H 434H | 18 | - | 166 | 118 | 80 | + | 384576 | 524935 | 634538 |

synchronisation. priorite. description generale



CORRECTIONS (G,S)



RESIDUS

TEMPS

(0 , 0)

DECALAGE FENETRE = 0
 DECALAGE TRAJECT = 0
 NOMBRE ECHOS = 4681

70m

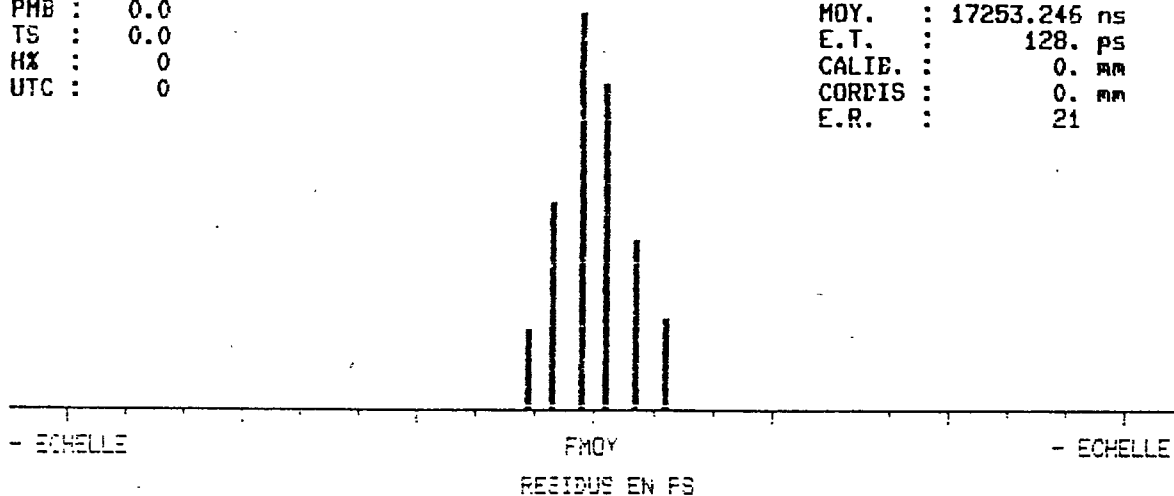
70m

STATION LASER-SATELLITES DU C.E.R.G.A.

L86082004.46D

PMB : 0.0
 TS : 0.0
 HX : 0
 UTC : 0

MOY. : 17253.246 ns
 E.T. : 128. ps
 CALIB. : 0. mm
 CORDIS : 0. mm
 E.R. : 21



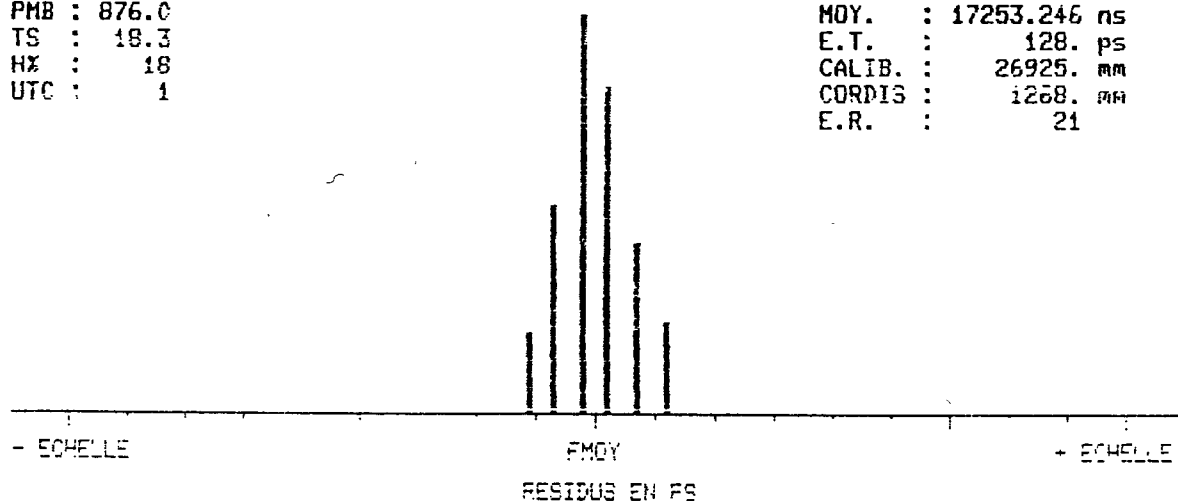
echelle : 2.000 ns largeur des canaux : 22. ps
 coord. du maximum : X= -44 ps Y= 150 pts

STATION LASER-SATELLITES DU C.E.R.G.A.

L86082004.46D

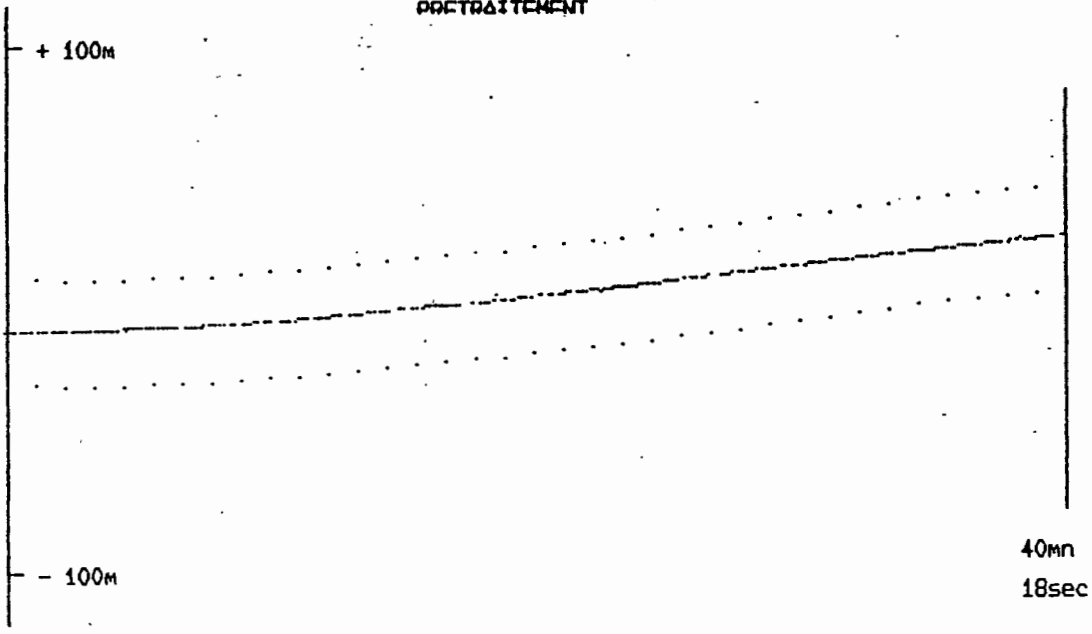
PMB : 876.0
 TS : 18.3
 HX : 18
 UTC : 1

MOY. : 17253.246 ns
 E.T. : 128. ps
 CALIB. : 26925. mm
 CORDIS : 1268. mm
 E.R. : 21



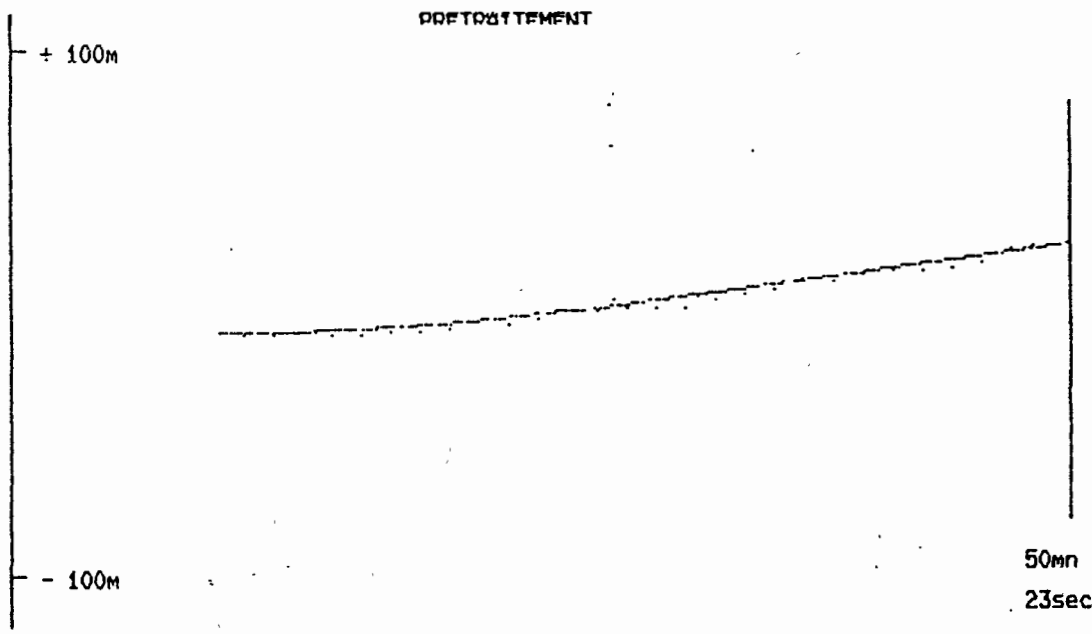
echelle : 2.000 ns largeur des canaux : 22. ps
 coord. du maximum : X= -44 ps Y= 150 pts

PROFONDITAMENT



40mn
18sec

PROFONDITAMENT

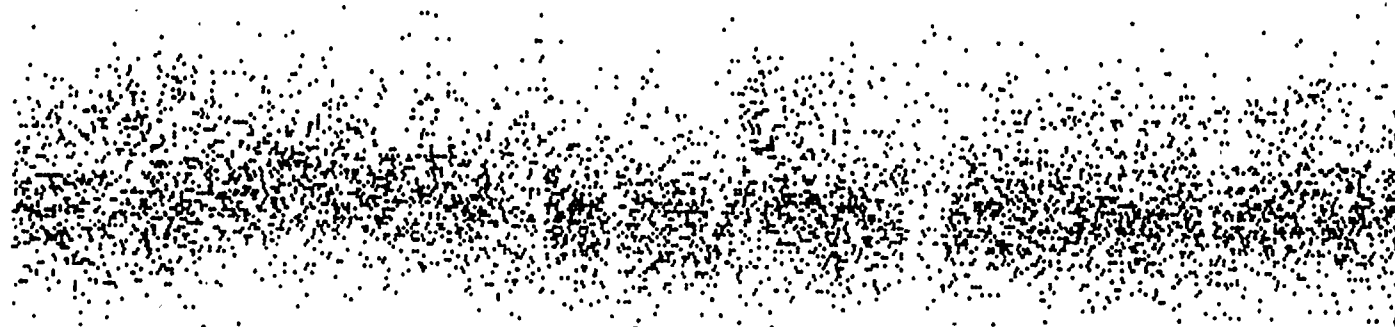


50mn
23sec

PRETRAITEMENT

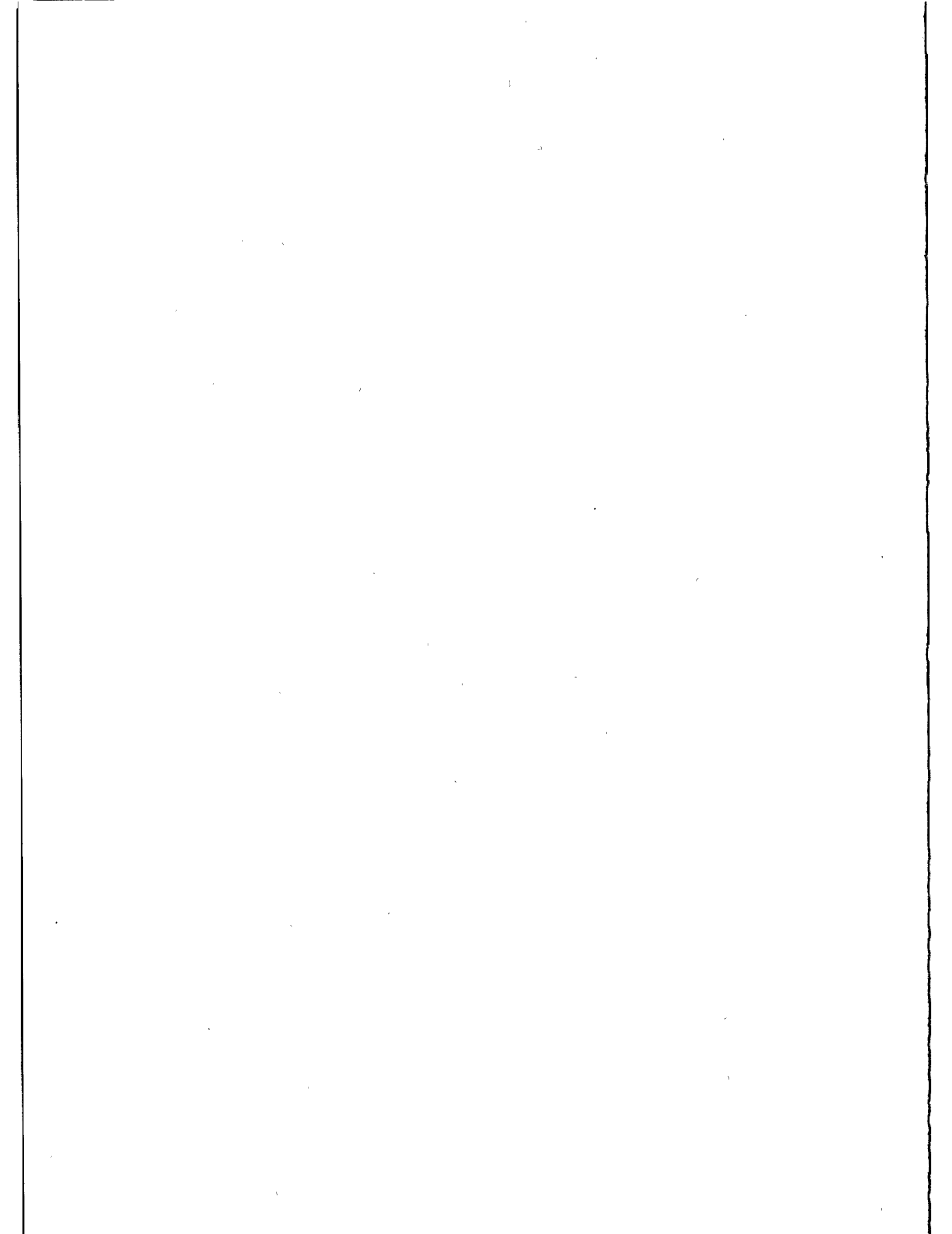
+ 15cm

- 15cm



40mn

18sec



THE SBG LASER RADAR STATIONS POTSDAM AND SANTIAGO DE CUBA
STATUS AND PERFORMANCE REPORT

L. Grunwaldt, H. Fischer, R. Neubert
Academy of Sciences of G.D.R.
Central Institute for Physics of the Earth
Potsdam 1500, G.D.R.

Telephone
Telex 15305

J. Del Pino
Cuban Academy of Sciences
Institute for Geophysics and Astronomy
Havana, Cuba

ABSTRACT

The systems are based on a modified 4-axis satellite tracking camera (SBG). Their basic concepts and technical performance are typical for 2nd generation devices. Blind tracking of LAGEOS using narrow beams is possible with the help of a star calibration method. The systems are operated with 2nd generation performance since 1981 and 1985, respectively. The Potsdam station is contributing continuously to the MERIT project since 1980. LAGEOS tracking at Santiago station started in December 1985.

1. Station 1181 Potsdam

The SBG telescope was developed in the early sixties as a photographic tracking camera and was operated at Central Institute for Physics of the Earth (ZIPE) since 1966. In its basic construction, it was a Maksutov-Schmidt system (effective diameter of receiver optics 32 cm) on a 4-axis mount with axes no. 1 and 2 fixed and axes 3 (along track) and 4 (cross track) moved during operation. Along track movement was controlled by punch tape with an accuracy sufficient for photographic tracking of GEOS type satellites (SBG mount see Fig.1).

The main modifications to allow laser tracking with the SBG was to mount an additional hinged Cassegrain mirror in front of the photographic unit and to drill a central hole through the main mirror. In this way the receiver optics and related electronics could be placed behind this mirror. A two-stage passively Q-switched ruby laser was mounted on the main tube and moved together with the telescope. By inserting and replacing the Cassegrain mirror, alternating photographic and laser observations became possible. This 1st generation system (laser pulsewidth 20 ns, visual tracking only) was operated successfully since 1974. First LAGEOS returns were obtained in September 1977.

Especially through the years 1979-81, the system was upgraded to a 2nd generation device (possibility of automatic observations, ranging errors of a few decimeters for all existing laser satellites). The main hardware modifications were:

- Equipment of the 3rd and 4th axis with step motor drives and digital encoders for precise positioning, 2nd axis with a theodolite for accurate control of inclination.
- On-line computer control of the mount and related electronics (digital range gate, laser firing etc.). For this purpose, an IEC 625 type interface with a desktop computer (8 - 24 kByte operational memory) as a controller is used.
- Replacement of the former laser transmitter (20 ns) by a 5 ns ruby laser [1].

There are some limitations in further upgrading the system: because of the optical-mechanical layout of the SBG mount there is no possibility to install a Coudé focus. So both laser and receiver have to be moved together with the mount being unfavourable especially for more sophisticated lasers with shorter pulsewidth. Additionally, the mount errors for a 4-axis mount are not so easy to handle and can be controlled exactly only by star calibrations limiting this method to night and twilight observations.

A program system for satellite position prediction, on-line mount control, data reduction and orbital elements improvement from own measurements was developed [2]. Additionally, from star observations an error model for the 4-axis mount can be derived leading to an absolute pointing accuracy of about

+/- 30" which is sufficient for most tracking purposes with wider diffraction angles of the laser. Totally blind tracking of LAGEOS using narrow beams (20 - 30") can be attained by observing the positions of some stars along the track of the satellite and finding the true setting angles of the mount by matching the observed and the catalogue positions of the stars via the computer. In this way the pointing accuracy can be improved to about +/- 10" which is strongly enhancing the reliability of LAGEOS tracking, especially using the long-term predictions of the LAGEOS position edited by the University of Texas [3] to produce osculating elements for the given pass.

The station 1181 Potsdam is contributing continuously to the MERIT project since the short campaign 1980.

2. Station 1953 Santiago de Cuba

To improve the INTERKOSMOS station distribution of highly automated stations and according to the good experience with the Potsdam equipment, a second SBG mount was upgraded according to the main construction principles described above. Some slight modifications as enhancement of the laser output energy and simplification of receiver optics were done. The station was equipped in cooperation between G.D.R., U.S.S.R. and Cuba. After the installation in summer/autumn 1985, first performance tests were carried out during Dec.1985/Jan.1986 proving that the main performance data are similar to the Potsdam device. In Fig.2 and 3 typical range-noise histograms on a pass-by-pass basis for both stations are shown. For the Santiago station it was gained from the performance test period, for the Potsdam station it is derived from the whole MERIT main campaign. A comparison of some technical data between both stations can be found in Table 1.

Table 1: Technical data of SBG stations 1181 and 1953

| Location | Potsdam, G.D.R. | Santiago de Cuba |
|--------------------|------------------------------|-------------------------|
| Station number | 1181 | 1953 |
| Laser type | Ruby, TEM ₀₀ | Ruby, TEM ₀₀ |
| Pulsewidth/ns | 5 | 5 |
| Max. output/mJ | 200 | 800 |
| Min. divergency/" | 20 | 20 |
| Q-switch | Dye cell | Dye cell |
| Receiver type | RCA C 31034A | FEU 79 |
| Quantum eff./% *) | 10 | 3-5 |
| Bus controller | HP 9825 S | EMG 666 B |
| Oper. memory/kByte | 24 | 8 |
| Time base | ZIPE time service (Cs-clock) | LORAN-C |
| First operation | March 1974 **) | December 1985 |

Remarks: *) $\lambda = 694 \text{ nm}$
**) First generation system

REFERENCES

- [1] Grunwaldt, L. et al.:
First Satellite Ranging Results Using a Dual-Pulse Ruby Laser
Proc. 4th Intern. Workshop on Laser Ranging Instr., vol II
Edt. by P. Wilson, Bonn (1982), p. 484-87
- [2] Neubert, R.:
HP 9825-based Software System for Laser Radar
Proc. 4th Intern. Workshop on Laser Ranging Instr. (Software Session), Edt. by P. Shelus
The Univ. of Texas Publ. in Astron. 19 (1982), p.77-88
- [3] Schutz, B.E. et al.:
LAGEOS Ephemeris Predictions
Proc. 4th Intern. Workshop on Laser Ranging Instr., vol. I
Edt. by P. Wilson, Bonn (1982), p. 145-71

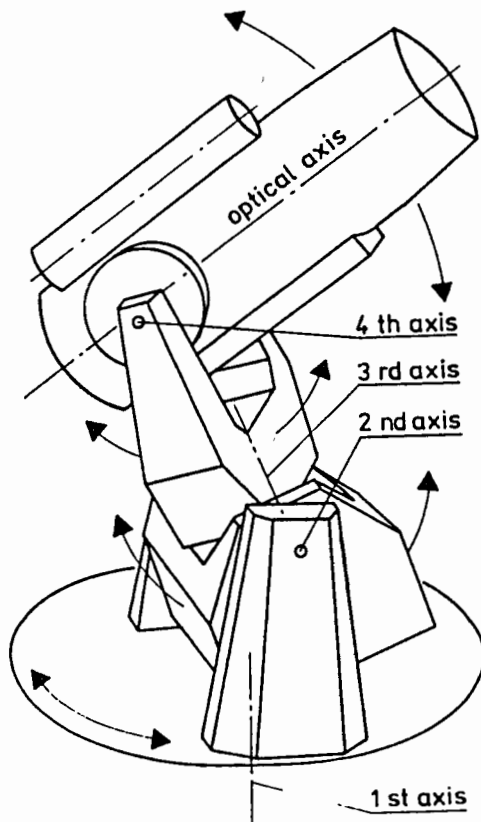


Fig. 1
Schematic drawing of the SBG - mount

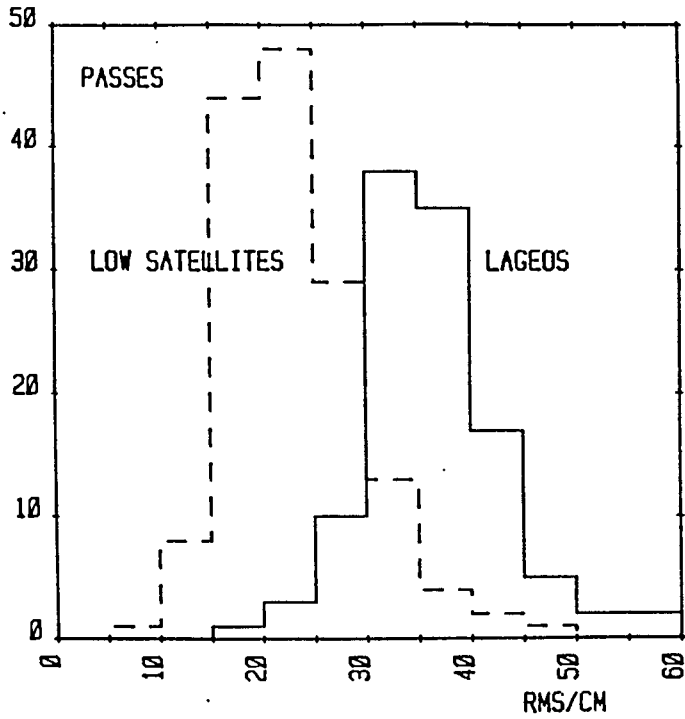


Fig. 2: Pass-by-pass range noise histogram for station 1181 Potsdam, data from the MERIT main campaign

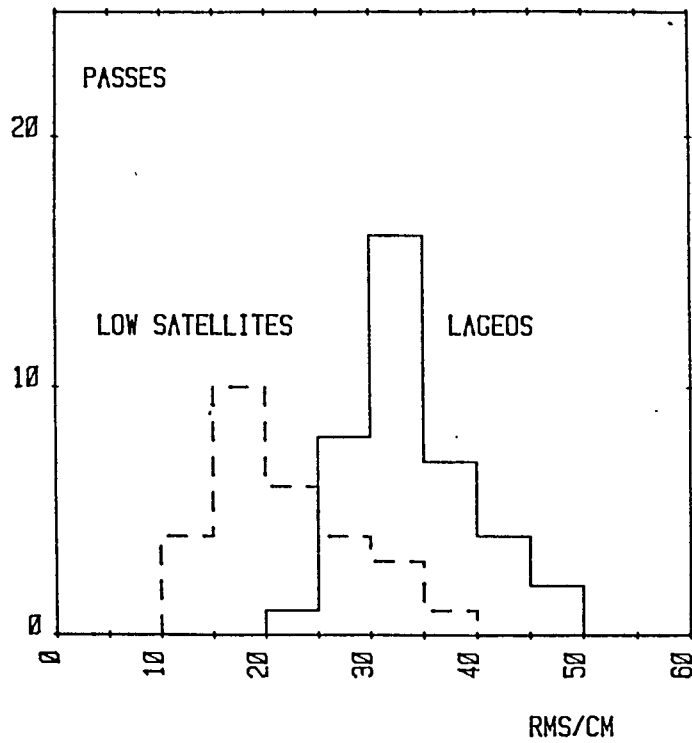
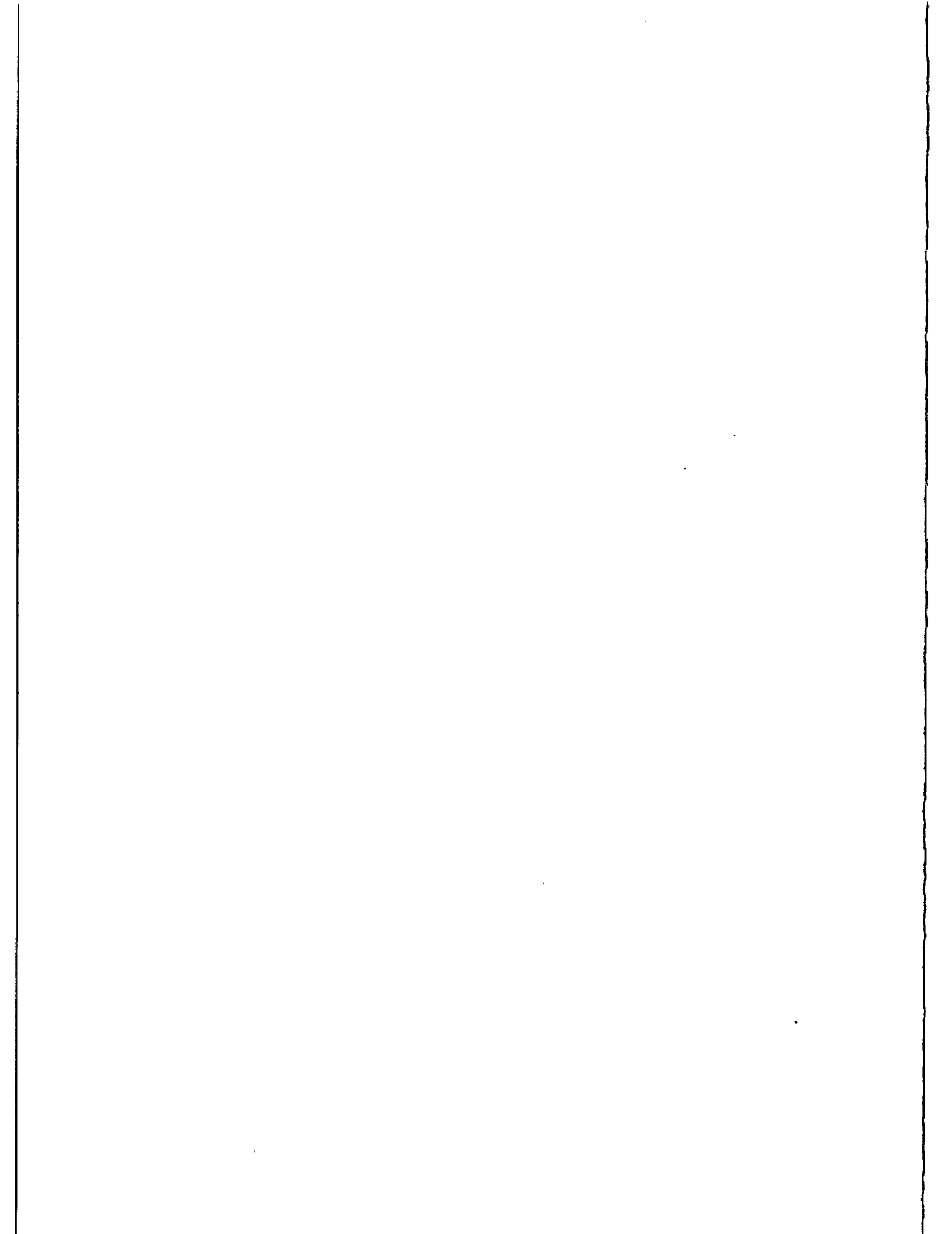


Fig. 3: Pass-by-pass range noise histogram for station 1953 Santiago de Cuba, data from performance test period December 1985 - January 1986



AMBIGUITY AND RESOLUTION OF A MODE-LOCKED
PULSE TRAIN LASER RADAR

R. Neubert, B. Ritschel, L. Grunwaldt
Academy of Sciences of G.D.R
Central Institute for Physics of the Earth
Telegrafenberg A 17, Potsdam 1500, G.D.R.

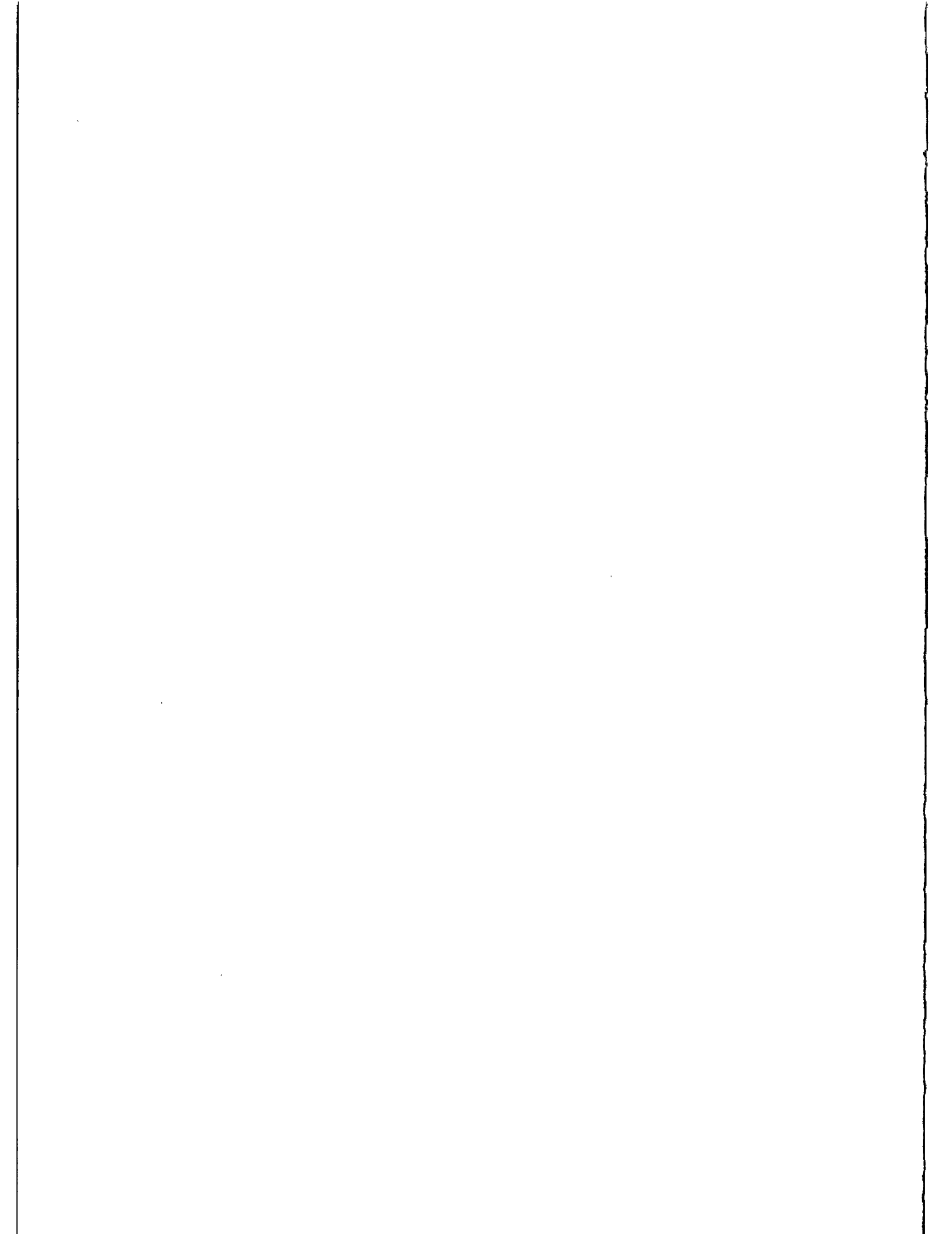
Telex 15305

ABSTRACT

The accuracy of a multipulse laser radar has been studied with indoor experiments and computer simulation. For the experiments a mode-locked Nd-YAG laser producing 7 to 9 pulses of 4.6 ns spacing at 10 Hz repetition rate is used. The frequency-doubled pulses are divided by a beamsplitter and recombined at the photomultiplier which is working at the single photoelectron level. The time-of-flight data are treated by cross-correlating the empirical distributions corresponding to the two light paths. This leads to an estimate of the time-of-flight difference. Using a large amount of data sets, the following parameters are determined:

- a) the percentage of estimates shifted by more than half a pulse spacing
- b) the standard deviation of the unshifted estimates.

For the parameters of our system, the percentage of "good" estimates is higher than 90% if more than 200 measurements are used. A standard deviation of about 100 ps is obtained under the same conditions. These results are obtained using electrostatic PMT's with about 500 ps jitter. Good agreement between the experiments and computer simulations is found. Thus the simulation method is used to determine the system performance in a wider parameter range.



Fernsehelektronik Berlin). Assuming that the start- and stop-time fluctuations are equal and independent in this case, the RMS start-time noise can be calculated to be 100-140 ps. For the experiments with PMT receiver, the SP 109 was always used. Thus, the jitter of the RCA C 31034A can be estimated by quadratic subtraction of the start noise to be around 350 ps. From this example it can be seen, that the start-time noise has only small influence on the overall resolution in our experiments.

The precision of the cross-correlation method

The generally adopted method for treating the data of a mode-locked train laser radar is to calculate first the frequency distributions of the calibration- and the ranging-measurements separately, and then to determine the time shift for maximum correlation of the two distributions. An example distribution is shown in Fig.2. The two subdistributions according to path 1 and 2 are well separated from each other by roughly 60 ns. Convoluting both distributions, Fig.4 was obtained. In this figure the convolution sum is plotted like a polygon linking the points separated by the bin width of 250 ps. The maximum can be determined very accurately using some interpolation method. In our case we obtain for the time shift of maximum correlation (61.16 ± 0.1) ns.

To investigate the precision of the method, the measurements of this and several other experiments were arranged into groups. Then the cross-correlation method was applied to each group so that an ensemble of time shifts is obtained from which statistical estimates for the precision can be gained. The parameters under consideration are:

1. the percentage of time shift results deviating from the real value not more than half a pulse separation (this quantity called "uniqueness")
2. the RMS error of the results deviating not more than half a pulse separation

These parameters are plotted in Fig. 5 and 6 in dependence of the quantity of measurements. As a normalized measure of the data quantity we are using $(1/n_1 + 1/n_2)^{1/2}$, where n_1 and n_2 are the number of measurements for path 1 and path 2, respectively. This is just the probable error of the ranging average for a single pulse system, expressed in terms of the standard deviation of a single time interval measurement. To estimate the uniqueness (resp. ambiguity) and precision from the measurements, 10 runs of 1000 points each are used. The total ensemble of 10000 measurements is arranged into groups of $n_1 + n_2 = 60, 120, 240, 480$ individual measurements. For each group the cross-correlation method is applied resulting in the generation of an ensemble of ranges from which the interesting average parameters are estimated. The return rates for the two light paths are slightly changing

from run to run. Therefore averages for the parameter $(1/n_1 + 1/n_2)^{1/2}$ have to be determined also. The resulting experimental values for the uniqueness and precision are plotted with the symbol "+" in Fig. 5 and 6.

For comparison with theoretical values and to obtain more general results (including different shapes of the laser signal like reduced pulse numbers), computer simulations were carried out assuming the photodetection process to be described by Poisson statistics and the timing jitter to have a Gaussian distribution. The simulator is a pseudo random number generator which outputs two possible numbers: 0 (corresponding to no detection) and 1 (detection). The probabilities of the two states are determined by the average number of photoelectrons (s) of the pulse according to:

$$P(0) = \exp(-s); \quad P(1) = 1 - \exp(-s)$$

The simulator is called for each consecutive pulse of the group using the pulse intensities as input parameters. When the first positive answer occurs, the corresponding pulse number is stored together with some added Gaussian timing noise. By repeating this process, 5000 simulated time intervals for both the calibration and the ranging channel are generated and stored into the memory. In this process, the average return rate for the calibration is set to be 50% and for the other channel 25%.

To estimate now the performance parameters of the system in dependence on the amount of measurements, example realizations are selected from simulated measurements and then treated by the cross-correlation method in the same way as is done with the real measurements.

The selection of the individual values from the memory is done by calling an equally distributed pseudo random number generator to determine the addresses. 500 example realizations are used to estimate the performance parameters, i.e. the uniqueness and the RMS error of a cross-correlation result.

To compare the experimental values with the simulations, the average shape of the time interval histogram is needed. It has been approximated by 9 Gaussian peaks with Gaussian envelope according to

$$h = a_0 \sum_{k=-4}^4 \exp(k^2/U) \cdot \exp((t - t_k)^2 / 2\sigma^2) \quad (1)$$

The average experimental parameters are $U = 4.61$, $\sigma = 386$ ps. The separation of consecutive pulses is

$$\Delta t = t_{k+1} - t_k = 4.55 \text{ ns.}$$

So the relative resolution is $C = \sigma / \Delta t = 0.0848$. Using these parameters the results marked in Fig. 5 and 6 by "*" are generated. They agree reasonably well with the experimental points, especially for the uniqueness (Fig.5). This

agreement is somewhat surprising because the laser pulse shape fluctuations are not directly modelled in the simulations. Instead, the pulse shape is chosen in agreement with the observed histograms. Note further that the simulated results showed almost no dependence from n_1 / n_2 if the above introduced parameter $(1/n_1 + 1/n_2)^{1/2}$ is kept constant. This is proved in the range $n_1/n_2 = 1 \dots 10$.

For the conditions used in our experiments, the following conclusions can be drawn:

- the performance of the system can be reasonably well determined by the described simulation method
- 200 measurements for both calibration and ranging are required to have 90 per cent probability of correct assignment of the data (not shifted by a multiple of the pulse separation)
- the standard deviation of a result generated from 200 measurements is in the order of 100 ps.

The good representation of the experiments by the simulation encouraged us to study the dependence of the system performance from the laser pulse shape and the timing resolution more detailed. Some of the results are graphically represented in Fig.7 and 8. In these figures, both the uniqueness parameter (broken lines, 1 at the vertical scale corresponds to 100%) and the ratio of the RMS error of the cross-correlation result to the single-shot timing jitter (full lines) are plotted in dependence on the amount of measurements. The relative RMS error as defined describes the effect of averaging.

In Fig.7 for a fixed laser pulse shape the influence of the timing resolution is represented. As a measure of the resolution, the parameter C (defined as the ratio of the overall RMS jitter of the timing system to the pulse separation of the laser pulses) is used. The time resolution is visualized by the probability distributions of the time intervals, i.e. the shapes of the histograms for very large amounts of measurements.

As can be seen from Fig.7, the timing resolution has a very small influence on the uniqueness (resp. ambiguity) but some effect on the relative RMS error. This behaviour is to be expected. We conclude from Fig.7 that the resolution parameter C should be smaller than 0.2. Note that for a given resolution of the timing system, the parameter C can be adjusted by the separation of the laser pulses which is possible by choosing the laser resonator length.

The number of pulses in a laser pulse group is represented by the parameter U. More precisely, this is the overall width of the probability distribution of the time intervals according to equ.(1). The parameter U is chosen to be $U = 6$ in Fig.7.

The dependence of the system performance on the parameter U

for a fixed resolution ($C = 0.1$) is shown in Fig.8. As expected, the parameter U has almost no effect on the error, but strong influence on the ambiguity. Fig.8 may be used to determine the amount of data to reach a given uniqueness level. A uniqueness of 90% in connection with $U = 2$ is reached for $n_1 = n_2 \approx 50$. For $U = 1$ only 20 measurements are needed in both channels to reach 90% uniqueness. There are some methods to minimize the parameter U including laser design, the combined use of nonlinear optical effects and well matched start detectors. With generally available technology, $U = 1...2$ should be a realistic value.

Conclusion

From the results of this study we conclude that the mode-locked train laser radar remains to be an attractive variant. Its main limitation, the ambiguity, can be reasonably overcome using a sufficient data quantity. The minimum data amount for a given probability of correct assignment can be gained from this paper. As a guide to good performance, one should restrict the number of pulses per group to a minimum and adjust the pulse separation to roughly 10 times the timing jitter. A special advantage of the rigorous use of single photoelectron detection is the low level of systematic errors. This gives the possibility to attain normal point errors near 1 cm even by using conventional electrostatic photomultiplier tubes.

REFERENCES

- [1] Silverberg, E.C.: The Feedback Calibration of the TLRS Ranging System
Proc. 4th Intern. Workshop on Laser Ranging Instr.,
Austin 1981
Edt. P. Wilson, Bonn 1982, p. 331-37
- [2] Hamal, K. et al.: INTERKOSMOS Laser Radar, Version Mode-Locked Train
Proc. 5th Intern. Workshop on Laser Ranging Instr., vol.II
Herstmonceux 1984
Edt. J. Gaignebet, Bonn 1985, p. 214-18
- [3] Neubert, R.: Simulation Studies on the Statistics of a Multipulse Laser Radar Working at the Single Photoelectron Level
Nabl. Isk. Sput. Zemli, Prague 23 (1984), p.93-102
- [4] Fischer, H.: Empfangsdiskriminator fuer Satellitenentfernungsmessung mit verbessertem Zeitverhalten
Radio Fernsehen Elektronik, Berlin 31 (1982) 8, p.491-92

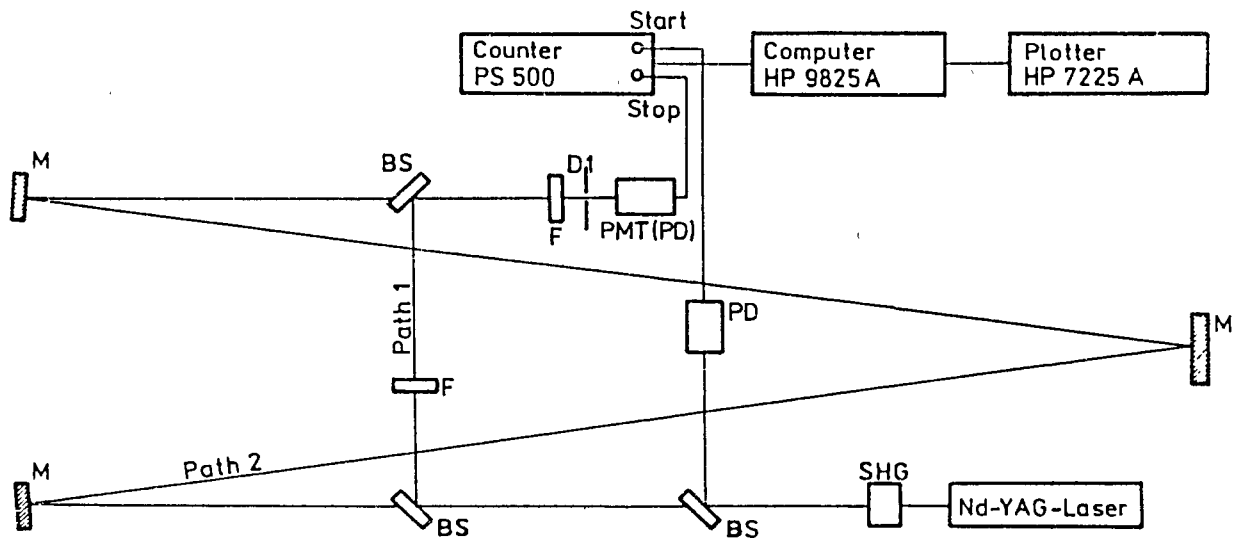


Fig. 1: Scheme of the experimental setup

BS - beam splitter, D - diaphragm
 F - neutral density filter, M - mirror
 PD - photo diode

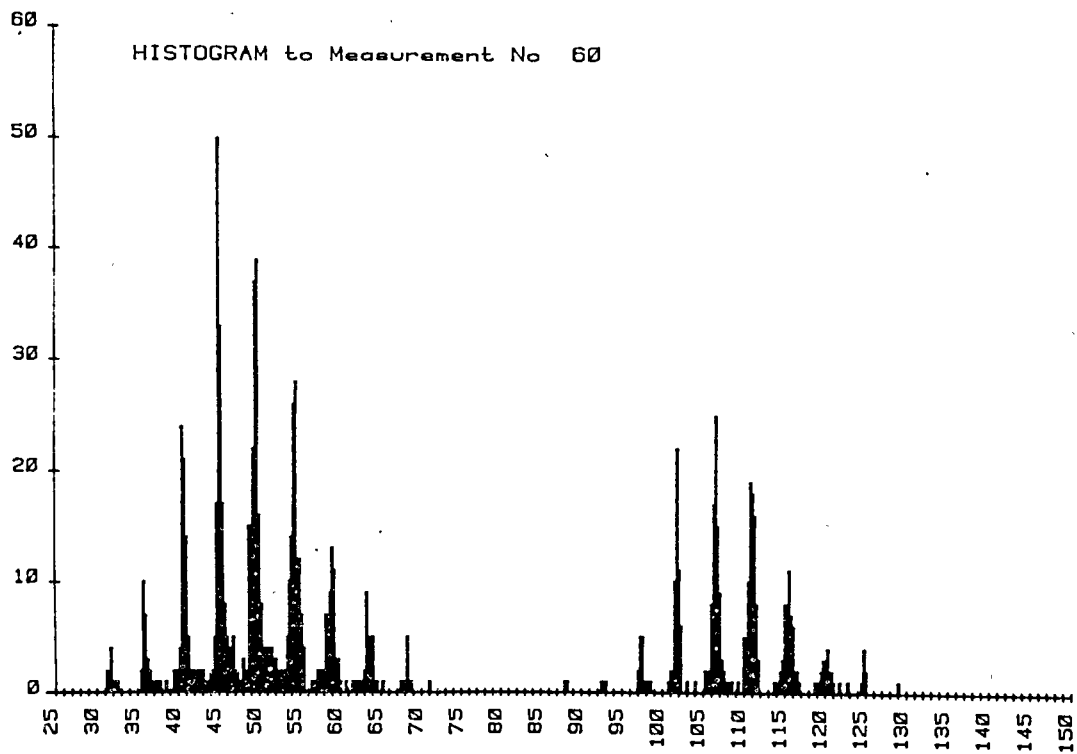


Fig. 2: Histogram of the time of flight values for a typical ranging experiment
 Abscissa: Time interval in ns
 ordinate: Number of measurements

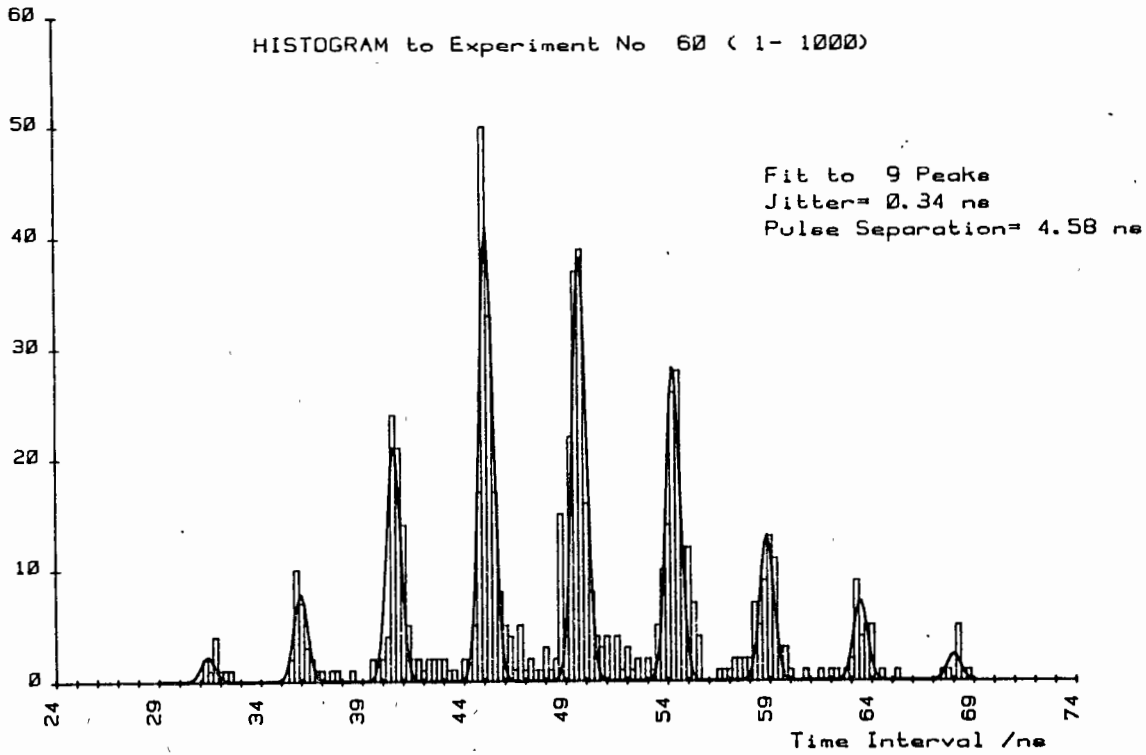


Fig. 3: Least square fit of a sum of Gaussian functions to the calibration part of experiment No. 60 (Fig. 2) bin width: 0.25 ns, RMS resolution: 0.34 ns, peak separation: 4.58 ns

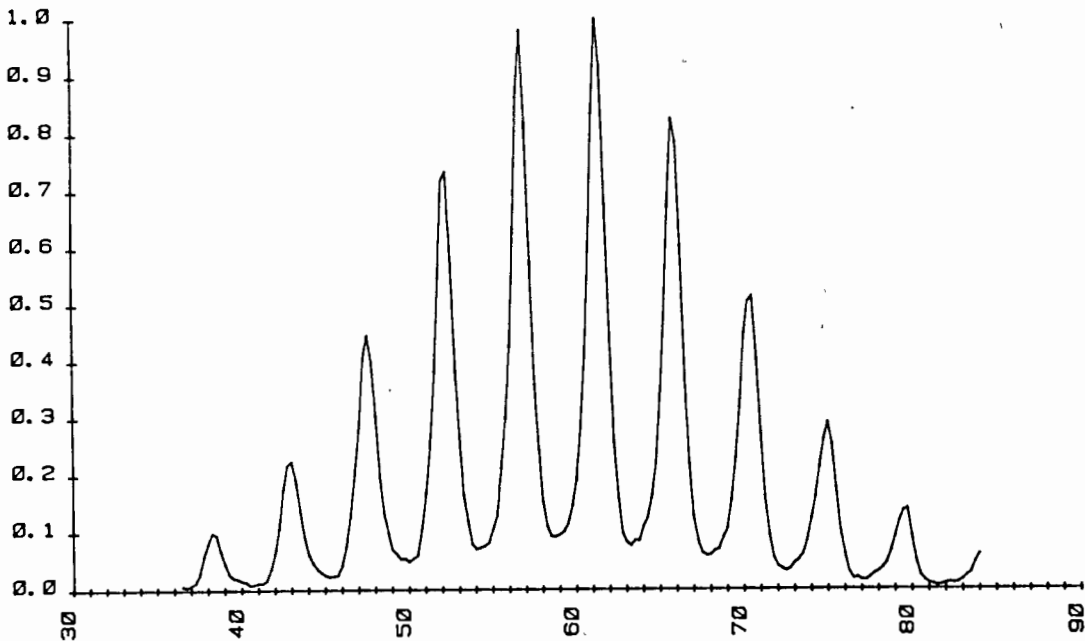


Fig. 4: Empirical cross-correlation to experiment No. 60 (convolution sum of the histograms corresponding to ray path 1 and 2 resp.)

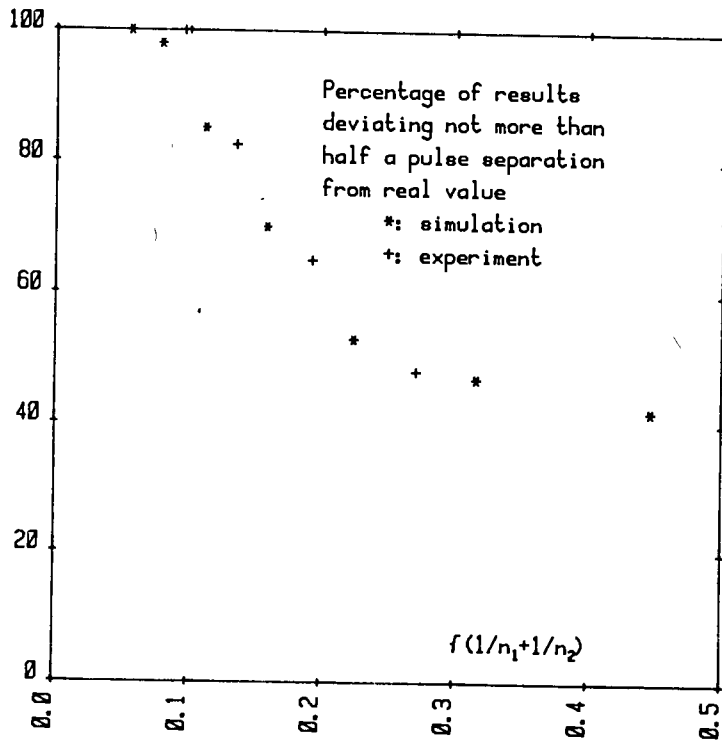


Fig. 5: Uniqueness in dependence of the amount of measurements: comparison of experiment and simulation.
 n_1 - number of measurements for path 1
 n_2 - number of measurements for path 2

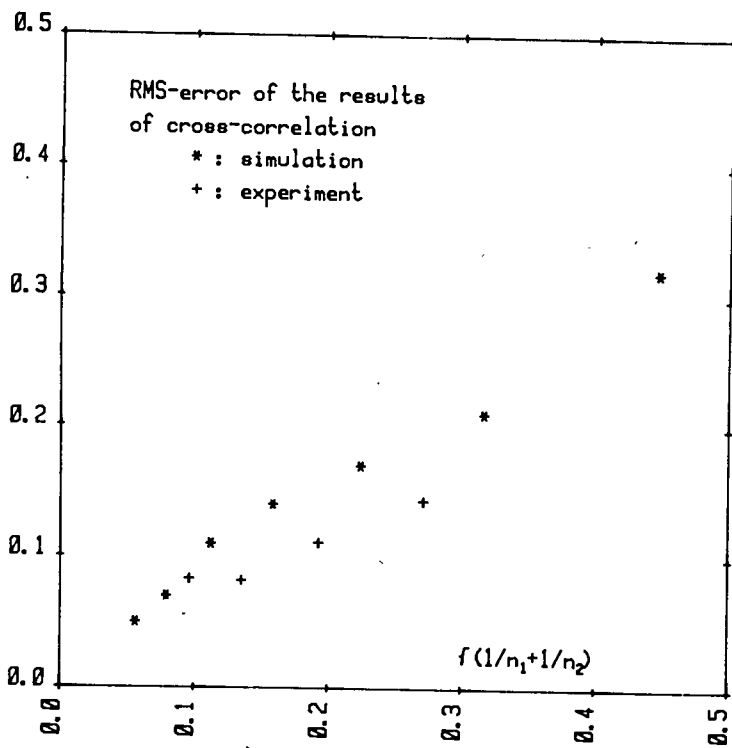


Fig. 6: RMS-error of the time shift corresponding to maximum cross-correlation: comparison of experiment and simulation

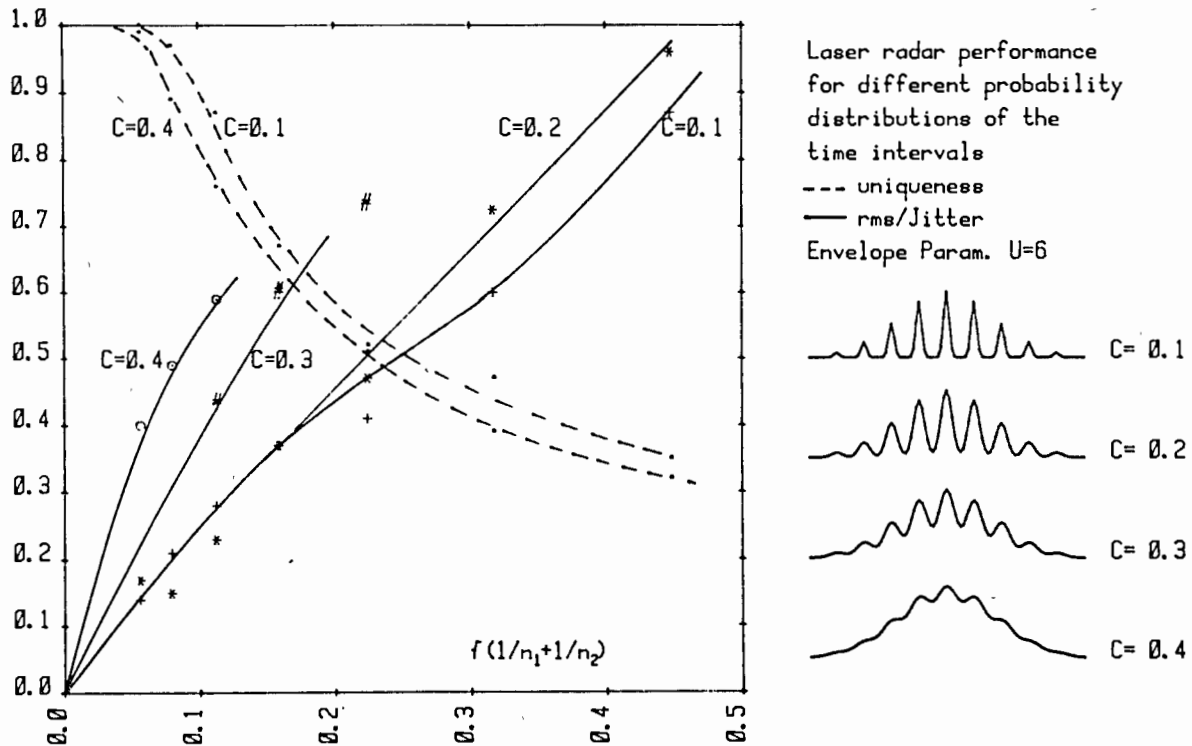


Fig. 7: Uniqueness and error obtained from simulations: dependence from timing resolution

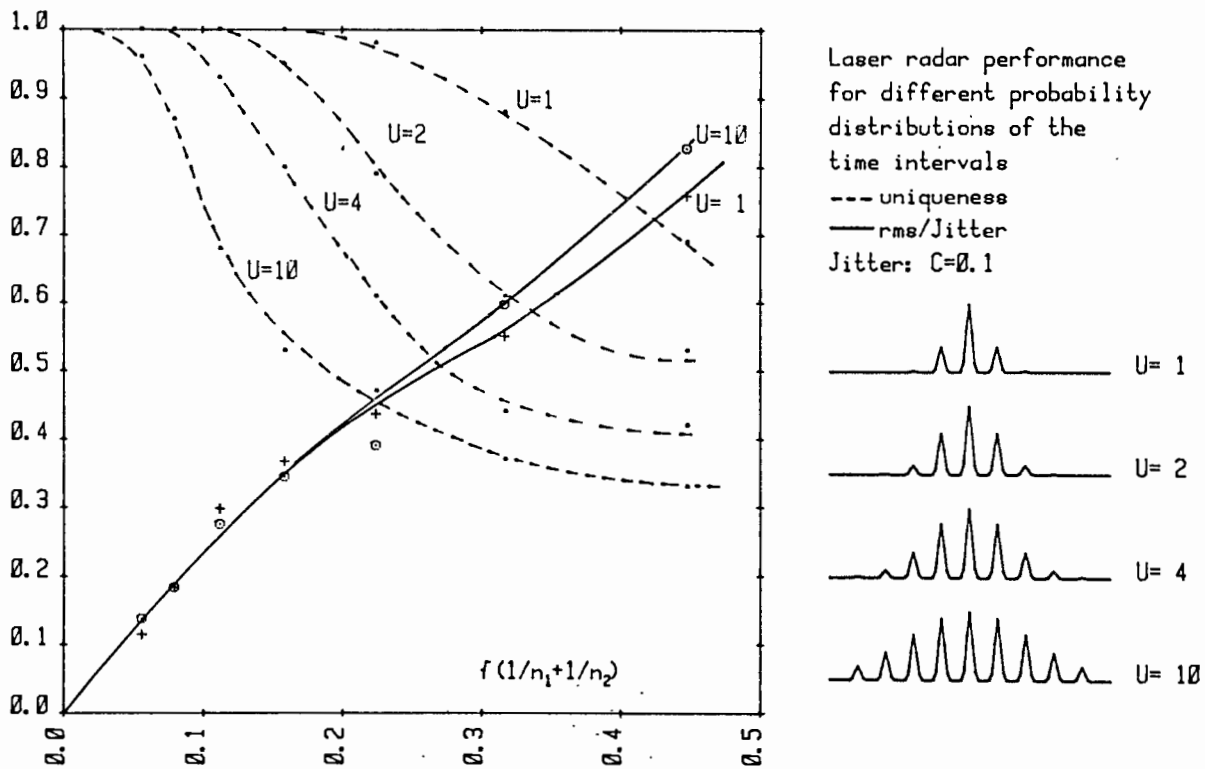


Fig. 8: Uniqueness and error obtained from simulations: dependence from the number of peaks

3.GENERATION LASER RADAR, VERSION MODE LOCKED TRAIN PROPOSAL

K. Hamal, I. Prochazka
Czech Technical University
Faculty of Nuclear Science and Physical Eng.
Brehova 7, 115 19 Prague 1 - Czechoslovakia -

Telephone (1) 848840
TWX 121254 FJFI C

ABSTRACT

To range the satellites and the Moon at the 3rd generation level ($\text{rms} < 9 \text{ cm}$), laser transmitters generating mostly single pulse are exploited. Following the idea of E. Silverberg (4WLRI, 1981) and B. Greene (5WLRI, 1984) we propose to exploit the full train of mode locked pulses. The simplification of the laser transmitter is tremendous, the laser output average power may be 3 to 5 times higher for the same material damage threshold. To avoid the ambiguity in range determination we propose to use the transient digitizers as the START/STOP discriminators. The ambiguity is removed by START/STOP signal crosscorrelation on the shot by shot basis for satellite/multi-photon/ranging. Assuming the Moon ephemeris quality, the possible ambiguity in Moon ranging at single photoelectron level may be removed by ranging data processing.

3.Generation laser radar /version mode locked train/proposal

REQUIREMENTS : RMS single shot (3cm (200 picoseconds)

JITTER budget main contributors - detector
- laser pulse
- discriminator

DETECTOR jitter contribution :

$$\begin{array}{ll} \text{RMS /multi PE detection/} & \sqrt{[\text{pulse energy}]^{-1}} \\ \text{Normal point accuracy} & \sqrt{[\text{average power}]^{-1}} \end{array}$$

PROJECT PROPOSAL

LASER - mode locked train, 3-5ML pulses, pulse HAFW 30psec

DETECTOR - microchannel PMT

DISCRIMINATORS - Tranzient digitizer /Tektronix 7912AD/

bandwidth 400MHz, 10nV/div sensitivity

discriminators software modelled

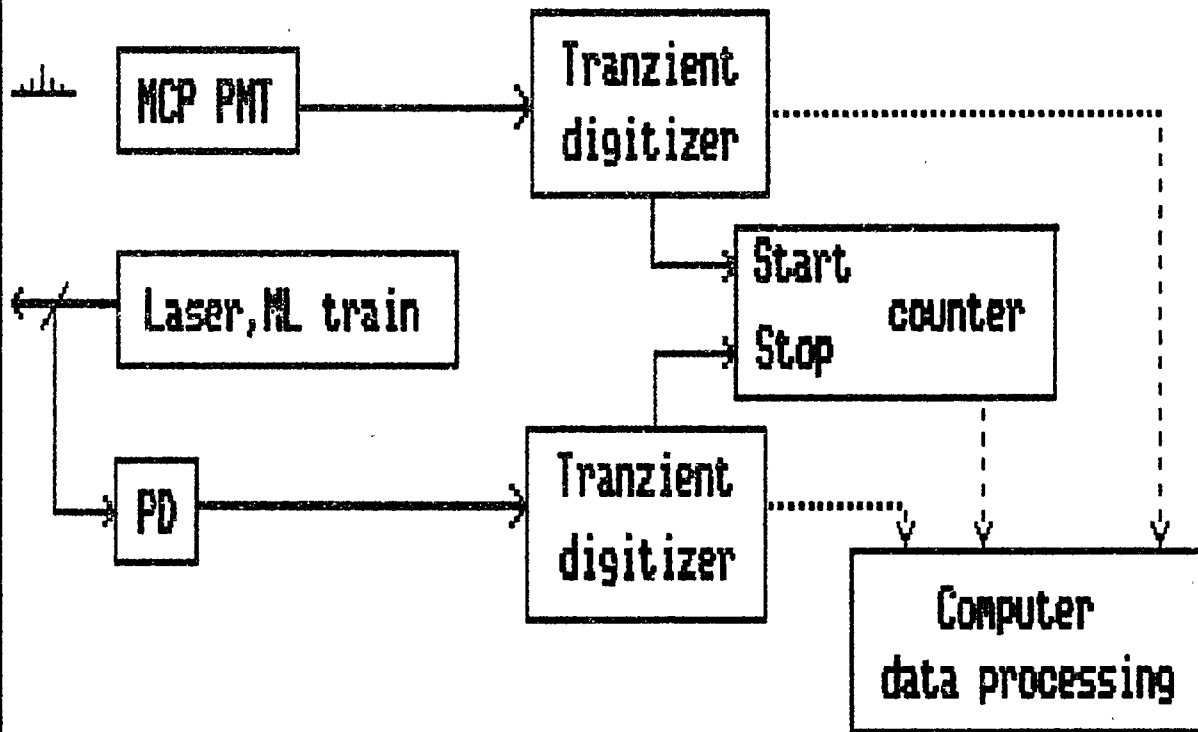
nonlinearities compensated

Start/Stop events data crosscorrelated

K. Haral, I. Prochazka
3.Generation/version mode locked train/proposal

1

Proposed block scheme



_____ signal pass
 data flow

| Jitter contributions: | multi PE | single PE |
|-------------------------|----------------|-----------------|
| photomultiplier (MCP) | 65 psec | 100 psec |
| transient 2x + PD | 30 psec | 30 psec |
| counter (HP53700) | 35 psec | 35 psec |
| laser pulse (fwhm 30ps) | 3 psec | 12 psec |
| RESULTING | 80 psec | 110 psec |

Summary / conclusion

PROPOSED SYSTEM ADVANTAGES: /in comparison to single pulse/

- * LASER : simple / no slicer/
- * AVERAGE POWER : 3-5 times higher for the same damage threshold, shorter pulses available
- * SIGNAL PROCESSING : start/stop discriminators software modelled, the time walk, nonlinearity etc. software compensated
- * CALIBRATION : both real time and pre/post pass possible, the signal strength is not critical
- * AMBIGUITY : due to the ML train
satellite / multi PE ranging / NO
Moon /single PE, excellent ephemeris/ LOW/NO

PROPOSED SYSTEM LIMITATIONS /in comparison to single pulse/

- * DATA QUANTITY : additional 2 x 1 KBytes per shot
- * SOFTWARE : more complex, data processing time consuming

K. Hanal, I. Prochazka
3. Generation/version mode locked train/proposal

3

THE NEW SATELLITE LASER RANGING SYSTEM
AT CAGLIARI OBSERVATORY

A. Banni
International Astronomic Station of Latitude
Cagliari - Italy

Telephone (39) 70 657657
TWX 790326 OSSAST I

V. Capoccia
Vitroselenia S.p.A.
Cagliari

Telephone (39 70 99952
TWX 791090

ABSTRACT

About one year ago the restructuring of our laser station was begun, with the technical assistance of the Vitroselenia Company of Cagliari.

The work consists of the total substitution of tracking, control and data acquisition equipment.

In carrying out the work the prime consideration was that of the reliability and precision of each single component.

The new station is expected to become operative in the first months of 1987.

1. TRANSMISSION-RECEPTION PULSES SYSTEM

At present we have available a first-generation Q-switched Ruby Laser that was custom-built for us by Apollo Lasers Inc.

This system remained inactive for about three years for various reasons, most of which of a technical nature.

Therefore we are now in the process of verifying the efficiency of the Pochels Cells assembly, the Q-switching system, the optical alignments, the electrical system and also the tracking system (fast diode, PMT, signal amplifiers).

The characteristics of our Ruby Laser Transmitter are given in Table 1.

For the transmission and reception of the laser shot we use a single reflector telescope of the Cassegrain-coude' type, the lenses of which were made in Florence.

In the previous system, transmission, reception and TV control were carried out by means of three distinct telescopes, with consequent problems of mechanical inertia, optical alignment and electromechanics.

We therefore designed an optical diagram that couples the three optical paths with the use of dichroic mirrors and beam splitters with minimum variations in the percentage of signal power loss.

As for mounting, we have available the base of a Contraves EOTVOS-B cinetheodolite the electromechanical components of which have been replaced, partly because they were obsolete and partly because they had deteriorated.

The characteristics of the telescope are given in Table 1 and the optical diagram is described in Figs 1a and 1b.

Table 1 .

RUBY LASER SPECIFICATION

| | |
|-------------------------|---|
| Oscillator Rod | 1x7.5 cm AR coated ruby |
| Amplifier | 1.3x15 cm AR coated ruby |
| Q-Switch | 1 cm clear aperture, KD*P pockels cell |
| Cavity configuration | Flat-Flat, pulse-on switching |
| Wavelength | 694.3 nm |
| Line width | 0.3 A fwhm typical |
| Output Energy | 1 Joule in 5 ns pulse width |
| Beam divergence | 3 mrad |
| Repetition Rate | 60 per minute, maximum |
| Main Mirror | 50 cm Quartz and aluminium |
| Equivalent Focal Length | 5 m |
| Field of View | 0.0003-0.006 mrad |

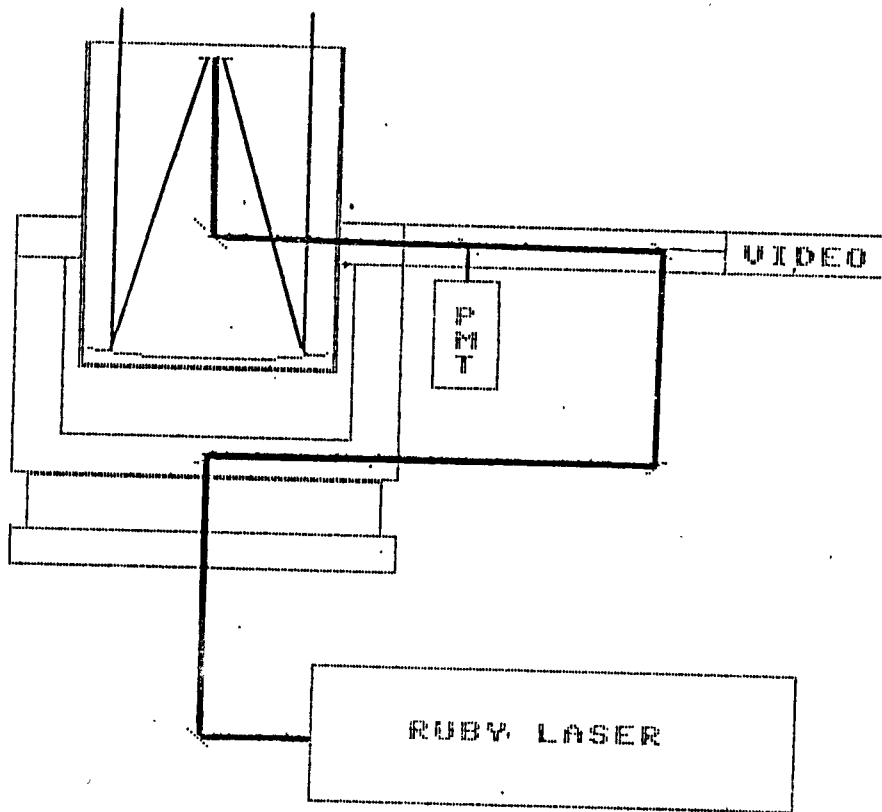


FIGURE 1a
OPTICAL DIAGRAM

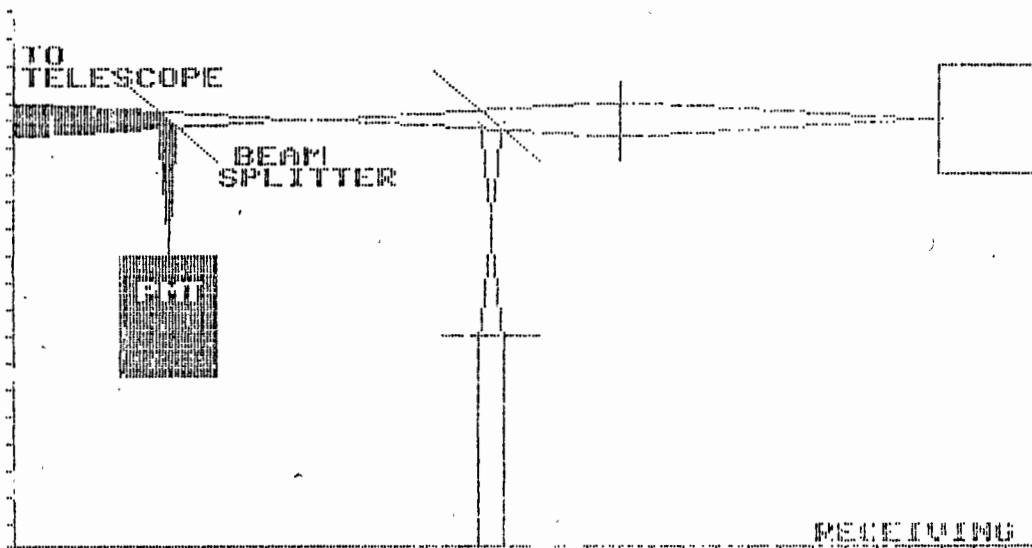
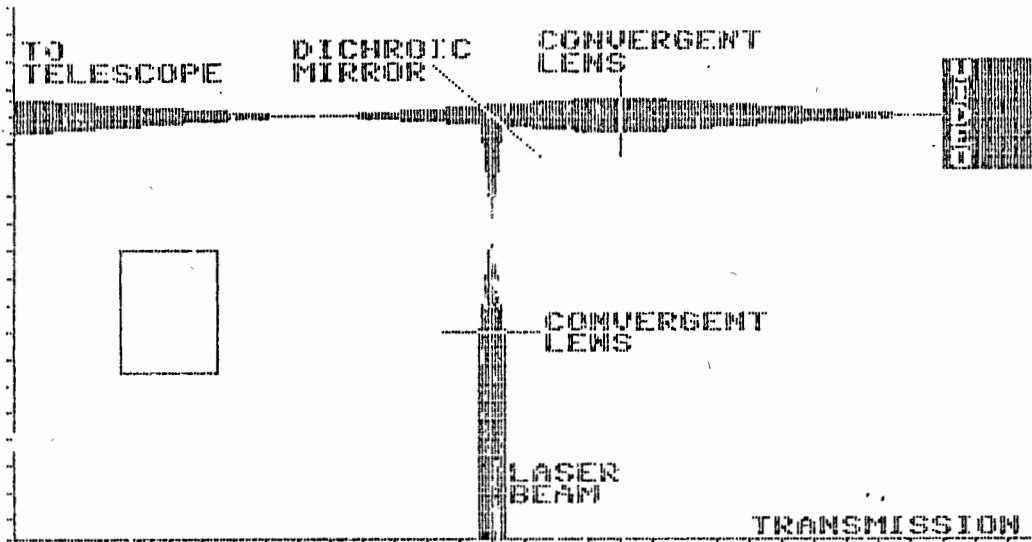


FIGURE 1b

2. FOLLOWING MOVEMENTS

For azimuth and elevation drives the cinetheodolite was equipped with servomotors of the type with direct current and low inertia which are coupled to the axes with gear wheel - worm screw couples.

The motors for following are driven by servoamplifiers and their speed is read by speedometer dynamos.

The speedometer dynamos, which make up the velocity feedback towards the servoamplifiers, are keyed on the same axis as the motors themselves.

The guiding servoamplifiers, built with LSI technology, are switching converters with bidirectional, high-speed response pulse wave modulation (PWM).

The controls are governed by a microprocessor which carries out the following duties:

- Control of the drive units
- Acquisition of angle data
- Closing of speed and position loops
- Limit switches
- Dialoguing with computer personnel

The microprocessor directly governs the function of following control by means of the position feedback supplied by the encoders.

The azimuth and elevation encoders used are of the absolute type with a 16 bit angular resolution; they consist of an optical-mechanical part and a card containing all the electronic interfacing to the data acquisition and control microprocessor.

In order to optimize the angle readings the encoders were installed close to the two rotational axes with a system for the taking up of mechanical play such as to guarantee aim accuracy with a tolerance of <0.1 degrees.

Table 2

SERVOMOTOR AND ABSOLUTE ENCODER

| | |
|------------------------------|---------------|
| NOMINAL TORQUE | 77 Ncm |
| NOMINAL EFFECTIVE POWER | 240 Watt |
| SPEEDOMETER DYNAMO LINEARITY | 0.18% |
| ENCODER OUTPUT CODE | BINARY |
| NUMBER OF BIT | 16 |
| AIM ACCURACY | 0.0017 rad |
| ZERO ADJUSTMENT | by dip switch |

3. DATA ACQUISITION SYSTEM

As in the case of following control, the data acquisition sub-system is also governed by a microprocessor which carries out the following tasks:

- a). time reading at the instant it receives the stop signal from the PMT;
- b) telescope position reading;
- c) Reading of time interval recorded by the time interval counter;
- d) temperature, humidity and pressure sensor readings;
- e) Dialogue with computer personnel.

The clock is triggered by the 1 Mhz sample frequency of our Master Clock and therefore gives a resolution of 1 us.

Furthermore, the clock is equipped with an output at various frequencies for the laser control trigger.

Readings are carried out serially at the moment in which the stop signal is received from the photomultiplier in the order given above.

The entire system will be managed by an IBM or IBM compatible personal computer to facilitate the management of both the follow control and data acquisition sub-system and the files of data acquired during satellite rangings.

In Table 3 the salient characteristics of the system are described.

Table 3

DATA ACQUISITION SYSTEM FEATURES

| | |
|-------------------------|------------------|
| CLOCK RESOLUTION | 1 us |
| CLOCK PRECISION | not yet verified |
| PULSE TRIGGER FREQUENCY | 1Hz-10Hz |
| HP COUNTER RESOLUTION | 20 ps |
| HP COUNTER PRECISION | 100 ps |

Table 4

STATION SITE DATA

| | |
|----------------|--------------------------|
| STATION NUMBER | 9999 (Punta Sa Menta) |
| LATITUDE | 39° 08' 32" |
| LONGITUDE | 8° 58' 12" |
| ALTITUDE | 202 m ssl |
| CAVU | Average 120 days an year |

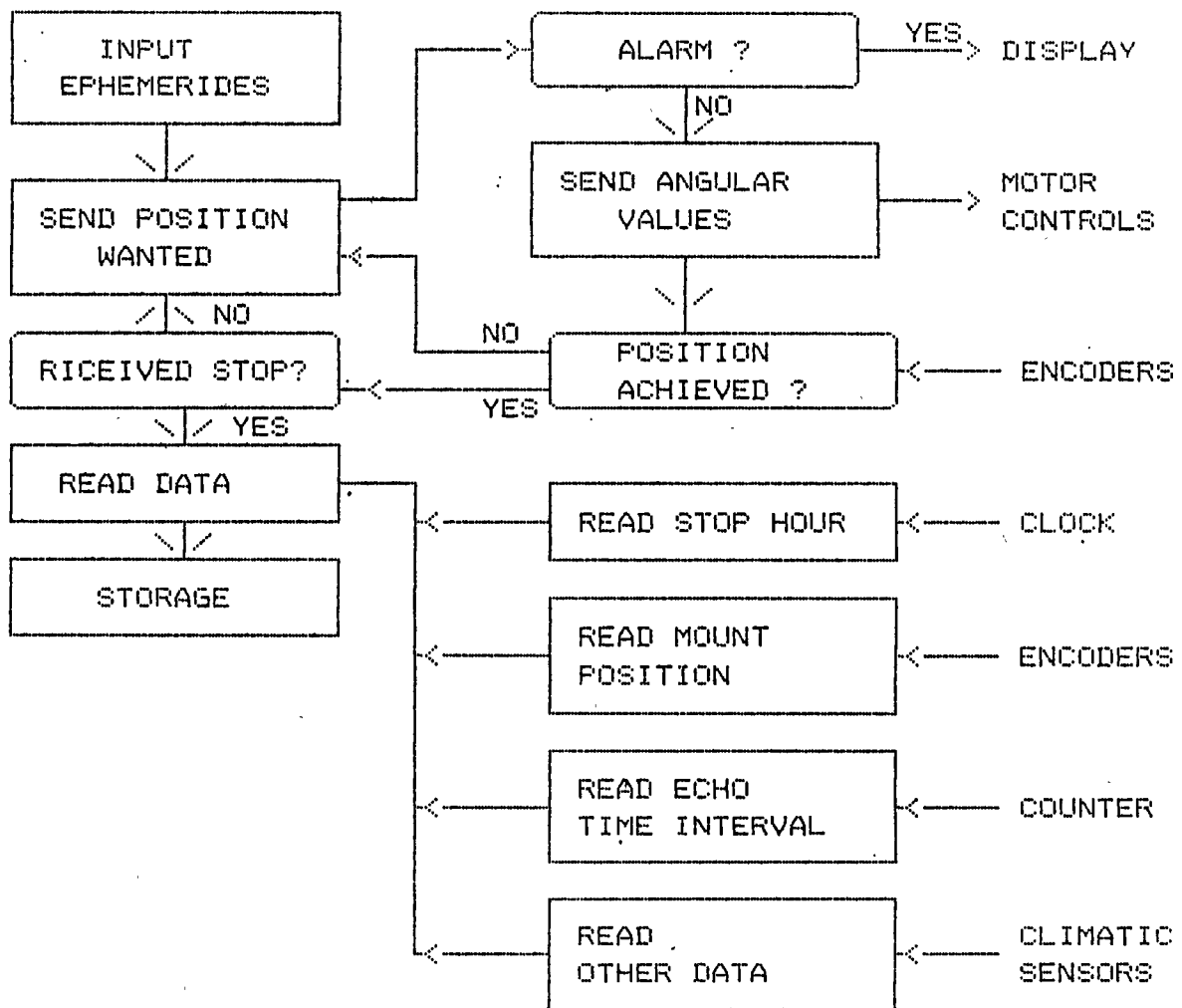


Figure 3
CONTROL PROGRAM FLOW CHART

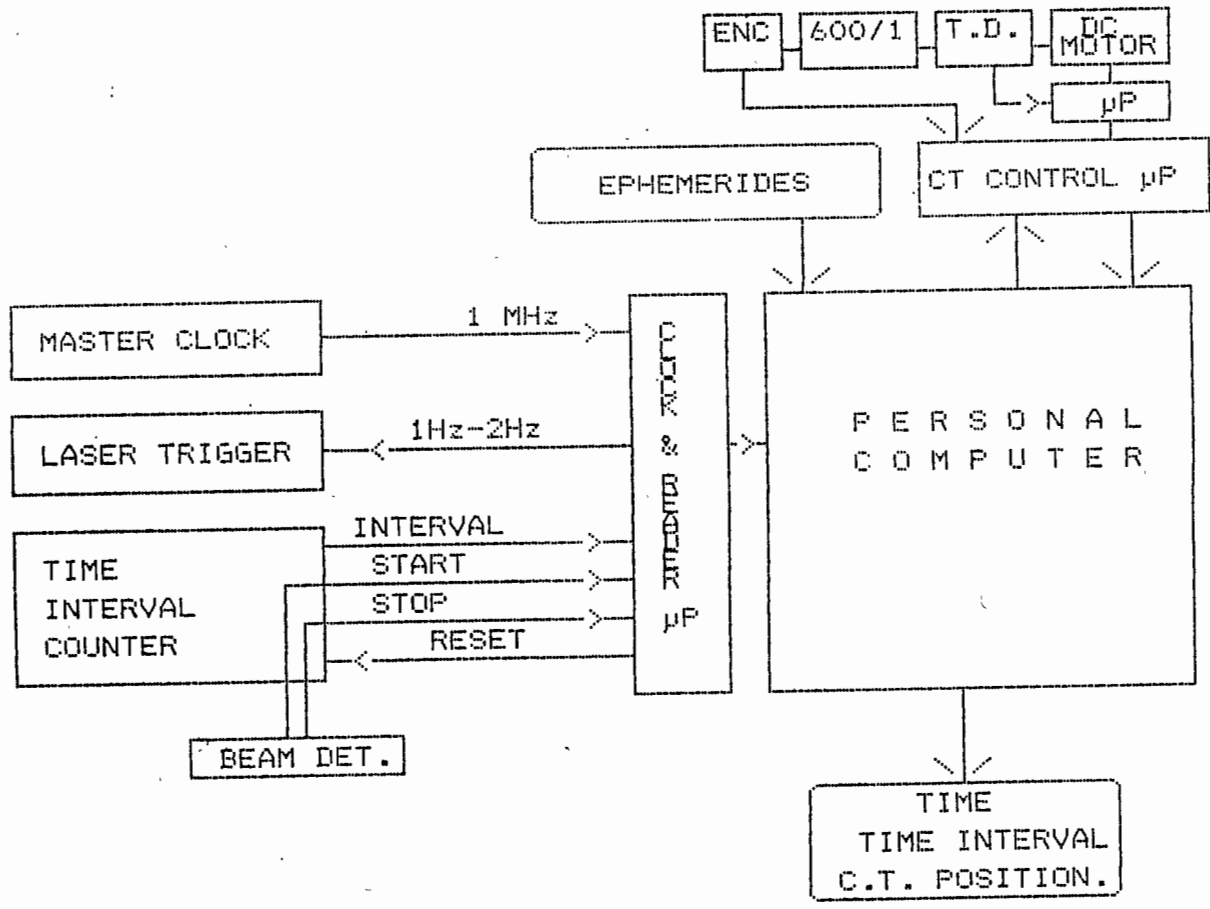
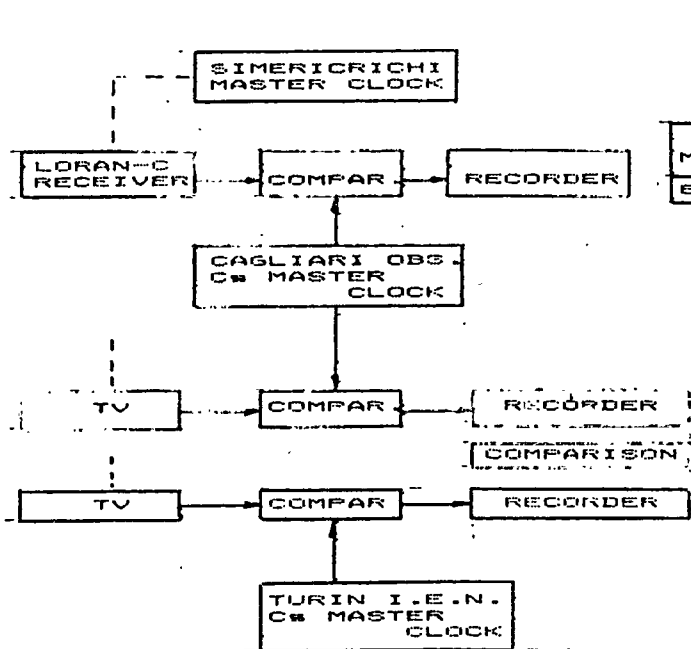


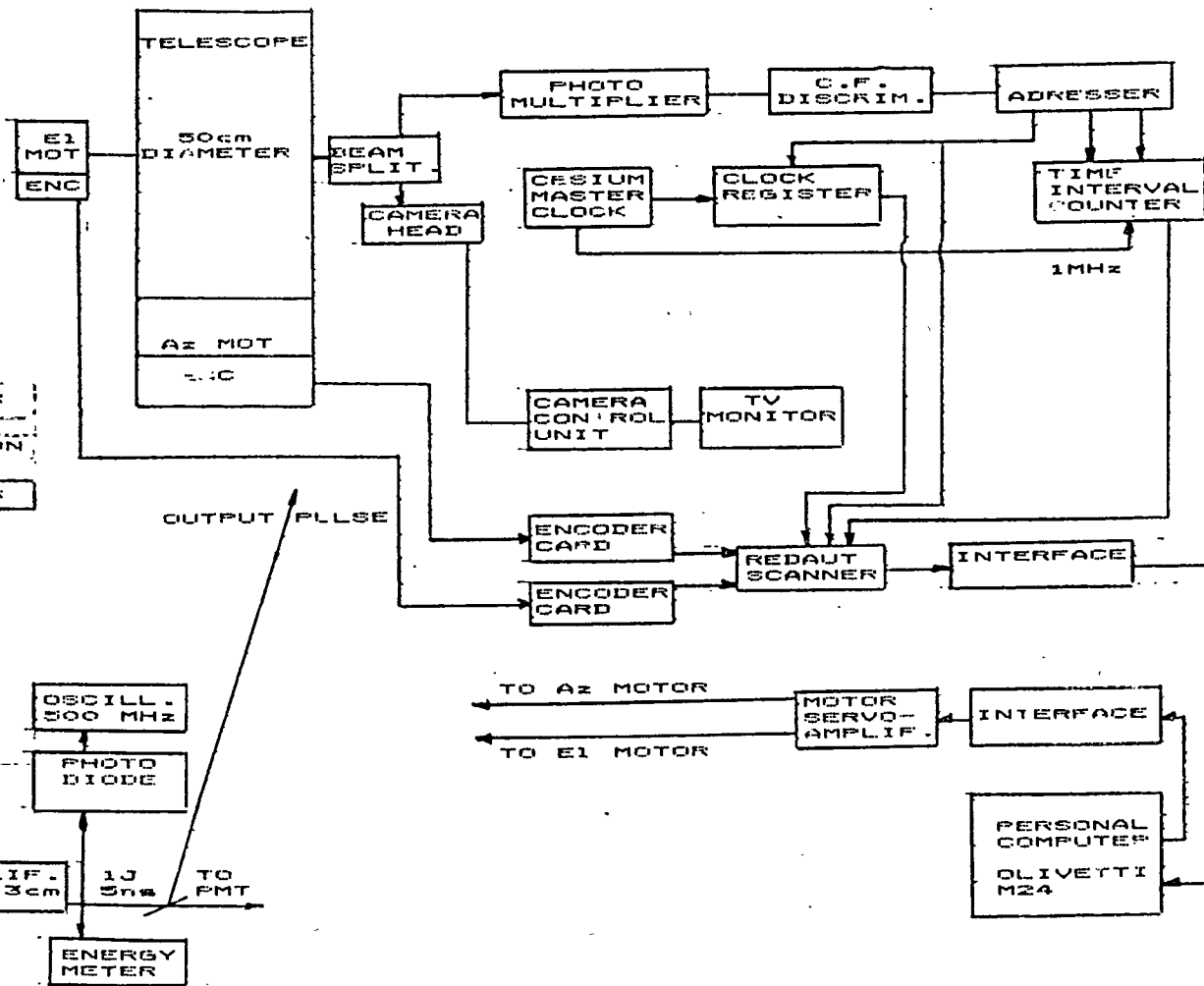
Figure 2
CONTROL BLOCK DIAGRAM

CAGLIARI LASER STATION

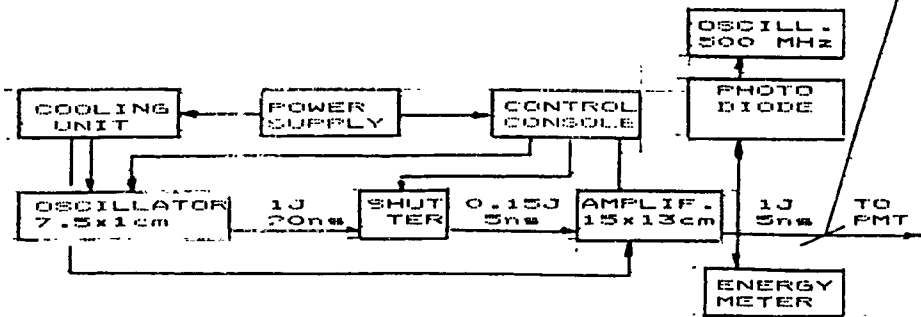
TIME SYNCHRONIZATION



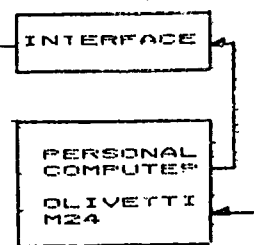
ECHO RECEIVER AND DATA RECORDING SYSTEM



LASER TRANSMITTER SYSTEM



TRACKING SYSTEM



REFERENCE

Cugusi L., Messina F., Proverbio E.
A LASER RANGE TRACKING STATION FOR GEODYNAMIC SATELLITES
,Proceedings of the Second Workshop on Laser Tracking
Instrumentation, Prague 1975

Cugusi L.
THE SATELLITE LASER RANGING SYSTEM AT CAGLIARI OBSERVATORY
Proceedings on Third Workshop on Laser Ranging
Instrumentation, 1978

ZIMMERWALD SATELLITE OBSERVATION STATION

P. Kloeckler, Th. Schildknecht
Astronomical Institute
University of Berne
Sidlerstrasse 5
CH - 3012 Berne - Switzerland -

Telephone +4131 65 85 91
Telex 912643 PIBE CH
Mark-3/Quick-Com AIUB

1986 STATION REPORT AND ESTIMATE OF SYSTEMATIC ERRORS

1986 STATION REPORT AND ESTIMATE OF SYSTEMATIC ERRORS

ZIMMERWALD SATELLITE OBSERVATION STATION

P. KLOECKLER AND TH. SCHILDKNECHT

ASTRONOMICAL INSTITUTE
UNIVERSITY OF BERNE
SIDLERSTRASSE 5
CH - 3012 BERNE
SWITZERLAND
TELEPHONE: +4131/65 85 91
TELEX: 912 643 pibe ch
MARK-3/QUICK-COM: AIUB

1. STATION REPORT AS PER SEPTEMBER 1, 1986

LASER

Measurements proved that the emitted laser energy in the mean was never above 5 millijoules, a fraction of the permitted energy with the Quantel 402 DP laser. Yet already at this output level the KD*P doublers had to be reworked quite frequently. The reason for this is suspected insufficient mechanical stability, and possibly uneven energy profile of the beam.

The average frequency of the laser shots also was never up to the expected 9 Hz or so, but mostly lingered around 5 Hz. This in turn reduced data-yield. Active/passive mode-locking in the near future will improve this situation.

An unnoticed breakdown in primary laser cooling caused destruction of a ND-YAG window and consequently a break in observations between July and September 1985.

The pulse-selector (Krytron switch) proved unreliable and will be replaced by the end of this year.

TRANSMIT OPTICS

The lenses of the Galilei telescope were replaced by a more precise set with better coatings, thus affording better transmittance and far field.

RECEIVER

After the protective shutter had been installed, and 1 GHz bandwidth provided for the timing channel, the microchannel plate photomultiplier (Hamamatsu R1294U) was tried with some good results.

99% of the data, though, have been gathered with the conventional photomultiplier model D341B by EMI.

A HP5370A time interval counter was purchased in spring 1986 and added to the system. Due to the computer limitations mentioned

below, it could be used only for calibration purposes so far. Intercomparison with our time digitizer showed a small reduction in digitizing noise, but no noticeable difference in systematics.

COMPUTER

The software was extended by some degree; most prominent extensions were the possibility of communicating via GE-Mk 3 (making telex transmission of QL data obsolete), improved tracking support and data screening.

The station computer PDP/11-40 under RT-11 and only 64 kbyte of RAM limited the program evolution, and many new concepts could not yet be implemented. Because of this, and the increasing failure rate, we decided to introduce a new computer, most possibly during 1987.

TIME SYSTEM

The station was fitted with a BVA quartz oscillator as principal time-base. This type of oscillator is reported to yield the best short-time stability.

OPERATIONS

Tracking efforts were considerable, but yields moderate. The weather limited observations, as well as the bad nocturnal coverage by LAGEOS in summer 1986. Much time was put into calibrations, to finally be able to specify an error budget.

Some special efforts were taking place in the fall of 1985, when the dutch MTLRS was visiting Mte. Generoso in southern Switzerland. SLR, terrestrial LR and GPS observations were gathered. Results are presently under review.

FUTURE IMPROVEMENTS AND ADDITIONS

The modifications of the laser for active/passive mode-locking and spatial filtering are under way. The computer replacement (most probably by a DEC Microvax) and an exchange of angle-encoders will be the most prominent upgrades at the station in 1986/7. We also hope, by modification of the building structure, to gain space for a new laser table. The purpose is to rearrange the laser related equipment to facilitate a mechanically more stable setup, and to solve the radio interference problem into the electronic system.

2. PRECISION ESTIMATE OF ZIMMERWALD LRS

This summary report covers the period September 1984 through August 1986. More detailed information is available on request.

2.1 MODELLING AND ENVIRONMENTAL ERRORS

The survey error is not being specified because we describe a stationary system.

Refraction corrections are especially sensitive to the pressure measurement. From barometer trips from the State Standards Laboratory, we conclude that the mercury barometer at our station is not beyond doubt. This situation is being cleared,

and for the reported period a worst case estimate used.¹ No measurements are made below 30°.

2.2 RANGING MACHINE ERRORS

SPATIAL VARIATION

No test of this has been made due to the lack of external calibration. We trust that our mode-locked QUANTEL laser performs equal to those tested at GSFC. Any remaining spatial effect should tend to average out due to our rather erratic tracking.

TEMPORAL VARIATION

As we perform in-pass calibration, temporal effects are minimized. However, the calibration measurements have been averaged over the whole pass so far. The mean has been rounded to 1/10 of a nanosecond, introducing a rounding error which should not introduce systematics.

AMPLITUDE DEPENDENCE

The system was mostly operated in the 1-10 photon region (LAGEOS). Stronger returns were noticed on the display and the beam immediately widened, thus limiting time-walk. Any excess amplitudes could be detected after screening and appropriate measures taken.

CALIBRATION PATH

The internal path geometry can be sufficiently well measured. On the other hand there is a piece of optical fibre for feedback, the delay of which has to be measured electro-optically. The method employed ensures an uncertainty of less than 100 picoseconds (a value which can be improved in the future.)

CALIBRATION (METEOROLOGICAL CONDITIONS)

Not applicable because of internal calibration.

MOUNT MODEL

Mount eccentricity is removed by the internal calibration.

TIMING ERRORS

Daily TV comparisons ensure an accuracy of ± 1 microsecond; an additional allowance is made for the drift of the TV delay-constant, which is checked yearly by clock transport. Since this method allows only "a posteriori" time comparison, the QL data epochs are of LORAN accuracy. (± 5 μ s worst case).

We finally wish to remark that we miss a specification of the short-time stability of the flight-time clock (scale factor) ! We urge that this issue be discussed at the next opportunity !

¹Note: A fault in the mechanical readout of the barometer has been found meanwhile; no adjustment is made of the data because the error was judged negligible.

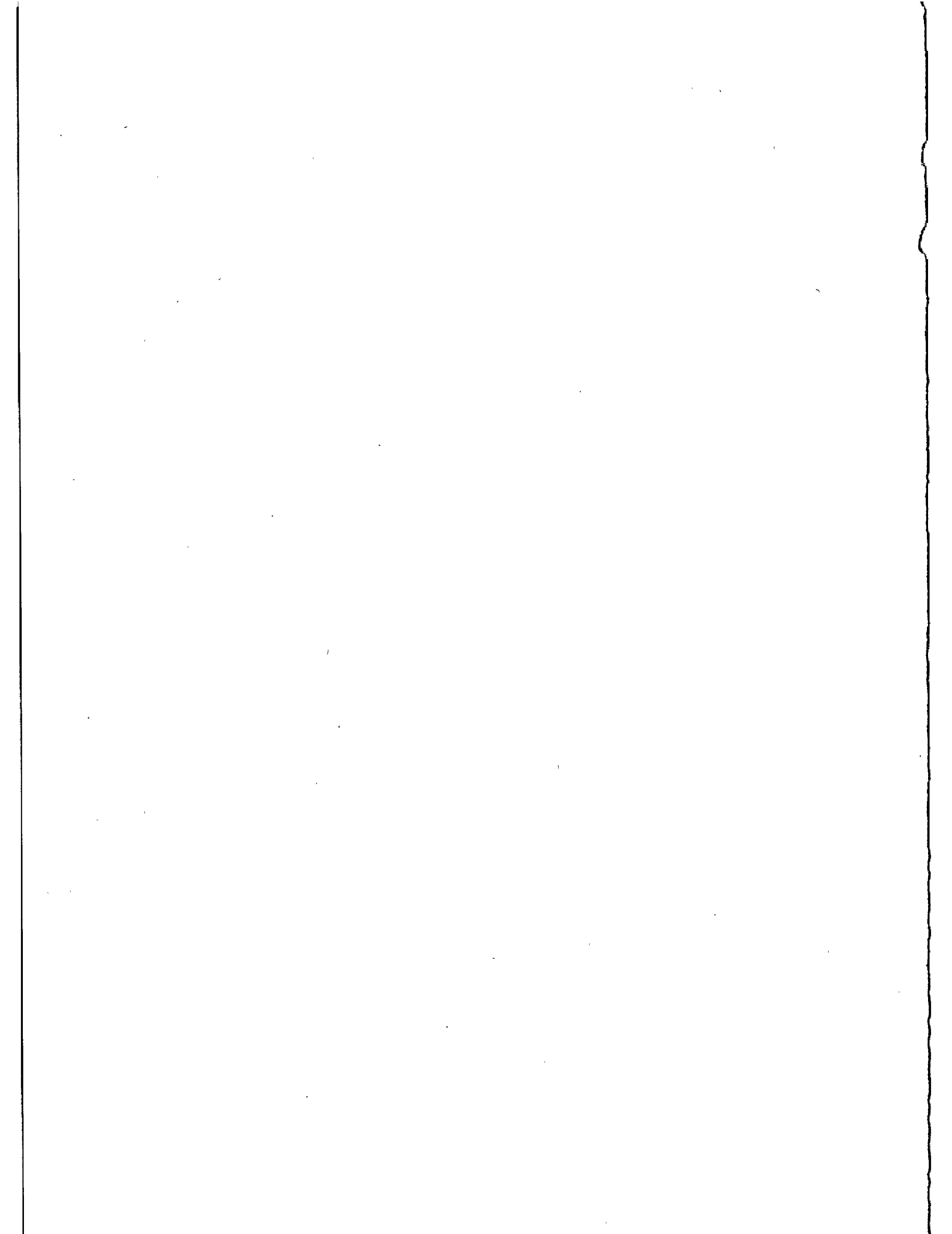
RANGING ERRORS (CM)

| | PASS | DAY | MONTH | INDEF. |
|---|------|------|-------|--------|
| MODELLING ENVIRONMENTAL ERRORS | | | | |
| ATMOSPHERIC PROPAGATION (MODEL) | .5 | .5 | .5 | .5 |
| ATMOSPHERIC PROPAGATION (METEOROLOGICAL MEASUREMENTS) | 1.0 | 1.0 | 1.0 | 1.0 |
| SPACECRAFT CENTER OF MASS | .2 | .2 | .2 | .2 |
| GROUND SURVEY OF LASER POSITION | - | - | - | - |
| DATA AGGREGATION | - | - | - | - |
| R.S.S. | 1.2 | 1.2 | 1.2 | 1.2 |
| RANGING MACHINE ERRORS | | | | |
| SPATIAL VARIATION | 1.0 | .5 | .5 | .5 |
| TEMPORAL VARIATION | 1.0 | .3 | .1 | .1 |
| SIGNAL STRENGTH VARIATION | 3.0 | 3.0 | 3.0 | 3.0 |
| CALIBRATION PATH (SURVEY) | 1.5 | 1.5 | 1.5 | 1.5 |
| CALIBRATION PATH (METEOROLOGICAL CONDITIONS) | - | - | - | - |
| MOUNT ECCENTRICITIES | .1 | .1 | .1 | .1 |
| R.S.S. | 3.70 | 3.50 | 3.40 | 3.40 |

RANGING ERRORS (CM)
TIMING ERRORS (MICROSEC)

| | | | | |
|----------------------|-----|-----|-----|-----|
| PORTABLE CLOCK SET | 1.0 | 1.0 | 1.0 | 1.0 |
| BROADCAST MONITORING | 1.0 | 1.0 | 1.0 | 1.0 |
| R.S.S. | 1.5 | 1.5 | 1.5 | 1.5 |

ESTIMATED RANGING ERRORS FOR SATELLITE LASER RANGING SYSTEM
ZIMMERWALD LRS (7810) 1984-1986



THE NEW CERGA LLR STATION

Ch. Veillet, J.E. Chabaudie, Ch. Dumoulin, D. Feraudy
J.G. Langlois, J.F. Mangin, J. Pham-Van, J.M. Torre
C.E.R.G.A.
Avenue Copernic
06130 Grasse - France -

Telephone 93 36 58 49
Telex 470865 F

ABSTRACT

The new Cerga Lunar Laser Ranging station is presented with its main characteristics. The new YAG laser delivers at 10 Hz two beams 300mJ each in green with a 300 ps pulse. The new transmitting/receiving/pointing package is described as well as the computer environment. The first series on a single night (obtained after the workshop) are finally shown.

1/ Introduction

The CERGA LLR station has been operating for four years with results increasing both in quantity and quality. It used a ruby laser with a 3ns/3J pulse and 10 shots per minute. Fig. 1 shows the progression in data quantity and diversity (various reflectors ...). Since April 1984, the normal point accuracy has been stable around 16 cm on the Moon distance. The CERGA station has been the most productive in 1985, and more than 2/3 of the UT determinations made from LLR that year have used CERGA data.

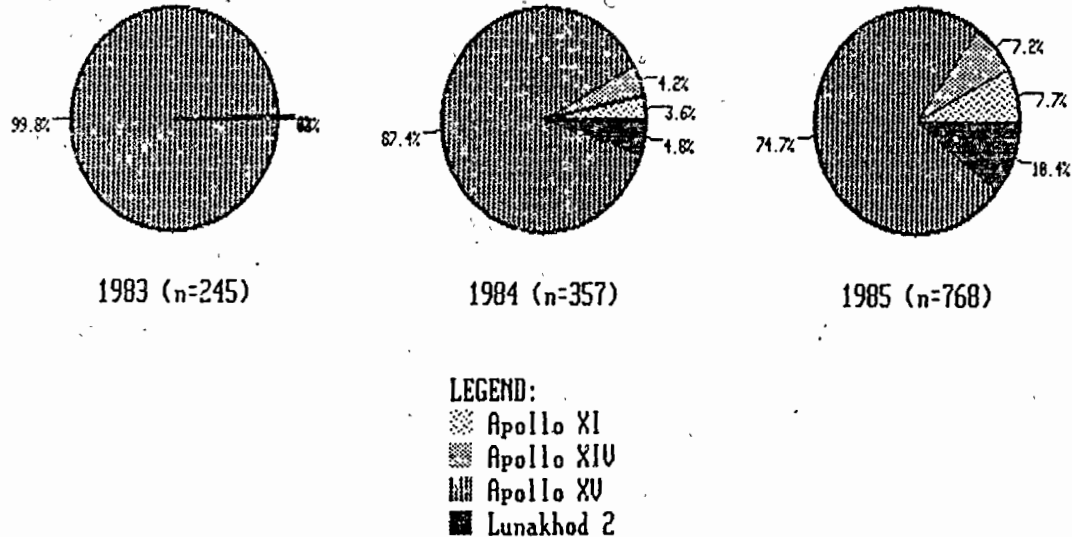


Fig. 1 - Normal point total number and repartition over reflectors - *n* is the number of normal points obtained with the old ruby laser at the CERGA LLR station for the given year.

In order to improve the accuracy of the data, an upgrade on two years has been planned for 1985 and 1986, including a new computer, a new laser and the new transmitting/receiving equipment linked to different laser rate and wavelength.

2/ The laser

Fig. 2 shows the implementation of the new Quantel Nd-YAG laser components on the granite. The oscillating cavity can work in both active/passive (dye cell) or active/active modes. After the slicer, each pulse is 1 mJ in 300 ps in active/active mode, or roughly .4 mJ in 200 ps in active/passive mode, both at a 10 Hz pulse rate and in infra-red. Two consecutive 7mm rod amplifiers permit to reach 200 mJ in active/active mode. This pulse is divided in two equal pulses, both of them being finally amplified on its own third amplifier (9mm rod), a delay line insuring a simultaneity of the start at the granite edge. The final energy is 600 mJ in infra-red per 300 ps pulse and per beam at 10 Hz.

By changing the Fabry-Perot glass at the cavity output edge, other pulse lengths in active/passive mode can be obtained down until 35 ps. They can be used for exemple for accuracy tests on the electronics. If the active/active mode is easier to work with (there is dye check and maintenance), it is less stable in energy. This mode has been used at the beginning till December 1986. The active/passive mode is now used due to a much better stability.

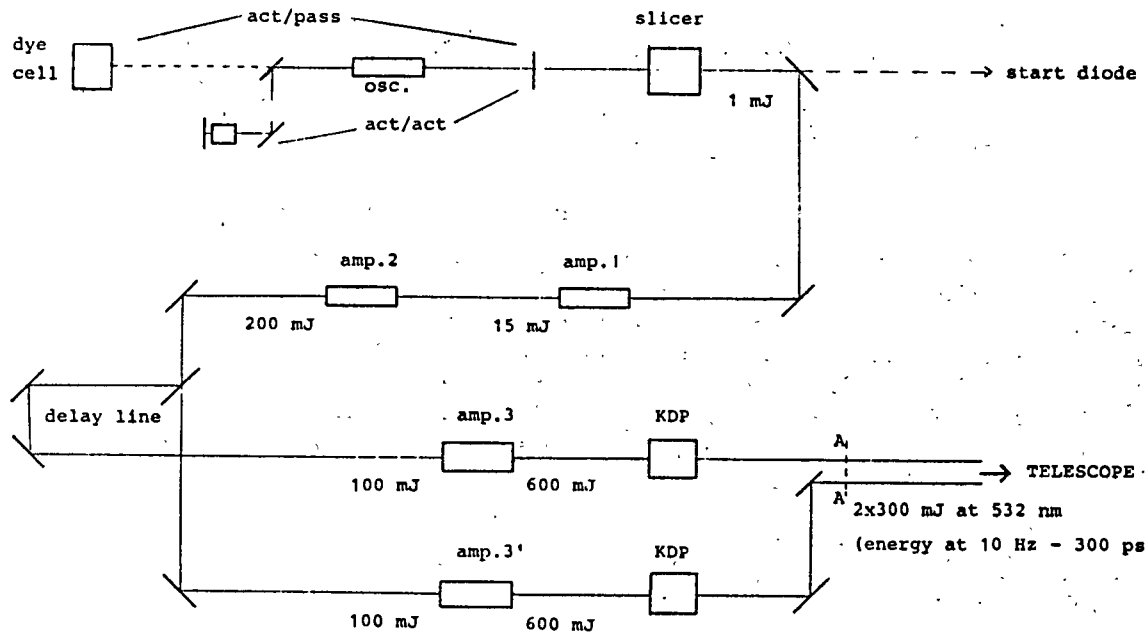


Fig. 2 - Laser configuration - Energies are given at 10 Hz rate for 300 ps pulses.

The shape of the two beams at the edge of the laser and on the telescope aperture can be seen on Fig. 3. Each beam has a 9 mm diameter after the last amplifier. The two beams are made parallel at the laser edge with a 9 mm separation. At the matching lens level, the laser spots are tangent and roughly 15 mm wide. This double beam configuration has been chosen in order to increase by a factor 2 the emitted energy without increasing the risks of damaging the optical components, and for only 20% of laser total cost.

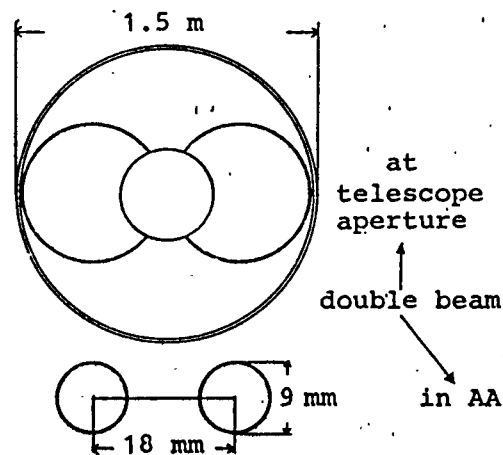


Fig.3 - Double beam configuration

3/ The transmitting/receiving/pointing package

The general design of this package is shown on Fig. 4. This system is mounted on the telescope and is moving with the telescope azimuthal motion. It has been designed in order to minimize the number of optical components encountered by the returns. The transmitted beam is entering the telescope after the matching lens (ML) and a reflection on a rotating mirror (RM1). This mirror itself starts the laser when in transmission position. Its speed is monitored by the computer in order to insure that the returns are entering the receiving path through the hole of the second rotating mirror, in fact a rotating hole (RM2). RM2 allows to send the pointed field on a COD camera and then to view the pointed area on a TV screen when RM1 is not transmitting nor RM2 receiving (most of the time).

A diaphragm adjustable from 5 to 60° is located at the telescope focus (F) on the return path. A dichroic glass (D) sends the green returns on the PMT through the filter wheel (FW) within an afocal system. The red way is free in R where an eye-piece can be used, waiting for a receiving package at 1.06 m.

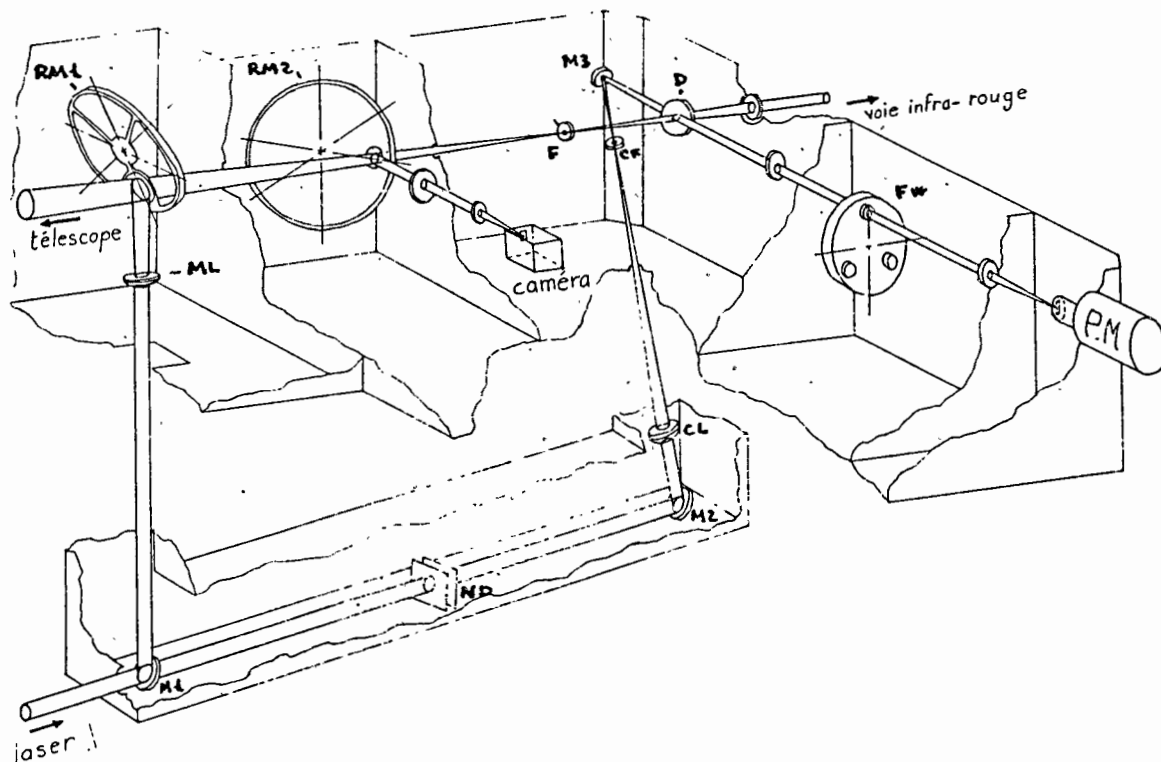


Fig. 4 - Transmitting/receiving/pointing package - See text for information.

The internal calibration path is shown on the same figure. The light transmitted by the first mirror M1 (lower left) is sent on the receiving package through neutral densities (ND) for attenuation, a second mirror M2 and a converging lens CL focusing the calibration in a point CF conjugate of the telescope focus. After M3, the calibration go through the dichroic glass (D) and follows the return path till the PMT.

4/ The computer and its environment

The new computer (PDP 11/73) has been installed in September 1985 and has monitored the ruby station ten months before the laser change. Its environment is shown on Fig. 5. The main characteristics of the configuration is that the PDP is not concerned with telescope pointing and guiding. At the beginning of each observing session, the data needed for pointing the Moon (9 reference craters and the five reflectors) and close stars are sent from the PDP to a microcomputer Victor S1. This small computer is sufficient for running the telescope for all the night with a very friendly software.

The PDP is thus only busy with the real time monitoring of the station : rotating mirrors enslavement, event acquisition (laser starts, internal calibration and in gate events), gate commands, ... The event-timer has one channel for the laser start and three other for events (calibration or/and gate events). Its resolution is 50 ps. A link is planned between the PDP and a CCD camera used for pointing stars or features on the Moon. It could be used for an automatic pointing (planned for the end of 1987). A data processing is made at the end of each series providing with the normal point (if there are identified returns). At the end of the night, these data can be used for a UTO determination.

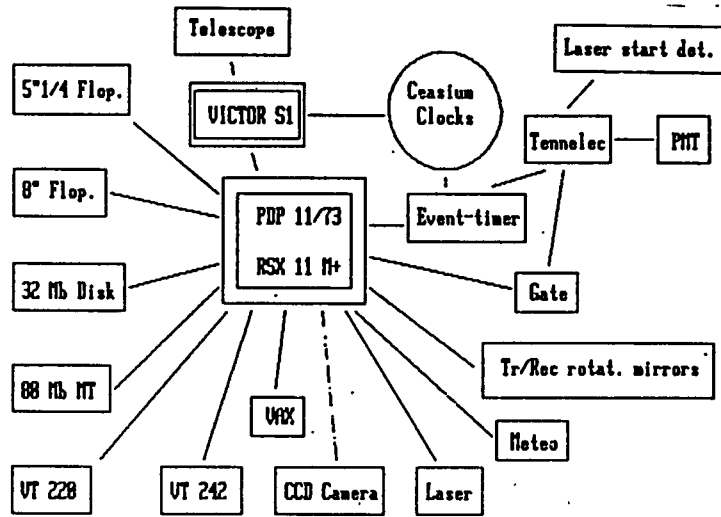


Fig.5 - Computer environment

The PDP is linked to the VAX computer located at the CERGA down and the normal points can be sent from the station on the VAX and from there on the CNES CDC computers.

5/ Conclusion

The system described here is working since the end of September 1986. It is planned to spend 6 months to test and improve the various components of the station recently modified or changed (laser, electronics, mechanics and software). It is thus too early to give some conclusions on the efficiency of the new station. The next paragraph added after the workshop will show the first results, but no information on energy or error budgets can be extracted from these data. The PMT, the laser and the internal calibration were not at there normal efficiency ... and the timing electronics was not tuned at this time for minimal jitters and biases.

The year 1987 should proof the quality both in accuracy and in efficiency that we hope to have with this new LLR station.

6/ First results ...

Fig. 6 shows a plot of the residuals for four normal points obtained in November 1986 (ns on the round-trip). The dotted line shows the fit done to determine UT0 from the data. It can be seen that the prediction used for the observations was very poor. The value finally found using X and Y prediction from BIH is :

$$UT0 - UTC = -0.09024 \text{ s } (\sigma = .00127) \text{ at } JD = 2446759.673591$$

The weighted rms of the residuals is 4.5 cm on the Moon distance.

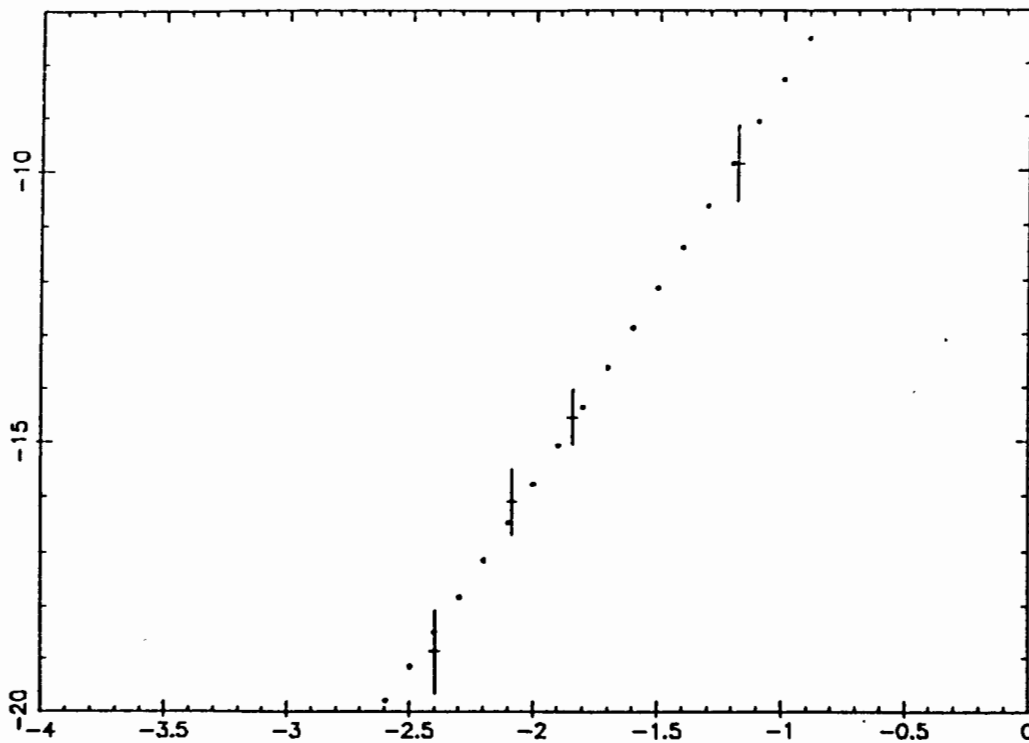


Fig. 6 - First normal point residuals - November 1986 - Residuals for four normal points in ns relative to the hour angle of the Moon (in hr). See text for more information

RECENT IMPROVEMENTS AND FUTURE PLANS AT THE UNIVERSITY OF HAWAII
LUNAR AND SATELLITE RANGING STATION

M.L. White
Lure Observatory
Institute for Astronomy
University of Hawaii
Kula, HI 96790

Telephone (808) 878-1215
Telex 7238459

ABSTRACT

Significant improvements have been made to the University of Hawaii laser ranging station during 1986. A new data processing and software development computer has been installed, and the real-time ranging computer has been upgraded. The ranging electronics and optical systems have been improved. These improvements and future station plans are discussed in this paper.

RECENT IMPROVEMENTS AND FUTURE PLANS AT THE UNIVERSITY OF HAWAII LUNAR AND SATELLITE LASER RANGING STATION

I. Computer Hardware Improvements

During 1986 at Hawaii, major improvements have been made to the computer hardware. Due to the increased demand on the ranging computer by lunar operations, and the necessity for on site lunar data analysis, a new Micro PDP-11 computer was purchased and installed at the observatory's administrative office in Waikoa. The new computer will free up the real-time ranging computer for operations, while allowing the majority of software development and lunar data analysis to be done at Waikoa. Future lunar data analysis requires near real-time normal point formation. The operation's crew will hand carry lunar data on a removable 26 megabyte disk cartridge to the Waikoa data processing center where the Micro PDP-11 will be used create normal points and earth rotation/polar motion solutions. The lunar data products will be entered on the G.E. Mark 111 system the morning after the data is acquired.

Concurrently, plans were developed and hardware purchased to expand the real-time operating computer backplane from 18 to 22 bits, increase the virtual memory to 1.25 megabytes and increase the data storage capacity to 52 megabytes. These changes will significantly speedup real-time execution and streamline operational procedures.

II. Optical Improvements

A new receive package was installed in the Multi-Lens-Telescope (MLT), greatly improving lunar ranging efficiency. During normal lunar operation the MLT alignment must be routinely compared to a guide camera to insure correct telescope pointing. The new receive package allows the operator to verify the telescope pointing and alignment by the electro-mechanical movement of a movie camera into the same location as the photo multiplier tube. The new receive package allows one operator to perform a task in several minutes which previously took two operators nearly 30 minutes.

The MLT has 160 individual turning mirrors which direct incoming light to a common focus. These turning mirrors were refastened after the epoxy, previously used to hold the mirrors in place, deteriorated. The deterioration of the epoxy caused the mirrors to become loose and unstable. The old epoxy was not as moisture resistant as expected. The new epoxy was applied in large quantities and is moisture resistant. A dramatic improvement in MLT alignment stability was observed as a result of applying the new epoxy. A complete MLT alignment is now required every 2 months rather than every 2 weeks.

A 1 angstrom bandpass filter was purchased and successfully tested in the lunar receiver. The double peak, polarized interference filter substantially improved the signal-to-noise ratio on illuminated lunar targets and during daylight lunar ranging.

Due to the unique design of the MLT, which consists of 80 individual light paths of varying lengths, a light pathlength compensator is needed. The compensator consists of 3 cylinders of solid glass that fit in the optical path of the MLT, delaying the longer path lengths. As is often the case with unique optical components, substantial fabrication time is required. After nearly two years since placing the order for the compensator, it is expected to be delivered by the end of 1986.

III. Ranging Machine Improvements

Plans to install a new Micro-Channel Plate (MCP) detector in the satellite and lunar systems have been approved. As part of the MCP package, new Tennelec discriminators will replace the currently used Ortec 934 discriminators. The new detectors are likely to be installed and acceptance tested by early 1987. Other future ranging machine improvements include new 50 pico-second vernier cards for the University of Maryland event timer currently used in the lunar system.

IV. Calibration

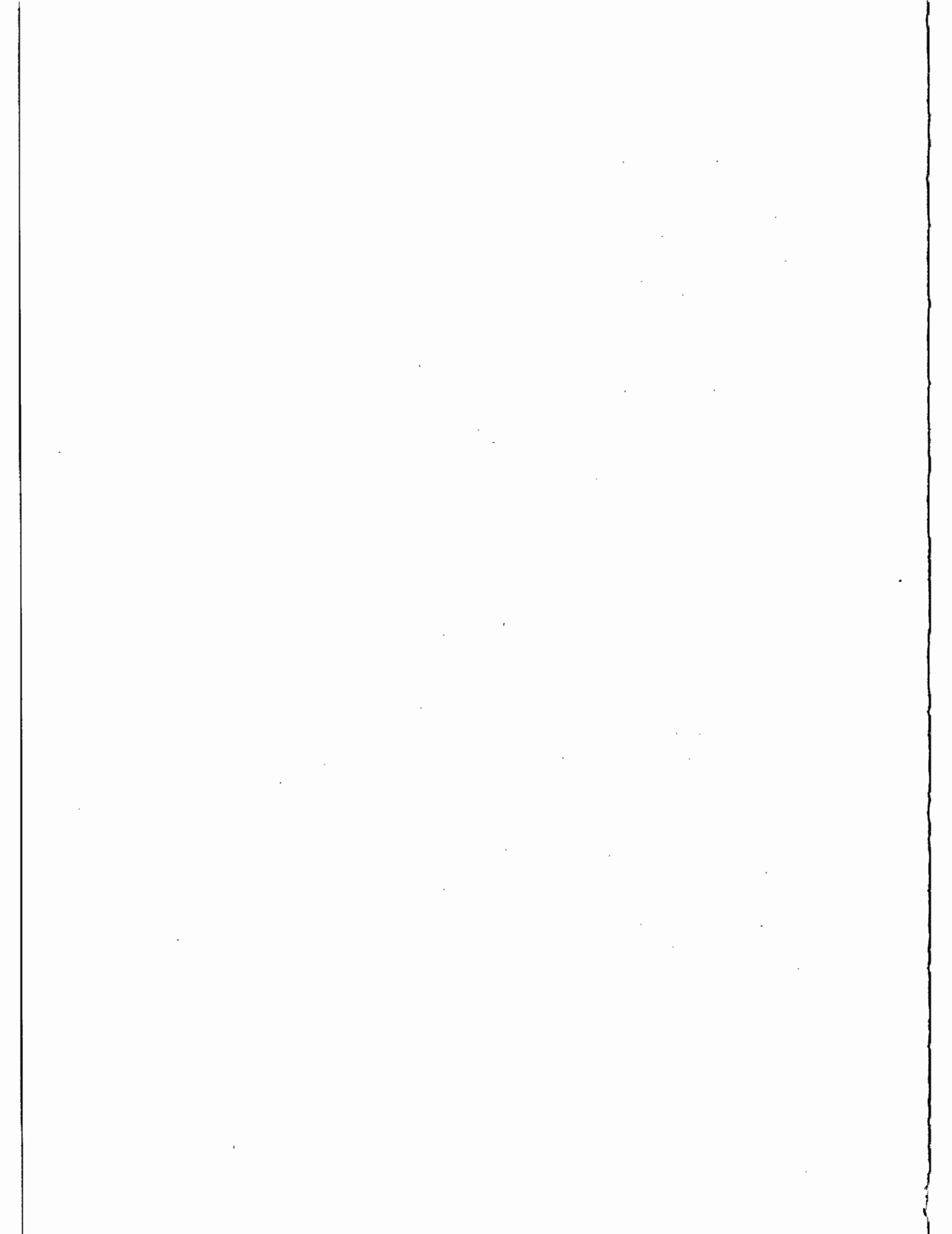
Currently, both the the lunar and satellite calibration are accomplished by ranging to an external calibration board located approximately 1 kilometer from the station. Internal calibration will be implemented by early 1987. The satellite system internal calibration will be easily accomplished due to the uniquely, simple design of the transmit/receive optics. The lunar system however, has a separate transmit and receive telescope making internal calibration more difficult. The use of a lengthy, single mode fiber optic cable will be required, and considerable testing will be necessary to verify calibration accuracy. Unlike the satellite system which uses a single stop epoch timer, the lunar system uses a multi-channel event timer, making real-time calibration possible. In both the satellite and lunar system the external calibration board will continue to be used as a verification of the internal calibration.

V. Observing Schedule

Over the past 2 years, the Hawaii ranging station has generally scheduled 2 observing shifts, back to back during the evening, Monday through Friday. The 2 shifts range to LAGEOS and the moon with LAGEOS as the first priority. This schedule resulted in a considerable loss of lunar data when optimal ranging times occurred over the weekend, and occasional loss of LAGEOS data, when LAGEOS moved out of the night-time window. As of August 1986, the station began scheduling one shift during optimal lunar ranging periods (including weekends), and scheduling the second shift to maximize lageos coverage. This new scheduling scheme, though sometimes complicated in the case of lunar scheduling, has greatly improved lunar coverage and contributed to increased lageos tracking efficiency.

VI. Conclusion

The University of Hawaii laser ranging station has provided very consistent state-of-the-art satellite ranging measurements to the scientific community for the past six years. During the past 3 years, the station has regularly provided lunar ranging data in quantities previously unobtained, and with normal point accuracies of less than 2 centimeters. The improvements discussed in this paper will allow the station to maintain state-of-the-art status by improving the ranging system accuracy and precision by a factor of 2 to 3, providing increased satellite and lunar coverage, and providing real-time earth rotation/polar motion solutions.



THE McDONALD OBSERVATORY LASER RANGING STATION : MLRS

J.R. Wiant, P.J. Shelus
McDonald Observatory and Department of Astronomy
University of Texas at Austin
Austin, Texas 78712-1083 - USA -

Telephone (512) 471 4461
TWX 910874 1351

ABSTRACT

Since the last Workshop of this type, which had been held in England some two years ago, a number of changes have been made with respect to laser ranging operations at McDonald Observatory near Fort Davis, Texas. First and foremost is the fact that all lunar operations on the 2.7 m (107") McDonald reflector have been discontinued and our entire operations, both lunar and LAGEOS, have been totally assumed by the stand-alone, dedicated 76 cm (30") based system now known as the McDonald Laser Ranging Station, MLRS. Since the MLRS system has been the subject of many reports in the past, this paper will only summarize the up-grades and improvements which have been made to that system over the past two years. These improvements include, but are not limited to, a new high-energy, short-pulse Quantel Nd-YAG laser capable of ranging both to the moon and to LAGEOS, a second Data General NOVA-based computer and Winchester-type hard-disk system providing for improved observing capabilities as well as for data pre-processing and analysis, the installation of 21-bit encoders and a new telescope bearing for improved tracking and pointing, as well as new timing and photomultiplier equipment. All of the relevant changes will be presented and discussed together with the impact of those improvements on the MLRS data yield, both with respect to the moon and to LAGEOS.

This work is being supported by the National Aeronautics and Space Administration under Contract NAS5-29404 to McDonald Observatory and the University of Texas at Austin from the Goddard Space Flight Center in Greenbelt, Maryland.

Introduction

The McDonald Observatory and Department of Astronomy of the University of Texas at Austin continues to operate the McDonald Laser Ranging Station (MLRS) for the NASA Crustal Dynamics Program under contract to Goddard Space Flight Center. The MLRS is a dual purpose installation designed for laser ranging operations to both lunar and artificial satellite targets. The station is located on the grounds of the Observatory, about 17 miles north of Fort Davis, Texas. Various operational, programmatic, and logistical support is also provided by several personnel associated with the Department of Astronomy on campus at the University of Texas in Austin. Since the MLRS system and its operations have been the subject of so many reports in the past, this paper will only summarize the up-grades and improvements which have been made to that system over the past two years (since the last laser ranging workshop).

Hardware Changes

The 18-bit absolute encoders on both axes of the alt-alt telescope were removed and replaced with 21-bit encoders. Only minimal software changes were required to take full advantage of the increased angular resolution and the expected pointing and tracking improvement was recognized immediately. The full extent of MLRS pointing and tracking capabilities has still not been fully realized however because of suspected bearing problems (especially for the telescope yoke). Work on this sub-project continues.

A single, short-pulse, dual-power laser was supplied to us by NASA/Goddard to replace the original two-laser system of the MLRS. With the help of Grant Moule, from the Australian laser ranging station at Ororral, this new laser went from shipping crate to operational status at the MLRS within nine calendar days. The advantages of the new laser system over the old are numerous. Alignment and calibrations need now only be performed for a single laser. There is possible a very rapid changeover from lunar to LAGEOS operations and vice-versa (~20 seconds). A more convenient physical arrangement allows for easier maintenance. And, of course, the ability to range the moon with a 200 picosecond pulse (instead of the 3 nanosecond pulse of the former system) has not been lost on the LLR analysts.

The Varian "super-tube" photomultiplier was recovered from the TLRS, when that system was up-graded to a more powerful laser, and this new tube was then incorporated within the MLRS. This new PMT has been observed to reduce the RMS of both the internal calibration and the data themselves by a factor approaching two over their former values. Further, the Varian is considerably less "noisy" than the previous tube used. A cloud on the horizon is the possible contamination of data quality caused by a potential time-dependent "beam-walk" problem across the face of the tube.

In order to establish the capability of performing simultaneous data acquisition and data reduction at the MLRS, some additional funding provided to us by the U. S. Naval Observatory allowed us to purchase and install an entire second Data General Nova computer system within the MLRS operating environment. In addition to a new CPU, there were two 160 M-Byte Winchester disk systems (with associated dual-controllers), an additional 9-track magnetic tape deck, and various communications peripherals purchased. As an additional benefit of this new computer system is the fact that two data streams can be simultaneously processed (when no observing is being performed) and we can temporarily share equipment to retain full observational capability (at the expense of data reduction) if there is an equipment failure. An IBM PC/AT Microcomputer was purchased with various peripheral hardware and software items as we seek to do "smart" terminal emulation in anticipation of the eventual "death" of our old and venerable Tektronix 4025 graphics terminals. Finally, an Apple Macintosh PC microcomputer was purchased for documentation preparation, the making of schematic

drawings, monthly reporting, and direct file transfers between the Austin and the Observatory portions of this project.

In an attempt to alleviate as many seeing-related problems as possible at the MLRS, an air conditioning unit was purchased and installed in the MLRS telescope room. This unit provides active temperature and humidity control during non-operating hours. Operations have been streamlined since this installation because far less time need now be spent in waiting for the telescope to come to thermal equilibrium with its surroundings after the dome has been opened in anticipation of ranging operations.

Finally, after 15 years of faithful service, our LORAN-C receiver has been retired. Its role in providing accurate epoch monitoring at the station has been taken over by a Global Positioning System (GPS) receiver. Also, we have abandoned our attempts to incorporate the computer controlled narrow-pulse filter in the MLRS receive system.

Software and Logistical Changes

As might be expected, a myriad of software changes were incorporated into the MLRS computing systems in concert with most of the hardware changes mentioned above. Fortunately, because the MLRS was originally designed to be a software intensive one, these software changes could be designed, coded, and debugged "off-line", well before the implementation of the actual hardware changes. Thus, in most instances, they could be incorporated into the system without requiring additional station down-time except for that which was required for the actual hardware changes themselves. Further, many routine changes were made in the data processing systems to accommodate data format and electronic communications up-dates and up-grades. Again, each of these was completed and implemented with a minimum of difficulty, all the time maintaining active communications with the outside world.

As far as MLRS observing operations go, it is safe to say that since December 1985, the station has finally realized a large percentage of its original observational potential. Day-time LAGEOS ranging is now accomplished with the same ease as night-time ranging and the lunar system has become as reliable as the 2.7-m system was. In reality, over the past year or so, only the weather has been our major problem (see the illustration of MLRS data statistics for both the moon and LAGEOS). With that in mind, a great deal of time and effort has been expended to examine the trade-offs between cost and data throughput to provide for the most cost effective operation of the dual lunar and artificial satellite capabilities of the MLRS. To that end we have strongly recommended that a minimum of two-shift operation always be present at a dual-capable station like the MLRS. In that scenario, one of the shifts is relatively fixed in an eight hour per day, five day per week schedule to concentrate on the LAGEOS target. The second shift is quite variable and "chases the moon" as efficiently as possible, in concert with whatever physical and personnel constraints may exist. Each shift, wherever possible, attempts to take the other crew's target as a "target of opportunity". To the best of our ability and within the constraints of our budget, those are the procedures which we try to emulate at the MLRS.

Using this scenario for our observing operations, it is easy to see that the scheduling of the LAGEOS crew is quite straightforward and can be implemented with little difficulty. For maximum lunar data throughput things get a bit more difficult. We attempt to maximize our coverage at the lunar quarters (completely ignoring week-ends). During a lunar ranging session we attempt to obtain a minimum of three Apollo 15 reflector observations with as wide an hour angle spread as possible; all remaining time is spent on observing the other three accessible lunar targets and/or observing any potential LAGEOS "targets of opportunity". At the present time, a successful lunar observation is considered to be made when a total of 25 photon returns have been identified (in real-time) by the observing crew.

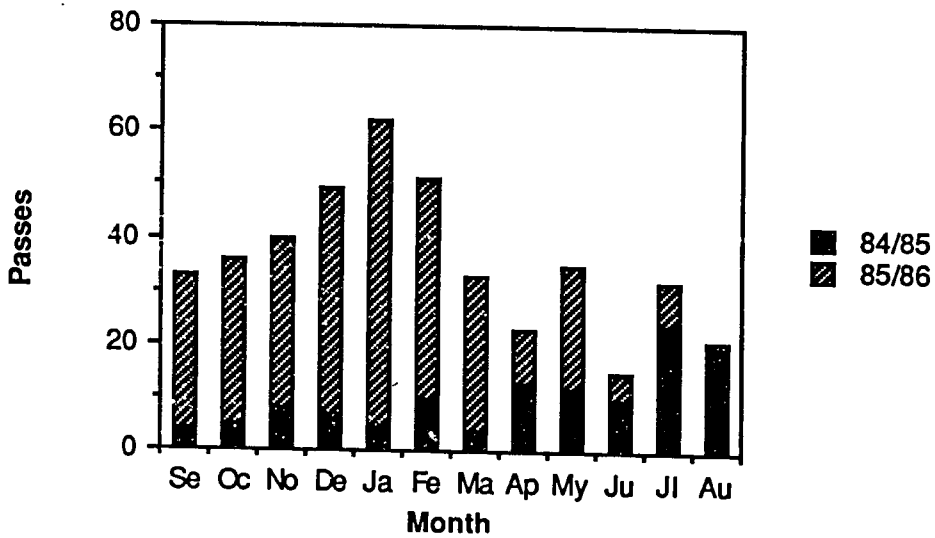
On other matters, as reported elsewhere in these workshop proceedings, we have established real-time Earth orientation computations at the MLRS, using lunar data. Normal lunar laser ranging data is identified, filtered, compressed, formatted, and analyzed on-site, and when sufficient data exists, an Earth orientation reduction is performed. The results are electronically transmitted to the U. S. Naval Observatory (and to other interested parties), usually within hours of the data taking.

Finally, the MLRS Operational Readiness Review was satisfactorily completed in the summer of 1985, testifying to the fact that the MLRS has indeed taken its place in the world among the other fine stations in the international laser ranging network. The road to the completion of the MLRS was a long and a hard one and, at times, many of us had our doubts as to whether or not it would ever come up to the standards which were set by our old 2.7-m system. To the future, we look forward to the time when the MLRS might be moved from its present "saddle-site" to one which is much more favorable, in order that it might be truly raised to its full observational potential.

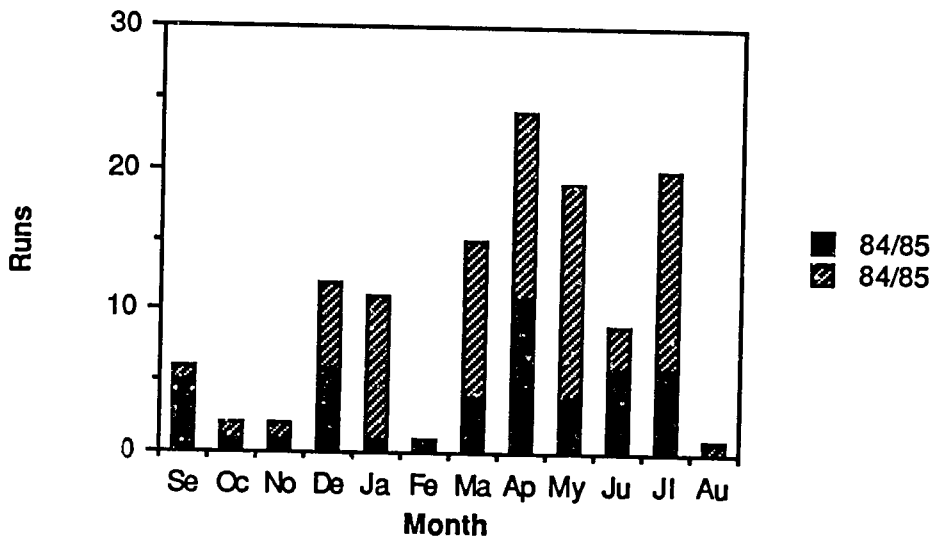
Acknowledgements

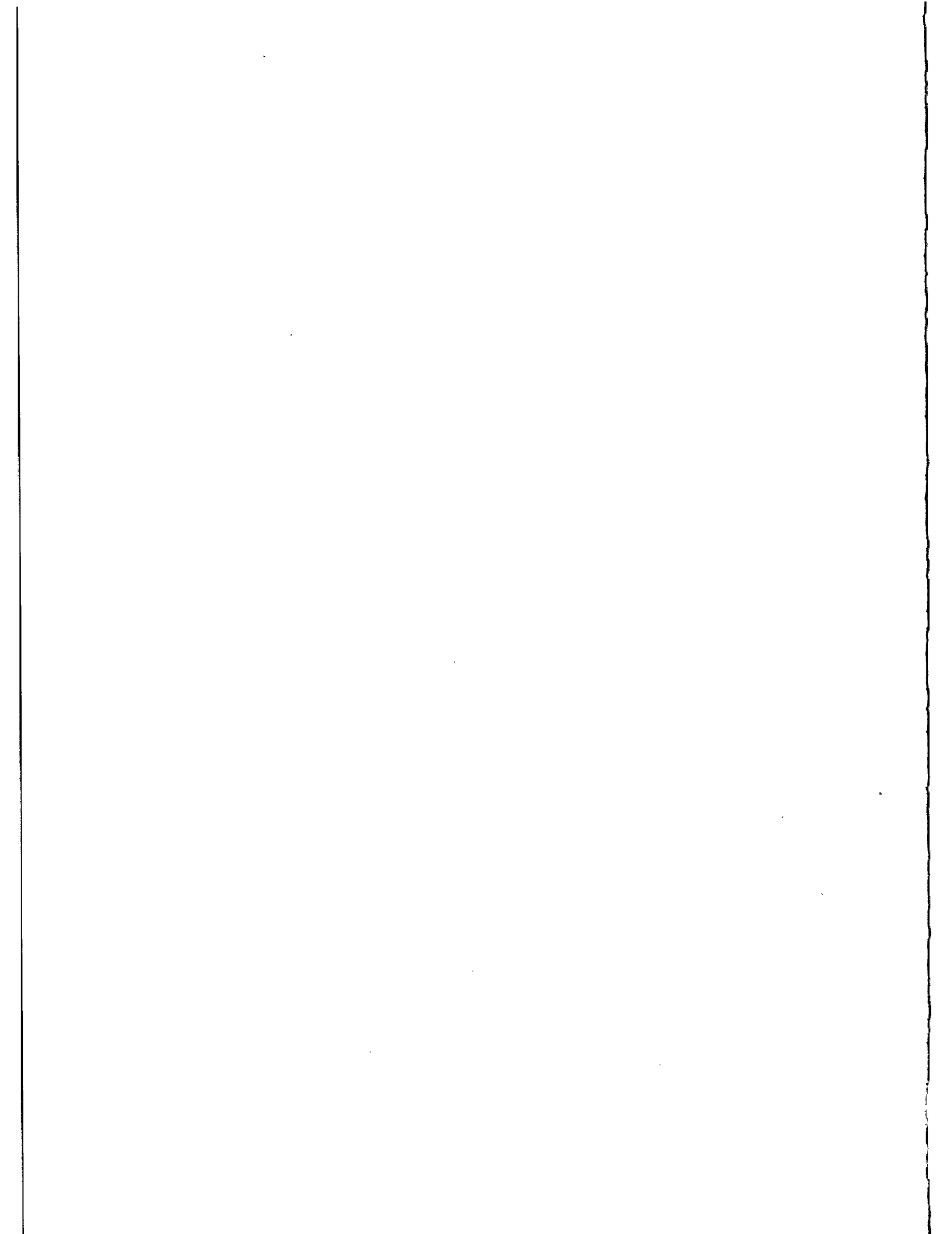
The authors acknowledge that this work is being supported at McDonald Observatory and the University of Texas at Austin by National Aeronautics and Space Administration Contract NAS5-29404 out of Goddard Space Flight Center, Technical Officer Mr. Robert L. Appler.

MLRS/LAGEOS Statistics



MLRS/Lunar Statistics





START DETECTOR FOR THE MODE LOCKED TRAIN LASER RADAR

I. Prochazka
Czech Technical University
Faculty of Nuclear Science and Physical Eng.
Brehova 7, 115 19 Prague - Czechoslovakia -

Telephone 848 840
TWX 121254 FJFI C

ABSTRACT

The start detector + discriminator for the mode locked train laser radar is described. The device is based on the semiconductor optical switch. The jitter test experiment using streak camera and the optical sampling application of the detector is described.

START DETECTOR FOR THE MODE LOCKED TRAIN LASER RADAR

I. Procházka

The Interkosmos laser radar is using the mode locked train transmitter since 1983 /1/. The laser emits the train of pulses HAFW<30psec, spaced at 2.00 nanoseconds (see fig.1). To start the ranging electronics channel, the appropriate detector/discriminator capable of responding to the train of pulses was to be developed. The most common set up consisting of fast photodiode followed by constant fraction discriminator is far from optimum, because no discriminator available is able to respond to a single pulse from a narrow spacing train with low jitter. A special type of a fast fixed threshold detector/discriminator was developed by Cech /2/ and applied 1983-85. It was based on the fast photodiode followed by tunnel diode monostable circuit and pulse forming circuit. The jitter and time walk 150psec at the dynamical range 1:2 was achieved. To meet the high requirements of picosecond ranging using the train, the new principle of detector/discriminator was developed.

Its electrical scheme is on fig.2. The circuit is based on the in house built semiconductor opto switch (OS). The switch is working in the avalanche regime generating on its output the uniform signal (see fig.3) of several volts with fast leading edge 10mV/picosec. The OS switches at the fixed signal level, thus the first pulse higher than this level is causing generation of the electrical output pulse. Taking into account the pulse duration <30psec, the fixed threshold discriminator technique is no drawback for the application.

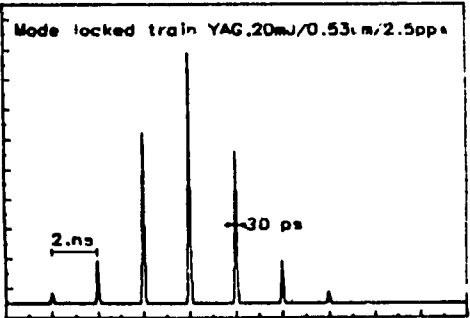
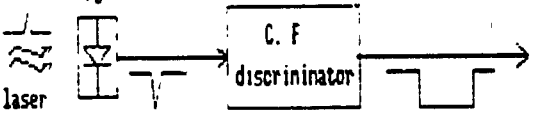
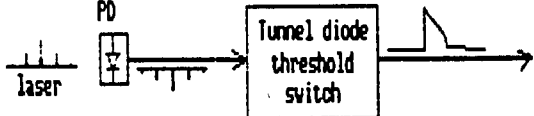
The jitter of the device was tested and the circuit optimised using the train of 10-30psec laser pulses and a streak camera (Hamamatsu 979) as a detector. The camera was triggered by the circuit output, the laser pulse was displayed. The digitised data from the camera were processed in the on line computer. The jitter of the device may be determined from fluctuations of the pulse position on the streak screen taking into account the trigger jitter of the camera itself (18psec measured by the manufacturer). On fig.5 there is a plot of consequent streak records. The excellent overlap of the pulses/trains may be seen. Using a streak camera, the jitter ranging 10-40picosecond was measured. The actual value of the jitter depends on the laser pulse length and amplitude fluctuations. Using pulses longer than 50picoseconds, the trigger jitter was about 0.4 times the pulse length.

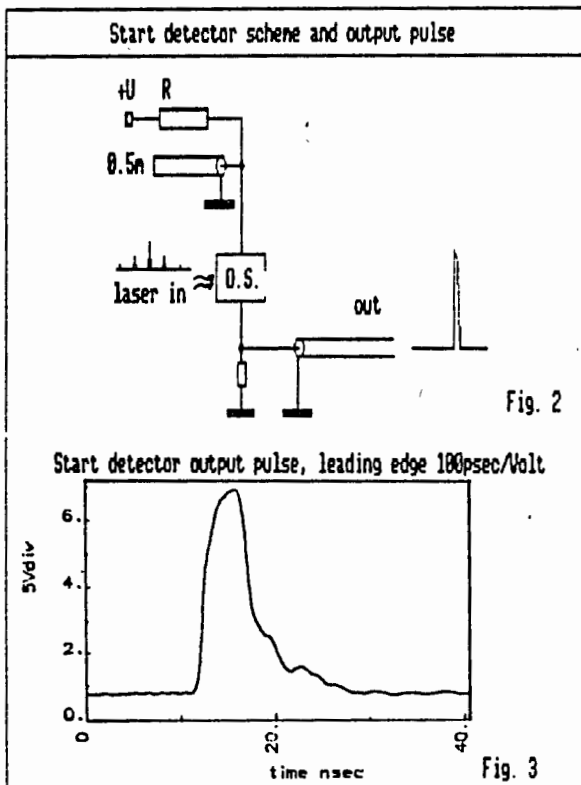
Using two identical circuits set to different trigger levels and a high resolution time interval meter, the simple sampling scheme may be constructed. One detector starts the counter the second it stops. On fig. 6 there is a histogram of measured times. The peaks separation corresponds to the laser resonator round trip, the peaks width determines the jitter $(2 \times \text{Start} + \text{counter})$ typ. 50-70psec. The quality of mode locking may be estimated from the background. For comparison, on fig.7 there is the analogical histogram of measurements taken on the passively

mode locked laser oscillator incorrectly adjusted, transmitting multiple pulses. The laser output was monitored simultaneously on the streak camera. The background is of order higher. Thus, the pair of the START circuits may be used for quick check of the mode locked train transmitter in the quasi sampling mode with effective bandwidth of 5GHz. The possibility to monitor the mode locking quality is attractive especially in connection with passively mode locked laser for picosecond pulses generation.

Literature

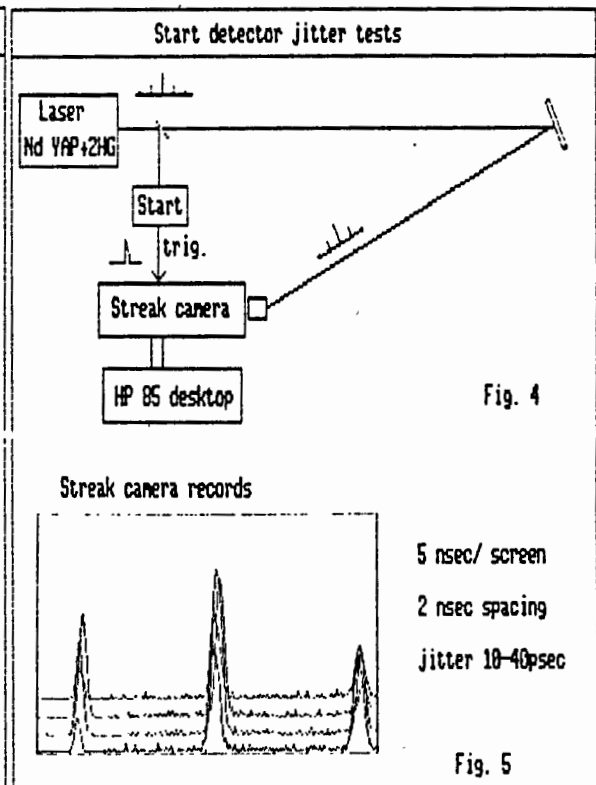
- 1/ K.Hamal et all, Interkosmos laser radar, version mode locked train proceedings of 5-WLRI, Herstmonceux, Sept. 1984, edited by J. Caignebet
- 2/ M.Cech, Start discriminator for the mode locked train laser, in /1/

| Start detector requirements | Available start detector/discriminator schemes |
|---|---|
| <p style="text-align: center;">SLR Transmitter output pulse</p>  <p style="text-align: right;">Fig. 1</p> <p>Requirements:</p> <ul style="list-style-type: none"> - process train of psec pulses with few (1..6)nsec spacing - low jitter < 50 psec - dynamical range > 10 : 1 - rugged and simple - simple adjustment/test procedures | <p>1/ Standard scheme :</p>  <ul style="list-style-type: none"> - not applicable for mode locked train of pulses with nsec spacing because of C.F. discriminator time response <p>2/ Scheme by M.Cech (5-th WLRI, Herstmonceux, 1984)</p>  <ul style="list-style-type: none"> - applied in Helwan, 1983..1985 nissions - jitter/time walk 150 psec / dyn.ratio 2:1 only - delicate set up |
| <p>I.Prochazka Start Detector For Mode Locked Train Laser Radar</p> <p style="text-align: right;">1</p> | <p>I.Prochazka Start Detector For Mode Locked Train Laser Radar</p> <p style="text-align: right;">2</p> |



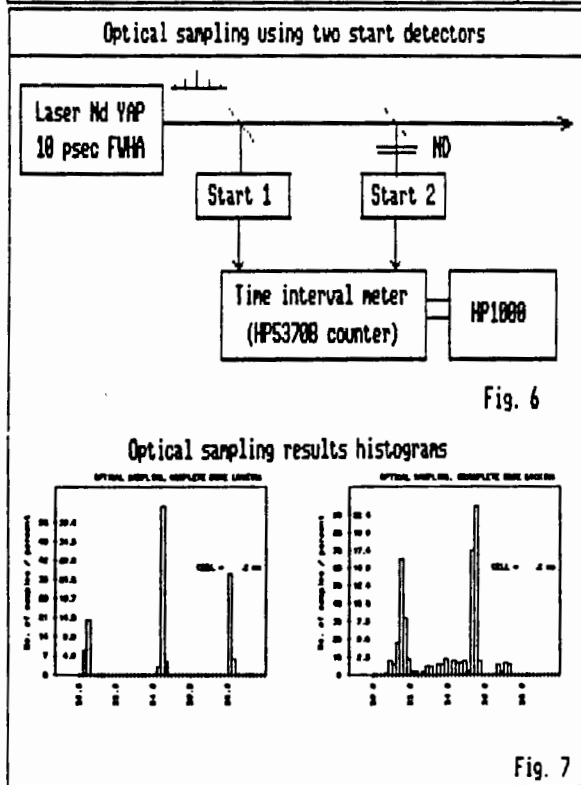
I. Prochazka
Start Detector For Mode Locked Train Laser Radar

3



I. Prochazka
Start Detector For Mode Locked Train Laser Radar

4



I. Prochazka
Start Detector For Mode Locked Train Laser Radar

5

Start detector summary

Start detector/discriminator performance:

- process train of picosecond ML pulses with nsec spacing
- fast fixed threshold discrimination
- uniform, high amplitude output
- internal delay (1 nsec
- jitter (40 psec
- dynamic range) 20 : 1
- optical sampling capability :

* passive mode locking check

* equivalent bandwidth 5 GHz

- changing bias voltage, serves as a laser monitoring PD
- applied in Helwan 1986,

calibration ranging jitter before 520ps after 300 ps

system stability before 150ps after 120 ps

I. Prochazka
Start Detector For Mode Locked Train Laser Radar

6

· AMBIGUITY AND RESOLUTION OF A MODE-LOCKED
PULSE TRAIN LASER RADAR

R. Neubert, B. Ritschel, L. Grunwaldt
Academy of Sciences of G.D.R.
Central Institute for Physics of the Earth
Telegrafenberg A 17, Postdam 1500 - G.D.R. -

Telephone
Telex 15305

ABSTRACT

The accuracy of a multipulse laser radar has been studied with indoor experiments and computer simulation. For the experiments a mode-locked Nd-YAG laser producing 7 to 9 pulses of 4.6 ns spacing at 10 Hz repetition rate is used. The frequency-doubled pulses are divided by a beamsplitter and recombined at the photomultiplier which is working at the single photoelectron level. The time-of-flight data are treated by cross-correlating the empirical distributions corresponding to the two light paths. This leads to an estimate of the time-of-flight difference. Using a large amount of data sets the following parameters are determined :

- a) The percentage of estimates shifted by more than half a pulse spacing.
- b) The standard deviation of the unshifted estimates.

For the parameters of our system, the percentage of "good" estimates is higher than 90 % if more than 200 measurements are used. A standard deviation of about 100 ps is obtained under the same conditions. These results are obtained using electrostatic PMT's with about 500 ps jitter. Good agreement between the experiments and computer simulations is found. Thus the simulation method is used to determine the system performance in a wider parameter range.

The use of the full mode-locked pulse train for laser radar is advantageous because of laser simplicity and efficient use of its energy. However, because of the ambiguity problem, this concept found only limited applications as yet [1], [2]. The ambiguity of such a laser was discussed in an earlier paper [3] on the basis of computer simulation. In the following we report on comparison of the simulation results with laboratory experiments.

Experimental setup

The simplified optical diagram of the setup is shown in Fig.1. The signal of the mode-locked Nd-YAG laser is split into three parts. A first part is reflected by a beam splitter (BS) to a silicon photodiode (PD) which is connected to the start input of the PS-500 time interval counter via a leading edge trigger. The stop receiver (usually a PMT) is illuminated with very weak signals reaching it along two different ray paths:

- the short calibration path 1
- the longer ranging path 2

The attenuation to the single-photoelectron level is achieved by neutral density filters (F). By choice of the filters, the signal level is adjusted in such a way, that 10 to 50% of the laser shots are causing the emission of one electron from the PMT photocathode. Thus, the stop of the counter occurs randomly by a photon arriving along path 1 or path 2. The single-photoelectron pulses from the PMT are detected by a constant-fraction discriminator [4] to reduce the timing noise caused by PMT gain fluctuations.

The main specifications of the passively mode-locked Nd-YAG laser, which has been designed in our laboratory, are given in Table 1.

Table 1: Specifications of the Nd-YAG laser

| | |
|--|---|
| Energy of pulse train ($\lambda = 1.06 \mu\text{m}$) | 3 mJ |
| Number of pulses per train | 7-9 |
| Pulse separation | 4.6 ns |
| Pulse width | 68 ps *) |
| Repetition rate | 10 Hz |
| Laser rod dimensions | 5 x 75 mm. |
| Optical resonator type | large radius mirrors |
| Resonator length | 69 cm |
| Modelocker | Soviet dyes 3955 or 3274 in methanol |

*) Average value for $\lambda = 1.06 \mu\text{m}$, estimated by the two-photon fluorescence method

For second harmonic generation, a KDP crystal is used. To

have definite polarization of the laser, Brewster plates are introduced into the optical resonator.

Time resolution tests

Starting point for the analysis of the measurements is the frequency distribution (histogram) of the time-of-flight values. This distribution is calculated usually from 1000 measurements. A typical example is shown in Fig.2. To determine the resolution of the system, the part of the distribution corresponding to one ray path is necessary only. As an example the left-hand part of Fig.2 is plotted in Fig.3 with higher resolution of the abscissa. The pulse structure of the laser is well resolved, but to take into account the partial overlap of the individual pulses, the distribution is analyzed using a least-square fit of a sum of Gaussian functions. To reduce the number of free parameters, the separation and width of the peaks have been assumed to be equal. The RMS width of the peaks obtained in this way can be used as a measure of the overall time resolution. The most important contribution to the timing noise is the fluctuation of the PMT delay (jitter). This quantity depends on PMT type and sample and its working conditions (voltage divider, illuminated area). Some contributions are also given by the amplitude fluctuations. This effect depends on the discriminator performance. Some results of resolution tests for different PMT tubes obtained in earlier experiments are shown in Table 2.

Table 2: Time resolution of the system

| PMT type | Sample No. | RMS - Jitter (ps) *) | |
|--------------|------------|----------------------|----------------|
| | | No diaphragm | 1 mm diaphragm |
| RCA C 31034A | 47105 | 540 | 370 |
| FEU 79 | 4665 | 530 | 530 |
| FEU 136 | 2053 | 600 | 470 |

*) Overall jitter including start, i.e. no deconvolution applied. Start photodiode type SP 109 directly connected to the counter (HP 5370 in these experiments).

It can be seen that the restriction of the illuminated area has some effect on the resolution, especially for the RCA C 31034A tested. The best resolution was obtained with this tube as yet, but with selected samples of other electrostatic PMT even better results might be attained. To determine the contribution of the start-time noise, some experiments were carried out using a silicon photodiode for the stop too. Using the HP 5082-4220 type in both channels, a RMS resolution of 300 ps was obtained. This value could be improved to 150-200 ps using the fast SP 109 photodiode (VEB Werk fuer

Fernsehelektronik Berlin). Assuming that the start- and stop-time fluctuations are equ. and independent in this case, the RMS start-time noise can be calculated to be 100-140 ps. For the experiments with PMT receiver, the SP 109 was always used. Thus, the jitter of the RCA C 31034A can be estimated by quadratic subtraction of the start noise to be around 350 ps. From this example it can be seen, that the start-time noise has only small influence on the overall resolution in our experiments.

The precision of the cross-correlation method

The generally adopted method for treating the data of a mode-locked train laser radar is to calculate first the frequency distributions of the calibration- and the ranging-measurements separately, and then to determine the time shift for maximum correlation of the two distributions. An example distribution is shown in Fig.2. The two subdistributions according to path 1 and 2 are well separated from each other by roughly 60 ns. Convolutin^r both distributions, Fig.4 was obtained. In this figure the convolution sum is plotted like a polygon linking the points separated by the bin width of 250 ps. The maximum can be determined very accurately using some interpolation method. In our case we obtain for the time shift of maximum correlation (61.16 ± 0.1) ns.

To investigate the precision of the method, the measurements of this and several other experiments were arranged into groups. Then the cross-correlation method was applied to each group so that an ensemble of time shifts is obtained from which statistical estimates for the precision can be gained. The parameters under consideration are:

1. the percentage of time shift results deviating from the real value not more than half a pulse separation (this quantity called "uniqueness")
2. the RMS error of the results deviating not more than half a pulse separation

These parameters are plotted in Fig. 5 and 6 in dependence of the quantity of measurements. As a normalized measure of the data quantity we are using $(1/n_1 + 1/n_2)^{1/2}$, where n_1 and n_2 are the number of measurements for path 1 and path 2, respectively. This is just the probable error of the ranging average for a single pulse system, expressed in terms of the standard deviation of a single time interval measurement. To estimate the uniqueness (resp. ambiguity) and precision from the measurements, 10 runs of 1000 points each are used. The total ensemble of 10000 measurements is arranged into groups of $n_1 + n_2 = 60, 120, 240, 480$ individual measurements. For each group the cross-correlation method is applied resulting in the generation of an ensemble of ranges from which the interesting average parameters are estimated. The return rates for the two light paths are slightly changing

from run to run. Therefore averages for the parameter $(1/n_1 + 1/n_2)^{1/2}$ have to be determined also. The resulting experimental values for the uniqueness and precision are plotted with the symbol "+" in Fig. 5 and 6.

For comparison with theoretical values and to obtain more general results (including different shapes of the laser signal like reduced pulse numbers), computer simulations were carried out assuming the photodetection process to be described by Poisson statistics and the timing jitter to have a Gaussian distribution. The simulator is a pseudo random number generator which outputs two possible numbers: 0 (corresponding to no detection) and 1 (detection). The probabilities of the two states are determined by the average number of photoelectrons (s) of the pulse according to:

$$P(0) = \exp(-s); \quad P(1) = 1 - \exp(-s)$$

The simulator is called for each consecutive pulse of the group using the pulse intensities as input parameters. When the first positive answer occurs, the corresponding pulse number is stored together with some added Gaussian timing noise. By repeating this process, 5000 simulated time intervals for both the calibration and the ranging channel are generated and stored into the memory. In this process, the average return rate for the calibration is set to be 50% and for the other channel 25%.

To estimate now the performance parameters of the system in dependence on the amount of measurements, example realizations are selected from simulated measurements and then treated by the cross-correlation method in the same way as is done with the real measurements. The selection of the individual values from the memory is done by calling an equally distributed pseudo random number generator to determine the addresses. 500 example realizations are used to estimate the performance parameters, i.e. the uniqueness and the RMS error of a cross-correlation result.

To compare the experimental values with the simulations, the average shape of the time interval histogram is needed. It has been approximated by 9 Gaussian peaks with Gaussian envelope according to

$$h = a_0 \sum_{k=-4}^4 \exp(k^2/U) \cdot \exp((t - t_k)^2 / 2\sigma^2) \quad (1)$$

The average experimental parameters are $U = 4.61$, $\sigma = 386$ ps. The separation of consecutive pulses is

$$\Delta t = t_{k+1} - t_k = 4.55 \text{ ns.}$$

So the relative resolution is $C = \sigma / \Delta t = 0.0848$. Using these parameters the results marked in Fig. 5 and 6 by "*" are generated. They agree reasonably well with the experimental points, especially for the uniqueness (Fig.5). This

agreement is somewhat surprising because the laser pulse shape fluctuations are not directly modelled in the simulations. Instead, the pulse shape is chosen in agreement with the observed histograms. Note further that the simulated results showed almost no dependence from n_1 / n_2 if the above introduced parameter $(1/n_1 + 1/n_2)^{1/2}$ is kept constant. This is proved in the range $n_1/n_2 = 1 \dots 10$.

For the conditions used in our experiments, the following conclusions can be drawn:

- the performance of the system can be reasonably well determined by the described simulation method
- 200 measurements for both calibration and ranging are required to have 90 per cent probability of correct assignment of the data (not shifted by a multiple of the pulse separation)
- the standard deviation of a result generated from 200 measurements is in the order of 100 ps.

The good representation of the experiments by the simulation encouraged us to study the dependence of the system performance from the laser pulse shape and the timing resolution more detailed. Some of the results are graphically represented in Fig.7 and 8. In these figures, both the uniqueness parameter (broken lines, 1 at the vertical scale corresponds to 100%) and the ratio of the RMS error of the cross-correlation result to the single-shot timing jitter (full lines) are plotted in dependence on the amount of measurements. The relative RMS error as defined describes the effect of averaging.

In Fig.7 for a fixed laser pulse shape the influence of the timing resolution is represented. As a measure of the resolution, the parameter C (defined as the ratio of the overall RMS jitter of the timing system to the pulse separation of the laser pulses) is used. The time resolution is visualized by the probability distributions of the time intervals, i.e. the shapes of the histograms for very large amounts of measurements.

As can be seen from Fig.7, the timing resolution has a very small influence on the uniqueness (resp. ambiguity) but some effect on the relative RMS error. This behaviour is to be expected. We conclude from Fig.7 that the resolution parameter C should be smaller than 0.2. Note that for a given resolution of the timing system, the parameter C can be adjusted by the separation of the laser pulses which is possible by choosing the laser resonator length.

The number of pulses in a laser pulse group is represented by the parameter U. More precisely, this is the overall width of the probability distribution of the time intervals according to equ.(1). The parameter U is chosen to be $U = 6$ in Fig.7.

The dependence of the system performance on the parameter U

for a fixed resolution ($C = 0.1$) is shown in Fig.8. As expected, the parameter U has almost no effect on the error, but strong influence on the ambiguity. Fig.8 may be used to determine the amount of data to reach a given uniqueness level. A uniqueness of 90% in connection with $U = 2$ is reached for $n_1 = n_2 \approx 50$. For $U = 1$ only 20 measurements are needed in both channels to reach 90% uniqueness. There are some methods to minimize the parameter U including laser design, the combined use of nonlinear optical effects and well matched start detectors. With generally available technology, $U = 1..2$ should be a realistic value.

Conclusion

From the results of this study we conclude that the mode-locked train laser radar remains to be an attractive variant. Its main limitation, the ambiguity, can be reasonably overcome using a sufficient data quantity. The minimum data amount for a given probability of correct assignment can be gained from this paper. As a guide to good performance, one should restrict the number of pulses per group to a minimum and adjust the pulse separation to roughly 10 times the timing jitter. A special advantage of the rigorous use of single photoelectron detection is the low level of systematic errors. This gives the possibility to attain normal point errors near 1 cm even by using conventional electrostatic photomultiplier tubes.

REFERENCES

- [1] Silverberg, E.C.: The Feedback Calibration of the TLRS Ranging System
Proc. 4th Intern. Workshop on Laser Ranging Instr.,
Austin 1981
Edt. P. Wilson, Bonn 1982, p. 331-37
- [2] Hamal, K. et al.: INTERKOSMOS Laser Radar, Version Mode-Locked Train
Proc. 5th Intern. Workshop on Laser Ranging Instr., vol. II
Herstmonceux 1984
Edt. J. Gaignebet, Bonn 1985, p. 214-18
- [3] Neubert, R.: Simulation Studies on the Statistics of a Multipulse Laser Radar Working at the Single Photoelectron Level
Nabl. Isk. Sput. Zemli, Prague 23 (1984), p.93-102
- [4] Fischer, H.: Empfangsdiskriminator fuer Satellitenentfernungsmessung mit verbessertem Zeitverhalten
Radio Fernsehen Elektronik, Berlin 31 (1982) 8, p.491-92

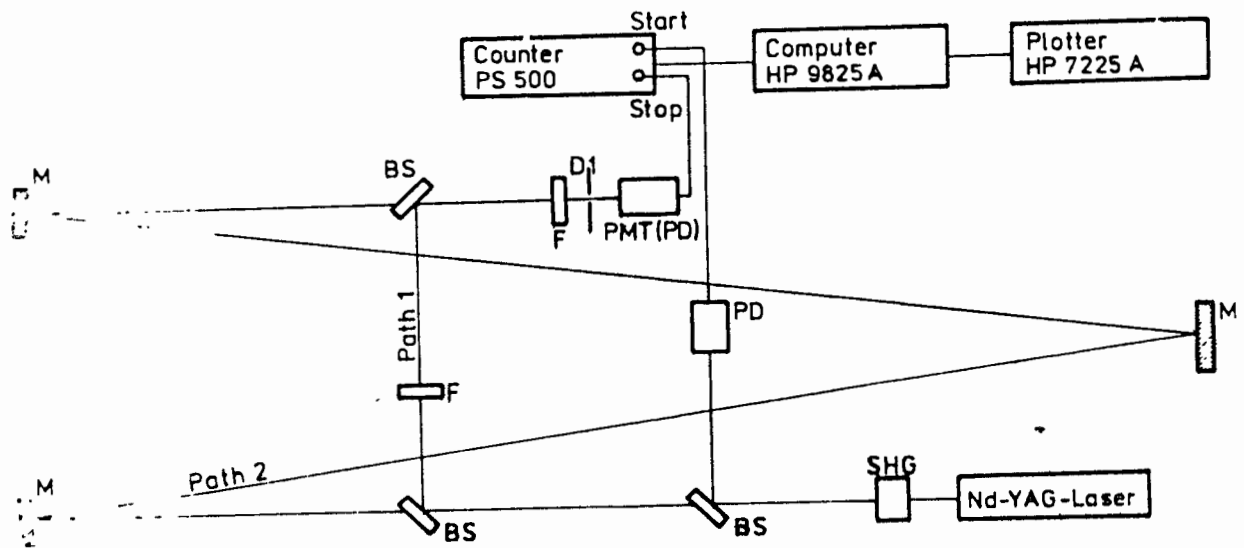


Fig. 1: Scheme of the experimental setup

BS - beam splitter, D - diaphragm
 F - neutral density filter, M - mirror
 PD - photo diode

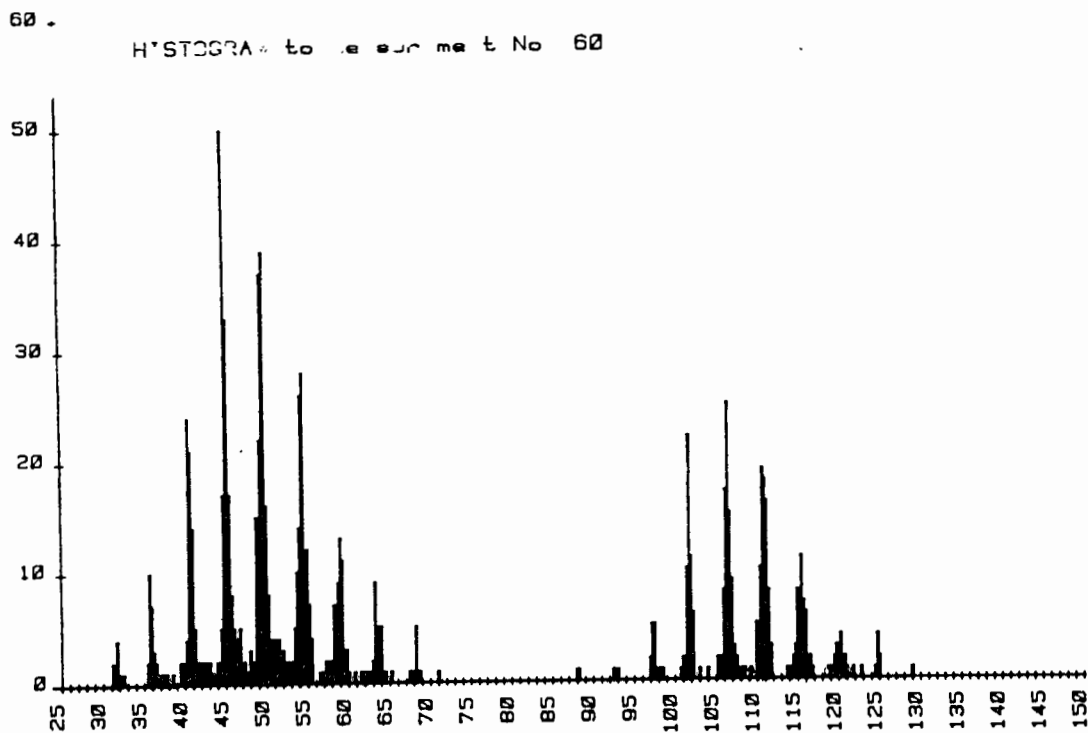


Fig. 2: Histogram of the time of flight values for a typical ranging experiment
 Abscissa: Time interval in ns
 ordinate: Number of measurements

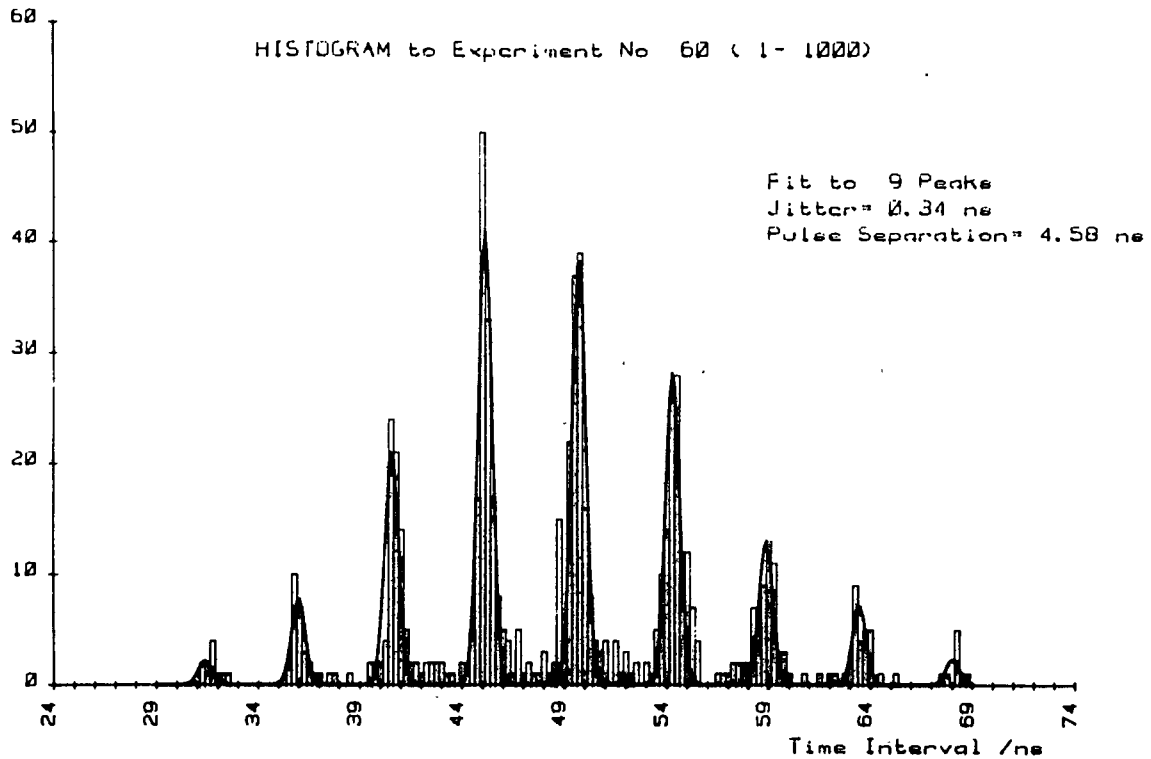


Fig. 3: Least square fit of a sum of Gaussian functions to the calibration part of experiment No. 60 (Fig. 2) bin width: 0.25 ns, RMS resolution: 0.34 ns, peak separation: 4.58 ns

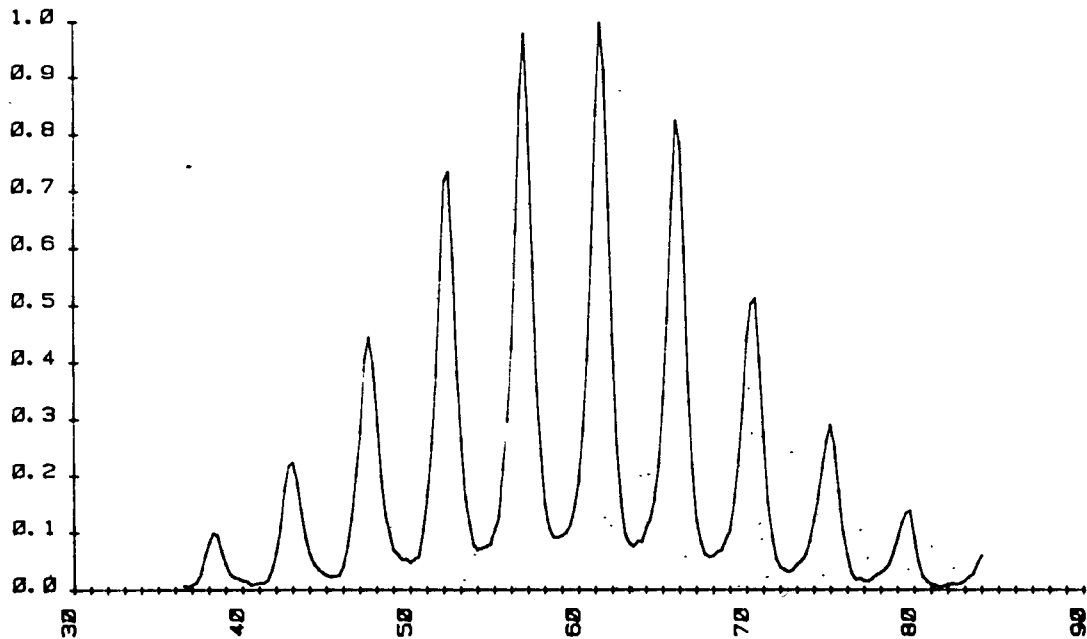


Fig. 4: Empirical cross-correlation to experiment No. 60 (convolution sum of the histograms corresponding to ray path 1 and 2 resp.)

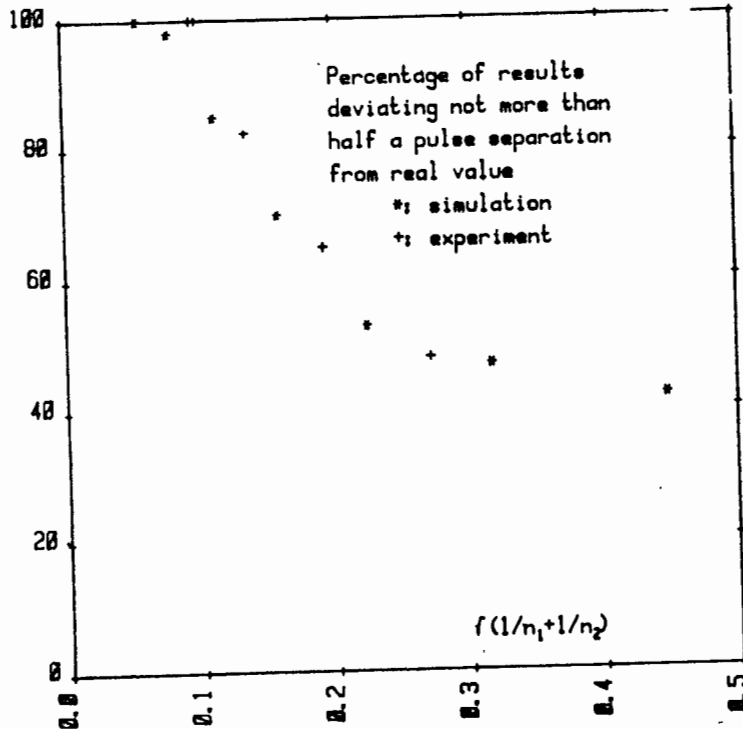


Fig. 5: Uniqueness in dependence of the amount of measurements: comparison of experiment and simulation.
 n_1 - number of measurements for path 1
 n_2 - number of measurements for path 2

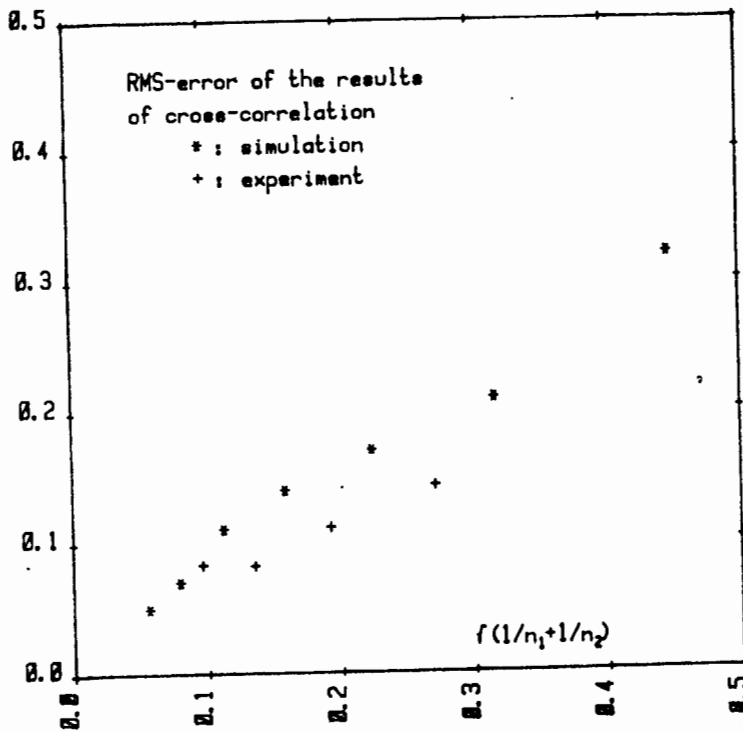
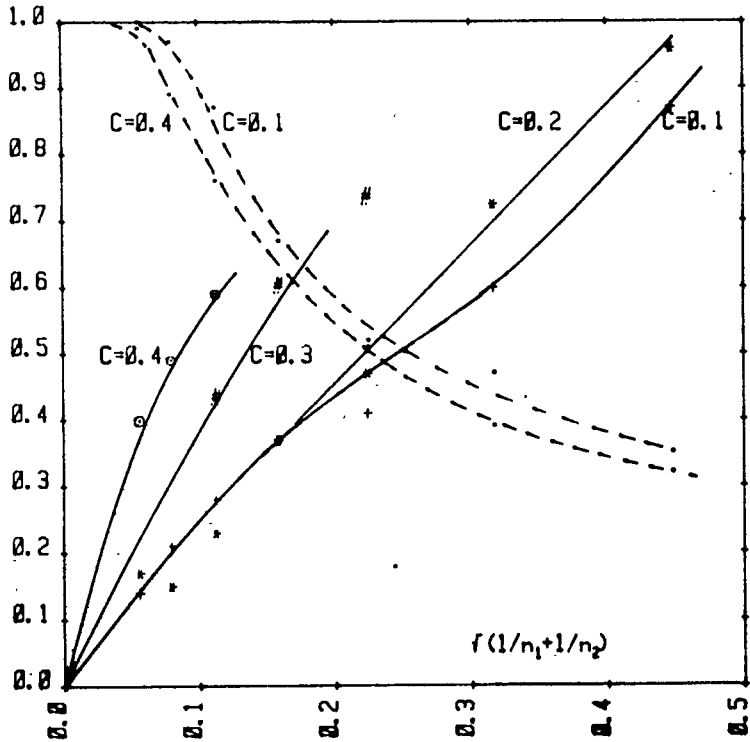


Fig. 6: RMS-error of the time shift corresponding to maximum cross-correlation: comparison of experiment and simulation



Laser radar performance
for different probability
distributions of the
time intervals
--- uniqueness
— rms/Jitter
Envelope Param. U=6

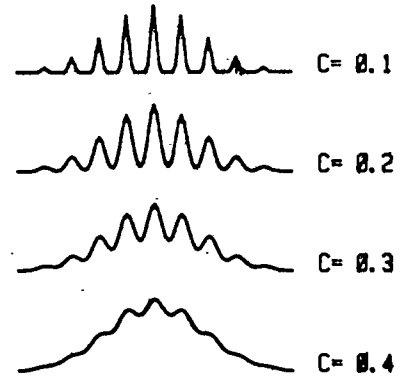
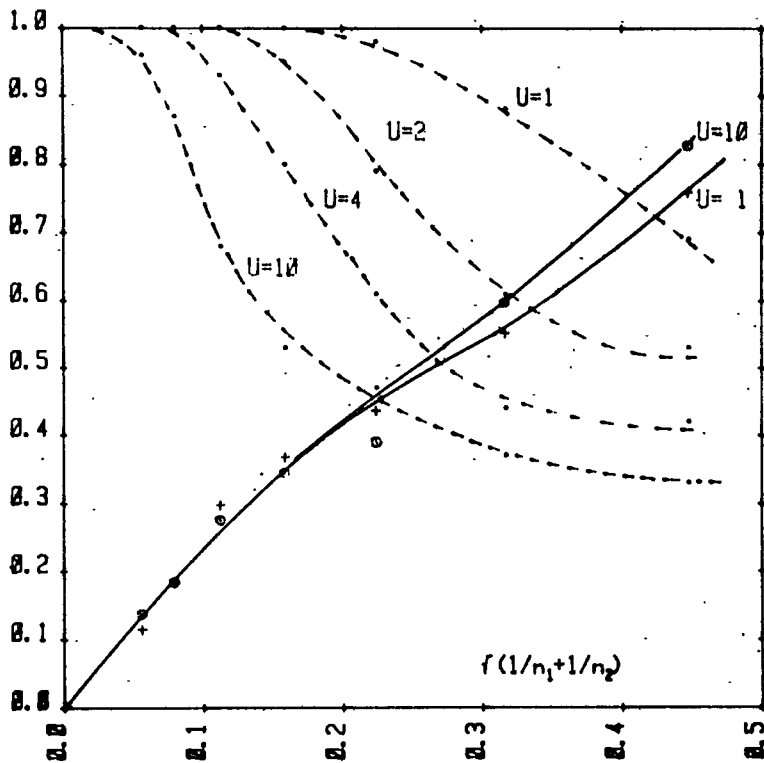


Fig. 7: Uniqueness and error obtained from simulations:
dependence from timing resolution



Laser radar performance
for different probability
distributions of the
time intervals
--- uniqueness
— rms/Jitter
Jitter: C=0.1

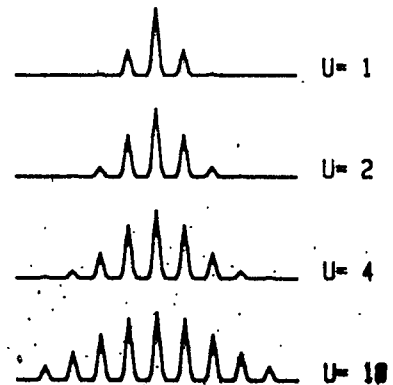
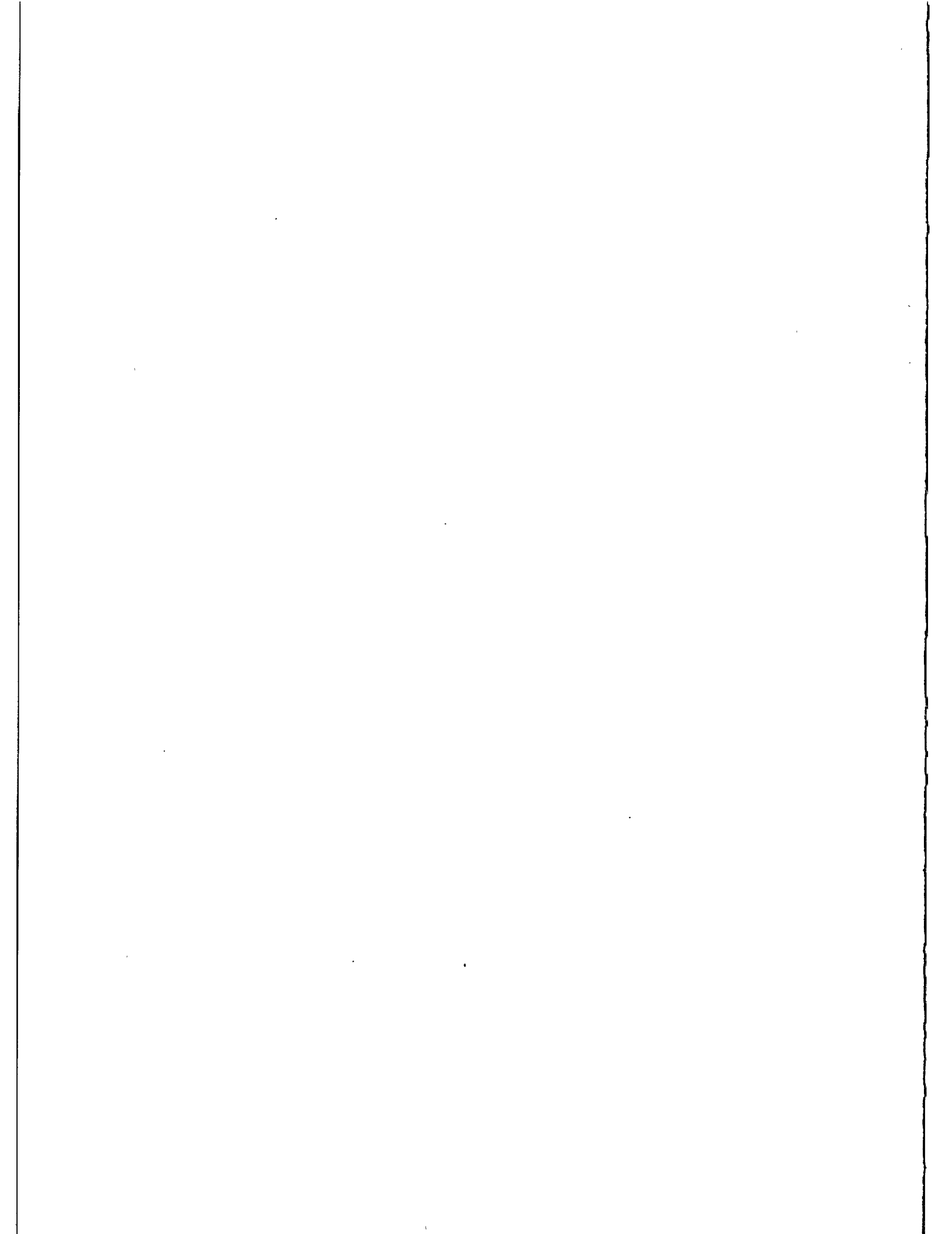


Fig. 8: Uniqueness and error obtained from simulations:
dependence from the number of peaks



MICROCHANNEL/DYNODE PHOTOMULTIPLIERS COMPARISON EXPERIMENT

I. Prochazka, K. Hamal
Czech Technical University
Faculty of Nuclear Science and Physical Eng.
Brehova 7, 115 19 Prague - Czechoslovakia -

Telephone 848840
TWX 121254 FJFI C

J. Gaignebet
C.E.R.G.A.
Avenue Nicolas Copernic
06130 Grasse - France -

Telephone 93 36 58 49
Telex 470865 CERGA F

ABSTRACT

The calibration/comparison experiment for PMTs jitter measurement is described. The Tranzient digitizer interfaced to a minicomputer together with the powerful software package is used as a high performance discriminator and time interval meter with jitter typ. 23 psec. The transit time jitter and time walk for single PE and multi PE response of the MCP PMT Varian and dynode PHT RCA 8852 were measured.

MICROCHANNEL/DYNODE PHOTOMULTIPLIER COMPARISON EXPERIMENT

I.Procházka, K.Hamal, J.Gaignebet

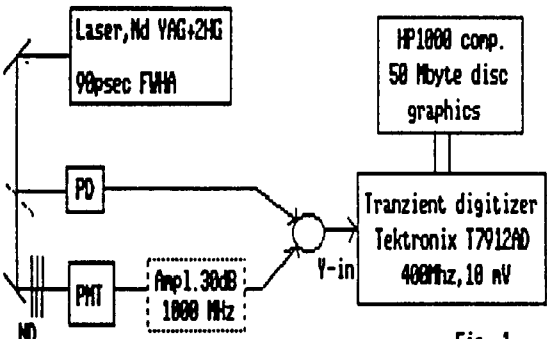
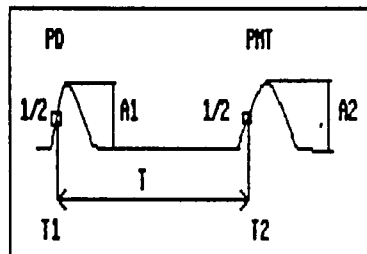
Analysing the 2G or 3G laser ranging system jitter budget one may conclude, that the photomultiplier contribution is the most significant. The transit time jitter and the time walk (transit time versus amplitude dependence) are the dominant parameters. The goal of this work was to measure the transit time jitter and the time walk of the microchannel and the dynode PMT. Although these parameters have been measured by several authors before (/1/,/2/ and others), the discrepancies between them and between the experience from the field was existing. That is why this measurement/comparison experiment was carried out.

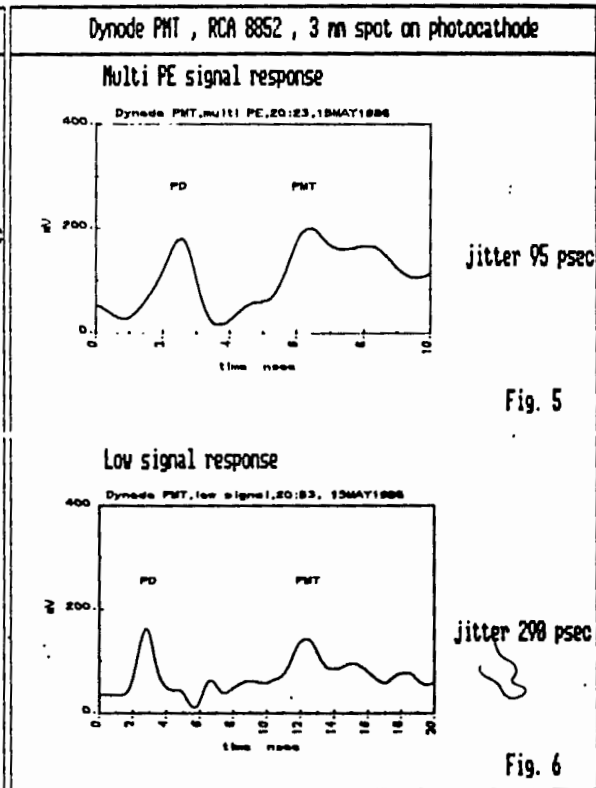
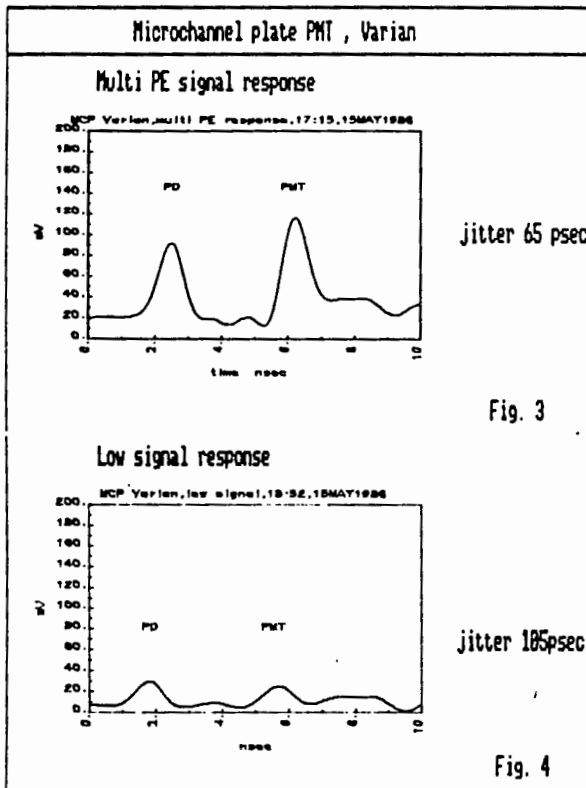
The experimental set up is on fig. 1. The single pulse from Nd YAG, frequency doubled laser, FWHM of 90psec is illuminating the fast vacuum photodiode and /after an appropriate attenuation/ the PMT photocathode. To reduce the effect of transit time dependence on the illumination spot position /1/, the light spot size on the dynode PMT photocathode was reduced to 3mm. Using the ND filters, the PMT input signal was set to 1 to 50 photoelectrons. The outputs of the photodiode and the PMT were added and fed to the Transient digitizer Y-input. The optional amplifier 1000MHz/30dB was used for MCP photomultiplier at low signals. The Transient digitizer Tektronix, bandwidth 400MHz, min. 10mV/div, 512x512 pixels array is interfaced to the HP1000 computer system. The Transient together with the computer hardware/software package are used as a high performance discriminator and short intervals meter. The recording speed exceeds 10frames per second. The records are off-line processed and data analysed. The example of the Transient output is on fig. 2. The first pulse corresponds to the photodiode, the second to the PMT output. The PMT output pulse amplitude A_2 and the pulses mutual distance T are the main process output parameters. The fluctuation of T is caused by the Transient, photodiode and PMT jitters. The Transient and photodiode jitter contributions were calibrated /3/ and found to be 23psec. The constant fraction (1/2) discriminator (software modelled) was used for all the measurements.

The examples of the records are on the figures 3 to 6 for the microchannel and dynode and multi PE and low signal, respectively. The results are plotted on fig.7 and 8 where is a graph of a photomultiplier transit time difference as a function of signal strength. The vertical bars represent the jitter for given signal strength.

Literature:

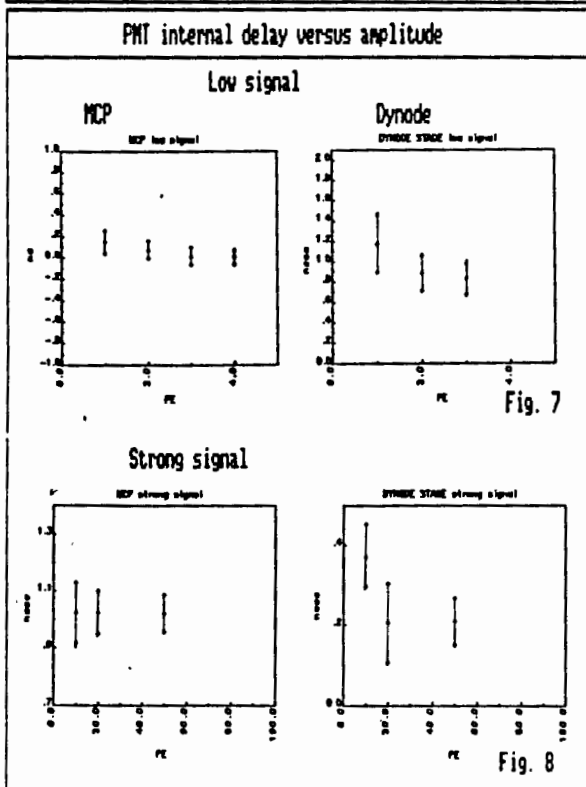
- 1/ S.K.Poultney, Single photon detection and timing, experiments and techniques, Advanced electronics and electron physics, Vol.31, 1972
- 2/ J.J.Degnan, Satellite laser ranging, current status and future prospects, IEEE, Geoscience nad remote sensing, Vol.GE-23, No.4
- 3/ I.Prochazka, Picosecond laser ranging using photodiode in this proceedings

| INTERKOSMOS SATELLITE LASER RADAR NETWORK | | PMT measurement goals | |
|---|--|--|--|
| <p>MICROCHANNEL/DYNODE PHOTOMULTIPLIERS COMPARISON EXPERIMENT</p> <p>I. Prochazka, K. Hanal Czech Technical University Faculty of Nuclear Science and Physical Engineering Brehova 7, 115 19 Prague, Czechoslovakia</p> <p>J. Gaignebet C.E.R.G.A, Grasse France</p> | | <p>Goals</p> <p>- measurements :</p> <ul style="list-style-type: none"> * jitter at single/multi PE signal level * time walk (int. delay/amplitude) dependence * ultimate jitter limits <p>- comparison :</p> <ul style="list-style-type: none"> * microchannel plate PMT Varian * dynode type PMT RCA8852 (3mm spot) | |
| I. Prochazka, K. Hanal, J. Gaignebet Microchannel/Dynode Photomultiplier Comparison Exper. | | 0 | I. Prochazka, K. Hanal Microchannel/Dynode Photomultiplier Comparison Exper. |
| PMT test experiment | | PMT test chain characteristics | |
|  <p style="text-align: center;">Fig. 1</p> | | <p>Laser - Nd YAG + 2HG, 90 psec FWHM</p> <p>Transient - 400MHz, 10 mV / div</p> <p>T7912AD - sweep speed 20 psec/pixel (MCP) 40 psec/pixel (dynode)</p> <p>- amplitude resolution 512 levels</p> <p>jitter - Pd (vacuum) + Transient 23 psec</p> | |
| <p>Transient record processing :</p>  <p style="text-align: center;">Fig. 2</p> | | <p>Limitation - dynamic range 5 : 1</p> | |
| I. Prochazka, K. Hanal J. Gaignebet Microchannel/Dynode Photomultiplier Comparison Exper. | | 2 | I. Prochazka, K. Hanal J. Gaignebet Microchannel/Dynode Photomultiplier Comparison Exper. |



I. Prochazka, K. Hanal J. Gaignebet
Microchannel/Dynode Photomultiplier Comparison Exper. 4

I. Prochazka, K. Hanal J. Gaignebet
Microchannel/Dynode Photomultiplier Comparison Exper. 5



PMT jitter comparison summary

| | | PMT type | |
|--------|--------|----------|----------|
| | | M C P | Dynode |
| | | Varian | RCA8852 |
| Jitter | 1 PE | 185 psec | 298 psec |
| | 10 PE | 100 psec | 150 psec |
| | 100 PE | 65 psec | 95 psec |

I. Prochazka, K. Hanal J. Gaignebet
Microchannel/Dynode Photomultiplier Comparison Exper. 6

I. Prochazka, K. Hanal J. Gaignebet
Microchannel/Dynode Photomultiplier Comparison Exper. 7

DETECTORS FOR III.GENERATION LASER RANGING SYSTEMS

Z. Neumann
Astronomical Institute
Czechoslovakia Academy of Sciences
Telephone (0204) 999201

ABSTRACT

Possible detectors are described and their properties jitter, gain, spectral response and noise are considered. The avalanche photodiodes are described in some detail.

The accuracy of transit time depends on - laser pulse width, accuracy of time counter, time property of photodetecting element, frequency properties of cables, type of discriminator, time properties of electronic circuits.

It is possible to generate a pulse width below 100 ps by mode-locking, it influences the detection accuracy (at one photoelectron level) by 40 ps approximately (see lit./1/, relation 2.14). In case of one photoelectron detection level, the accuracy almost does not depend on the type of the discriminator used (see lit./3/ table 1). The top time counters reach the accuracy level better than 40 ps (HP 5370). There are cables for frequencies over 10 GHz and with a convenient arrangement (discriminator as near as possible to the detector) the influence of cables is below 10 ps. It is possible make electronic circuits with jitter below 20 ps. Thus, the transformation of light pulse into the electric one by a photodetector is the main effect that determinates the transit time accuracy.

The case of a photodetector for a start impulse is relatively simple. It is possible to use an intensive light pulse so that no amplification is necessary. The absorption process is fast enough and it implies that the time properties depend on passive elements (encasing, parasitic capacity, inductance etc.). It is possible realize photodetectors, see lit./10/,/11/, such as having a jitter below 10 ps. For the start impulse we can use photoresistor, PIN photodiode, Schottky photodiode etc.

The case of a photodetector for the stop impulse is more difficult. One photoelectron or some photoelectron detection level implies the need of a high subsequent amplification ($10^6 - 10^7$). Up today solution by the usage of photomultipliers is limited. The photomultipliers reach a sufficient gain, however, the principle of photomultiplier activity causes the best photomultipliers having the jitter of approximately 500 ps (see lit./3/,/4/). Therefore, the photomultiplier limits the resultant accuracy to a value of appro-

ximately 7 cm.

What are the possibilities of improving ? The usage of microchannel plate photomultipliers is one solution. They reach a sufficient gain of 10^7 and maybe also a convenient jitter with regard to their time response of approximately 250 ps (FWHM). The comparison of this value with the time response of best photomultipliers (approximately 5 ns) and with their jitter (see lit./3/,/4/) shows the probable jitter of microchannel photomultipliers being of about 30 ps.

The other possibility is to look for some other devices acting on an other principles. The need to detect a single photon implies the necessity of amplifying in the same device where the photon is detected. So, main attention among semiconductor devices is directed to the avalanche photodiode.

The amplifying effect of avalanche photodiodes is based on the knocking-out the electrons from a valence in to a conduction band by high energetic electrons and holes. Heterogeneous photodiodes, instead of homogeneous ones, are used to decrease the dark current. They consist of absorption and avalanche regions, see fig. 1 . Photon is detected in the

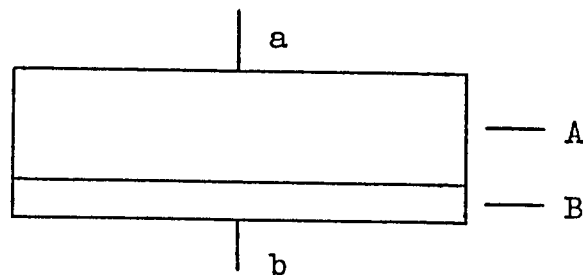


Fig. 1 Schematic illustration of an avalanche photodiode
A - absorption region, B - avalanche region, a - negative outlet, b - positive outlet

absorption region (A). The free electron penetrates into the avalanche region (B) where it induces an avalanche propagation. Arise free electrons get out by the b outlet, the holes penetrate through absorption region to the a outlet.

Avalanche photodiodes from germanium, silicon or A^3B^5 semiconductor (mainly $In_xGa_{1-x}As_yP_{1-y}$) are under consideration from technology point of view.

Avalanche photodiode, as an amplifier, can operate in two modes - linear amplifier mode and photon counting mode. In the first case, it reaches the gain of approximately 10 to 100 which is a very small value for usage in laser ranging system. In the other case, an avalanche photodiode operates either nearly below breakdown voltage or (a short time) over breakdown voltage. In this mode, the gain reaches a value of 10^6 or higher (for silicon see lit./6/,/9/). This is sufficient for a one photoelectron detection level, too.

The type of the semiconductor used implies a spectral response, see fig. 2 . We can see that all materials are able

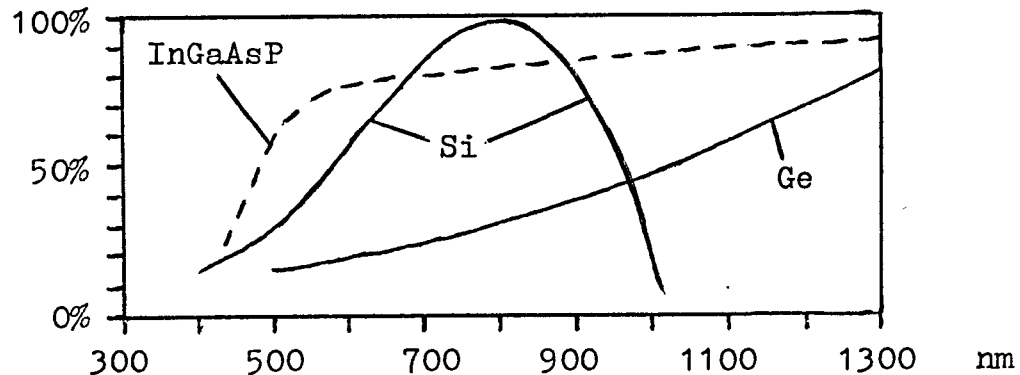


Fig. 2 Spectral response of semiconductor materials
 Comment spectral response of InGaAsP changes according to the relation of components

to detect the radiation with 532 nm wavelength as well as with 1064 nm wavelength.

Total photodiode quantum efficiency at concrete wavelength is determined mainly by the value of absorption coefficient at this wavelength and by the thickness of the absorption layer (and also by antireflection improvement etc.). To obtain a reasonable quantum efficiency (over 10%), a minimal thickness of the absorption layer ought to be of 10 μm

(for 532 nm) and 5 um (for 1064 nm) in case of germanium, of 20 um (for 532 nm) and 100 um (for 1064 nm) in case of silicon and of 1 um (for both wavelength) in case of InGaAsP.

The jitter of an avalanche photodiode is determined mainly by the thickness of the absorption layer. A photon is absorbed randomly on any place of the absorption layer. Due to the different speed of light (approximately 10^8 m.s^{-1}) and electron (approximately 10^5 m.s^{-1}), the delay between a photon coming into the photodiode and the electrical pulse leaving out the photodiode changes according to the place of photon absorption. The jitter implying from this effect reaches approximately 50 ps (10 um layer) and 25 ps (5 um layer) for germanium, 100 ps (20 um layer) and 500 ps (100 um layer) for silicon and 5 ps (1 um layer) for InGaAsP.

The signal-to-noise ratio is not constant (depending on gain) at avalanche photodiodes, as it is in the case of photomultipliers, but it decreases as the gain increases. This dependence is shown on the equation /1/ (according lit./7/)

$$s:n = \frac{K_1 \cdot P^2 \cdot M^2}{(K_2 \cdot P + 2 \cdot e \cdot I_d) \cdot M^2 \cdot F \cdot K_3 + K_4}, \quad /1/$$

where K_1 to K_4 are constants, M is the gain, P is the optical power, I_d is the dark current, e is the electronic charge and F is the excess noise factor depending on the semiconductor material. If the ionization coefficients of electrons and holes are equal, the noise power increases as M^3 but the signal one only as M^2 . When the ionization coefficients are very different, the noise power increases also as M^2 . The biggest difference between the ionization coefficients reveals silicon. In the case of InGaAsP the difference depends on the ratio between the components.

It is reasonable to describe the noise properties of a

photodetector for laser ranging instruments by the frequency of noise pulses instead by its noise power. According to data from lit./6/ - the dark current 18 nA and a gain of $2 \cdot 10^4$ (at temperature 25°C) - it is possible to compute the frequency of noise pulses of 5 MHz. According to data from lit./9/ - the dark current 10^{-13} A and the gain 250 (at the temperature -22°C) - the frequency is equal to 2500 Hz. It is possible to compute, according to data from lit./8/ - dark current $3 \cdot 10^{-10}$ A and the gain 100 - the frequency of noise pulses 20 MHz for InGaAsP .

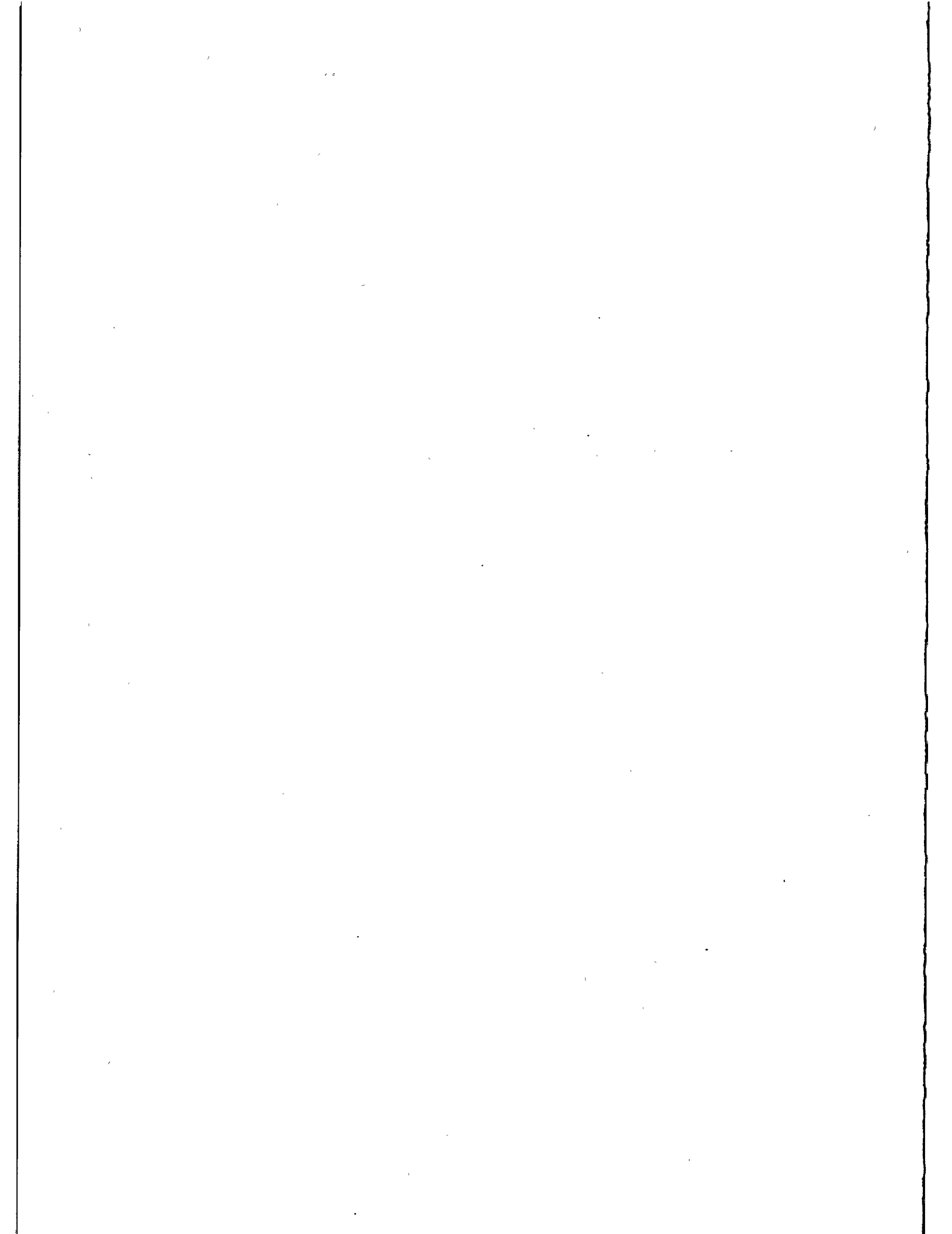
Conclusion : The microchannel photomultipliers and silicon avalanche photodiodes with an approximately 20 μm thick absorption layer (and probably cooled) are convenient for stop impulse detection of 2. harmonic of the Nd:YAG laser for III. generation laser ranging instruments.

Only silicon avalanche photodiodes with approximately 20 μm thick absorption layer (for small jitter) in the photon counting mode seem to be convenient for stop impulse detection of 1064 nm wavelength. The quantum efficiency (due to thin absorption layer and small absorption coefficient) is small, of about 2 to 3%.

For the future, after improving the technology, the InGaAsP avalanche photodiodes seem to be most perspective photodetectors (see lit./7/ pages 413-414). A detection of not only 532 nm, but also of 1064 nm wavelength radiation with high quantum efficiency and a very small jitter will be probably possible in the case of convenient ratio between the components. The jitter will be probably so small to make it reasonable to consider their usage in a two-colour laser instruments (instead of streak camera). Different ionization coefficients enable to reach small noise. The gain 10^6 or more will be probably reached in the photon counting mode.

Literature

- /1/ Matti Paunonen : Studies on the Metsáhovi Satellite Laser Ranging System
- /2/ Centre National D'Études Spatiales, GRGS : Starlette
- /3/ K. Hamal, I. Procházka, J. Gaignebet : Mode Locked Train YAG Laser Calibration Experiment, Observations of Artificial Earth Satellites 23/1984
- /4/ R. Neubert, B. Ritschel, L. Grunwald : Ambiquity and Resolution of a Mode-locked Train Laser Radar, paper on the International Scientific Seminar "Laser Satellite IInd and III^d generation ", 26-30 May 1986, Sofia
- /5/ Specification VPM-221D (2 MCP's) Photo Plate Detector, Varian
- /6/ private information
- /7/ T.P. Pearsall : GaInAsP Alloy Semiconductors, John Wiley and Sons, 1982
- /8/ Kishi, Y and others : Liquid-phase-epitaxial growth of InP/InGaAsP/InGaAs Buried-structure avalanche photodiodes, Electronic Letters, Vol.20, page 165
- /9/ Photonics Spectra, June 1986, page 52
- /10/ Roth, W., Schumacher H., Beneking H. : Fast Photoconductive GaAs detectors made by laser stimulated MOCVD, Electronic Letters, Vol.19, nom.4, page 142
- /11/ Wang S, Y., Bloom D. M. : 100 GHz Bandwidth Planar GaAs Schottky Photodiode, Electronics Letters, Vol.19, nom.14. page 554



THE USE OF GEIGER MODE AVALANCHE PHOTODIODES FOR PRECISE
LASER RANGING AT VERY LOW LIGHT LEVELS :
AN EXPERIMENTAL EVALUATION

S.R. Bowman, Y.H. Shih, C.O. Alley
Department of Physics and Astronomy
University of Maryland
College Park, Maryland 20740 - USA -

Telephone (301) 454 - 3405
Telex 908787

ABSTRACT

Measurements have been conducted to determine the utility of commercially available silicon avalanche photodiodes as detectors in single photon ranging systems. When cooled and operated in a gated Geiger mode these detectors offer an attractive alternative to photomultipliers.

Seven different types of diodes were evaluated for Geiger mode operation. Characteristics such as dark noise and temporal response were used to select the best diode types. Response time studies were conducted on the selected diodes at very low light levels using a mode-locked frequency doubled Nd-YAG laser and a picosecond resolution streak camera system. Single photon response time distributions with standard deviations as small as 90 picoseconds were observed.

Detection efficiency at the singles level was also studied. Using a parametric down conversion process to generate a source of correlated photon pairs, the absolute single photon detection efficiency was measured at 532 nanometers. Efficiencies of 28 % were observed and changes in the detection efficiency with gating voltage were studied.

Results from low and moderate intensity laser ranging with Geiger mode diodes are discussed. The ranging results acquired at the Goddard Optical Test Facility include both terrestrial targets and the Laser Geodynamics Satellite, LAGEOS.

measurements. In this application "echo" pulses are not a significant problem.

Qualitatively the theory of Geiger mode operation is quite simple. The combination of low temperature and a high reversed biasing potential produces an essentially carrier-free region in the junction and depleted intrinsic region of a PⁿN diode, Figure 1. When a carrier is produced in the depleted region it will move into the high field region of the junction and undergo avalanche amplification as large as 10^9 . The resulting current pulse will continue until voltage across the diode falls to below the breakdown voltage.

Geiger mode operation is easy to observe. The circuit in Figure 2 is cooled to -60°C using dry ice. Reverse bias is applied through a current limiting resistor to bring the diode to within a few volts of breakdown. An additional gating voltage pulse is capacitively coupled onto the diode. In this way the diode can be overvoltaged by as much as several hundred volts during the time of an expected signal. (If the diode is kept in almost total darkness the full voltage can be applied continuously. Most of the silicon diodes tried exhibited dark count rates of less than 100 Hertz at this temperature.) When the diode does break down the resulting pulse is large, usually several volts. This is a great advantage when working with lasers or other electrically noisy devices.

DETECTION EFFICIENCY

To determine their usefulness as laser ranging detectors, several different avalanche photodiodes were purchased. They were selected for large active area, high responsivity, and low cost. Each was tested for Geiger mode operation. Diodes that either failed to exhibit Geiger mode or had dark count rates above one kilohertz were rejected. Figure 3 illustrates relative measurements made to determine the optimum diode operating conditions. Measurements were made to determine detection efficiency and temporal response.

Accurate measurements of the detection efficiency of silicon Geiger diodes were made using a technique first described by D.N. Klyshko.⁵ Conceptually, this is a very simple technique. A single weak laser beam passes through a nonlinear crystal that is phase matched for non-collinear parametric frequency halving. With proper spectral filtering, the result will be two very weak beams having the same wavelength. In fact, energy conservation requires that an equal number of photons, N , are simultaneously created in each beam. Two very sensitive detectors are used to count photons in each beam. The number of counts in each beam, N_1 and N_2 , are recorded. Also, the number of coincidence counts, N_c , is recorded. The absolute detection efficiencies, η_1 and η_2 can then be calculated from the simple relations:

$$N_1 = \eta_1 N \quad N_2 = \eta_2 N \quad N_c = \eta_1 \eta_2 N.$$

Figure 4 details the actual device set up to realize the Klyshko technique at the wavelength of interest, 532 nanometers. The results of measurements using two RCA C30902E diodes were maximum single photon detection efficiencies of 21

$\pm 3\%$ and $28 \pm 3\%$.

TEMPORAL RESPONSE

In addition to detection efficiency, the temporal response of the diodes was studied. Three important properties of the Geiger pulse were measured. They were amplitude stability, pulse risetime, and internal delay time jitter.

Amplitude fluctuations are a potential source of timing error in any ranging system.⁶ Fortunately, the amplitude of the Geiger pulse is very stable. Under normal conditions "good" diodes have only a few percent variation in pulse amplitude, Figure 5. If the diode is operated at high count rates (greater than 5 kilohertz for d.c. biasing), it will not recharge completely before each firing. The result is a wide spectrum of pulse heights. Some diodes, particularly the RCA C30954E, exhibited frequent echo pulses within 10^{-4} seconds of the leading pulse. The amplitudes of the echo pulses varied substantially again, probably due to lack of charging time.

Rise time measurements on the Geiger diode pulses are summarized in Table 1. All were measured with a load impedance of 50 ohms. A weak dependence of the risetime on temperature and voltage was observed. Lowering the temperature or raising the voltage could shorten the risetime by as much as a factor of two. The fastest rise attained was 1.0 nanosecond. This may be limited by the impedance of the diode packaging, a TO-18 can and socket.

Internal delay jitter was measured in two different ways. The first was to trigger a Hamamatsu C1000 Streak Camera System with the output of a Geiger diode. This system incorporates a C1583 streak camera with a streak trigger jitter of 5 picosecond as measured by the company. After a thousand laser firings, the width of the distribution of camera streaks was measured. Comparing this with the distribution produced by triggering from an ultrafast PIN diode, the internal jitter in the Geiger diode can be found. For the single photon intensity level, the standard deviation of the distribution was 90 picoseconds. These distributions clearly show an increase in the 10% full width trigger jitter from 190 to 360 picoseconds when the moderate intensity was reduced by 10^7 to the single quanta level. This increase in the internal delay jitter at low light levels can be explained in terms of the carrier transit time of the depleted region. At very low intensities the carriers which start the avalanche in the junction are formed throughout the depleted region. The structure of the RCA C30902E diode on which these measurement were made is such that the depletion region and junction are 15 and 2 microns thick, respectively.⁷

Similar results were obtained when the detector was used for terrestrial ranging. Figures 6 and 7 show histograms of the timing spread for ranges to a terrestrial corner cube reflector. With only a factor of 10 difference in the intensities used, the broadening of the distribution is clear. In addition to a 39% increase in the standard deviation, the mean value shifted later by 200 picoseconds. These measurement have 40 picosecond uncertainty associated with the timing electronics used.

Although Geiger mode photodiodes offer many advantages to photomultipliers in the measurement of weak light pulse epochs, they do have a serious drawback. After the avalanche pulse occurs, the diodes experience a relatively long deadtime associated with the carrier lifetimes in silicon. The minimal recovery time was not studied here but is thought to be of the order of 10^{-7} seconds. In this research the recovery time was limited by the RC time constant of the biasing circuit, 10^{-4} seconds. As a result the GM diodes used here were basically single stop detectors. This leads to significant noise blanking when the diodes are used in the presence of high background lighting, photon flux rates above 10^5 Hz. To resolve this problem work is currently under way on a multiple diode detecting package.

RANGING RESULTS

As a final test of utility of the GM photodiodes, laser ranging sessions were conducted using a single RCA C30902E diode as detector. The ranging test were conducted at the 1.2 meter precision tracking telescope on the Goddard Optical Test Site in Greenbelt Maryland. Strong return rates were achieved from the Laser Geodynamics Satellite (LAGEOS) using only two millijoules of transmitted laser energy. The LAGEOS satellite is in a nearly circular orbit with an altitude 6000 kilometers. For ranging at the single photon level, a chi squared fit to a second order polynomial using a typical two minute sample of the resulting timing residuals gave a standard deviation of 192 picoseconds. Figure 8 shows ranging residuals from a typical LAGEOS ranging session where higher laser energies are used to get a nearly one to one signal rate.

Lunar ranging data has also been acquired using the GM photodiode receiver. The results shown in Figure 9 were obtained in five minutes using 100 millijoule pulses under marginal atmospheric conditions. JPL analysis of this data gave a standard deviation of 168 picoseconds or a range uncertainty of 2.8 centimeters.

CONCLUSION

Measurements were conducted with silicon avalanche photodiodes used in a cooled Geiger mode to determine their usefulness in satellite laser ranging systems. Single photon detection efficiencies were measured to be 28% for 532 nanometers. Timing jitters of the single photon responses were found to have a standard deviation of 90 picoseconds. The high quality lunar and satellite ranging results obtained here prove the commercially available GM photodiodes to be an excellent alternative to photomultipliers both in terms of cost and performance.

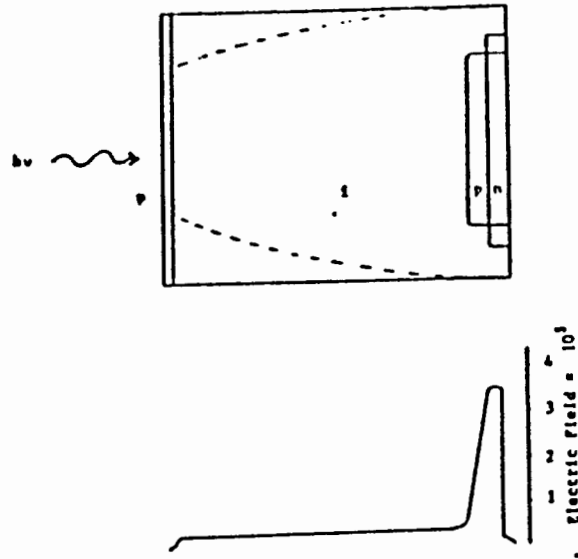
ACKNOWLEDGMENT

The authors would like to thank Bob Hyde for his initial suggestion of this research topic. Thanks also go to John Rayner, Jack Bufton, and Liming Ding for their assistance during this work.

TABLE 1
TYPICAL GEIGER MODE PROPERTIES OF APD'S TESTED
T = +60°C

| | |
|-------------------------|---|
| RCA C309021S | $V_{Brk} = 165 \text{ V}$, $T_{Rise} = 3 \text{ ns}$ Dark count = 16 Hz @ $V_{Brk} + 20 \text{ V}$ |
| RCA C30902E | $V_{Brk} = 170 \text{ V}$, $T_{Rise} = 1.2 \text{ ns}$ Dark count = 100 Hz @ $V_{Brk} + 40 \text{ V}$ |
| RCA C30948E | $V_{Brk} = 192 \text{ V}$, $T_{Rise} = 1.7 \text{ ns}$ Dark count = 50 Hz |
| RCA C30954E | $V_{Brk} = 140 \text{ V}$, $T_{Rise} = 3 \text{ ns}$ Dark count = 70 Hz @ $V_{Brk} + 20 \text{ V}$ |
| RCA C30955E | No Geiger mode |
| NDL 1202 | $V_{Brk} = 135 \text{ V}$, $T_{Rise} = 1 \text{ ns}$ Dark Count = 2 kHz @ $V_{Brk} + 15 \text{ V}$ |
| NDL 5100 (Germanium) | $V_{Brk} = 30 \text{ V}$, $T_{Rise} = 5 \text{ ns}$ very noisy, triggered immediately, amplitude only 10mV |

REACH-THROUGH APD STRUCTURE



From P.P. Webb et al. "Properties of Avalanche Photodiodes,
R.C.A. Review 35, (1974), 251.

FIGURE 1

GEIGER MODE PHOTODIODE BIASING CIRCUIT

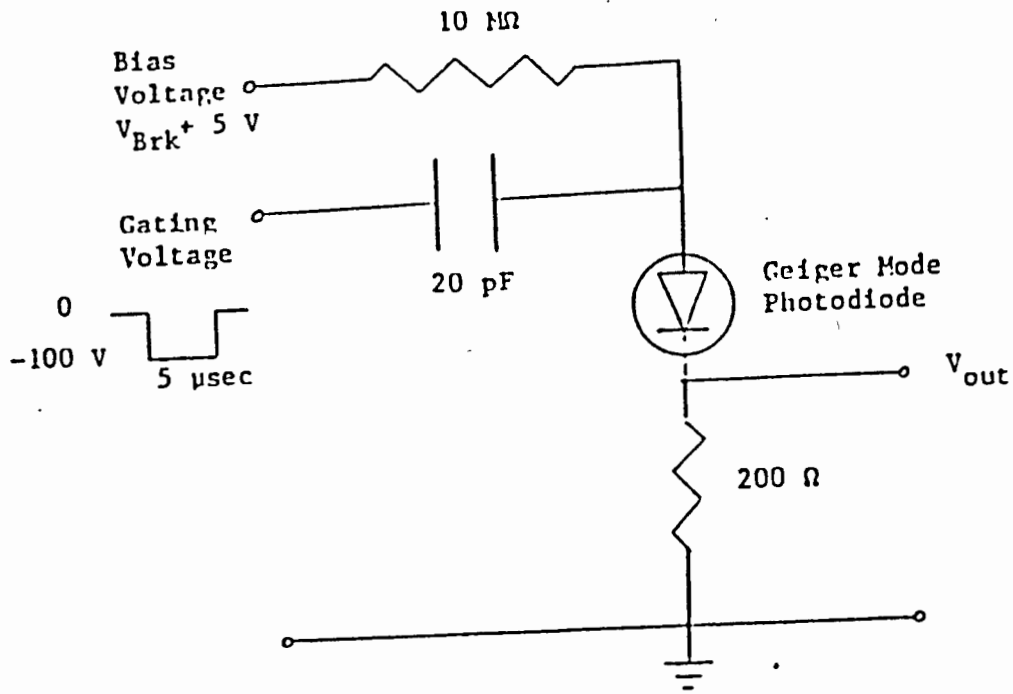


FIGURE 2

GEIGER MODE PHOTODIODE PERFORMANCE VS. VOLTAGE

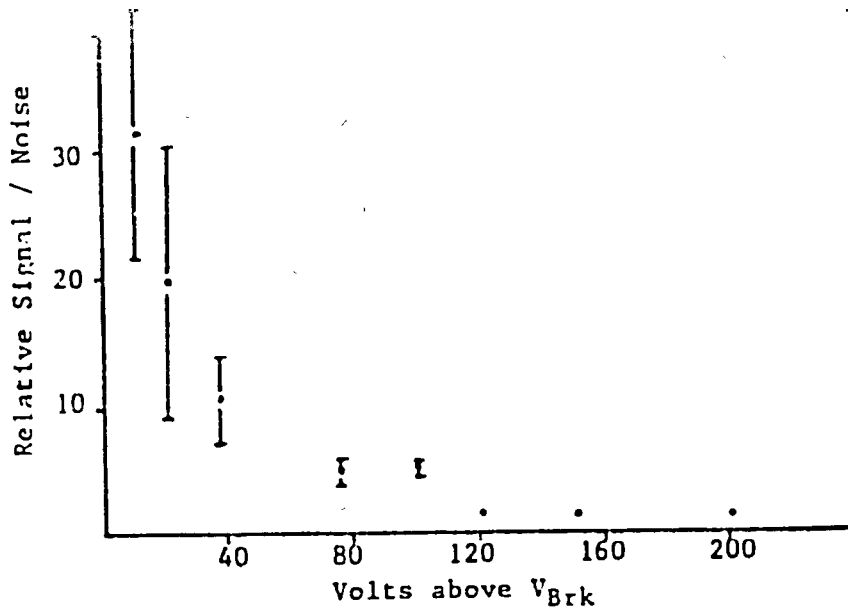
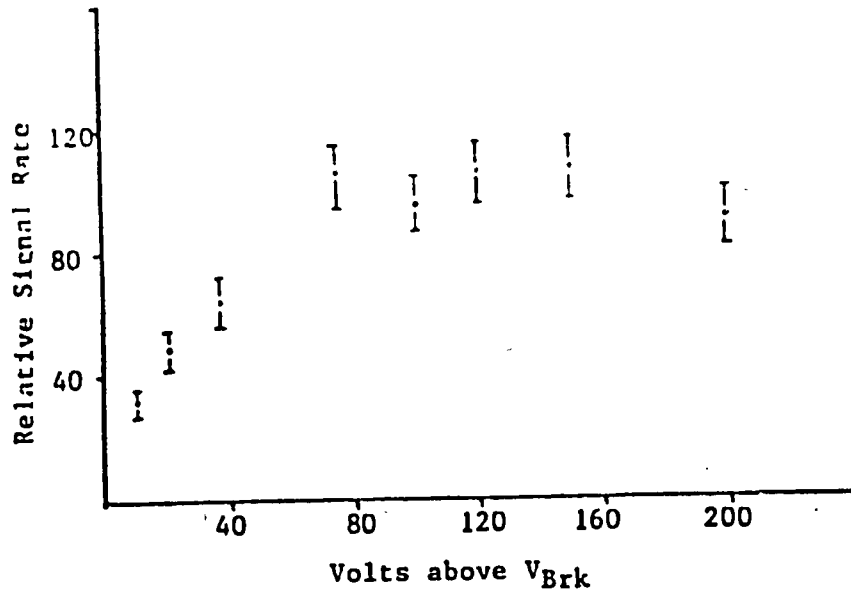


FIGURE 3

KLYSHKO DETECTION EFFICIENCY MEASUREMENT

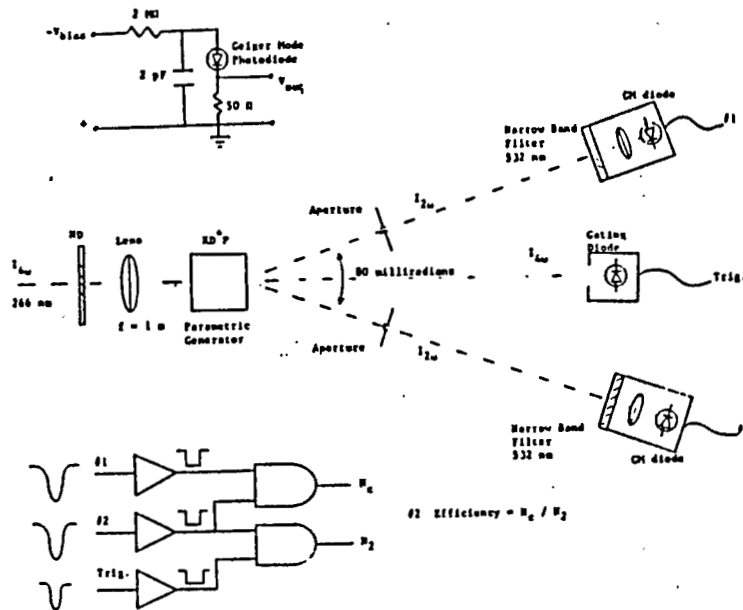
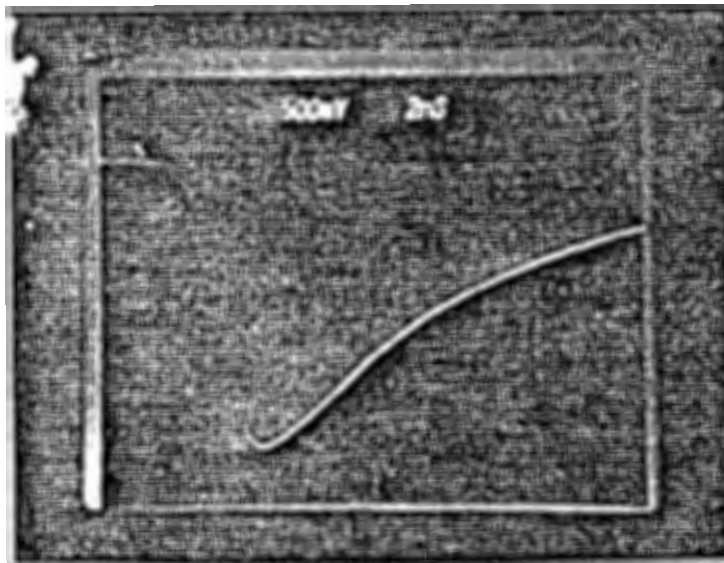


FIGURE 4



RCA30902E DIODE SN 40889, V_{gate} = +50 V, V_{bias} = -160 V
 Three Pulses, Risetime = 1.2 ns (10-90%)
 measured with Tektronics 7104 Oscilloscope

FIGURE 5

TERRESTRIAL RANGING WITH GM PHOTODIODE, ND = 9

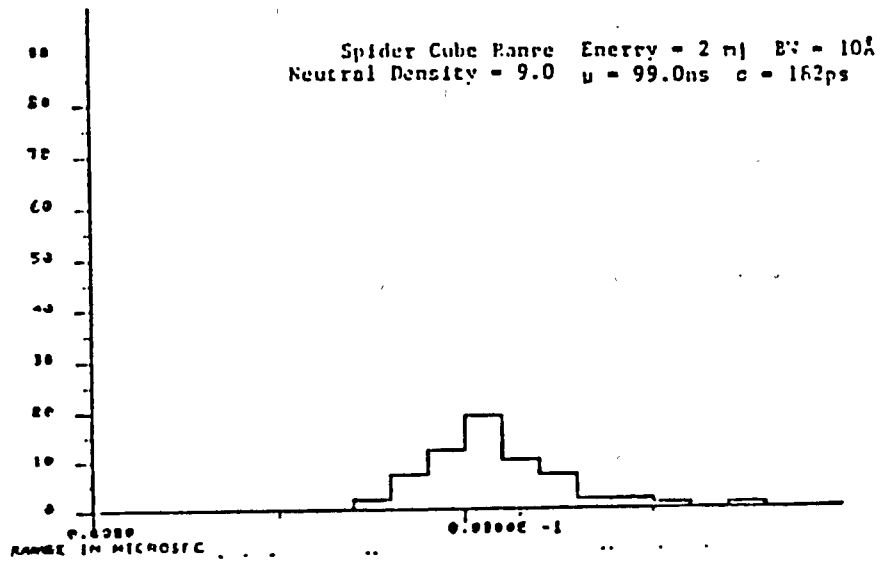


FIGURE 6

TERRESTRIAL RANGING WITH GM PHOTODIODE, ND = 10

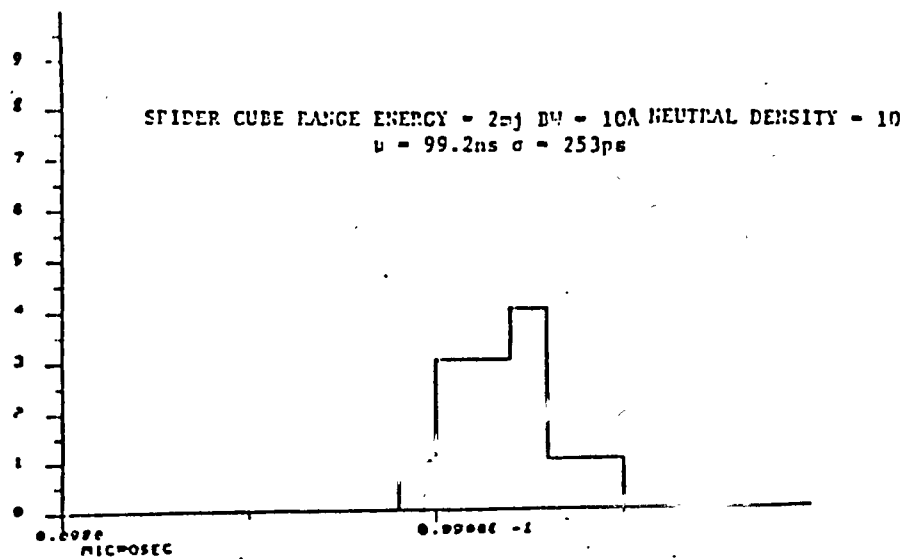


FIGURE 7

SATELLITE RANGING RETURNS

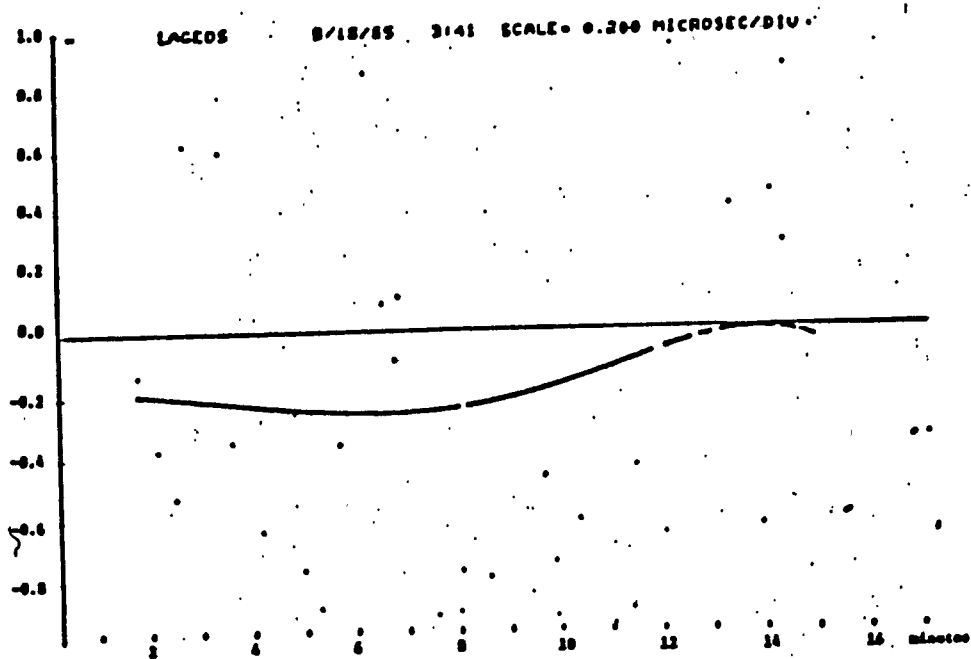


FIGURE 8

LUNAR RANGING RETURNS

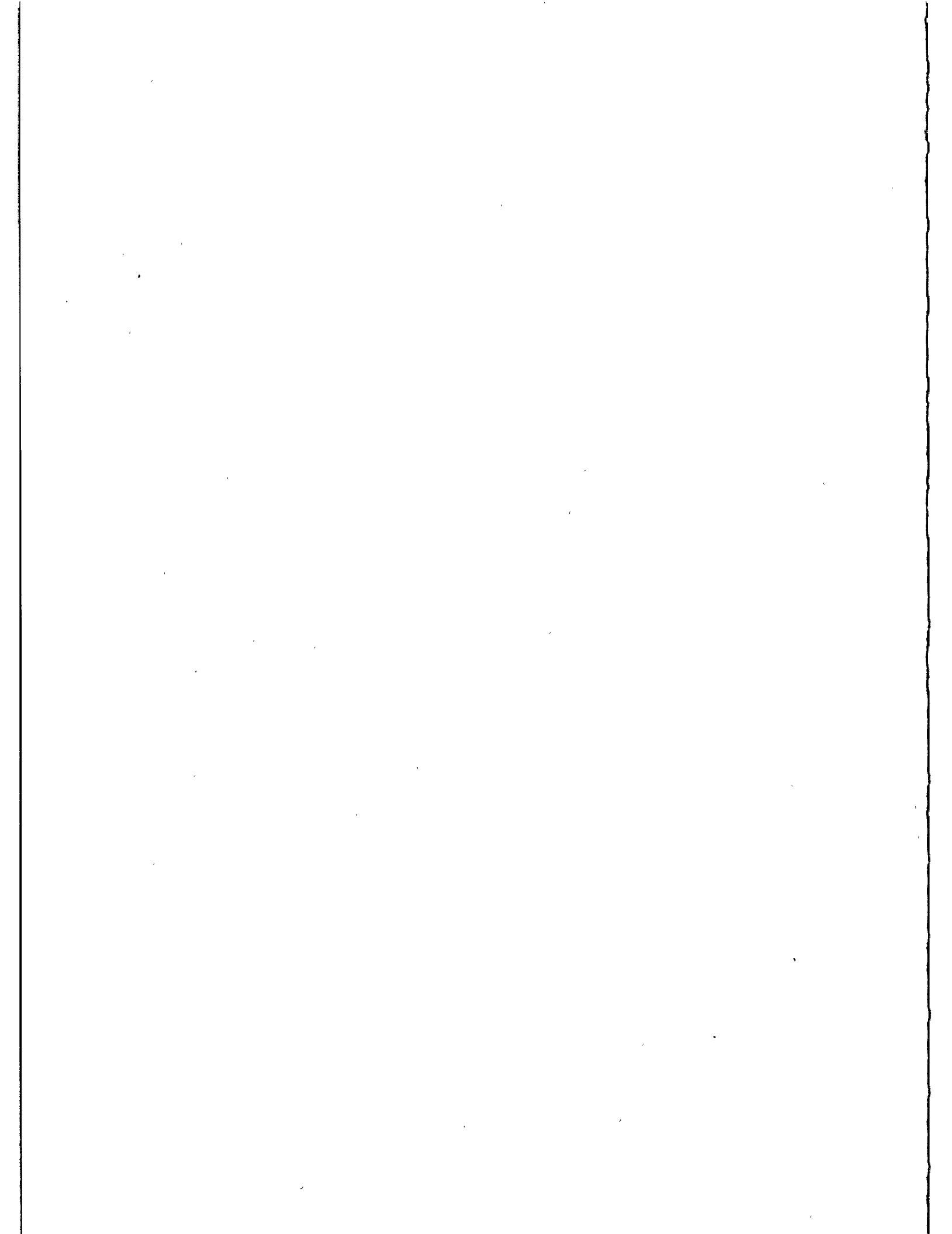
HADLEY 8143 8/26/86



FIGURE 9

REFERENCES

1. R.J. McIntyre, "The Distribution in Gains in Uniformly Multiplying Avalanche Photodiodes : Theory," IEEE Transactions on Electron Devices, ED-19 (1972), 703.
2. T.E. Ingerson, et al., "Photon counting with photodiodes," Applied Optics, 22 (1983), 2013.
3. P.A. Ekstrom, "Triggered avalanche detection of optical photons," J. Appl. Phys., 52 (1981), 6974.
4. P.P. Webb and R.J. McIntyre, "Recent developments in silicon avalanche photodiodes," RCA Engineer, 27-3 (1982), 96.
5. D.N. Klyshko, "Use of Two Photon Light for Absolute Calibration of Photoelectric Detectors," Sov. J. Quantum Electron. 10 (1980), 1112.
6. T.M. Zagwodzki, Test Techniques for Determining Laser Ranging System Performance, NASA Technical Memorandum TM82061 (Goddard Space Flight Center, Greenbelt, MD. Jan. 1981).
7. Webb and McIntyre, p.100.



SINGLE PHOTON SOLID STATE DETECTOR
FOR RANGING AT ROOM TEMPERATURE

K. Hamal, H. Jelinkova, I. Prochazka, B. Sopko
Czech Technical University
Faculty of Nuclear Science and Physical Eng.
Brehova 7, 115 19 Prague, Czechoslovakia

Telephone 848 840
Telex 121254 FJFI C

ABSTRACT


To detect return signal at satellite/lunar laser ranging stations, mostly photomultipliers are exploited. There is a strong interest to exploit solid state detector. We developed a solid state detector operating at single and multiphoton level at room temperature. The quantum efficiency is 10/2% at 0.53/1.06 μ m. The timing jitter at single photon detection is 100/220 psec at 0.53/1.06 μ m. Two modes of operation: active and passive quenching have been exploited.

Photodiode for ranging

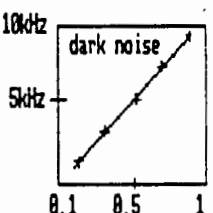
RANGING DETECTOR - REQUIREMENTS

| | |
|--------------------|--------------------------|
| JITTER | LOW |
| QUANTUM EFFICIENCY | HIGH |
| WAVELENGTH | 0.4 - 1.08 μm |

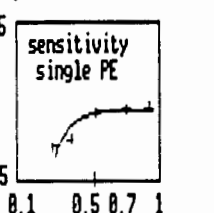
DESIGN



R. H. HAITZ, J. APPL. PHYS., 35, 1964, 1370
 BREAKDOWN VOLTAGE CCA 26V, $-20\text{mV}/^\circ\text{C}$



dark noise



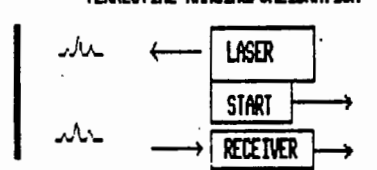
sensitivity single PE

Volts above break

K. Hana, H. Jelinkova, I. Prochazka, B. Sopko
 Single Photon Solid State Detector For Ranging ...

Optical scheme/laser


TERRESTRIAL RANGING/CALIBRATION



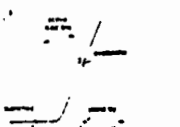
diffused target

YAG LASER/SHG
 MODE LOCK TRAIN 2-3 PULSE
 PULSE DURATION 30 ps
 ROUND TRIP TIME 2ns

MODES OF OPERATION



PASSIVE/GEIGER

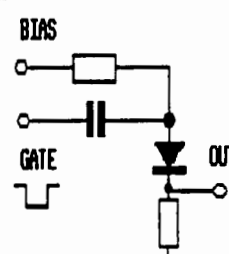



ACTIVE/SPAD

S. Gova, JQE-19, 1983, 630

K. Hana, H. Jelinkova, I. Prochazka, B. Sopko
 Single Photon Solid State Detector For Ranging ...

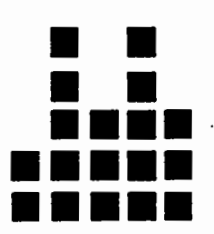
Passive Quenching/Geiger mode 0.53 μm





PD/GEIGER → ORTEC → COUNTER → COMPUTER

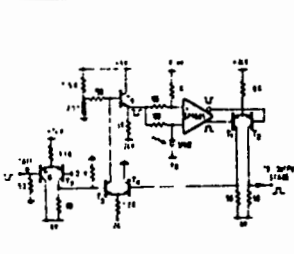
SINGLE PHOTON DETECTION JITTER

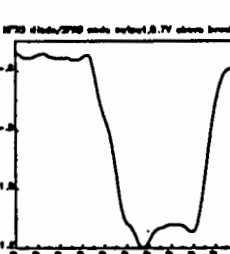
| | | |
|---------|-------|---|
| RAW | 112ps |  |
| START | 30ps | |
| COUNTER | 36ps | |
| LASER | 10ps | |
| ORTEC | 20ps | |
| TARGET | 30ps | |

DECONVOLUTED 90ps .80 90 100 110 120 ps

K. Hana, H. Jelinkova, I. Prochazka, B. Sopko
 Single Photon Solid State Detector For Ranging ...

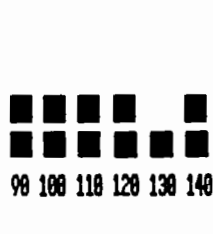
Active Quenching/Spad mode 0.53 μm





PD/SPAD → COUNTER → COMPUTER

SINGLE DETECTION JITTER

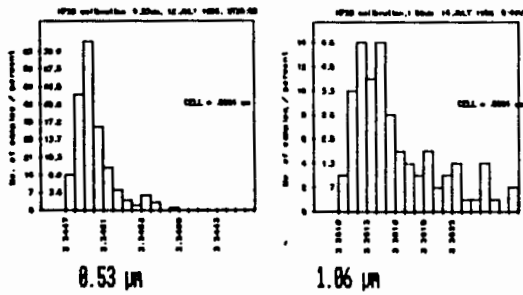
| | | |
|--------------|-------|---|
| RAW | 125ps |  |
| START | 30ps | |
| LASER | 10ps | |
| COUNTER | 36ps | |
| TARGET | 30ps | |
| DECONVOLUTED | 110ps | |

90 100 110 120 130 140 ps

K. Hana, H. Jelinkova, I. Prochazka, B. Sopko
 Single Photon Solid State Detector For Ranging ...

Active Quenching: 0.86 μm

SINGLE PHOTOELECTRON RANGING

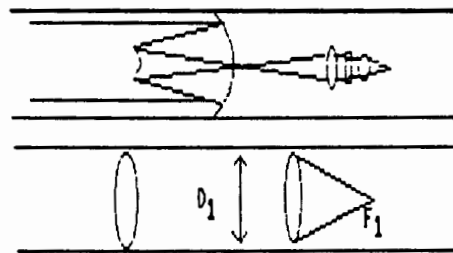


1.06 PHOTON PENETRATES NEUTRAL REGION

| | |
|--------------|-------|
| RAW | 225ps |
| START | 30ps |
| LASER | 18ps |
| ORTEC | 20ps |
| COUNTER | 36ps |
| TARGET | 30ps |
| DECONVOLUTED | 220ps |

Field of View / Max. Beam Divergence

RECEIVER OPTICS



TRANSMISSION EFFICIENCY

$$\eta = \frac{\beta_{\text{diode}}^2 (f_1/D_1)^2}{\beta_R^2 \cdot D^2}$$

IF $\beta=45\mu\text{m}$, $f_1/D_1=1$, $\eta=1$ $\beta_R \text{ LIMIT} = \frac{45 \cdot 10^{-3}}{D}$

| | | | | |
|--------------------|------|----|------|------|
| TELESCOPE DIAMETR | 1.5M | 1M | 0.6M | 0.3M |
| MAX. FIELD OF VIEW | 6° | 9° | 15° | 30° |

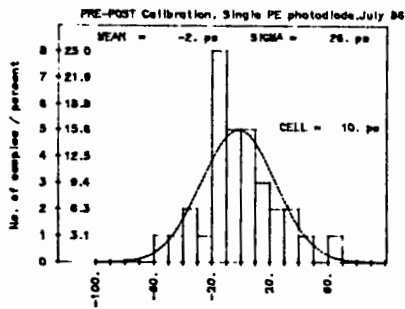
K. Hanal, H. Jelinkova, I. Prochazka, B. Sopko
Single Photon Solid State Detector For Ranging ...

5

K. Hanal, H. Jelinkova, I. Prochazka, B. Sopko
Single Photon Solid State Detector For Ranging ...

6

System Stability



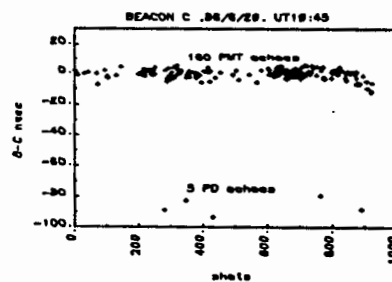
PERIOD JULY 1986
SERIES 100-200 ECHOES
WAVELENGTH 0.53 μm
SINGLE PHOTOELECTRON

K. Hanal, H. Jelinkova, I. Prochazka, B. Sopko
Single Photon Solid State Detector For Ranging

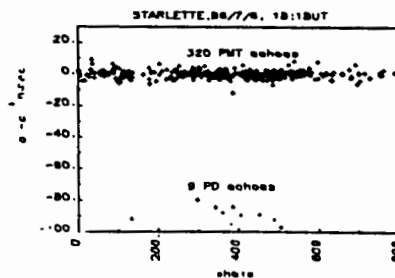
7

Satellite Ranging

BEACON-C




STARLETTE



K. Hanal, H. Jelinkova, I. Prochazka, B. Sopko
Single Photon Solid State Detector For Ranging

8

| HPSS diode ruggedness | |
|---|--|
| <p>Diode used as a SLR experimental receiver detector, the system was alligned using corner cube at 100n, accidentally, the MD were nissing lasing with the full power</p> <p>total energy 70 nJ power flux density 7.000 GW/cm²</p>  <p>NO DAMAGE</p> | |
| <p>K. Hanal, H. Jelinkova, I. Prochazka, B. Sopko Single Photon Solid State Detector For Ranging ...</p> | |

| Summary / Single Photon Detectors Review | | | | |
|---|-------------|------|--------------|--------------------|
| | Hanal et al | | PMT dyn./MCP | Bowman et al |
| | Geig | SPAD | | |
| JITTER psec | 0.53 | 98 | 118 | 298 185 253/162/98 |
| | 1.06 | 220 | 220 | |
| QUANTUM EFFICIENCY % | 0.53 | 10 | 10 | 10-30 28 |
| | 1.06 | 2 | 2 | 0.3 |
| DARK COUNT kHz | | 6 | 6 | < 0.1 |
| DEAD TIME incl. discrim | | | 150ns | 60ns 100 μs |
| OUTPUT PULSE per Photoel. | 2 V | NIM | | 2-50mV 3 V |
| RUGGEDNESS | excellent | | low/very low | excellent |
| FIELD OF VIEW | 9"/1n | | no limit | |
| TEMPERATURE | room | | room | -68°C |
| DISCRIMINATOR | yes | no | yes | yes |
| POWER SUPPLY | 30V | | 2.5kV/5kV | 160 V |
| GATE | TTL | NIM | HV/HV | 50 V |
| <p>K. Hanal, I. Prochazka, H. Jelinkova, B. Sopko Single Photon Solid State Detector for Ranging at Room.</p> | | | | 9 |

"CONSTANT FRACTION" DISCRIMINATORS IN FEW
AND MULTIPHOTOELECTRON LASER RANGING

W.A. Kielek
Departement of Electronics
Institute of Radioelectronics
Warsaw University of Technology
Nowowiejska str. 15/19 00-665 Warsaw - Poland -

Telephone 21007653 or 253929
Telex 813 307

ABSTRACT

The report explains some not widely known properties of c.f. discriminators used in nuclear techniques when using in laser ranging, as for instance mean value of timing point walk with signal energy, and the possibility of jumps in results in some conditions. Accuracy optimization methods are given for the case of the absence of jumps.

"CONSTANT FRACTION" DISCRIMINATORS IN FEW-
AND MULTIPHOTOELECTRON LASER RANGING

W.A. Kielek
Department of Electronics
Institute of Radioelectronics
Warsaw University of Technology
Nowowiejska str. 15/19 00-665 WARSAW, POLAND

Telephone 21007653 or 253929
Telex 813 307

ABSTRACT

The report explains some not widely known properties of c.f. discriminators used in nuclear techniques when using in laser ranging, as for instance mean value of timing point walk with signal energy, and the possibility of jumps in results in some conditions. Accuracy optimization methods are given for the case of the absence of jumps.

1. GENERALITIES

Almost all so called "constant fraction" discriminators use the principle of work as follows [1], [2], [3], [4]: from the input signal attenuated in accordance with fraction value, the input signal unattenuated but properly delayed is subtracted, and resulting signal is examined for zero - crossing. After that subtraction, one obtains the signal

$$\psi(t) = f \cdot f(t) - f(t - T_d) \quad (1)$$

where: f - fraction, T_d - delay, $f(t)$ - input signal.

This operation is done using for instance block schemes as at Fig. 1. All ORTEC, TENNELEC 454 and 455, EC&G and almost all other c.f. discriminators used in nuclear technics follow this principle of work. The independence of timing point on the amplitude of incoming pulses is preserved in case of constant deterministic shape of them. This situation is illustrated at the Fig. 2. There is the single zero - crossing only in case of that deterministic pulse signal case.

The signal at the PMT output, it is the sum of random Poisson number of PMT single-photoelectron responses, each of deterministic shape, but of random amplitude. The single realisation of that signal can be described by the formula:

$$f(t) = \sum_{i=1}^K g_i f_{SER}(t - t_i - \tau_i) \quad (2)$$

where: K - Poissonian number of photoelectrons realised, g_i ,

t_i , τ_i - random variables: PMT gain, times of PE generation at the photocathode, and delay in PMT, respectively; $f_{SER}(t)$ - deterministic shape of single PE (photoelectron) response of PMT. Due to existence of the sum $t_i + \tau_i$ in parentheses of formula (2), it is clear that probability density of PMT delay curve has got the same effect on the accuracy as the laser pulse shape, and the "equivalent" laser pulse can be introduced, of the shape of the convolution of laser pulse and PMT delay density curve. In case of single - photoelectron signal the shape of the signal is the same in each realisation. It is also true when the signal is composed of few or many PE but the length of the laser pulse and PMT delay density curve is very short in comparison with the single electron response pulse of the PMT tube.

2. POSSIBILITY OF JUMPS

When it is not the case, the shape of the input signal is random, not the same in each realisation. For few PE in realisation of the signal, and sufficiently small relation between widths of f_{SER} and convolution of the laser pulse and PMT delay density curve, the width of f_{SER} is not enough to make one smooth pulse signal. There is the group of separated f_{SER} pulses with breaks between them. The signal can be also of the form of the multi - top single pulse. In both such cases the resulting signal at the input of the zero - crossing sensitive trigger can have more than one zero - crossing (Fig. 3). The time position of work of the discriminator jumps from the right position to the first zero - crossing. This effect produces the increase in standard deviation and decrease in the mean value of results.

Especially severe influence on the results can have this effect, when the laser signal is not well limited in time, for instance when the main signal pulse stands at some pedestal of weaker radiation (e.g. when using pulse chopper), or when laser pulse is a Gaussian pulse. For such signal, in few - and multi - PE work there exists the possibility to obtain the jumps in results in the direction to decrease the result by few nanoseconds.

This phenomenon is illustrated at the Fig. 4 (Gaussian signal pulse). Single photoelectrons generated by the weak laser radiation before main part of the signal can move in some realizations the time point of work of zero - crossing trigger from the right position to the wrong position few ns before the right one.

At low energies, there is no this effect due to small probability of generation of photoelectrons far before the central part of the laser pulse. At higher energies, when the photoelectron number is high, there exists the high probability of compensation of the influence of the first photoelectrons by the subsequent ones. The probability to obtain false zero - crossing at the summing point in the circuit is again small. The max. probability lies in the medium energy region, between 20 and 1000 PE, dependent on parameters such as fraction, filtration and delay.

It can be deduced from signal model and formula (1) that

probability of jumps should be smaller when: increasing the delay of delay line, or / and the filtration F, or / and the fraction value f. These statements are confirmed by simulations and experiment in laboratory and at the 1-st generation laser stations. Simulation results are given at Figs. 5 and 6.

3. WALK IN THE CASE OF ABSENCE OF THE JUMPS

But also when the jumps are absent, there is no possibility to obtain no delay walk with energy when using c.f. or fixed threshold discriminators. Suppose the symmetrical shape of the "equivalent" laser pulse. In case of the single photoelectron in the signal, the mean position of this photoelectron is in the centre of this pulse, say zero, due to equal probabilities of negative and positive values of PE position. But in case of two photoelectrons, the probability of positive value of position of both photoelectrons is 25% only. Then, the probability of existence of at least 1 PE on the left side from the zero position is 75% (50% for single PE). For very high PE number, the PMT output signal has got the shape of the f_{SER} convolution with the "equivalent" laser pulse shape, and the timing point goes to the negative position in accordance with the fraction value. Then, for the signal following (2), the walk is unavoidable even in the ideal case of no walk for deterministic signal shape. Some results for walk obtained from simulations are given at Fig. 5.

4. STANDARD DEVIATION

There exists the proof, that normalised to the pulse half-width random error, approximately, for large PE number, follows the formula:

$$\sigma_{\Delta}/T = g_1 \alpha^{1/2} N^{-1/2} \quad (3)$$

where α is the mean square of the normalised to unity PMT gain, N is the mean PE number, T - half of width of the pulse, or σ parameter of Gaussian pulse.

The g_1 coefficient obtained by simulations is given at the Fig. 6.¹ Fortunately, no jumps are present up to 20 PE energy level. Well limited in time (for instance trapezoidal) waveforms without wide pedestal do not produce the jumps. In case of absence of jumps, this discriminator is quite good, especially for the random error.

The theoretical formula I obtained (remarks about method in [5]) for g_1 coeff. dependent on f, F and w (fraction, filtration and g_1 normalised delay respectively) when the signal and filter (PMT) response is of the form of Gaussian pulse is as follows:

$$g_1^2 = \left\{ f^2 \exp \left[- \frac{z+1}{2z+1} A^2 \right] + \exp \left[- \frac{z+1}{2z+1} B^2 \right] + \right. \\ \left. - 2f \exp \left[- \frac{z+1}{2z+1} \left\{ \frac{w^2}{2} \left(z + \frac{1}{2} \right) + \left(\frac{\ln \frac{1}{f}}{w} \right)^2 \right\} \right] \right\} \cdot \\ \cdot \frac{z+1}{z \sqrt{2z+1}} \cdot \left\{ B \exp \left[- \frac{B^2}{2} \right] - f A \exp \left[- \frac{A^2}{2} \right] \right\}^{-2} \quad (4)$$

where: $w^2 = \frac{T_d^2}{\sigma^2 + \sigma_F^2}$, T_d - delay time at Fig. 1, $z = (\sigma/\sigma_F)^2$
 $F = (8 \ln 2)^{1/2} \cdot \sigma_F/\sigma$

$$A = \frac{w}{2} - \frac{\ln \frac{1}{f}}{w}, \quad B = -\frac{w}{2} - \frac{\ln \frac{1}{f}}{w}, \quad \sigma, \sigma_F - \text{parameters}$$

of Gaussian signal and filter response, respectively. Computations from formula give the results as at the Figs. 7, 8, 9.

The case of f equals 1, there is also the case of Short Circuited Delay Line shaping and zero crossing detection. The results indicate that proper choice of parameters can give the same standard deviation as for max. likelihood estimation [6].

5. CONCLUSIONS

- A. The mean value change is unavoidable when using C.F. timing in case of changing the energy level from 1 to few PE. That change is proportional to the width of the convolution of laser pulse and PMT delay density curve.
- B. Above 10-20 PE energy jumps in results can exist. This effect is absent for laser pulse waveforms well limited in time.
- C. Probability of jumps decreases when increasing the filtration (f_{SER} width), fraction, delay, and charge sensitivity of zero-crossing trigger or comparator.
- D. In the absence of jumps, for proper values of F , T_d , f parameters, Gedcke-Mc Donald type c.f. discriminator is good, especially for standard deviation, and is only slightly poorer in mean value walk than the c.f. discriminator with peak value memorization [5].
- E. Standard deviation reaches the minimum for much higher delay values than the value which is needed to obtain constant fraction work for the deterministic signal.

REFERENCES

1. D.A.Gedcke, W.J. Mc Donald. Nucl. Instr. Methods 55, 1 (1967).
2. M.R.Maier, P.Sperr. Nucl. Instr. Methods 87, 13 (1970).
3. T.J.Paulus, M.O.Bedwell. "High Speed Timing Electronics and Applications of Hybrid Electronics in Nuclear Instrumentation". ORTEC Inc.
4. Instructions and data sheets for ORTEC and other c.f. discriminators.
5. W.Kielek. V-th Workshop on Laser Ranging Instrumentation, Proceedings, p. 112-118.
6. I.Bar David. IEEE Trans. on Information Theory, IT-15, 31 (1969).

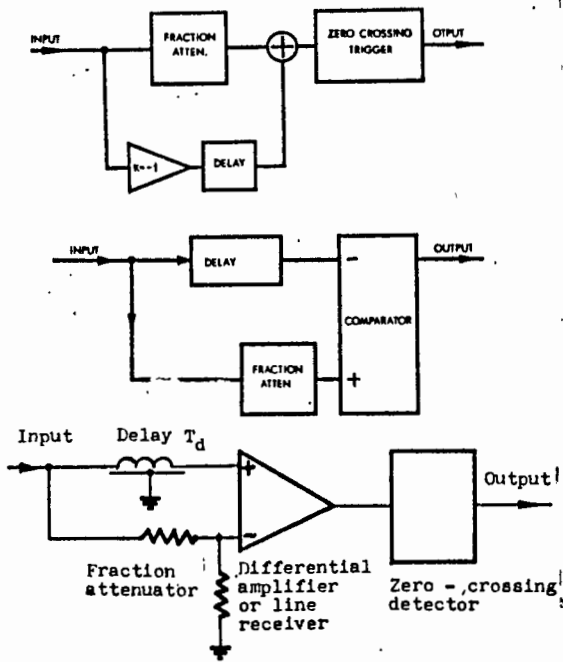


Fig. 1 Variants of principal scheme of nuclear "c.f." discriminators

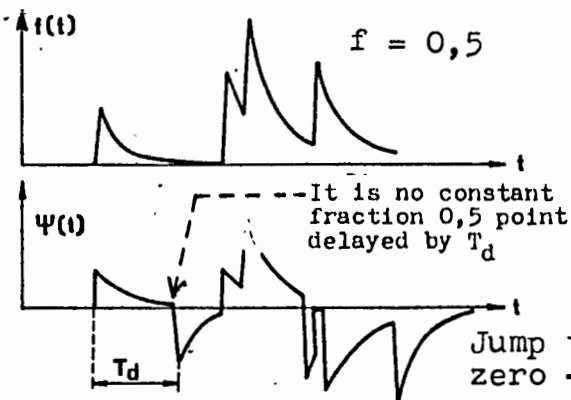


Fig.3 Illustration of work of the circuits from Fig.1, few PE, stochastic signal

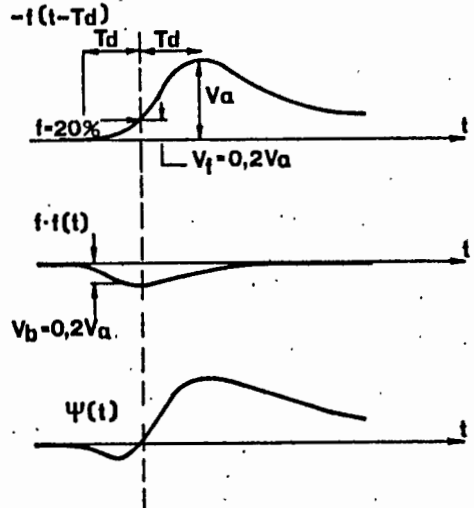


Fig.2 Illustration of work of the circuits from Fig.1, deterministic in shape single signal pulse

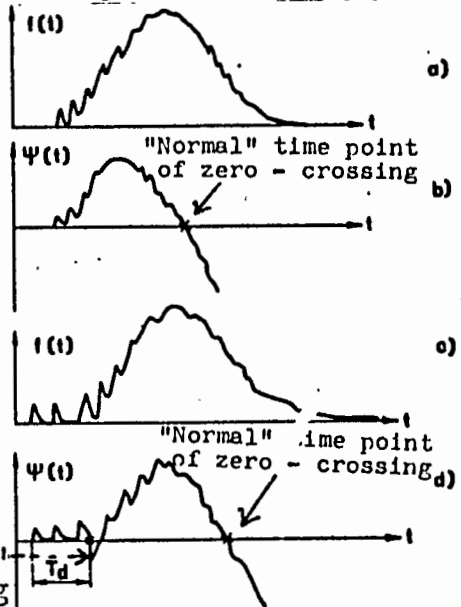


Fig.4 The same as at Fig. 3, 50+1000 PE, small filtration F(f_{SER} width divided by half-width of the laser pulse)

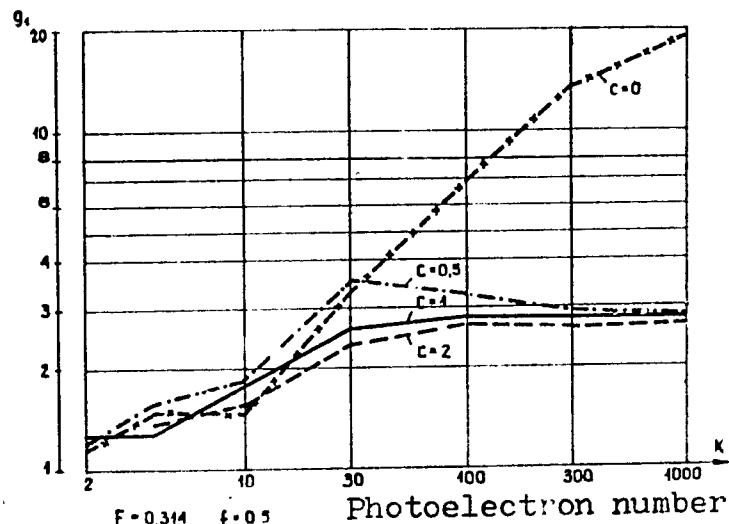


Fig. 6a

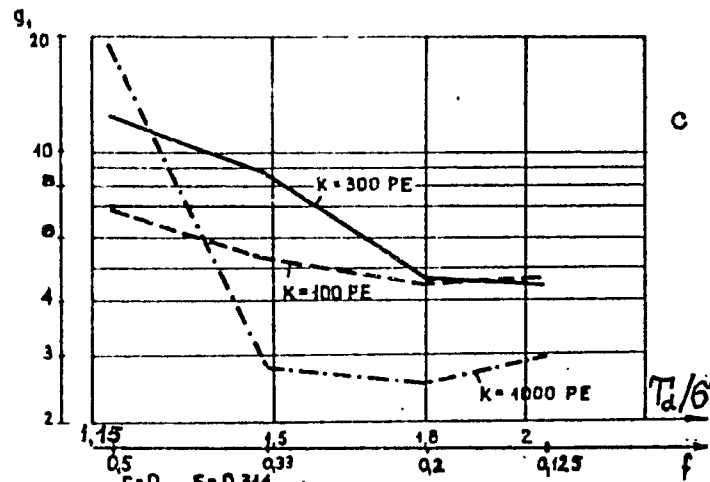


Fig. 6b

Fig. 6. g_1 values obtained from simul. a/ vs energy and charge sensitivity, b/ vs energy and filtration, c/ vs energy and normalised delay T_d/σ (fraction value changes also)

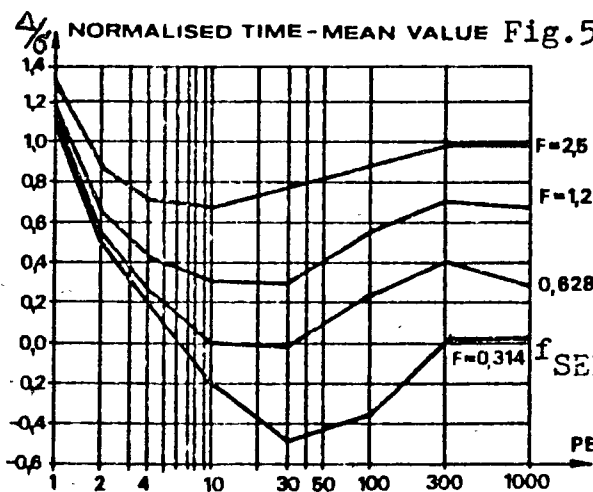
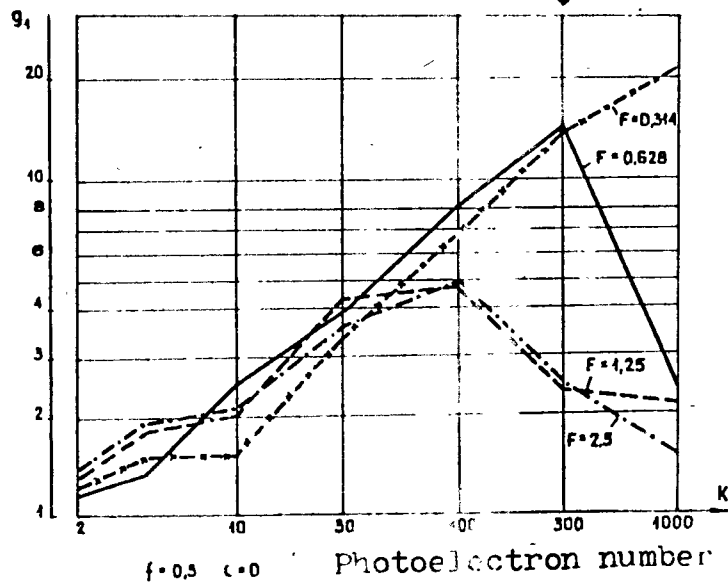


Fig. 5. Change in mean value of result vs energy obtained from simulations (F it is the f_{SER} width divided by σ_{SER} parameter of Gaussian laser pulse).

$$f_{SER} = \exp[-t/5\sigma] - \exp[-t/\sigma]$$

in all simulations

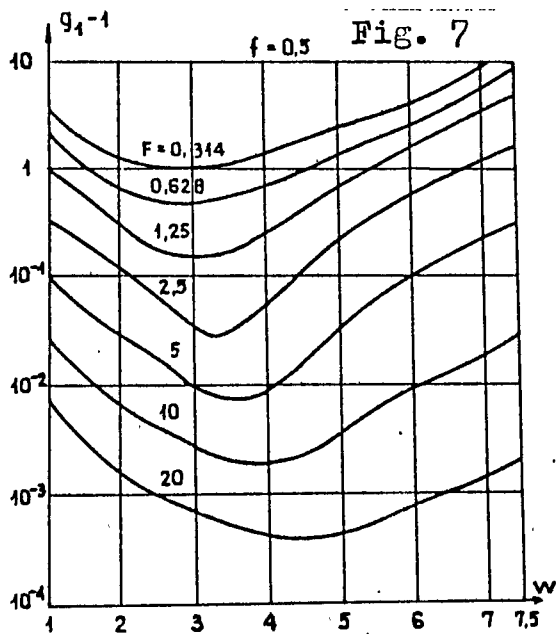
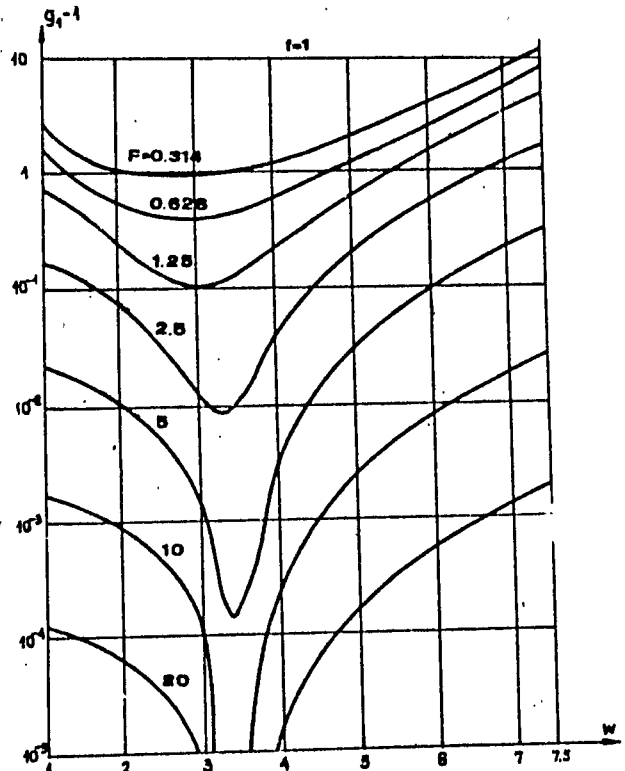
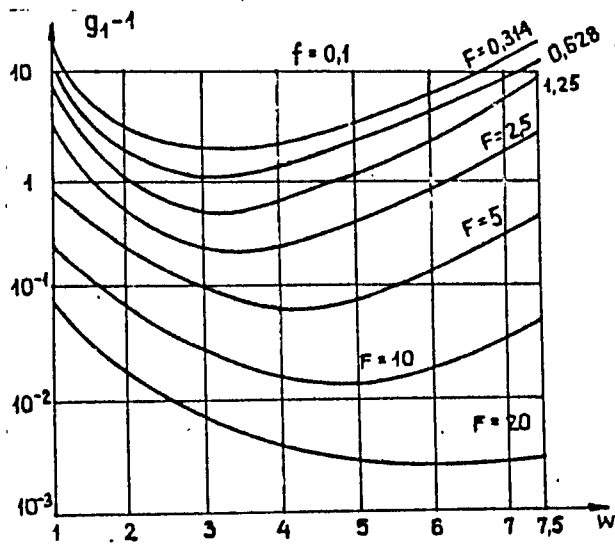


Fig. 7. g_1-1 values vs delay W and filtration F for 3 values of fraction f .

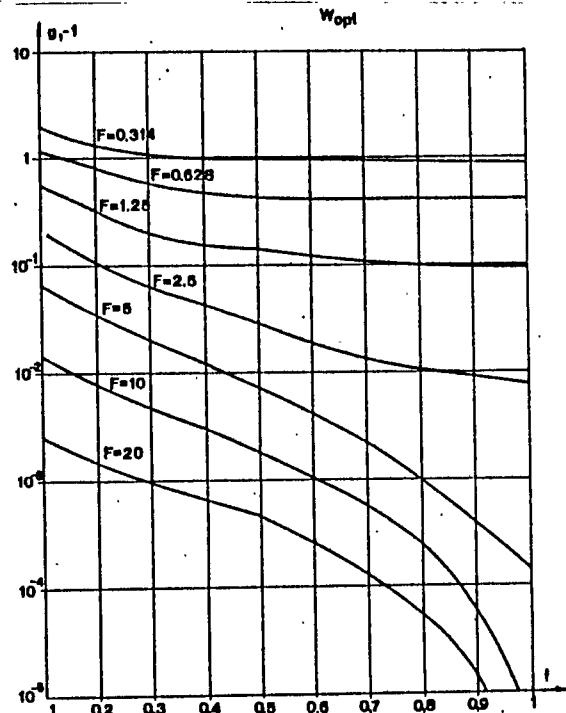
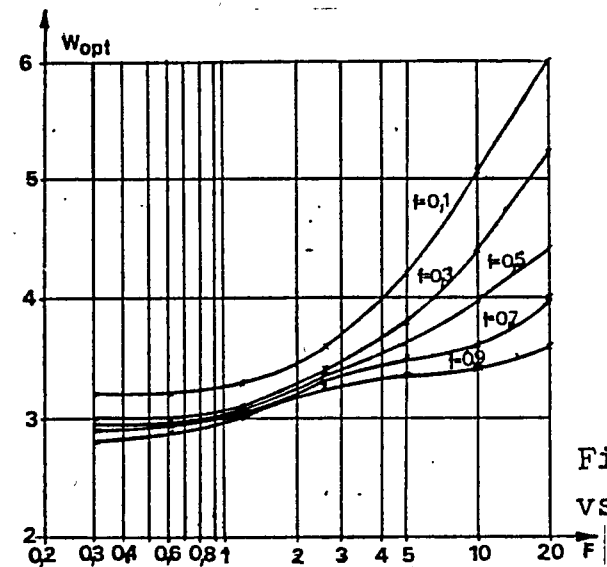


Fig. 9. g_1-1 values for W_{opt} vs fraction f and filtration F

Fig. 8. Optimum delay w_{opt} values vs filtration F and fraction f .

CALIBRATION OF SUB-PICOSECOND TIMING SYSTEMS

B.A. Greene
Division of National Mapping
P.O. Box 31
Belconnen ACT 2616 - Australia -

Telephone (6162) 525095
Telex AA 62230

ABSTRACT

The difficulties of calibrating picosecond precision timing systems are discussed. A wide range of techniques are considered, and a minimum configuration for rigorous calibration is described. High speed techniques that lend themselves to full automation are evaluated in the context of a fully operational system.

CALIBRATION OF SUB-PICOSECOND TIMING SYSTEMS

B.A. Greene

1. Introduction

The recent development of timing systems with picosecond and even sub-picosecond accuracy has stimulated a requirement to calibrate such systems. In SLR systems the systematic errors are of overriding importance, and even if real time surveillance of the absolute accuracy [1] of the SLR system as a whole is maintained, it is still essential to be able to calibrate the timing sub-system independently. Once calibrated, it is a tool which can then be used to characterise the errors, systematic and otherwise, in other sub-systems.

The principal requirements for timing system calibration are to establish

- . stability
- . continuity ('smoothness')
- . linearity

If these characteristics are properly established, then the absolute accuracy of the timing system is rigorously proven.

In the context of a time interval measurement system, stability can be defined as the RMS error associated with a straight line fit of zero slope against time for a constant (not necessarily known) time interval.

Linearity is defined as the degree to which system error is proportional to length of time interval measured.

Continuity is defined as the degree to which linearity and stability are maintained as the time interval between test (calibration) points is reduced continuously.

A rigorous calibration procedure must examine all of these parameters.

In this paper we discuss several calibration techniques, and the role they can play in establishing system accuracy in terms of which of the above criteria are adequately tested.

2. Delay Line Calibrations

An established calibration technique for nanosecond timing systems utilizes an array of switchable coaxial delay lines, which have been pre-measured and are thus of 'known' delay. Even if it is assumed that the original calibration of each delay line was accurate without limit, this technique is unsuitable for picosecond calibrations because

- cable ageing causes delay changes
- cable flexing causes delay changes
- typical switch repeatability is only 3 ps RMS
- cable delays are temperature dependent
- coaxial connect-reconnect repeatability is only 3 ps RMS

This technique can be adapted to produce sub-picosecond tests of stability only. If the cable temperature is controlled such that the delay is stable to 0.5 ps RMS, then long term stability tests can be conducted on the timing system. A typical temperature sensitivity for coaxial cable is 0.03% per degree (C). Although temperature servos have been developed which can offer .001°C temperature control, it is in practice difficult to control coaxial cable to better than 0.1°C for each 50 ns of delay. That is, 0.5 ps stability can be readily obtained up to about 17 ns of delay. This is of little use if time interval units (TIUs) are used directly (i.e. in time interval mode) to measure satellite range. However, if precision TIU's are used as the high precision vernier of an epoch timing system, it is not necessary for them to count beyond 20 ns. Thus temperature stabilised delay lines can be used for 0.5 ps stability tests throughout the range of use of the TIU.

3. Variable Delay Lines

Rigid coaxial delay lines have been manufactured for calibrating the linearity and continuity of timing systems. These systems proliferated during a period when 100 ps timing system accuracy was the achievable limit, and could be expected to be inadequate for picosecond calibrations. This is the case, although some well constructed variable (rigid) coaxial delays can produce 3 ps RMS linearity and repeatability. Their stability will depend on delay length chosen, heat sources and sinks attached to the delay, and mechanical wear.

4. Dual Oscillator Techniques

It is now possible to obtain crystal oscillators which have sub-picosecond stability over 1 second, and ageing rates which are undetectable over 20 minutes with present instrumentation. The relative phase of two such oscillators provides a very slowly and linearly time varying delay for calibration purposes. This calibration technique is in everyday use at some SLR sites [2,3], using less stable oscillators for coarser (50 ps) calibrations. Provided that care is taken in generating the pulses to the timing system from the crystal output frequencies, this technique can give 1 ps linearity and accuracy, and sub-picosecond continuity checks.

5. Phase Locked Loop Method

An alternative oscillator phase technique utilises a single high stability oscillator and another oscillator phase-locked to it. The phase angle is programmable allowing selection of the relative phase of the crystals and thus a time interval. This technique gives linearity and continuity test capability, but is inherently noisier than the dual oscillator technique (above).

The noise attributable to the phase locking process can be brought down to around 5 ps if great care is taken with the circuit design. In addition, several picoseconds of systematic error arise from non-linearities in state-of-the-art phase angle programming circuits.

6. Optical Delay Line (ODL)

The time required for light to travel up to 10 m in air is virtually independent of environmental parameters [4]. To effect a 0.5 ps change in observed optical delay, environmental changes of the following order would be required:

$$\begin{array}{l} P = 30 \text{ mb} \\ \text{or} \\ P_w = 200 \text{ mb} \\ \text{or} \\ T = 10^\circ\text{C} \end{array}$$

[where P is atmospheric pressure, P_w is water vapour pressure, and T is air temperature]

The use of an optical delay line provides excellent linearity, accuracy, continuity, and stability. For example, if the delay elements are used to form a one-way light path, 100 microns of displacement of either end will cause a 0.33 ps change in the delay. Since the delay path can be very accurately controlled, to within a few microns, femtosecond resolution and accuracy can be obtained for differential delays.

For a two-way (folded path) calibration range, only 1.5 m of travel is required to produce a delay change of 10 ns. Such a path length is both simple to control environmentally and quite simple to automate for translation with 0.1 mm accuracy. Thus high resolution verniers with up to 10 ns full scale count can be absolutely calibrated to 0.66 ps under program control.

The technique is usually limited by the characteristics of the optical transmitter and receiver used to generate and detect the light pulse which transits the delay so accurately formed. Using a 30 ps FWHM diode laser transmitter, and a 30 ps risetime detector, sub-picosecond relative accuracy, stability, and resolution can be achieved, provided environmental parameters are controlled.

7. Ensemble Techniques

The process of refining the accurate determination of time interval is analagous to that of defining time itself. The well established technique of using clock ensembles and optimised algorithms for manufacturing a timescale can be readily adapted to the time interval problem.

The use of as large an ensemble as possible of time interval counters is suggested by two factors arising from a very limited development program for TIUs for the Natmap Laser Ranging System (NLRS) at Orroral:

- . no single TIU was ever constructed or tested which had better than 8 ps RMS single-estimate uncertainty for time interval.
- . even the very best units ever tested at Orroral would exhibit occasional and inexplicable short term (minute) systematic excursions of up to 4 standard errors of a single estimate as measured from the long term average. Over a long period (20 mins) these units would produce sub-picosecond (averaged) stability of a mean estimate.

Since the Orroral program goal was to produce 5 ps RMS single estimate random errors with 0.5 ps systematic error, it was necessary to aggregate the performance of many TIUs to damp out excursions and to statistically reduce time interval errors.

A feature of the ensemble technique is that it requires very compact TIU design, so that a large number of TIUs can be fed an electronic signal over short paths, and so that complete environmental control of the ensemble is possible.

It has been found that the ensemble techniques are very effective in improving the resolution and linearity of TIU systems. Ensemble techniques do not yield absolute accuracy, but do facilitate absolute accuracy calibration of systems by improving linearity. The decay of accuracy of an ensemble is also significantly slower than that of individual TIUs, allowing less frequent resort to absolute accuracy calibrations, which can be tedious to execute rigorously.

The ensemble techniques can be used to calibrate individual TIUs simply by examining the performance of the unit in comparison to the ensemble mean. In general, if the ensemble is well behaved, errors in the individual TIUs can be readily identified. The technique lends itself very well for total automation, but is clearly not rigorous.

8. Calibration Techniques for the NLRS

Although the NLRS has the capability to apply any of the above calibration techniques, in practice the only techniques routinely used are:

- . optical delay line
- . fixed (stable) cable delays
- . ensemble

The NLRS is constrained to operate almost totally automated. Thus only techniques which can lend themselves to total automation can be routinely used. The optical delay line method, which is the only rigorous technique listed above, is used very infrequently because it is not totally automated (here defined as requiring no user intervention whatsoever).

The timing system philosophy for the NLRS uses a large ensemble to reduce random error and give momentum to the system (the ensemble characteristics change more slowly than those of its elements). These ensembles can then be monitored very infrequently using a primary (rigorous) test such as ODL.

Such a complex calibration technique is not required to monitor the ensembles for accuracy. In practice a very simple approach is used, called fixed delay epoch measurement (FDEM).

For FDEM, two electronic pulses are obtained from a fixed, stable, delay cable built into the timing system. One NLRs timing ensemble measures the epoch of the first pulse, whilst a second ensemble measures the epoch of the second. The pulses are sourced such that they are totally random in phase with respect to the time base of the epoch timing system. Thus the full count range of the ensembles will be sampled if many measurements are taken. The delay is obtained by subtracting epochs. An error in either ensemble, at any point in its range, will cause the distribution of delay estimates to depart from the ideal. This is most easily seen as an increase in the spread of the distribution.

Because the delay is fixed, the error space of the ensemble measuring the second epoch is not sampled randomly. That is, the point in its range which is sampled is 100% correlated with the sample point of the first ensemble. Thus it is possible for errors to compensate and go undetected. The probability of this is reduced significantly if more than one delay is used.

The utility of this technique, which is used before every tracking operation, has been borne out by occasional applications of rigorous tests such as ODL.

The three techniques in routine use at Orroval are thus applied in the following way:

- (a) On every shot. On each shot, at least 34 estimates of epoch are made. The ensemble size is large enough to give a good reduction in systematic drift and random error over individual TIU elements. Individual TIU readings are processed through a double-pass filter which utilises the recent performance history of a TIU to adjust its reading before comparing it to the ensemble mean in the filter process. Units may be 'accepted' or 'rejected'. Consistent rejection implies a need for repair or recalibration.

Also on each shot, a real-time calibration of system delay is made. This is essentially an ODL calibration in which the delay is not known a priori to better than 200 ps, because of long term drift in the apparatus. However, the system delay so measured can be and is used in an FDEM sense. The calibration curve is displayed, shot by shot, in real time, with picosecond resolution, so that the operator (if present) can monitor the overall system performance, including timing. The data is continuously analysed in real time, and statistics presented to the operator. Only gross errors of over 40 ps would be detected at this stage because the detector used (MCP-PMT) has around 40 ps RMS error itself, and can walk 40 ps during a typical SLR pass.

- (b) Before each pass.

Before each pass, over 3000 samples of timing system performance are taken in FDEM mode, under total software control. The FDEM algorithm in use calculates the signal delays to each ensemble, and trims them into equality before the pass commences (usually only a few ps adjustment).

- (c) Occasionally the granularity and accuracy of the timing system are checked independently. A good test for continuity of the timing system is obtained by taking a delay line and heating it for 1 minute and then allowing it to cool. The thermal relaxation produces a delay continuum. If the delay is sampled at 50 Hz, delay changes of 20 fs can be sampled. Figure 1 shows a typical result from a continuum test of this kind, showing individual delay measurements. Strong structure at the picosecond level is evident, but the results show very good performance overall.

The accuracy calibration used is the ODL technique, applied infrequently because of its need for operator intervention.

Finally, system stability checks are carried out periodically. A typical stability plot for the NLRS timing system is shown in Figure 2. Each point plotted is a normal point of 400 ensemble estimates of a fixed and stable delay. The RMS error of a straight line fit to the data shown is around 0.6 ps, which is a typical result. The suggestion of a cyclic systematic error is present in the data. This has been seen in ODL tests also, so it is likely to be attributable to the timing system.

9. Comments

The electronic measurement of time interval to the picosecond level is exceedingly complex. The NLRS timing system can only approach picosecond performance on a statistical basis. That is, it is beyond our present technology to adjust a delay by 5 picoseconds and be 100% confident that the TIU single sample reading, or even that of a TIU ensemble, will change by 5 picoseconds. However, if many hundreds of estimates are made, delay changes of less than 1 ps can be accurately determined by TIU ensembles.

REFERENCES

1. Greene, B.A., "Calibration of Sub-Millimetre Precision Satellite Laser Ranging Systems", proc. Sixth International Workshop on Laser Ranging Instrumentation, to be published.
2. Sinclair, A., Royal Greenwich Observatory, UK, Private Communication.
3. Steggerda, C. University of Maryland, USA, Private Communication.
4. Owens, J.C., "Optical refractive index of air dependence on pressure temperature and composition", Appl. Opt., Vol 6, No 51, 1967.

Figure 1
TIMING CONTINUUM TEST

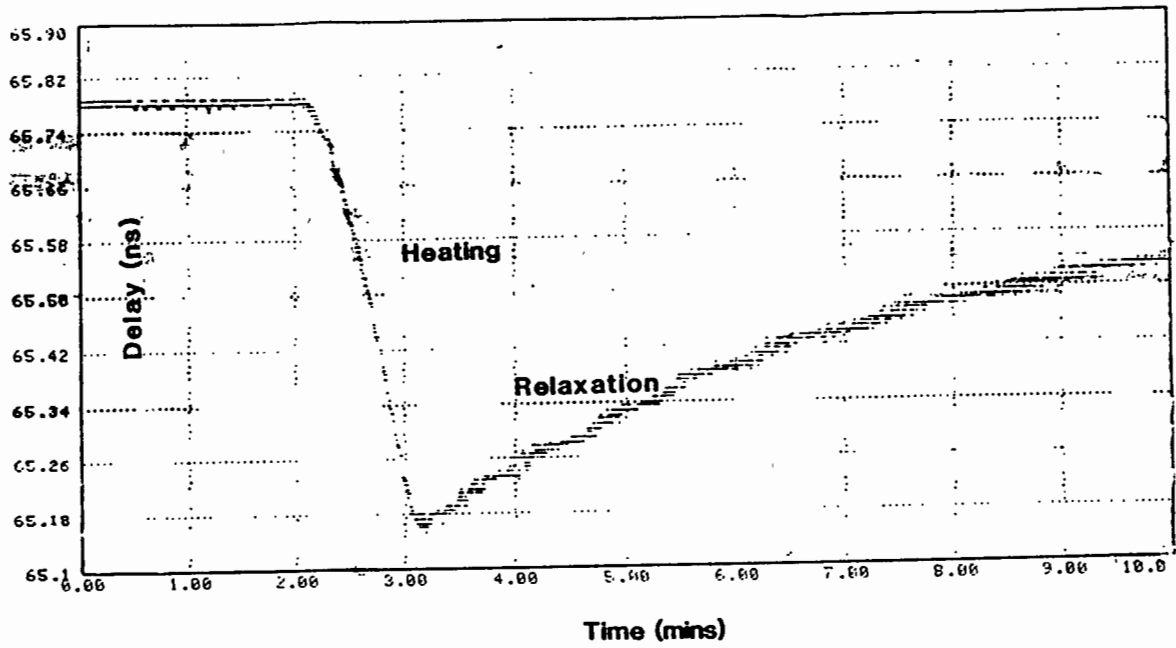
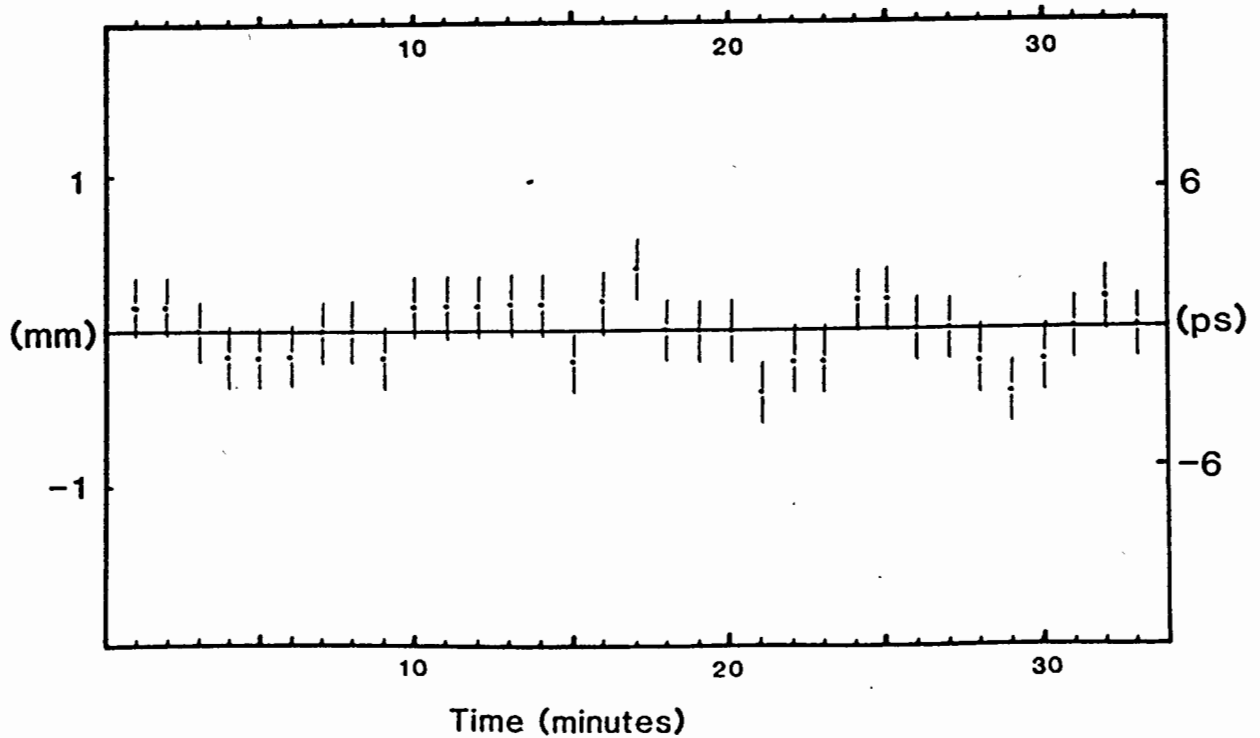


Figure 2
NLRS TIMING STABILITY



RECENT ADVANCES IN THE GLTN TIMING AND
FREQUENCY INSTRUMENTATION

P. Dachel, and A1
Bendix Field Engineering Corporation
One Bendix Road
Columbia, Maryland 21045 - USA -

Telephone (301) 964 7189
TWX 198120 BENFLD COLB

ABSTRACT

The stringent epoch time requirements necessary for the Goddard Laser Tracking Network to satisfy its global geodetic survey programs have consistently pushed the state of the art. As geophysical baseline accuracy requirements have approached the sub centimeter level, new time and frequency technologies have been sought.

This paper will describe the early Global Positioning Satellite (GPS) time transfer receiver development. The GPS receiver development program at the Naval Research Laboratory for NASA was the forerunner of many commercial efforts which have led to unitized construction and firmware controlled receivers. Along with the GPS receiver development, NASA worked with other U.S. and international timing organizations to develop strategies to optimize the use of these receivers by forming a global timing network for geophysical measurements. Through the use of "common look" techniques a laser tracking site may observe a GPS satellite simultaneously with the data reduction center which is in turn synchronized to UTC via USNO. Using this common look technique, orbital & spacecraft clock systematic errors may be minimized.

With a need for greater synchronization accuracy also grew the need for improved short term frequency stabilities. In the past, where less accurate geodetic measurements were being performed, much of the low level phase noise and frequency instabilities were seen as random processes. Recent investigation has shown that many of these frequency instabilities have systematic signatures which contribute to measurement error. To meet the sub centimeter accuracy goal of the Crustal Dynamics Program the need for picosecond short term stabilities in generation, distribution and monitoring systems is becoming a necessity. System options are described which will allow a spectrally pure crystal oscillator (better than 2 picoseconds over a 50 millisecond interval) to be frequency locked and steered to epoch time accuracies of 100 nanoseconds via the GPS system.

Prior to the inception of the Goddard Laser Tracking Network (GLTN) ten years ago, NASA required that satellite support stations be synchronized within ± 25 microseconds. The GLTN need for ± 1 microsecond world-wide time synchronization required the development of new methods for maintaining time synchronization.

Recognizing that conventional means of timekeeping using LORAN-C, HF and VLF could not practically achieve the required ± 1 microsecond global clock synchronization, the cesium portable clock was used to provide time synchronization. Periodic portable clock trips were made to each station to determine the station's nominal LORAN-C value. Each station's cesium clock offset from U.S. Naval Observatory (USNO) time was plotted from daily LORAN-C values, time steps were calculated to synchronize station time to USNO time, and the station was directed to make the proper equipment adjustments to achieve the recommended time step.

With the improvement of laser equipment and the demand for more accurate ranging, the need for sub-microsecond timing has become a valid requirement.

This need prompted investigation and development of satellite timing receivers in a combined effort between the Naval Research Laboratory and NASA.

The Navigational Technology Satellite receiver was developed as a forerunner to the GPS Time Transfer Receiver now being used for sub-microsecond time transfer.

GPS TIMING

Techniques are being developed to utilize GPS timing for the GLTN, with a goal of world-wide time synchronization to the greatest feasible accuracy.

To utilize the time transfer capability of the GPS, a timing receiver was developed by the Naval Research Laboratory (NRL) for NASA, was tested at field sites, and was used in time transfer experiments (References 1 and 2). The first commercial GPS time transfer receiver was built by Stanford Telecommunications Incorporated (STI). This receiver was evaluated for possible use in the GLTN. The STI and the NRL receivers are operated from a keyboard similar to that of a personal computer. The cost of the STI receiver was approximately one half that of the NRL receiver and it was more suitable for mobile installations. More recently a third receiver, the Frequency and Time Systems (FTS) Model 8400 was evaluated and found to be the best suited for GLTN operations because of its smaller size, unit construction and lower cost.

Figures 1 and 2 compare time transfer data obtained with an FTS 8400 GPS receiver or the identical Trimble 5000A and a cesium portable clock at several timing installations. Portable clock time was compared to USNO time before and after these trips. The measurements were supplemented by TV Line 10 measurements which were accurate to +/- 50 nanoseconds with respect to USNO.

Figure 3 lists current deployments of FTS 8400 GPS timing receivers in the GLTN.

GLTN GPS DATA COLLECTION

GPS time position measurements are made daily at the GLTN stations. The stations collect GPS data twice a day for each visible satellite. The raw time position reading is recorded during the 10-minute satellite observation pass. This data point along with the date, time, and satellite vehicle number are recorded for each measurement. The measurement data are transmitted to the NASA Communications Center in the daily Laser Operations Report (LOR). Also transmitted in the LOR is information concerning station time steps, frequency changes, power outages, equipment problems, etc.

AUTOMATED TIME POSITION SYSTEM (ATPS)

The Automated Time Position System is the means by which station time is monitored and analyzed for the GLTN. The ATPS

- o provides daily time position determination
- o calculates long term cesium frequency drift
- o predicts the date the station tolerances exceed 1 microsecond
- o evaluates the validity of data and data analysis methods

The System includes several computer programs that (1) read the LOR data into the ATPS data bases, (2) permit the manual entry, editing, deletion, and listing of data files and (3) perform the analysis of the timing measurements. The system is coded in FORTRAN and runs on a VAX computer

cluster. The cluster consists of two VAX-11/780 computers and one VAX 8600 computer. The analysis program is operator inactive and produces a printed data output. The data output consists of the source listing data from the data files used in the analysis, a least-squares calculation of the original source data, and a line printer graph of the original and least-squares data plot.

GPS COMMON VIEW

Utilizing the GPS common view technique described in Reference 3, orbital and spacecraft clock systematic errors can be minimized.

A common view/near common view GPS time transfer experiment was conducted in 1983 to determine the accuracy of GPS time transfer receivers for the GLTN (Reference 4). The experiment was conducted between the Bureau International de l'Heure (BIH), Paris, France, the Institute Fur Angewandte Geodasie (IFAG), Wettzel, Germany and the GLTN data reduction center at Columbia, Maryland. The local time bases incorporated HP5061 (Option 004) Cesium standards or hydrogen masers. Results of the experiment showed the overall accuracy to be consistently better than 100 nanoseconds. Recent improvements in the GPS system have permitted common view accuracies approaching 10 to 20 nanoseconds. (Reference 5).

Efforts are underway to utilize GPS common view techniques on a day-to-day operational basis in the GLTN (Figure 4).

TIME INTERVAL MEASUREMENT ERRORS

The GLTN utilizes Hewlett Packard 5370 time interval counters with an atomic standard for the time base. The 5370 has a 20 picosecond single shot resolution, however, the accuracy is typically +/- 40 picoseconds. The accuracy of the time interval measurement is influenced by the summation of:

- o trigger level
- o input signal noise
- o interval timing jitter
- o time base short term stability

Event timers developed by the University of Maryland and by the Division of National Mapping (Australia) reduce the internal timing jitter and improve the short term stability. The University of Maryland unit uses a 200 MHz oscillator phase locked to the atomic standard.

IMPROVEMENTS IN SHORT TERM STABILITY

Improved short term stability oscillators that can be steered to UTC via the GPS are being developed.

Austron, Inc. and the GLTN are developing a low noise disciplined frequency standard (Reference 6) that utilizes a microprocessor controlled system which automatically locks the frequency of a precision BVA crystal oscillator to an atomic standard having superior long term stability.

With the use of a third-order servo technique, the instrument is able to correct the frequency offset and aging of the internal BVA oscillator. If the frequency of the atomic standard is altered (due to loss of lock, loss of signal or failure) the unit will continue to apply corrections to the internal BVA oscillator. These corrections are calculated from data accumulated while the atomic standard is stable. These corrections are automatic and do not disturb the phase. This technique minimizes the effect of aging of the BVA oscillator and holds the unit to within +/- 3 parts in 10^{12} per day.

The short term stability (50 milliseconds to 100 seconds) of the low noise disciplined frequency standard is represented in Figure 5. The internal BVA oscillator has a short term stability σ ($\tau = 0.2$ to 30 seconds) $\approx 5 \times 10^{-13}$ and an aging rate of 1×10^{-11} per day. Frequency steering of the low noise disciplined oscillator by the atomic standard to epoch time accuracies of 100 nanoseconds via the GPS system can be achieved.

REFERENCES

1. J. Oaks, J. Buisson, C. Wardrip, "GPS Time Transfer Receivers for the NASA Transportable Laser Ranging Network", NASA/GSFC x-814-82-6, April, 1982.
2. J. Oaks, A. Franks, S. Falvey, M. Lister, J. Buisson, S. Wardrip and H. Warren, "Prototype Design and Initial Test Evaluation of a GPS Time Transfer Receiver", NRL report 8608, July 27, 1982.
3. D. W. Allan and M. A. Weiss, "Accurate Time and Frequency Transfer during Common-View of a GPS Satellite", Proceedings of 34th Annual Frequency Control Symposium, 1980.
4. C. Wardrip, J. Buisson, J. Oaks, et al., "An International Time Transfer Experiment", Proceedings of the 37th Annual Frequency Control Symposium, 1983.
5. M. A. Weiss, "Weighting and Smoothing of Data in GPS Common View Time Transfer", Proceedings of the 17th Annual Precise Time and Time Interval Applications and Planning Meeting, 1985.
6. B. Bourke and B. Penrod, "An Analysis of a Microprocessor Controlled Disciplined Frequency Standard", Proceedings of the 37th Annual Frequency Control Symposium, 1983.

| <u>FEB 5 1985</u> | <u>MOBLAS 1 TAHITI</u> | <u>GPS SV</u> | <u>PC VS USNO USING GPS</u> | <u>PC VS USNO CALCULATED</u> | <u>(GPS-USNO)-(PC-USNO)</u> |
|-------------------|----------------------------|-------------------|---------------------------------|----------------------------------|-----------------------------|
| | | 06 | 2.003 | 1.991 | +0.012 * |
| | | 08 | 1.996 | 1.991 | +0.005 |
| | | 09 | 2.009 | 1.991 | +0.018 |
| | | 11 | 2.012 | 1.991 | +0.021 |
| | | 13 | 1.999 | 1.994 | +0.005 |
| | | 12 | 1.995 | 1.997 | -0.002 |

ALL VALUES IN MICROSECONDS

TIMES VERIFIED BY PORTABLE CLOCK CLOSURES WITH USNO.

* ± 200 NANoseconds DUE TO SATELLITE AND PORTABLE CLOCK ERRORS.

FIGURE 1 - GPS VS PORTABLE CLOCK TIME TRANSFER.

| <u>DATE</u> | <u>LOCATION</u> | <u>(PC VS USNO) USING GPS</u> | <u>(PC VS USNO) CALCULATED</u> | <u>(GPS-USNO) - (PC-USNO)</u> |
|-------------|------------------------|-----------------------------------|------------------------------------|-------------------------------|
| FEB 12 1985 | CSIRO, AUSTRALIA | 2.087 | 1.989 | 0.098 * |
| FEB 13 1985 | NATMAP, AUSTRALIA | 2.050 | 2.030 | 0.020 |
| FEB 14 1985 | TIDBINBILLA, AUSTRALIA | 2.160 | 2.068 | 0.092 |
| FEB 16 1985 | MOBLAS 5, AUSTRALIA | 2.243 | 2.159 | 0.084 |
| FEB 19 1985 | TELCOM, AUSTRALIA | 2.262 | 2.262 | 0.000 |
| FEB 20 1985 | CSIRO, AUSTRALIA | 2.275 | 2.296 | -0.021 |
| FEB 22 1985 | HOLLAS, HAWAII | 2.395 | 2.406 | -0.011 |

ALL VALUES IN MICROSECONDS

USNO CLOSURE ON FEB 8 AND FEB 27, 1985

* ±200 NANoseconds DUE TO SATELLITE AND PORTABLE CLOCK ERRORS.

FIGURE 2 - GPS VS PORTABLE CLOCK TIME TRANSFER

| <u>STATION</u> | <u>DATE OF INSTALLATION</u> |
|----------------------------|---------------------------------|
| MOBLAS-2 ISRAEL | SEPTEMBER 85 |
| MOBLAS-5 WESTERN AUSTRALIA | OCTOBER 85 |
| MOBLAS-6 MEXICO | MAY 86 |
| HOLLAS HAWAII | APRIL 86 |
| SAO-2 PERU | AUGUST 86 |
| NATMAP AUSTRALIA | OCTOBER 85 |
| MLRS TEXAS | JUNE 86 |
| TLRS-1 GORF | NOVEMBER 85 |
| TLRS-2 GORF | NOVEMBER 85 |
| MATERA | NOVEMBER 86 (PROPOSED) |

FIGURE 3 - DEPLOYMENT OF FTS-8400 GPS TIME TRANSFER MONITORS

FREQUENCY COMPARISON OF VARIOUS STANDARDS

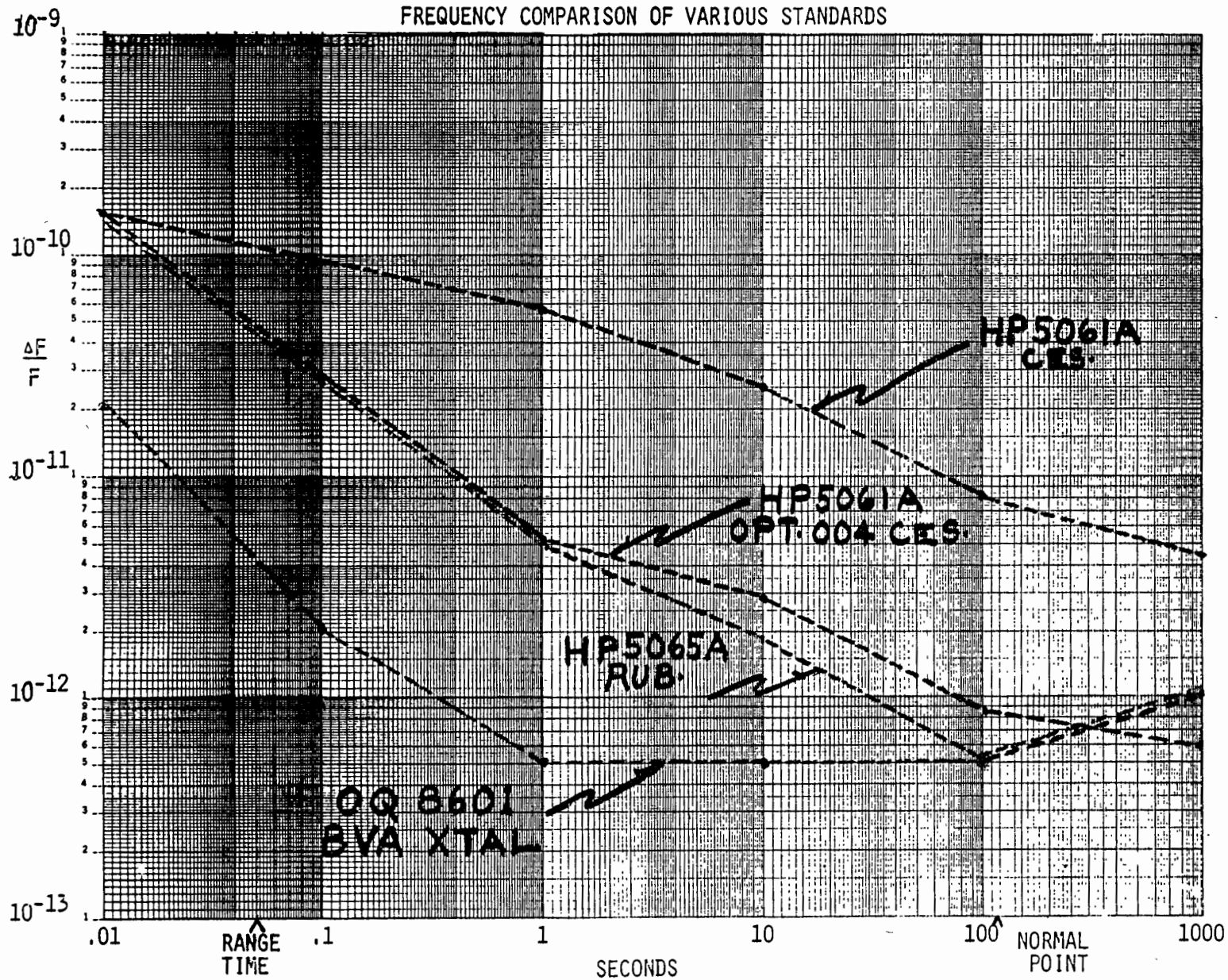
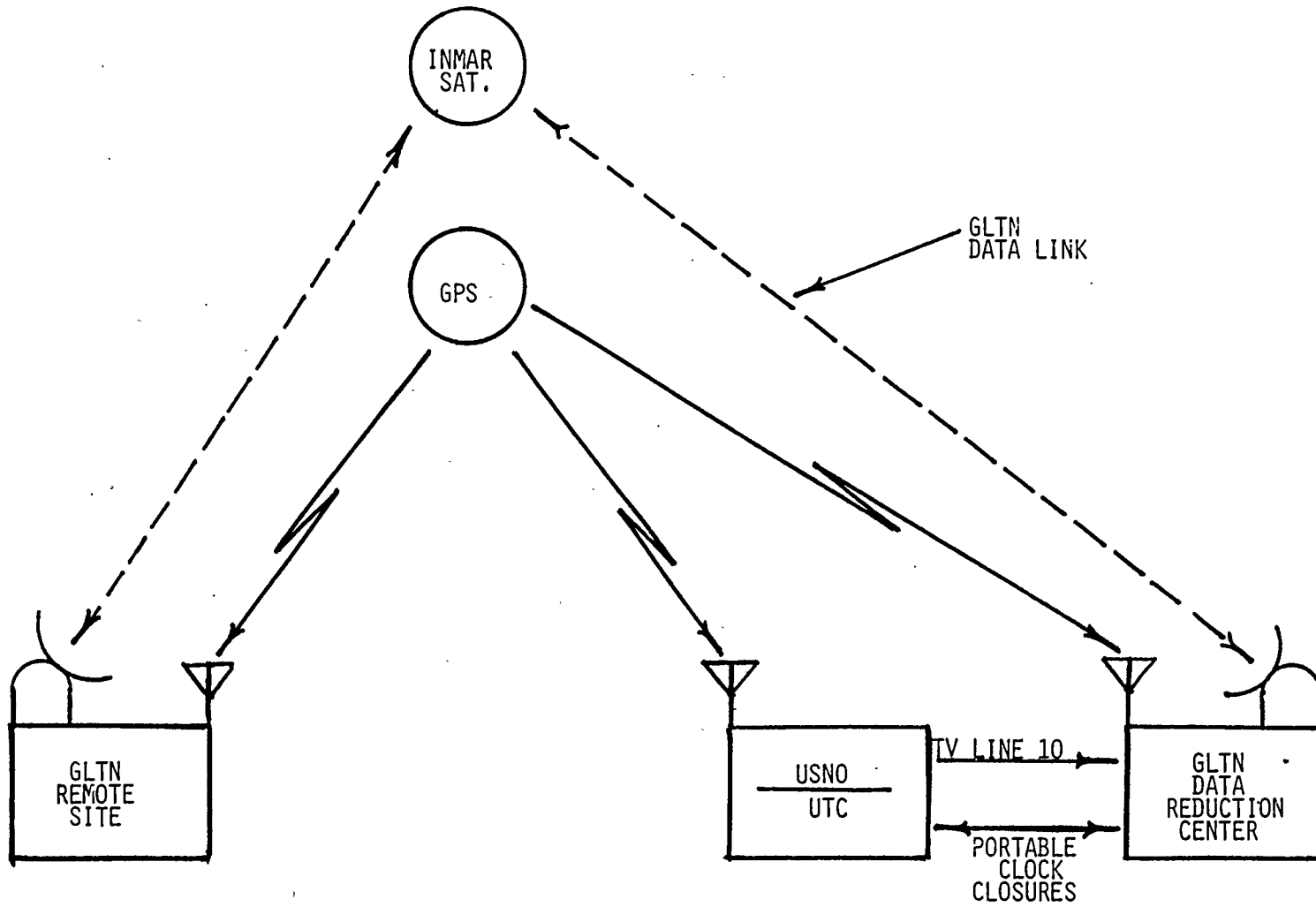


FIGURE 5

FIGURE 4



GPS "COMMON LOOK" &
GLTN DATA TRANSFER METHODS

Prior to the inception of the Goddard Laser Tracking Network (GLTN) ten years ago, NASA required that satellite support stations be synchronized within ± 25 microseconds. The GLTN need for ± 1 microsecond world-wide time synchronization required the development of new methods for maintaining time synchronization.

Recognizing that conventional means of timekeeping using LORAN-C, HF and VLF could not practically achieve the required ± 1 microsecond global clock synchronization, the cesium portable clock was used to provide time synchronization. Periodic portable clock trips were made to each station to determine the station's nominal LORAN-C value. Each station's cesium clock offset from U.S. Naval Observatory (USNO) time was plotted from daily LORAN-C values, time steps were calculated to synchronize station time to USNO time, and the station was directed to make the proper equipment adjustments to achieve the recommended time step.

With the improvement of laser equipment and the demand for more accurate ranging, the need for sub-microsecond timing has become a valid requirement.

This need prompted investigation and development of satellite timing receivers in a combined effort between the Naval Research Laboratory and NASA.

The Navigational Technology Satellite receiver was developed as a forerunner to the GPS Time Transfer Receiver now being used for sub-microsecond time transfer.

GPS TIMING

Techniques are being developed to utilize GPS timing for the GLTN, with a goal of world-wide time synchronization to the greatest feasible accuracy.

To utilize the time transfer capability of the GPS, a timing receiver was developed by the Naval Research Laboratory (NRL) for NASA, was tested at field sites, and was used in time transfer experiments (References 1 and 2). The first commercial GPS time transfer receiver was built by Stanford Telecommunications Incorporated (STI). This receiver was evaluated for possible use in the GLTN. The STI and the NRL receivers are operated from a keyboard similar to that of a personal computer. The cost of the STI receiver was approximately one half that of the NRL receiver and it was more suitable for mobile installations. More recently a third receiver, the Frequency and Time Systems (FTS) Model 8400 was evaluated and found to be the best suited for GLTN operations because of its smaller size, unit construction and lower cost.

Figures 1 and 2 compare time transfer data obtained with an FTS 8400 GPS receiver or the identical Trimble 5000A and a cesium portable clock at several timing installations. Portable clock time was compared to USNO time before and after these trips. The measurements were supplemented by TV Line 10 measurements which were accurate to ± 50 nanoseconds with respect to USNO.

Figure 3 lists current deployments of FTS 8400 GPS timing receivers in the GLTN.

GLTN GPS DATA COLLECTION

GPS time position measurements are made daily at the GLTN stations. The stations collect GPS data twice a day for each visible satellite. The raw time position reading is recorded during the 10-minute satellite observation pass. This data point along with the date, time, and satellite vehicle number are recorded for each measurement. The measurement data are transmitted to the NASA Communications Center in the daily Laser Operations Report (LOR). Also transmitted in the LOR is information concerning station time steps, frequency changes, power outages, equipment problems, etc.

AUTOMATED TIME POSITION SYSTEM (ATPS)

The Automated Time Position System is the means by which station time is monitored and analyzed for the GLTN. The ATPS

- o provides daily time position determination
- o calculates long term cesium frequency drift
- o predicts the date the station tolerances exceed 1 microsecond
- o evaluates the validity of data and data analysis methods

The System includes several computer programs that (1) read the LOR data into the ATPS data bases, (2) permit the manual entry, editing, deletion, and listing of data files and (3) perform the analysis of the timing measurements. The system is coded in FORTRAN and runs on a VAX computer cluster. The cluster consists of two VAX-11/780 computers and one VAX 8600 computer. The analysis program is operator inactive and produces a printed data output. The data output consists of the source listing data from the data files used in the analysis, a least-squares calculation of the original source data, and a line printer graph of the original and least-squares data plot.

GPS COMMON VIEW

Utilizing the GPS common view technique described in Reference 3, orbital and spacecraft clock systematic errors can be minimized.

A common view/near common view GPS time transfer experiment was conducted in 1983 to determine the accuracy of GPS time transfer receivers for the GLTN (Reference 4). The experiment was conducted between the Bureau International de l'Heure (BIH), Paris, France, the Institute Fur Angewandte Geodasie (IFAG), Wettzel, Germany and the GLTN data reduction center at Columbia, Maryland. The local time bases incorporated HP5061 (Option 004) Cesium standards or hydrogen masers. Results of the experiment showed the overall accuracy to be consistently better than 100 nanoseconds. Recent improvements in the GPS system have permitted common view accuracies approaching 10 to 20 nanoseconds. (Reference 5).

Efforts are underway to utilize GPS common view techniques on a day-to-day operational basis in the GLTN (Figure 4).

TIME INTERVAL MEASUREMENT ERRORS

The GLTN utilizes Hewlett Packard 5370 time interval counters with an atomic standard for the time base. The 5370 has a 20 picosecond single shot resolution, however, the accuracy is typically +/- 40 picoseconds. The accuracy of the time interval measurement is influenced by the summation of:

- o trigger level
- o input signal noise
- o interval timing jitter
- o time base short term stability

Event timers developed by the University of Maryland and by the Division of National Mapping (Australia) reduce the internal timing jitter and improve the short term stability. The University of Maryland unit uses a 200 MHZ oscillator phase locked to the atomic standard.

IMPROVEMENTS IN SHORT TERM STABILITY

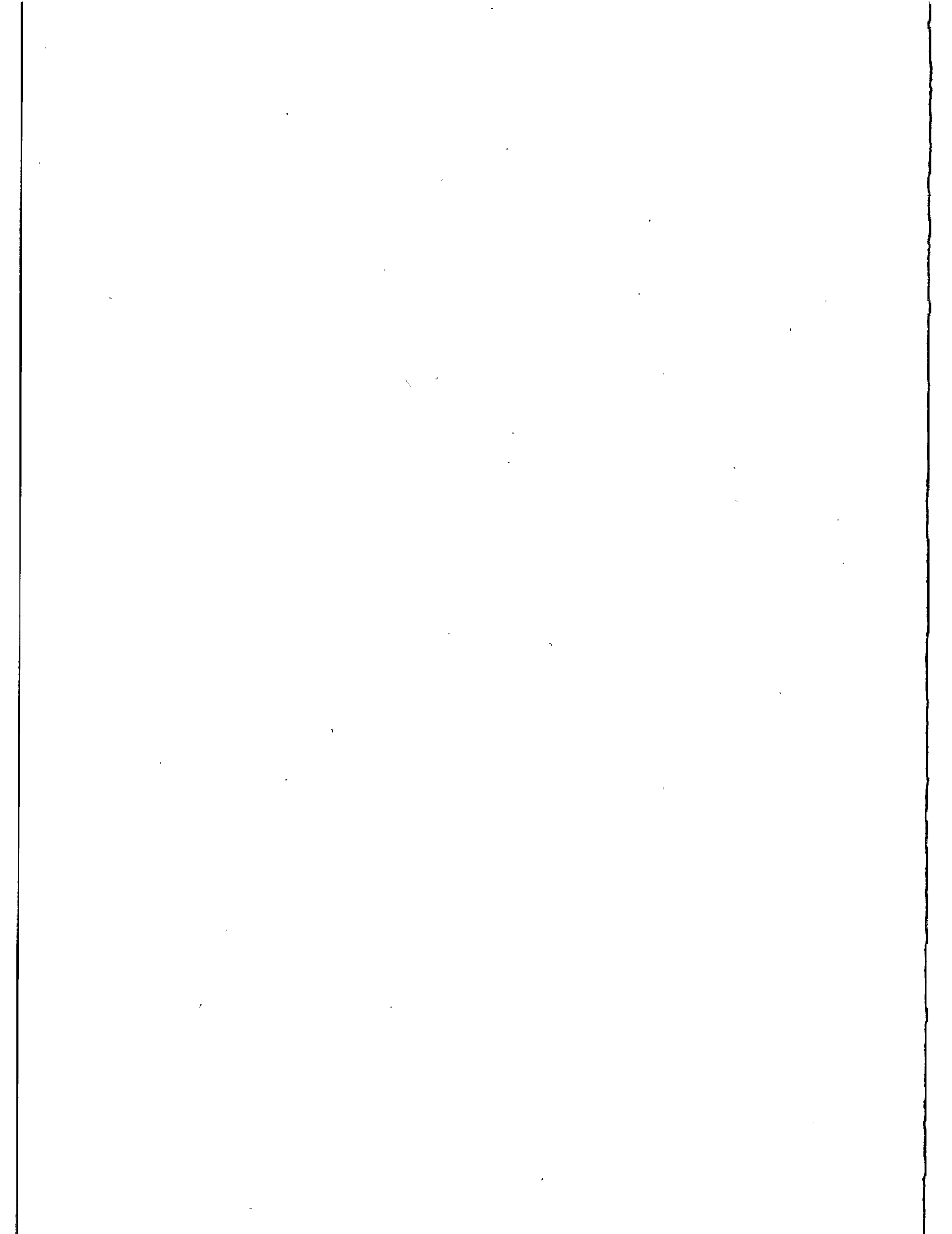
Improved short term stability oscillators that can be steered to UTC via the GPS are being developed.

Austron, Inc. and the GLTN are developing a low noise disciplined frequency standard (Reference 6) that utilizes a microprocessor controlled system which automatically locks the frequency of a precision BVA crystal oscillator to an atomic standard having superior long term stability. With the use of a third-order servo technique, the instrument is able to correct the frequency offset and aging of the internal BVA oscillator. If the frequency of the atomic standard is altered (due to loss of lock, loss of signal or failure) the unit will continue to apply corrections to the internal BVA oscillator. These corrections are calculated from data accumulated while the atomic standard is stable. These corrections are automatic and do not disturb the phase. This technique minimizes the effect of aging of the BVA oscillator and holds the unit to within +/- 3 parts in 10^{12} per day.

The short term stability (50 milliseconds to 100 seconds) of the low noise disciplined frequency standard is represented in Figure 5. The internal BVA oscillator has a short term stability σ ($\tau = 0.2$ to 30 seconds) $\cong 5 \times 10^{-13}$ and an aging rate of 1×10^{-11} per day. Frequency steering of the low noise disciplined oscillator by the atomic standard to epoch time accuracies of 100 nanoseconds via the GPS system can be achieved.

REFERENCES

1. J. Oaks, J. Buisson, C. Wardrip, "GPS Time Transfer Receivers for the NASA Transportable Laser Ranging Network", NASA/GSFC x-814-82-6, April, 1982.
2. J. Oaks, A. Franks, S. Falvey, M. Lister, J. Buisson, S. Wardrip and H. Warren, "Prototype Design and Initial Test Evaluation of a GPS Time Transfer Receiver", NRL report 8608, July 27, 1982.
3. D. W. Allan and M. A. Weiss, "Accurate Time and Frequency Transfer during Common-View of a GPS Satellite", Proceedings of 34th Annual Frequency Control Symposium, 1980.
4. C. Wardrip, J. Buisson, J. Oaks, et al., "An International Time Transfer Experiment", Proceedings of the 37th Annual Frequency Control Symposium, 1983.
5. M. A. Weiss, "Weighting and Smoothing of Data in GPS Common View Time Transfer", Proceedings of the 17th Annual Precise Time and Time Interval Applications and Planning Meeting, 1985.
6. B. Bourke and B. Penrod, "An Analysis of a Microprocessor Controlled Disciplined Frequency Standard", Proceedings of the 37th Annual Frequency Control Symposium, 1983.



THE DEVELOPMENT OF A DUAL FREQUENCY EVENT TIMER

C.A. Steggerda
Department of Physics and Astronomy
University of Maryland
College Park, Maryland 20742

Telephone (301) 454 3406
Telex 908787

ABSTRACT

The fundamental concepts and equations of the Event Timer are discussed. The evolution of the Event Timer since the Herstmonceux conference and the specifications are stated. New circuits are described which reduce the RMS jitter to the range of 15 picoseconds. Under ideal conditions, over a period of one hour, the stability and the RMS variation of 1000 point mean points is in the order of one picosecond. Plans for a 5 picosecond resolution Timer are presented.

INTRODUCTION

About five years ago I started developing an Event Timer or chronograph, using the dual frequency vernier system. Described two years ago at the Herstmonceux conference, the Event Timer is near completion and I hope to have at least two Timers built by the end of this year. One of the Event Timers will go to the Yunnan Observatory of the Peoples Republic of China when Mr. Wang Ben-Chun returns to China. Others will be used by Dr. Alley for time synchronization experiments and satellite and lunar ranging.

This paper is organized into three parts. The first part is a description of the fundamental concepts and the equations of the Event Timer. The second part describes the specifications and describes how the Event Timer has evolved since the Herstmonceux conference. The third part concerns the measurement of jitter and a new circuit which improves the jitter characteristics. Final concluding remarks describe a possible new next Event Timer.

Part 1 Fundamental Concepts of the Event Timer

Figure 1 shows the essence of the dual frequency Event Timer concept. One of the dual frequencies, F_1 , is produced by a 200 MHz tunable crystal oscillator which is synchronized to a 5 or 10 MHz standard. The 200 MHz oscillator runs continuously to drive a 26 bit synchronous counter which is the time generator. The time generator has exactly 50,000,000 states so it repeats every $\frac{1}{4}$ second.

The second of the dual frequencies, F_2 , is produced by a delay line oscillator which is tuned by other circuits to operate at 199.2217899 MHz called 199* MHz. F_1 and F_2 come into synchronization every 257 cycles of F_1 and 256 cycles of F_2 . F_2 is derived from F_1 by the equation $F_1 - F_2 = F_2/256$.

An event, either from the test circuit or an outside source, stops, then restarts the 199* MHz restartable oscillator to drive a 9 bit counter called the A register. Constantly monitoring the two frequencies is a comparator which reacts to the rising edges of F_2 and transitions in state of F_1 . The result of this operation is that the comparator reacts to the nearest co-incidence of the rising edges of F_1 and F_2 . When the F_1 and F_2 rising edges are in closest synchronization, the comparator gives a Sync. pulse which latches or stores the state of the 26 bit time generator and stops the 9 bit A counter.

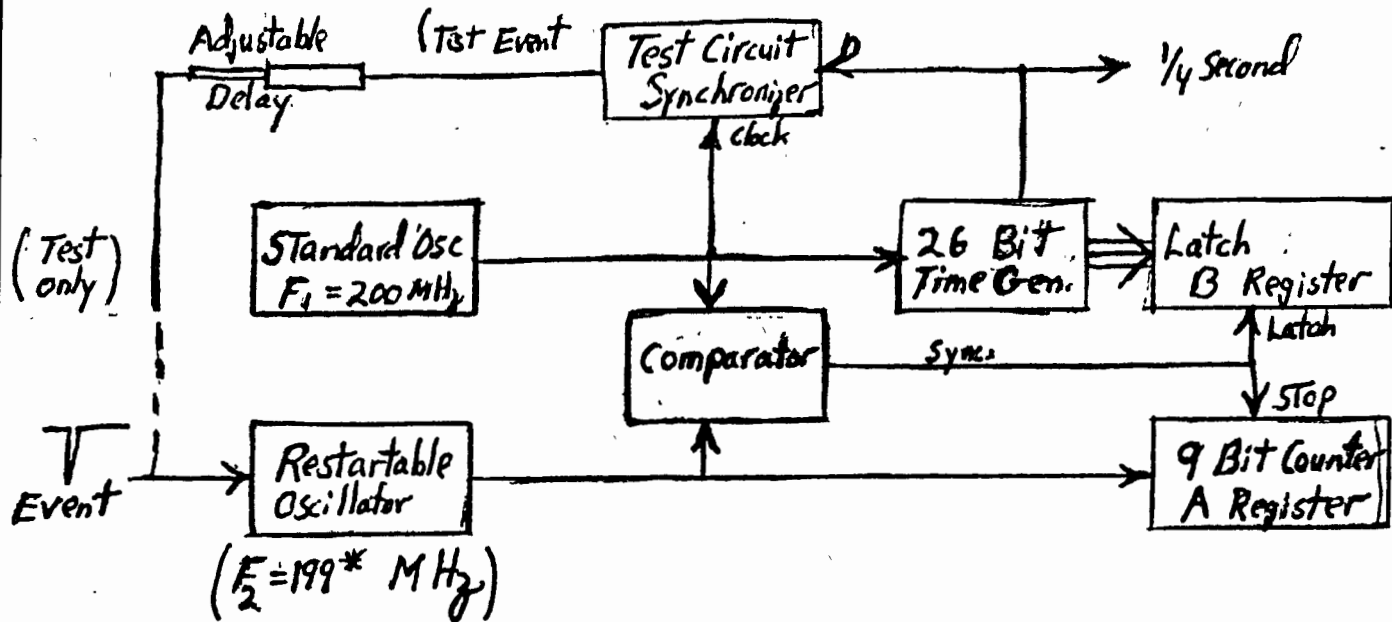
From the contents of the A and B registers, the epoch of the event can be computed within a $\frac{1}{4}$ second interval. The epoch of the event is = Time of Sync. (represented by the number latched in the B register) - the A register count times 5.01953125 n.s.. (5.01953125 n.s. is the period of 199* MHz.)

The vernier action occurs because the period of F_1 and F_2 differ by 19.53125 p.s.. Using the test circuit, which produces an event synchronized to the 200 MHz standard every $\frac{1}{4}$ second, we find that A and B repeat every $\frac{1}{4}$ second. In figure 2, if the event is delayed by 19.53125 p.s., the Sync condition occurs one cycle sooner, A and B are both decreased by 1.

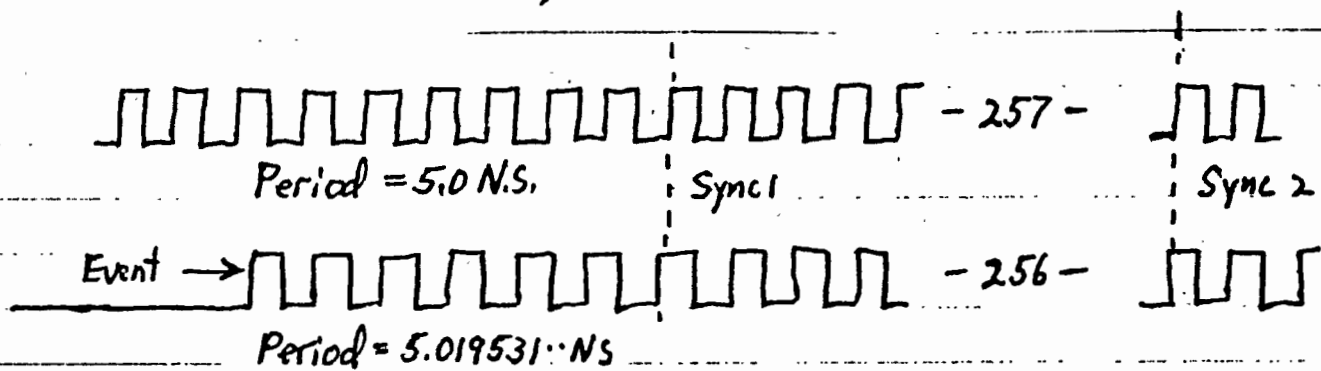
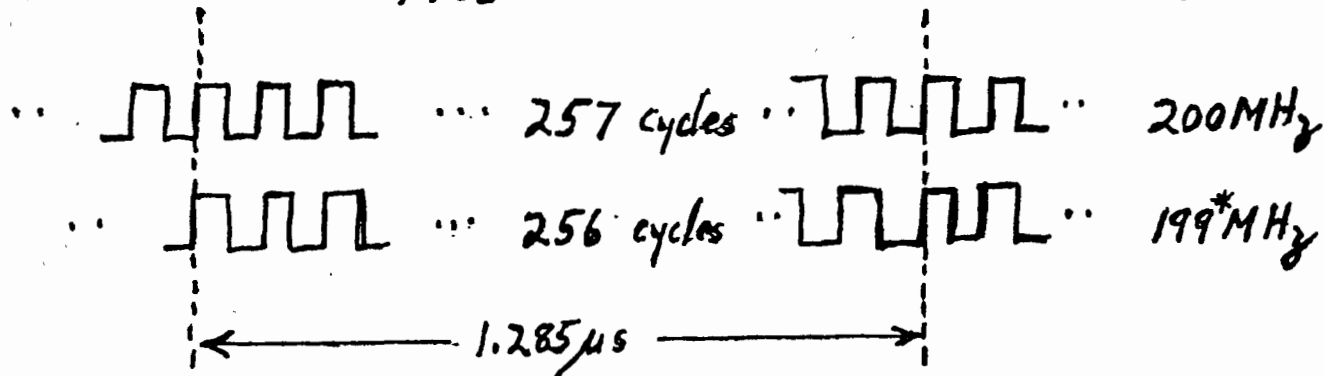
The equation Epoch = $(B-A)(5.0 - A(19.531 \times 10^{-3})$ n.s.
and Epoch' = $[(B-1)-(A-1)] 5.0 - (A-1)(19.531 \times 10^{-3})$ n.s.
give Epoch' = Epoch + 19.53125 p.s.

Fundamental Concepts of the Event Timer

Figure 1



$$F_1 - F_2 = F_2 / 256 \quad \therefore \quad F_2 = 199.2217899 \text{ MHz}$$



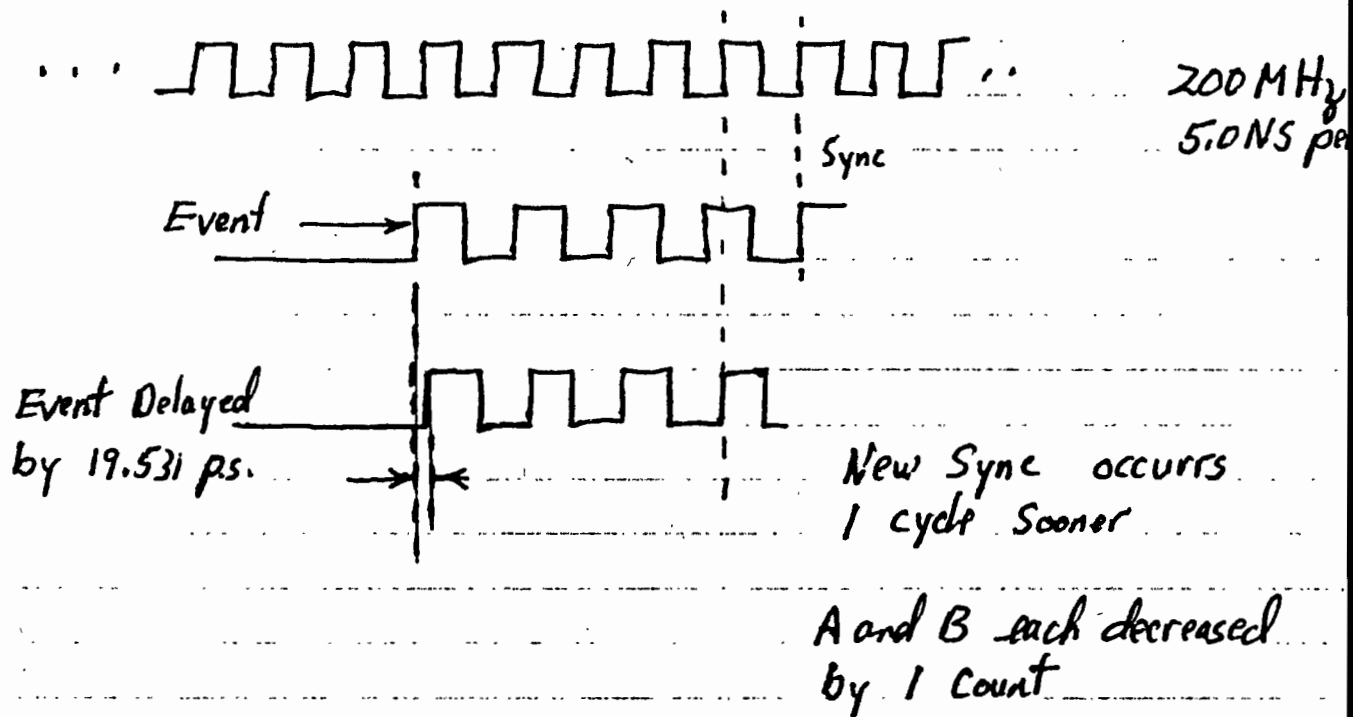
$$\text{Epoch} = \text{Time at Synchronization} - A (5.01953125) \text{ N.S}$$

$$\text{Epoch} = B(5.0) - A(5.01953125) \text{ N.S.}$$

$$\text{Epoch} = (B-A)5.0 - A(19.531 \times 10^{-3}) \text{ N.S.}$$

Fundamental Concepts Continued

figure 2



$$\text{Epoch}' = [(B-1) - (A-1)] 5.0 - (A-1)(19.531 \cdot 10^{-3}) \text{ N.S.}$$

$$\text{Epoch}' = (B-A) 5.0 - A(19.531 \cdot 10^{-3}) + 19.531 \cdot 10^{-3} \text{ N.S.}$$

$$\text{Epoch}' = \text{Epoch} + 19.531 \cdot 10^{-3} \text{ N.S.}$$

In General

$$\text{Epoch} = [(B+257N) - (A+256N)] 5.0 - (A+256N)(19.531 \cdot 10^{-3})$$

$$\text{Epoch} = (B-A)(5.0) - A(19.531 \cdot 10^{-3}) + [5.0 - 256(19.53125 \cdot 10^{-3})] N$$

" 0

$$\text{Epoch} = (B-A)(5.0) - A(19.531 \cdot 10^{-3})$$

If we can continue increasing the delay of the test event, the Sync. point will come closer and closer to the event. The actual Event Timer is built such that when A becomes equal to about 15, the first Sync. is ignored whereby the next Sync. point 1.285 u.s. later is used. At this time, the A register jumps 256 counts and the B register jumps 257 counts. In fact, any Sync point can be used to compute epoch. In fact, for the Nth synchronization point

$$\text{Epoch} = [(B + 257N) - (A + 256N)] 5.0 - (A + 256N)(19.531 \times 10^{-3})$$

$$\text{Epoch} = (B - A)5.0 - A(19.531 \times 10^{-3}) + N(5.0 - 256(19.531 \times 10^{-3}))$$

but $5.0 - 256(19.531 \times 10^{-3}) = 0$

$$\text{Epoch} = (B - A)5.0 - A(19.531 \times 10^{-3}) \quad \text{n.s.}$$

Thus the epoch of the test pulse may be moved about in the 1/4 second interval. Either the first or second Sync. point is used to generate A and B from which the epoch can be computed.

Part 2

Block Diagram and Specifications

Figure 2 shows a partial block diagram of the Event Timer. This diagram is useful primarily to show input and output functions.

The Event Timer has been expanded to have two independent verniers. It is thus possible to measure the epoch of two events up to and including co-incidence. Each event can arrive on its own cable, or, the events may be combined to feed both verniers in which case the first vernier arms the second.

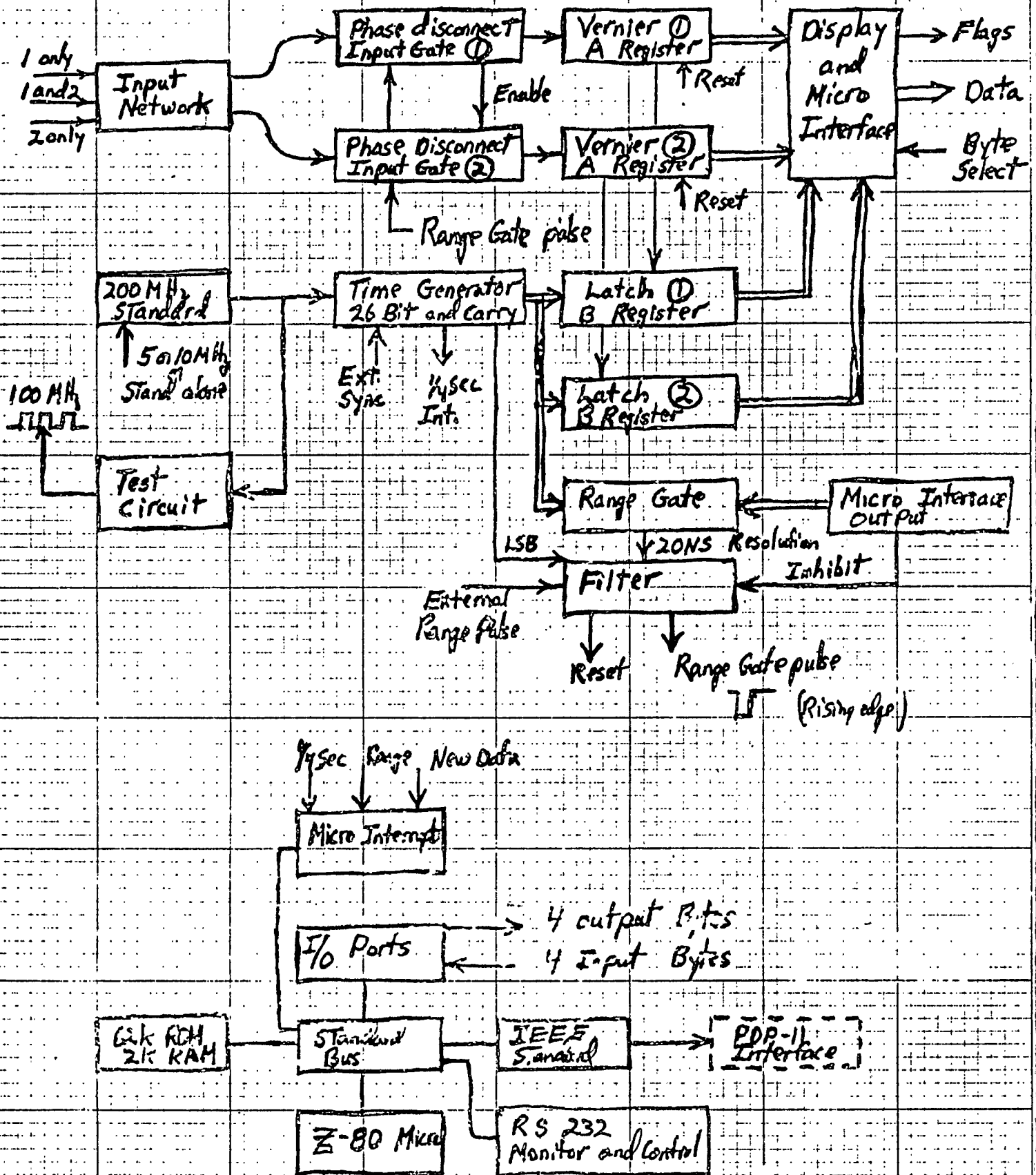
There are three inputs, each terminated in 50 ohms. In one mode, input 1 drives vernier 1 only, and input 2 drives vernier 2 only. In the second mode, input 3 drives both verniers. The input networks accept negative NIM type pulses going from an initial value of 0 volts to an amplitude of -.5 to -1.0 volts. Verniers respond to leading edges, so the pulses may be any width greater than 1 n.s..

The 200 MHz standard is a 66.66... Mhz voltage controlled crystal oscillator with a times 3 multiplier and a very narrow band filter. The oscillator is phase locked to either 5 or 10 Mhz standards, or, the oscillator may be operated without a standard at a frequency very close to 200 Mhz..

The time generator consists of a 24 bit synchronous counter and two $\div 2$ prescalers adjusted so that the rising edges of all bits are synchronous. A 27th bit carry is provided to prevent ambiguity problems if events occur near the 1/4 second point. The 26 bits and 27th bit carry are supplied to latches 1 and 2. The 24 bit synchronous counter number is compared with a 24 bit number supplied by the microprocessor to form a range gate to enable the Event Timer. The output of the comparator is filtered by a glitch supressor to form both a reset pulse for the A registers and a rising edge to enable the input gate portions of the phase disconnect circuits. The microprocessor supplies an inhibit pulse to the glitch supressor to prevent false range gate pulses while the numbers are being updated in the comparator. The range gate may be opened on the next 20 n.s. clock pulse following an external NIM type pulse.

Partial Block Diagram of Event Timer

figure 3



The phase disconnect circuit ① is enabled by the trailing edge of the range gate pulse. Phase disconnect circuit ② is enabled by either the same range gate pulse if the verniers are to be enabled simultaneously, or, phase disconnect circuit ② may be enabled when circuit ① has received an event to allow operation in the serial mode.

The outputs from the A and B registers are displayed with LED readouts and are stored in two 40 bit storage registers. The Z-80 microprocessor receives program interrupts when new data is available, when the range gate goes off, and when the 1/4 second pulses are generated from the time generator. The microprocessor reads in the data one byte at a time and can tell how much data is available by reading data status flags. Because the A and B registers act as storage registers along with the two 40 bit storage registers of the interface, it is possible to store four epochs, two from each vernier before the data must be read out. This feature provides for very rapid acquisition of data for very close targets.

The micro computer has 62K of ROM and 2K of RAM. The system operates the IEEE bus and RS-232 type monitors. Programs have been developed in FORTH language to calculate epoch and time of day and various tests for the Event Timer.

The Event Timer in conjunction with the Z-80 can give range data to the mainframe system computer at a rate of 172 ranges per second or every 5.8 milliseconds. However, the Event Timer can operate by itself every 7 microseconds or at a rate exceeding 100,000 ranges per second for each vernier.

Through the kindness of Messieurs Dachel and Ingold of the Bendix Corporation, the Allen Variance and the harmonic content of the 200 MHz standard were measured. Jeff Ingold's report is shown in figure 4.

CHARLES A. STEGGERDA

figure 4

9-4-86

200 MHz PHASE LOCKED OSCILLATOR

VECTRON S/N 628441 PHASE LOCKED TO NP 2 VS NP 4

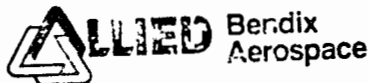
| TAU | ALLAN VARIANCE (σ_y^2) | FLOOR |
|------------|---------------------------------|-----------|
| 0.1 second | 1.00 E-11 500 samples | 6.49 E-12 |
| 1.0 | 2.39 E-12 500 | 8.43 E-13 |
| 10 | 2.08 E-13 100 | 1.00 E-13 |
| 100 | 3.30 E-14 5 | 1.53 E-14 |

HARMONICS

2ND (400 MHz) > 56 dB down from CARRIER
3RD (600 MHz) > 60 dB down from CARRIER
4TH (800 MHz) > 60 dB down from CARRIER

SUB HARMONICS & SPURIOUS RESPONSE

> 70 dB down from CARRIER



9-4-86

JEFF INGOLD

964-7188

Part 3 Jitter Measurements and a New Phase Disconnect Circuit

Consider again the basic block diagram of figure 1. If an event is generated precisely every $1/4$ second and this event is synchronized to the 200 MHz standard, then the A counter and B latch will repeat the same numbers every $1/4$ second. This in fact does happen, the same epoch being calculated for 10 to 20 minutes at a time with no jitter.

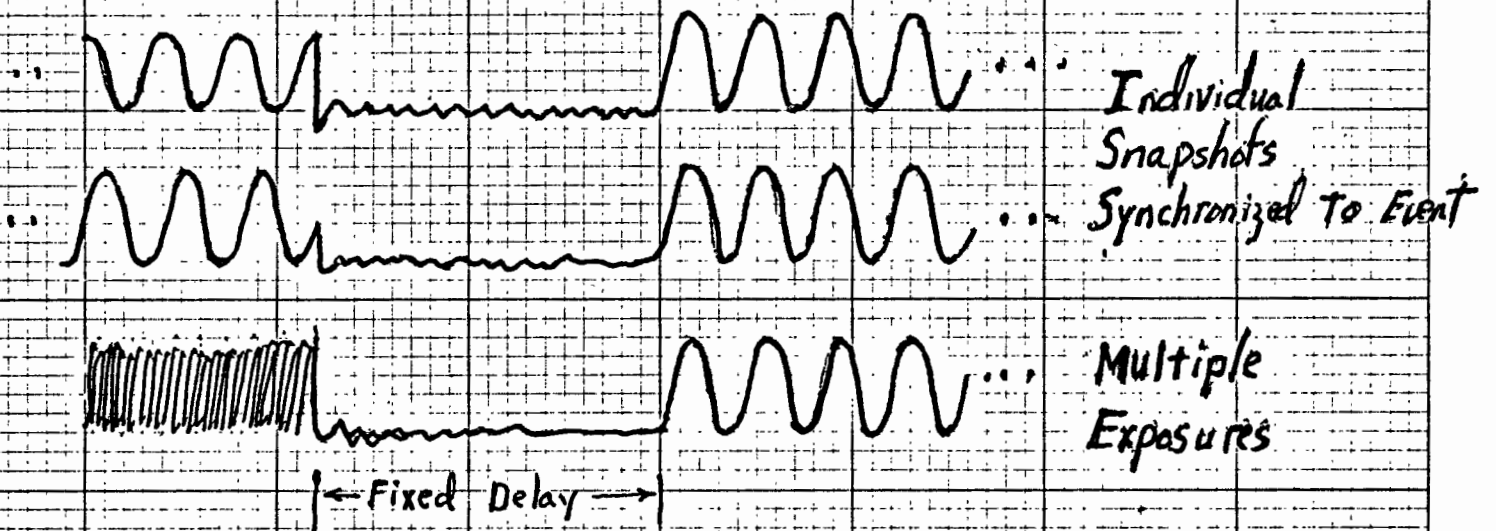
This test mode is not however the way the Event Timer is to be used. In operation the range gate operates 10 to 100 times a second in varying patterns according to the laser firing and the expected return time. A more valid test would replace the $1/4$ second period pulse with a pulse from an ordinary free running pulse generator running at 30 pps.. In this mode an event is generated that is synchronized to the 200 MHz standard but comes at a random time in the $1/4$ second interval. In this mode the A counter value should be constant and the B latch value should constantly change. The Event Timer of 6 months ago however had a jitter of up to 8 counts on the A counter when the range gate was moved randomly yet the A count was very stable if the range gate was opened at precise intervals as generated by the time generator. Measurement of the interpolator assembly of the Hewlett Packard 5370 universal counter revealed the same problem, which is understandable since the Event Timer verniers are directly related to H.P. interpolators.

It appears that an improvement can be made in the system jitter if F_2 , the 199* MHz oscillator, is stopped and restarted in a controlled manner. In the original fixed delay phase disconnect circuit, a 10 n.s. pulse synchronized to the event to be measured, stops and restarts F_2 . Before this synchronization process, the event is in no way synchronized to F_2 , and so the oscillator is stopped at any point in its cycle as shown in figure 5. When the oscillator is restarted, the initial conditions vary depending on what part of the cycle the oscillator was stopped. The changing initial conditions cause a phase jitter in F_2 relative to the event which then is measured as a system jitter.

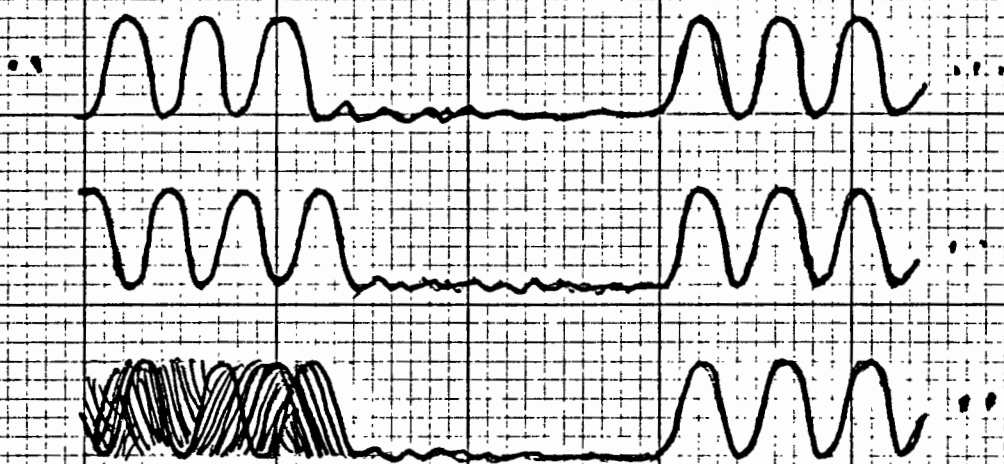
The Action of Phase Disconnect Circuits

Figure 5

A. Fixed Delay Phase Disconnect F_2 Waveforms (Pin 11)



B. Variable Delay Phase Disconnect F_2 Waveforms



A different way to stop F_2 would be to allow the oscillator to complete its current cycle and always stop at the same minimum voltage. Then, after the transients have subsided, restart the oscillator synchronized to the event. This variable delay phase disconnect technique has the same conditions at turnoff but a variable delay time for the transients to subside. The fixed delay phase disconnect technique has differing energies stored in the oscillator at turn off but a fixed delay time for the transients to subside. The variable delay seems to result in less phase noise. Further improvements can be made by increasing the delay before restart.

Jitter measurement have been made on five H.P. restartable oscillators in the Event Timer. The test event was a 100 MHz square wave synchronized to the 200 MHz standard. The range gate was opened randomly on the next 20 n.s. window by a free running pulser running at about 30 p.p.s.. The range gate opening is synchronized by the 50MHz least significant bit of the time generator to prevent slicing of the event pulse. 100 sample runs were made for all values of the vernier and the RMS jitter was calculated. The results are shown in figures 6,7, and 8.

Use of this variable delay phase disconnect circuit has resulted in a reduction of jitter from perhaps 35 p.s. RMS to the order of 15 p.s. RMS at this time. Further improvements may be possible. While this reduction may not be important in Lageos tracking where there is an abundance of data to smooth out the jitter, this should be a decided advantage in Lunar ranging where every data point is precious.

Again, using the above described test of measuring a 100 MHz square wave at random times, a test was made over a period of one hour of the stability of the system. During the test, the delay line was not changed, the temperature was held constant at 22.5 C., and 1000 measurements were made and averaged every two minutes. The mean value of each 1000 measurements is plotted in figure 9.

Further tests, which have not been done as yet, would measure the linearity of the vernier. In this linearity test, the standard used to generate the test signal would be allowed to slowly drift with respect to the standard of the Event Timer. If measurements were made at precisely known times, the rate of drift could be measured and a projected ideal vernier could be formulated. The deviation from this ideal vernier would measure the linearity error.

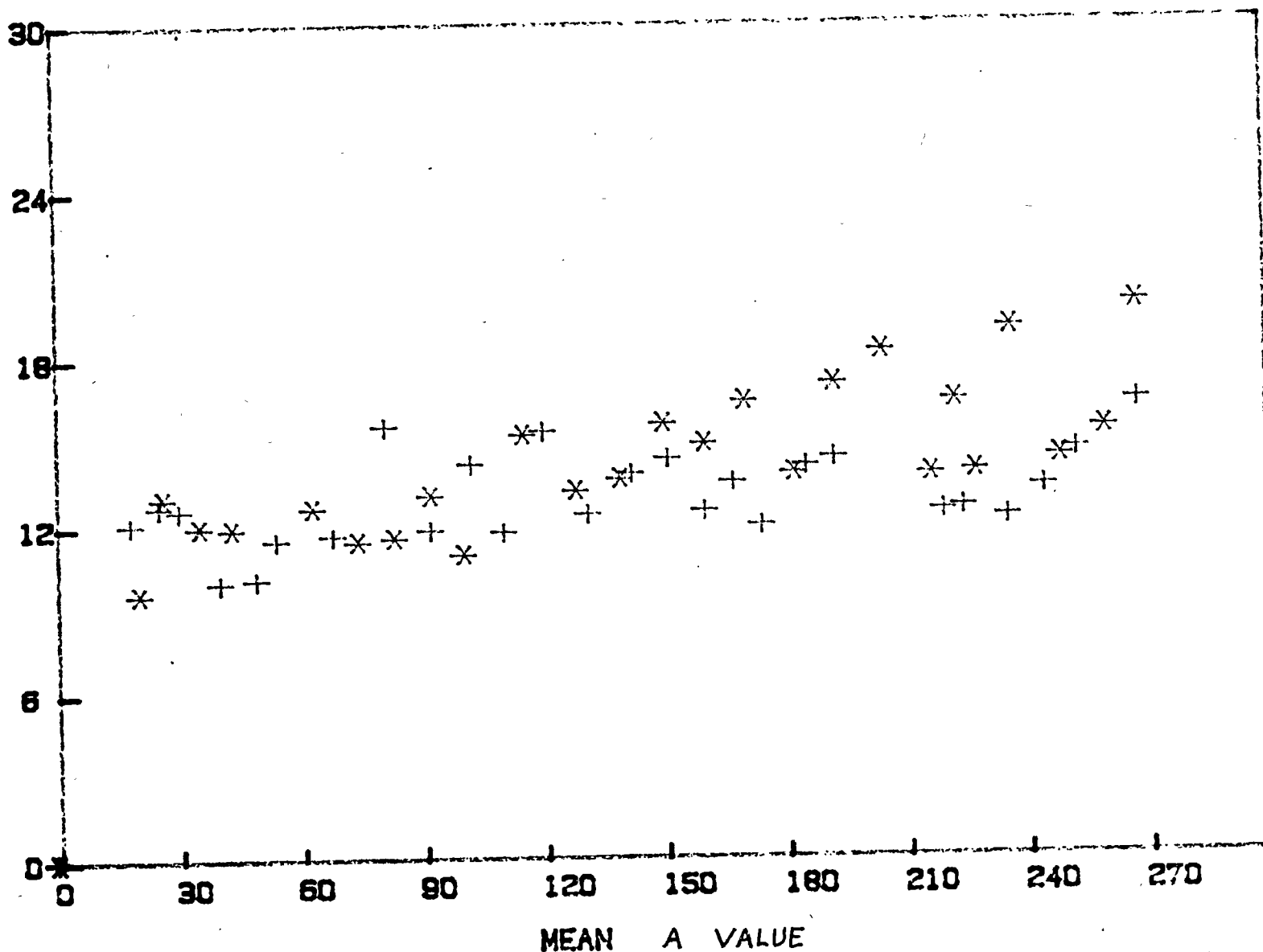
EVENT TIMER RMS JITTER

+ - Chip 2
* - Chip 5

RMS PS.

CHIP#1 CHIP#2 CHIP#3 CHIP#4 CHIP#5 CHIP#6

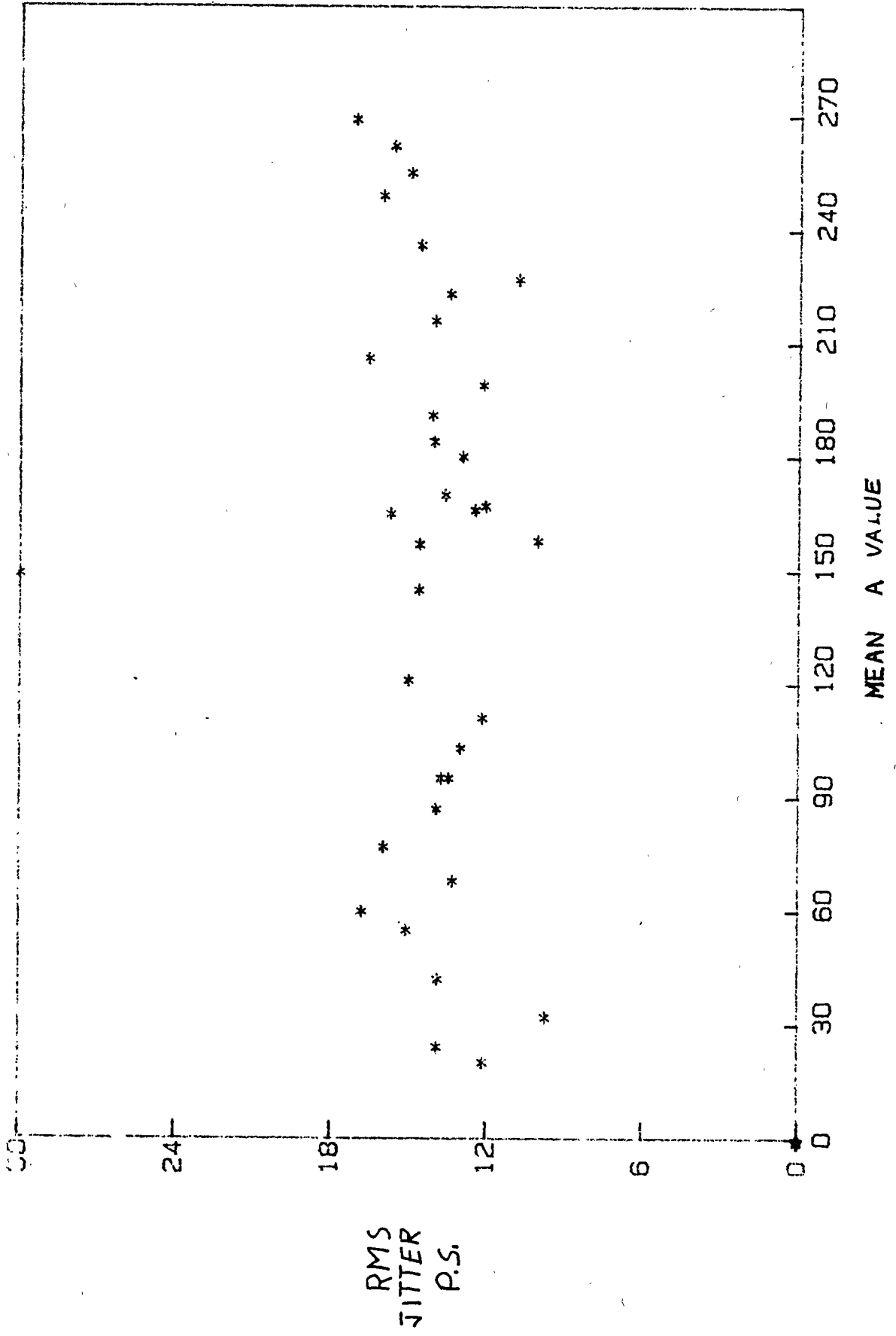
figure 6



EVENT TIMER RMS JITTER

figure 7

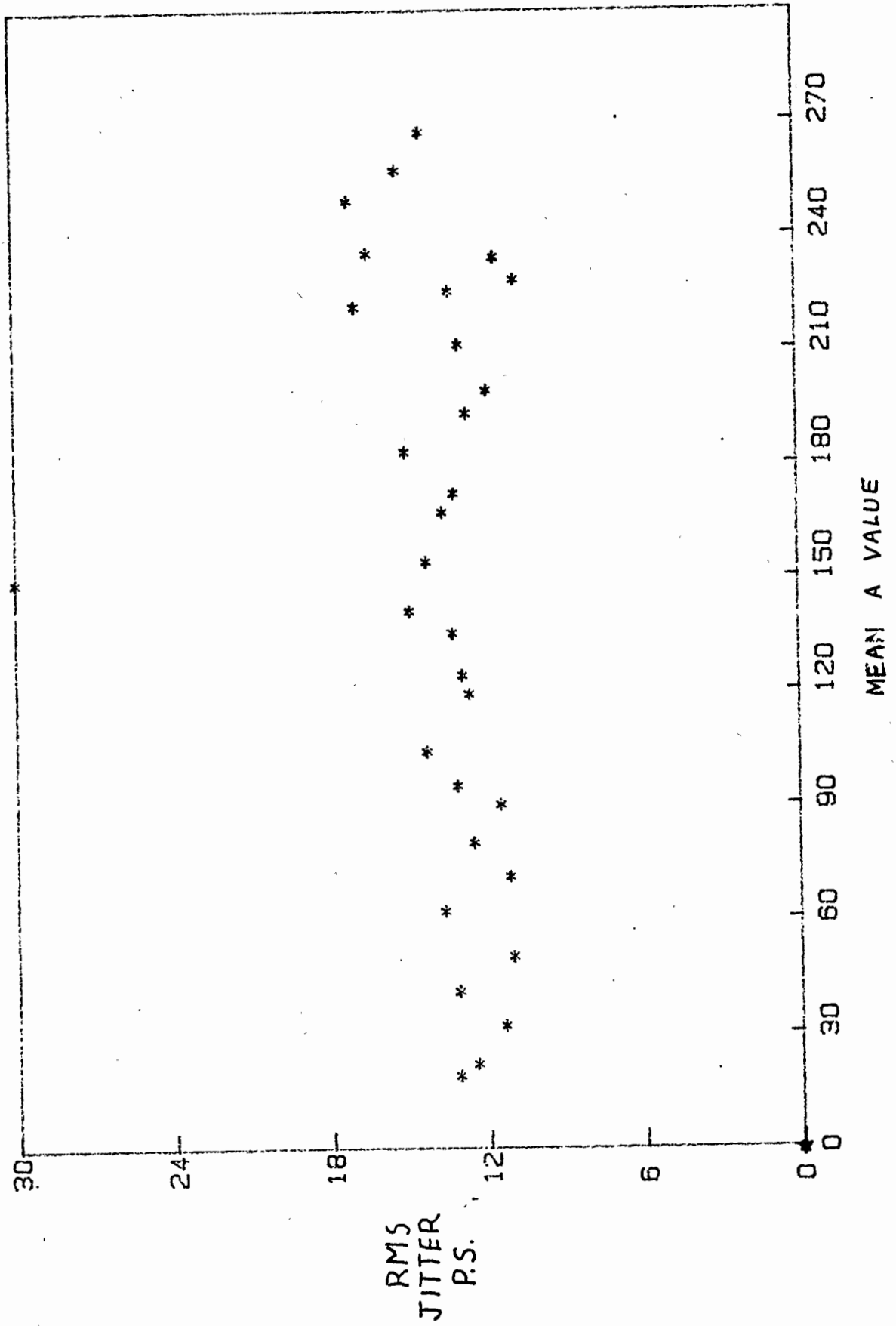
CHIP #1A



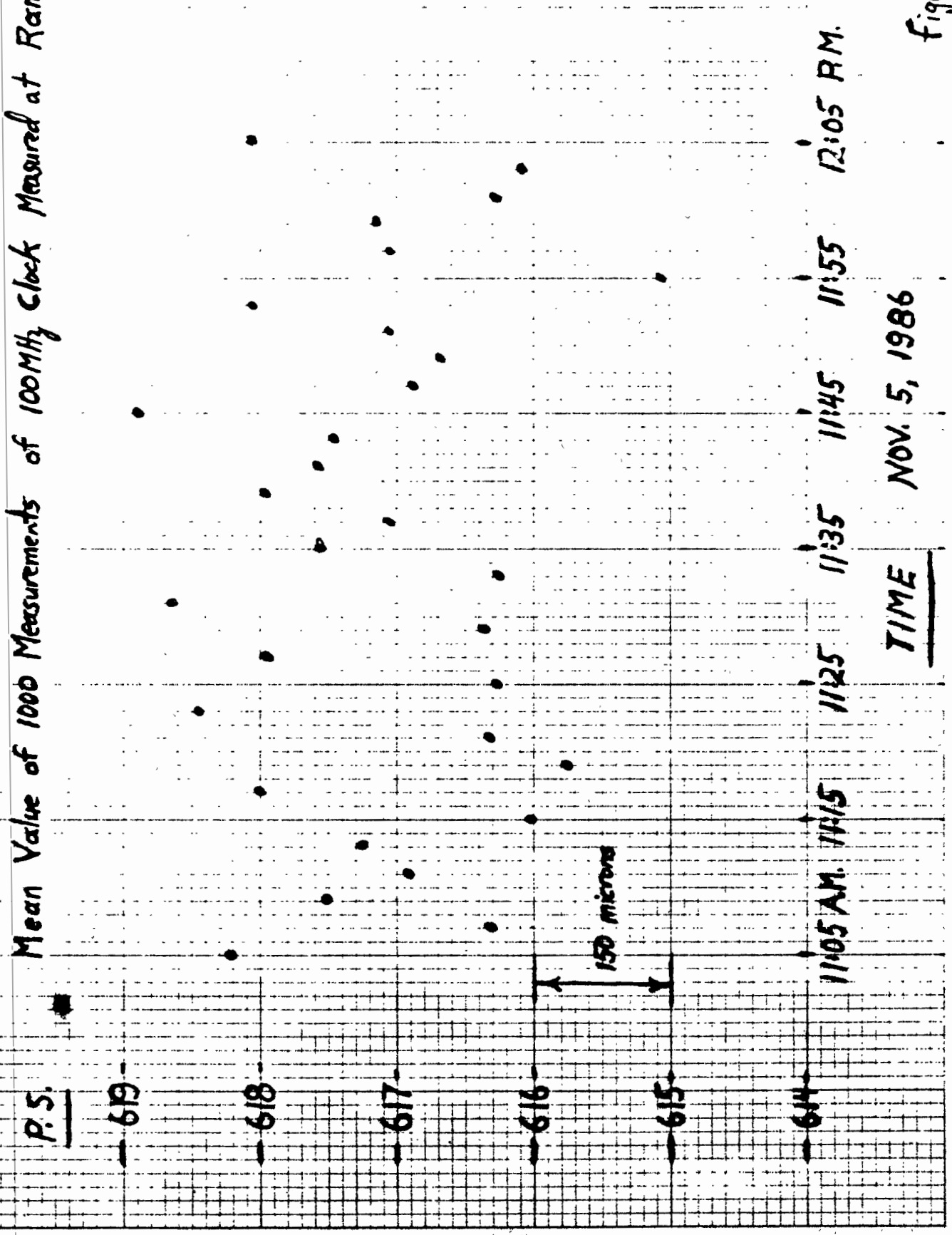
EVENT TIMER RMS JITTER

Figure 8

CHIP4A



Mean Value of 1000 Measurements of 100MHz Clock Measured at Random



TIME

NOV. 5, 1986

Figure 9

Finally, I have been asked whether a 10 p.s. resolution Event Timer could be made using the H.P. restartable oscillator. It is not practical to use the H.P. chip in its present form because the transmission line oscillator cannot be stably tuned to the required 199.610136.. MHz. In this mode of operation there would be 513 of the 200 MHz. cycles for 512 of the offset frequency giving a resolution of 9.76 p.s.

If, as is shown in figure 10, an entirely new restartable oscillator were to be made, I believe that it is possible to design an Event Timer based of the standard frequency of 400 MHz. Using 512 as the offset frequency divider instead of 256, the restartable oscillator frequency becomes 399.2202729 MHz with a period of 2504.882813 p.s.. The resolution of the Event Timer is 4.88 picoseconds. Hopefully, the RMS jitter could be less than 5 p.s..

Design of 400 MHz Event Timer

Figure 10

- 1) $F_1 = 400 \text{ MHz}$
- 2) Time generator is a 27 Bit Synchronous Counter consisting of 3 $\div 2$ prescalers and the present 24 Bit counter.
- 3) Resolution of Range Gate 20 N.S.

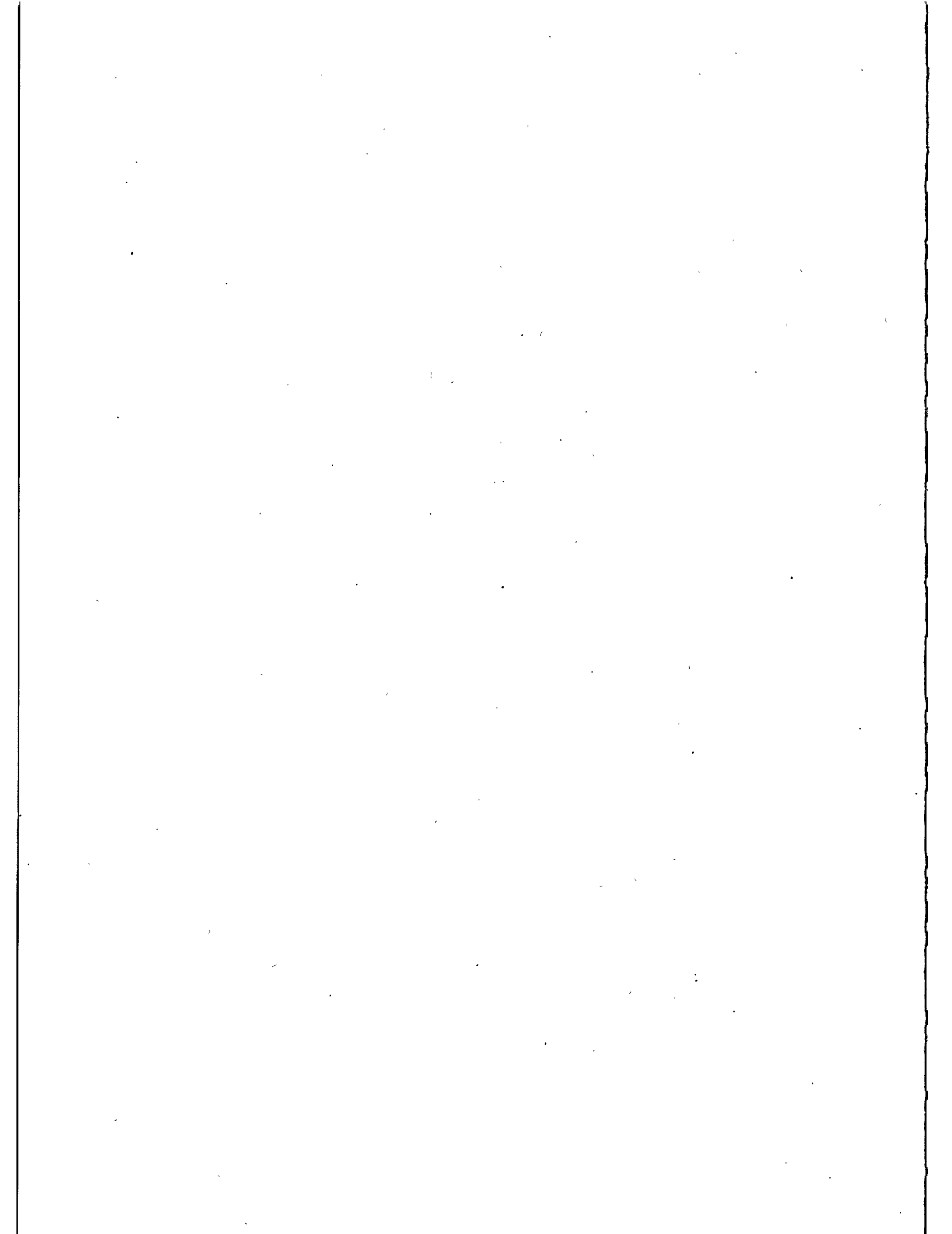
$$F_1 - F_2 = F_2 / 512 \quad F_2 = 399.2202729 \text{ MHz}$$

$$\frac{400 \text{ MHz}}{513} = .77972 \dots \text{ MHz Beat Frequency}$$

$$2500 \left(\frac{513}{512} \right) = 2504.882813 \dots = \text{period of } F_2 \text{ P.S.}$$

$$\text{Period of } F_1 = 2500 \text{ P.S.}$$

- 4) Resolution of Vernier = 4.8828 p.s.



STABLE SATURABLE DYE FOR 1.06 μM

K. Hamal, H. Jelinkova
Czech Technical University
Faculty of Nuclear Science and Physical Eng.
Brehova 7, 115 19 Prague 1 - Czechoslovakia -

Telephone 848840
TWX 121254 FJFI C

ABSTRACT

Most of the second generation Satellite and Lunar ranging stations and practically all of the 3. generation ones exploit pico-second pulses to ensure the required accuracy. To synchronize the modes and to Qswitch the resonator, either an active or passive modulator or combination of them, may be used. To apply a passive modelocker/Qswitch, some characteristics of the saturable modulator (bleacher) are required.

STABLE SATURABLE DYE FOR 1.06 μm

Karel Hamal, Helena Jelinkova

Most of the second generation Satellite and Lunar ranging stations and practically all of the 3. generation ones exploit picosecond pulses to ensure the required accuracy. To synchronize the modes and to Qswitch the resonator, either an active or passive modulator or combination of them, may be used. To apply a passive modelocker/Qswitch, some characteristics of the saturable modulator (bleacher) are required:

- compatibility with the Nd transition and host (YAG, YAP, Nd glass, etc) (wavelength, absorption cross-section, lifetime, saturation intensity)
- short/long term stability
- acceptable solvent
- to range Satellites/Moon, the desirable pulse duration is 30-100 psec (3. generation) and 30 psec or less for 4. generation /1/.

We have worked to develop saturable dye having performances closed the mentioned ones above. The parameters of the resulting saturable dye ML51 /2/ are summarized in the table 1. Some other dyes are mentioned for comparison.

The photostability has been estimated from the following experiment: the sample of the dye was illuminated by the cw high pressure xenon flash lamp XBO500 /3/. The exposure time of the photodecomposition was measured and the slope was compared for different dyes (Fig.1.).

To investigate modelock/Qswitch properties, we have used different laser configuration:

(1) /4/ The YAG rod was cut at 1 deg near the back mirror, the perpendicular surface on the opposite side acted as the output mirror. A 5 mm cell, containing 2 cc of no flowing dye, was placed at the Brewster angle between the back mirror and the YAG crystal. The optical length of the resonator was 30 cm. The single mode operation was accomplished by an iris 1 mm in diameter. The output energy was 3 mJ in a train of two or three pulses, the replate was 2.5 Hz. The pulse duration and the output energy fluctuation were detected and statistically processed using a diagnostics chain consisting of the second harmonic generator, the streak camera Hamamatsu C-979 (10 psec resolution) interfaced with the SIT camera and temporal analyzer, the HP85 console and

the computer HP 1000. The resulted pulse duration at 0.53 μm was 30 psec RMS, the output energy 3mJ, $RMS = 3\%$ (Fig.2A). The corresponding power density is 3 GW/cm². To examine the output spatial structure of the beam, the detection chain /5/, consisting of the CCD Fairchild camera, Quantex singleframe memory and HP 1000 has been used. The beam profile is closed to the Gaussian. (Fig.3.) The divergence is 1 mrad, close to the diffraction limit. The corresponding brightness is 3.10^{15} W/cm² sr.

(2) To prove the saturable dye in the active/passive arrangement, we put it to Quantel laser system at CERGA (fall 1983). The oscillator contains a dye cell and a active modelocker. The records of the output pulse train and selected pulses are on Fig.4. The transmission of the bleacher has been set to obtain required 5-7 pulses within FWHM envelope. The replate was 10 Hz. A similar experiment was carried out at U. of Maryland /10/ using Kodak 9740 and ML51. Pulse widths were between 20-50 psec, however the shot to shot energy stability of the cavity dumped single pulse was poor.

(3) The ML51 was applied in two wavelength experiment /6/. To obtain picosecond ranging accuracy, the pulse duration should be minimized. The oscillator consisted of the concave 5m, 100%, back mirror in contact with 2 mm flowing dye cell. The YAG rod 3 mm in diameter 2deg/2deg AR coated was pumped in Quantel head. The front mirror was a quartz plate 0.25 mm thick. The duration was 14 psec at 0.53 μm , when deconvoluted. The pumping energy was varying up to 2.3 times above the modelock threshold and no change in the pulse duration or stability has been observed.

(4) The saturable dye was used to modelock the YAP laser /7/. The laser setup was similar to the experiment in (1). The raw value of the pulse duration was 10 psec, actually equal to the temporal resolution of the streak camera.

Generally, we did not observed any damage of any optical element throughout all experiments and during long term exploitations in different laser configurations. The saturable dye ML51 has been used at the INTERKOSMOS satellite laser station in Egypt since 1982 /1/, for two wavelength experiment /9/, for the ophthalmology and in several other lasers, occasionally, the dye lasts in the cell for several months.

LITERATURE

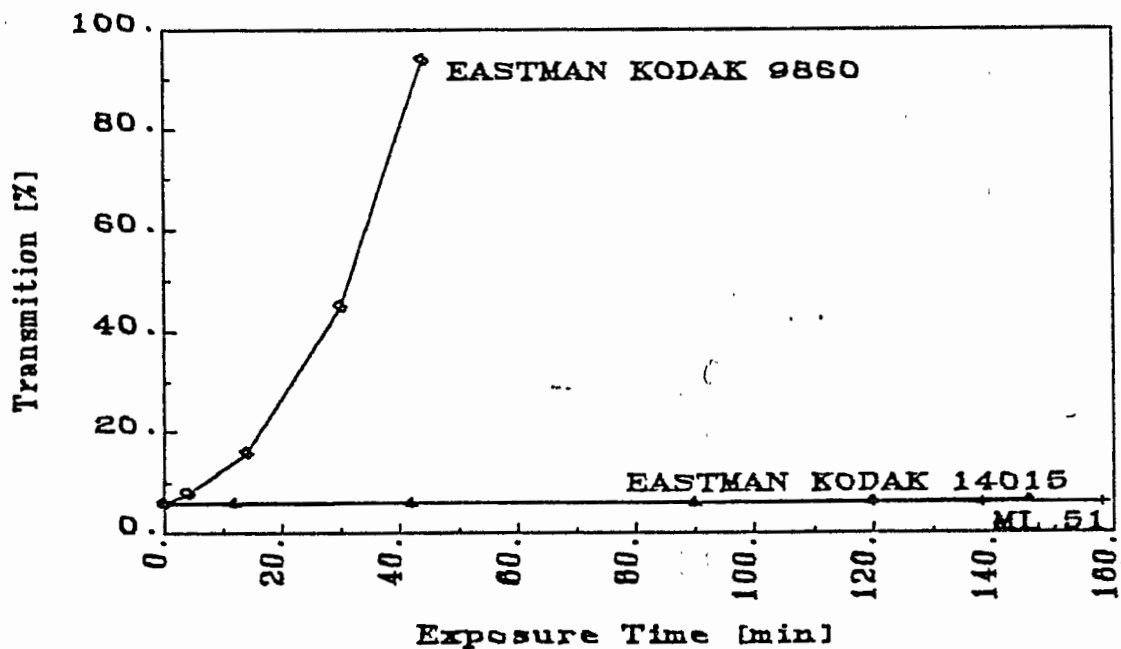
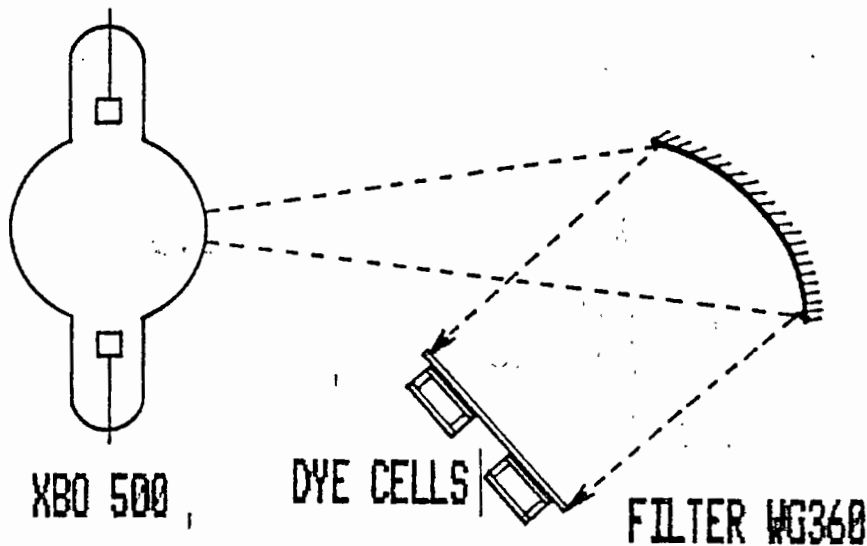
- /1/ Proceedings of the V. International Workshop on the Laser Ranging Instrumentation, Greenwich, 1984.
- /2/ K. Hamal, H. Jelinkova, V. Hruskova, CLEO, Baltimore, May, 1985
- /3/ B. Kopański et al, Appl. Phys., 15, 1982, p. 29.
- /4/ H. Jelinkova, in /1/
- /5/ H. Jelinkova, in this Proceedings.
- /6/ J. Gaignebet et al, in this Proceedings.
- /7/ K. Hamal, to be published.
- /8/ K. Hamal et al, in /1/.
- /9/ V. A. Babenko et al, Quantum Electronics, 7, 1980, p. 1796, (in Russian).
- /10/ W. Koechner, Solid-State Laser Engineering, Springer-NY, 1986
- /11/ I. Prochazka, in this Proceedings.
- /12/ M. Košelja, MS thesis.

| Parameters of saturable dyes | | | | |
|--|--------------|-------------|-------------|--------------|
| | ML51 /2/ | 3955 | Kodak 9740 | Kodak 9860 |
| Solvent | dichloethane | etylalcohol | chlorbenzen | dichloethane |
| Molec. weight | 631 | 688 | 762 | |
| λ_{MAX} (nm) | 1010 | 1040 /9/ | 1049 | |
| σ_{MAX} (10^{-10} cm ²) | 5.54 | | 6.2 | |
| σ_{1000} (10^{-10} cm ²) | 0.45 | 3.2 /9/ | 5.7 | 3.5 |
| τ (ps) | 37+/-2 | 40 /9/ | 8.3 /10/ | 9.3 /10/ |
| I_s (MW/cm ²) | .112 | 7.3 /9/ | 40 /10/ | 56 /10/ |

Tab. 1.

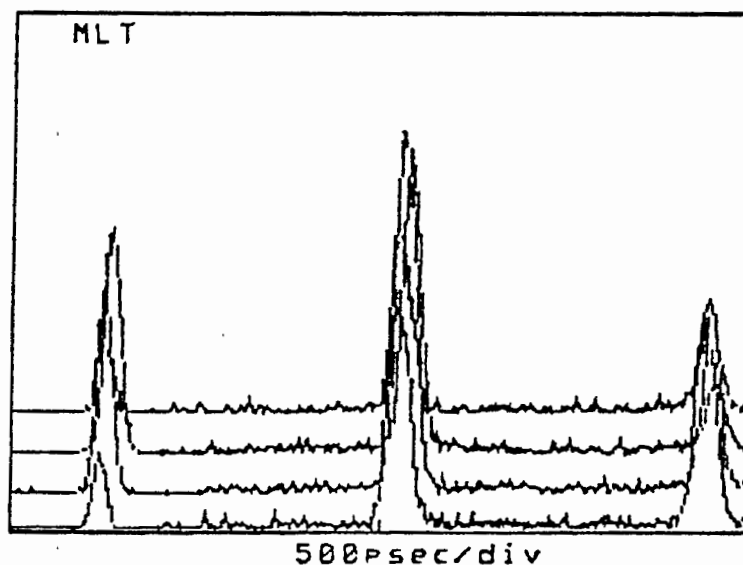
PHOTOSTABILITY TEST

EXPERIMENTAL ARRANGEMENT

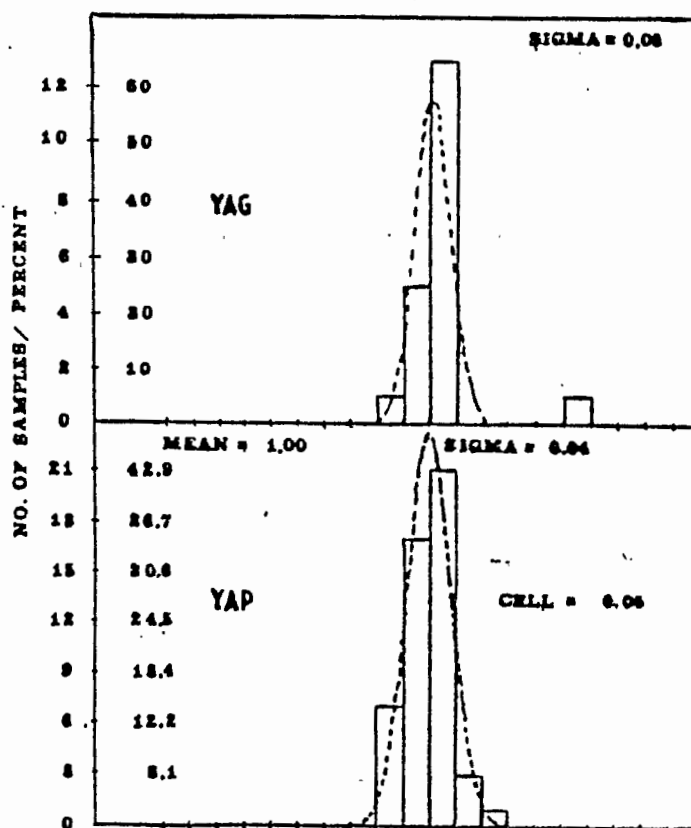


K. Hanal, H. Jelinkova
Stable Saturable Dye For 1.06 μ m

LASER OUTPUT



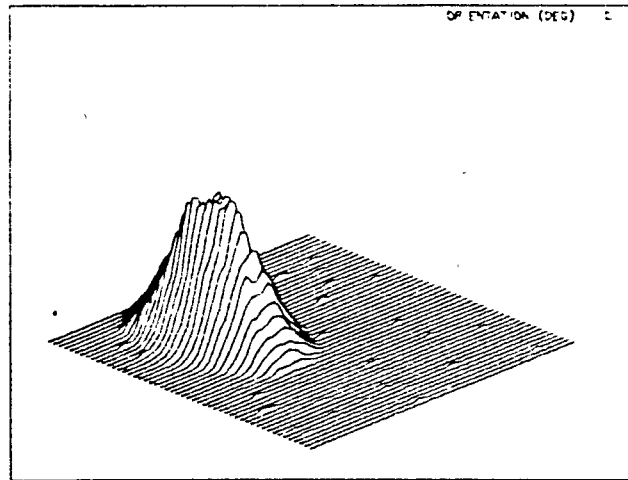
MODELOCKED TRAIN
(STREAK)



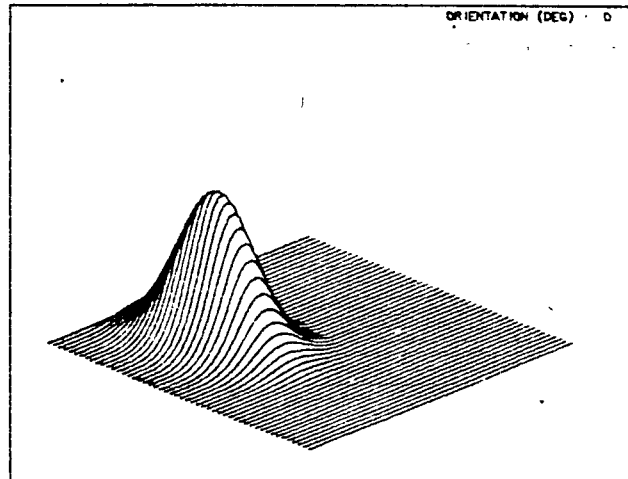
ENERGY STABILITY
HISTOGRAM

SPATIAL STRUCTURE OF THE OUTPUT BEAM

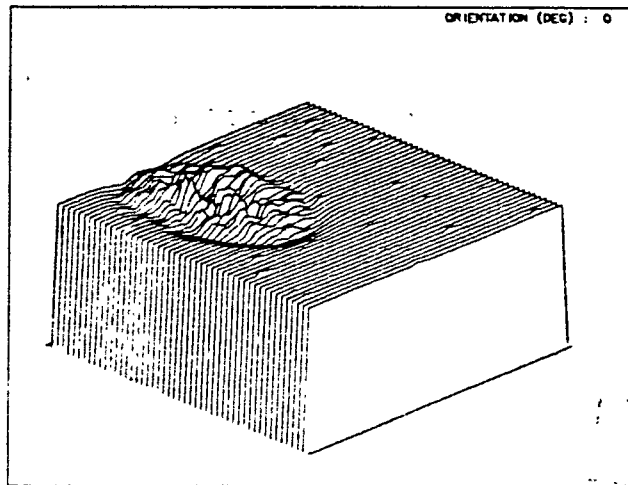
OSCILLATOR BEAM
DIVERGENCE 1 MRAD



GAUSS PROFILE
(THEORY)

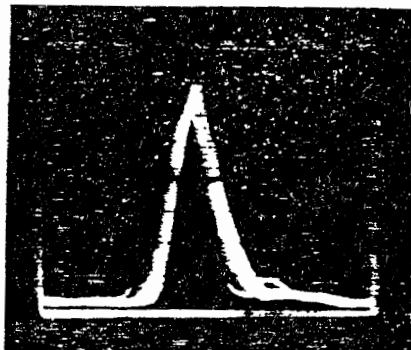
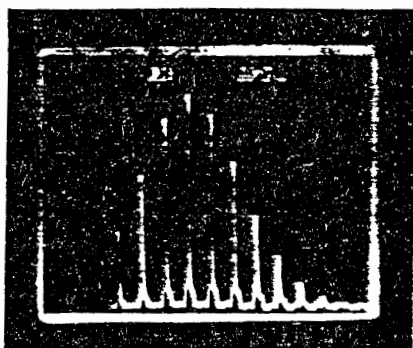


DIFFERENCE ~ 8%



INTERKOSMOS SATELITE LASER RADAR NETWORK

ACTIVE/PASSIVE MODE LOCKED LASER OUTPUT TRAIN



K. Hamal, H. Jelinkova
Stable Saturable Dye For $1.06\mu\text{m}$

SPATIAL STRUCTURE OF THE DOUBLED Nd : YAG
LASER TRANSMITTER BEAM

H. Jelinkova, P. Valach
Czech Technical University
Faculty of Nuclear Science and Physical Eng.
Brehova 7, 11519 Prague 1 - Czechoslovakia -

Telephone 848840
TWX 121254 FJFI C

J. Del Pino
Cuban Academy of Sciences
Institute for Geophysics and Astronomy
Santiago de Cuba

ABSTRACT

The beam spatial structure of the passively mode-locked Nd : YAG oscillator/amplifier/SHG laser radar transmitter has been examined.

To analyze the laser beam structure, an on line diagnostic chain, giving a three-dimensional graphic display, the contours and the two dimensional Fourier transformation of the output pattern was implemented at the Interkosmos indoor calibration facilities.

The beam was studied in every point of the laser transmitter and the IR Gaussian beam structure changes due to the outside oscillator optical elements were eliminated from the system. The SH beam profile was investigated from the point of view of temperature dependent efficiency and the pointing stability. The difference between the spatial shape of pulse IR and SH was found and the changes between them were tried to be compensated by the help of the tandem scheme of two SHG crystals.

SPATIAL STRUCTURE OF THE DOUBLED Nd:YAG LASER TRANSMITTER BEAM

H.Jelinkova, P.Valach, J.del Pino

INTRODUCTION

A Nd:YAG laser (YAG, YAP, etc.) allows to generate picosecond pulses for laser ranging. However, up to now, a lack of detectors in the near IR requires the radiated frequency to be multiplied into the second resp.third harmonics. To apply a second harmonic generator (SHG) into the laser transmitter scheme, the homogeneous, Gaussian IR output beam is required. Every change of the laser system configurations (resonator readjustement, active or passive elements temperature dependence, pumping inhomogeneity, etc.) causes significant changes of the Gaussian beam structure. Applying the new technology giving the fast accurate response, we have got the possibility to optimize the laser system performance. Consequently, the spatial structure of the transmitter output SH beam has been investigated.

EXPERIMENTAL ARRANGEMENT

The laser system configuration /1,2,3/, we employed, consists of passively mode-locked Nd:YAG oscillator, isolation saturable dye cell, expanding telescope, single pass amplifier and KDP doubling crystal (Fig.1.). According to /4/ the image in the focal plane of a well corrected lens coincides with the beam far field pattern (in Fraunhofer region). Therefore, in the laboratory, the beam farfield was observed in the focus of the 2.5 m thin lens by the help of the CCD array (Fairchild 320 x 489 cells). The CCD output signal was digitized using Quantex image memory (256 x 256 cells, 8 bits, 100 MHz) and stored on line on the magnetic disc of the host computer (Fig.2.).

IR BEAM

To understand the beam distortion through the laser transmitter, the beam was examined at different points (Fig.1, Fig.3) (behind the oscillator (A), the isolation cell (B), the expanding telescope (C), the amplifier (D)). The oscillator output beam structure was clean, near Gaussian, with the divergence of the one mrad (Fig.3A). The greater increment to the distortion was made by the isolation 5 mm thick Brewster angled dye cell (Fig.3B). The improvement was

obtained by tilting the dye cell to 1 degree. Resultant divergences in every measured points are summarized in Tab.1.

SH BEAM

In general case, the index of refraction of the negative nonlinear crystal, which is mostly used in SHG, depends on the incidence angle θ , the temperature T and the basic radiation wavelength λ . Every change of these parameters causes the index matching condition modification.

In our experiment, the temperature dependence of the SHG was investigated in detail.

1) The temperature of the SH crystal was varied from the 16°C to 37°C and the index matching angle was found for every examined temperature. From Fig.4 it can be seen that there is no variation in the efficiency within the experimental limit and therefore in the measured temperature interval the optimal thermal region for dominating SH output does not exist.

2) The index matching angle was alligned for the 24°C and the temperature dependence of the efficiency and the spatial structure was investigated. For the KDP crystal type II the temperature dependence is expressed by /5/:

$$\Delta T = \frac{0,44\lambda}{L} \cdot \left(\frac{\partial n_e^{2\omega}}{\partial T} - \frac{\partial n_o^{\omega}}{\partial T} \right)^{-1}$$

where λ is the wavelength of the incident wave, L is the crystal length, T is the temperature. For the KDP crystal (10x10x30 mm) which was used to SH conversion $\Delta T_{CALC} = 5.8^\circ\text{C}$. (ΔT is the interval in which the efficiency is more than 1/2 of maximum value). This calculated value coincides with the experimental measured data plotted on Fig.5 from which follows $\Delta T_{EXP} = 6.2^\circ\text{C}$. The independent experimental determination was done by the integration of the CCD output spatial structure.

From the measuring of the temperature dependence of the far field SH beam spatial structure (Fig.6) follows that inside the temperature range 24°C-32°C, the SH beam has mostly clean profile and due to the diffraction aperture effect, the contour has a little elliptical form. Within the range 10°C-22°C, the beam profile was deformed and in the temperature range 36°C-52°C, the most significant feature observed was the appearance of a double spot alternating regularly with the homogeneous elliptical one. In all cases, the center of the beam has been shifted with changing temperature.

In Fig.6. it is seen that the far field beam structure of the SH beam has the elliptical form. This distortion of the spatial structure in one direction follows from the fact that due to the double refraction of the nonlinear crystals, the extraordinary ray deviates in the anisotropy or walk off angle. The beam of the SH radiation is therefore deviated from the original (IR beam) direction and from this fact the aperture effect follows which decreases the efficiency of the SHG and changes the shape of the pulse (Fig.7.B). We try to use the tandem scheme /7/ for the compensation of this deviation. The resulted spatial beam structure is on Fig.7.C.

SUMMARY

The laser transmitter system was designed to have an optimum farfield beam spatial structure what implies a good farfield and a higher efficiency of the SH radiation beam. The measurement of the temperature dependence of the SH crystal showed the strong dependence of the efficiency, of the spatial structure and of the pointing accuracy on temperature changes.

LITERATURE

- /1/ Jelinkova H., Proceedings of the Vth International Workshop on Laser Ranging Instrumentation, Greenwich, England, 1984.
- /2/ Hamal K., Hruskova V., Jelinkova H., Proceedings of CLEO 1985, Baltimore, USA.
- /3/ Hamal K., Jelinkova H., "Stable Saturable Dye for 1.06 μm ", in this Proceeding.
- /4/ Born M., Volf E., "Principles of Optics", Pergamon Press, 1964.
- /5/ Koechner W., "Solid-State Laser Engineering", New York, Springer Verlag, 1976.
- /6/ Tarasov L.V., Dmitrijev V.G., "Prikladnaja Nelinejnaja Optika", Moskva, Radio i Svjaz, 1982 (in Russian).
- /7/ Volosov V.D. et al., Sov. J. Quantum Electron., 6, p.1163, 1976.

Tab.1. Laser System Divergence

A) Isolation cell - Brewster angle

| Measured point | X [mrad] | Y [mrad] |
|----------------|----------|----------|
| A | 1 | 0.9 |
| B | 1.7 | 1.1 |
| C | 0.8 | 0.6 |
| D | 0.7 | 0.6 |

B) Isolation cell - 1 deg angle

| Measured point | X [mrad] | Y [mrad] |
|----------------|----------|----------|
| A | 1 | 0.9 |
| B | 1.1 | 0.9 |
| C | 0.6 | 0.6 |
| D | 0.6 | 0.6 |

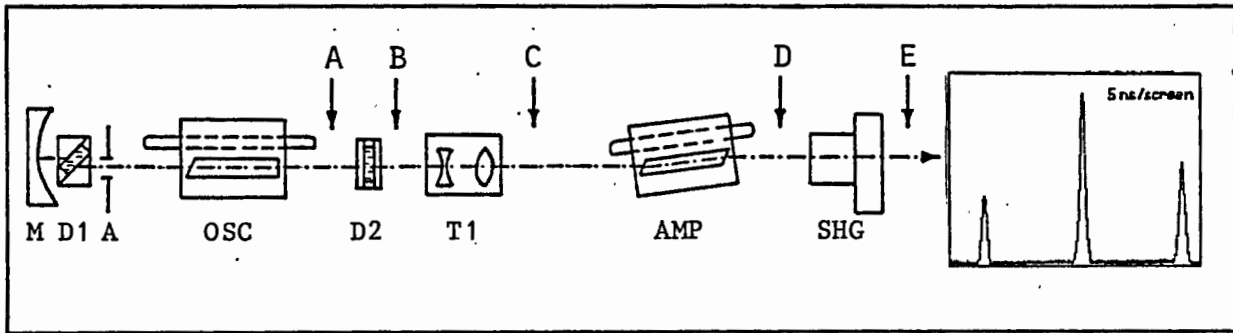


Fig.1. Block diagram of the optical lay-out of the Nd:YAG laser transmitter.

| | | | |
|-----|-----------------|-----|--------------------------|
| M | End mirror | D2 | Dye cell |
| D1 | Dye cell | T1 | Telescope |
| A | Aperture | AMP | Amplifier head |
| OSC | Oscillator head | SHG | KDP II Frequency doubler |

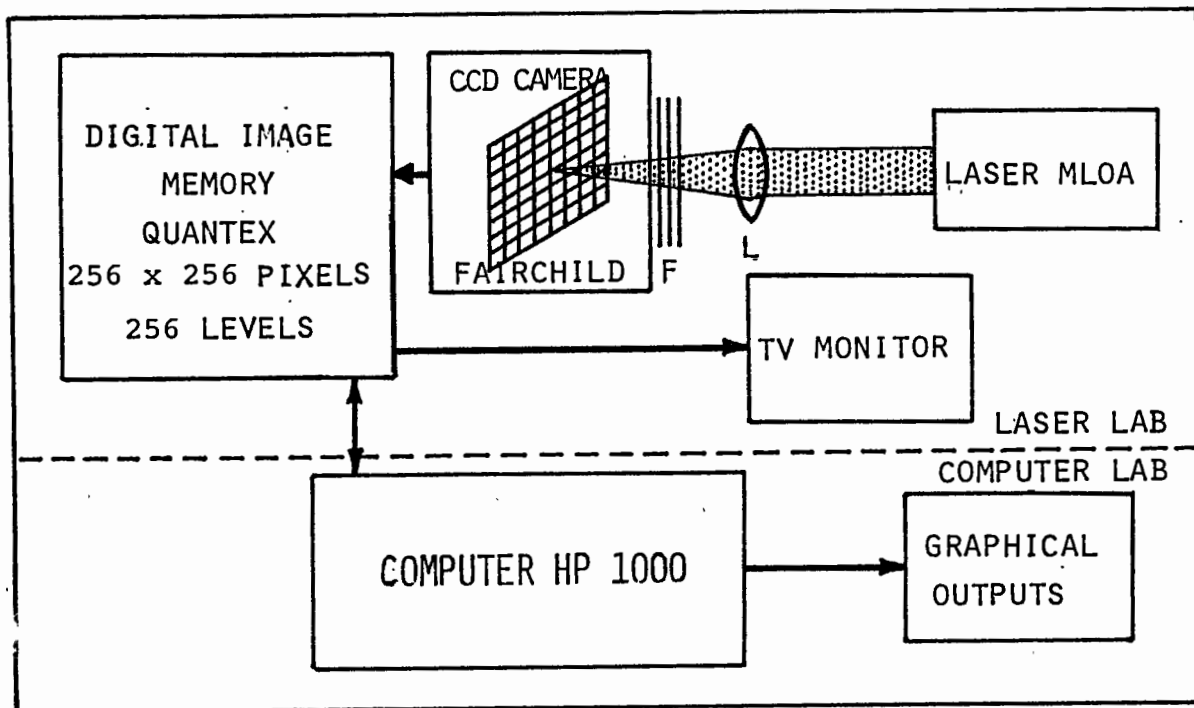


Fig.2. The experimental set up of the farfield beam spatial structure measurements. (F - neutral density filters, L - 2.5 m lens.)

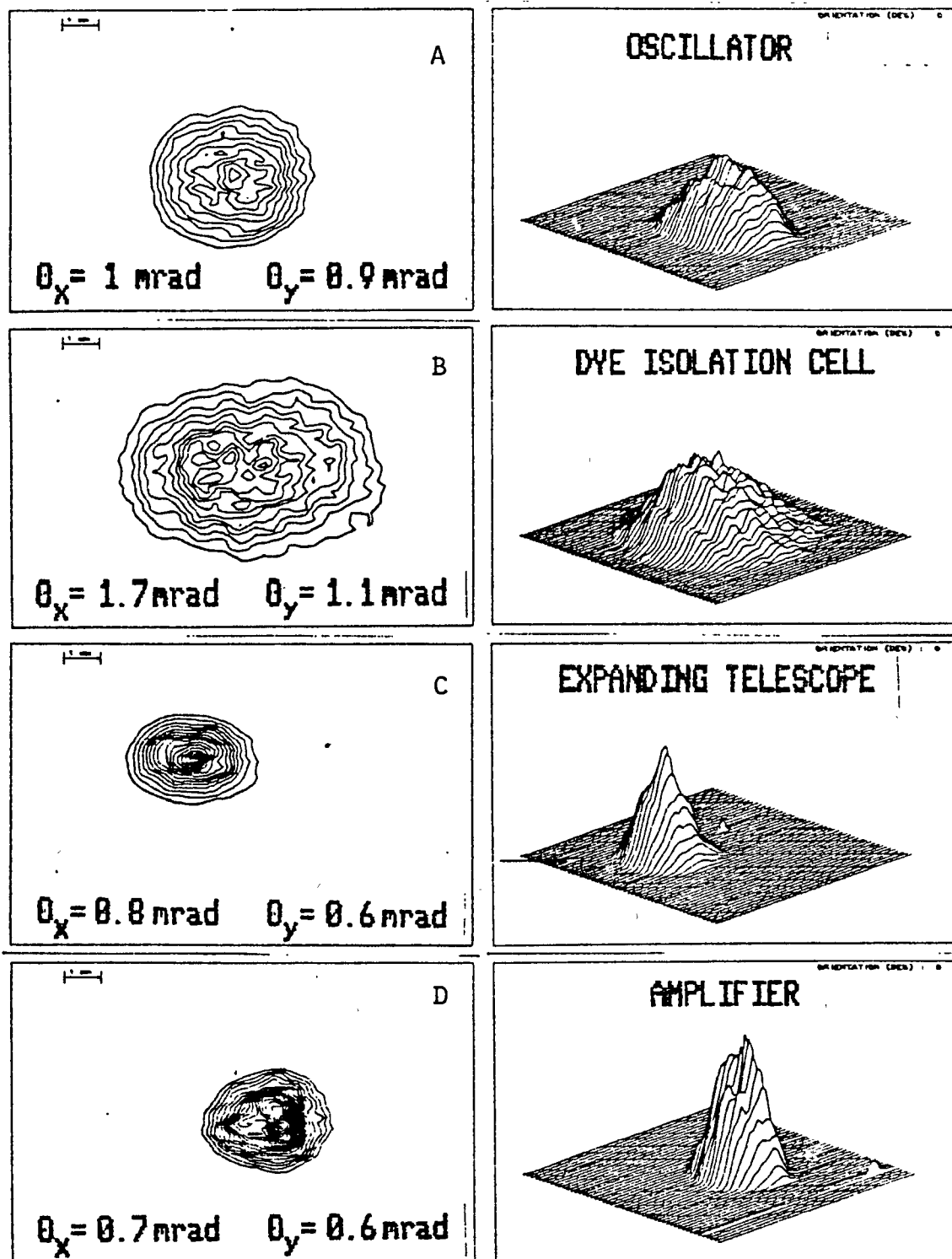


Fig.3. The IR far field beam spatial structure.

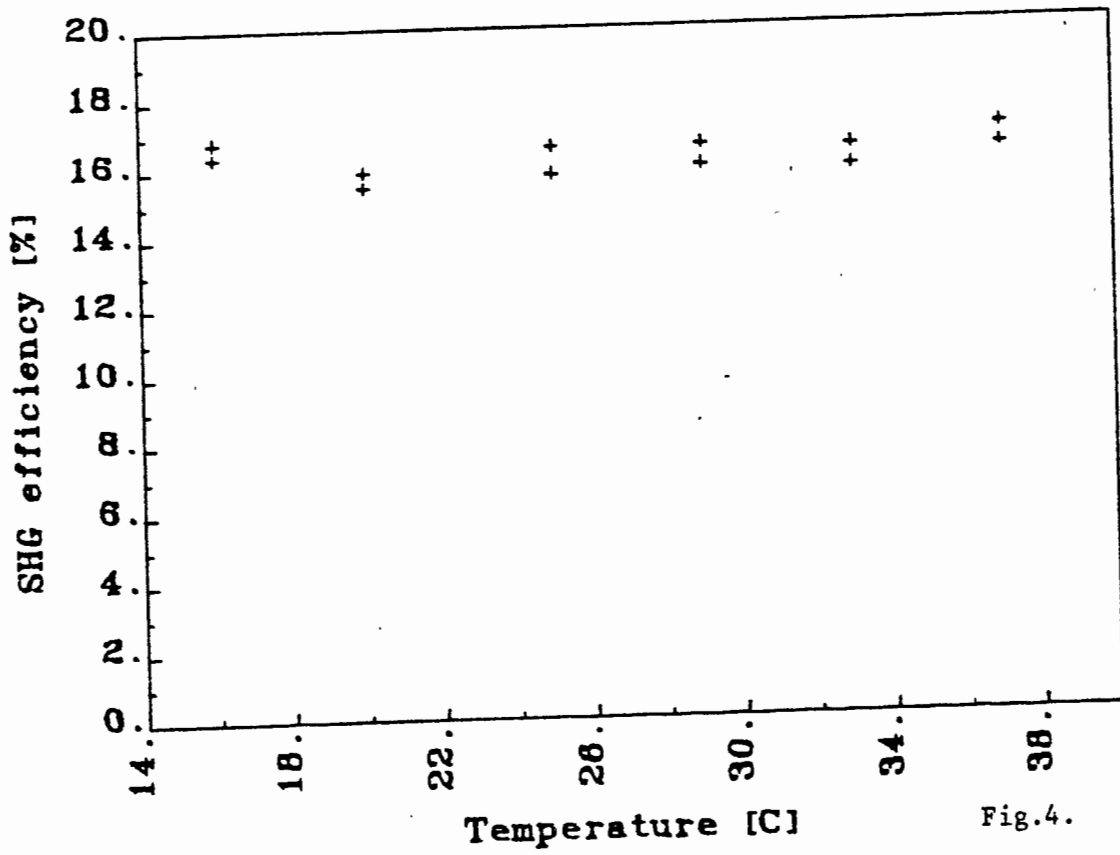


Fig.4.

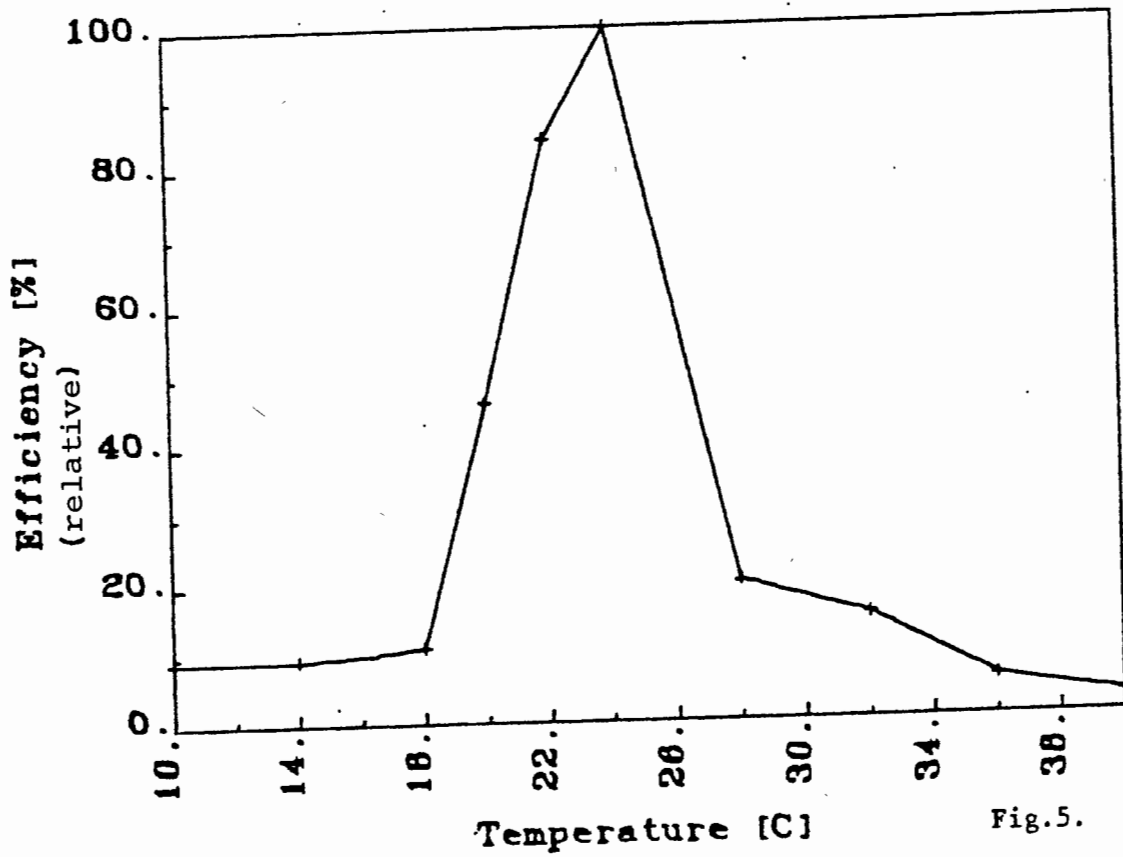


Fig.5.

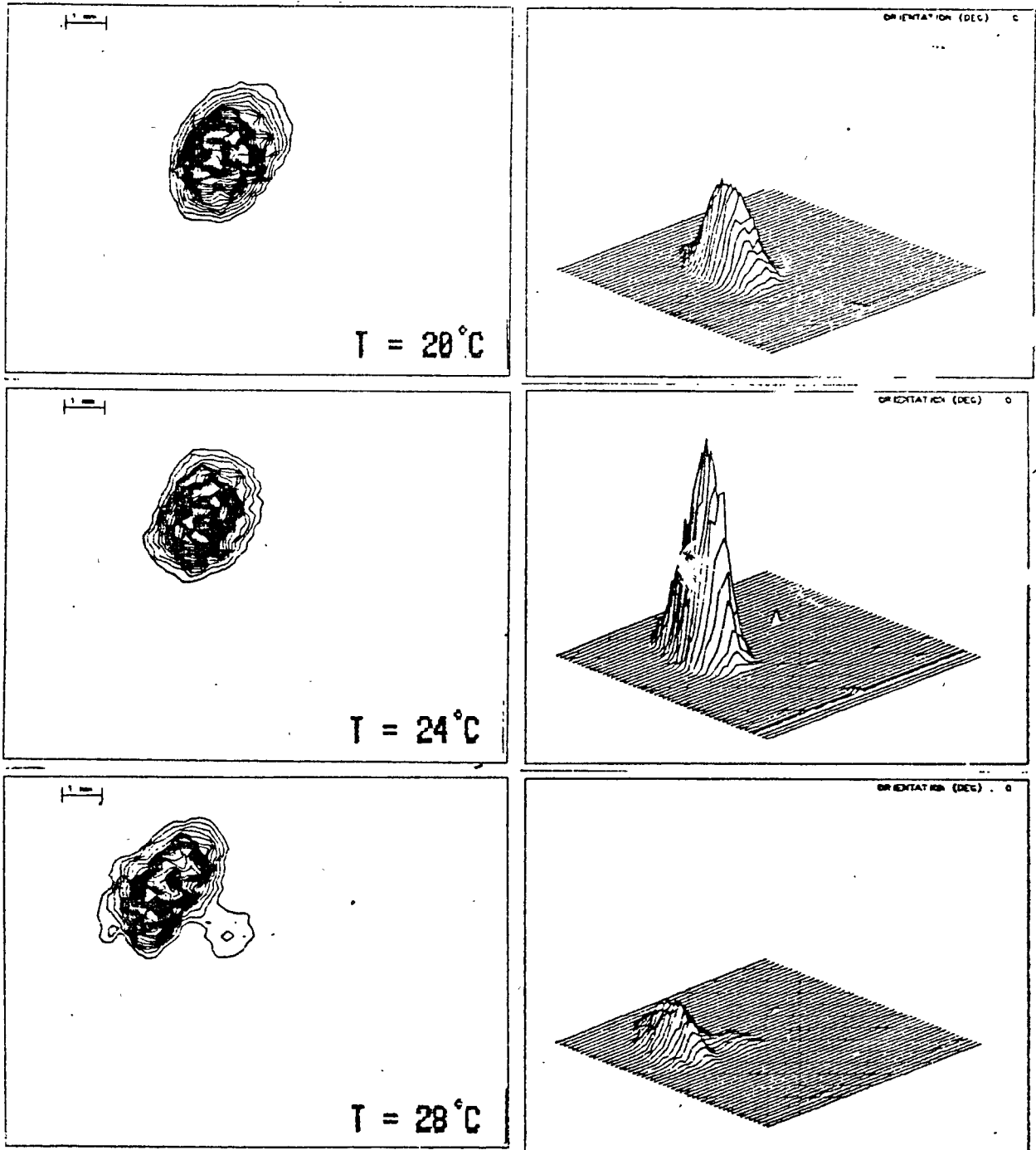


Fig.6. Temperature dependence of the far field SH beam structure.

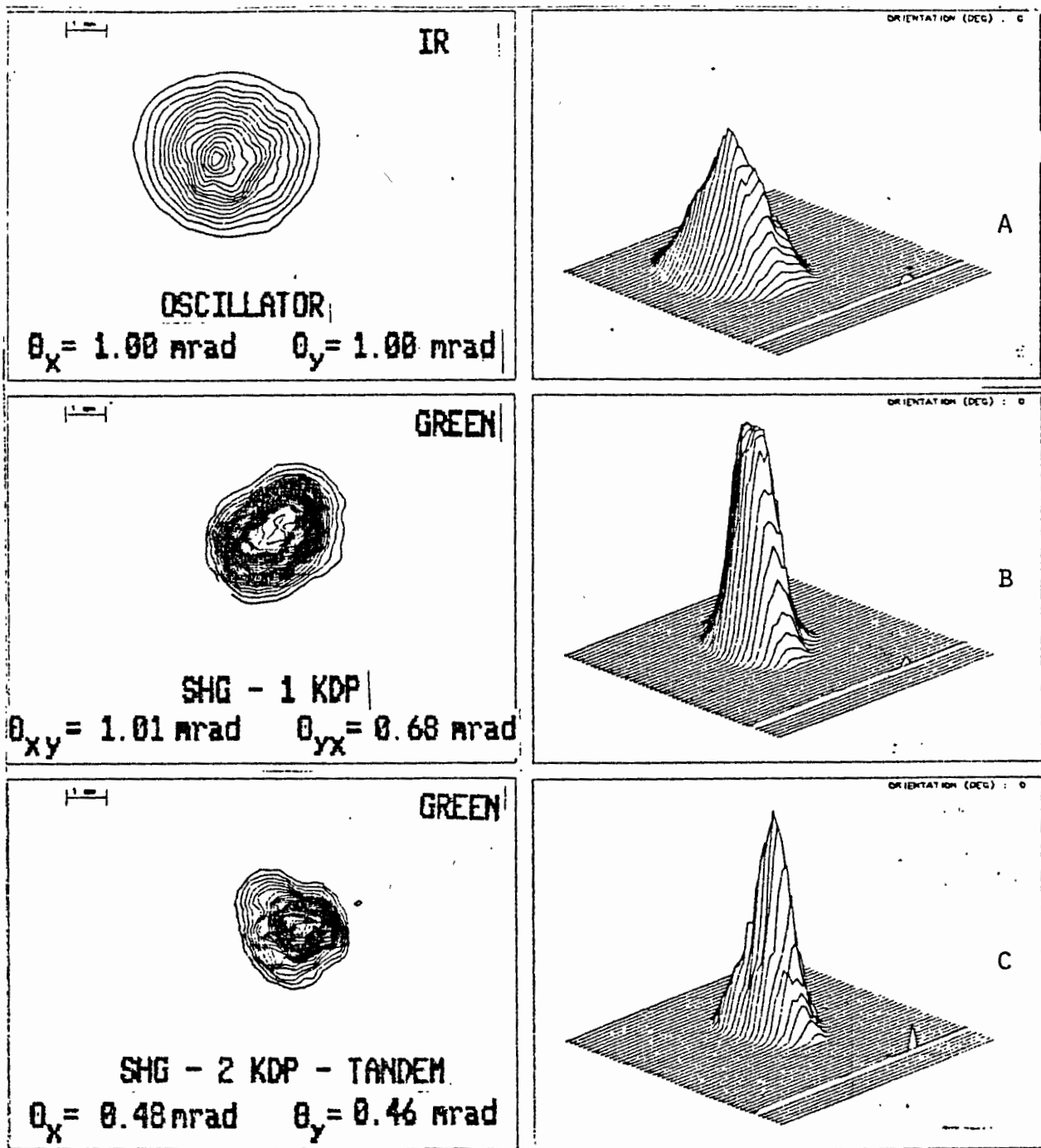


Fig.7. Aperture effect compensation

SOME SPECIAL REQUIREMENTS
TO LASERS FOR SATELLITE LASER RANGING

L. Jiyu
Wuhan Technical University of
Surveying and Mapping
23 Lo-yu Road, Wuhan
The People's Republic of China

ABSTRACT

When designing or improving an SLR system it will be necessary to take into consideration that which laser should be selected. This paper has given an outline of some special requirements to select a suitable laser.

At present solid-state lasers are used to measure the distances not only between a ground station and the satellite specially equipped with retroreflectors far off several thousand kilometers, but also between a ground station and the moon set by five retroreflectors arrays far off about 380 thousand kilometers. Laser pulses generated by a solid-state laser are not modulated with any way, but used directly to measure the distances. In this case, what requirements are proposed for lasers? This paper will try to discuss them.

Some Special Requirements to lasers for Satellite Laser Ranging

Liu JiYu
Wuhan Technical University of
Surveying and Mapping
23 Lo-yu Road, Wuhan
The People's Republic of China

Abstract

When designing or improving an SLR system it will be necessary to take into consideration that which laser should be selected. This paper has given an outline of some special requirements to select a suitable laser.

At present solid-state lasers are used to measure the distances not only between a ground station and the satellite specially equipped with retroreflectors far off several thousand kilometers, but also between a ground station and the moon set by five retro-reflector arrays far off about 380 thousand kilometers. Laser pulses generated by a solid-state laser are not modulated with any way, but used directly to measure the distances. In this case, what requirements are proposed for Lasers? This paper will try to discuss them.

It is known that the received photons per pulse for SLR systems, N are given as follows:

$$N = \frac{16E\lambda A_s A_r \tau_t \tau_r \tau^2 \gamma}{\pi^2 h c \delta_t^2 \delta_s^2 D^4} \quad (1)$$

Where,

- E = transmitted energy per pulse, in joule;
- λ = laser wavelength, in meter;
- A_s = effective area of Satellite-borne retroreflectors, in cm^2 ;
- A_r = effective area of the received objective of a received telescope, in cm^2 ;
- τ_t = transmitter optical transmission;
- τ_r = receiver optical transmission;
- τ = one-way atmospheric transmission which is a function of zenith distance, site altitude, locality, visibility and wavelength;
- γ = reflectivity of the satellite-borne retroreflectors, generally $\gamma = 0.8$;
- h = Planck's constant, $h = 6.625 \times 10^{-27}$ erg second;
- c = light velocity, in meters/second;
- δ_t = full angular divergence of a transmitted laser beam, in arc;
- δ_s = reflected laser beam divergence by the satellite-borne retroreflectors, in arc;
- D = distance between the ground station and the laser satellite, in cm.

It is seen from the above equation that the parameters, $E\lambda\delta_t$ are dealt with the lasers. How their magnitudes are selected is a problem which laser is designed to satisfy some requirements for an SLR system. Therefore it is very useful to discuss their selections.

Table 1: Lasers used by worldwide SLR systems

| country | wavelength | pulsewidth | transmitted power | Repetition rate | Detector type |
|-----------|------------|---------------------------|-------------------|-----------------|---------------------------------|
| Australia | 532 nm | 5-7 nsec | 250 mJ | 1 pps | 2233 Amperex |
| " | 694.3 nm | 6 nsec | 350 MW | 8 ppm | RCA 7265 |
| " | 694.3 nm | 6 nsec | 1 J | 12 ppm | RCA 31034 |
| Austria | 530 nm | 100 ps | 100 mJ | up to 10 Hz | |
| " | 694.3 nm | 3 ns, 6 ns | 2.5 J, 4 J | up to 0.25 Hz | |
| Brazil | 694.3 nm | 6 nsec | 350 MW | 8 ppm | RCA 7265 |
| China | 532 nm | 5 nsec | 20 MW | 1 Hz | GDB 49 |
| " | 694.3 nm | 20 nsec | 80 MW | 30 ppm | |
| Cuba | 694 nm | 30 nsec | 50 MW | 15 ppm | RCA 8852 |
| Ecuador | 694.3 nm | 35 nsec | 1 J | 0.25 pps | FEU-84 |
| Egypt | 694 nm | 30 nsec | 50 MW | 15 ppm | RCA 8852 |
| " | 694 nm | 4 nsec | 200 MW | 15 ppm | RCA 8852 |
| W-Germany | 532 nm | 200 pps | 0.25 J | 4 pps | Varian Static Crossed Field 154 |
| " | 539 nm | 400 pps | 10 mJ | 10 Hz | RCA 8850 |
| Finland | 694.3 nm | 20 nsec | 50 MW | 4 ppm | RCA C 31034 |
| France | 694.3 nm | 3 nsec | 1.5 J | 6 ppm | RCA 31034 |
| " | 694 nm | 3.5 nsec | 3 J | 10 ppm | centroid detection |
| DDR | 694.3 nm | 20 nsec | 0.5 to 1 J | 10 ppm | RCAC 34034A |
| Greece | 694.3 nm | 25 nsec | 4.5 J | 8 ppm | RCA 7265 |
| Hungary | 694 nm | 20 nsec | 0.5 J | 0.5 Hz | FEU-84 |
| India | 694.3 nm | 20 nsec | 1 J | 1 pps | RCA 8852 |
| Japan | 694.3 nm | 15 ns, 4 ns (with slicer) | 0.3 J | 0.1 pps | RCA 7265 |
| " | 532 nm | 200 ps | 250 mJ | 4 pps | static crossed field |
| Netherla. | 694.3 nm | 1.8 nsec | 700 mJ | 15 ppm | RCA 8852 |
| " | 539 nm | 400 ps | 10 mJ | 10 Hz | RCA 8852 |
| Peru | 694.3 nm | 6 nsec | 350 MW | 8 ppm | RCA 7265 |
| Poland | 694 nm | 25 nsec | 1.5 J | 7 ppm | RCA 8852 with CFD |

Table 1 (Continuous)

| country | wavelength | pulsewidth | transmitted power | Repetition rate | Detector type |
|----------------|------------|--------------|-------------------|-----------------|-----------------|
| Spain | 694 nm | 27 nsec | 0.7 J | 6 ppm | RCA 31034A |
| Switzerla. | 694 nm | 17 nsec | 1.5 J | 0.25 Hz | RCA 7265 |
| United Kingdom | 532 nm | 150 ps | 30 MJ | 10 Hz | Varian VPM 152S |
| USA (Texas) | 694.3 nm | 3 nsec | 0.4 J | 20 ppm | RCA 31034A |
| " " | 532 nm | 100 ps | 0.4 J | 10 Hz | RCA 8852 |
| " " | 532 nm | 100 ps | 35 MW | 10 Hz | Varian 152S |
| " (Hawaii) | 694 nm | 5 nsec | 750 mJ | 1 pps | 56 TVP |
| " (Colorado) | 694 nm | 5 nsec | 750 mJ | 1 pps | 56 TVP |
| " (CA) | 694 nm | 5 nsec | 750 mJ | 1 pps | 56 TVP |
| " (GSFC) | 532 nm | varied | varied | 1 pps | 56 TVP |
| " " | 532 nm | 5-7 nsec | 250 mJ | 1 pps | 56 TVP |
| " " | 532 nm | 0.2-0.4 nsec | 250 mJ | 1 pps | 56 TVP |
| " (CA) | 532 nm | 5-7 nsec | 250 mJ | 1 pps | Amperex 56 TVP |
| " (GSFC) | 532 nm | 0.2-0.4 nsec | 250 mJ | 1 pps | Amperex 56 TVP |
| " (Maui) | 532 nm | 500 ps | 0-6 J | 3 Hz | Amperex XP2233 |
| USSR | 694.3 nm | 20 nsec | 50 MW | 0.7 Hz | FEU-79 |
| " | 694.3 nm | 25 nsec | 1 J | 0.33 Hz | FEU-84 |

On the basis of the materials published by the Fourth International Workshop on Laser Ranging Instrumentation held at the University of Texas in Austin, Texas USA, October 12-16, 1981 the essential specifications of the lasers operating in worldwide SLR systems are shown in the Table 1. The used laser wavelengths are of three types of 6943 Å, 5320 Å and 5390 Å, corresponding with three laser medium of ruby, Nd:YAG and Nd:YAP crystal. The longer laser wavelength used is to the benefit of detections with the view of the transmission traveled in the atmospheric layer (see Table 2). Under the condition of the smallest zenith distance there is not greater difference between

Table 2: Atmospheric transmission at different wavelengths and zenith distances, from Mastrocinque

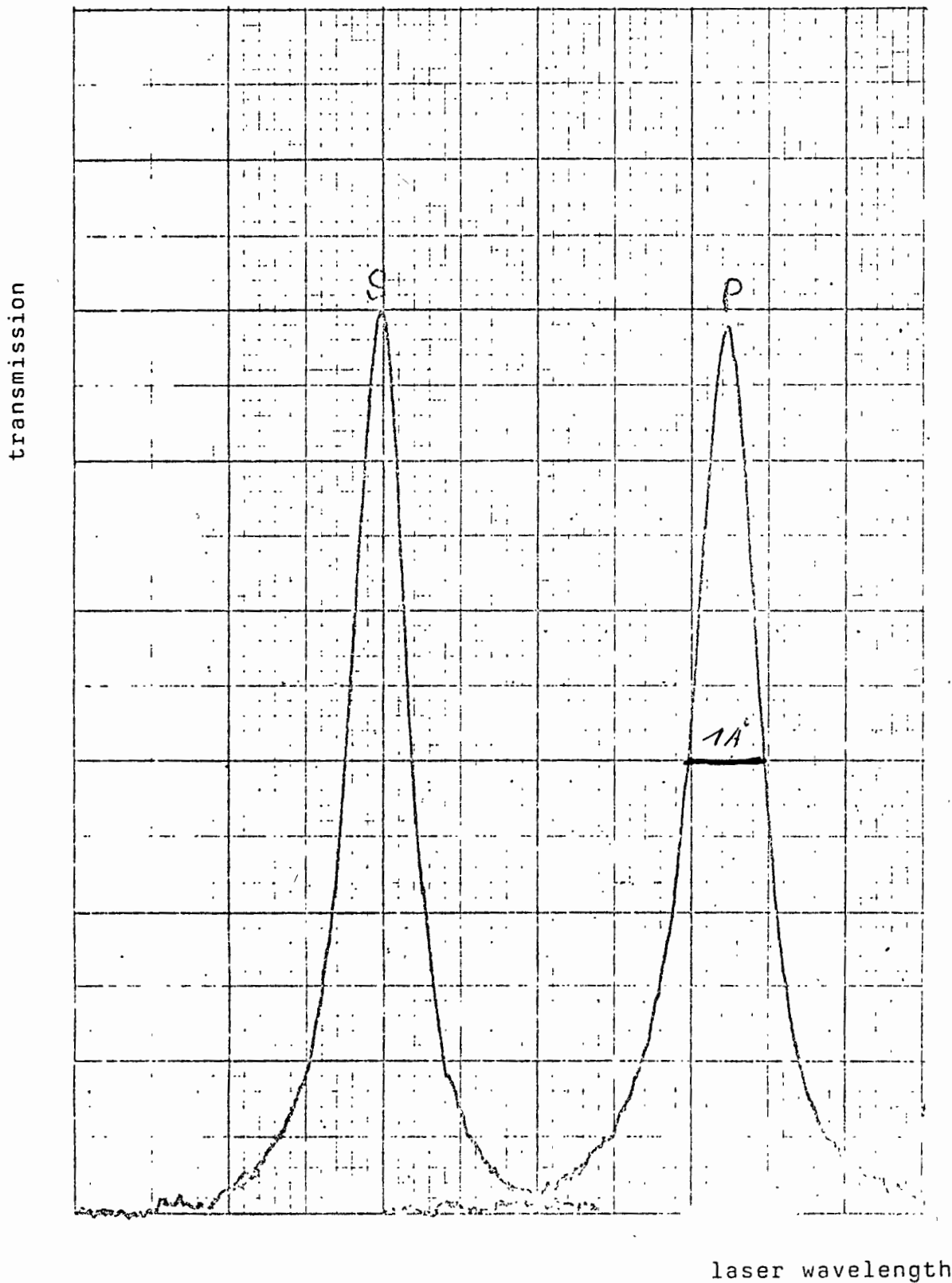
| λ (nm) | $\tau(0^\circ)$ | $\tau(60^\circ)$ | $\tau(70^\circ)$ |
|----------------|-----------------|------------------|------------------|
| 760 | 0.79 | 0.63 | 0.50 |
| 694.3 | 0.77 | 0.58 | 0.45 |
| 532 | 0.67 | 0.45 | 0.30 |
| 380 | 0.44 | 0.20 | 0.09 |

atmospheric transmission at different wavelengths. However, the smaller the elevation is, the greater the transmission difference gets. For example, the atmospheric transmission of 6943 Å laser will be 50 % higher than that of 5320 Å laser obtained with a second harmonic generator (SHG) when the elevation is equal to 20°. It is known that the SHG halves the wavelength of 1064 nanometers generated by Nd:YAG laser to 532 nanometers which is in the visible region of the spectrum. If there should be any photoelectronic conversion device which is of higher efficiency of quantum for a infrared laser it would be of great advantage for SLR systems to directly use the laser beam generated by the laser system without

SHG, such as 1064 nm laser falling within an atmospheric window. When omitting the SHG for which maximum conversion efficiency is up to 30 percent (energy) the latter is equivalent to increase the transmitted energy of about 70 percent. On the other hand, it will be seen from equation (1) that the received photons varies as the laser wavelengths. Under the condition of the same parameters the number of the received photons is increased with an increased wavelength. It will be possible to execute normal SLR with the smaller transmitted energy produced by a simplified laser.

If there is any significant drift for the laser wavelengths this will produce three bad effects. First is a transmission decrease for a telescope. It is known that the coatings of all optical components are compatible with a certain operation wavelength. The greater the drift of the laser wavelength is, the smaller the transmission for a transmitted laser beam gets. Second is an attenuation increase for a narrowband filter. In order to heighten the signal-to-noise ratio a narrowband filter is used in a receiver based on PMT. Due to a very narrow FWHM, such as that of $1 \pm 0.2 \text{ \AA}$, the attenuation of the narrowband filter for the returned laser will be greatly increased when there is any greater drift (see Fig.). For example, when the drift of laser wavelengths is equal to $\pm 0.5 \text{ \AA}$ the transmission gotten through the narrowband filter will be decreased to 50 percent. Third is a reduction of the conversion efficiency from a light pulse to an electronic one. The peak conversion for a photocathode is compatible with a certain wavelength. Due to the drifted wavelength the conversion efficiency can not be impinged in the peak region. It will be seen from these that the stability of the laser wavelength is very important to insure the optimal operation for SLR systems. The spectral line stability should be better than a few subangstroms.

It will be seen from Table 1 that in 44 lasers used by worldwide SLR systems the minimal transmitted energy is 10 millijoules, the maximum 4.5 joules; the minimal pulsewidth is 100 picoseconds,



Transmission of double peak polarized interference filters produced by DayStar Filter corporation, California, USA

the maximum 35 nanoseconds. It was pointed out that the more narrow the laser pulsewidth, the smaller the pulsewidth error [Liu, 1985]. In practice the relationship was also found with constraining the laser pulsewidth. For example, the pulsewidth was constrained from 25 nsec to 6 nsec by means of a pulse chopper in an SAO SLR system so that the ranging accuracies increased to at least 50 percent [Tapley, et al, 1982]. From the following equation it can be demonstrated:

$$M_w = \frac{k_p \tau_p}{\sqrt{N_r}} \quad (2)$$

Where,

M_w = pulsewidth error;

τ_p = FWHM of a laser pulse;

N_r = number of received photoelectrons;

k_p = coefficient depending on different detection.

However, to use the pulse chopper for a narrow laser pulsewidth is a temporary improvement means. Due to its reject for a sizable fraction of the laser energy it is not efficient. An essential and efficient means is to employ the new laser which can not only generate laser pulses as short as 30 psec, but also operate in a pure fundamental TEM₀₀ mode. The latter can produce the smallest beam divergence, the highest power density, and, hence, the highest brightness. Furthermore, the radial intensity profile is uniform and uniphase [Koechner, 1976]. The experiment by GSFC demonstrated that the requirements can be satisfied essentially when using modelocked Nd:YAG lasers. Their repeatability and rangemap measurements have shown less than 2 cm peak-to-peak variation in 100 point mean. The repeatability and rangemap measurements for PTM Q-switched and Q-switched lasers were of more than 6 cm peak-to-peak variation in 100 point mean [Degnan and Zagwodzki, 1982]. It will be seen from the above

that modelocked Nd:YAG (or YAP) lasers should be substituted for Q-switched ones. The latter has also other problem leading to a wavefront error. Its source and magnitude have been discussed in another paper [Liu, 1985]. For at least decreasing the wavefront error SLR systems do not employ also the Q-switched lasers, but the modelocked ones.

From what has been said above, we know that it is suitable for lasers to be able to generate the following pulses:

- stable wavelength laser pulses, so as to insure the optimal operation for SLR systems. If there should be any device which can effectively detect infrared lasers it would be very beneficial to use longer laser wavelength for SLR;
- higher repetition laser pulses, so as to acquire more ranging data in one satellite pass; but due to limitations of thermal transients which disturb the fine balance within the optical resonator and high peak power nonlinear effects which can lead to the irreversible breakdown of materials subnanosecond laser pulses are limited to about 20 pps repetition rate [Hyde and Whitehead, 1982];
- short sharp laser pulses, so as to improve the accuracy for measurements to the time interval between a transmitted and returned laser pulse;
- powerful peak laser pulses. so as to be able to measure the distances not only to the satellite-borne retroreflectors, but also to the moon-borne retroreflector array;
- purer fundamental laser pulses, so as to obtain an uniform and uniphase intensity profile for precise SLR.

Acknowledgement: The author would like to express his hearty gratitude to the Institut für Angewandte Geodäsie, Frankfurt, FR Germany, for its support.

11
References

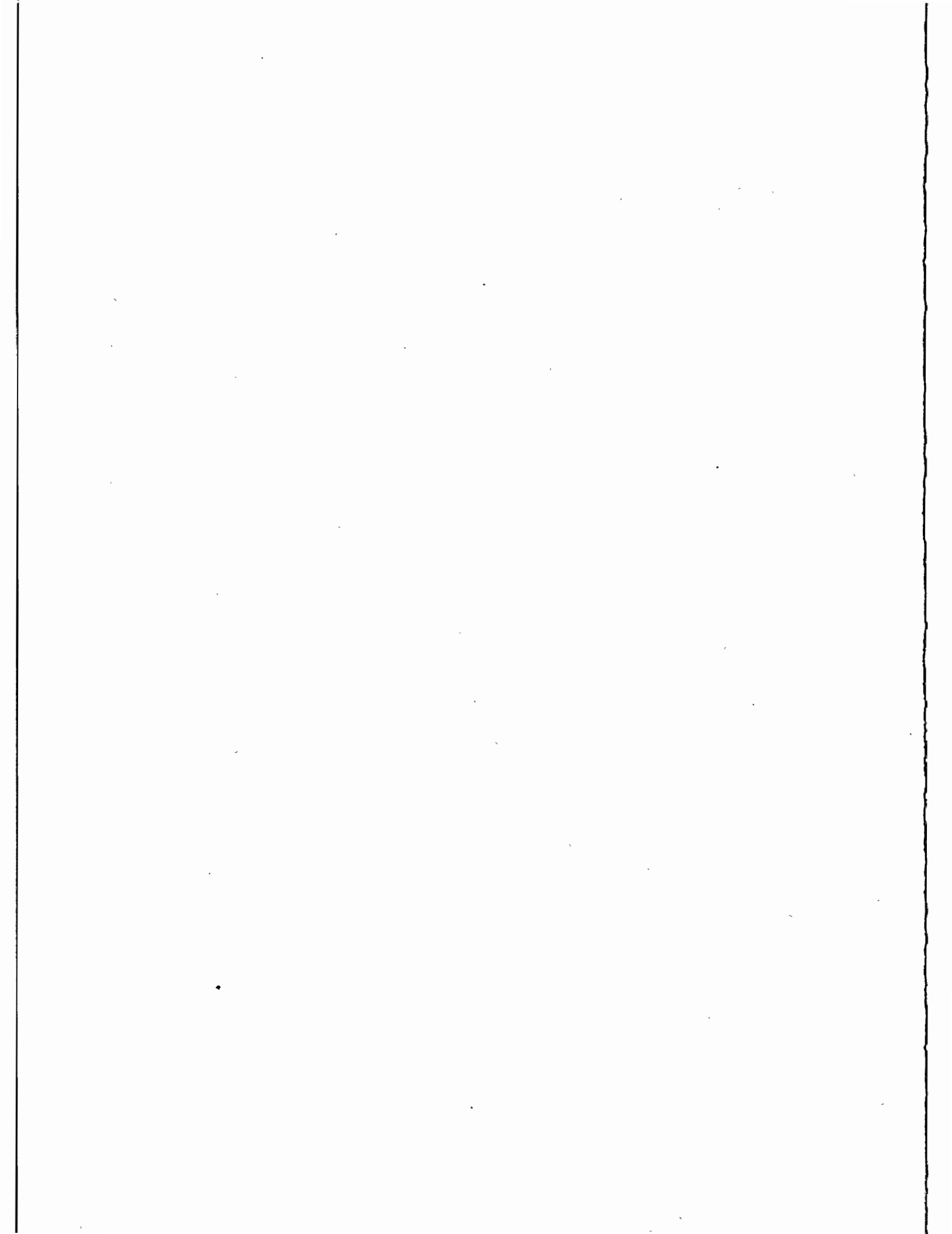
- [1] G. Mastrocinque, Feasibility of Satellite Tracking with a Dual-wavelength Laser Ranging System
ESA Journal, 1985, Vol. 9, pp 273-286

- [2] Liu Jiyu, Satellite Laser Ranging Errors

- [3] W. Koechner, Solid-state Laser Engineering, 5.1.9 Mode Selecting techniques
Springer-Verlag, Berlin, 1976

- [4] J.J. Degnan and T.W. Zagwodzki, A Comparative Study of Several Transmitter Types for precise Laser Ranging
Proceedings of the Fourth International Workshop on Laser Ranging Instrumentation, published by the Geodetic Institute, University of Bonn, 1982, pp. 241 - 250

- [5] R.L. Hyde and D.G. Whitehead, Some Problems of Short Pulse, Low Energy, High Repetition Rate Lasers Applied to Satellite Ranging Systems
Proceedings of the Fourth International Workshop on Laser Ranging Instrumentation, published by the Geodetic Institute, University of Bonn, 1982, pp. 251 - 259



ANALYSIS AND PERFORMANCE OF A PASSIVE
POLARIZATION TELESCOPE COUPLING SWITCH
FOR LUNAR LASER RANGING

S.R. Bowman, J.R. Rayner, C.O. Alley
Department of Physics and Astronomy
College Park, MD 20742

Telephone (301) 454 3405

ABSTRACT

A passive polarization switch is an attractive way to couple a laser transmitter and receiver to a telescope because it is so simple. However, few laser ranging stations have implemented such a switch because of concern about depolarization of the beam by the target. Here we show that the amount of depolarization is less than one might expect by considering the case of the Apollo lunar reflectors.

ANALYSIS AND PERFORMANCE OF A PASSIVE
POLARIZATION TELESCOPE COUPLING SWITCH
FOR LUNAR LASER RANGING

S. R. Bowman, J. R. Rayner, C. O. Alley
Department of Physics and Astronomy
College Park, MD 20742

Telephone (301) 454-3405

ABSTRACT

A passive polarization switch is an attractive way to couple a laser transmitter and receiver to a telescope because it is so simple. However, few laser ranging stations have implemented such a switch because of concern about depolarization of the beam by the target. Here we show that the amount of depolarization is less than one might expect by considering the case of the Apollo lunar reflectors.

INTRODUCTION

In order to separate the transmitted from the returned beams, some sort of switch is required. Most laser ranging systems incorporate a rotating mirrored chopper wheel for the switch. While this approach is conceptually simple it can lead to some practical problems. The wheel must spin stably while staying in phase with a high repetition rate laser. The limited extinction ratio between the two paths requires some additional blocking mechanism. Also, for realistic spin rates this type of switch is too slow for terrestrial ranging.

For the Goddard/Maryland Lunar Ranging System, a passive polarization switch was chosen.¹ It has the advantage of being very simple to implement, consisting of only a thin film Brewster angle polarizer and a zero order quarter wave plate. It has the disadvantage of losing some return light due to depolarization, but this is more than compensated for by its reduction of the noise by a factor of two. This section examines the efficiency of such a switch for lunar ranging.

DEPOLARIZATION FROM APOLLO REFLECTORS

After the second harmonic generator a half wave plate is used to rotate the linear polarization to the vertical, Figure 1. The "S" polarization is reflected off a thin film polarizer and passes through a zero order quarter wave plate into the telescope. (The zero order plate is needed to prevent temperature variation from affecting the polarization state.) Returning light of the correct polarization will become "P" polarized after a second trip through the quarter wave plate. Using Jones's calculus the polarization state can be computed each step of the way.²

Define a coordinate system on the optical table as shown in Figure 2. Transmission of the "S" polarization through the $\lambda/4$ plate gives a polarization state

$$U_s = \frac{1}{2} \begin{pmatrix} 1-i \\ 1+i \end{pmatrix} \quad (1)$$

Multiple reflections off the telescope mirrors will change the polarization state. However measurements of this effect show it to be small. A helium neon laser with an arbitrarily oriented linear polarization was transmitted through the telescope. The attenuation of the transmitted beam by a crossed linear polarizer was measured at many telescope positions. The linearly polarized intensity was found to be preserved to within 5%. Since this change is small and is reversed upon returning through the telescope, it is ignored here. It cannot be ignored, though, that the polarization axis will rotate as the telescope tracks in azimuth. This effect combined with the changing orientation of the moon as it passes overhead will be accounted for by a rotation transformation of the corner cube array.

PASSIVE POLARIZATION SWITCH

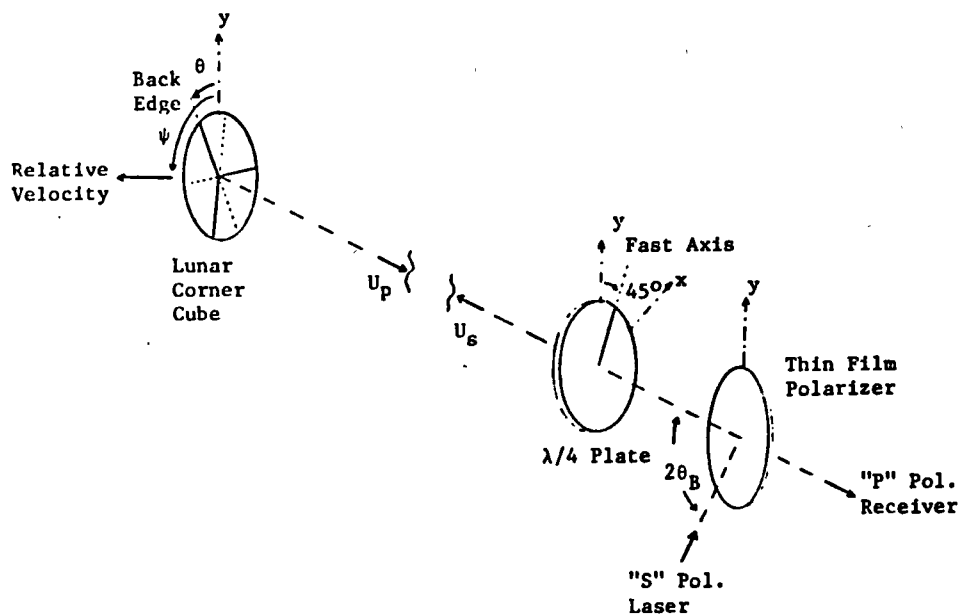


FIGURE 1

What happens to the polarization of a beam when reflected from a total internal reflection corner cube was first studied by E.R. Peck.³ R.F. Chang et al.⁴ extended the analysis to include far field diffraction of linear polarization from a corner cube. In a similar calculation, the Fraunhofer diffraction pattern for normally incident, circularly polarized light from a corner cube can be determined. Then the efficiency of the passive polarization switch can be evaluated once the velocity aberration effect is accounted for.

Upon reflection from a lunar corner, the incident beam is broken up into six wedge shaped beams. In general, each of these beams will have a different polarization. These six polarization states, \underline{V}^n , can be calculated from the equation

$$(\underline{V}_x^n, \underline{V}_y^n) = \underline{C}^n \cdot \underline{U}_s. \quad (2)$$

The authors mentioned above have calculated the polarization matrix \underline{C}^n consistent with the coordinates chosen here for the case of one back corner edge parallel to the "y" axis.

$$\begin{aligned} \underline{C}^1 &= \xi \underline{1} + \sqrt{1/2} \eta \underline{g}_z + \zeta \underline{g}_y + \sqrt{3/2} \eta \underline{g}_x \\ \underline{C}^2 &= \xi \underline{1} + \sqrt{2} \eta \underline{g}_z + \zeta \underline{g}_y \\ \underline{C}^3 &= \xi \underline{1} + \sqrt{1/2} \eta \underline{g}_z + \zeta \underline{g}_y - \sqrt{3/2} \eta \underline{g}_x \\ \underline{C}^4 &= \xi \underline{1} + \sqrt{1/2} \eta \underline{g}_z - \zeta \underline{g}_y - \sqrt{3/2} \eta \underline{g}_x \\ \underline{C}^5 &= \xi \underline{1} - \sqrt{2} \eta \underline{g}_z + \zeta \underline{g}_y \\ \underline{C}^6 &= \xi \underline{1} + \sqrt{1/2} \eta \underline{g}_z - \zeta \underline{g}_y + \sqrt{3/2} \eta \underline{g}_x \end{aligned} \quad (3)$$

In terms of the total internal reflection coefficients r_s and r_p

$$\begin{aligned} \xi &= \frac{1}{16} (r_s + r_p) [3(r_s + r_p)^2 - 2(r_s - r_p)^2] \\ \eta &= \frac{\sqrt{2}}{16} (r_s + r_p)^3 \\ \zeta &= -i \frac{\sqrt{3}}{16} (r_s + r_p)^2 (r_s - r_p). \end{aligned} \quad (4)$$

For an arbitrary azimuthal orientation of the corner, the matrix \underline{C}^n must be rotated about the "z" axis. It is easy to see that only the "x" and "z" Pauli matrix components are affected by a rotation of angle θ . To transform \underline{C}^n to $\underline{C}^n(\theta)$, one only need substitute

$$\underline{g}_x(\theta) = \begin{pmatrix} \cos 2\theta & \sin 2\theta \\ \sin 2\theta & \cos 2\theta \end{pmatrix} \quad \text{and} \quad \underline{g}_z(\theta) = \begin{pmatrix} \cos 2\theta & \sin 2\theta \\ \sin 2\theta & \cos 2\theta \end{pmatrix}. \quad (5)$$

Combining the last few equations gives the polarization state vectors, \underline{V}^n , for the six normally reflected beams from an azimuthally rotated total internal reflection corner cube. In order to evaluate the efficiency of the polarization switch, the components of each \underline{V}^n that are transmitted and rejected must be found. Transforming back through the $\lambda/4$ plate shows that:

$$\underline{U}_p = \frac{1}{2} \begin{pmatrix} 1 & +i \\ 1 & -i \end{pmatrix} \quad (6)$$

is the transmitted polarization state. The components of the \underline{v}^n 's in the \underline{U}_p and \underline{U}_s directions are

$$\begin{aligned} \gamma_p^n &= \underline{v}^n \cdot \underline{U}_p = \begin{cases} \tau\xi + \zeta & (\text{for odd } n) \\ \tau\xi - \zeta & (\text{for even } n) \end{cases} \end{aligned}$$

and

$$\gamma_s^n = \underline{v}^n \cdot \underline{U}_s = \eta \delta_n e^{i2\theta}, \quad (7)$$

where the complex numbers δ_n are given in Table (1).

The normalized reflected electric field from the n th subaperture of the j th corner cube in the array can now be written as

$$\underline{A}_j^n = [\gamma_p^n(\theta_j) \underline{U}_p + \gamma_s^n(\theta_j) \underline{U}_s] \exp(i\Delta_j). \quad (8)$$

The phase Δ_j is the overall optical delay for the j th corner. For even slight variations in the physical dimensions or temperatures of the corners, the optical delay will vary over one wavelength. For this reason the following analysis assume Δ_j to be random.

Records of the construction of the lunar corner reflector packages show that all the corners in the arrays were carefully oriented alike.⁵ Therefore, the subscript on θ_j can be dropped.

After propagating back from the moon, the beam from each of the corner cubes will be spread by diffraction. For the j th corner the field component in the \underline{U}_p direction at a point Q will be

TABLE 1

| n | δ_n |
|-----|---------------------|
| 1 | $\sqrt{3/2} - 1/2$ |
| 2 | $+i$ |
| 3 | $-\sqrt{3/2} - 1/2$ |
| 4 | $-\sqrt{3/2} + 1/2$ |
| 5 | $+i$ |
| 6 | $\sqrt{3/2} - 1/2$ |

$$u_j^P(Q, \theta) = \frac{1}{\pi a^2} \exp(i\Delta_j) \int_0^a \rho d\rho \int_0^{2\pi} \gamma_p(\phi, \theta) e^{-ik\rho \sin\alpha \cos(\phi-\psi)} d\phi \quad (9)$$

Here (ρ, ϕ) are polar coordinates on the corner aperture and (α, ψ) are the angles locating the point Q relative to the center of the diffraction pattern. Dividing by the area of the corner, πa^2 , normalizes the amplitude for $\alpha = 0$. Rewriting the ϕ integral in terms of the six subapertures gives

$$u_j^P(Q, \theta) = \frac{1}{\pi a^2} \exp(i\Delta_j) \sum_{n=1}^6 \gamma_p(\theta) \int_0^a \rho d\rho \int_{\theta+(2n+1)\pi/6}^{\theta+(2n+3)\pi/6} \exp[-ik\rho \sin\alpha \cos(\phi-\psi)] d\phi \quad (10)$$

With the definition of $x = k a \sin\alpha$ and the use of the Bessel series expansions

$$e^{+iy \cos\beta} = J_0(y) + 2 \sum_{\ell=1}^{\infty} (-1)^\ell J_\ell(y) \cos(\ell\beta) \quad (11)$$

and

$$\int_0^x y J_\ell(y) dy = 2\ell x \sum_{m=0}^{\infty} \frac{(\ell + 2m + 1)}{(\ell + 2m + 2)(\ell + 2m)} J_{\ell+2m+1}(x)$$

the amplitude component becomes

$$u_j^P(Q, \theta) = \frac{1}{3x} \exp(i\Delta_j) J_1(x) \sum_{n=1}^6 \gamma_p^n + \frac{8}{\pi x} \exp(i\Delta_j) \sum_{\ell=1}^{\infty} (-1)^\ell \sin(\ell\pi/6) \sum_{n=1}^6 \gamma_p^n \cos\{\ell[\pi(n+1)/3 + \theta - \psi]\} * \sum_{m=0}^{\infty} \frac{(2m+\ell+1)}{(2m+\ell)(2m+\ell+2)} J_{2m+\ell+1}(x) \quad (12)$$

If the laser pulse duration is long enough, the fields from all of the N corners will superimpose. In the approximation that N is large, the transmitted intensity will be

$$I^P(Q, \theta) = \left| \sum_{j=1}^N u_j^P \right|^2 = N |u_j^P|^2 \quad (13)$$

Likewise, the rejected intensity will be

$$I^S(Q, \theta) = \left| \sum_{j=1}^N u_j^S \right|^2 = N |u_j^S|^2 \quad (14)$$

The polarization switch efficiency can now be written as

$$e(Q, \theta) = |u^P|^2 / [|u^P|^2 + |u^S|^2] \quad (15)$$

where the subscript j is now superfluous.

For small x, the J_1 term dominates the expression for u^P and the efficiency approached unity. Realistically though, the diffraction pattern is never centered on the receiver. It was shown earlier that

$$4.0 \leq |\alpha| \leq 7.3 \text{ microradians.} \quad (16)$$

as a result of velocity aberration. Figure 2 shows the switch

POLARIZATION SWITCH EFFICIENCY
FROM APOLLO REFLECTOR ARRAY

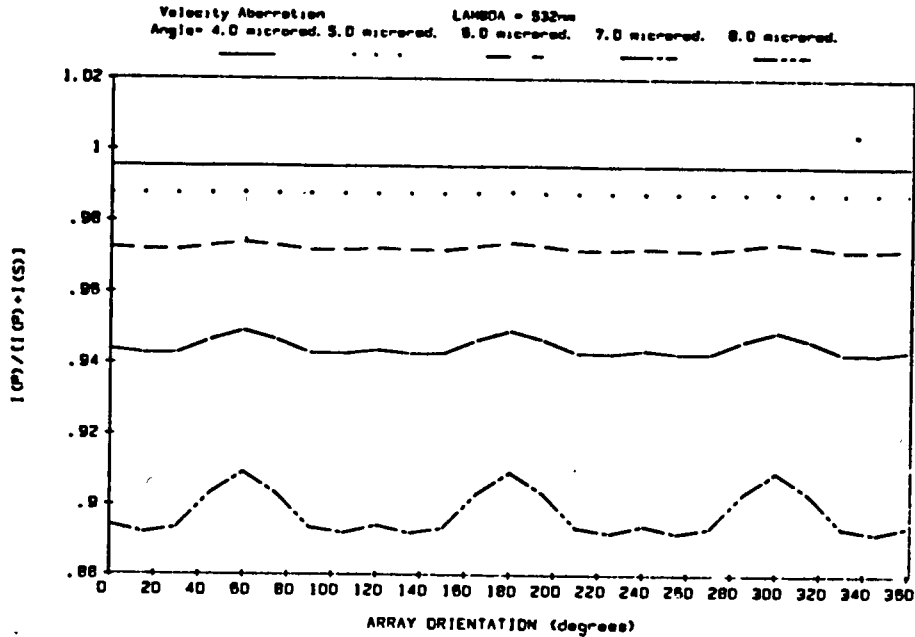


FIGURE 2

efficiency for several intermediate velocity aberration angles. It is clear from these curves that the depolarization is a weak function of the corner array orientation, $\theta = \psi$. More importantly though, the passive switch efficiency is better than 90% for all cases.

From the example calculation for lunar targets one would expect the depolarization losses to increase for other targets as the velocity aberration increases, although the exact calculation depends on the details of the targets structure. This means that the highest losses would be expected for the lowest satellites since they have the highest relative velocity. In practice, the passive polarization switch has been found to work very well for LAGEOS, BE-C, and GEOS-A.

CONCLUSIONS

Passive polarization switches are a simple, efficient way of coupling the laser and receiver to a laser ranging telescope. For lunar ranging operations, depolarization losses of less than 10% can be expected. Additional advantage is gained in noise reduction by the filtering of the unwanted polarization.

REFERENCES

1. The idea of using a polarization switch for coupling the laser and detector was originally suggested by Professor Douglas G. Currie about 1976. Its first use was reported in: C.O. Alley et al., "Experimental Range Measurements at the Single Photo-Electron Level to the GEOS-A and BE-C Satellites," Third International Workshop on Laser Ranging, Lagonisi, Greece, May 1978.
2. R.C. Jones, "A New Calculus for the Treatment of Optical Systems," J. Opt. Soc. Am., 31 (1941), 488.
3. E.R. Peck, "Polarization Properties of Corner Reflectors and Cavities," J. Opt. Soc. Am., 52 (1962), 253.
4. R.F. Chang et al., "The Far Field Diffraction Pattern for Corner Reflectors with Complex Reflection Coefficients", J. Opt. Soc. Am., 61 (1971), 431.
5. Laser Ranging Retro-Reflector Array for the Early Apollo Scientific Experiment Package, Final Report to Aerospace Systems Division The Bendix Corporation, Arthur D. Little, Inc., Cambridge, Mass., June 30, 1969.
6. M. Born and E. Wolf, Principles of Optics, (New York: Pergamon Press, 1985), p. 394.

AN ACCURATE TEST OF THE AZIMUTH AXIS OF A 1.2M
ALT-AZ TELESCOPE MOUNT FOR THE LUNAR LASER
RANGING AND THE ANALYSIS OF THE RESULTS

H. Feng, Y. Xiong, Y. Zhang, J. Wang
Yunnan Observatory
Academia Sinica
P.O Box 110
Kunming - China -

Telephone 729 46
Telex 64040 YUOBS.FN

ABSTRACT

The wobble of the azimuth axis of a 1.2m Alt-Az telescope mount for the Lunar Laser Ranging is measured by means of an accurate method. The systematic error is separated out and the random wobble is found to be about $0''.08$. The relation between the systematic error and the structure of the mount is also given in this article.

I. Introduction

Because of the long distance between the Earth and the Moon, the lunar laser ranging works approximately to the threshold of detection for the current laser ranging technology. In addition, the aim actively pursued by all the lunar laser ranging stations today is to make the lunar laser ranging by means of the absolute pointing of a telescope so as to increase in the number of days for the ranging. But the necessary condition is that the telescope should have highly accurate pointing. However, the pointing is based on the stability of the axis system. It is known that because of the error in the level adjustment or mechanical faults of the mount even the effects of the environments, the azimuth axis of the mount can not coincide with the direction of the plumb line of the station. The deviation consists of the systematic error and random wobble. Our aim is to seek for an accurate testing method, analyse the measured data, extract the systematic error from them and make an exactly quantitative estimate of the random wobble. It is hopeful to make compensation for the systematic error extracted when a computer is used to correct the telescope pointing. Moreover, some very interesting details related to the structure of the telescope mount are also found as the systematic error is analysed.

II. The Measuring Method

The most direct method for determining the deviation of the azimuth axis from the local plumb line is that the shift of a fine bubble, which is put at the top of the azimuth axis, is observed when the mount turns around the axis. Our measuring method still follows this principle, but the measurement accuracy is greatly improved.

The Talcott level used on the Zeiss transit instrument is adopted and one of the graduations is measured to be 1.17 arcsec (at about 20°C). The level bubble is fixed on an adjustable support which is installed at the top of the azimuth axis. Two small measuring telescopes, each with a micrometer, are used to determine the position of either end of the bubble, respectively. As two measuring telescopes may be pointed to the targets within a short range and one graduation of the bubble may be equivalent to 130 divisions on the micrometer. And it is easy to estimate the readout of $1/5$ division on the micrometer. In this way the readout resolution may be up to $1/500$ arcsec. Of course, the actual measurement accuracy can not be so high, which is limited by the factors such as the sighting accuracy, the manufacture precision of the bubble, the effects of the environment and so on.

When the measurement is carried out the bubble is firstly put in the direction paralleled to the altitude axis. As the mount is turned at 10° around the azimuth axis, the positions of the two ends of the bubble are determined by the micrometers separately and the mean of the two readouts represents the position of the center of the bubble. Then place the bubble in the direction perpendicular to the altitude axis

and repeat the steps of the measuring method mentioned above. We have made the measurement of 46 circles in all (with 36 measuring points and 37 readouts per circle). The measured data of the last 20 circles are used for the quantitative calculation and analysis. When the measurements of half of the 20 circles are made, the bubble is parallel with the altitude axis, and for the other half is perpendicular to the altitude axis.

III. The Results and their Analyses

When the measured results are shown graphically, it is not difficult to find that the systematic error is evidently included in the results and there appears good repeatability between the circles (Fig.1).

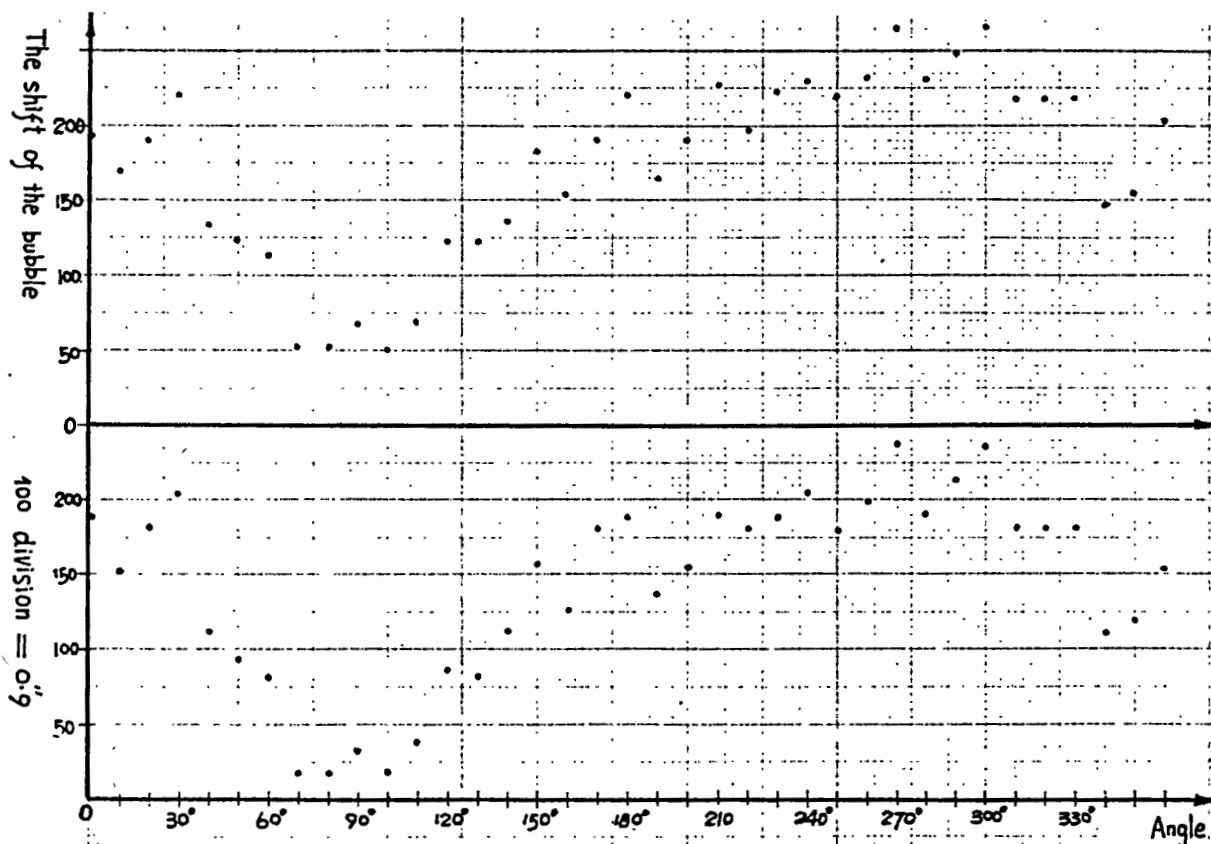


Fig.1. The positions of the bubble as the mount is turned at 10° around the azimuth axis

Using a trigonometric polynomial to fit the data, we can obtain the corresponding harmonic components. The first harmonic mainly originates from the level adjustment error of the mount, while the phases of the maxima of the third harmonic just correspond to the three bearing points of the mount, respectively. And it is of interest to note that the results also contain a twelfth harmonic, of which the amplitude is considerable and stable. The twelfth harmonic corresponds just right to the twelve oil pads of the revolving stage (Fig2).

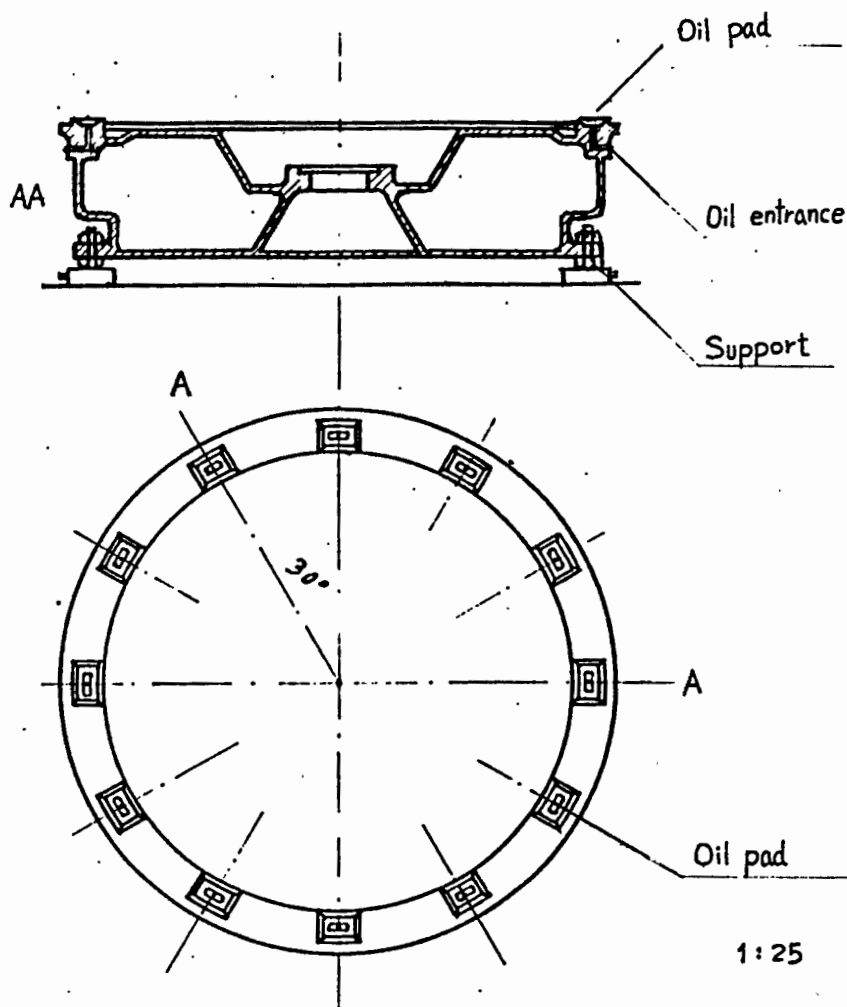
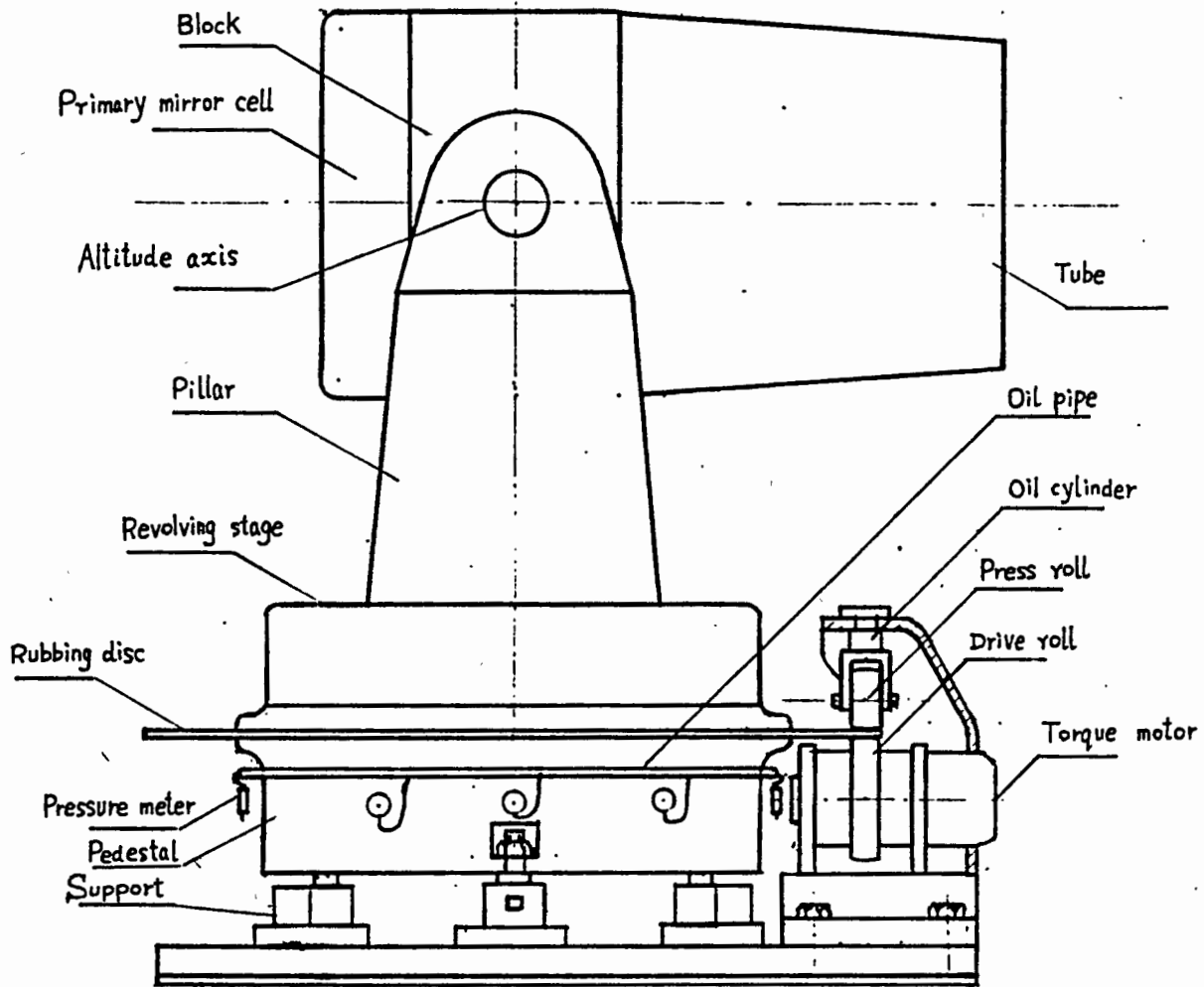


Fig.2. The twelve pads of the hydrostatic oil bearing

As for the second and fourth harmonics, they all originate from the deviation of the azimuth axis caused by the coupling of the drive roll with the rubbing disc (Fig.3). The drive roll is located at one side of the mount and its influence upon the azimuth axis may be regarded as the superimposition of both of the rigid and flexible compositions. The rigid composition influences the first harmonic and the flexible one produces the second and fourth harmonics. This analysis has been proved by the experiments. When the coupling of the driving roll with the rubbing disc is released, the second and fourth harmonics would nearly disappear and the first harmonic would have an obvious change. In addition, it is also found that both of the amplitude and phase of the first harmonic will have a slow and smooth change owing to the effects of the weather on the concrete pier, on which rests the mount. On the contrary, no notable variations would happen in the components, such as the third and twelfth harmonics, etc., which express the internal properties of the azimuth axis. It is necessary to note that a time-dependent linear term is included in the results, although its value



1:25

Fig.3. Azimuth axle drive assembly and its effects on the azimuth axis

is very small. The reason why there exists the linear term is that the measured value at 0° point at the beginning of the measurement may not be in accordance with that at the end of the measurement after running a circle. But if the measurement is repeatedly made at the 0° point in a short period, the measured values tally well with each other. Only in a rather long time interval when the measurement at the same point is made, the level bubble can shift in the same direction. It is considered that the reason why this phenomenon appears is that a substitute is used as the support of the bubble, of which the structure at either end is extremely unsymmetric. Even if there is no temperature gradient in the surrounding environment, the bubble will shift in the same direction owing to the time-dependent variation in the temperature within the dome. Therefore, it is reasonable to introduce the linear term to the measured results. It does not represent the internal characteristics of the axis, but shows that there is a linear variable term in the data, caused by the effects of the external environment on the measuring device.

Finally, the following formula is adopted to fit the measured data.

$$Y = a_1 \cos x + b_1 \sin x + a_2 \cos 2x + b_2 \sin 2x + a_3 \cos 3x + b_3 \sin 3x + a_4 \cos 4x + b_4 \sin 4x + a_{12} \cos 12x + b_{12} \sin 12x + kx + c \quad (1)$$

For the data of every circle (the 37 measured values are expressed by Y_i), the twelve coefficients awaiting determination in the above equation can be calculated by the least square method. From the residua $\Delta Y_i = Y_i - Y$ and equation (2) the root-mean-square of the fitting error M_f may be obtained, of which the mean is about 0.08.

$$M_f = \sqrt{\sum \Delta Y_i^2 / (37 - 12)} \quad (2)$$

The R.M.S. of the fitting contains the random wobble of the axis and the measuring error. The quantitative estimation should be made for our measuring method. It is found in the process of the analysis of the measured data that the random wobble of the axis does not happen in some small districts. So in this case the relation between the shift S of the bubble and the rotation angle θ can be determined accurately (Fig.4). The data θ_i, S_i can be fitted by a quadratic curve $S = a \theta^2 + b \theta + c$, which represents the motion model without wobble. The residua ΔS_i of the measured values S_i with respect to the fitting curve can be used to estimate the measuring accuracy. The R.M.S. error in the measurement is

$$M_s = \sqrt{\sum \Delta S_i^2 / (N - 3)} \quad (3)$$

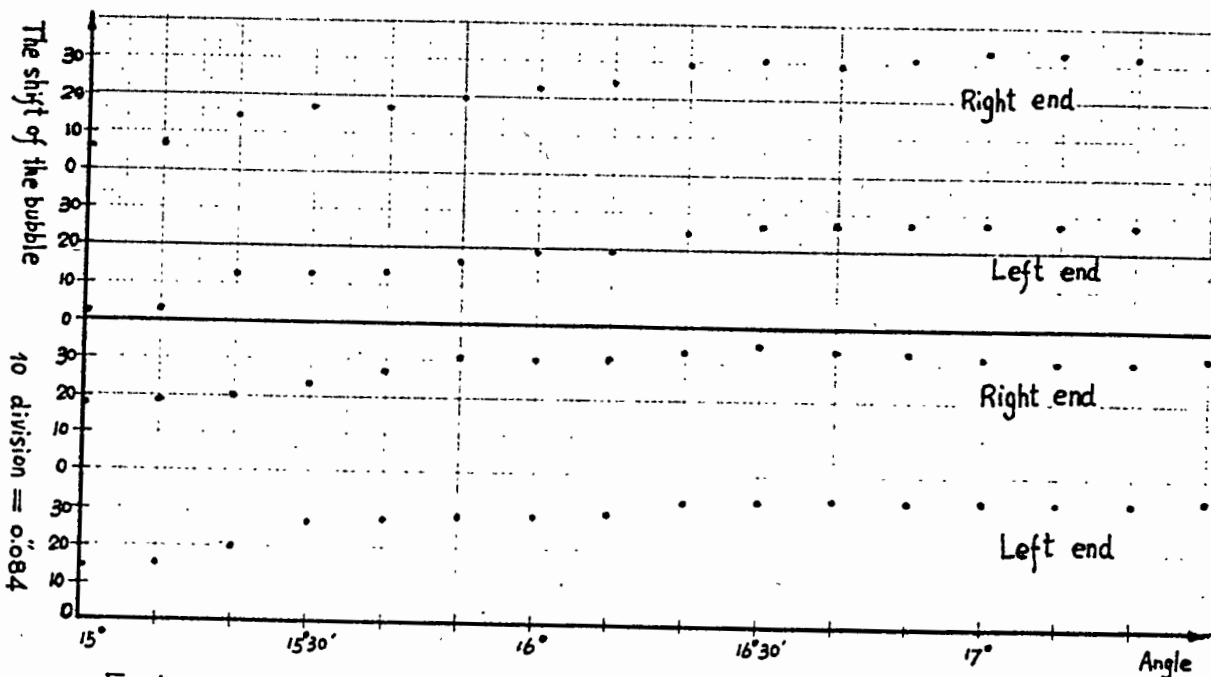


Fig.4. The relation between the shift of the bubble and rotation angle

where N is the number of the measuring points. A certain district of 3° is chosen where a measurement is made at every

10'. Fig. 4 shows two measured results. The repeatability of two measurements is very good and the root-mean-square error of the measurement is 0.015. Therefore, the values obtained from formula(2) primarily are the random wobble of the axis.

The data of 20 circles are listed in Table 1 and Table 2, where A_i represents the amplitude of the i th harmonic.

IV. Conclusions

(1) It can be seen from the data listed in Table 1 and Table 2 that the r.m.s. errors calculated from the measured data of every circle are quite approximate to one another. The standard deviation is used to express their dispersion, of which the value is about 0.01, being equivalent to the measuring error. It is shown that the tested result for the wobble of the azimuth axis is reliable.

(2) The systematic error model measured in a direction is different from that in the direction perpendicular to the former one. It is shown that a rigid model can not be used to describe the wobble of the axis. Hereafter, the correction for the telescope pointing must be made separately according to the results measured in the two directions.

(3) The first harmonic is affected by the influence of the environment on the concrete pier, but the other harmonics mainly have relation to the structure of the mount, and therefore they are all relatively stable. From now on, the first harmonic will be determined by the monitor of the relation between the first harmonic and the environments or by the observation of stars. Then the effect of the wobble of the azimuth axis on the telescope will be limited within the range approximate to that of the wobble of the azimuth axis stated in this paper. This is undoubtedly advantageous to the realization of the lunar laser ranging by means of the absolute pointing.

Unit: arc second

| N | A ₁ | A ₂ | A ₃ | A ₄ | A ₁₂ | M _f |
|------------|----------------|----------------|----------------|----------------|-----------------|----------------|
| 1 | 0.432 | 0.174 | 0.218 | 0.087 | 0.226 | 0.066 |
| 2 | 0.681 | 0.232 | 0.237 | 0.071 | 0.211 | 0.069 |
| 3 | 0.664 | 0.154 | 0.273 | 0.101 | 0.221 | 0.064 |
| 4 | 0.921 | 0.229 | 0.265 | 0.127 | 0.261 | 0.081 |
| 5 | 0.869 | 0.194 | 0.276 | 0.102 | 0.238 | 0.082 |
| 6 | 0.740 | 0.207 | 0.247 | 0.108 | 0.233 | 0.078 |
| 7 | 0.705 | 0.175 | 0.232 | 0.089 | 0.212 | 0.068 |
| 8 | 0.743 | 0.176 | 0.209 | 0.084 | 0.206 | 0.080 |
| 9 | 0.665 | 0.171 | 0.221 | 0.105 | 0.257 | 0.095 |
| 10 | 0.730 | 0.192 | 0.246 | 0.106 | 0.238 | 0.078 |
| mean | 0.715 | 0.190 | 0.242 | 0.098 | 0.230 | 0.076 |
| σ_x | 0.124 | 0.024 | 0.022 | 0.015 | 0.018 | 0.009 |

Table1 The bubble is parallel with the altitude axis.

Unit: arc second

| N | A ₁ | A ₂ | A ₃ | A ₄ | A ₁₂ | M _f |
|------------|----------------|----------------|----------------|----------------|-----------------|----------------|
| 1 | 2.014 | 0.478 | 0.203 | 0.086 | 0.159 | 0.094 |
| 2 | 2.046 | 0.470 | 0.209 | 0.080 | 0.161 | 0.091 |
| 3 | 2.056 | 0.465 | 0.228 | 0.095 | 0.140 | 0.096 |
| 4 | 2.235 | 0.462 | 0.259 | 0.137 | 0.146 | 0.077 |
| 5 | 2.338 | 0.481 | 0.222 | 0.124 | 0.150 | 0.074 |
| 6 | 2.323 | 0.463 | 0.212 | 0.119 | 0.131 | 0.059 |
| 7 | 2.265 | 0.482 | 0.245 | 0.123 | 0.143 | 0.074 |
| 8 | 2.159 | 0.466 | 0.233 | 0.111 | 0.143 | 0.063 |
| 9 | 2.190 | 0.499 | 0.243 | 0.122 | 0.176 | 0.075 |
| 10 | 2.141 | 0.475 | 0.245 | 0.124 | 0.155 | 0.064 |
| mean | 2.177 | 0.474 | 0.230 | 0.112 | 0.150 | 0.077 |
| σ_x | 0.109 | 0.011 | 0.017 | 0.018 | 0.012 | 0.012 |

Table2 The bubble is perpendicular to the altitude axis.

DOUBLE PEAK POLARIZED INTERFERENCE FILTERS

M.L. White
Lure Observatory
Institute for Astronomy
University of Hawaii
Kula, HI 96790

Telephone (808) 878-1215
Telex 7238459

ABSTRACT

A new type of high transmission, narrow bandpass filter is tested at the University of Hawaii's Lunar Laser Ranging Observatory. In this article, the Daystar double peak, polarized interference filter is described. The filter performance is characterized through the evaluation of several tests.

DOUBLE PEAK POLARIZED INTERFERENCE FILTERS

I. Introduction

The Daystar double peak interference filter utilizes a solid spacer birefringent etalon. The etalon is cut to a half wave thickness and the refractive index of the etalon material is such that both orthogonal transmission modes are supported. This results in the transmission of both the vertical and horizontal light components at a desired wavelength. A single peak filter of the same type would pass only one polarization component resulting in a 50% loss of transmission at the desired wavelength. Finding birefringent material of acceptable quality and cutting the material at perfect half-wave plate thicknesses are the major limiting factors in the construction of double peak filters. Therefore, sources for these filters are limited.

Following are specifications for the filter described in this paper:

Transmission Wavelength: 532 Nanometers

Bandwidth: 1.0 Angstrom FWHM +/- 0.2 angstrom

Transmission: 28% per channel (This gives an actual throughput for our application of 28%)

Blocking: Full short side to x-ray optical density = 6.0
Long side to 900 nanometers optical density = 5.0

Clear Aperture: 32 mm.

Filter components: Instrument quality, 60-40 scratch dig. Anti-reflection coated air/glass interfaces for minimum of 0.2 % reflectance. Installed in a temperature regulated oven providing +/- .05 angstrom on band control and minimum +/- 1.0 angstrom off-band search capability.

II. Test Results

The filter was first tested on the University of Hawaii's, Mees Observatory solar spectrograph. The digitized signal from a silicon vidicon tube was used to measure the transmitted light through the filter and then without the filter. A graph was then plotted comparing the amount of light transmitted at 532 nanometers with no filter in place with the amount of light transmitted at 532 nanometers with the filter in place. The filter transmission was measured to be 28% with a FWHM bandpass of 1 angstrom (figure 1). At this time it was noted that the recommended on band temperature setting was not correct. In order to tune the filter on band, the recommended temperature had to be raised approximately 3 degrees centigrade to achieve maximum transmission at 532 nanometers. This was easily accomplished with the adjustable temperature controller, although the controller was near its maximum setting. The manufacturer doubted that the temperature calibration performed at the factory was nearly one angstrom off. However, the additional

tests performed also indicated that to achieve optimum transmission the filter temperature had to be raised.

The filter was then placed in the station's satellite calibration receive package. The average return signal off of the calibration target board was measured with a receive energy monitor through the filter and then without the filter in line with the detector. The comparisons of these two sets of data revealed that about 75% less energy was received with the filter in line with the detector than was received when the filter was not in line. This test was more subjective than the first and had an error factor of approximately plus or minus 10%.

Finally, the filter was tested during actual lunar ranging. The histograms in figures 2 and 3 show the number of photo-electron events obtained during several runs. It is difficult to apply a transmission efficiency number to the results, since one can only compare the data to other ranging data taken on nights when seeing conditions might be considerably different. A test of this nature is greatly affected by seeing conditions and equipment performance on a given night. However, when comparisons are made with lunar data taken with a four angstrom filter with a transmission of about 40%, the data rate is within expectation.

III. Test Considerations

Angle of Incident Energy and Effects of Temperature Variance

Particular emphasis was placed on controlling the angle of incidence during these tests. When a narrow bandpass filter is tilted from the normal, the pass band will broaden while shifting its center to the shorter wavelengths. When testing the filter on the solar spectragraph a real-time display was monitored while the filter tilt was adjusted for maximum red shift.

Increasing the filter's correct operating temperature will shift the bandpass towards the longer wavelengths. Likewise, decreasing the filter's normal room temperature will shift the band pass toward the shorter wavelengths. The change in bandpass as a function of temperature depends on the spectral location of the filter and falls within a range of .15 to .4 angstrom per degree centigrade change. The Daystar 1 angstrom filter is installed in a temperature regulated oven providing +/- .05 angstrom on band control with a maximum +/- 1.0 angstrom off band search capability.

IV. Conclusions

The filter performed at a level of efficiency consistent with the manufacturer's specifications with the exception of the discrepancy noted with the temperature controller. Daystar originally agreed to provide a filter with a throughput of 25%. The completed filter, however, was measured to have a throughput of 28%. This is an excellent overall transmission for a 1 angstrom bandpass filter and it should be useful to any lunar ranging station desiring to improve the receiver, signal-to-noise ratio. The problem with the temperature controller should lead future users of this filter type to verify on-band tuning since any deviation from the filter's correct operating temperature will lead to a significant change in the bandpass.

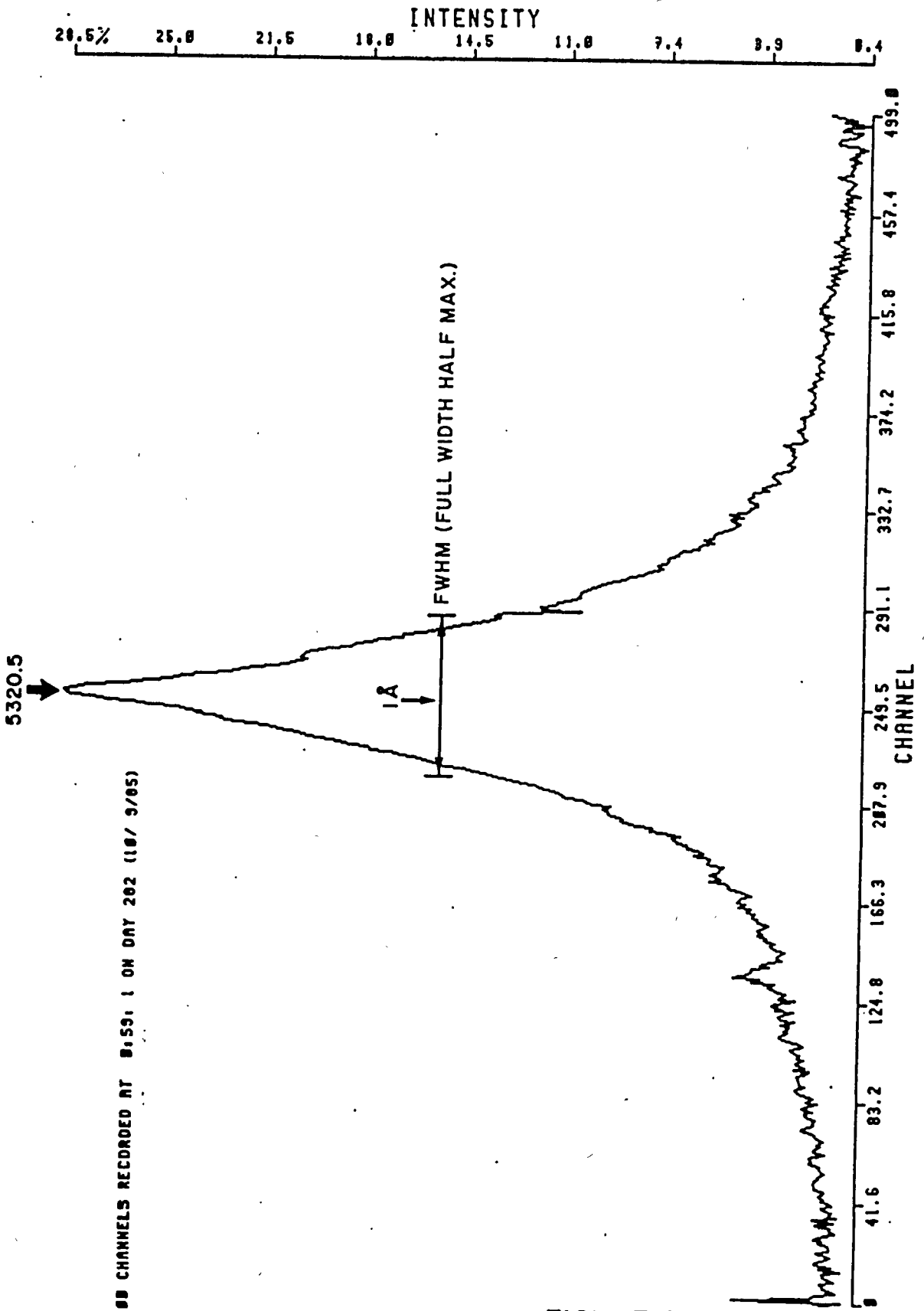
The filter was originally expected to increase the station's coverage through the maximum lunar illumination period. However, when the filter was tested during several full moon periods, a significant improvement in the signal to noise ratio was not observed. The background noise was considerably reduced as expected however, very few lunar events were observed. It is possible that more attempts at full moon ranging are needed to verify this result. More recently, other lunar stations have reported limited ranging success

during full moon that cannot be entirely related to increased lunar noise during full moon. This has led to some speculation that the Apollo reflectors lose some efficiency as they heat up during maximum lunar illumination.

Recently, the LURE Observatory achieved its first daylight lunar ranges. As a consequence normal lunar operations will be extended into daylight hours. More testing of the 1 angstrom double peak filter will be conducted during daylight hours where a significant improvement in the signal to noise ratio can be expected.

V. Acknowledgments

Special thanks to Dr. Donald Mickey for developing the solar spectrograph test and to the University of Hawaii, Institute for Astronomy for use of the Mees solar spectrograph. Thanks also to Richard Dawe and Lou Macknik for help with graphs and test ideas.



500 CHANNELS RECORDED AT 8:59:1 ON DAY 202 (10/ 9/05)

FIGURE 1

HISTP(8.30)

Data histogram for Input File : LUN31210.279

LUNAR Data Histogram

| 460 DATA RECORDS WITH | | 560 RANGES | |
|-----------------------|----------|------------|--------|
| Less than | 50.0000 | 211 | !***** |
| 50.0000 TO | 52.0000 | 3 | !*** |
| 52.0000 TO | 54.0000 | 2 | !** |
| 54.0000 TO | 56.0000 | 3 | !*** |
| 56.0000 TO | 58.0000 | 2 | !** |
| 58.0000 TO | 60.0000 | 1 | !* |
| 60.0000 TO | 62.0000 | 1 | !* |
| 62.0000 TO | 64.0000 | 3 | !*** |
| 64.0000 TO | 66.0000 | 7 | !***** |
| 66.0000 TO | 68.0000 | 2 | !** |
| 68.0000 TO | 70.0000 | 4 | !**** |
| 70.0000 TO | 72.0000 | 4 | !**** |
| 72.0000 TO | 74.0000 | 5 | !***** |
| 74.0000 TO | 76.0000 | 5 | !***** |
| 76.0000 TO | 78.0000 | 4 | !**** |
| 78.0000 TO | 80.0000 | 7 | !***** |
| 80.0000 TO | 82.0000 | 2 | !** |
| 82.0000 TO | 84.0000 | 3 | !*** |
| 84.0000 TO | 86.0000 | 30 | !***** |
| 86.0000 TO | 88.0000 | 31 | !***** |
| 88.0000 TO | 90.0000 | 2 | !** |
| 90.0000 TO | 92.0000 | 3 | !*** |
| 92.0000 TO | 94.0000 | 0 | ! |
| 94.0000 TO | 96.0000 | 0 | ! |
| 96.0000 TO | 98.0000 | 3 | !*** |
| 98.0000 TO | 100.0000 | 3 | !*** |
| 100.0000 TO | 102.0000 | 4 | !**** |
| 102.0000 TO | 104.0000 | 0 | ! |
| 104.0000 TO | 106.0000 | 3 | !*** |
| 106.0000 TO | 108.0000 | 4 | !**** |
| 108.0000 TO | 110.0000 | 3 | !*** |
| 110.0000 TO | 112.0000 | 3 | !*** |
| 112.0000 TO | 114.0000 | 1 | !* |
| 114.0000 TO | 116.0000 | 0 | ! |
| 116.0000 TO | 118.0000 | 1 | !* |
| 118.0000 TO | 120.0000 | 1 | !* |
| 120.0000 TO | 122.0000 | 2 | !** |
| 122.0000 TO | 124.0000 | 2 | !** |
| 124.0000 TO | 126.0000 | 2 | !** |
| 126.0000 TO | 128.0000 | 2 | !** |
| 128.0000 TO | 130.0000 | 1 | !* |
| 130.0000 TO | 132.0000 | 4 | !**** |
| 132.0000 TO | 134.0000 | 4 | !**** |
| 134.0000 TO | 136.0000 | 0 | ! |
| 136.0000 TO | 138.0000 | 4 | !**** |
| 138.0000 TO | 140.0000 | 4 | !**** |
| 140.0000 TO | 142.0000 | 2 | !** |
| 142.0000 TO | 144.0000 | 1 | !* |
| 144.0000 TO | 146.0000 | 2 | !** |
| 146.0000 TO | 148.0000 | 4 | !**** |
| 148.0000 TO | 150.0000 | 2 | !** |
| More than | 150.0000 | 163 | !***** |

A TOTAL OF 560 DATA POINTS PROCESSED

APOLLO 15
OCTOBER 6, 1985 2:10 A.M.
20 MINUTE RUN
1 Å 30^m

FIGURE 2

```

HISTP(8.30)
Data histogram for Input File : LUN01236.279
LUNAR Data Histogram
40 DATA RECORDS WITH 43 RANGES
Less than 50.0000 6 !*****
50.0000 TO 52.0000 0 !
52.0000 TO 54.0000 0 !
54.0000 TU 56.0000 0 !
56.0000 TO 58.0000 0 !
58.0000 TU 60.0000 0 !
60.0000 TU 62.0000 0 !
62.0000 TO 64.0000 0 !
64.0000 TU 66.0000 0 !
66.0000 TO 68.0000 0 !
68.0000 TO 70.0000 0 !
70.0000 TO 72.0000 0 !
72.0000 TO 74.0000 0 !
74.0000 TO 76.0000 1 !*
76.0000 TU 78.0000 0 !
78.0000 TO 80.0000 0 !
80.0000 TU 82.0000 0 !
82.0000 TO 84.0000 0 !
84.0000 TO 86.0000 1 !*
86.0000 TO 88.0000 5 !*****
88.0000 TO 90.0000 5 !*****
90.0000 TO 92.0000 0 !
92.0000 TO 94.0000 0 !
94.0000 TO 96.0000 0 !
96.0000 TO 98.0000 0 !
98.0000 TO 100.0000 0 !
100.0000 TO 102.0000 0 !
102.0000 TO 104.0000 0 !
104.0000 TO 106.0000 0 !
106.0000 TO 108.0000 1 !*
108.0000 TO 110.0000 0 !
110.0000 TU 112.0000 1 !*
112.0000 TO 114.0000 1 !*
114.0000 TO 116.0000 1 !*
116.0000 TO 118.0000 0 !
118.0000 TO 120.0000 0 !
120.0000 TO 122.0000 0 !
122.0000 TO 124.0000 0 !
124.0000 TO 126.0000 0 !
126.0000 TO 128.0000 1 !*
128.0000 TO 130.0000 2 !**
130.0000 TO 132.0000 0 !
132.0000 TO 134.0000 0 !
134.0000 TO 136.0000 0 !
136.0000 TO 138.0000 0 !
138.0000 TO 140.0000 0 !
140.0000 TO 142.0000 0 !
142.0000 TO 144.0000 0 !
144.0000 TO 146.0000 0 !
146.0000 TO 148.0000 0 !
148.0000 TO 150.0000 1 !*
More than 150.0000 17 !*****
A TOTAL OF 43 DATA POINTS PROCESSED

```

APOLLO 11
OCTOBER 6, 1985 2:36A.M.
20 MINUTE RUN
1 Å 30^m

FIGURE 3

FILTER ADVANTAGES

- GOOD TRANSMISSION, 28%, FULLY BLOCKED.
- DURABLE. (Survived Sounding Rocket Crash).
- COMPACT. (2" x 3")
- EASY TO CONTROL TEMPERATURE.
- SINGLE PASS BAND.
- WORKS IN SYSTEMS AS FAST AS $f/20$.
- REASONABLE COST \sim \$3,000.00 U.S.

FILTER DISADVANTAGES

- LIMITED NUMBER OF VENDORS AVAILABLE.
- DIFFICULT TO MANUFACTURE.
- SENSITIVE TO $>1^\circ$ DEVIATION FROM NORMAL.

EFFECTS OF TELESCOPE DESIGN ON LASER BEAM POINTING ACCURACY

R. Korakitis
Department of Topography
National Technical University of Athens
Heroon Polytechniou 9
GR-157 73 Zografos - Greece -

Telephone (01) 777 3613
Telex 215032 GEO GR

ABSTRACT

This work presents some studies about the effects of the optical design of the telescope on the beam pointing accuracy of the SLR system at Dionysos Satellite Geodesy Observatory.

A brief description of telescope and mount is given, with emphasis on components critical to beam alignment. Possible torsional flexure of the horizontal axis is examined and is found to be unimportant.

The path of the laser beam through the mount is softwaremodelled and beam deviations upon exit are computed for different positions of adjustable optical components. At the same time, it is shown that precession of the beam, due to improper alignment, has practically no effect on the optical path length, so no system delay changes are expected for different orientations of the mount. This prediction is experimentally confirmed down to the performance limit of the system (about 2 cm).

1. Introduction

This work reports some results of studies, conducted at Dionysos Satellite Geodesy Observatory, concerning the mechanical and optical performance of the mount and telescope used in the Satellite Laser Ranging system. The purpose of the studies is to establish the accuracy limit of the system with regard to laser beam pointing and system delay stability, since the mount was originally designed to be used with a 1st generation Ruby laser, having much lower precision capabilities.

In the first part, a brief description of mount and telescope is given, indicating components critical to mechanical and optical adjustments. A possible torsional flexure of the horizontal axis is examined both theoretically and experimentally and is found to be unimportant.

The second part describes the laser beam path and its software model. In this model, all optical components are suitably represented and ray-tracing results show how each individual adjustment affects the alignment of the beam and the optical path length. For all reasonable values of beam deviation, the path length does not depend on the orientation of the mount. The last section of the work describes the experimental verification of this prediction, through system delay measurements at various orientations.

2. Characteristics of the mount

The SLR system at Dionysos uses a conventional altitude over azimuth design, with separate transmit and receive optics and a coude optical path. The overall lay-out of the mount and telescope is shown in Fig.1.

Both rotation axes are realized by pairs of conical roller bearings and their exact orientation can be adjusted by suitably located screws. A precision level permits alignment of the primary (azimuth) axis within 3 arcsec of the local vertical. Similarly, the tilt of the secondary (altitude) axis is adjustable to within 3 arcsec of the horizontal plane. In addition to the roller bearings, the altitude axis is supported by preloaded bronze bushings, in order to minimize flexure. Rotation angles of the axes are read by optical encoders, which have a resolution of 1 millidegree and are situated by the respective drive gears. The rotation of the axes is accomplished by step-motors having a resolution of 0.001 per step and repeatability 1 millidegree (RMS). Therefore, the positioning accuracy of the mount is limited to about 5 arcsec.

With regard to the distribution of masses, one should note that the center of mass (CM) of the receiving telescope lies behind the altitude axis (when the telescope is in the horizontal plane), whereas the CM of the transmitter lies in front of the axis. Since the corresponding moments have opposite direction, the altitude axis is rotationally balanced. However, these moments can cause a torsional flexure of the steel tube that realizes the axis. The rotation angle of this axis (i.e. the altitude) is determined at the transmitting end of the tube, where the altitude drive and the encoders are situated, so any torsional flexure will show itself as a vertical deflection of the receiving telescope. A rough estimate of the magnitude of this deflection can be made using elementary elasticity theory [1]:

To a first approximation, the deflection angle ϕ due to torsional flexure of a thin cylindrical tube is given by:

$$\phi = \frac{M l}{G r^2 S}$$

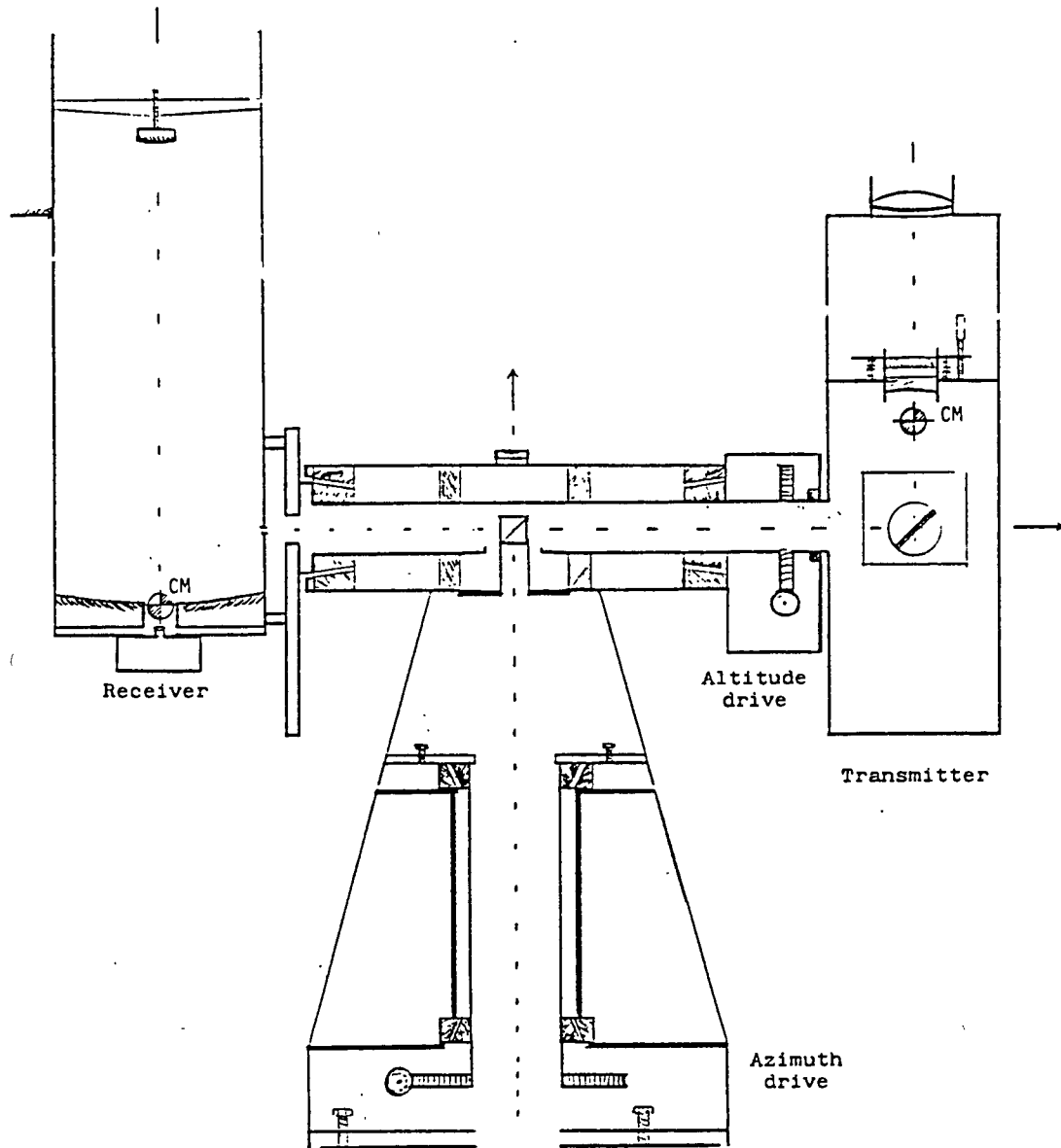


Fig. 1 : Mechanical lay-out of mount and telescopes

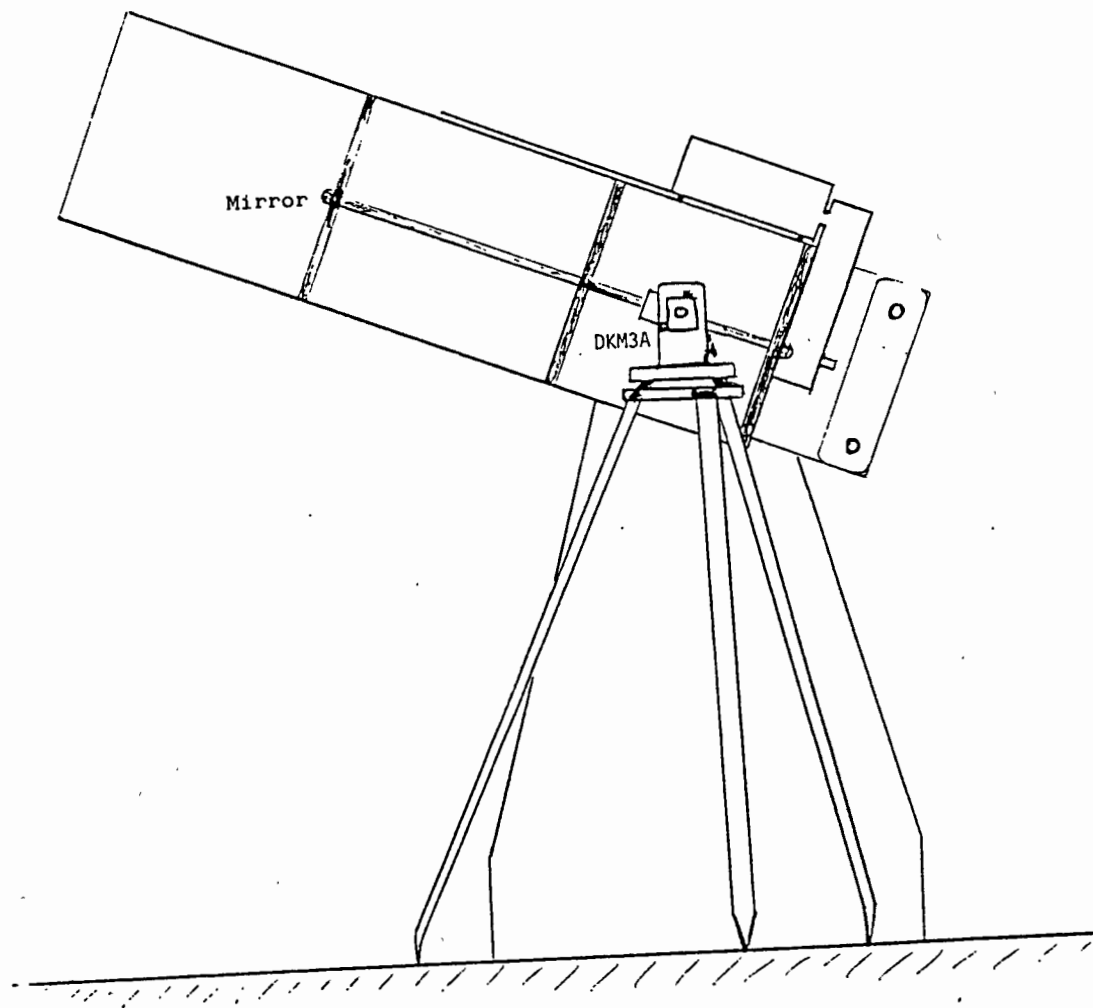


Fig. 2 : Set-up for the torsional flexure experiment

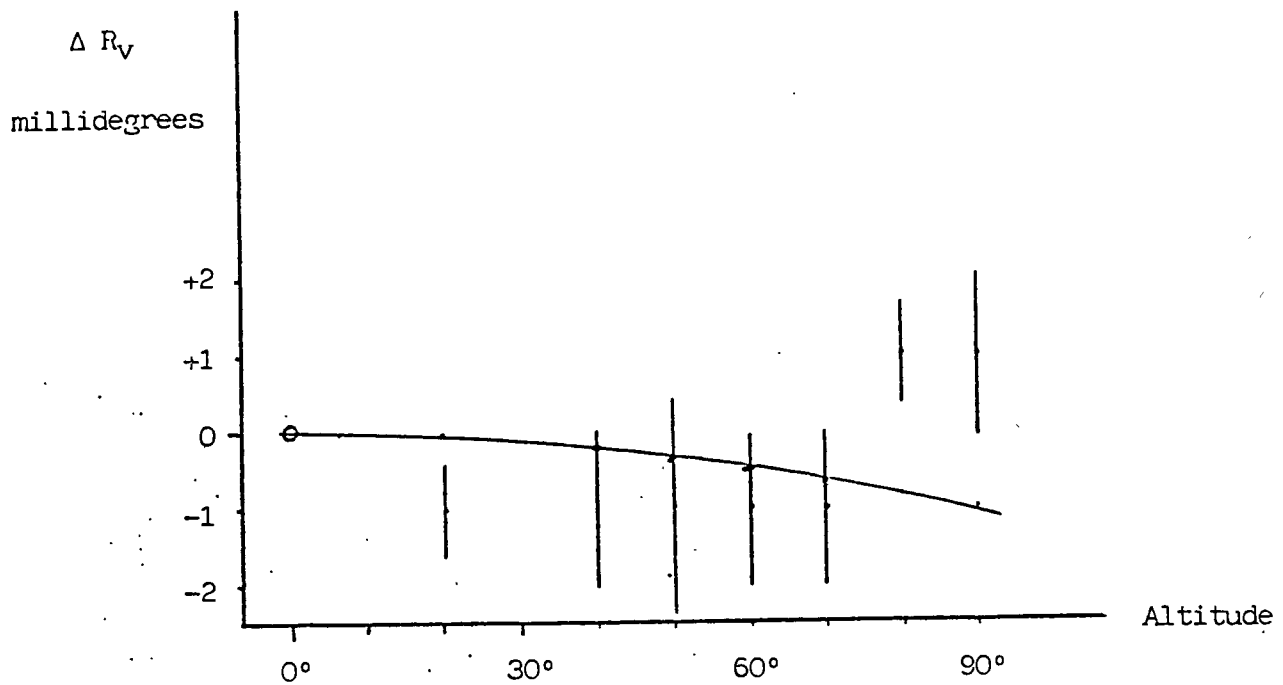


Fig. 3. Vertical reading differences (theodolite-telescope) vs. altitude. ΔR_v defined to be zero at $v = 0^\circ$. The solid curve shows the effect of the expected torsional flexure.

where the symbols and their values for this particular case are:

| | |
|---------------------------------------|---|
| M = the applied torque | = 100 kgr* × 20 cm × cosv |
| l = the length of the tube | = 100 cm |
| G = the shear modulus of the material | = 8 × 10 ⁵ kgr* cm ⁻² |
| r = the radius of the tube | = 10 cm |
| S = the cross-section of the tube | = 157 cm ² |

Therefore, the maximum deflection (at altitude $v=0^\circ$) is about 16 microradians or $0^\circ.001$. Since the predicted value of the deflection is similar to the positioning accuracy of the axis, torsional flexure is considered to be unimportant. In any case, an experimental check was performed as follows:

A small mirror was fixed on the outside wall of the receiving telescope, perpendicular to the optical axis. A precision theodolite, type Kern DKM3A, was placed by the receiver so that its horizontal axis roughly coincided with the altitude axis of the mount (Fig.2). The theodolite was used as an autocollimator, projecting the image of an illuminated crosshair to the mirror. In this way a direction, approximating the optical axis, was realized that remained fixed with regard to the receiver. The altitude of the telescope was varied and the encoder readings were compared with the corresponding readings of the vertical angle of the theodolite. Two independent series of such measurements were taken and the mean values of the differences are shown in Fig.3, along with the expected value of the deflection. No systematic deviation that can be attributed to torsional flexure is evident. The deviation of the measurements near the zenith, currently under further investigation, is probably connected with the behaviour of the anti-backlash torque motors of the altitude drive.

3. The laser beam path model

A general schematic of the laser beam path is shown in Fig 4. Upon exit from the laser unit, the beam is twice deflected through 90° by dichroic mirrors that separate the 532nm radiation from the IR. The laser beam, after expansion, is directed to the 1st mirror of the coude path that sends it upwards, along the vertical (azimuth) axis of the mount.

In order to facilitate the alignment of the beam, an auxilliary optical setup is under construction by the vertical axis. It mainly consists of an autocollimator and a fixed mirror, that will realize a permanent reference direction for the laser beam. A sample of the laser beam will be brought into this path by inserting a pellicle beam-splitter. At the same time, this setup will permit direct viewing through the transmitting telescope, enabling thus a direct check of the pointing of the telescope using observations of stars.

The alignment procedure consists of three main parts:

- Adjustment of the last dichroic mirror, together with expander, for pitch, yaw and linear position. Then, adjustment of the 1st coude mirror for pitch, yaw and transverse linear position so that the beam exactly follows the azimuth axis of the mount.
- Adjustment of the 2nd coude mirror, which actually is a right-angle prism situated at the intersection of the axes, for pitch, yaw and linear position so that the beam follows the altitude axis.

When these adjustments are completed, the laser beam should not precess when the mount is rotated to different orientations. At present, that can be achieved within 15 arcsec but this figure is expected to decrease using the alignment setup described earlier.

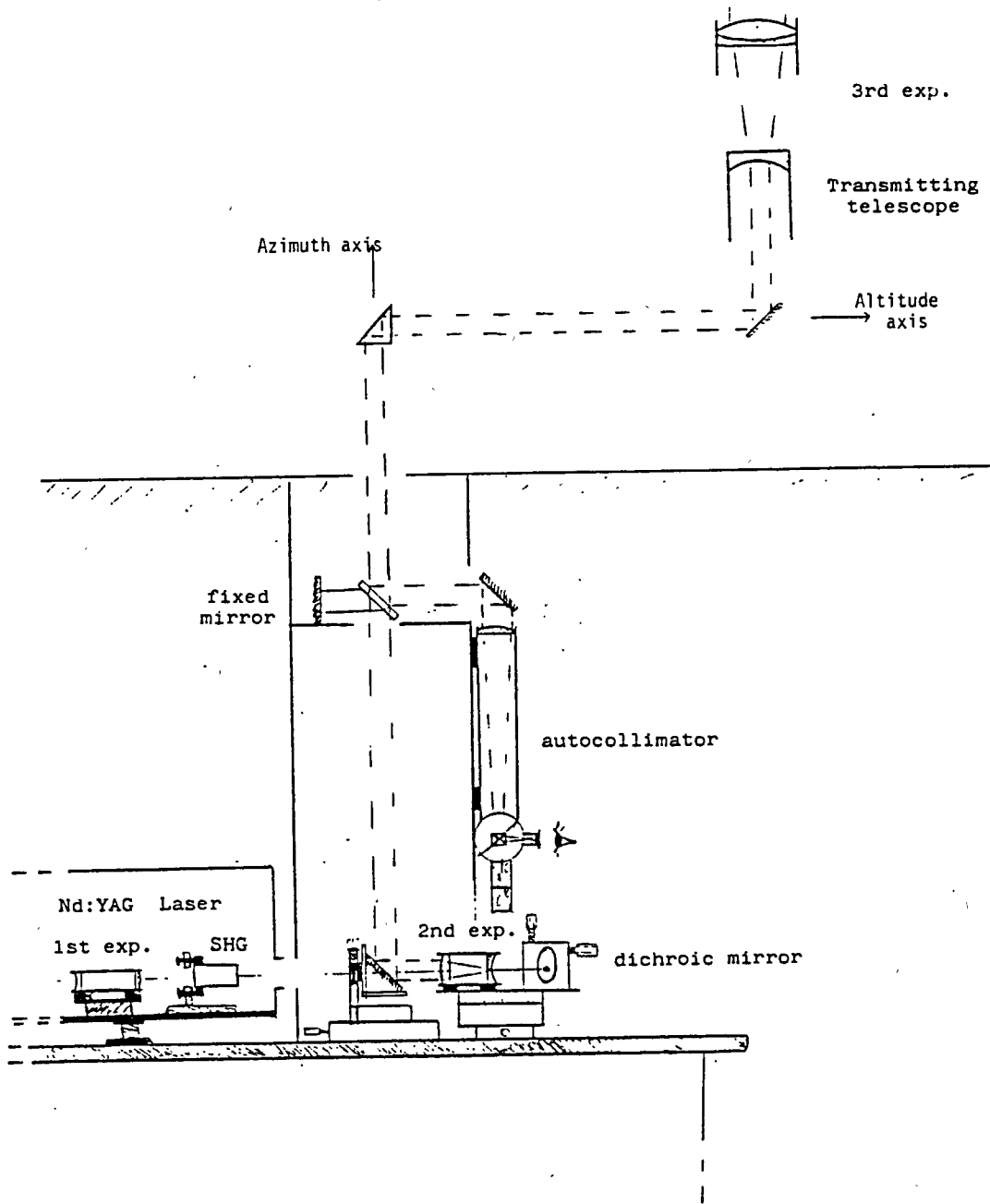


Fig. 4 : Schematic of the laser beam path

- c. The last step involves the adjustment of the 3rd coude mirror, located inside the transmitter, in order to bring the exit laser beam into alignment with the pointing direction of the mount (common direction of transmitter and receiver optical axes). In addition, the final beam expander adjusts the full angle divergence of the beam in the range 10 to 100 arcsec.

Referring to Fig.1, one should note the internal calibration path that is established inside the receiver end of the altitude axis. A very small drop of clear glue, at the hypotenuse face of the central coude prism, scatters some radiation towards the receiver. There, a small prism deflects it towards the main mirror so that it can be acquired by the detection package.

In order to study quantitatively the effects of the several adjustments needed for the alignment of the beam, the optical path was modelled in the computer. This software model analytically treats the deflections of the beam at all mirrors and prisms in the path, the position and orientation of which can be varied in accordance with the degrees of freedom of the actual components. The starting point and initial direction of the laser beam, as it leaves the 2nd expander, is taken into account, as well as the distances between the components, which were measured using a Chesterman stainless-steel tape.

The computations are performed using matrix representations of vectors in three rectangular coordinate systems: the $\{X_0, Y_0, Z_0\}$ system remains fixed in space, with Z_0 along the azimuth axis of the mount (local vertical) and Y_0 towards the local astronomical North. The $\{X_1, Y_1, Z_1=Z_0\}$ system is produced by rotating the previous one around Z_0 through the azimuth angle A ; the X_1 axis is along the altitude axis of the mount. Finally, the $\{X_2=X_1, Y_2, Z_2\}$ system is derived by rotating the previous one around X_1 through the altitude angle v ; the Y_2 axis is along the optical axis of the transmitting telescope. The program outputs the direction of the laser beam upon exit, expressing it as an angular deviation from the Y_2 axis towards a certain direction in the $\{X_2, Z_2\}$ plane. Figures 6 and 7 are typical examples of the output, showing different locii of beam deviations for constant azimuth or altitude and for different adjustments of the components. In addition, the program computes the total path length, from the starting point of the beam up to a fixed plane outside the last lens of the system, where a retroreflector can be actually placed.

At present, the effects of the final beam expander are computed using the paraxial approximation. Since the overall alignment precision will increase with the installation of the auxiliary optics, a revised program is under development that will perform accurate ray-tracing using the exact refraction matrices.

It is worth mentioning that the program also handles the possibility that the two rotation axes of the mount are skew lines. In such case, the beam will rotate around the Y_2 axis without changing its direction, in the paraxial approximation. In reality, though, the direction of the beam may be affected and this problem is another motivation for developing the exact treatment.

It is apparent that a similar program can be used to study any other telescope design as well, provided that all relevant positions and orientation of components are properly introduced.

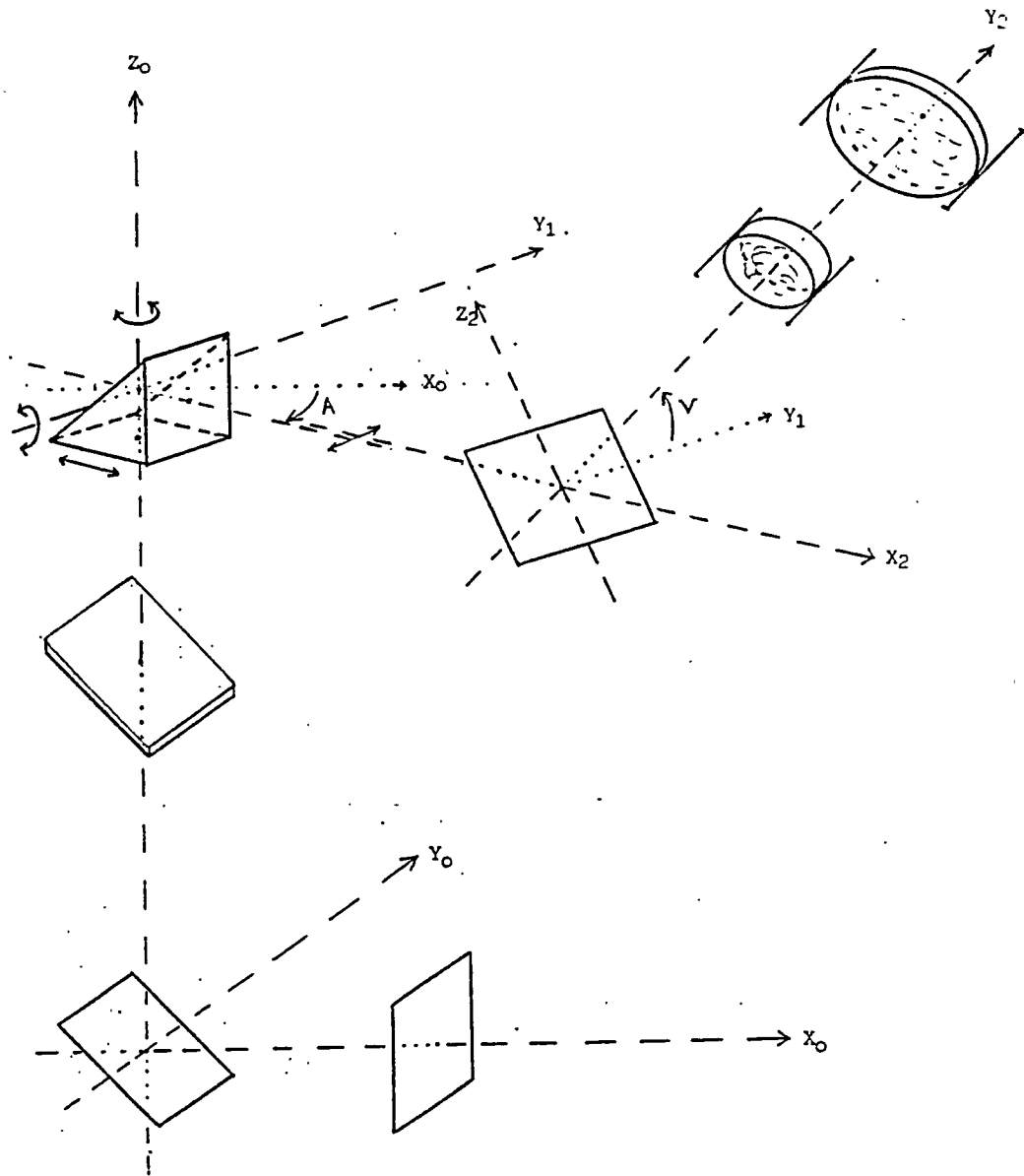
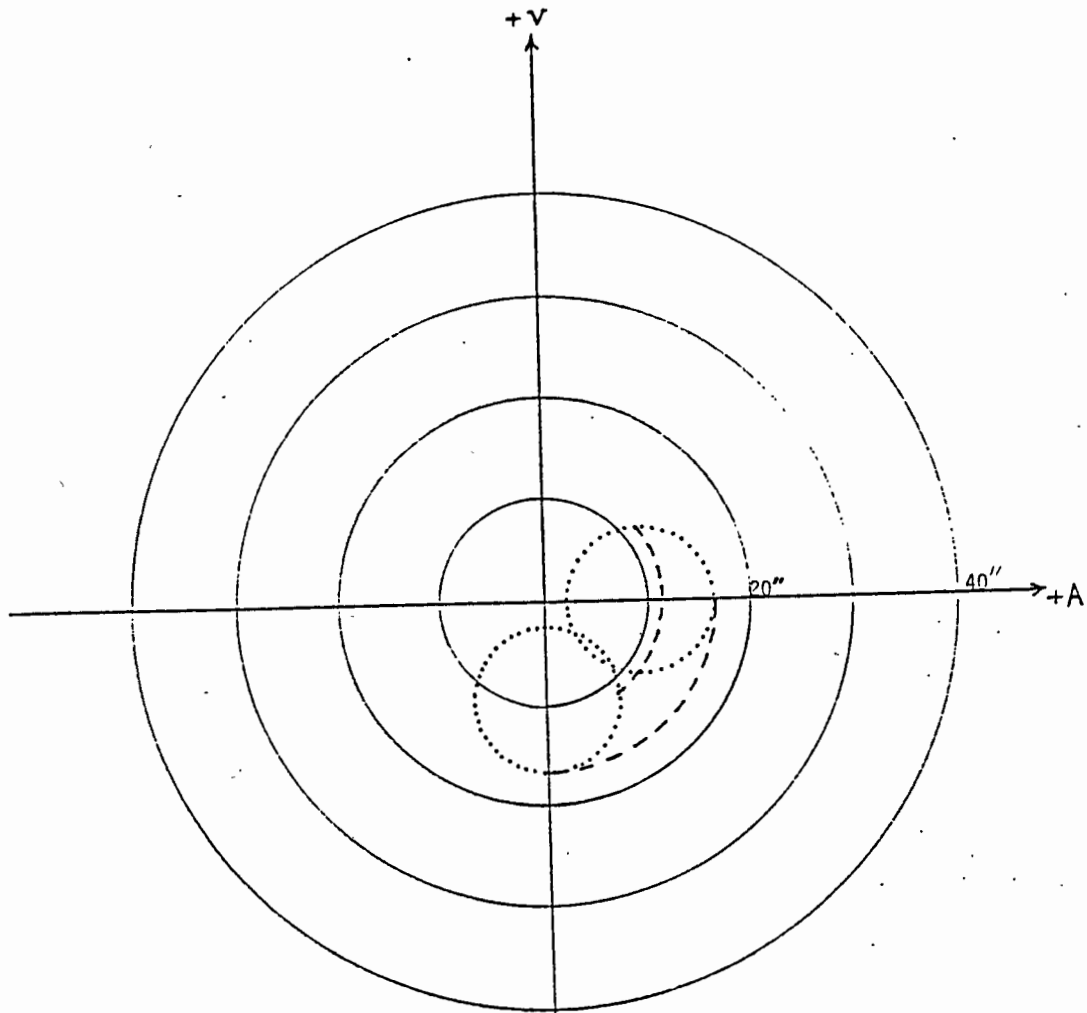
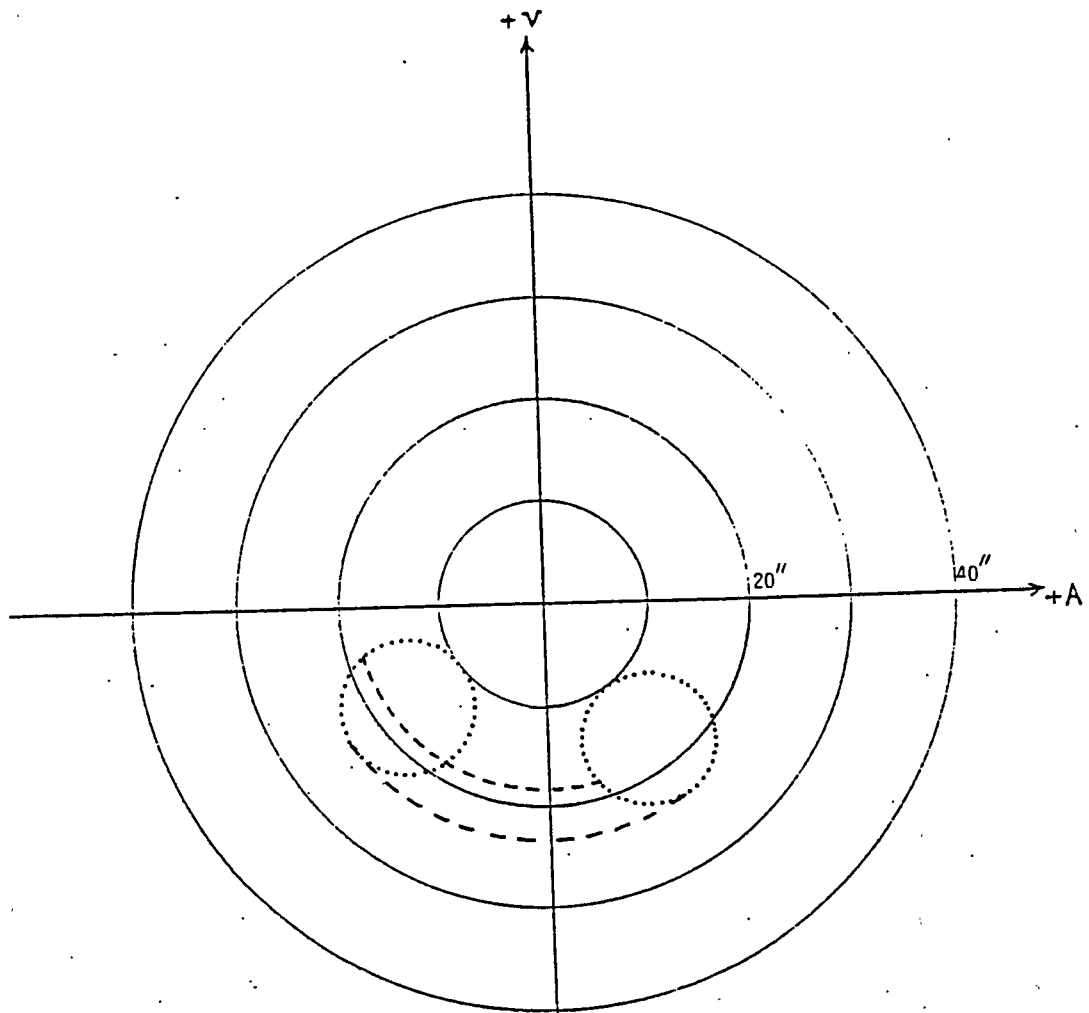


Fig. 5 : Geometry of the laser beam path model



Initial beam tilt : $20''$ to $-Z_0$
 Prism displacement: 0 mm
 angular dev. : $-20''$ az
 $0''$ alt

Fig. 6 : Laser beam deviation curves
 at constant azimuth (dashed lines)
 and constant altitude (dotted lines)



Initial beam tilt : $10''$ to $-Y_0$ and $18''$ to $-Z_0$
 Prism displacement: 0 mm
 angular dev. : $-20''$ az
 $-20''$ alt
 Hor. axis displaced by 1 mm

Fig. 7 : Laser beam deviation curves
 at constant azimuth (dashed lines)
 and constant altitude (dotted lines)

4. System delay measurements

As was mentioned earlier, the software model of the mount includes the total path length of the laser beam, which is directly related to the overall system delay. The computations indicate that the path length is only affected either by a linear displacement of the central coude prism or by the skewness of the two rotation axes. However, for any fixed adjustment of components, the path length is invariant for every orientation of the mount, at least for reasonably small beam deviations (up to several arcminutes!). The implication is that, once the alignment of the beam is even approximately correct, the system delay should not change with orientation of the mount.

This prediction was experimentally tested by measuring the travel time of the laser pulse from a point behind the last dichroic mirror, where a fiber optic link to the START photodiode of the system was placed, to a retroreflector at the transmitter exit and back. The travel time was measured at several different values of azimuth and altitude of the mount and a total of 40 individual measurements were taken in each position. The results are shown in figures 8 and 9 and no variation larger than the resolution of the measurements (about 2 cm [2]) is evident. In addition, one should note that the measurements were taken when the spatial profile of the laser beam was greatly distorted by a damaged SHG crystal. Therefore, a second test is scheduled, to be done after the installation of a new SHG crystal and which will also include a stability check of the internal calibration path.

5. Conclusion

It has been shown that the particular telescope design of the SLR system at Dionysos Observatory presents some problems regarding the alignment of the beam in the coude path, which are studied using a software model of the mount. The results of the study dictate several improvements that can be made to increase the pointing accuracy of the system, with beneficial effects on received energy and return rate. On the other hand, it has been shown, both theoretically and experimentally, that the mount is free from appreciable flexure and is quite immune to system delay (i.e. calibration) changes for different orientations.

I would like to thank Mr. D. Paradissis for his kind help during the flexure test of the telescope.

REFERENCES

1. R.Feynman : "Lectures on Physics" , Addison Wesley Publ. Co. , 1964
2. R.Korakitis : "Performance considerations of the SLR system at Dionysos Observatory", 2nd WEGENER-MEDLAS Conference, Athens, 1986

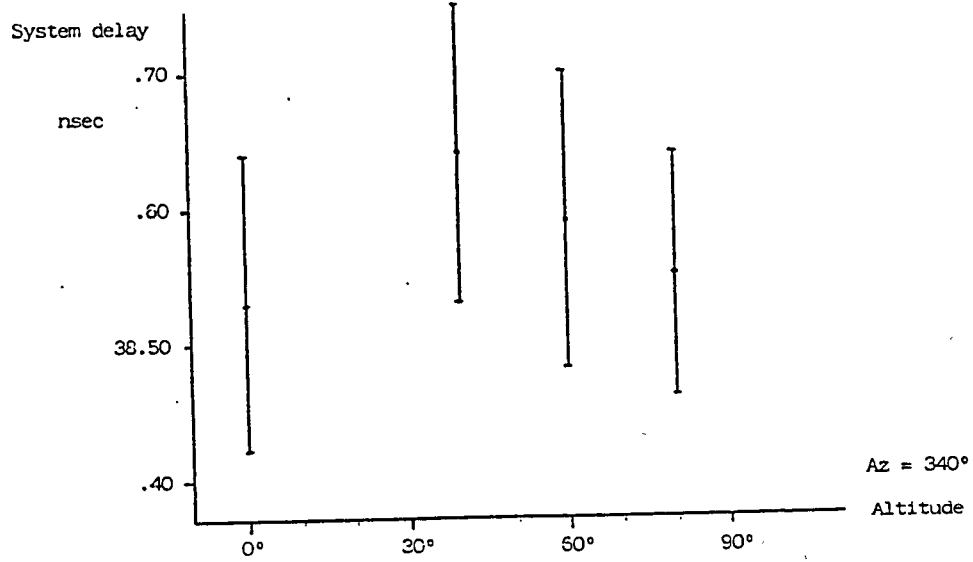
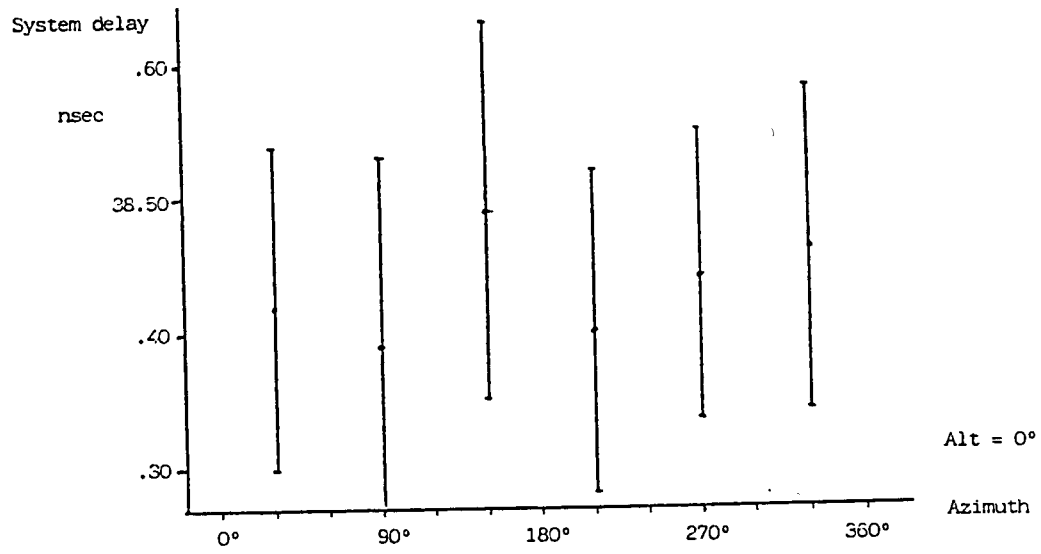
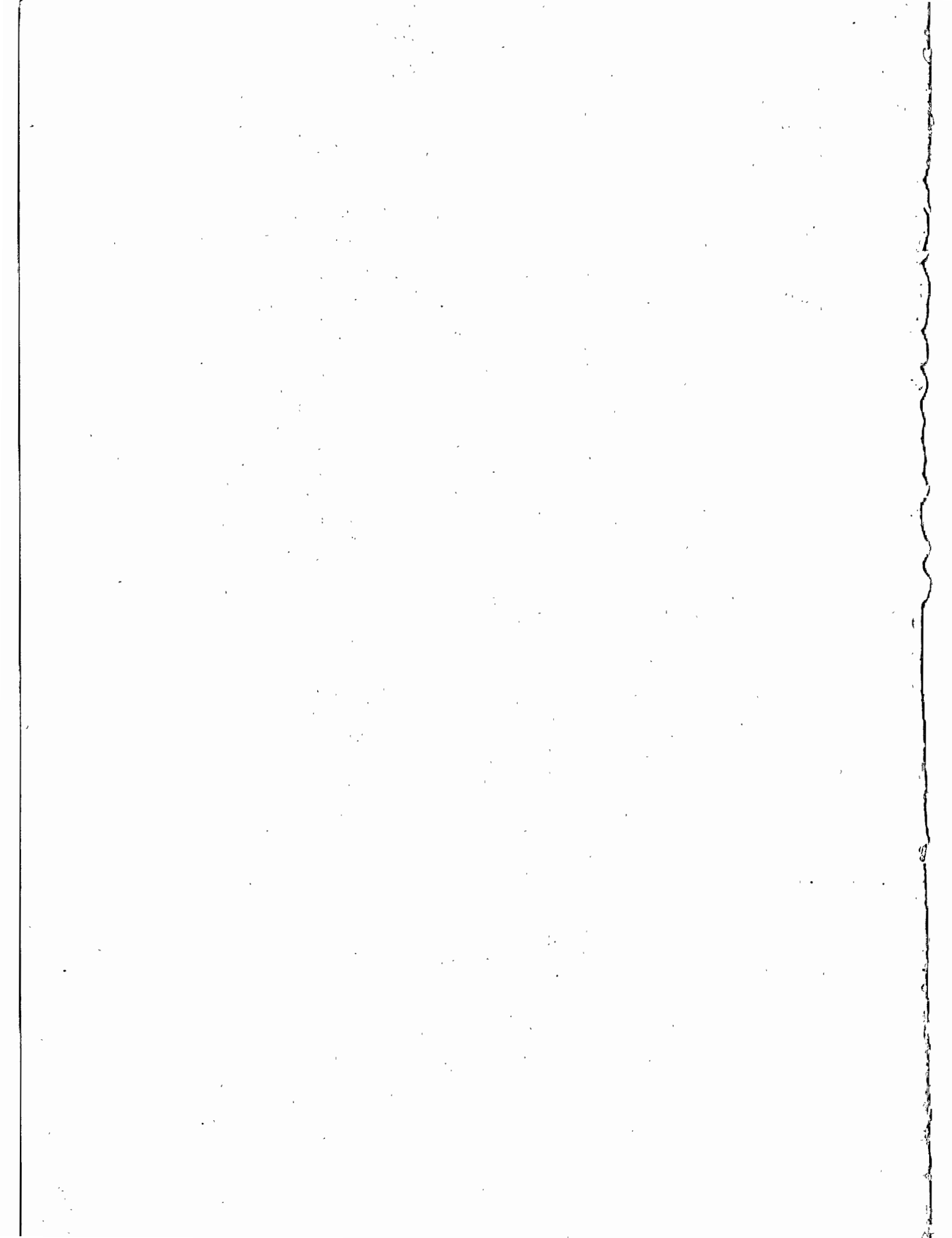
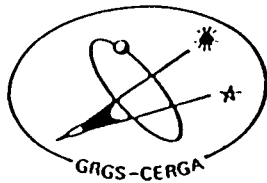


Fig. 8,9 : System delay measurements





SIXTH INTERNATIONAL WORKSHOP

ON LASER RANGING INSTRUMENTATION

ANTIBES JUAN-LES-PINS



6^e COLLOQUE INTERNATIONAL
SUR L'INSTRUMENTATION
DE LA TELEMETRIE LASER

EDITED BY / EDITE PAR :

- JEAN GAIGNEBET
- FRANCOISE BAUMONT

WE WISH HEREBY TO EXPRESS OUR THANKS TO /
NOUS TENONS A REMERCIER ICI :

- MINISTERE DES AFFAIRES ETRANGERES
- ASSOCIATION INTERNATIONALE DE GEODESIE
- UNION GEODESIQUE ET GEOPHYSIQUE INTERNATIONALE
- INSTITUT NATIONAL DES SCIENCES DE L'UNIVERS
- CENTRE NATIONAL D'ETUDES SPATIALES
- AEROSPATIALE
- BRASSARD MICHELET INDUSTRIES
- QUANTEL
- SOCIETE D'ETUDES ET DE CONSTRUCTION D'INSTRUMENTS ASTRONOMIQUES

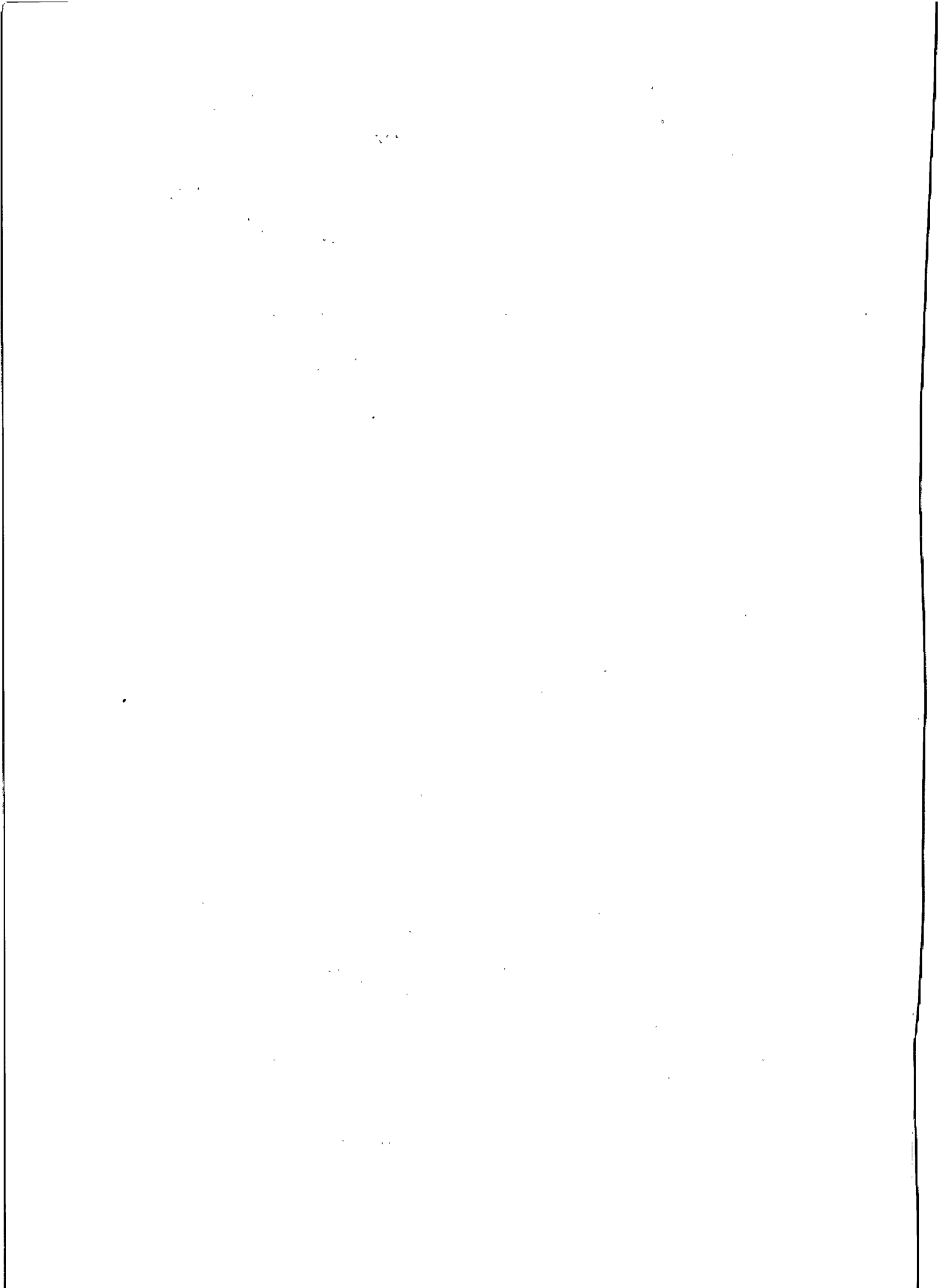


TABLE OF CONTENTS

=====

| | PAGE |
|--|------|
| WELCOMING ADDRESS J.P. Rozelot | V |
| PREFACE J. Gaignebet | VII |
| RESOLUTIONS | XI |
| LIST OF PARTICIPANTS | XVI |
| <u>SCIENTIFIC RESULTS AND FUTURE GOALS OF LASER RANGING</u> | |
| Chairman : F. Barlier (Invited Papers) | |
| I. Ciufolini | |
| New Relativistic Measurements With Laser Ranged Satellites | 1 |
| <u>NORMAL POINTS</u> Chairman : D. Lelgeman | |
| R. Kolenkiewicz et al. | |
| Comparison Of Lageos Satellite Ranging Normal Points | 11 |
| <u>SATELLITE MOBILE STATIONS</u> Chairman : P. Wilson | |
| T. Varghese, M. Hernick | |
| Sub Cm Multiphotoelectron Satellite Laser Ranging | 21 |
| T. Varghese et al. | |
| TLRS-1 ; System Upgrade And Performance Results | 33 |
| N. Sasaki, Y. Suzaki | |
| Satellite Laser Ranging System At The Simosato Hydrographie Observatory And The Transportable system, HTLRS | 45 |
| Z. Wen-Yao, T. De Tong | |
| Progress In SLR At Shanghai Observatory | 59 |
| K. Hamal et al. | |
| Interkosmos Laser Radar, Version Mode Locked Train | 69 |
| F. Pierron et al. | |
| Upgrades And New Developments On Satellite Laser Ranging Station From Grasse | 73 |
| L. Grunwaldt et al. | |
| The SBG Laser Radar Stations Potsdam And Santiago De Cuba Status And Performance Report | 93 |
| K. Hamal et al. | |
| 3. Generation Laser Radar, Version Mode Locked Train Proposal | 109 |
| A. Banni, V. Capoccia | |
| The New Satellite Laser Ranging System At Cagliari Observatory | 113 |
| P. Kloeckler, Th. Schildknecht | |
| Zimmerwald Satellite Observation Station | 123 |

LUNAR AND COMBINED Chairman : K. Hamal

Ch. Veillet et al.
The New CERGA LLR Station 129

M.L. White
Recent Improvements And Future Plans At The University Of
Hawaïi Lunar And Satellite Ranging Station 135

J.R. Wiant, P.J. Shelus
The McDonald Observatory Laser Ranging Station : MLRS 139

DETECTORS : SOLID STATE AND PMT Chairman : S.R. Bowman

I. Prochaska
Start Detector For The Mode Locked Train Laser Radar 145

R. Neubert et al.
Ambiguity And Resolution of A Mode Locked Pulse
Train Laser Radar 149

I. Prochaska, J. Gaignebet
Microchannel/Dynode Photomultipliers Comparison Experiment 161

Z. Neumann
Detectors For III Generation Laser Ranging Systems 165

S.R. Bowman et al
The Use Of Geiger Mode Avalanche Photodiodes For Precise
Laser Ranging At Very Low Light Levels : An Experimental Evaluation 173

K. Hamal et al.
Single Photon Solid State Detector For Ranging At Room Temperature 185

W.A. Kielek
"Constant Fraction" Discriminators In Few And Multiphotoelectron
Laser Ranging 189

TIMING AND EPOCH Chairman : C.A. Steggerda

B.A. Greene
Calibration Of Sub-Picosecond Timing Systems 197

P. Dachel et al.
Recent Advances In The GLTN Timing And Frequency Instrumentation 205

C.A. Steggerda
The Development Of A Dual Frequency Event Timer 225

LASERS Chairmen : F. Moya, H. Jelinkova

K. Hamal, H. Jelinkova
Saturable Dye For 1.06 μ m 243

H. Jelinkova et al.
Spatial Structure Of The Doubled Nd:YAG Laser Transmitter Beam 251

L. Jiyu
Some Special Requirements To Lasers For Satellite Laser Ranging 261

OPTICS, TRACKING AND MOUNTS Chairman : M.L. White

| | |
|--|-----|
| S.R. Bowman et al. Analysis And Performance Of A Passive Polarization Telescope Coupling Switch For Lunar Laser Ranging | 273 |
| H. Feng et al. An Accurate Test Of The Azimuth Axis Of A 1.2M Alt-AZ Telescope Mount For The Lunar Laser Ranging And The Analysis Of The Results | 281 |
| M.L. White Double Peak Polarized Interference Filters | 289 |
| R. Korakitis Effects Of Telescope Design On Laser Beam Pointing Accuracy | 297 |

CALIBRATION Chairman : M. Pearlman

| | |
|---|-----|
| T. Varghese System Characterization Of Moblas-7 For Colocation With TLRS-1 & 2 | 311 |
| R. Appler Calibration Error Sources | 323 |
| B.A. Greene Calibration Of Sub-Millimeter Precision Satellite Laser Ranging Systems | 331 |
| P. Kloeckler, T. Schildknecht Measuring And Modelling Pulse Discriminator Amplitude Dependence | 343 |
| H. Junginger MTLRS Ground Tests | 357 |
| J.D. Rayner et al. Zero Range Realtime Calibration | 373 |
| K. Hamal, I. Prochaska System Stability Using Mode Locked Train | 377 |
| L. Jiyu Satellite Laser Ranging Errors | 379 |

SOFTWARE BENCHMARKING AND COLOCATION Chairman : E. Vermaat

| | |
|--|-----|
| M.R. Pearlman Some Current Issues On Laser Collocations | 399 |
| A. Cenci Management Of The Laser Ranging Systems Colocation | 409 |
| D.L.F. Van Loon Eccentricity Vectors For Colocation Purposes | 441 |
| V. Husson, D. Edge Polyquick Collocation Analysis | 453 |
| A. Caporali Colocation Data Analysis : Dynamical Approach | 467 |
| R. Kolenkiewicz Geodyn Collocation Analysis And Its Comparison With Polyquick | 481 |

RAPID ON SITE DETERMINATION OF THE EARTH ROTATION

Chairmen : D. Smith, Ch. Veillet

- P.J. Shelus, R. Ricklefs
Real Time, On Site Earth Orientation Parameter Generation At
The MLRS Using Laser Ranging Data 493
- G.M. Appleby, A.T. Sinclair
A Note On The Use Of The CRS Lageos Ephemerides 499
- Ch. Veillet et al.
Real Time UT0 Determination At CERGA LLR Station 507
- P.J. Shelus
A Simple Software Scheduling Tool For Efficient Observing
Operations At A Lunar/Lageos Laser Ranging Station 511

HIGHT AVERAGE POWER AND NEW LASERS, NEW SATELLITES

Chairman : C.O. Alley

- S.R. Bowman et al.
A Neodimium YAG Active Mirror For The Amplification Of Mode
Locked Laser Pulses 523
- M. Sasaki
Japanese Geodetic Satellite "AJISAI" Launched In August 1986 527
- F.M. Yang
The Proposal Of Strictly Simultaneous Satellite Laser Ranging 549

TWO WAVELENGTH SYSTEMS AND STREAK CAMERA Chairman : B. Greene

- I. Prochaska, K. Hamal
Streak Camera Based Laser Radar Receiver. Its Performance and
Limitations 559
- J. Gaignebet et al., K. Hamal et al.
Two Wavelength Ranging On Ground Target Using Nd:YAG 2HG and
Raman 0.68 μm Pulses 565
- I. Prochaska, K. Hamal
Picosecond Laser Ranging Using Photodiode 577
- B.A. Greene
Multiple Wavelength Laser ranging 581
- F. Guerin, G. Cerutti-Maori
Problems Induced By Multicolor Telemetry On Laser Retroreflector
Development 593

SPECIAL STUDY GROUP ON LUNAR LASER RANGING

Report prepared by Ch. Veillet 623

LUNAR AND COMBINED (Additive)

- C.O. Alley et al.
First Lunar Ranging Results From The University Of Maryland
Research Station At The 1.2M Telescope Of The GSFC 625

The Vith International Workshop on Laser Ranging Instrumentation

recognizing the many contributions of the Centre d'Etudes et Recherche en Geodynamique et Astronomie to the success of the Workshop through its sponsorship and local supporting organization,

and further recognizing the exceptionally effective and untiring efforts of the Chairman of the Local Organizing Committee for the Workshop, Jean Gaignebet and its Scientific Secretary, Francoise Baumont,

Wishes to express its deep appreciation to the members of CERGA and especially to Dr. Gaignebet and Dr. Baumont for selecting such as attractive location and for providing excellent support.

PAPERS PRESENTED BUT NOT PUBLISHED

SCIENTIFIC RESULTS AND FUTURE GOALS OF LASER RANGING INVITED PAPERS

- X.X. Newhall et al.
Lunar Laser Ranging Results Review
- D.E. Smith
Tidal Dissipation With Lageos
- C. Yoder
Implication Of Tidal Dissipation On G'
- B.D. Tapley et al.
Lageos Results Review

LASERS

- R. Dewhurst et al.
A Passively Mode Locked Nd:YAG Laser Using A Half Symetry Unstable Resonator With Continuous Output Coupling
- B.A. Greene
Laser Design For Fifth Generation SLR System

OPTICS, TRACKING AND MOUNTS

- K. Hamal
Transmit Receive Switch

HIGH AVERAGE POWER LASERS AND NEW LASER SPACE BORNE SYSTEMS AND NEW SATELLITES

- D.M. Smith
Topex, Poseidon And ERS-1 Satellite For Laser Tracking
- I. Ciufolini et al.
The Status Of Lageos 2 ; Informal Discussion Prospects For A Lageos 3.

SYSTEM CHARACTERIZATION OF MOBLAS-7 FOR COLLOCATION WITH TLRS-1 & -2

T. Varghese
Allied Bendix Aerospace
BFEC, GLTN
Seabrook, MD 20706 - USA -

Telephone (301) 7318916 - 2867743
Telex 197700 GLTN

ABSTRACT

The Moblas 4-8 systems are characterized by separate transmission reception axial geometry and hence produce parallax in ranging to short range targets. The conventional targets for these systems are located at distances of approximately 3 km and produces significant errors during survey as well as range measurements due to terrain and environmental features. An optical package with dual capability for parallax - free short/long external ranging and internal calibration at levels better than 1 mm was designed and performance evaluated on the system. This paper describes the system characterization test results performed with the above configuration.

1.0 INTRODUCTION:

A major collocation effort has been under-way at the NASA Goddard Optical Research Facility between the Goddard Laser Tracking Network (GLTN) " standard " Moblas-7 (Mobile optical Laser ranging System) and TLRS-1 & 2 (Transportable Laser Ranging System) since May 1986. The goal of NASA Crustal Dynamics program is to obtain ranging agreement between these stations on simultaneously collocated passes under 1cm. This may appear to be an ambitious goal considering the complexity of the number of parameters involved. However, the technology incorporated into these systems are robust enough to yield results comparable to the set goals provided, sufficient care is taken in the calibration and satellite operation of the system. Considering the number of error sources ,systematic and otherwise, present in the system it was recognized to be important to characterize the system at the mm level to meet the above goal. The precision of the system has been considerably improved after receiver upgrade(1,2) whereby calibration RMS is typically 4-5mm and satellite RMS 7-8mm.

This paper describes some of the recent improvements in our calibration techniques to establish systematic errors at the few mm level. The results presented in this paper are preliminary; refinements in techniques and analyses will be published(3) elsewhere at a future time.

2.1 SYSTEM DESCRIPTION

The schematic of the data-loop comprising the transmitter and receiver is shown in fig.2-1 and the corresponding optical layout in fig.2-2. A beam splitter reflects part of the output onto a photodiode(PD) which initiates the time interval counting process. The receive optics consists of a 30 inch telescope (Cassegrain with a f/1.5 primary mirror) which images the target return-optical beam onto the MCP-PMT after collimation and spectral bandpass filtering (used only for daytime tracking) The output from PD/PMT is allowed to undergo constant fraction discrimination in the Tennelec TC 454 CFD which provides a NIM pulse output for the HP5370 to start/stop counting. A part of the output is also fed to the LeCroy224 Quad Integrator for energy measurement.

The separate transmission reception geometry of the ranging system reduces the effectiveness of the system for horizontal ranging on short range targets due to problems of parallax. The system has been traditionally ranging to targets 3 km away for calibration purposes.

The meteorological measurements are performed on station and can be significantly different from the target location. The topological constraints dictated putting up the target at heights of about 40 ft which when subject to temperature, wind and solar loading produces variations of several mm. The overall error due to all the above problems were around a cm. By establishing a target close to the station on a stable structure the above problems can be significantly reduced provided ranging can be performed without parallax.

2.2 PARALLAX-FREE OPTICAL RANGING

The schematic for parallax-free optical ranging is illustrated in fig.2.3. It consists of two mirrors M1 and M2 mounted on mirror mounts and are aligned parallel to each other within few arc-secs. The mirrors are mounted such that the line joining their centers makes an angle of 45 degrees with the reflecting surfaces of the mirrors and is orthogonal to the transmit receive axes. This arrangement is held together in a rotary fixture and can be swung into position for calibration and moved out of the way for satellite ranging. The reflectivity of M1 is 50% while that of M2 is 100%.

The partially transmitted beam leaving the system hits the target and retro-reflected to M1. M1 reflects part of the return beam to M2 which couples the light into the telescope and from there to the detector. A target can also be mounted on the system as a reference for internal calibration. The distance from the center of rotation to the internal target can be accurately measured using a vernier to better than a mm and thus provides a powerful tool to examine survey inaccuracy. This arrangement also provides a means to measure any changes in the path length of the system as a function of mount pointing angles and apply the corresponding correction to the satellite data.

2.3 RESULTS AND DISCUSSION

Fig.2.4 illustrates the system delay as a function of time for two targets measured over a period of two hours. Each division on the vertical axis is 1.5mm. The number shown along with each box is the ambient temperature in fahrenheit. The displacement of the two data sets is due to the wrong range value used in station processing of the data for internal calibration. The pertinent feature to examine here is the close agreement between internal and external calibration as a function of time. The difference between the system delays stays as a constant over the time interval of the experiment. When the system was stabilized over a period of time, the system delay did not vary more than a mm and this feature is depicted in fig.2.5.

The variation of system delay as a function of elevation and azimuth were also studied. Fig.2-6 &-7 illustrates the Az-El dependence under two alignment conditions of the coelostat which holds the coude optics. Although the nature of response differed, the magnitude of variation remained essentially the same.

Satellite passes were simulated using the target mounted on the telescope. Fig.2.8 illustrates the plot of system delay as a function of elevation angle for a 66 degree (PCA) elevation Lageos pass. It is clear that for the particular geometry of this pass, the system delay is a monotonically decreasing function (within the uncertainty of measurement) of elevation. Further experiments are planned for future to examine mm problems due to mount pointing angles and apply appropriate correction to the satellite data.

2.3 SUMMARY

The demonstration of a parallax-free optical ranging scheme has been accomplished with the means to study mm problems in horizontal ranging. The optical closure that can be realized between the transmit and receive axes can be used for the alignment of optical components following the telescope. The ability to verify survey ranges and characterize mm problems due to mount orientation angles are unique advantages of the system.

2.4 REFERENCES

- (1) "Sub-cm Multiphotoelectron Satellite Laser Ranging", Thomas Varghese, Michael Heinick, Sixth International Workshop on Laser Ranging Instrumentation, Antibes, France, Sept.1986.
- (2) Thomas Varghese, Technical Report, Allied-Bendix Aerospace, BFEC, #1909A-B-05/10/85-S-C.
- (3) Thomas Varghese (to be published)

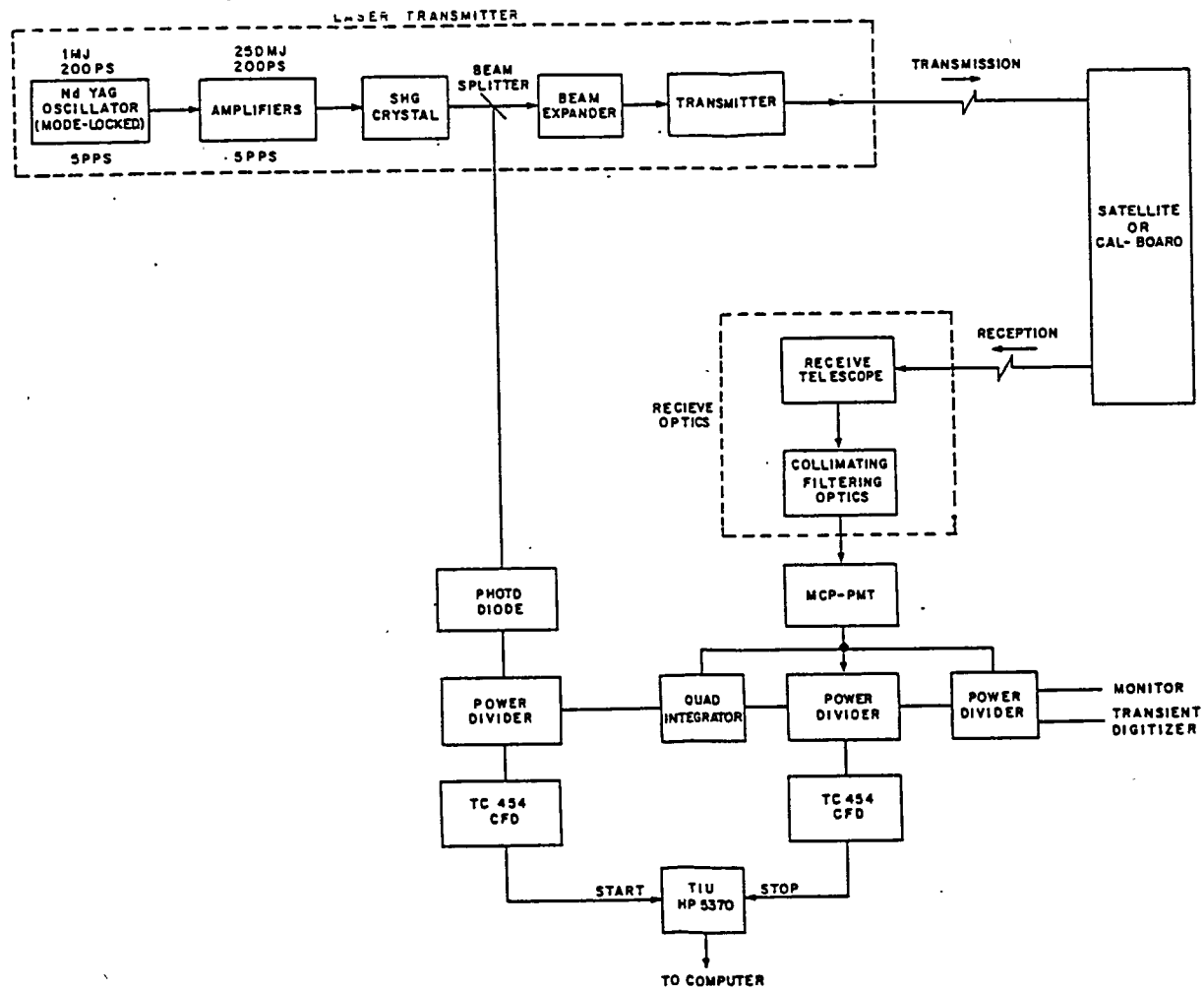


FIG. 2-1

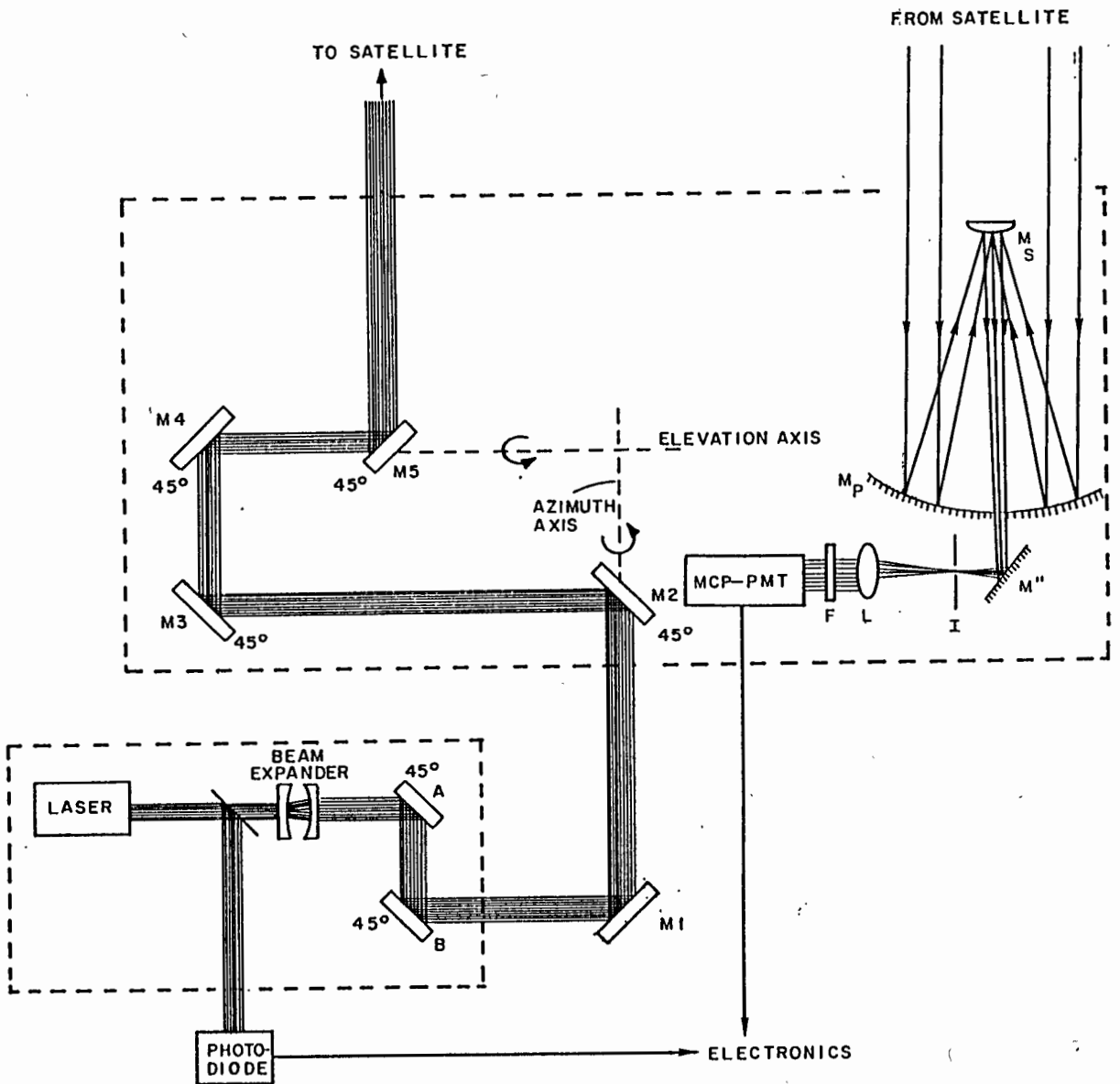


FIG. 2-2 SCHEMATIC OF OPTICAL LAYOUT

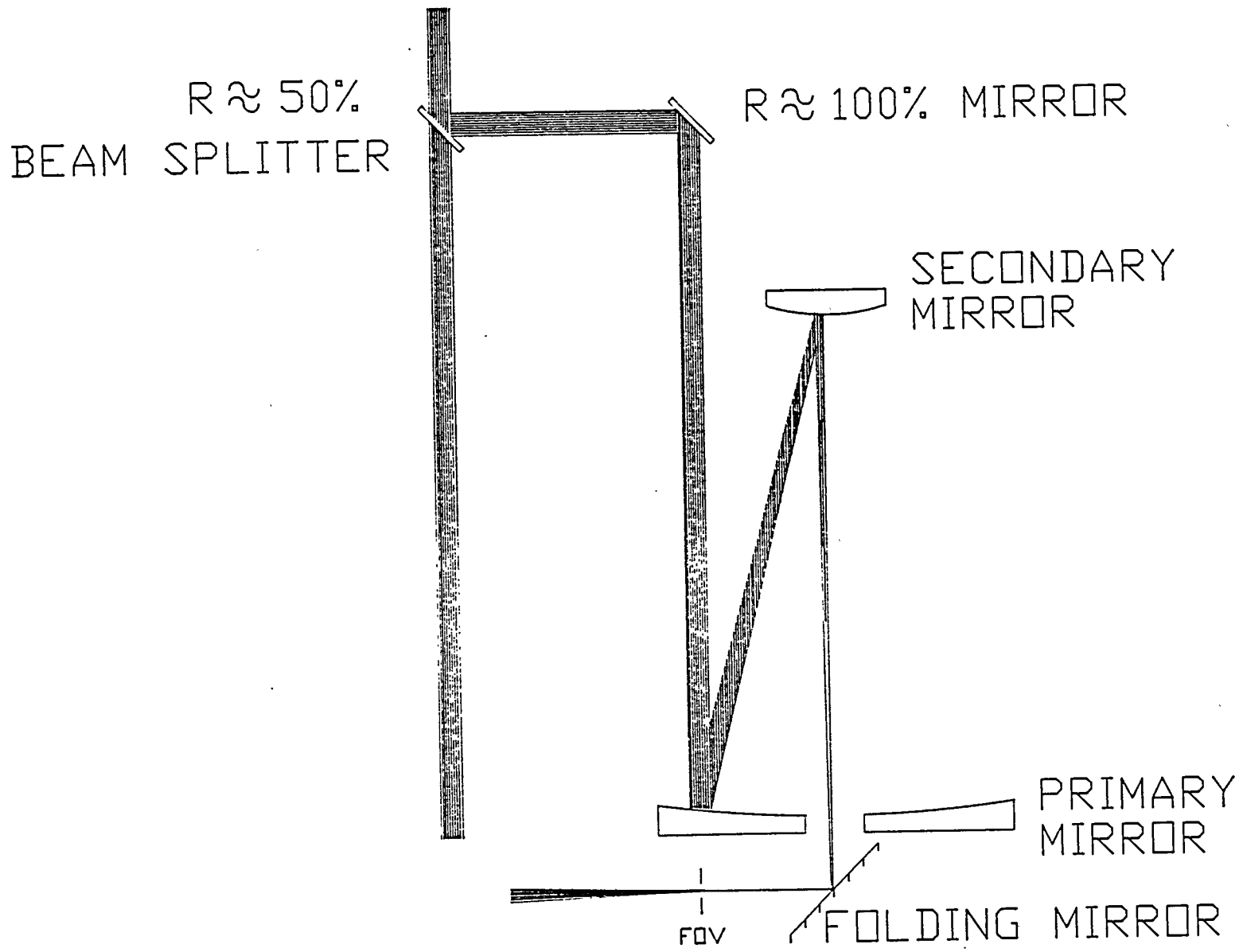
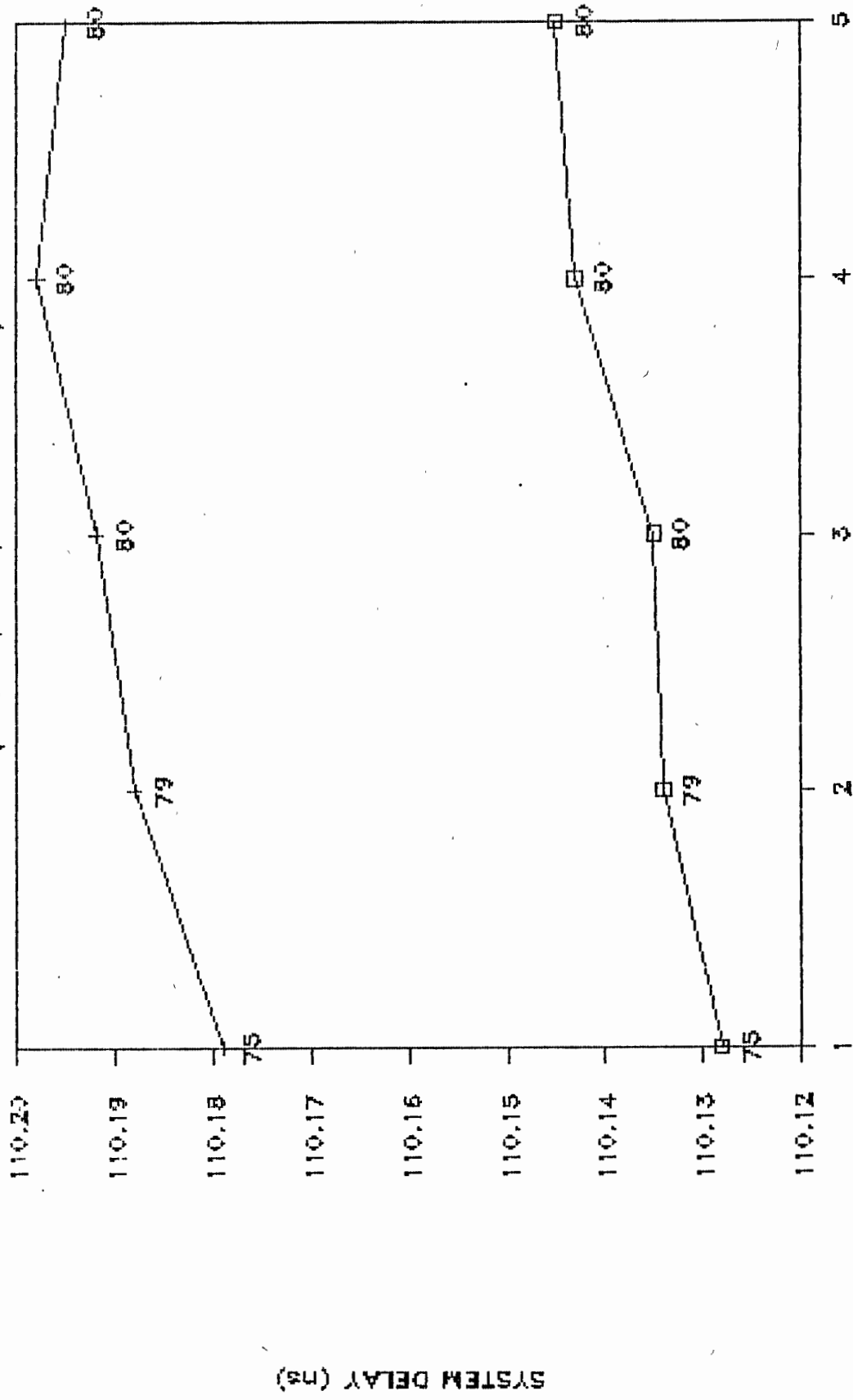


FIG. 2-3

MOBLAS-7 SYSTEM DELAY STABILITY VS TIME

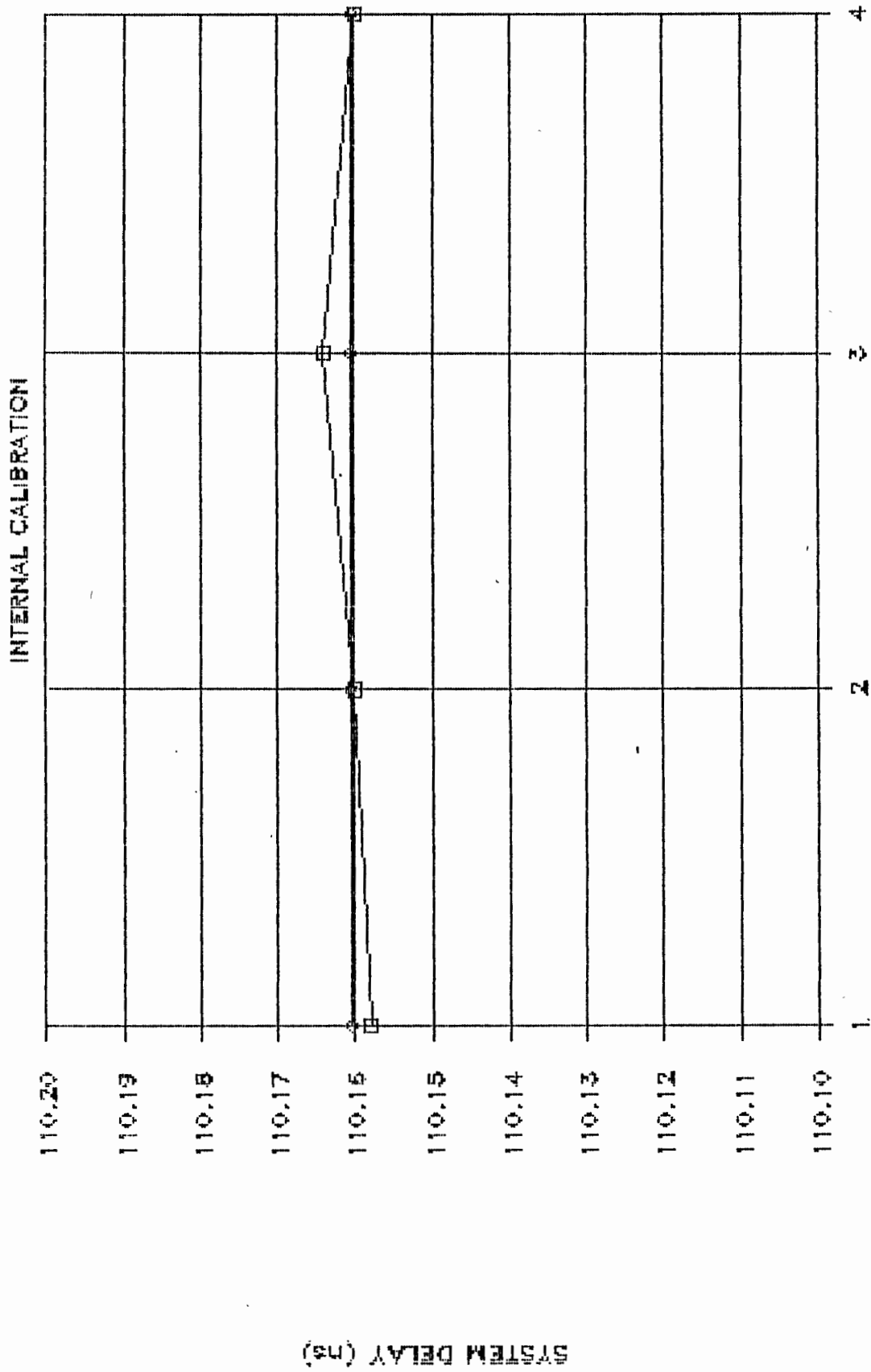
(SEP 18, 1986, 6 PM TO 8 PM)



□ IC + TGT #3 (RANGE 80 M)

FIG. 2-4

MOBLAS-7 SYSTEM DELAY VS TIME



◇ AVG

FIG. 2-5

MOBLAS-7 SYSTEM DELAY VS AZIMUTH

IC (ELEVATION 0-90)

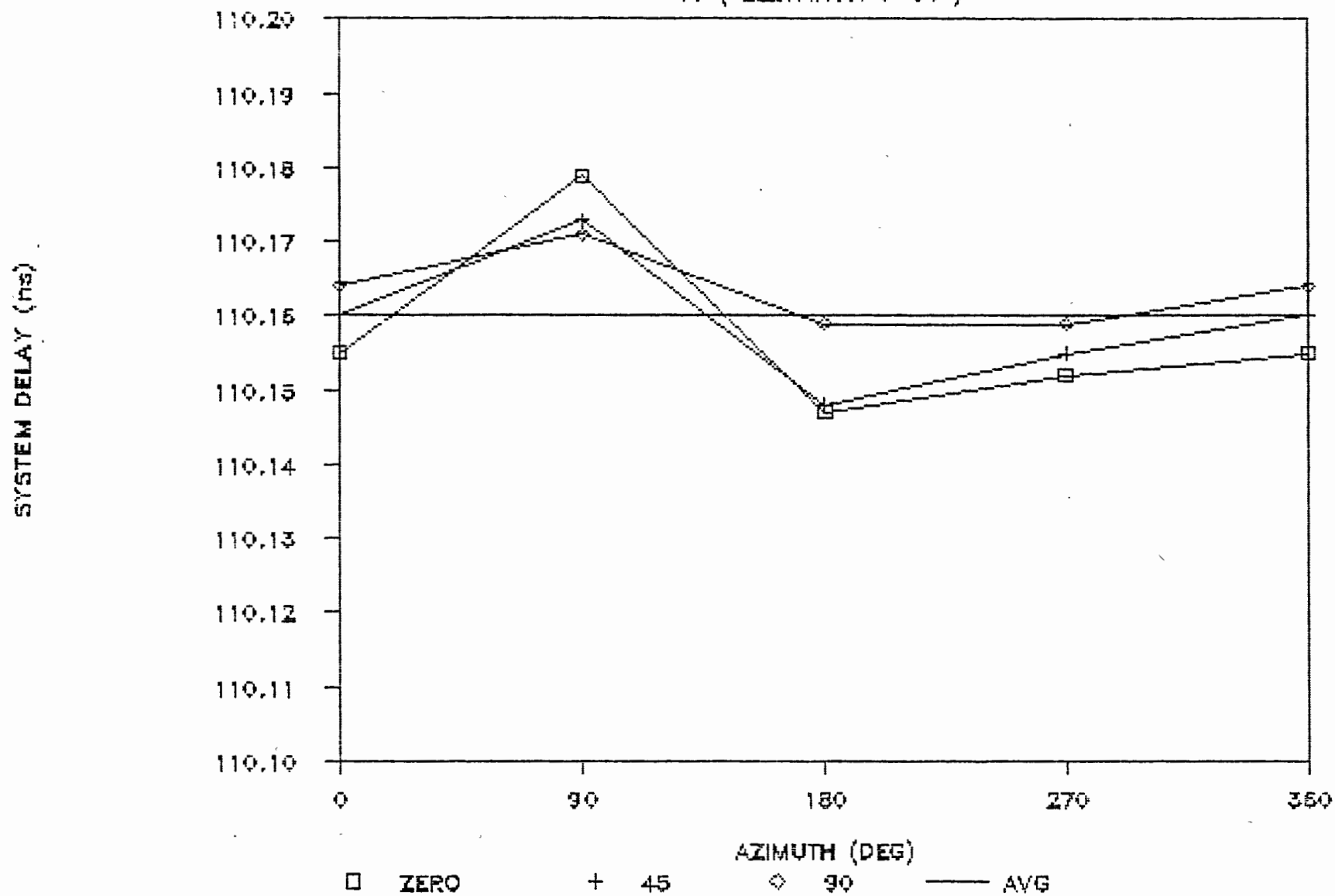


FIG. 2-6

MOBLAS-7 SYSTEM DELAY VS AZMUTH (EL 0 - 90)

INTERNAL CALIBRATION ON SEP 17, 1986

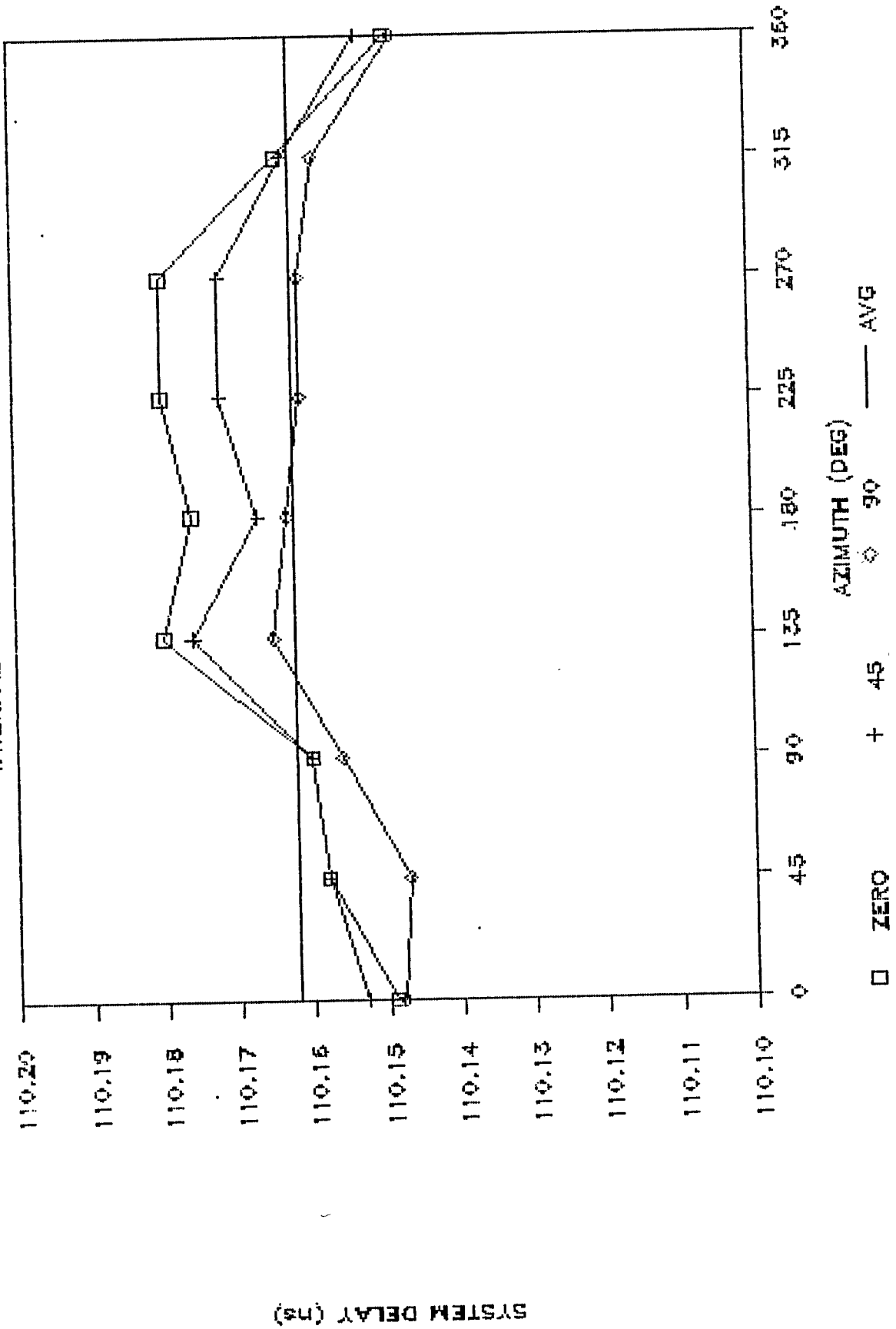


FIG. 2-7

M7 IC VS. EL

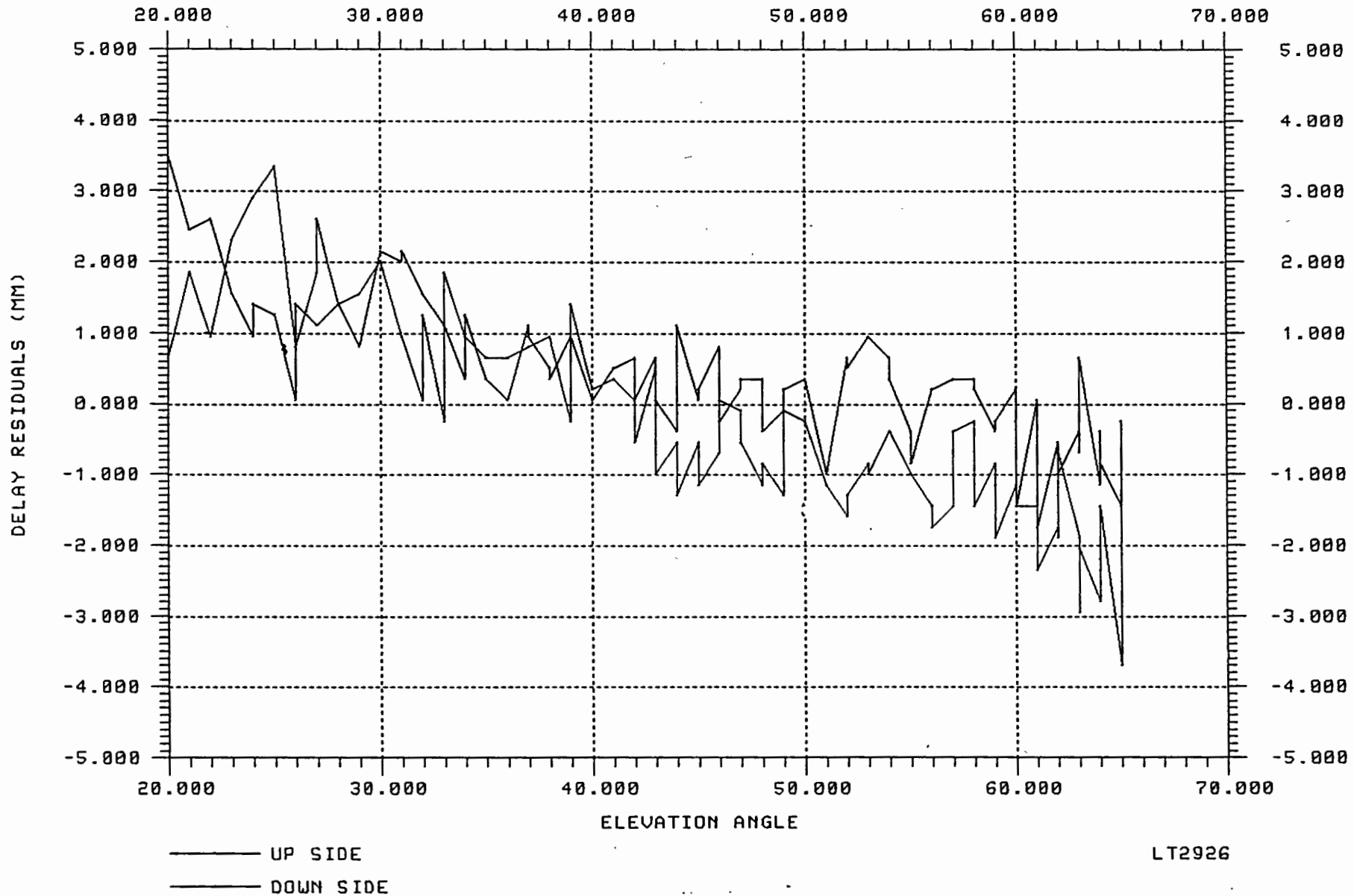


FIG. 2-8

CALIBRATION ERROR SOURCES

R.L. Appler
NASA/Goddard Space Flight Center
Greenbelt, Maryland 20771

Telephone (301) 286 8119
TWX 2579559 CDPO UR

ABSTRACT

Through gradual improvement in laser ranging hardware and software, we have reached an era where sub-centimeter ranging precision and two-minute normal point data at the millimeter level are routinely obtained at Moblas 7. Systematic error sources, once buried in the noise of measurements, are now being identified and investigations are underway to determine the means through which we can minimize these errors with sub-centimeter ranging accuracy as our near-term goal. An overview of some of the error sources and possible means to reduce their effect is presented.

CALIBRATION ERROR SOURCES

Robert L. Appler
NASA/Goddard Space Flight Center
Greenbelt, Maryland 20771

Telephone (301) 286-8119
TWX 2579559 CDPO UR

ABSTRACT

Through gradual improvement in laser ranging hardware and software, we have reached an era where sub-centimeter ranging precision and two-minute normal point data at the millimeter level are routinely obtained at Moblas 7. Systematic error sources, once buried in the noise of measurements, are now being identified and investigations are underway to determine the means through which we can minimize these errors with sub-centimeter ranging accuracy as our near-term goal. An overview of some of the error sources and possible means to reduce their effect is presented.

1. Introduction

Substantial hardware changes directly and/or indirectly influencing the time-of-flight measurements in satellite laser ranging have been incorporated into laser ranging instrumentation within the Goddard Laser Tracking Network. Laser pulse widths have been reduced to 200 picoseconds or less. Timing is within 100 nanoseconds of Universal Time. The jitter in the measurement of system and satellite delay is less than 30 picoseconds. Discriminator time walk as a function of signal amplitude at signals greater than three photoelectrons is negligible. Signals at three photoelectrons or less are rejected by gating. Photomultiplier time walk as a function of image position and signal level is virtually nonexistent. Better alignment techniques have been initiated. Multi-photoelectron ranging has substantially increased the signal-to-noise ratio. These and a multitude of other refinements in instrumentation and technique have brought the single-shot precision even in daylight LAGEOS ranging to the eight millimeter level on a regular basis at Moblas 7. Similar results should be seen on Moblas 4, 5, 6, and 8 after the installation of the microchannel plate detector and the Tennelec discriminator on these systems.

The enhanced ranging precision brought about by events discussed above increases our ability to identify the sources of systematic errors that exist. We are making an in-depth effort to uncover and diminish the effects of known error sources and we are constantly on the look out for new error sources to be identified and eliminated. The following areas are being scrutinized to determine whether systematic errors

leading to range biases are present or whether they indirectly cause range biases in other data loop optics, mechanics, or electronics:

- * System Timing
- * Optical/Mechanical Path
- * Data Processing Software
- * Atmospheric Model
- * Atmospheric Monitoring
- * Temperature and Humidity Control
- * System Calibration

As new sources of error are uncovered, these too, will be investigated and attempts will be made to eliminate, or at least, reduce them.

I. System Timing

Cesium clocks used in the network are known to have excellent long term stability but to exhibit significant short term phase and frequency jitter which may or may not translate into a systematic range bias. Distribution amplifiers and time code generators currently used in conjunction with the cesium clock were installed in the network during an era of much lower system precision and have looser specifications than is desired. The output of these devices provides epoch time to 100 ns when locked to epoch time obtained from the GPS receiver. The cesium also provides the clock frequency input to the time interval units used to measure system delay and the round trip time of flight to the satellite.

In an attempt to determine whether any systematic bias is contributed by the timing system, a spectrally pure disciplined crystal oscillator will be purchased, tested against a hydrogen maser, and then used as a standard of comparison against timing electronics presently in the network. If results indicate the need, network timing electronics will be upgraded to meet the more stringent performance requirements needed to achieve sub-centimeter system accuracy.

The time interval counters used in the GLTN will also be investigated to determine what timing error is introduced by its electronics when driven by the disciplined oscillator. Measures will be taken to correct resulting systematic biases.

II. Optical/Mechanical Path

Every system alignment of the optical path to the mechanical axes is subject to some alignment error which is difficult to routinely measure to an accuracy of a few millimeters. Systems where the transmit and receive optical paths are separated and especially in those systems using a Coude' path having four or five mirrors, are subject to translational errors as a function of mount pointing because of the very difficult task of aligning the optics to the mechanical axes exactly. Certainly, routine alignment which is necessary due to thermal and other shifts during operations does not permit the time necessary to achieve a "perfect" alignment, if indeed, a "perfect" alignment were possible to achieve.

Solar loading and other thermal effects, minor misalignment during laser repair and/or alignment, mechanical disturbances to the laser and mount, deviations of the azimuth axis from vertical due to settling and other causes, inadvertent relaxation of spring load when adjusting spring-loaded optical mounts represent some additional probable causes for alignment errors. Care must be taken to minimize most of these problems through proper mount design.

Some steps that can and must be taken to improve system alignment integrity include the use of special paints and/or shielding of critical mechanical components from the sun to minimize the effects of solar loading, making adjustments against spring loads, and designing adjustment mechanisms to work with gravity wherever possible.

III. Data Processing

A thorough investigation must be made to insure that all measurement resolution available by the hardware is used during the processing of data. For instance, is epoch time analyzed to a resolution of 100 ns? Is atmospheric pressure analyzed to a resolution of 0.1 millibar? Are temperature effects on range analyzed at a resolution of 0.1 degree C? If the answer to any of these and/or similar questions is no, immediate steps must be taken to see that all available resolution is used in processing data.

Similar questions relate to correction during data processing for known sources of range biases such as:

- * Use of neutral density filters during system calibration.
- * Correction for parallax resulting from the use of near-in calibration targets.
- * Minor changes in optical path caused by residual alignment errors after system alignment.
- * Range bias as a function of return signal amplitude.

Care must be taken in all of these areas to eliminate these and other similar sources of data processing error as well as in the verification of system and data processing software to ensure that avoidable errors are not introduced.

IV. Atmospheric Model

Marini and Murray of NASA Goddard Space Flight Center developed an atmospheric model for refraction which has been the Network standard for many years. Dr. Jim Davis and Dr. Tom Herring of the Massachusetts Institute of Technology have added coefficients to the Marini-Murray model which improve the model from an accuracy of approximately 1 centimeter to one of approximately 0.5 centimeters.

Although not a source of ranging system error, the error in the atmospheric model still produces a systematic error in the range value. Until such time that two color ranging can be implemented into the network, at least the updated Davis-Herring version of the model must be used in satellite range determination.

V. Atmospheric Monitoring

Care must be taken in regard to the location of atmospheric monitoring instrumentation on a site and in the calibration of that instrumentation. The pressure sensor should be placed as close to the elevation axis as possible and any tubing required between the sensor and the axis should have its open end pointed upward in order to avoid the trapping of air in the tube--thereby introducing an error in the actual pressure. Temperature sensors should be placed sufficiently far from artificial heat sources and protected from direct incidence of the sun so as to avoid an error in the reading in the ambient temperature. Significant range biases have been introduced in the past because of improper placement of these instruments.

VI. Temperature and Humidity Control

In order to minimize their effects on wavefront propagation, laser alignment and power, data loop electronic stability, etc., it is imperative that environmental control be given high priority. Errors in range measurement can be significant if the environment is not maintained to high tolerances. The effect of heat on instrument reliability is already well known. Temperature and humidity control is being heavily stressed now in the network and measures have already been taken or are being taken to hold these parameters constant to practical levels.

VII. Calibration

System calibration errors are deeply interwoven with the error sources discussed above. Station timing, optical/mechanical alignment, data processing, etc., when combined, lead to an unacceptable level of systematic errors. In addition to these errors, which are internal to the system, another perhaps larger source of error lies in the system calibration, itself.

Target boards and corner cubes are traditionally placed at distant ranges in order to minimize parallax problems encountered in those systems which transmit on one path and receive on another. Newer systems having a common transmit and receive path, perhaps by tradition rather than for any other reason, have continued using these distant targets. As a consequence, atmospheric ambiguities continue to compromise the measurement range to the target during the surveying process and during system calibration. In addition to atmospheric concerns, the target heights have been excessive in order to accommodate site conditions. As a consequence, small, random changes

in target verticality have led to significant calibration biases. Errors in the survey of a station monument as well as errors in the determination of system eccentricities compound the problem.

Recent steps have been taken to minimize the effects of parallax and atmosphere. Unfortunately, only preliminary data has been taken and it is too early to report on the results at this time, although the data appears encouraging. Dr. Thomas Varghese of Bendix Field Engineering has developed an anti-parallax attachment for Moblas 7 to demonstrate the enhanced precision possible with such a device. This device can be used for near-in ranging as well as for internal calibration (IC) wherein the IC feedback optics covers the total optical path so as to avoid any subtle alignment errors leading to an incorrect determination of system delay via internal calibration itself. It provides an independently calibratable optical path which can be subtracted from the total time of flight from transmit start to detect stop so as to be able to accurately determine true system delay. This can be done in all pointing directions. The system delay thus determined can be compared against near targets as a redundant check on calibration.

In addition to the parallax-free internal calibration system discussed above, short, concrete reinforced piers are gradually being installed in the network to minimize the atmospheric and target instability problems. These piers are virtually identical to the first order surveying monuments which have proved to be very stable at the millimeter level. When used at the Goddard Optical Research Facility, each system ranges on the same corner cube with negligible parallax. As a result, any minor changes in the target position does not negate the use of the target as a valuable means to achieve system intercomparisons.

An open corner cube has been developed by NASA Goddard to provide another means to check system calibration. This cube has an effective aperture of 0.5 m to permit ranging by Moblas 7 without parallax. great care has been taken in the design to insure that the range between the vertex point and the laser system reference point can be surveyed to an accuracy of about 1 mm. Unfortunately, there has not yet been time available to check out this device.

VIII. Summary

As discussed above, ranging precision is currently at the subcentimeter level on Moblas 7. Some sources of error known to exist include:

- System Timing
- Optical/Mechanical Alignment
- Time Tagging
- Data Processing
- Atmospheric Model
- Atmospheric Measurements
- System Calibration

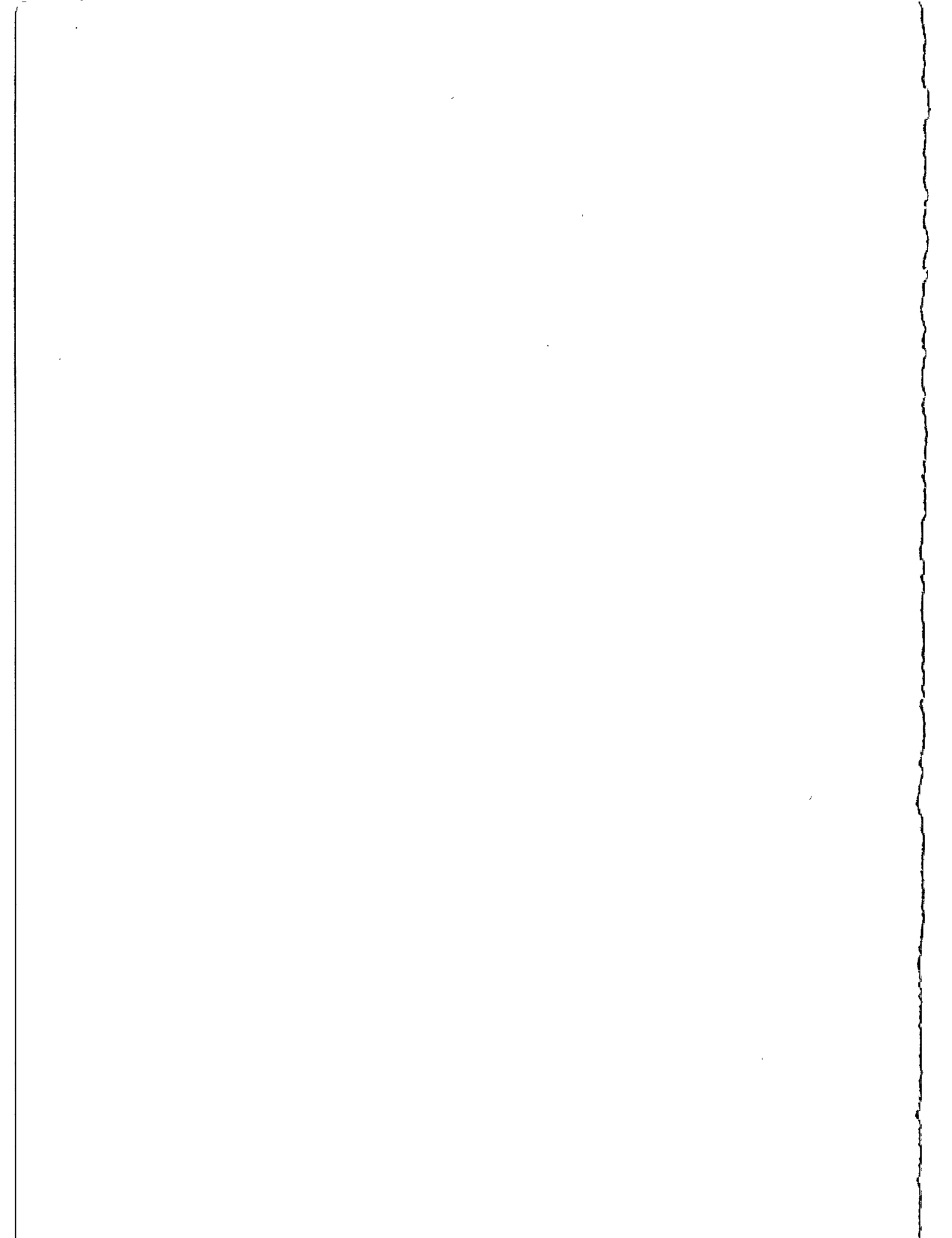
The measures being taken to implement hardware/software changes are discussed.

It is clear that the degree to which system accuracy can approach system precision depends upon the amount of success achieved in the elimination of these and other errors.

It is hoped that this paper will assist anyone who is not aware of the potential problems mentioned to take advantage of the experience of others to avoid known pitfalls during the development or modification of a laser ranging system.

ACKNOWLEDGMENT

Special thanks go to Dr. Tom Varghese of Bendix Field Engineering Corporation and Dr. Mike Pearlman of the Smithsonian Astrophysical Observatory who through their work or through useful suggestions have helped in providing information included herein. Also to be thanked are other members of the Bendix Engineering and Data Services teams and to Dr. Robert Coates, Manager of the Crustal Dynamics Project who made possible the presentation of this paper at the Sixth International Workshop on Laser Ranging Instrumentation.



CALIBRATION OF SUB-MILLIMETRE PRECISION SATELLITE
LASER RANGING SYSTEMS

B.A. Greene
Division of National Mapping
P.O. Box 31
Belconnen ACT 2616 - Australia -

Telephone (6162) 525095
Telex AA 62230

ABSTRACT

The deficiencies of the calibration procedures in general use by SLR stations are examined in the context of sub-millimetre precision systems and their calibration requirements. It is shown that calibration accuracies of a few millimetres are possible if great care is taken with conventional procedures. Two new calibration techniques which yield sub-millimetre accuracy are proposed, and the results of applying one of these to a fully operational SLR station are presented.

CALIBRATION OF SUB-MILLIMETRE PRECISION SATELLITE LASER RANGING SYSTEMS

B.A. Greene

1. Introduction

The precision of satellite laser ranging systems has improved dramatically over the past 10 years. It is now possible to obtain, within 2 minutes, over 400 range measurements to satellites 1-10 000 km distant, with each measurement having associated with it an uncertainty of only 8 mm. Data of this quality and quantity allow the satellite position to be described with a statistical uncertainty of 0.4 mm each 2 minutes ('normal' points). Even better performance can be expected in the future.

Clearly, the accuracy of the measurement will depend on systematic error terms which must be removed from the data by means of system calibration. In this paper the characteristics and in particular the deficiencies of existing calibration techniques are reviewed. It is found that no existing technique can provide sub-millimetre accuracy and thus allow removal of all systematic errors to below the noise level of the 2-minute satellite range normal point presently being obtained.

Two new techniques for calibration are then proposed.

2. Current Calibration Techniques

There are currently two modes of calibration in general use in operational laser ranging systems. These are:

- . target board calibration
- . real-time calibration

Target board calibrations utilise a sequence of range measurements to a fixed terrestrial target to determine the system constant delay. These calibrations are normally carried out to a target 0.2 - 4.0 km distant on a regular basis, and always before and after a ranging operation (satellite pass). This technique is deficient in several ways:

- . It includes a component of system delay which is not replicated in ranging mode - the horizontal path;
- . It gives the system delay before and after the pass, not during the pass, which is the time of interest;
- . Because the range is short, critical errors in elapsed time measurement are not sampled in those systems utilising time-interval techniques;
- . The technique is limited by survey accuracy, which is sometimes poor because of inaccessibility of system reference points;

- . Because the range measured is so short, the return signal enters an electromagnetic environment which can be different from that experienced by a satellite return (electromagnetic asymmetry);
- . Because of the way calibrations are made, the system is very open to abuse. It is not rare for post-ranging calibrations to be continued by operational crews until a 'satisfactory' result is obtained.

To overcome these disadvantages, the real-time calibration (RTC) technique was pioneered by the University of Texas. This technique uses real-time optical feedback to the detector, via the same (identical) path as the range measurement uses, to determine on a shot-by-shot basis the system delay. A great benefit of the technique is that any system hardware element, even in the measurement chain, can be modified, repaired, or replaced without adversely affecting the system delay or the calibration accuracy, as the system delay is measured during the ranging process each time. Another major benefit is that the calibration data is securely written into the 20-30 000 long record of ranging, and is virtually tamper-proof, so a true record of station calibration is assured.

The RTC technique also has several disadvantages:

- . the range is still very short, so electromagnetic asymmetry will apply;
- . the calibration (feedback) path does not usually include all of the transmit and receive optics, so some categories of system delay associated with (e.g.) misalignment of optics may pass undetected, and cause systematic errors.

Figures 1-4 show the result of real-time calibration of a state-of-the-art SLR system, the Natmap/NASA Laser Ranging System at Orroral (Australia). The time walk of this system is evident in these figures, which show actual RTC results for 4 consecutive LAGEOS passes taken in July 1986, plotted as 1 minute normal points. Also clearly evident is that pre- and post-calibration techniques would show differences of up to 2 mm, with no indication possible of how the system temporal drift took place in terms of time distribution.

According to the theory of RTC, time walk in a system monitored by RTC is irrelevant, since RTC gives the system delay as a function of time. However, it is not common for analysis centres of SLR data to allow a time-varying system delay, despite the physical impossibility of it being anything other than time-varying. This has been because very few stations can determine time-dependent system delay during ranging, and also because errors arising from taking system delay as a constant are rarely greater than 5 mm. A 5 mm maximum error has, until recently, been acceptable.

3. Real Time Differential Range Calibrations

The data shown in Figures 1-4 is typical of Orroral calibration (RTC) data. It contains some interesting features which suggest fine temporal structure within the system delay at the 1-2 minute scale. A second real-time calibration, to a target at a different range from that used for the existing RTC, should reflect all real temporal structure in the RTC estimate of system delay. In addition, if the range difference between the two targets was known, then the accuracy of the system can be

determined, since the difference in system delays should equal the range difference between targets.

Since it is trivial to obtain optical mounts, rails, and components which can be positioned to 0.1 mm or better, an extremely precise accuracy calibration of the system is possible, if the system is based on epoch timing, as all submillimetre systems must be. Epoch timing is essential because even events closely spaced in time, such as two calibration pulses, will be jointly random in phase with respect to the epoch timing system timebase, and so will sample the error space randomly, as desired. If the differential range is never varied, some sectors of error space are never sampled due to the fixed phase relationship between calibration pulses. That is, the first event is random in phase with respect to the system time base, but the phase of the second is completely determined. In practice it has been found that only a few differential range settings are required to establish accuracy, with occasional changes to the differential delay sufficing to maintain it. For a properly designed timing system the error due to completely ignoring the fact that the two calibration epochs are correlated is never more than 0.5 mm RMS.

The result of applying real-time differential range (RTDR) calibration to the NLRS is shown in Figures 5 and 6. The range difference used was 19.0 picoseconds, and the two real time calibrations can be seen together in Figure 5 against elapsed time. In Figure 6 the difference between the two calibrations minus the known range difference (system error) is plotted against elapsed time. The accuracy specification of the NLRS at this time was 0.5 mm, and the calibration data for this pass gives:

| | | | |
|-----------------------------|---|-------|----|
| True range difference | : | 19 | ps |
| Average measured difference | : | 17.95 | ps |
| Standard deviation | : | 3.0 | ps |
| Mean error | : | 1.05 | ps |

Clearly, despite the evident loss of calibration after approximately 20 minutes of ranging, the specification is met. The error from 20 minutes onwards was due to a temperature change in one part of the timing system. When these excursions can be controlled, a specification of 0.25 mm RMS is achievable, as can be seen from the initial data segment of Figure 6. Absolute calibration using RTDR methods is contributing significantly to the refinement of timing circuits and techniques for SLR.

The RTDR method allows tracking of system delay to 0.1 mm accuracy. However, it suffers from the same principal deficiencies as the conventional RTC method from which it was derived, i.e.

- . electromagnetic asymmetry
- . some potential errors (optical) not sampled.

Testing using the actual ranging environment whilst electrically and magnetically shielding detector and timing systems can determine the impact of transient electromagnetic fields on the SLR system. Independent tests can be made by generating optical pulses using high speed laser diodes to avoid electromagnetic transients, and observing the performance of the SLR system under calibration. As a result of such testing at the NLRS, conventional PMTs are completely magnetically shielded in mu-metal cases for operations. At the 0.5 mm level MCP PMTs do not exhibit bias in magnetic fields such as are generated by typical SLF laser systems.

The sampling of all possible errors in a SLR system requires additional calibration techniques.

4. Terrestrial Target Array Calibration

SLR systems normally define their site coordinates in relation to a number (at least three) of intervisible prime geodetic marks within 100 m of the SLR system. It is normal for all marks on the site, or in the case of a mobile SLR, on the pad, to be subordinate to these prime marks, which can be surveyed and located to 1 mm RMS in 3 coordinates.

State-of-the-art SLR systems can provide 0.5 mm precision over virtually any range, as well as possessing sub-arcsecond precision readout of angular position. If these capabilities were utilised to connect the SLR system directly to the prime geodetic markers, many advantages could be obtained:

- . The accuracy of the SLR system could be determined in the context of conventional geodetic measurements. Although the SLR system can be accurately calibrated by RTDR, a second calibration is afforded by the closure calculations when surveying the control marks. In this application the marks are used as ultra-high precision terrestrial targets, the redundancy in which yields a measure of system accuracy.
- . Monitoring of tilt, subsidence, and local movement is automatic. This is useful for fixed stations, and for mobile systems allows the concept of a highly mobile 'padless' design. That is, a mobile SLR which does not require a concrete pad or the normal marks contained in/on it. This greatly enhances mobile SLR productivity and flexibility.
- . A proliferation of instruments (and errors) is avoided, as the ranging system surveys itself onto the site, and maintains its own coordinates.
- . If the geodetic markers are fixed in any major datum, very good initial offsets for mount modelling of the telescope can be obtained from the terrestrial targets alone. Similarly, mount model recovery can be expedited, even if the marks have not been fixed.
- . Any desired reference point in the SLR system can be solved for.

In practice, a specially constructed target must be placed very precisely on each marker. Ranging to at least 3 targets produces a sub-millimetre solution for horizontal coordinates. The 3-D error ellipsoid is elongated in the vertical direction, because all targets are approximately coplanar. However, arcsecond precision elevation angle observations readily produce sub-millimetre vertical coordinates over 100 m distances. Once angle and range observations have been combined, the solution can be obtained. Six targets, randomly distributed in azimuth, are recommended. This allows for one or two marks to be damaged, obscured, or inaccessible at any time, whilst still providing adequate redundancy for sub-millimetre solution.

The technique is clearly sensitive to survey errors in the ground geodetic marks. In practice it is not difficult to isolate one or two errors from the solutions. Scale errors can also be easily detected, although not attributed. In general, if a sub-millimetre solution is not possible

initially, with the geodetic marks constrained in 3 dimensions by the ground survey results, then the mark coordinates must be unconstrained, and small adjustments made as the optimum solution for station coordinates is sought. Releasing the constraint on the marker coordinates is not done unless the SLR system has successfully calibrated at all other levels. This procedure could be necessitated by ground survey error, target installation (on mark) error, or atmospheric model error. Standard geodetic techniques can apply to the establishment and maintenance of the station coordinates and system delay determined by this technique.

The single weakness in this technique is that elevation-dependent misalignments which can cause systematic error are not sampled. An additional, infrequent, calibration technique must be applied to measure these errors. This technique involves the erection of a simple calibration jig which allows retroreflectors to be placed at any point in the transmitted beam, and RTC to be executed as elevation angle is altered. Rigorous testing is tedious and time consuming, but is required very infrequently. Mobile systems could be taken to a standard calibration facility, whilst fixed systems can more readily program the effort required on-site.

References

1. E.C. Silverberg, "The feedback calibration of the TLRS ranging system", in Proc. Fourth International Workshop on Laser Ranging Instrumentation, (University of Texas, Austin, Oct 12-16 1981). Bonn: Geodetic Institute, University of Bonn, 1982, pp. 338-351.
2. B.A. Greene, "Epoch timing for laser ranging", in Proc. Fifth International Workshop on Laser Ranging Instrumentation, (Herstmonceux Castle, September 10-14, 1984). Geodetic Institute, University of Bonn, 1985, pp. 247-250.

Figure 1

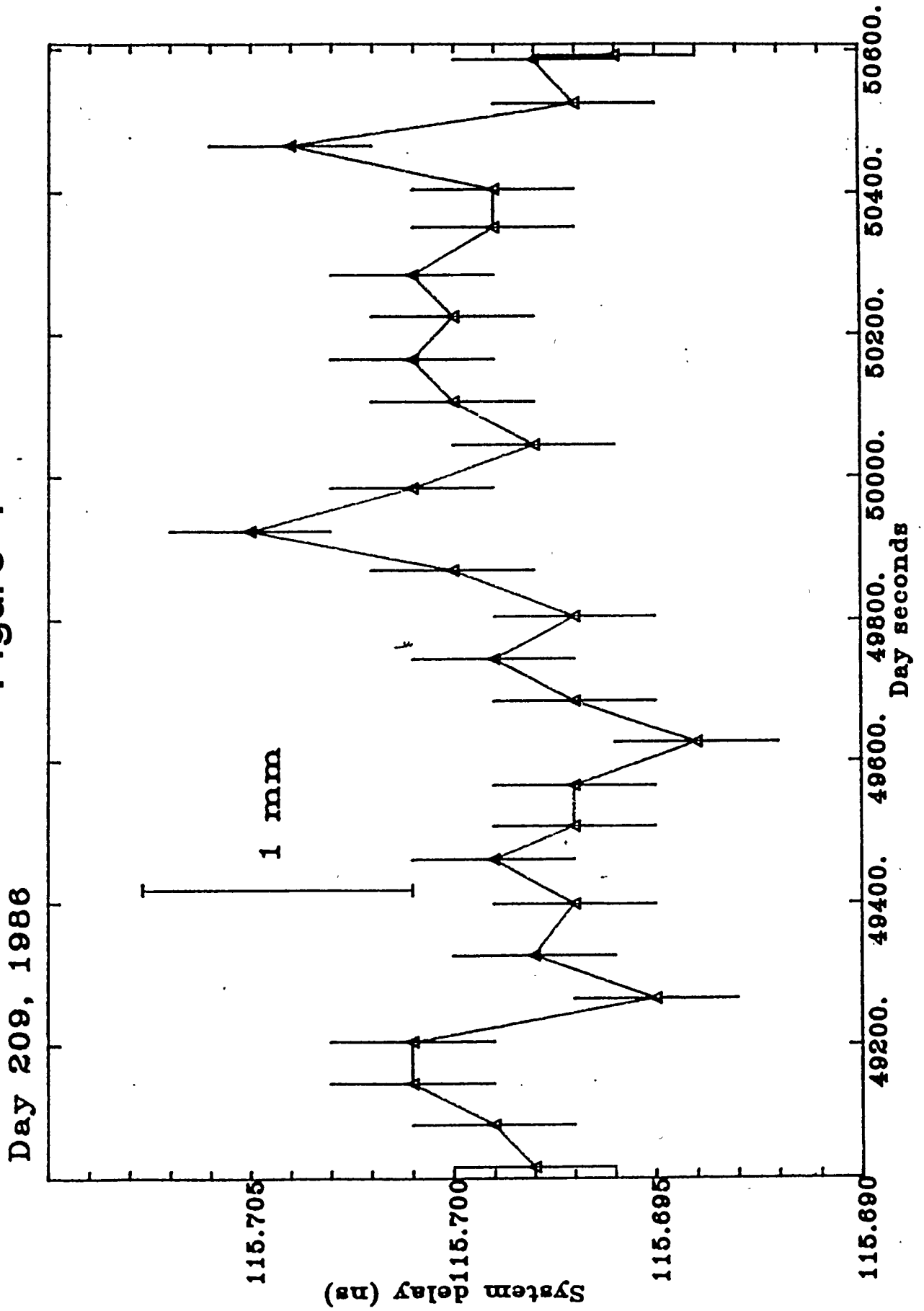


Figure 2

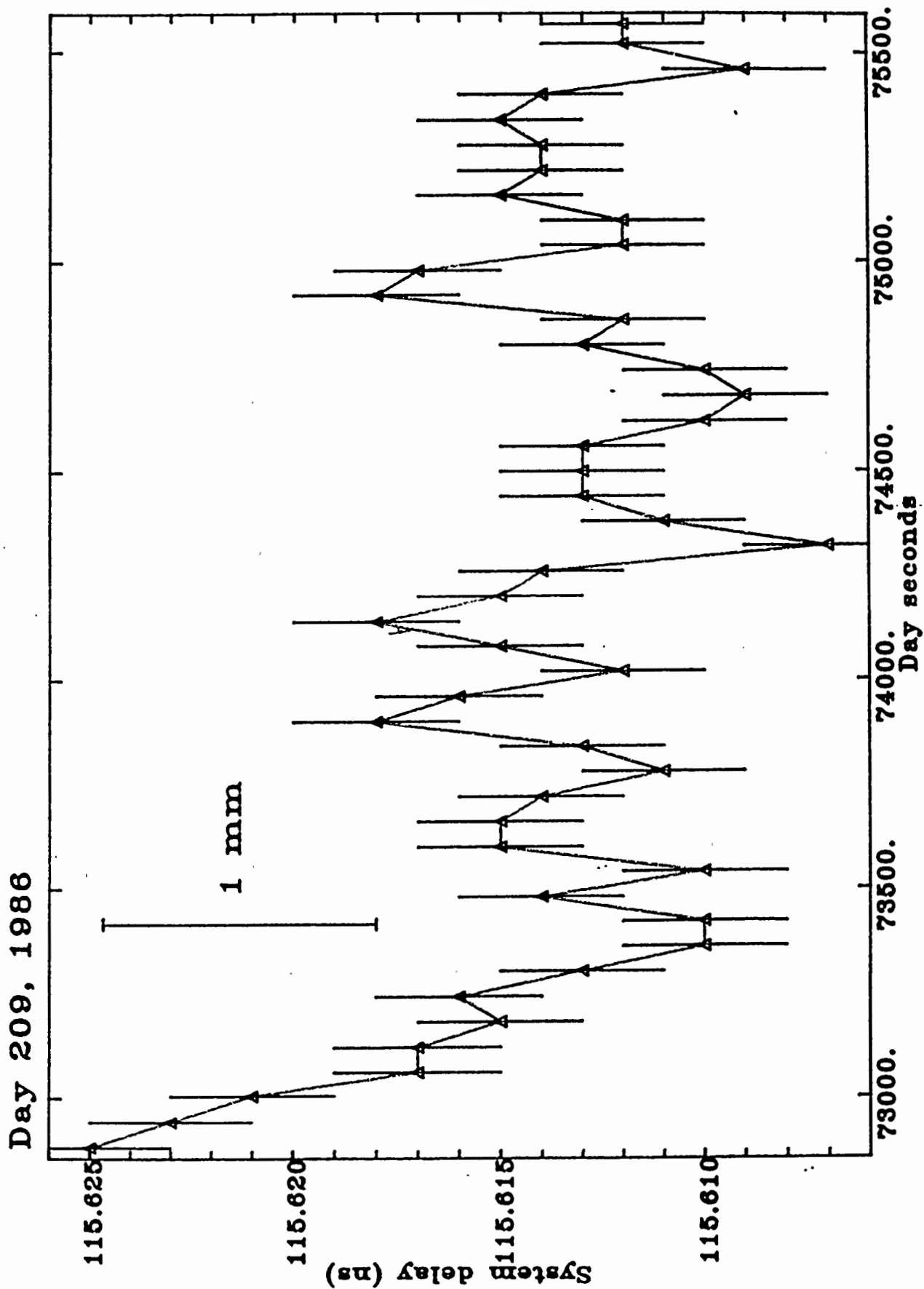


Figure 3

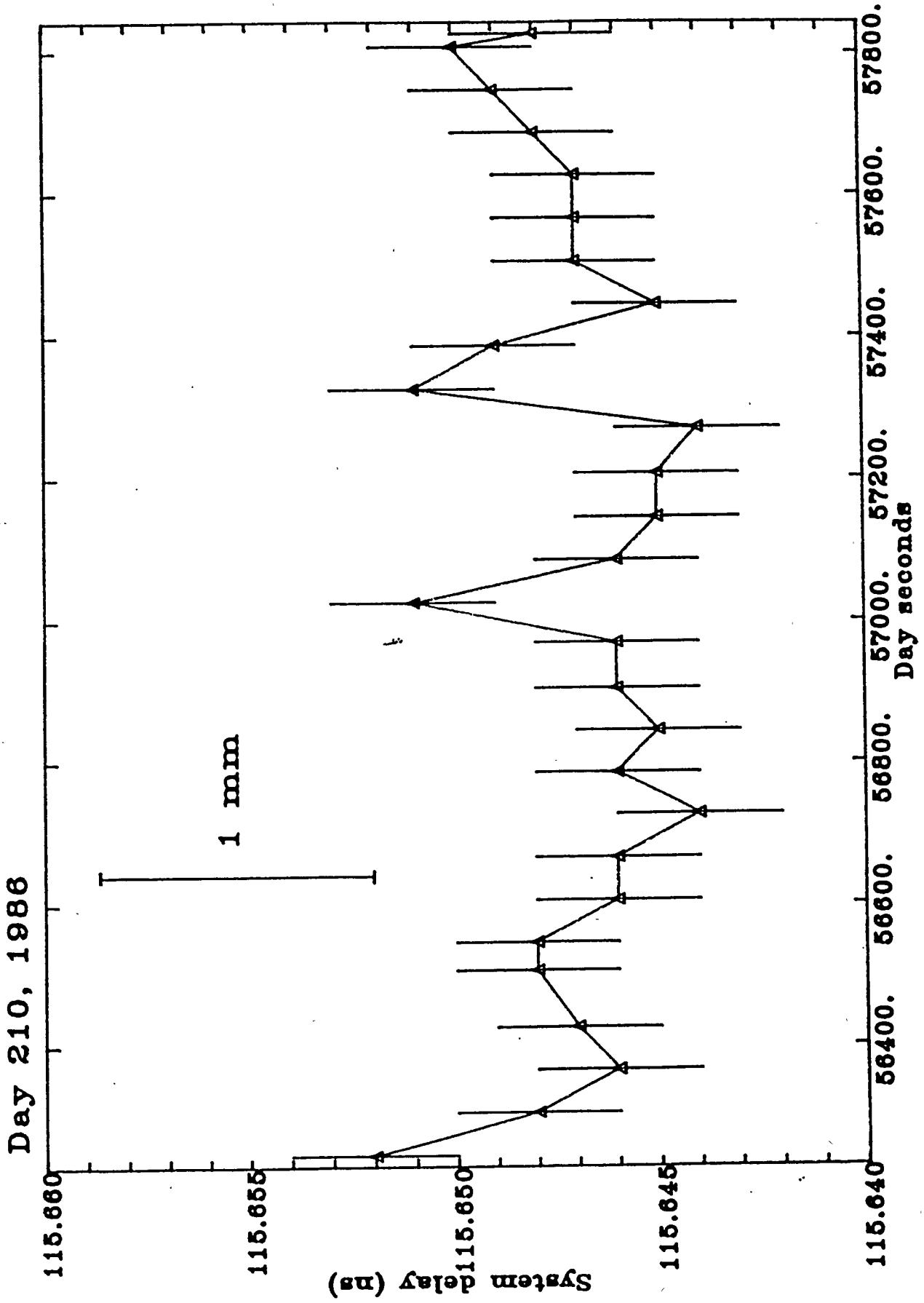
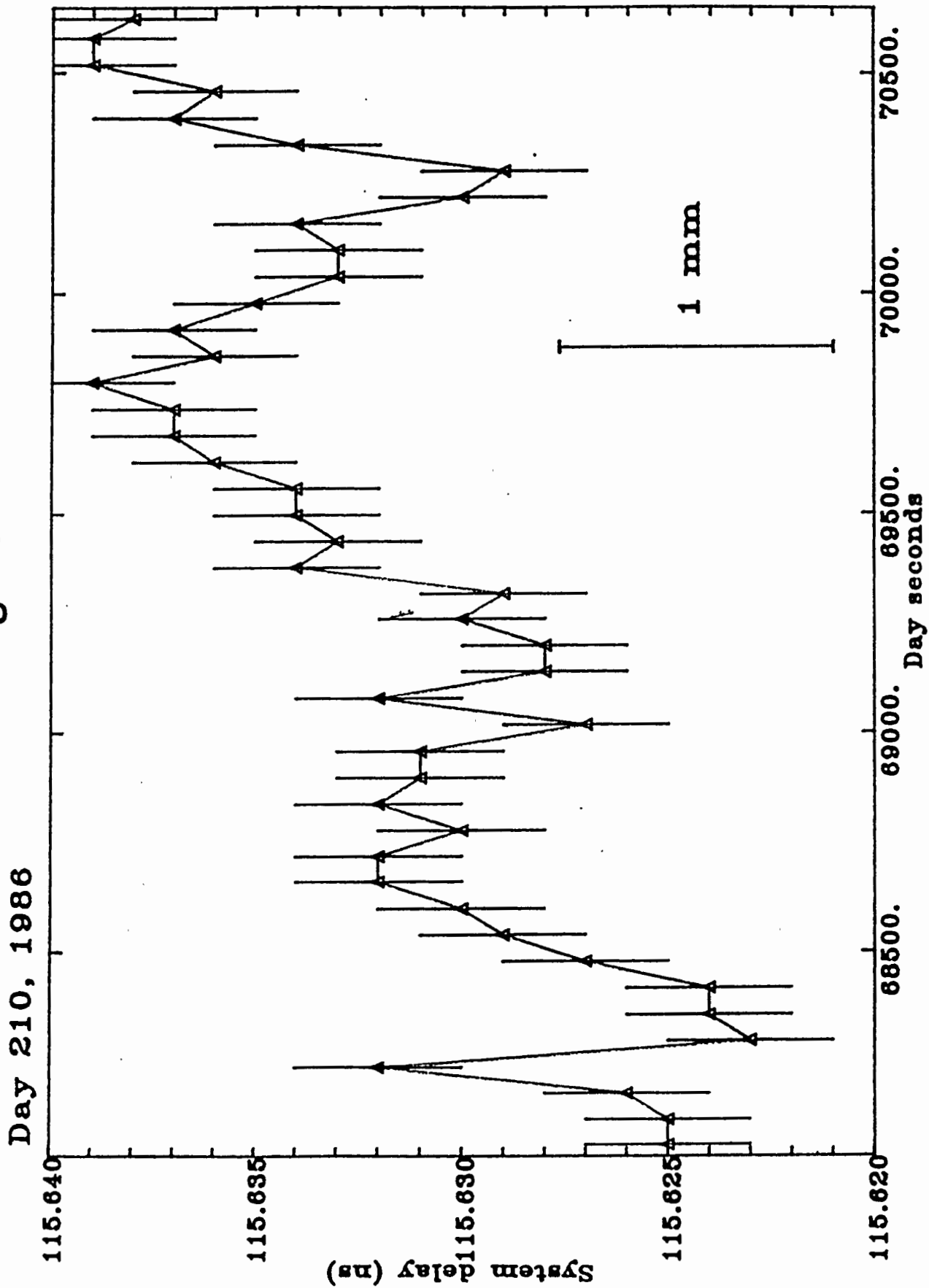


Figure 4



Calibrations

Real-Time Differential Range (RTDR)

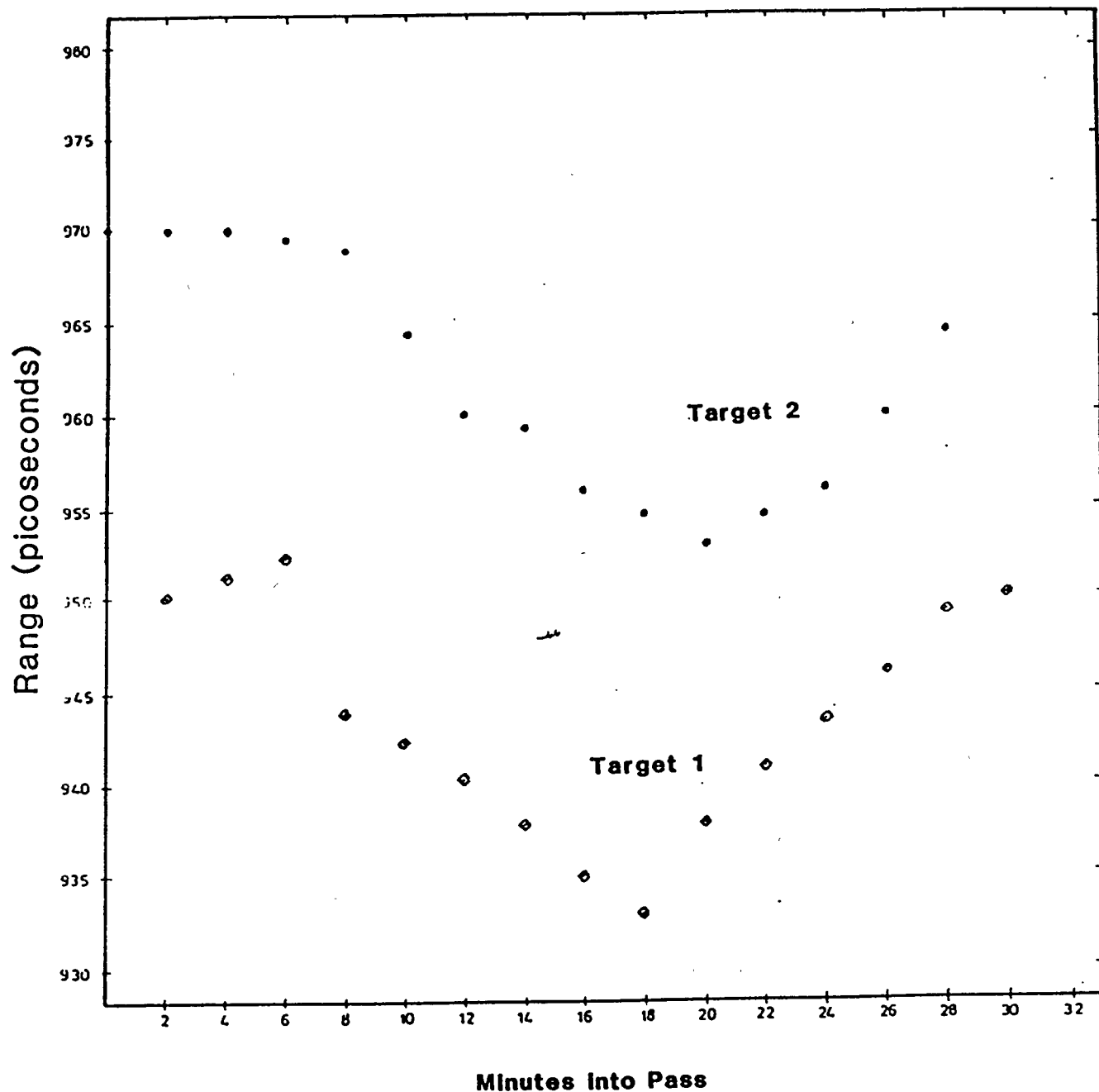


Figure 5

NLRS ACCURACY

Determined by Real-Time Differential Range Calibrations

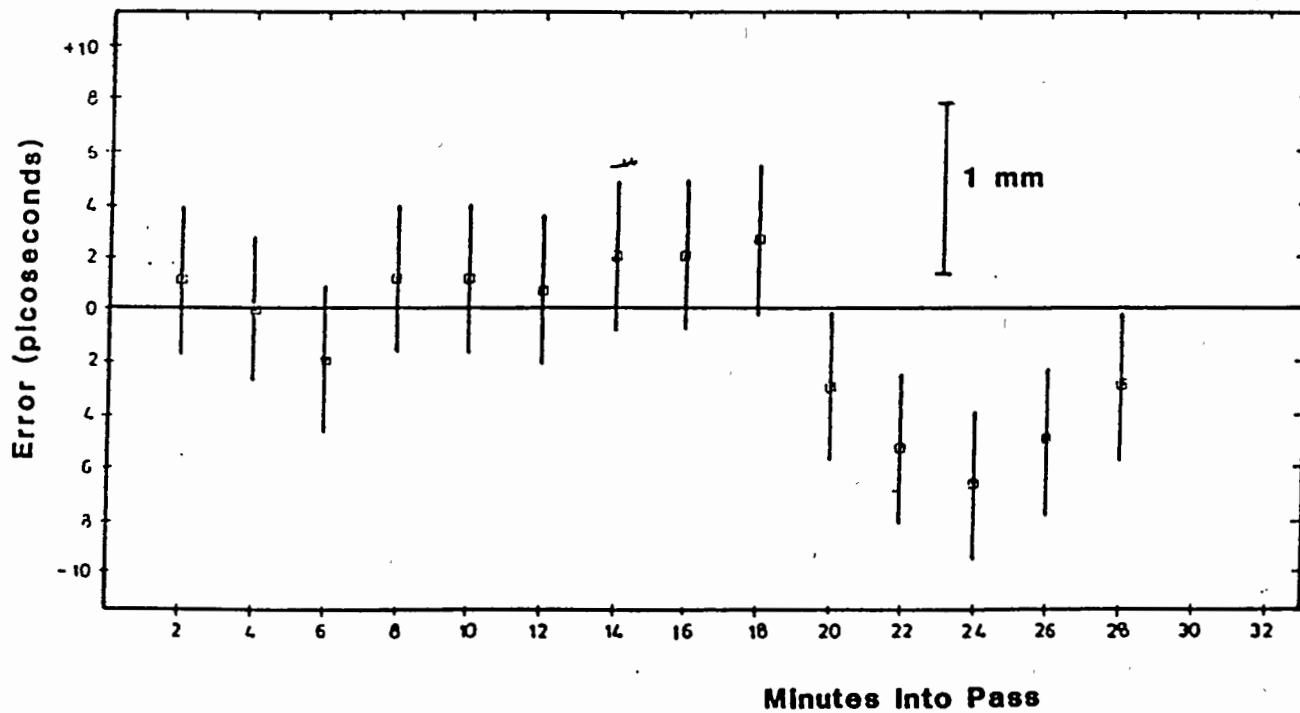


Figure 6

MEASURING AND MODELLING PULSE DISCRIMINATOR AMPLITUDE DEPENDENCE

P. Kloeckler, Th. Schildknecht
Zimmerwald Satellite Observation Station
Astronomisches Institut
Sidlerstasse 5,
CH - 3012 BERNE - Switzerland -

Telephone 4131 65 85 91
Telex 912643 PIBE CH

ABSTRACT

Amplitude dependence of the return pulse discriminator contributes significantly to the ranging-machine error budget, if multiphoton ranging is considered. Constant fraction discriminators of improved design are most commonly used to reduce this dependence, yet these must be - and remain - well adjusted. Even then, a rest of doubt remains, because characterizations are often done in an ideal, not real, test environment.

The present paper introduces a characterization method which confronts the discriminator under test with a real ranging environment. The same setup is also used to monitor the performance during the ranging session.

Several discriminator types have thus been investigated, and attempts undertaken for computer-modelling of remaining systematic errors.

1. AGAIN: THE TIME-WALK PROBLEM

This problem, as illustrated in Fig.1 for a simple fixed-threshold discriminator, seemed solved when the stations changed to picosecond lasers and single-photon ranging. This resulted in a very limited dynamic range of echo-pulse amplitudes; multi-photon events were deliberately purged from the data by signal attenuation and data screening. Any remaining amplitude dependence was taken care of by a constant fraction discriminator and hence deeply buried in the timing noise caused by the photomultiplier. (5..15 cm r.m.s.)

However, after some operational experience with the new or upgraded systems it was found that multiphoton-events were sometimes quite numerous -perhaps caused by "hot spots" in the laser beam- and operators had to be alert to react accordingly.

With the advent of microchannel-plate photomultipliers, the situation changed again. The r.m.s. values dropped to the 1..3 cm level, and millimetre precision ranging to satellites became feasible. Systematic errors had to be reduced accordingly: better constant-fraction discriminators were selected | 2 |.

Another trend that became apparent was the revival of multi-photon ranging with stations affording large telescope apertures and more powerful lasers: the dynamic range of the received signal became larger again and had to be well controlled for the ultimate in precision.

The japanese satellite AJISAI with its great effective cross-section and diameter imposes such a pulse distortion (Fig.2), so that it was suggested to use some sort of leading edge detection to preserve the inherent ranging precision of the observing stations.

To conclude this brief review, we suggest that the discriminator problems are far from solved, and it is certain that new products and concepts will continue to be introduced into the LRS's. Prior to their introduction, however, they have to be sufficiently well characterized to make sure that no additional systematic errors will bias the low r.m.s. data.

2. CHARACTERIZATION OF TIMING CHANNELS

CHARACTERIZATION MEANS DETERMINATION OF ALL RELEVANT SYSTEM PARAMETERS WITH REGARD TO ALL RELEVANT VARIABLES (TIME, TEMPERATURE, GEOMETRY, AMPLITUDE, NOISE ETC.).

In practice, though, only a few parameters are characterized, while others are either thought to be less relevant, have been measured once by some reputed agency | 2 |, or it is depended upon the manufacturer's specifications. This attitude is possible because a total system delay is elaborated frequently in which all individual parameters are lumped together. Nevertheless, we sometimes would like to determine individual parameters for optimization.

An ideal setup for characterizing a typical timing channel (consisting of: optoelectronic detector, solid-state amplifiers, cables, pulse discriminator and time-interval digitizer) would include an optical pulse source, a variable attenuator, some pulse amplitude measuring device, a background events counter, an oscilloscope or pulse digitizer and a computer. (Fig.3)

Our practical installation, though presented earlier | 3 |, is depicted in Fig.4. We use our actual ranging equipment for the characterization, with only a few additions: a lid on the receiving telescope with an iris diaphragm for control of background illumination, a counter and a second fast photodiode to provide an additional, low jitter stop-channel. A pulse generator for simulating pulses of variable width (from 1 ns FWHM) exists, but is not used for amplitude characterizations because of inevitable time shifts when attenuating the pulse. The internal feedback path used for in-pass calibration readily can be used for characterizing a chain of devices, which are intended to work together. The advantages against testing individual devices separately in the laboratory are numerous:

- *A similar electro-magnetic environment is effective as when actually ranging to satellites
- *Optical attenuation introduces no variable delays (as electrical attenuation might do)
- *Possibility of verification any time and on site
- *Pulse shapes¹, amplifier distortions, cable bandwidth limitations and background noise as in real LRS

3. TESTS

3.1 DEVICES UNDER TEST

Two types of discriminators have been tested so far:

-FIXED THRESHOLD: Various models (LeCroy 120, 623 and 4202, the latter included in the time digitizer) differ mainly in the number of channels and the minimal thresholds available. Threshold in the 4202 can be set as low as -5 mV, thus affording additional receiving gain. Their amplitude response is smooth and naturally reflects the leading edge of the input signal. It easily can be modelled (viz. Appendix). They behave well also with sub-nanosecond pulses.

¹ One fundamental limitation of the concept is the failure to simulate the target depth function. We have to trust that the transmitted pulse shape is only slightly altered by the satellite's reflectors.

-CONSTANT FRACTION: The earlier "network-standard" Ortec model 934 has caused serious time-walk problems even with the 3 ns FWHM pulses of our conventional photomultiplier | 3 |. The device is not specified for sub-nanosecond pulses. Minimum threshold is -30mV, but it was found that up to -100 mV operation was not satisfactory. Adjustment of minimum walk is a cumbersome procedure.

A successor (ETL 103 model) features an automatic walk adjustment utilizing a slow feedback loop to keep the DC/level at the input zero. It also allows a minimum threshold setting of -5 mV, and contains a faster trigger circuit.

The new Tennelec 454 model arrived just recently; hence we cannot comment much on its merits. Initial tests indicate a significant improvement in performance and ease of adjustment. However, it was noted that a slewing effect near threshold also exists.

3.2 TEST PROCEDURE

The program for internal calibration was run, which operates the laser and data acquisition. The stop ND-filter was placed in an initial position, attenuating the laser pulse to single-photon level. Then a short calibration run was performed to aid adjustment of the start ND-filter(to make sure that the start detector was operating in its specified amplitude range). After this, a few hundred calibration points were taken while opening the stop-ND filter to run through the dynamic amplitude range at the receiving side. After completion, the relevant variables were noted and the data-set screened. A following computer evaluation yielded the time-delay vs. amplitude curve.

As an optoelectronic detector, both photomultipliers and a PIN diode were used. Time intervals were measured with the LeCroy 4202 TDC and not with the HP counter for practical reasons.

3.3 RESULTS OF MEASUREMENTS

Some results are summarized in the table below and plotted in Figures 5-12:

Figs. 5 and 6 reflect the amplitude dependence of a typical constant-fraction and leading-edge discriminator, respectively. They were taken using a conventional photomultiplier.

In Figs.7 and 8, the effect of modelling the amplitude dependence of a fixed-threshold discriminator is shown. Here, the microchannel- detector was used.

Fig. 9 shows the effect of linearly modelling the same constant-fraction discriminator as in Fig.5. The slewing near threshold still visible in Fig. 5 was removed by raising the threshold.

In Fig. 10 the improved constant-fraction discriminator is characterized, using the diode detector.

Figs. 11 and 12 show the effect of modelling on the residuals of a satellite pass, which was AJISAI, observed by microchannel-plate.

The results of the amplitude dependence characterizations are summarized in the following table:

SUMMARY OF RESULTS

T I M E - W A L K
(ALL VALUES IN PICOSECONDS PEAK)

| DETECTOR TYPE: | D341 (PM) | R1294 (MCP-PM) | HP-5082 (DIODE) |
|----------------------------------|--------------|-------------------|--------------------|
| METHOD: | | | |
| CONSTANT FRACTION (NO MODEL) | | | |
| ORT 934 | ±210 @ 1:10 | | |
| | ±650 @ 1:50 | | |
| ETL 103 | ±460 @ 1:10 | | |
| | ±630 @ 1:30 | | |
| TENN 454 | | ±125 @ 1:10 | ± 55 @ 1:5 |
| | | ±175 @ 1:50 | ±285 @ 1:10 s |
| CONSTANT FRACTION (LINEAR MODEL) | | | |
| ORT 934 | ±200 @ 1:10 | | |
| | ±200 @ 1:50 | | |
| ETL 103 | ±210 @ 1:10 | | |
| | ±210 @ 1:30 | | |
| FIXED THRESHOLD (NO MODEL) | | | |
| LCR 4202 | ±780 @ 1:10 | ±120 @ 1:10 | |
| LCR 623 | ±725 @ 1:10 | | |
| FIXED THRESHOLD (LINEAR MODEL) | | | |
| LCR 4202 | ±325 @ 1:10 | | |
| FIXED THRESHOLD (GAUSS MODEL) | | | |
| LCR 4202 | | ± 80 @ 1:10 | |

s Note: TIME "SLEWING" NEAR THRESHOLD

4. REFERENCE

| 1 | J. J. DEGNAN

SATELLITE LASER RANGING: CURRENT STATUS AND FUTURE PROSPECTS
IEEE TRANS. ON GEOSCIENCE AND REMOTE SENSING
VOL. GE-23, NO. 4, JULY 1985, P. 398

| 2 | M. R. PEARLMAN

SLR GROUND TESTS
CIRCULAR DATED AUGUST 2, 1985

| 3 | P. KLOECKLER, I. BAUERSIMA

IN PASS CALIBRATION DURING LASER RANGING OPERATION
PROC. OF THE FIFTH INTERNATIONAL WORKSHOP ON LASER RANGING
INSTRUMENTATION, HERSTMONCEUX CASTLE, SUSSEX, ENGLAND
VOL. I, P. 194

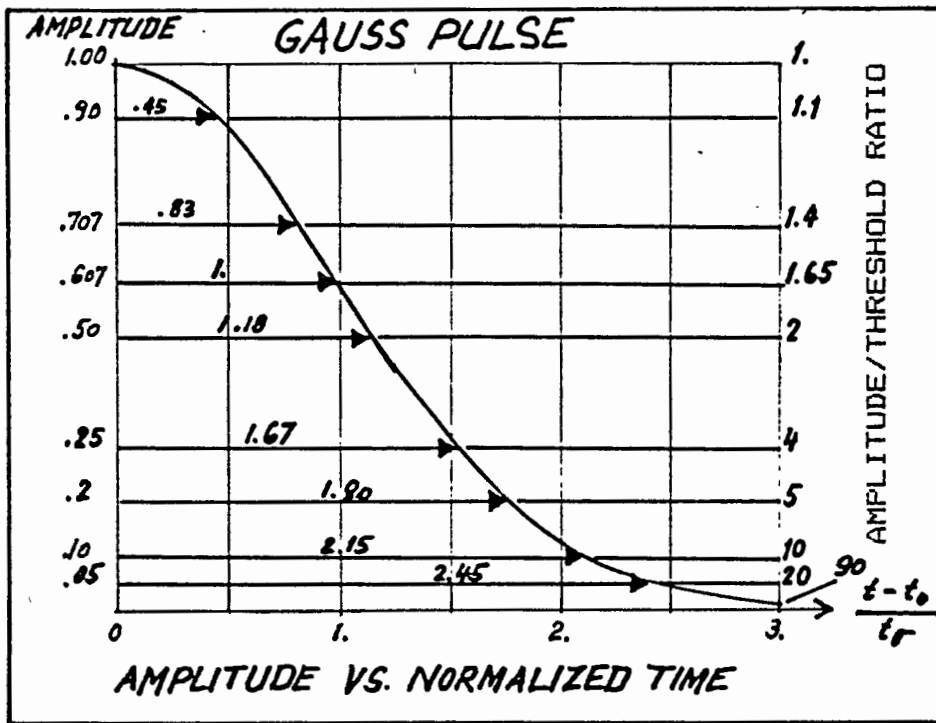


FIG. 1 CORRECTIONS FOR AMPLITUDE DEPENDENT ERROR:
(FIXED THRESHOLD DETECTION)
1 ns t_0 Pulse Width assumed

| A/T ratio: | correction in ns: |
|------------|-------------------|
| 1.0 | 0 |
| 1.65 | 1.00 |
| 5.0 | 1.80 |
| 10.0 | 2.15 |
| 90.0 | 3.00 |

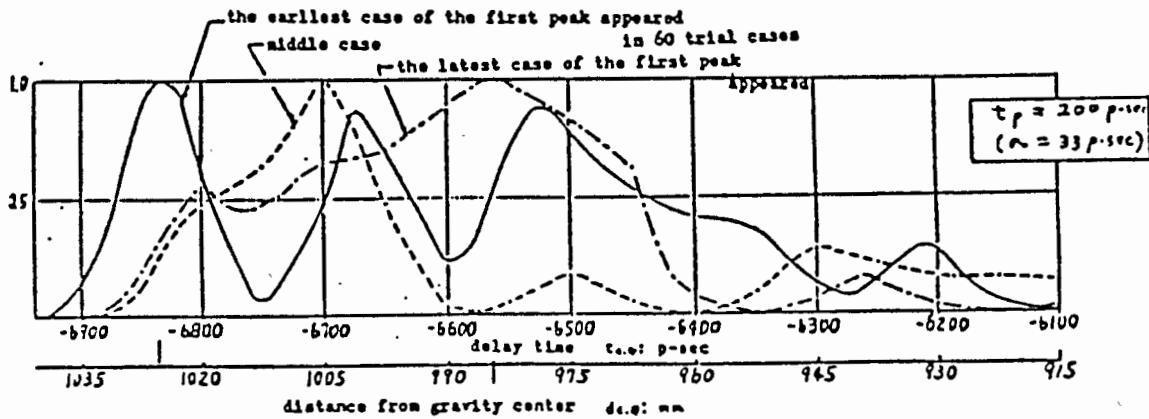


FIG. 2 RETURN PULSE FROM "AJISAI"
Results of Computer Modelling

Courtesy:
M. SASAKI
HYDROGRAPHIC DEPT.
OF JAPAN

FIG. 3 IDEAL SETUP FOR AMPLITUDE DEPENDENCE CALIBRATION

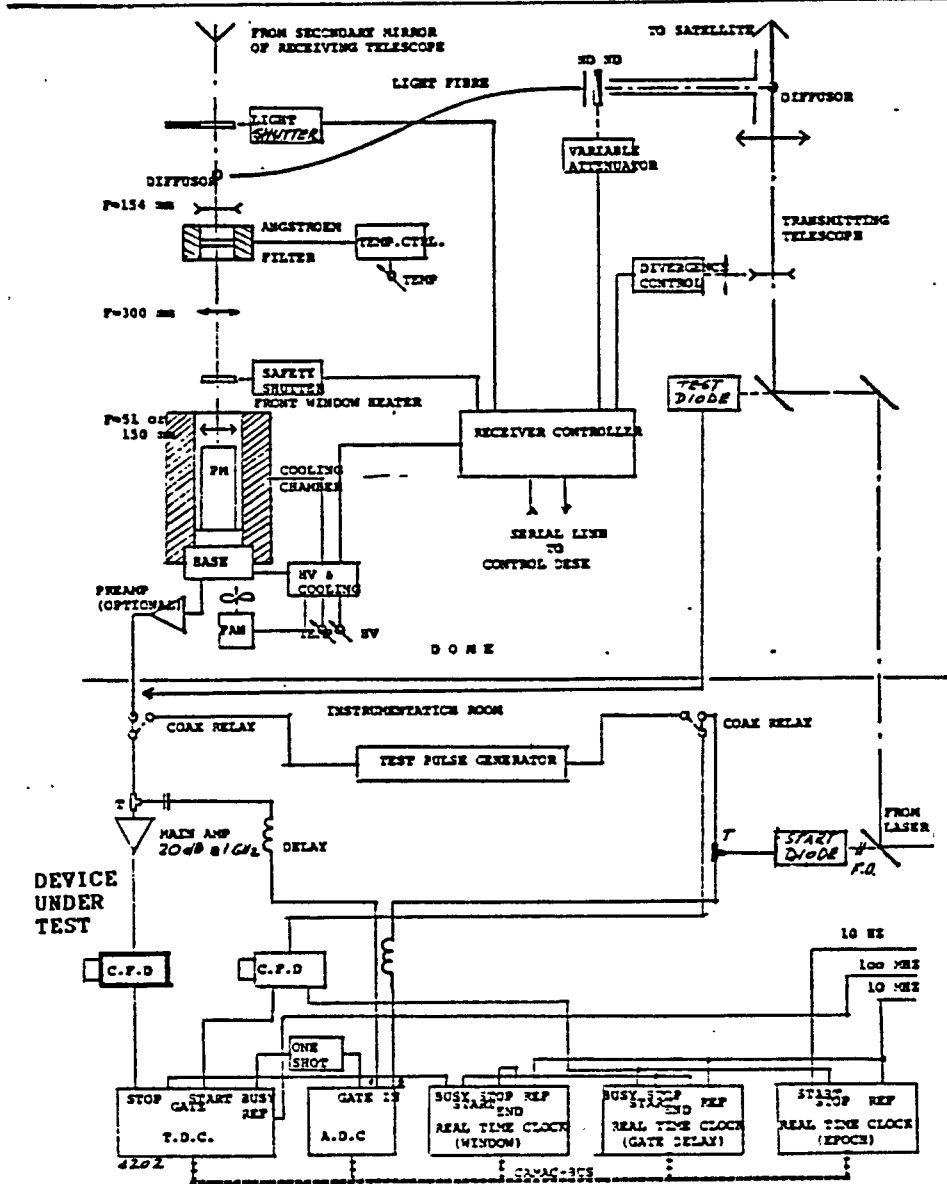
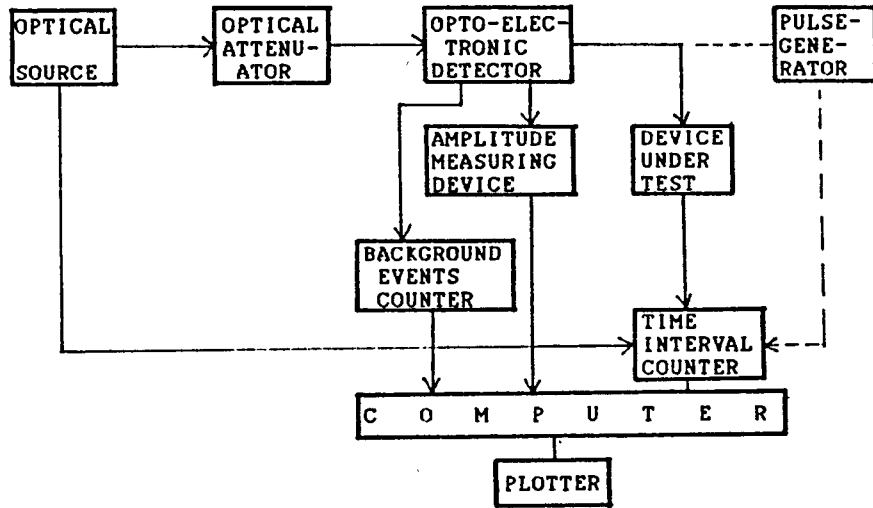
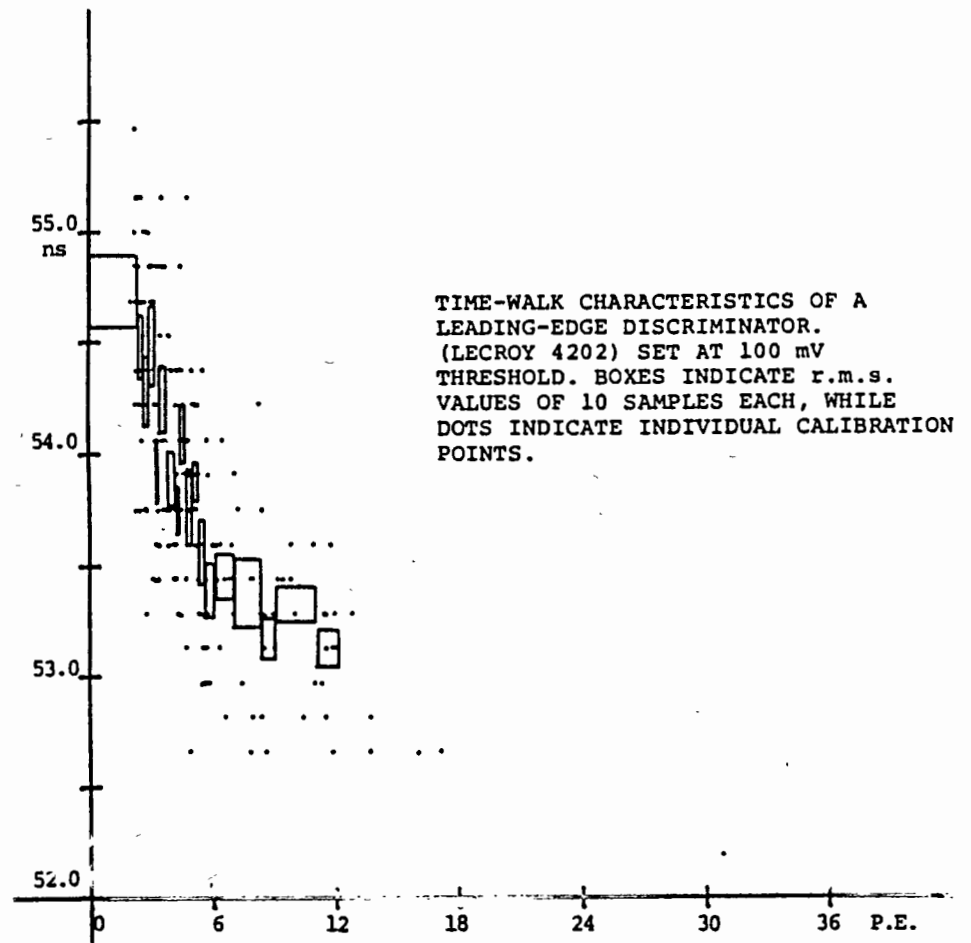
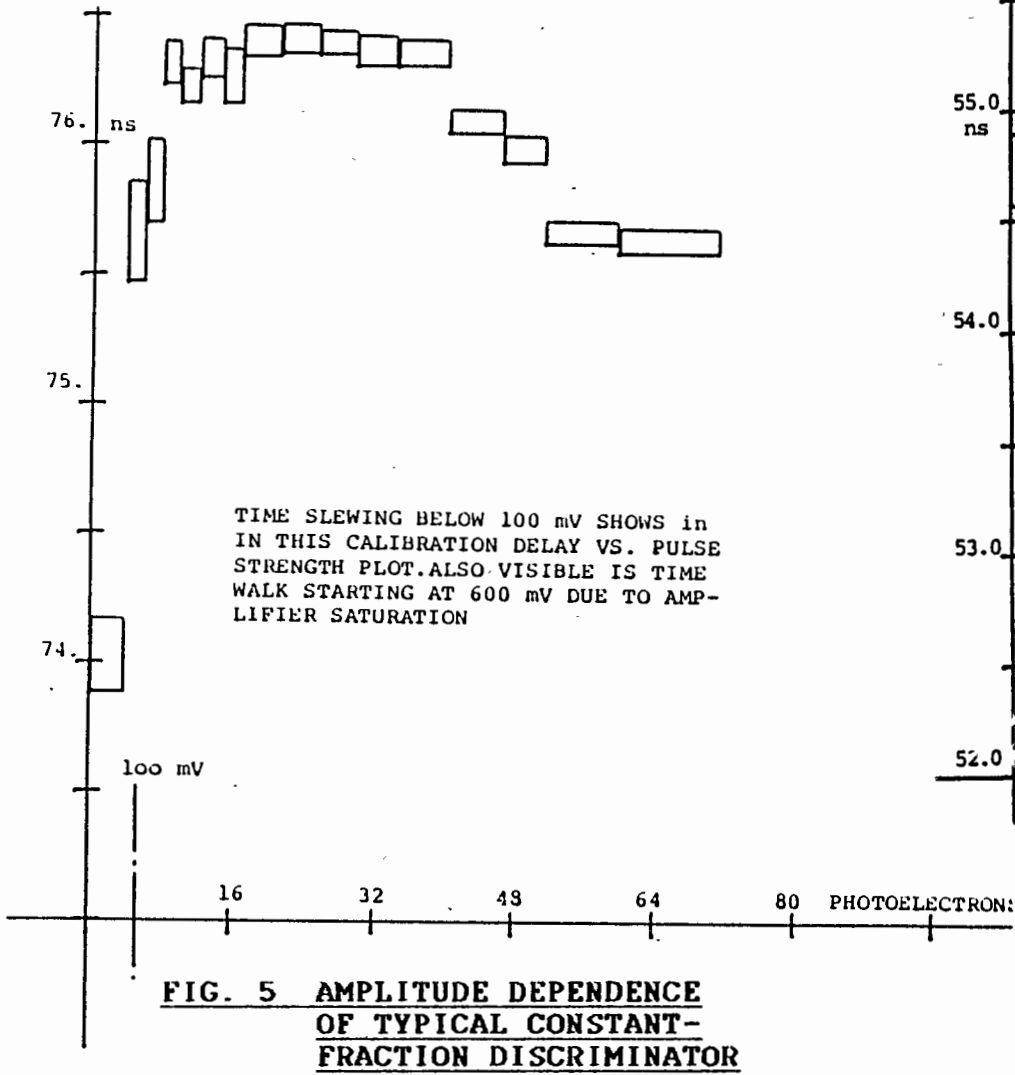


FIG. 4 CALIBRATION SETUP USING INTERNAL OPTICAL FEEDBACK



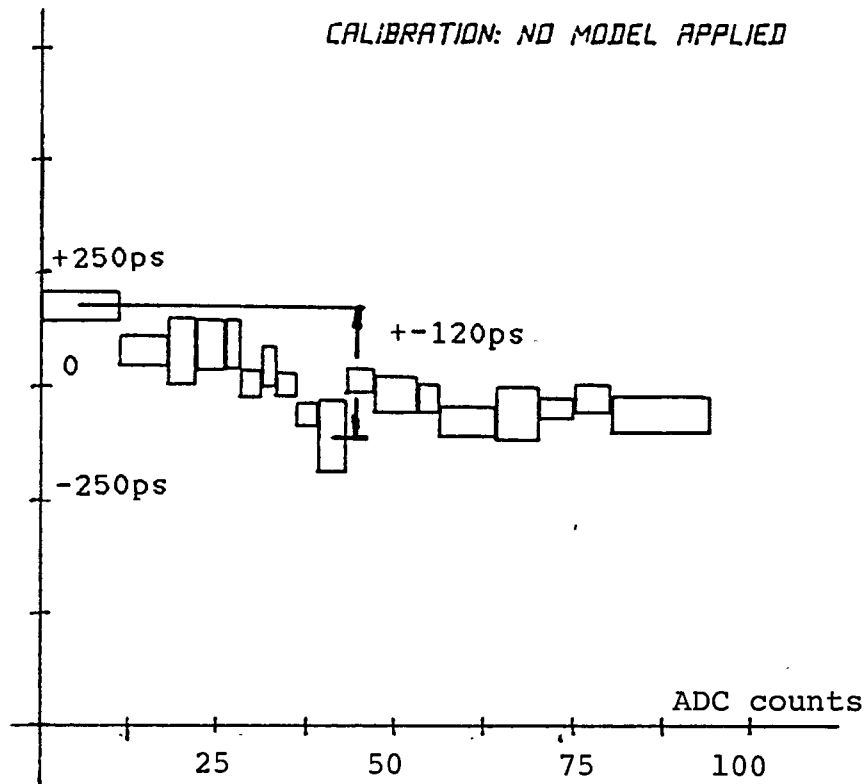


FIG. 7 FIXED-THRESHOLD DISCR.:
UNMODELLED

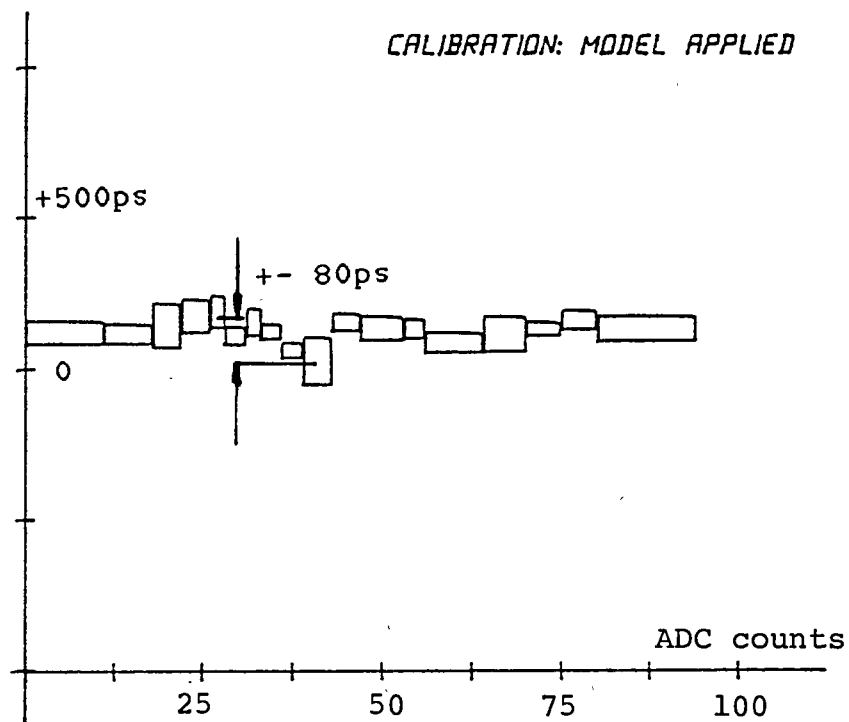
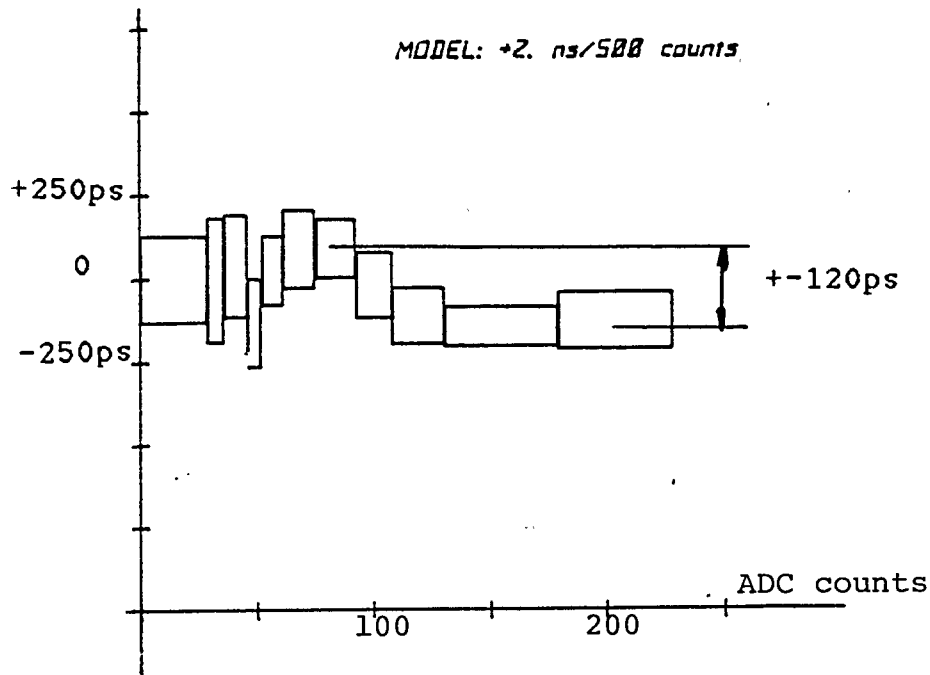
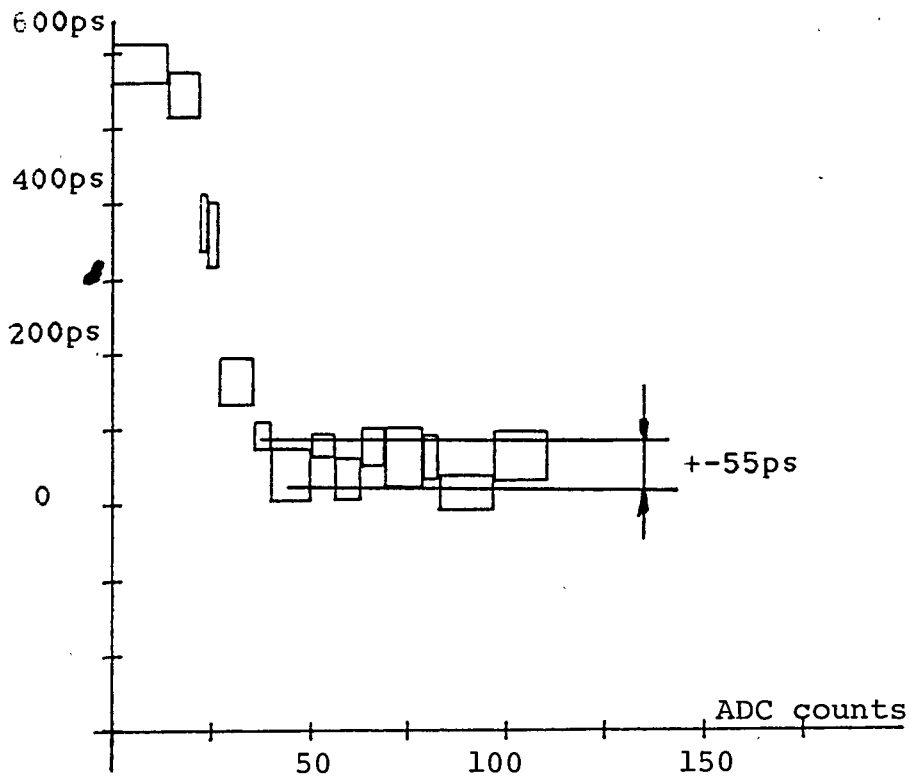


FIG. 8 FIXED-THRESHOLD DISCR.:
MODELLED



**FIG. 9 CONSTANT FRACTION DISCR.:
MODELLED**



**FIG. 10 IMPROVED CONST. FRAC. DISCR.
NOTE 'SLEWING' NEAR THRESHOLD**

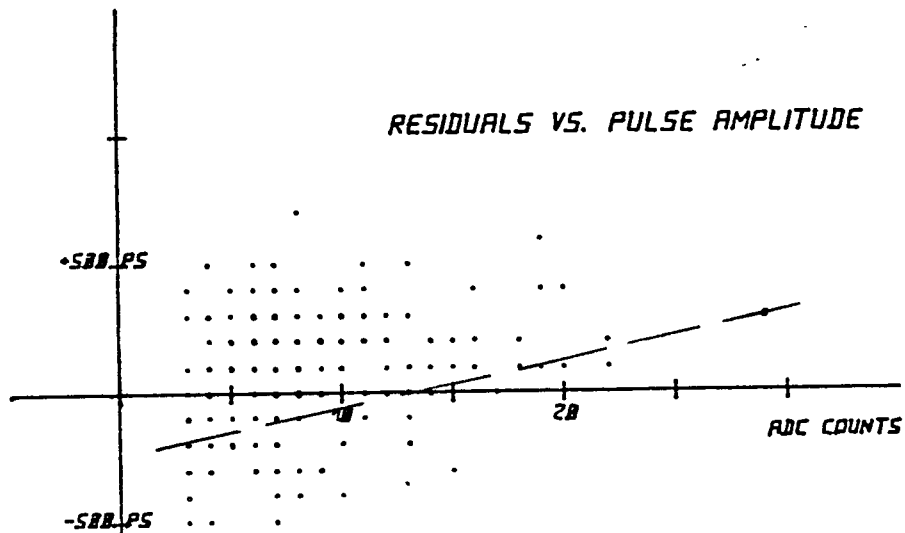


FIG. 11 "AJISAI" PASS
AFTER SCREENING:
FIXED THRESHOLD
NO MODEL

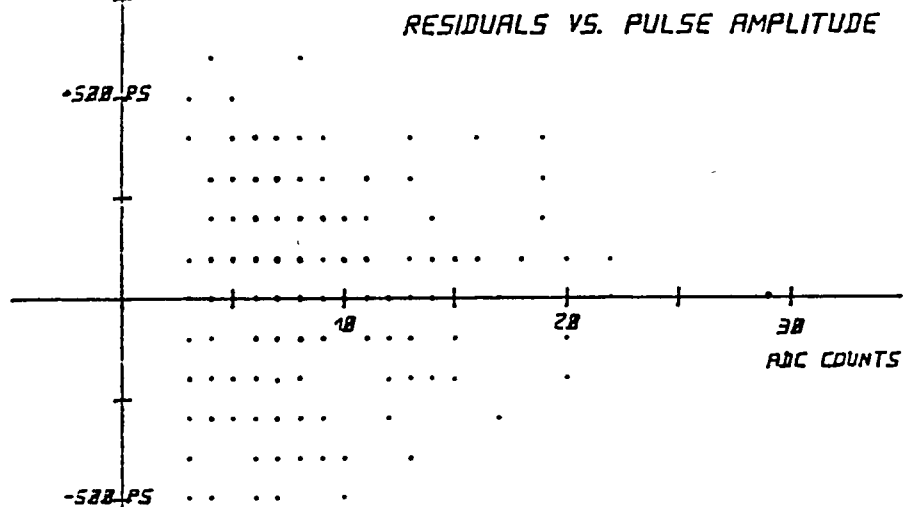


FIG. 12 SAME PASS
FIXED THRESHOLD
GAUSS-MODEL

APPENDIX COMPUTER MODELLING OF DISCRIMINATOR AMPLITUDE DEPENDENCE

A) LEADING EDGE

If Gaussian pulse is assumed:

$$u(t) = U_{th} = A * \exp - \frac{(t - t_0)^2}{(2 t_0)^2}$$

with: U_{th} threshold voltage
 A amplitude
 $t - t_0$ time correction to centroid
 t_0 half pulse width at $.607 * A$

we get for the time correction:

$$t - t_0 = .60 * t_{FWHM} \sqrt{-\ln(U_{th}/A)}$$

with: t_{FWHM} full pulse width at $.5 * A$

In the above formula, the term U_{th}/A must not become greater than 1. Threshold usually is defined as the amplitude where 50% firings occur. Here, care must be taken to use the smallest amplitude value permitted to fire the discriminator as U_{th} . Correction is most prominent with low amplitudes, and becomes very small above tenfold threshold. (viz. Fig. 1)

When the calibration values are evaluated, a table is created which contains correction values vs. amplitude. Intermediate values are linearly interpolated. For the whole procedure note Table A.1.

B) CONSTANT FRACTION

A linear correction, removing the slope, was applied. It then was found, that the remaining "roughness" was possibly of systematic nature, but its law is not easily found from the electronic circuitry involved.

FINAL REMARK

The chosen approach utilizing a table of correction data allows an empirical model which can be tested immediately. We finally wish to point out that all observation data remain unchanged; in particular the in-pass calibration points can be used at any time later-on to adjust or test the applied model.

CALIBRATION PROCEEDURE

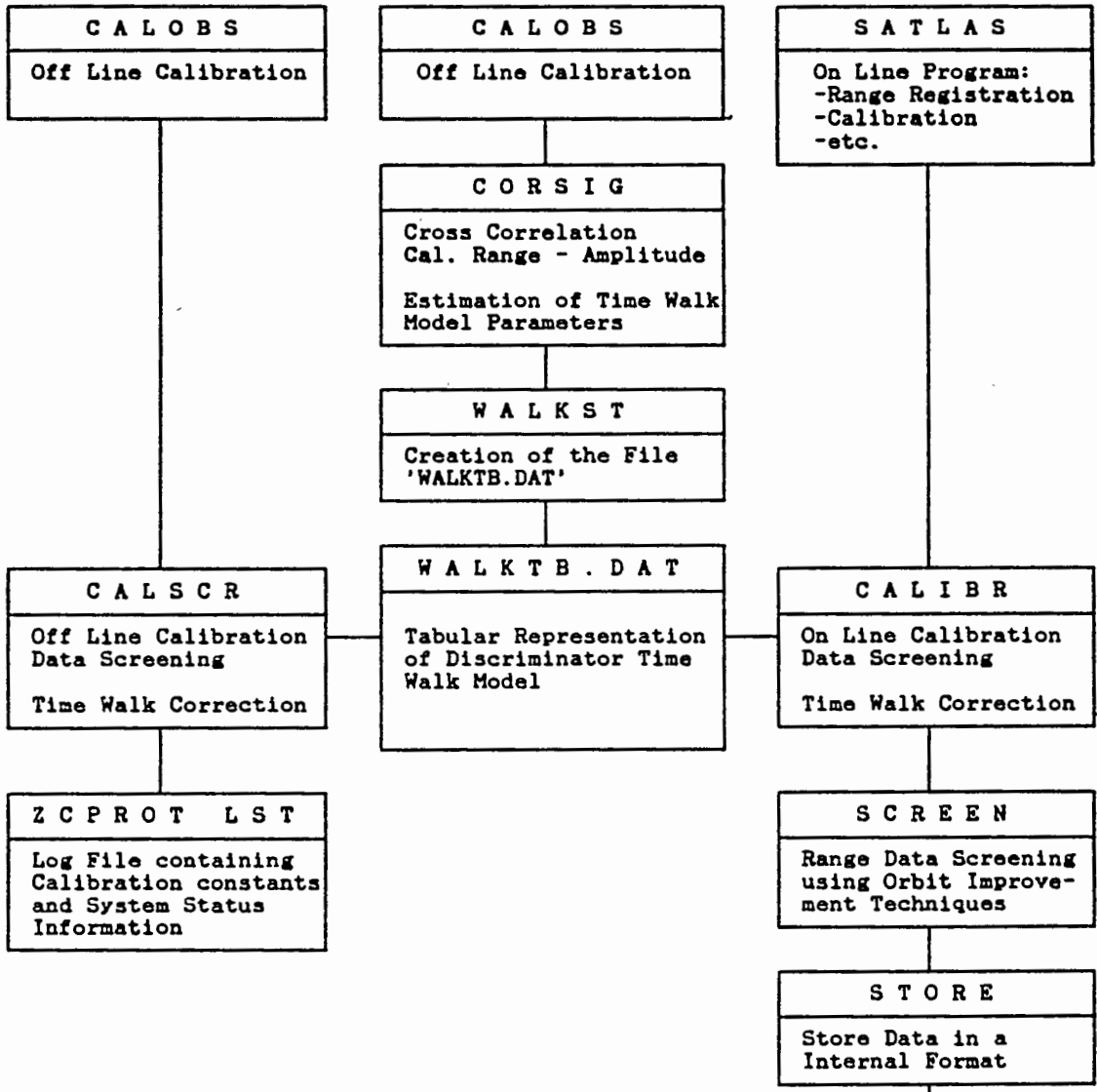
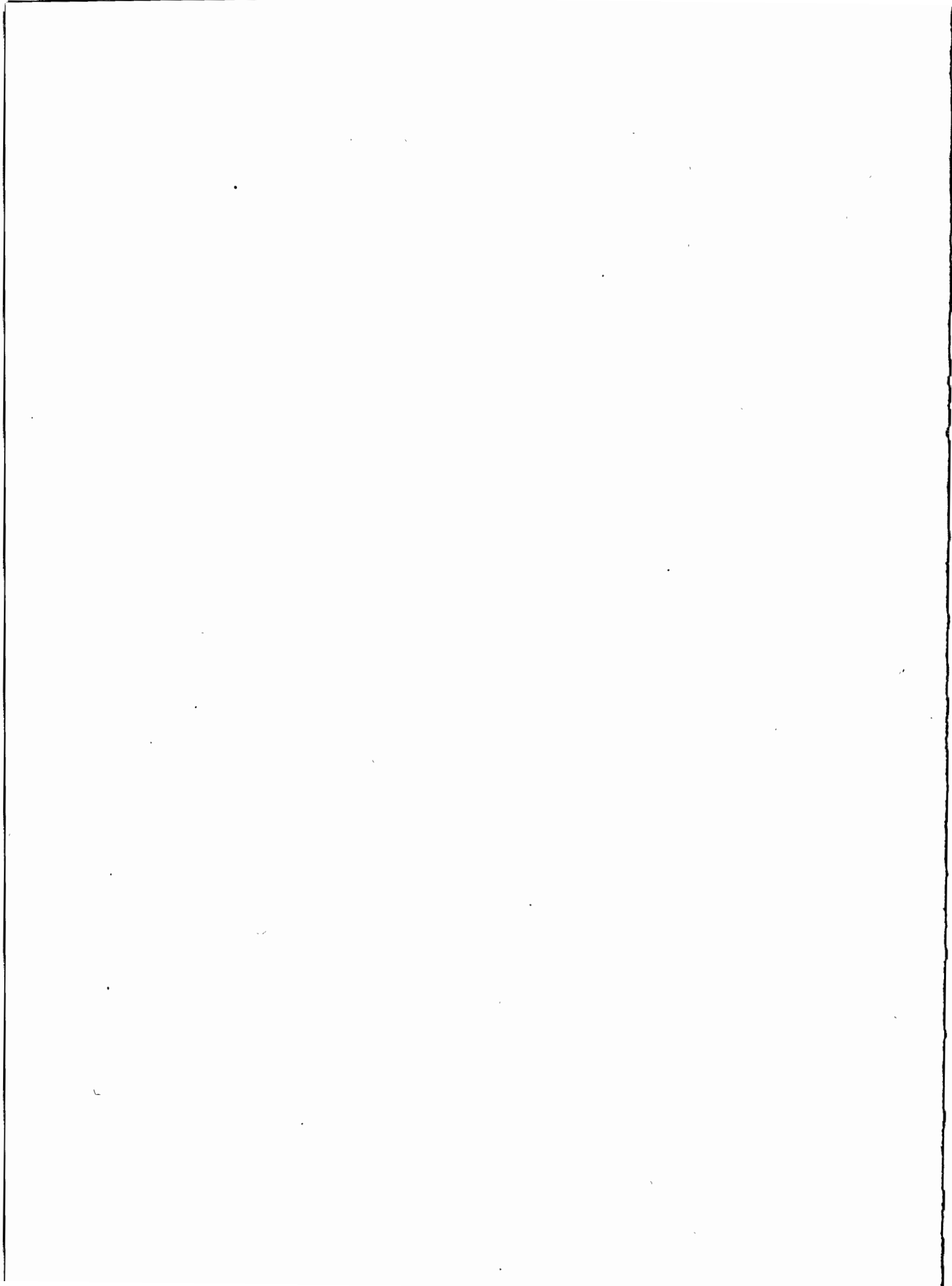


TABLE A.1 FLOWCHART FOR MODELLING OF AMPLITUDE DEPENDENCE



MLRS GROUND TESTS

H. Junginger
Institut für Angewandte Geodäsie
Satellitenbeobachtungsstation Wettzell
D-8493 Kötzing

Telephone (9941) 8643
Telex 69937 WESAT D

W. Beek
Delft University of Technology
Observatory for Satellite Geodesy
Postbox 581
NL-7300 AN Apeldoorn

Telephone (5769) 341
Telex 36442 SATKO NL

ABSTRACT

MLRS-1 and MLRS-2 performed a series of ground tests in 1985/86. Thereby they were using their internal as well as this target calibration capabilities. Five different test procedures are described and data are presented for each procedure at least from one MTLR-System. The mean RMS of MTLRS calibration normal points was found to range between less than .4 and 1 cm, well within the system specifications. No indications for systematic biases at the 1 cm level could be found under normal MTLRS operation conditions.

1. Introduction

The two European Modular Transportable Laser Ranging Systems [1] operated by the Institut für Angewandte Geodäsie in Frankfurt / Federal Republic of Germany (MTLRS-1) and the Delft University of Technology / The Netherlands (MTLRS-2) were for the first time collecting data in Italy and Greece in 1986. Before the systems were shipped to these countries to start the WEGENER-MEDLAS observation campaign (Working Group of European Geo-Scientists for the Establishment of Networks for Earthquake Research - MEDiterranean LASer Project) they went through a series of collocation and performance verification tests. It is the purpose of this paper to report on the results of ground measurements done during this testing period.

The paper is organized as follows: In section 2 the internal calibration procedure for the MTLR-Systems is described because most of the tests are based on this capability. Furthermore an overview is given on the electronical devices in the time of flight detection circuits. Section 3 starts with a discussion of system stability over time periods typical for LAGEOS passes. Temporal variations of the time of flight caused by internal noise sources are superimposed to all data. For this reason they have to be well known before in the remaining parts of section 3 systematic dependences of range data on the PMT voltage, the laser beam wave front, the pointing direction of the mount, and on the signal strength can be studied. In section 4 the results of the ground tests are critically summarized.

2. Internal Calibration and Brief System Overview

In Fig. 1 the optical and opto-electronic components of the MTLR-Systems and the paths of transmitted and received light are shown schematically. Light pulses originating in the Nd:YAP Laser are transmitted through a neutral density filter package (which optionally allows attenuation), through various mirrors and prisms to the beam splitter assembly. There the laser beam is divided into two symmetric semi-circular beams which are guided through the mount into the telescope. A cross section of the emitted laser beam at the telescope exit is shown schematically in Fig. 2.

The tiny fraction of the transmitted light pulses which is reflected at any target is received by the same telescope. It follows a light pass common to the transmitted light up to the beam splitter assembly. There it is separated and guided into the detection package.

The MTLR-Systems are calibrated by fixing a retroreflector in the laser beam at the telescope entrance (see Figs. 1 and 2). The retroreflector is mechanically integrated in a cover which can be screwed on the entrance. During calibration and

MTLRS COUDE TELESCOPE

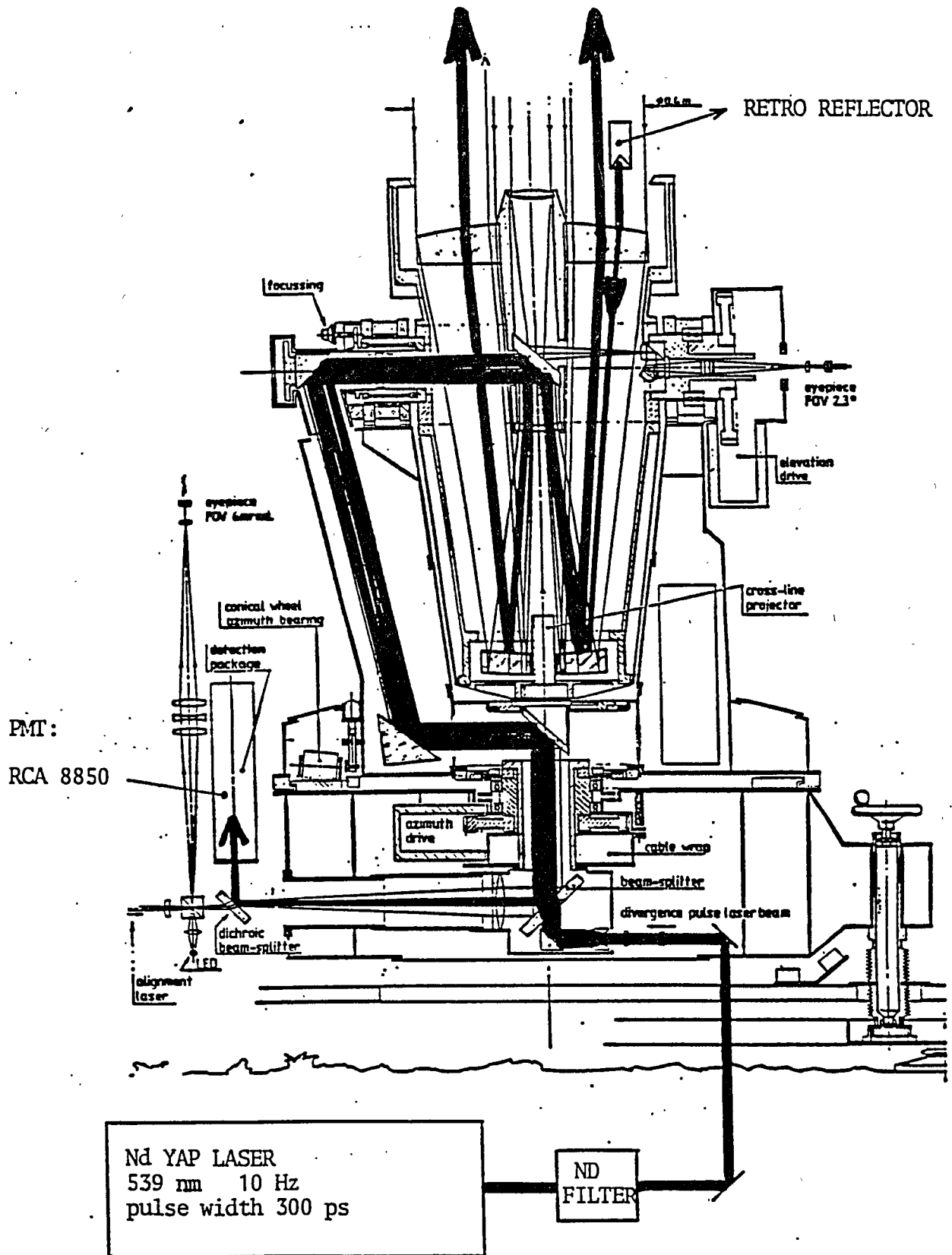


FIG 1 Light pathes through the MTLRS Coudé Telescope

during ground target measurements the transmitted light is attenuated by 8 to 12 orders of magnitude.

Since the retroreflector is fixed with respect to the telescope, the emitted laser beam rotates relative to the reflector when the mount is moved. This is evident from the optical design. In Fig. 2 a 90° rotation is shown. It can be achieved in three different ways: Either the azimuth of the mount is rotated by 90°, or the elevation is changed by -90°, or the elevation is moved by X° and the azimuth by X° - 90°. The rotation of the semi-circular beam halves with respects to the retroreflector puts constraints on the possible mount pointing directions during calibration. These constraints are important for the tests described in section 3.4.

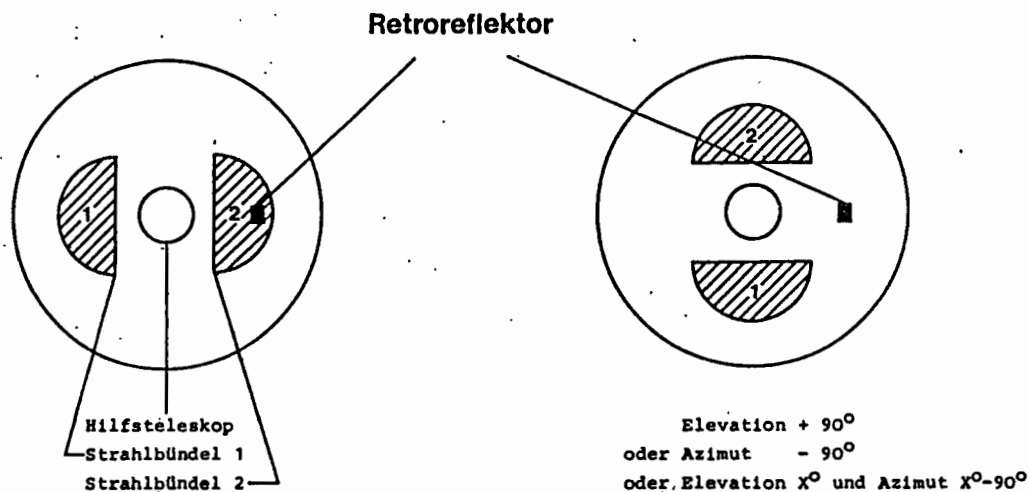


Fig. 2: Cross section through laser beam (hatched areas) at the telescope entrance in two different telescope positions.

Nearly all electrical and opto-electronic components of the MTLRS time of flight detection circuits are commercially available. As a reference their types are given in Table I.

TABLE I

| | |
|----------------------------------|--------------------------------------|
| Start-Detector | HP 5082-4207 |
| Constant Fraction Discriminators | ORTEC 934 |
| Range Counters | HP 5370A/B |
| Photo Multiplier Tube (PMT) | RCA 8850 |
| PMT High Voltage Supply | LABEN 8122 |
| PMT Amplifier | TRONTECH W500F |
| Frequency Standards | Cs (FTS 4010) or Rb (EFRATOM FRK) |

Table 1: Commercially available components of the MTLRS time of flight detection circuits.

3. Ground Tests

3.1 Stability Tests

During the collocation period in Matera starting in January and ending in March 1986, MTLRS-1 and MTLRS-2 went through a stability test which was done by calibrating continuously to the retroreflectors (as described in the previous section) for a bit less than one hour. Times of flight measured in this way are shown in Fig. 3 as a function of time together with single shot RMS-values and return rates. In the upper part of the figure data from MTLRS-1 are displayed, whereas the lower part shows data from MTLRS-2.

The full and dashed lines in the first panel of the figure distinguish average calibration values measured by the two MTLRS-1 range counters 1 and 2 within 5 minute bins. The RMS of the average calibration values is .03 ns which corresponds to .45 cm. The difference between the maximum and minimum bin averaged time of flight is .09 ns which corresponds to a range difference of 1.35 cm. The mean calibration value for MTLRS-1 is about 116.10 ns.

In the second panel single shot RMS-values are shown for each 5 minute bin and for each range counter. The RMS-values vary between .30 and .42 ns. There is a weak indication for about 20 ps greater RMS-values for counter 1. This could be caused by a quartz of inferior quality installed in this counter.

The third panel shows the mean return rates per bin measured by counters 1 and 2. They are defined as the number of accepted data points in one bin (for each individual counter), divided by the number of laser shots in the same bin. Because MTLRS lasers usually operate with a pulse frequency of 10 Hz, a return rate of 5% in a 5 minute bin means that 150 measurements contributed to a bin averaged calibration value. During the stability test the return rate was fluctuating between 5% and 8%.

The variations of the mean calibration values and of the single shot RMS-values in the MTLRS-2 data shown in the lower part of the figure are smoother than those for MTLRS-1. The mean calibration point RMS is .01 ns corresponding to .15 cm. The mean calibration value for MTLRS-2 is about 138.5 ns, the mean single shot RMS .36 ns, in agreement with the value characterizing MTLRS-1. The return rate varied during the MTLRS-2 stability test between 10% and 14%. Eventhough this is twice the MTLRS-1 return rate, both systems were testing at the same light intensity levels. MTLRS-2 has only one counter, therefore its return rate has to be compared with the sum of the MTLRS-1 return rates.

The differences in scatter of the MTLRS-1 and MTLRS-2 mean calibration- and single shot RMS-values have possibly statistical reasons. The numbers of data points contributing to the mean calibration values shown in Fig. 3 differ by a factor of 4 approximately between MTLRS-1 and MTLRS-2. A factor of 2 comes from the fact that MTLRS-1 data were measured with two counters whereas MTLRS-2 was only using one counter. Another factor of 2 is caused by the bin size which was chosen to be 5 minutes for MTLRS-1 and 10 minutes for MTLRS-2.

Assuming Gaussian statistics the RMS of bin averaged calibration values should be smaller than the single shot RMS by a factor of $1/\sqrt{N}$ (where N is the number of accepted data points within a bin). This leads (for the bin sizes and return rates shown in Fig. 3) to an expected RMS for bin averaged calibration values of .2 and .4 cm for MTLRS-2 and MTLRS-1 respectively, in reasonable agreement with the data.

Another meaningful number characterizing the temporal stability of Laser ranging systems over time periods typical for LAGEOS passes is the mean pre- minus post-calibration value. Before and after each measurement the MTLR-Systems are calibrated as described in section 2. The difference between these calibration values is the pre- minus post-calibration value.

For all measurements made during the Matera collocation period the mean pre- minus post-calibration values were found to be .8 cm and 1.0 cm for MTLRS-1 and MTLRS-2 respectively. They are slightly larger than those found during the Matera stability tests. However, they are within the system specifications.

3.2 PMT Test

In Fig. 4 mean calibration values, single shot RMS and return rates are shown as a function of the voltage applied to the MTLRS-1 and MTLRS-2 photo multiplier tubes (PMT). The voltage was changed from 30 V below the nominal PMT voltage (which is -2000 V for MTLRS-1 and -1900 V for MTLRS-2) to 30 V above the nominal voltage in steps of 10 V. It was the intention of this test to estimate the influence of instabilities in the high voltage power supply on range measurements.

The calibration values of both systems decrease with decreasing PMT voltage. This is in accordance with our expectations because the transit times of primary and secondary electrons in the PMT should decrease with increasing potential differences inside the tube.

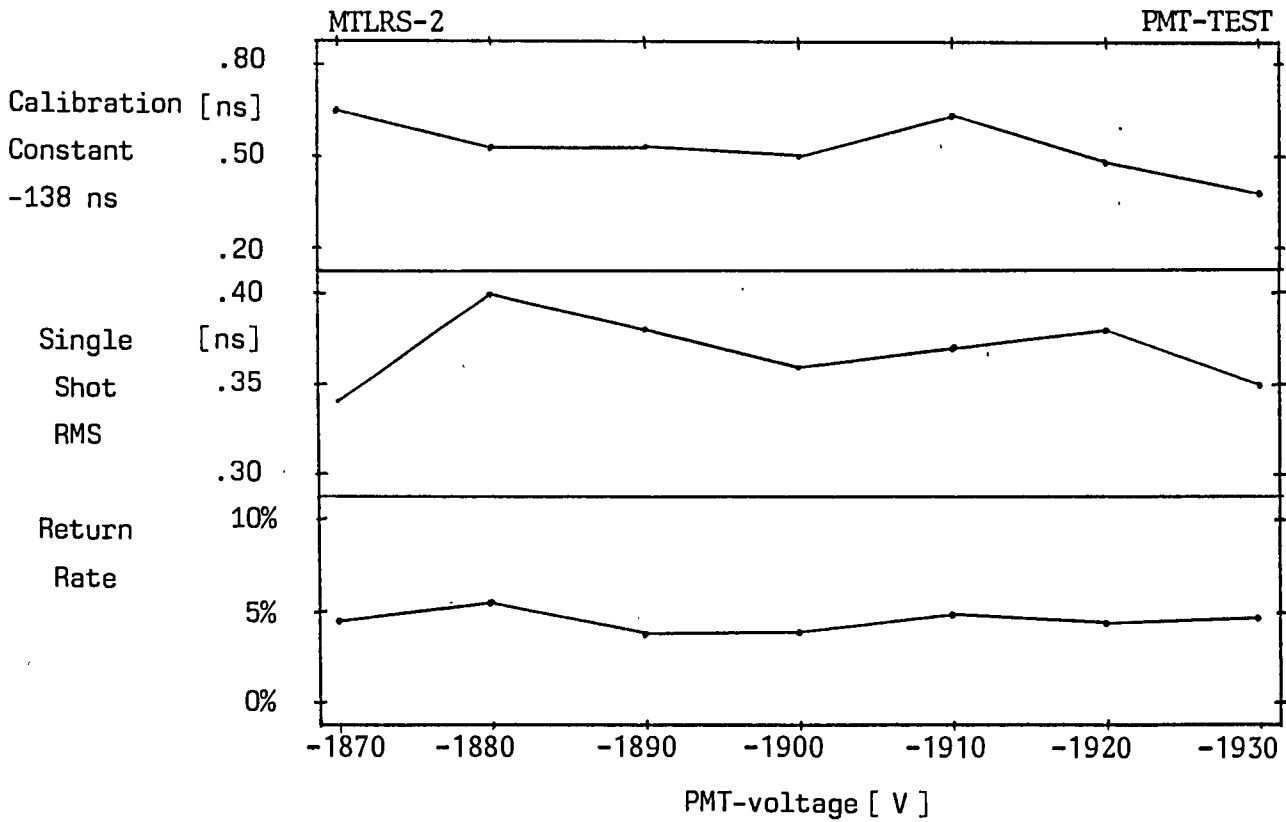
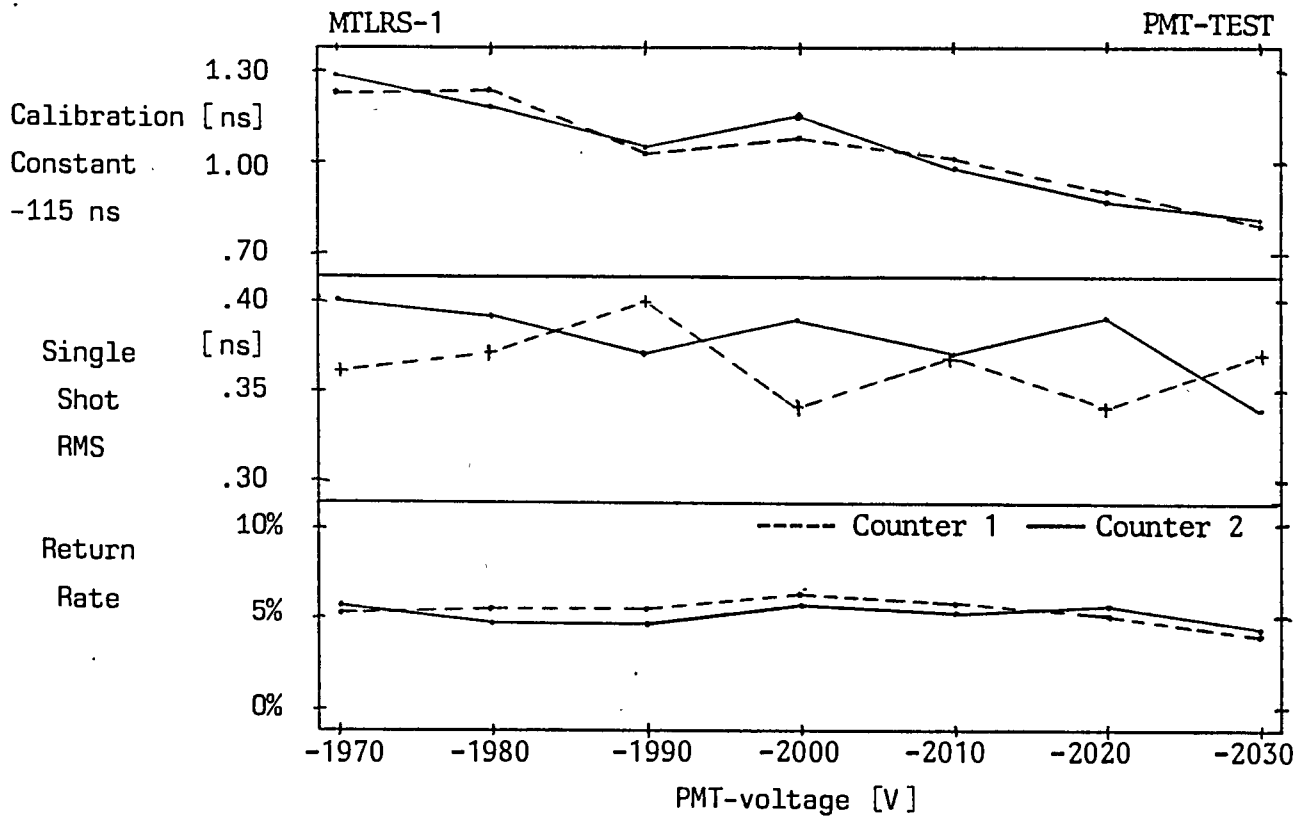


FIG 4 Influence of the PMT-voltage on the calibration constant. The nominal PMT-voltage is -2000 V for MTLRS-1 and -1900 V for MTLRS-2.

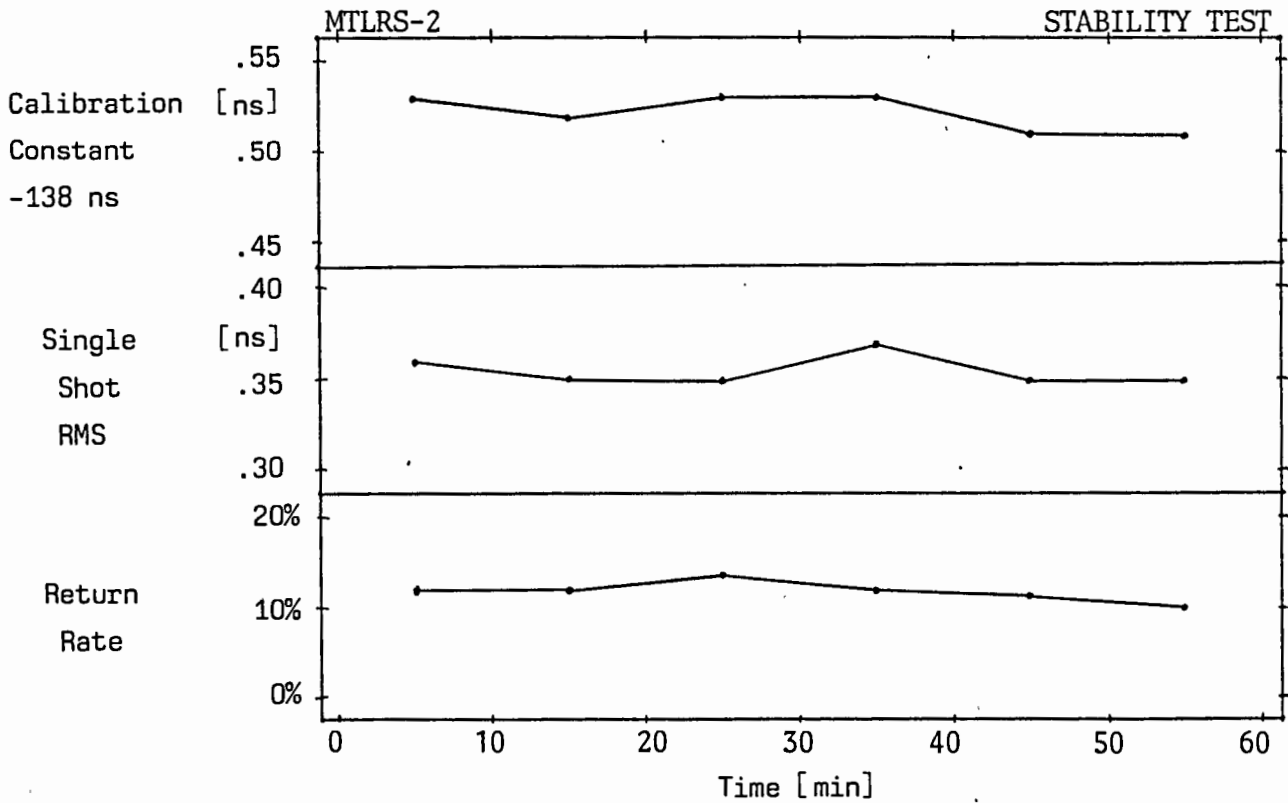
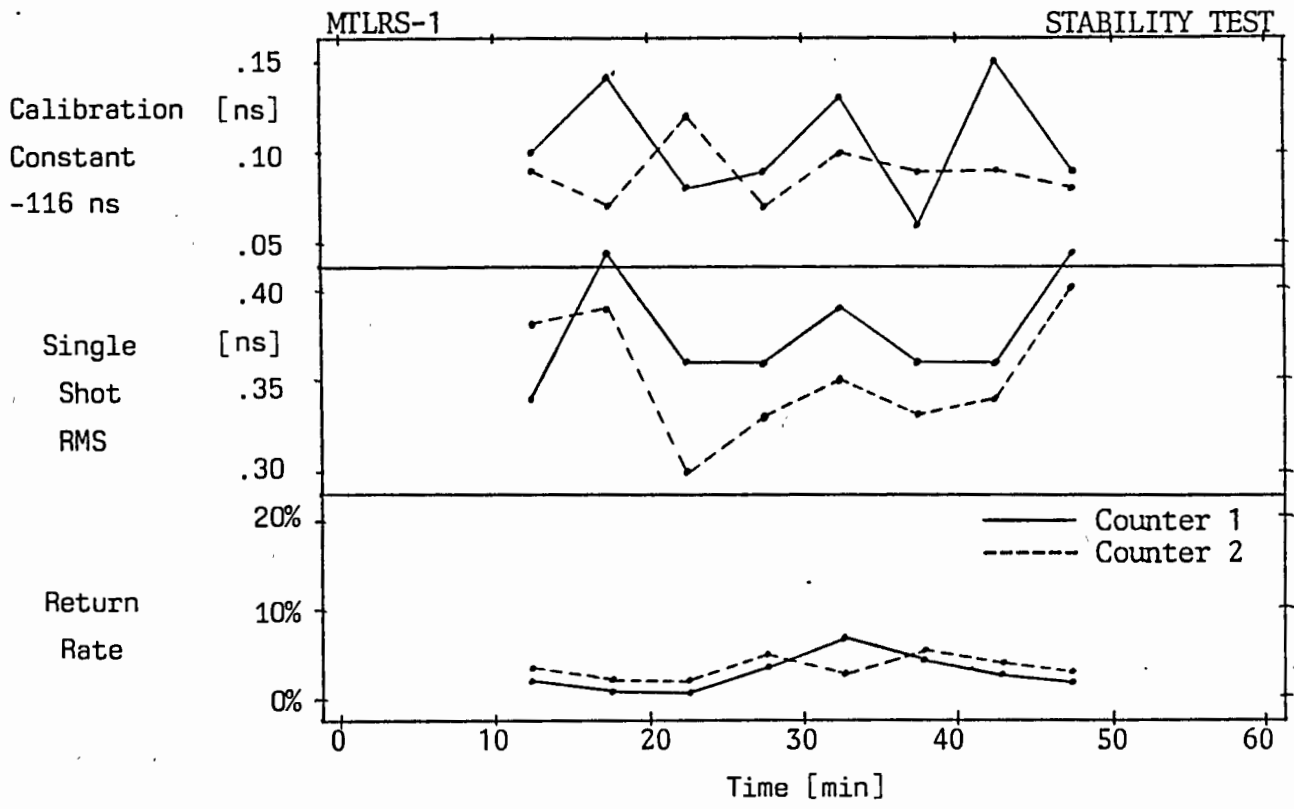


FIG 3 Calibration constant, single shot RMS, and return rate versus time. For MTLRS-1 5 min bins have been used. MTLRS-2 data were evaluated in 10 min bins.

The decrease of the calibration values with decreasing PMT voltage is not as smooth and steady (in particular for MTLRS-2) as might be expected. This can not be fully attributed to statistics. The main reason could be the uncertainty of the PMT voltage actually applied. It was adjusted in both systems with the adjustment knobs at the high voltage power supplies and not verified with a volt meter.

The calibration values changed by about .4 ns and .3 ns for MTLRS-1 and MTLRS-2 over 60 V. This corresponds to range differences of the order of 1 cm per 10 V deviation of the PMT voltage from its nominal value for both systems.

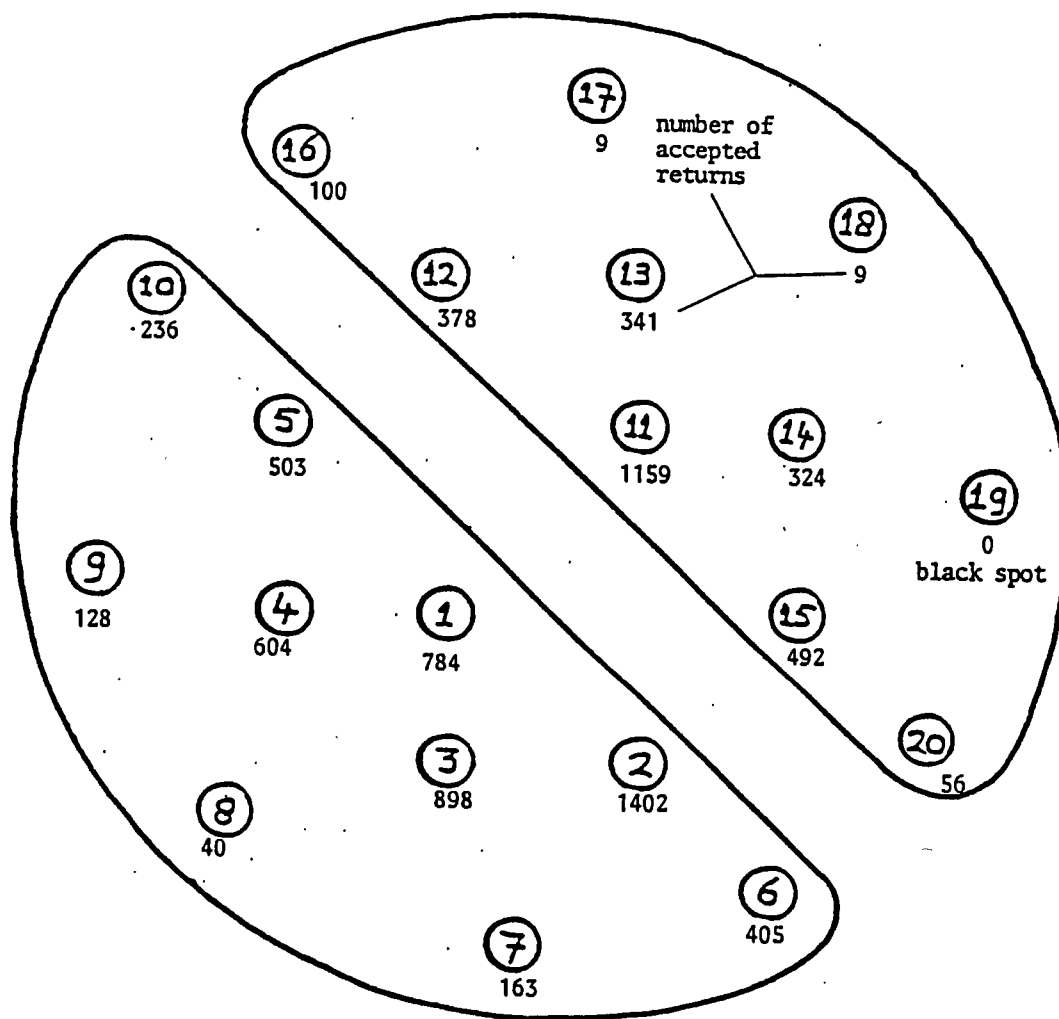


Fig. 5: Retroreflector positions in the MTLRS-2 beam during the Matera cube map test. The beam had a diameter of about 1.5 m at the target 1146 m from the system. The retroreflector positions are labeled with numbers between 1 and 20.

In order to estimate the influence of the PMT high voltage power supply on system stability we will investigate in the near future the temperature coefficient, switch on effects, and the long term stability of this device.

The single shot RMS values were not affected by the PMT voltage changes. For both systems the return rates during the PMT test were about 5%, indicating that MTLRS-1 was testing at about twice the light intensity used by MTLRS-2.

3.3 Cube Map Test

Wave front distortions originating very often from multi-mode laser operation can lead to biases which depend on the location of the target inside the transmitted laser beam. It is the purpose of the cube map test to detect these kind of biases.

MTLRS-2 tried a cube map test during the Matera collocation period. The test was originally planned to take place in two steps. The aim of the first step was to measure an intensity map of the beam. In a second step ranges as a function of the target location inside the beam should have been measured. Thereby it was foreseen to use the intensity information to compensate for intensity differences within the beam with the ND-filters.

The retroreflector used for the cube map test was at a distance of 1146 m from MTLRS-2. With maximum beam divergence the diameter of the beam at the target was about 1.5 m. In Fig. 5 the cross section of the beam at the target is shown schematically. The distribution of retroreflector positions inside the laser beam (seen towards MTLRS-2) is indicated. All positions are labeled by numbers between 1 and 20. The ranging time to one position was 2.5 minutes. Positions were changed by redirecting the mount. The number of accepted returns from each retroreflector position is also indicated in Fig. 5.

Mean times of flight, single shot RMS values, and total numbers of accepted returns are shown in Fig. 6 for the retroreflector positions indicated and labeled in Fig. 5. The sequence in which the data are presented was defined by the number of accepted returns contributing to a mean range.

Mean times of flight calculated for positions with more than 100 returns show an extremely smooth behaviour. All of them differ by less than 100 ps from each other, indicating no biases, eventhough the light intensity during these measurements varied by 1½ orders of magnitude.

The deviations of the times of flight for positions with less than 100 returns are larger. The maximum deviation is 300 ps for position 20 with 56 returns. All these positions are located on the outer semi-circle of the right beam half in Fig. 5.

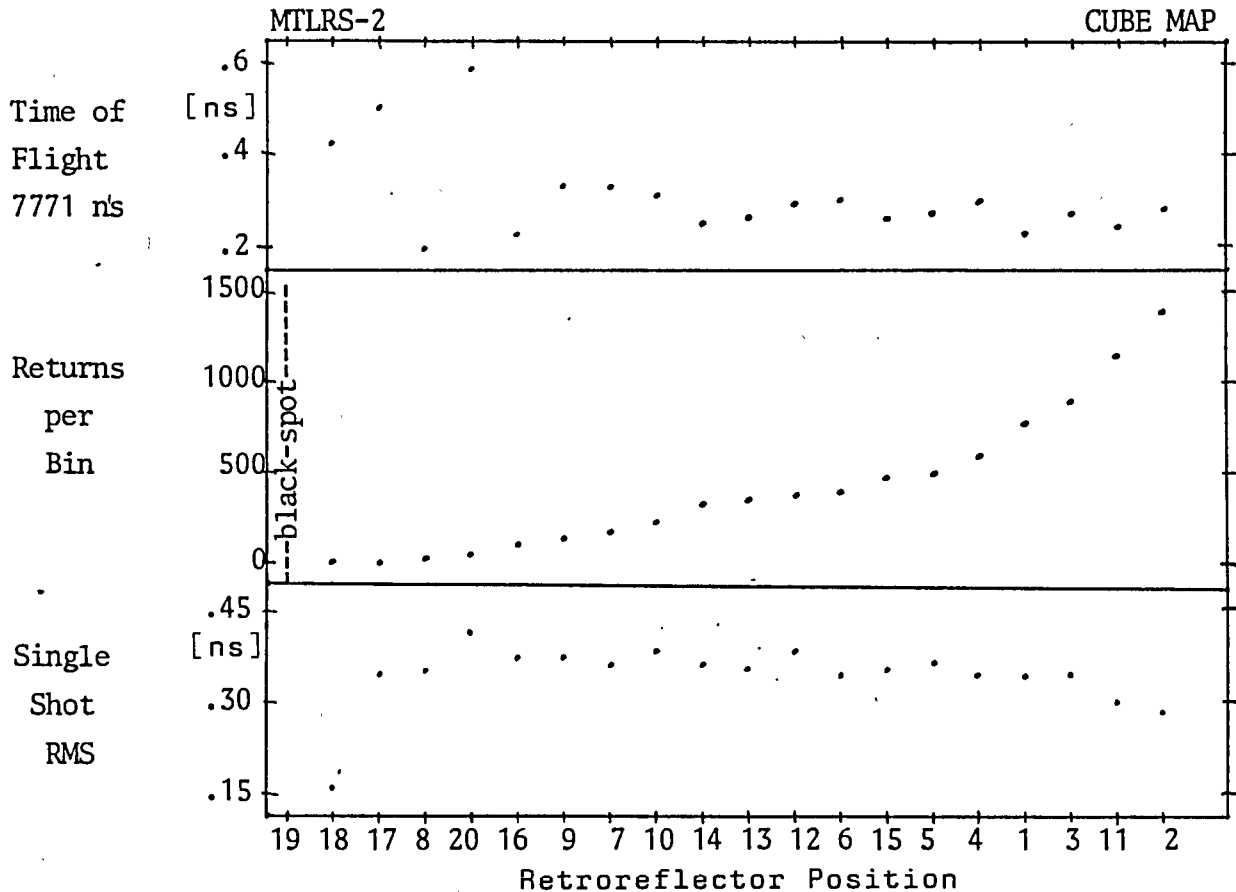


FIG 6 Range, single shot RMS, and number of returns measured during 2.5 min at the retroreflector positions marked and labeled in Fig. 5.

In order to verify whether there is or there is not a wave front distortion problem on the outer semi-circle, the second part of the test was planned, as described above. Unfortunately it was impossible to complete this step in Matera because of instrumental problems.

3.4 Mount Biases

Fig. 7 shows mean calibration values as a function of universal time which were measured by MTLRS-1 at the Goddard Optical Test Facility in June 1985. During the test which lasted for nearly 4 hours the mount was moved. Dots represent mean calibration values calculated from data within 51 sec bins. Vertical dashed lines separate intervals of different system states. System states are characterized by three parameters which are also indicated in Fig. 7: Azimuth and elevation of the telescope pointing direction and mean number of accepted calibration points per 51 sec bin. Horizontal dashed lines mark mean calibration values for each system state.

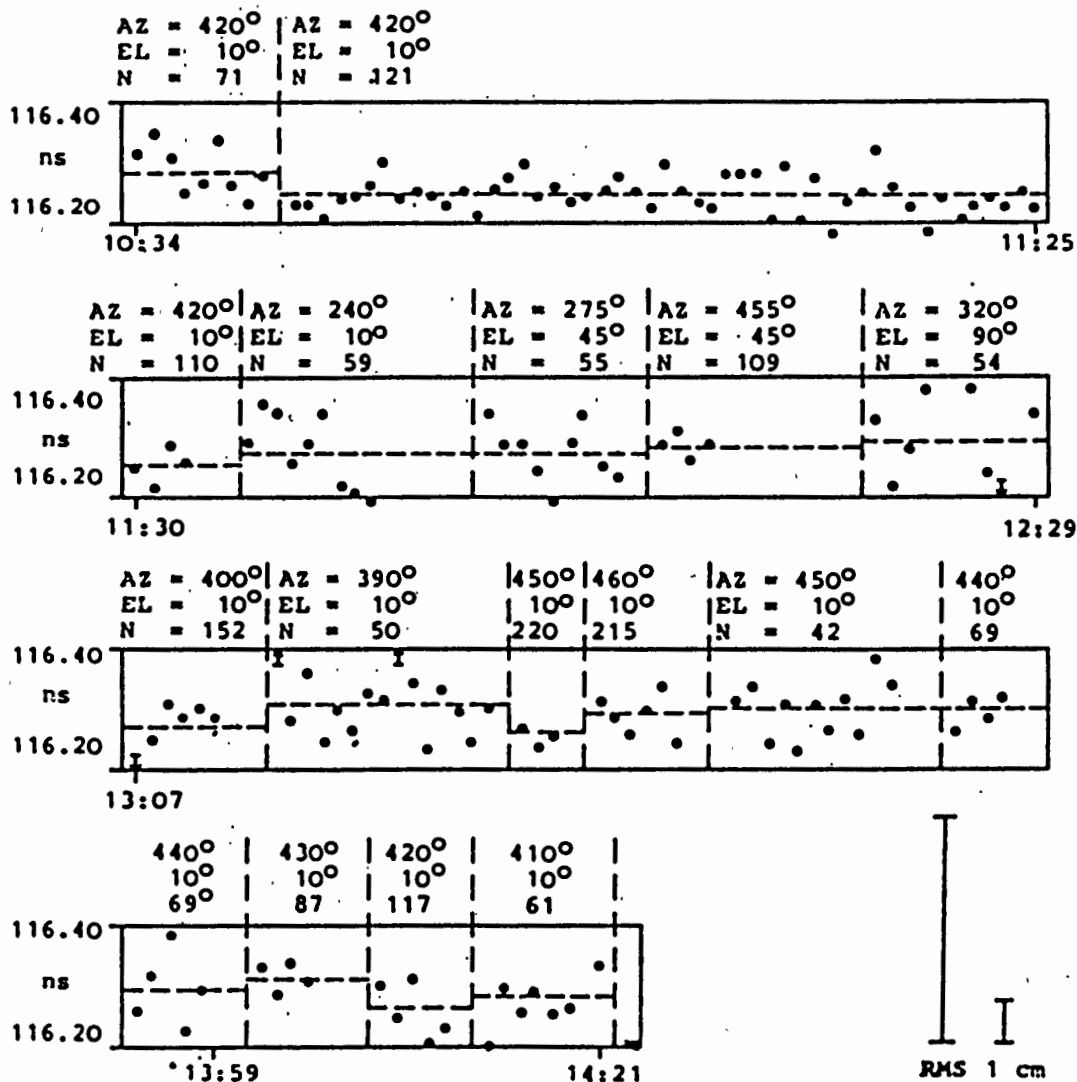


Fig. 7: MTLRS-1 calibration constants measured at GORF in June 1985. See text for details.

The test was done in three phases. In the first phase the telescope was in the normal calibration position and the system was running for about one hour. In the second phase the mount was moved in a way that the retroreflector for internal calibration was either at the same position within the beam as during normal system calibration, or at the conjugate position which is reached after a 180° rotation of the reflector (see Fig. 2). Thereby the constraints discussed in section 2 were taken into account. In the third phase of the test one beam half (see Figs. 2 and 5) was scanned azimuthally by the retroreflector in steps of 10°.

The difference between the maximum and minimum mean calibration value for the system states shown in Fig. 7 is 70 ps corresponding to a range difference of 1 cm. This is in excellent agreement with the tests discussed in sections 3.1 and 3.3. No significant systematic variation could be found in the data which is associated with the mount pointing direction.

3.5 Signal Strength

MTLR-Systems up to now do not directly measure pulse heights of PMT signals. Therefore indirect means have to be applied to infer the intensity level of light pulses received in the detection package. A number related to the received light intensity is the return rate defined in section 3.1. For low light intensities it is directly proportional to the latter. For higher intensities its slope decreases and goes to zero at return rates of 1 for very high intensities.

Fig. 8 shows mean calibration values as a function of the return rate measured by MTLRS-1 in two different tests. The calibration values shown in the upper panel of the figure are the system state averages from Fig. 7. In the lower panel data from a signal strength test in Matera are presented. During this test the light intensity was varied with ND-filters. One data point corresponds to one ND-filter setting. The ranging time for these data points varied from 30 minutes for very low intensities to 3 minutes for high intensities. The data point on the left hand side represents 100 range measurements, the data point on the right 1600.

A careful analysis of both data sets shown in Fig. 8 could not reveal a strongly significant tendency. There is a weak indication for decreasing calibration values with increasing return rates. However, it must be less than 30 ps between 0% and 30% return rate, where MTLRS is normally operated.

Fig. 9 shows the results of the MTLRS-2 signal strength test in Matera. Mean calibration values are plotted as a function of the ND-filter setting attenuating the transmitted laser light by factors of 10^{-10} to $10^{-12.5}$. All mean calibration values are within less than 50 ps of each other for light intensity variations over 2½ orders of magnitude.

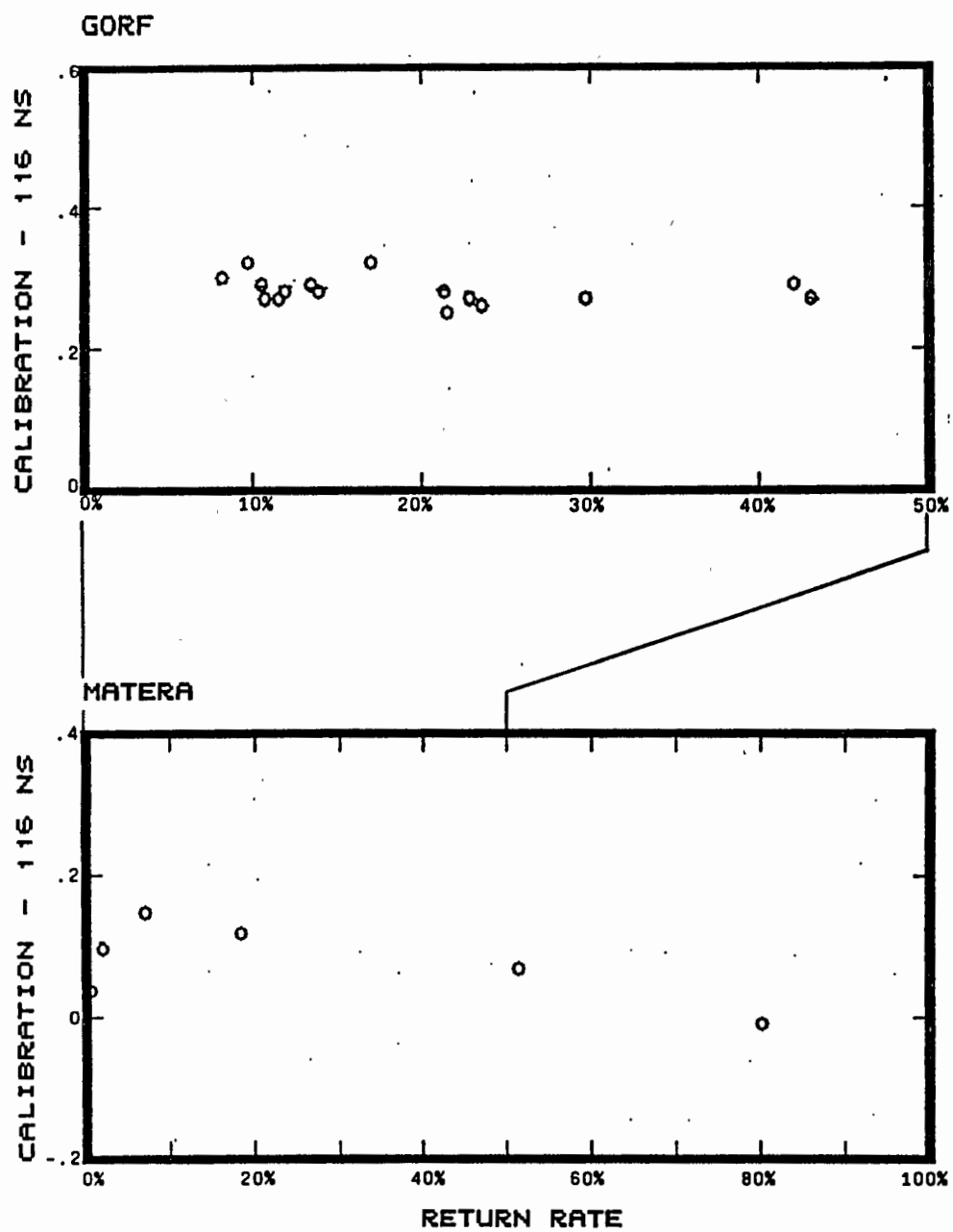


Fig. 8: Calibration constants for MTLRS-1 versus return rate.

MTLRS-2: SIGNAL STRENGTH TEST

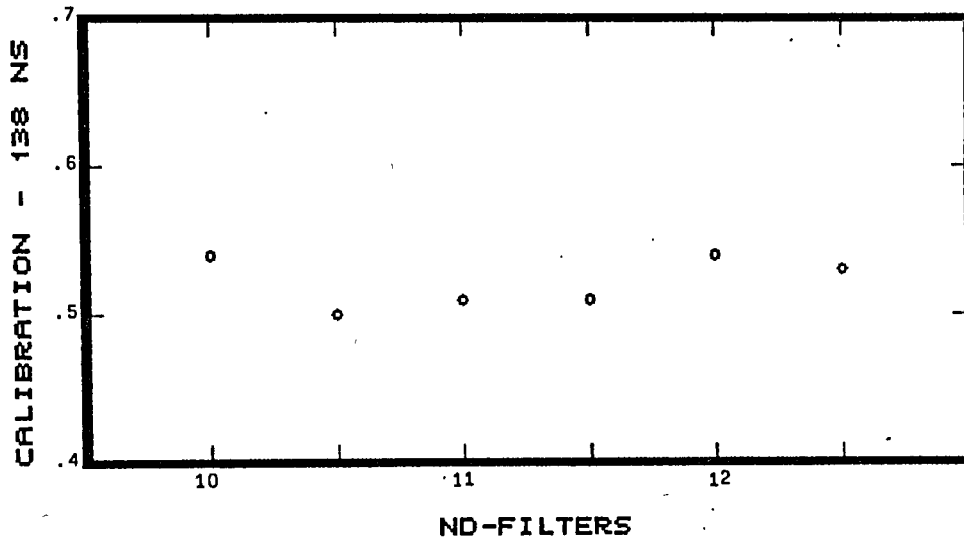


Fig. 9: Calibration constant for MTLRS-2 versus ND-filter setting.

4. Summary and Conclusions

Data from five different ground tests have been presented from at least one MTLR-System. Mean calibration RMS values were always found to be well below 1 cm which is in excellent agreement with the system specifications. No significant bias of the system could be identified.

During the Matera collocation the mean pre- minus post-calibration values for MTLRS-1 and MTLRS-2 were .8 and 1 cm, also within the system specifications but slightly above the RMS of the mean calibration values discussed in this paper. This probably could indicate that there are not yet identified noise sources either in the system hardware or in the operation procedures which can be eliminated. In order to do this we plan to continue and to complete the tests described here. We will try to clarify still open questions concerning for instance temperature effects, intensity dependent biases, wave front distortion, or PMT power supply stability.

Acknowledgements: We would like to thank L. Amberg, G. Blenski, W. Etling, U. Hessels, R. Motz, I. Nowak, N. Rodenburg, and D. Samson who spent many hours to discuss, to prepare and finally to do the described tests. Without their help this paper would not have been possible.

References

- 1 Wilson, P., and H. Visser, Development of the Modular Transportabel Laser Ranging System, Fifth International Workshop on Laser Ranging Instrumentation, Royal Greenwich Observatory, Herstmonceux, UK, Sept. 10 - 14, 1984

ZERO RANGE REALTIME CALIBRATION

J.D. Rayner, S.R. Bowman, C.O. Alley
Department of Physics and Astronomy
University of Maryland
College Park, MD 20742

Telephone (301) 454 34 05
Telex 908787

F.M. Yang
Shanghai Observatory Academia Sinica
Shanghai - China -

ABSTRACT

A real time feedback calibration system is described in which the range to a mirror mounted within .5mm of the elevation axis of the transmitting telescope is measured for each outgoing laser pulse.

In a general feedback calibration system a small portion of the outgoing laser pulse is fed back into the stop detector and its delay relative to the start pulse is measured by the timing electronics. One of the primary motivations for using feedback calibration is that some stations are unable to range to terrestrial calibration targets. There are, however, many other advantages to such a system. First it simplifies the ranging operations since the calibration is done automatically during the ranging session. Secondly, it eliminates the need for a surveyed calibration target, which is particularly advantageous in the case of mobile stations. Also, as we begin to talk of millimeter accuracies survey errors and target stability will become greater problems introducing errors at the centimeter level. At the millimeter level correcting for atmospheric delays in the calibration path which is close to ground and subject to temperature gradients and other local effects will also introduce errors.

In going from an external calibration target to an internal feedback calibration path you trade the surveying problem for one of measuring internal telescope delays. While trying to solve this problem we were reminded of a technique reported by John Degnan (1) at the last Workshop. Tom Zagwodzki and his coworkers installed an open corner with its vertex on the elevation axis of the telescope, to return some of the outgoing laser pulse to the receiving photomultiplier where it was used to start the timing electronics. This is a very elegant solution to the calibration problem since the ranging calibration is now zero. Unfortunately this scheme did not work as well in practice as it did in theory and was, at least temporarily, dropped by the Goddard group. This technique is not directly applicable at the single photoelectron level, since we would have to run the start pulse at the multi-photoelectron level in order to get a reliable start for each shot. The start and stop energies would then be different introducing a energy dependent calibration shift. By using a separate start detector optimized for fast response and low jitter we can remove start jitter from the system error budget. At the present time we are using a bulk GaAs Austin switch with a 20ps rise time as our start detector. It monitors the output of the laser oscillator and thus should provide a start pulse which is independent of laser energy. Since the start and stop channels are independent we must measure the the difference in their delays which we accomplish by timing the return from a small mirror placed at the elevation axis of the telescope. This gives us all the the advantages of a feedback calibration and some additional advantages specific to the zero range configuration of the feedback path. Since the feedback path exactly measures the delay to the reference point for the telescope there is no need for a separate measurement of the internal telescope delay. In fact, any angle dependent telescope delays will automatically be mapped out in the course of ranging, since the telescope delay is measured for each shot. In short, this system automatically measures virtually all calibration corrections without operator intervention.

There are several requirements imposed by the implementation of such a system. The most fundamental requirement is that the same telescope be used as transmitter and receiver, with the transmitted beam filling the telescope aperture. Next, there must be an attenuated path through the transmit/receive switch to allow a small portion of the feedback laser pulse to hit the stop detector. In addition the detector must be immune to the electrical noise associated with the laser firing. Finally, the timing electronics must be able to measure the very short calibration delay and still be able to measure the full range.

Since there is a good fit between these requirements and our system it was easy for us to implement a zero range calibration system. I will describe those features of our system which affect the feedback calibration. We have mounted a small mirror on a micrometer translation stage attached to the side of the telescope tube. By adjusting the micrometer the front surface of the mirror can be made to coincide with the elevation axis of the telescope. This can be checked by moving the telescope in elevation while viewing the mirror through a small telescope. Then if a point on the surface of the mirror seems to remain fixed it is on the elevation axis. Using this technique we were able to position the mirror to within .5 mm of the elevation axis. We use a passive polarization sensitive transmit/receive switch(2). This means that there is a feedback path from the telescope to the detector at all times. The detector is blocked when the laser fires by a rotating vane. We have modified this vane by cutting a hole in it which is then blocked by a ND 13 filter which attenuates the feedback laser pulse to the singles level. The detector is a solid state Geiger mode diode(3) which puts out a five volt pulse for a single photon input and thus is virtually immune to the electrical noise from the laser firing. Finally, for timing we use a four stop event timer with the start pulse being measured by the first stop and the calibration pulse measured by the second stop. This is one weakness of the system since the offset between the first and second stops of the event timer must be separately calibrated. For the present this calibration is limited to an accuracy of about 50 ps.

We have just started working with this system and there will undoubtedly be changes, particularly in the area of event timer calibration. Our preliminary studies suggest that this should be a viable method for automatically calibrating ranging systems at the millimeter level.

REFERENCES

1. T. W. Zagwodski, J. F. McGarry, J. J. Degnan, R.S. Chabot, J. G. Lessner, and J. B. Abshire, "Experimental Large Aperture Satellite Laser Ranging System", Proceedings of the Fifth International Workshop on Laser Ranging Instrumentation, pg.178.

2. S. R. Bowman et al , "Analysis and Performance of a Passive Polarization Telescope Coupling Switch for Lunar Laser Ranging", these Proceedings.
3. S. R. Bowman et al, "The Use of Geiger Avalanche Photodiodes for Precise Laser Ranging at Very Low Light Levels; An Experimental Evaluation", these Proceedings.

SYSTEM STABILITY USING MODE LOCKED TRAIN

K. Hamal, I. Prochazka
Czech Technical University
Faculty of Nuclear Science and Physical Eng.
Brehova 7, 115 19 Prague - Czechoslovakia -

Telephone 848840
TWX 121254 FJFI C

ABSTRACT

The calibration procedure of the INTERKOSMOS satellite laser ranging station is described. Several system configurations and calibration setups were tested within 1984 to 1986. The satellite ranging and calibration echo signal strength in single PE only. The receiver detector is the main contributor to the system jitter and stability. The jitter and stability performance of the dynode PMT and silicon photodiode HP S5 operating in Geiger mode were compared. Replacing the PMT by the HP S5 photodiode, the ranging jitter dropped from 300 psec down to 100 psec rms and the (pre-post) calibration differences spread dropped from 110 psec down to 26 psec.

| System configuration, station Helvan | CALIBRATION CONFIGURATIONS TESTED |
|---|--|
| <p>LASER Nd YAG+2HG, mode locked by ML51 dye train of 2-3 pulses, FWHM 30psec</p> <p>START - PD+tunnel diode switch by M.Cech /1985/ - optical threshold switch /1986/</p> <p>COUNTER - HPS368 /1983-1985/ - HPS3708 /1986/</p> <p>DETECTOR - dynode stage PMT RCA31834A, +15°C, spot diam. 2mm + two HP 120MHz amplifiers</p> <p>DISCRIMINATOR c.f. type, ORTEC 934A</p> <p>SIGNAL STRENGTH single PE echoes only guaranteed by low (echo/lasing) ratio for both calibration and satellite ranging</p> | <p>TARGETS :</p> <p>INTERNAL - pass composed of flat Ag mirrors+diff. screen</p> <p>EXTERNAL 100 METERS OR 500 METERS - corner cube - diffuse flat - mirror flat</p> <p>* The 100 meters target perpendicularity was maintained within 1 milliradian</p> <p>LASER OUTPUT BEAM DIVERGENCE</p> <ul style="list-style-type: none"> - minimal/collimated beam (30 arcsec) - standard for satellite ranging (1-2arcmin) - focus on the external target <p>* In each configuration at least 10 series of calibration runs, 200 echoes each, were completed</p> <p>* The best results were obtained for configuration : BEAM FOCUSSED ON EXTERNAL 100m DIFFUSE TARGET</p> |

K. Hanal, I. Prochazka
System stability using mode locked train

1

K. Hanal, I. Prochazka
System stability using mode locked train

2

| PRE-POS CALIBRATION DIFFERENCE, SYSTEM STABILITY | SYSTEM STABILITY / SUMMARY | | | | | | | | | | | | | | | | | | | | | | | | | | | | | | | | | | | | | | | | | | | | | | | | |
|--|----------------------------|---------|---------|--|-------|---------|--|----------------------|---------|------|------------------|----|----|------------------------|-------|--|---------|--|----|------------------------------|-------|----|------------------------|-----|-----|-----------------------------|--|----|-------------------------|--|--|-------|-----|-----|---------|--|-----|--------------------------------|--|--|--|---------|------|-----------------------------|-----|-----|----------------------|--|----|
| <p>DETECTOR USED - HPSS Silicon photodiode in Geiger mode</p> <p>CALIBRATIONS - 200 single PE echoes each - 10 to 50 minutes between consequent runs</p> <p>SINGLE SHOT 80 - 140 psec RMS</p> <table border="1" style="margin-left: auto; margin-right: auto;"> <tr> <td>PRE-POST CALIBRATION</td> <td>MEAN</td> <td>-2 psec</td> </tr> <tr> <td></td> <td>SIGMA</td> <td>26 psec</td> </tr> </table> | PRE-POST CALIBRATION | MEAN | -2 psec | | SIGMA | 26 psec | <table border="1"> <thead> <tr> <th>JITTER BUDGET (psec)</th> <th>1983-85</th> <th>1986</th> </tr> </thead> <tbody> <tr> <td>Laser pulse FWHM</td> <td>30</td> <td>30</td> </tr> <tr> <td>Ranging counter HPS368</td> <td>) 100</td> <td></td> </tr> <tr> <td>HPS3708</td> <td></td> <td>35</td> </tr> <tr> <td>Start detector/discriminator</td> <td>) 150</td> <td>30</td> </tr> <tr> <td>PMT /dynode/ RCA31834A</td> <td>298</td> <td>298</td> </tr> <tr> <td>Diode /HPSS in Geiger mode/</td> <td></td> <td>98</td> </tr> <tr> <td colspan="3">RESULTING (psec)</td> </tr> <tr> <td>(PMT)</td> <td>520</td> <td>300</td> </tr> <tr> <td>(Diode)</td> <td></td> <td>100</td> </tr> <tr> <td colspan="3">SYSTEM STABILITY (psec)</td> </tr> <tr> <td></td> <td>1983-85</td> <td>1986</td> </tr> <tr> <td>PMT (dynode) based receiver</td> <td>150</td> <td>118</td> </tr> <tr> <td>Diode based receiver</td> <td></td> <td>26</td> </tr> </tbody> </table> | JITTER BUDGET (psec) | 1983-85 | 1986 | Laser pulse FWHM | 30 | 30 | Ranging counter HPS368 |) 100 | | HPS3708 | | 35 | Start detector/discriminator |) 150 | 30 | PMT /dynode/ RCA31834A | 298 | 298 | Diode /HPSS in Geiger mode/ | | 98 | RESULTING (psec) | | | (PMT) | 520 | 300 | (Diode) | | 100 | SYSTEM STABILITY (psec) | | | | 1983-85 | 1986 | PMT (dynode) based receiver | 150 | 118 | Diode based receiver | | 26 |
| PRE-POST CALIBRATION | MEAN | -2 psec | | | | | | | | | | | | | | | | | | | | | | | | | | | | | | | | | | | | | | | | | | | | | | | |
| | SIGMA | 26 psec | | | | | | | | | | | | | | | | | | | | | | | | | | | | | | | | | | | | | | | | | | | | | | | |
| JITTER BUDGET (psec) | 1983-85 | 1986 | | | | | | | | | | | | | | | | | | | | | | | | | | | | | | | | | | | | | | | | | | | | | | | |
| Laser pulse FWHM | 30 | 30 | | | | | | | | | | | | | | | | | | | | | | | | | | | | | | | | | | | | | | | | | | | | | | | |
| Ranging counter HPS368 |) 100 | | | | | | | | | | | | | | | | | | | | | | | | | | | | | | | | | | | | | | | | | | | | | | | | |
| HPS3708 | | 35 | | | | | | | | | | | | | | | | | | | | | | | | | | | | | | | | | | | | | | | | | | | | | | | |
| Start detector/discriminator |) 150 | 30 | | | | | | | | | | | | | | | | | | | | | | | | | | | | | | | | | | | | | | | | | | | | | | | |
| PMT /dynode/ RCA31834A | 298 | 298 | | | | | | | | | | | | | | | | | | | | | | | | | | | | | | | | | | | | | | | | | | | | | | | |
| Diode /HPSS in Geiger mode/ | | 98 | | | | | | | | | | | | | | | | | | | | | | | | | | | | | | | | | | | | | | | | | | | | | | | |
| RESULTING (psec) | | | | | | | | | | | | | | | | | | | | | | | | | | | | | | | | | | | | | | | | | | | | | | | | | |
| (PMT) | 520 | 300 | | | | | | | | | | | | | | | | | | | | | | | | | | | | | | | | | | | | | | | | | | | | | | | |
| (Diode) | | 100 | | | | | | | | | | | | | | | | | | | | | | | | | | | | | | | | | | | | | | | | | | | | | | | |
| SYSTEM STABILITY (psec) | | | | | | | | | | | | | | | | | | | | | | | | | | | | | | | | | | | | | | | | | | | | | | | | | |
| | 1983-85 | 1986 | | | | | | | | | | | | | | | | | | | | | | | | | | | | | | | | | | | | | | | | | | | | | | | |
| PMT (dynode) based receiver | 150 | 118 | | | | | | | | | | | | | | | | | | | | | | | | | | | | | | | | | | | | | | | | | | | | | | | |
| Diode based receiver | | 26 | | | | | | | | | | | | | | | | | | | | | | | | | | | | | | | | | | | | | | | | | | | | | | | |

K. Hanal, I. Prochazka
System stability using mode locked train

3

K. Hanal, I. Prochazka
System stability using mode locked train

4

SATELLITE LASER RANGING ERRORS

L. Jiyu
Wuhan Technical University of
Surveying and Mapping
23 LO-Yu Road, Wuhan
The People's Republic of China

ABSTRACT

Satellite laser ranging systems are used effectively to determine earthcrustal dynamic parameters. The accuracy and reliability of SLR products are of extraordinary importance for an appearance of new scientific information. This paper has discussed all potential SLR errors and their magnitude, and given some recommendations for decrease, such as how to take meteorological data, how to approximate optimal calibration, how to control transit time jitter.

Satellite Laser Ranging Errors

by Liu Jiyu

Wuhan Technical University of Surveying and Mapping
23 Luyu Road, Wuhan, The People's Republic of China

ABSTRACT: Satellite laser ranging systems are used effectively to determine earthcrustal dynamic parameters. The accuracy and reliability of SLR products are of extraordinary importance for an appearance of new scientific information. This paper has discussed all potential SLR errors and their magnitude, and given some recommendations for decrease, such as how to take meteorological data, how to approximate optimal calibration, how to control transit time jitter.

ZUSAMMENFASSUNG: Um dynamische Parameter der Erdkruste zu messen, werden die Laserentfernungsmeßsysteme zu künstlichen Satelliten benutzt. Die Genauigkeit und Zuverlässigkeit der Ergebnisse der Laserentfernungsmessung besitzt außerordentliche Wichtigkeit für neue wissenschaftliche Erkenntnisse. Der Artikel hat alle potentiellen Fehler der Laserentfernungsmessung und ihren Größen diskutiert und zeigt einige Vorschläge, z. B. wie bessere meteorologische Daten zu gewinnen sind, wie ein optimale Kalibration durchzuführen ist und wie der Jitter zu verbessern ist.

Fixed and highly mobile satellite laser ranging systems, which located at 40 stations distributed in 19 countries, have been ranging to satellites for the Crustal Dynamics Research Program (acronym CDRP), Part of NASA's Geodynamics Program. In order to execute the CDRP a lot of fund have to be expended, for example, expending approximately \$ 2.8 million in FY 1986 [Edelson, 1985]. The accuracy and reliability of the products are of extraordinary importance for being able to provide valuable and exciting new scientific information on geodynamics. On the basis of unstable ranging products would scientists be able to make the reliable conclusions which, for example, will indicate that the rates of motion of the larger

tectonic plates are within 1 cm/yr? Therefore, it is very necessary to find out all potential source of SLR errors and to search out some methods for eliminating, at least decreasing them.

There have been some effective efforts to improve SLR accuracies, such as making use of pulsewidths as short as 30 picoseconds, micro-channel plate photomultipliers, zero-delay configuration and two-color laser. When a greater improvement is expected for SLR accuracies it will be very useful to systematically investigate all potential errors for SLR. This paper will try to achieve this purpose.

1. SLR Error Expression

It is known that a distance between a ground station and the satellite specially equipped with retroreflectors (laser satellite), D measured by SLR systems can be written as

$$D = \frac{C_0}{2n} \frac{N}{f} + d_0 \quad (1)$$

Where, C_0 = velocity of light in a vacuum;

n = effective refractive index on the laser pulse path;

N = number of a timing clock pulses recorded by a time interval unit (TIU);

f = clock frequency of the TIU;

d_0 = additional constant, including two portions: one is an equivalent length caused by a difference between the electro-optical centre and the mechanical centre of the SLR system, being simplified into system constant; another is a correction resulting from that the effective reflecting points of retroreflectors have to be reduced to the center -of- mass of the laser satellite, equaling 25.8 cm for LAGEOS, 7.5 cm for STARLETTE.

From the above distance equation the following error expression for SLR has been derived [Liu, 1985]:

$$M_D^2 = \left[\left(\frac{M_{C_0}}{C_0} \right)^2 + \left(\frac{M_n}{n} \right)^2 + \left(\frac{M_f}{f} \right)^2 + \left(\frac{M_N}{N} \right)^2 \right] \cdot D^2 + M_{d_0}^2 \quad (2)$$

Where, M = errors whose subscripts depend on the foregoing respective marks.

On the basis of the above expression we shall discuss all errors emerging from SLR as detailing as possible and give some recommendations for decreasing them.

2. Index Error, M_n

The Marini and Murray (MM) formula has been used to calculate atmospheric refraction corrections for SLR [Sylvania, 1974, Bufton, 1978, Tapley, et al, 1982]. The MM formula based on that of atmospheric refractive index in consideration of an elevation angle, site latitude and site altitude [Marini and Murray, 1973]. The surface level measurements of atmospheric pressure, temperature and relative humidity are required when using the MM formula [Bufton, 1978]. However, to the best of writer's knowledge some operators for SLR systems have taken the meteorological data only at one surface point near the earth surface. The height of the point is often lower than that of a transmitted and received telescope of SLR system, achieving several meters lower at the fixed station. How can these readings represent the meteorological data along the laser pulse path in an atmospheric layer? On the other hand, they have always taken one time for the meteorological data while observing one satellite pass, and reading in only ranging start. In general one satellite pass has to last in several decade minutes for LAGEOS. In such long time interval the meteorological data can not keep to the same values at all. When using the same data to calculate the overall refraction corrections, how can the ranging products escape the error effect due to not matching meteorological data? In this case there is a natural difference between the start and end ranging products of one satellite pass due to the only incoordinate refraction correction.

It was pointed out that atmospheric refraction corrections have achieved accuracies within a few cm at 20° elevation when only taking the meteorological data at the ranging site [Abshire and Gardner, 1984]. If taking in consideration of the above two man-made errors the correction accuracies have to be reduced again. When refractive indices calculated contain the error of $\pm 2 \times 10^{-8}$ the

distance error, M_{Dn} will achieve ± 2.4 cm for the atmospheric layer of 1200 km. If the difference between the temperatures is equal to only $\pm 0.5^\circ$ C the distance error will achieve ± 0.53 mm/km for a ground laser ranging under the condition of $P = 760$ mmHg, $-20 \leq t \leq +40^\circ$ C. In order to escape the man-made errors the following recommendations appear as being useful:

- the meteorological instruments have to be settled at least as high as the transmitted and received telescopes of SLR systems;
- the meteorological readings for each satellite pass should be made with a few times, for example, taking them in the start, mid and end of each satellite pass. We, of course, would better make use of an interpolation of the meteorological data at the weather stations of the region near a ranging station;
- the psychrometer and barometer have to be checked to send them to a meteorological bureau for a few times per year. For example, when the drift of the zero point of a barometer equals within only ± 2 mmHg the distance error due to this will achieve ± 0.76 mm/km for a ground laser ranging.

Applications of two-color laser ranging technique can omit not only the exact measurements of the meteorological data, but also improve the accuracy to one order of magnitude for measured distances [Liu, 1984]. When making use of the two-color technique for SLR we must not consider atmospheric refraction corrections. In recent years a few scholars have been investigating two-color laser applications in SLR systems and getting desirous progress [Abshire and Gardner, 1984, Mastrocinque, 1985]. However, pulsed two-color SLR systems require some advanced equipments, such as mode-locked multiple frequency lasers, streak camera receivers and atmospheric delay measurements with an accuracy of 0.5 cm or better. This restricts its wide applications at once.

It must be pointed out that the path curvature correction is less than 1 cm when the zenith angles do not exceed only 70 degrees. If the zenith angles are greater than ones, the path curvature corrections have to be taken into consideration. For example, when the zenith angle is equal to 74 degrees it is greater than 1.5 cm [see Fig. 1, Sylvania., 1974]. To neglect the 1.5 cm correction is equivalent to introduce the same as error.

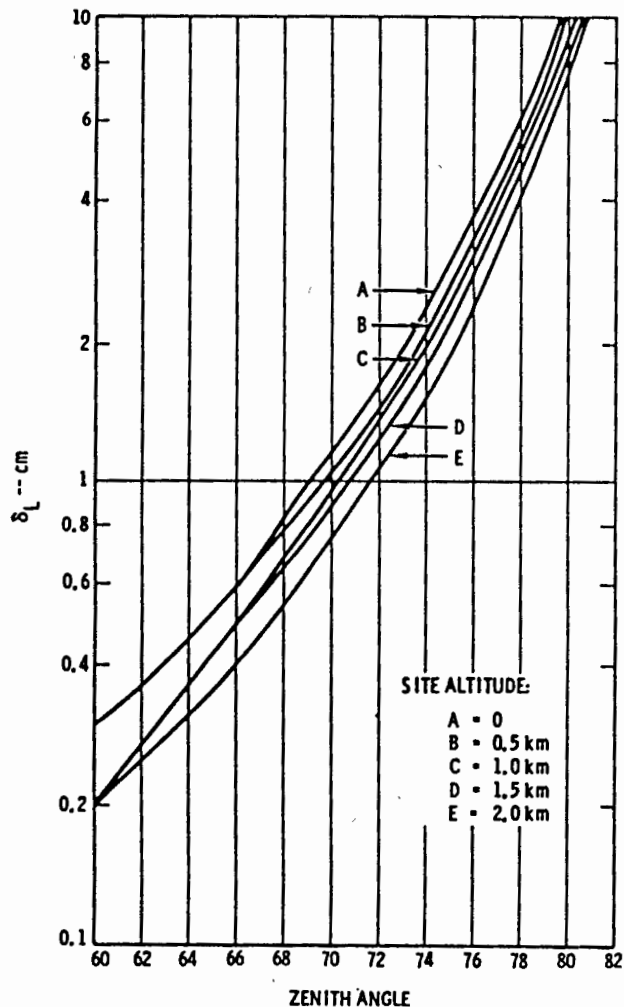


Figure 1 = Path Curvature Correction, from Sylvania

3. Velocity Error, M_{co}

The velocity of light, in a vacuum used for calculation of the foregoing distance, D was obtained by means of measurements at a field or laboratory, beginning at the year of 1676 by Roemer. The recently precise value (299792458 m/s) was also measured to make use of the laser metrology. The latter can only provide an accurate measurement, but not escape any error to influence the velocity value of light in a vacuum. It is known that there is an error for measurements all the time, but it will be different to have its size. Therefore, the following velocity value of light in a vacuum proposed by IUGG in August 1975 is very right:

$$C_0 = 299792458 \pm 1.2 \text{ m/s}$$

It is very necessary that the error of ± 1.2 m/s will be considered for laser ranging far off several thousand kilometers, even far off about 380 thousand kilometers, that is

$$\frac{M_{co}}{C_0} = \pm 4 \times 10^{-9}$$

For example, when only taking the elevation angles from 70° to 15° for LAGEOS the correspondent distances are equal to 6000 km to 9000 km. In this case, even if assuming all other sources of error are zero, the distance error, M_{DCo} produced only by the velocity error, ± 1.2 m/sec will achieve ± 2.4 cm to ± 3.6 cm. If the measured error of the velocity of light in a vacuum were to be decreased from ± 1.2 m/sec to at least ± 0.12 m/sec, the M_{DCo} would be able to be neglected. Except this the only velocity error, M_{DCo} makes the real accuracy can not achieve ± 1 cm for SLR. If we do not employ $C_0 = 299792458 \pm 1.2$ m/sec, but other values for the velocity of light in a vacuum, such as $C_0 = 299792.5 \pm 0.4$ km/sec, the velocity error will be much greater than that. This is very worthy to be considered.

4. Frequency Error, M_f

On the basis of the analyses to materials desirable discriminators have to match with an ideal time interval unit. For example, under the condition of using a constant fraction discriminator (CFD) the measurement accuracy for flight time depends essentially on the TIU. If an advanced event timer is used to measure the flight time, t_d the following expression can be given:

$$t_d = N_0 T_0 + t_1 - t_2 \tag{3}$$

- Where, N_0 = number of period of the clock pulse train;
- T_0 = period of the clock pulse train;
- t_1 = front part for the time interpolation;
- t_2 = additive part for the time interpolation.

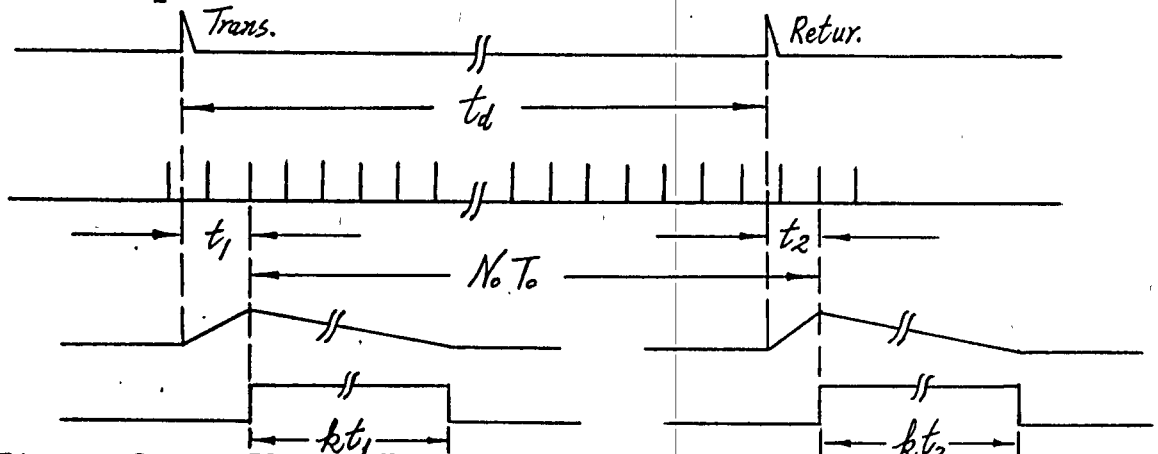


Figure 2 = Flight Time Measurement

When we select $T_o/T_r = k$, where T_r is the desired timing resolution, the following widths of the interpolating pulses are measured:

$$kt_1 = N_1 T_o, \quad kt_2 = N_2 T_o$$

Therefore, the flight time can be written as

$$\begin{aligned} t_d &= (N_o + \frac{N_1}{k} - \frac{N_2}{k}) T_o \\ &= (kN_o + N_1 - N_2) \frac{1}{kf} \end{aligned} \quad (4)$$

Where, f = clock frequency of the event timer;

k = stretching coefficient of the event timer;

N_1 = period number of the clock pulse for the front part;

N_2 = period number of the clock pulse for the additive part.

From the above equation the following error expression for the measured flight time can be acquired:

$$M_{td} = \pm (kN_o + N_1 - N_2) \frac{M_f}{kf^2} = \pm \frac{M_f}{f} t_d \quad (5a)$$

or written as

$$M_{Df} = \pm \frac{M_f}{f} D \quad (5b)$$

If $M_f/f < \pm 1 \times 10^{-9}$, the distance error, M_{Df} which varies as the measured distances to the satellite is not greater than ± 1 cm for the foregoing distance range.

5. Period Error, M_N

The period error consists of a resolution error, pulsewidth error, wavefront error, fluctuation error and timing error. If the resolution of the event timer is equal to 66.7 psec, its equivalent distance resolution will equal 1 cm. In this case the SLR system can only measure the distances for how many times of 1 cm, but not the distance portions within 1 cm. The time interval unit used by SAO

has a resolution of 0.1 nsec [1.5 cm, Pearlman, 1983]. The lower the distance resolution is, the greater the resolution error gets. In a word the resolution error is produced by the timer resolution which cannot be enough small.

The pulsewidth error results from that the energy of a laser pulse is not centralizing in a moment, but distributing in a shorter interval. For example, the pulse of 5 to 7 joules generated by the ruby laser system has the FWHM of 25 nsec for early SAO SLR system [Pearlman, et al, 1978]. Nd:YAG lasers with modelockers can generate light pulses as short as 30 psec [Puell, 1982, Degnan, 1985]. When the laser pulses impinge on a photocathode the conversion from a light pulse to an electronic pulse has to be distorted due to some disturbance. The pulsewidth error, M_W is of a random ranging one which varies as the laser pulse width and the number of received photoelectrons [Degnan, 1985]. It can be written as

$$M_W = \frac{k_p \tau_p}{\sqrt{N_r}} \tag{6}$$

Where, τ_p = FWHM of a laser pulse;

N_r = number of received photoelectrons;

k_p = coefficient depending on different detection.

An external pulse slicer, which consists of a Pockels cell and is situated between crossed polarizers, was used early in order to constrict the laser pulse width from 20 nsec to about 4.5 nsec [Degnan, 1985]. Due to its lower efficiency the cavity dumped Nd:YAG laser was substituted for it rapidly. At present modelocked Nd:YAG lasers are mostly used to obtain a shorter and single mode laser. It has been seen from the ranging results that the accuracies increased to at least 50 % after the pulse width was reduced from 25 nsec to 6 nsec by means of a pulse chopper in the SAO SLR systems [Tapley, et al, 1982].

The wavefront error is caused by the wavefront distortion of a transmitted and returned laser beam. It is known that individual radiation modes which are possessed of different spatial and temporal property, build up at their own rates in Q-switched lasers. When they appear out of the laser cavity these different spatial modes

will have different far field patterns. The latter is defined as the wavefront distortion of the transmitted beam. When the distorted wavefront beam is used to measure the distances to a laser satellite the satellite-borne individual retroreflectors will catch different wavefronts. The returned signal received by SLR systems is an ensemble of reflections from all those retroreflectors facing in the general direction of the ranging station. When the distortion returned signal is used to stop the operation of TIU this will have to produce a ranging error, so - called wavefront error. The latter measured by SAO has shown peak to peak change of 4,5 cm to 7.0 cm [Pearlman, 1983].

At present modelocked Nd:YAG or Nd:YAP lasers are used in the most modern SLR systems. The lasers operate in the fundamental TEM₀₀ mode. The latter produces the smallest beam divergence, the highest power density, and, hence, the highest brightness. Furthermore, the radial intensity profile is uniform and uniphase [Koechner, 1976]. This makes the laser beam transmitted by modelocked Nd:YAG lasers does not exhibit the wavefront distortion. The experiment data on the ground baseline have also demonstrated that the performance of modelocked lasers is far superior to that of other laser types [Degnan and Zagwodzki, 1982].

The fluctuation error is produced by the strength fluctuation of a returned laser pulse from the satellite-borne retroreflectors far off several thousand kilometers. The strength fluctuation makes the output signals from PMT become ones with a randomly varying amplitude. When the latter drives a discriminator, such as fixed threshold, rise time compensated and hybrids one, the varying signal amplitudes will produce time biases on the order of half the input pulse width. Even if using a constant fraction discriminator with a compensation circuitry for the varying signal amplitudes the strength fluctuation can not be compensated wholly due to the rapidly varying atmospheric. It will be seen from the experimental data that when changing input pulse amplitudes from 0.1 voltages to 4 voltages the time walk due to this will be equal to + 3 cm to -2 cm for ORTEC 934 CFD currently used in the NASA MOBLAS network [Degnan, et al, 1984]. The analogous experiment by SAO indicated that the average fluctuation error has achieved $\pm 2,2$ cm, the maximum ± 4.5 cm [Pearlman, 1983].

According to the experience of McDonald Observatory there will not be any significant signal strength effect to the calibration and satellite data when the SLR system operates indeed in the single photoelectron domain. However, it is necessary to monitor hard the operation. When there are significant multi-photoelectron events this will result in a high dynamic range in the returned signal strength [Ricklefs, et al, 1985].

Currently single-stop TIU's are used in almost all operatin SLR systems to measure the flight time. When an incoming noise exceeds the stop discriminator threshold it will be easy to produce pseudo-measurements for this sort of TIU. The timing error does not imply the pseudo-measurements at all, but the effects from the TIU own proterty which can not be as good as possible. It consists of an interpolated and triggered error. In order to measure precisely the flight time an interpolation counts are used in TIU (see Fig.2). For example, the interpolated error results fròm that the stretch-ing coefficient, k has not been calibrated to the nominal value. When the stretching coefficient offset incompatible with the nor-minal value achieves ± 0.5 the interpolated error is equal to 67 psec. The interpolated error resulting from a nonlinear spreading to the smaller components, $t_1 t_2$ can achieve ± 60 psec for 15 MHz event timer [Guan, et al, 1982]. The interpolated error for HP 5360 A Time Interval Counter is ± 1 nsec from 0° C to 50° C [HP, 1975].

The triggered error of TIU includes both an input trigger circuit error and error due to noise on input signal. It is known that the start and stop input signals are typically DC-coupled in TIU used by SLR systems. Any noise can superimpose on the baseline of the start or stop signals. This has to result in the triggered error. Therefore the advanced HP 5370A TIC with a 20 psec time resolution can only achieve the time measuring accuracy of 100 psec [Deghan, 1985].

6. Constant Error, M_{do}

The constant error contains a transit error, calibration error, sync error and satellite error. The transit error results from the transit time jitter for the photoelectrons from the photocathode to the anode in PMT. The transit time jitter is produced essentially by the following factors:

- the fluctuation of the photocurrent transmitted by the photocathode due to a strong scintillation of the returned laser from Satellite-borne retroreflectors;
- the variance of the position and size of the light spot illuminating on the photocathode;
- the unstability of DC power supply voltage for PMT.

For example, the transit time jitter varied with DC voltage between a pair electrodes has been given [Liu, 1983]:

$$M_{te} = \frac{M_u}{2U} \sqrt{\frac{2md^2}{eu}} \quad (7)$$

Where, m = electron mass, $m = 9 \times 10^{-28}$ grams;

e = electron charge, $e = 4.8 \times 10^{-10}$ statcoulombs;

u = DC voltage between a pair electrodes in statvolt;

d = distance interval between a pair electrodes in centimeter.

When there are nine dynodes in the PMT the overall transit time is equal to 18.8 nsec under the condition of $d = 0.7$ cm, $u = 155$ V. If the voltage change rate of DC power supply for the PMT, M_u/U equals ± 0.019 the overall transit time jitter will achieve ± 180 psec (± 2.7 cm). If $M_u/U = \pm 0.002$ the jitter will be equal to ± 19 psec (± 3 mm). It will be seen from this that a strictly regulating circuitry has to be used for the DC power supply to the PMT, so as to decrease the transit time jitter.

The experiment results measured by E. Bergstand to RCA 1P21 PMT indicated that the transit time difference between an illuminating centre and eccentric point on the photocathode with ± 3 mm is equal to 1.9 nsec (28.5 cm). It will be seen from this that a position stability of the illuminating point has to be required strictly for the photocathode. The variance with time can not be permitted during ranging.

It is will be known that in an illuminating region on the photocathode the photoelectrons from the respective transmitting points are not synced due to the photoeffect feature. Therefore the transit time is a statistical average for the photoelectrons. If the size of the illuminating spot on the photocathode varies as time, the average will be changed with it, so as to result in the transit time jitter.

The transit time jitter for microchannel plate photomultipliers (MCP/PMT) is much smaller than that for dynode chain PMT's. Experiment data have shown that the one sigma transit time jitter for an ungated ITT F4128 MCP/PMT was equal to about two centimeters for single photoelectron inputs, but one for the Amperex 2233B PMT achieved ten centimeters [Degnan, et al, 1984]. There is also faster impulse response for MCP/PMT'S. It will be seen from these that it is desirable to use MCP/PMT in SLR systems.

The calibration error varies as different calibration. It is the purpose of SLR calibration to control the change of the system constant which is produced by the jitter of an internal circuitry delay. When signals in SLR system are transferring from one circuit to other circuit it is necessary to spend a certain time. The spent time in circuitries is defined as the internal delay. Its value can be not only calculated on the basis of the circuitry parameters, but also determined by means of ground baselines whose lengths were measured precisely. If the system constant should not vary there would not be any error for corrected ranging data with one. In fact the system constant is of changing due to that of the internal delay. The latter of the start pulse gotten through the start channel can not compensate that of the stop pulse gotten through the stop channel. The system constant contains the difference between the internal delay of the start and stop pulse. The optimal calibration is defined as being able to eliminate the jitter influence. However, in practice there is any difficulty to achieve this purpose. For example, it can be demonstrated with the following experience [Mangin, 1982]:

On June 17, 1981: cal. = 199.0 nsec.

On September 16, 1981:

- Single round trip: cal. = 198.7 nsec,
- Double round trip: cal. = 198.5 nsec,
- Silverberg method: cal. = 198.7 nsec
- Internal target: cal. = 199.1 nsec.

According to the above calibration results we can calculate that one sigma is equal to ± 0.219 nsec (± 3.3 cm), and know:

- the results are varying with the different calibration method;
- there are the different results for the variant time.

Experience by SAO has also indicated the typical values for the jitter range' from ± 0.15 nsec to ± 0.20 nsec ($\pm 2 - \pm 3$ cm), not including PMT; when including PMT from ± 0.2 nsec to ± 0.3 nsec ($\pm 3 - \pm 4.5$ cm) [Pearlman, et al, 1982].

It will be known from the above experience data that the greater delay jitter has to be taken enough notice for precisely ranging. In order to approximate the optimal calibration a few SLR systems have employed some internal calibration, such as the feedback calibration of TLRS ranging system [Silverberg, 1982], the double calibration of MTLRS mobile system [Wilson, 1982] and the zerodelay system of Goddard new experimental facility [Degnan, 1985]. In writer's opinion there will be a much smaller jitter due to each other compensation for the start and stop delay when the start and stop pulse emerge in common from one channel circuitry based on a common PMT. If the SLR systems with the internal calibration were to make use of one common channel circuitry they would be able to approximate the optimal calibration mostly.

When making use of ground baselines for the SLR calibration the baseline length has to be measured precisely. For example, when baselines are measured to use AGA Geodimeter 8, due to its standard diviation of $\pm (5 \text{ mm} + 1 \times 10^{-6} D)$ the measured error for 5 km baseline will achieve ± 1 cm. If microwave distance measuring instruments

are used to measure the 5 km baseline the measured accuracy of ± 1 cm will be unable to be achieved at all. For example, when using MRA-5 Tellurometer the measured accuracy will only achieve ± 2.5 cm. The low measured accuracy for ground baselines will become into a limitation for the calibration accuracy except using still more precise baselines. In performing the SLR calibration the meteorological data must be taken for the calibration refraction correction. We would better take them on two end points of the ground baseline whose length is equal to several kilometers, so as to improve the calibration accuracy.

When the momentary time arriving at the satellite for the laser pulse can not be exactly reduced to UTC the following sync error will be produced [Liu, 1985]:

$$M_s = -V_s M_t \cos\alpha \quad (8)$$

Where, V_s = movement velocity of the satellite in the space,

M_t = ranging moment error in respect to UTC,

α = Satellite elevation.

It was pointed out that the best synchronization results have an RMS of a half microsecond, and the worst synchronization results have been a four microsecond RMS [Oaks, et al, 1982]. It was known that $V_s = 5698$ m/sec for LAGEOS; $V_s = 7400$ m/sec for STARLETTE [Mastrocinque, 1985]. If taking $M_t = \pm 4 \mu s$, $\alpha = 15^\circ$, we will know $M_{SL} = \pm 2.2$ cm for LAGEOS, $M_{SS} = \pm 2.9$ cm for STARLETTE. Assuming $M_t = \pm 7 \mu s$, we will obtain $M_{SL} = \pm 3.8$ cm, $M_{SS} = \pm 5.0$ cm. If using $M_t = \pm 0.5 \mu s$, we will get $M_{SL} = \pm 3$ mm, $M_{SS} = \pm 4$ mm. It will be seen from these calculated sync errors that there will be greater sync errors for both a high and low satellite when the moment error, $M_t \geq \pm 4 \mu s$ and the elevation is smaller. Therefore, an exact time synchronization has to be performed in order to reduce the sync error. It is better to use a Time Transfer Receiver (TTR) operating with the NAVSTAR Global Positioning System (GPS). Its time synchronization accuracy is expected to achieve a RMS of less than 50 nsec [Oaks, et al, 1982]. GPS TTR's were started to synchronize the time for some SLR systems, such as the mobile MTLRS system in Winter 1985.

The satellite error is caused by a deviation from the satellite center-of-mass (SCM) correction and a coherent fading effect. The satelliteborne retroreflectors are distributed on each laser satellite crust. The effective reflection points depending on a centroid of the incoming laser pulse have to be reduced to the satellite center-of-mass. For LAGEOS the SCM correction is theoretically equal to 258 mm. However, the SCM correction varies with a function of incidence angle, laser pulsewidth, detection means and receiver impulse response. The experimental data have shown that the SCM correction was changed from 245.7 mm to 253.8 mm when the laser pulsewidth was equal to 1 nsec to 61 psec. The SCM correction for centroid detection was 249 mm with a standard deviation of 1.7 mm [Degnan, 1985]. For gravity gradient satellites the incidence angle, θ between the laser beam and the axis of symmetry of the satellite can be approximately expressed [Carpenter, 1978]:

$$\theta = \arctan \frac{\cos \alpha}{\sin \alpha + \frac{D}{R}} \quad (9)$$

Where, D = distance between a ground station and laser satellite;
R = earth's radius.

It will be known from the above mention that the satellite error has to be produced due to the different pulsewidth, detection means and incidence angle. On the other hand, there is the so-called coherent fading effect for the returned beam. The latter is an ensemble of reflections from all those retroreflectors facing in the general direction of the observation station. Due to superimposing from the individual returned signals each other this results in a coherent interference for corresponding electric fields in the receiver. The coherent fading effect will cause a random timing error with a standard deviation of 77 psec [1.15 cm, Degnan, 1985].

7. Conclusions

From what has been said above, we know that the real accuracy for SLR can not achieve ± 1 cm proposed by them at all, but only a few centimeters for the executed experiments. SLR errors can be divided into two types:

- condition errors caused by exterior conditions in laser ranging,
- instrumentation errors caused by the properties which are not enough good for SLR systems,

and summarized in the following table:

| | | |
|--------------------------------|------------------------|--|
| Satellite laser ranging errors | condition errors | velocity error resulting from the measurement error for velocity of light in a vacuum; index error resulting from inaccurate meteorological data; satellite error resulting from the inaccurate satellite center-of-mass correction and coherent fading effect; sync error resulting from an inexact clock synchronization; calibration error resulting from the inexact measurement for the system constant; |
| | instrumentation errors | frequency error resulting from the difference between the nominal and real value of a clock frequency; resolution error resulting from the counter resolution which can not be enough small; timing error resulting from the counter property which of itself can not be as good as possible; fluctuation error resulting from the strength fluctuation of a returned laser pulse; pulsewidth error resulting from that the energy of a transmitted laser pulse is not centralizing in a moment; wavefront error resulting from the wavefront distortions of a transmitted and returned laser beam; transit error resulting from the transit time jitter for the photoelectrons from the photocathode to the anode in a PMT. |

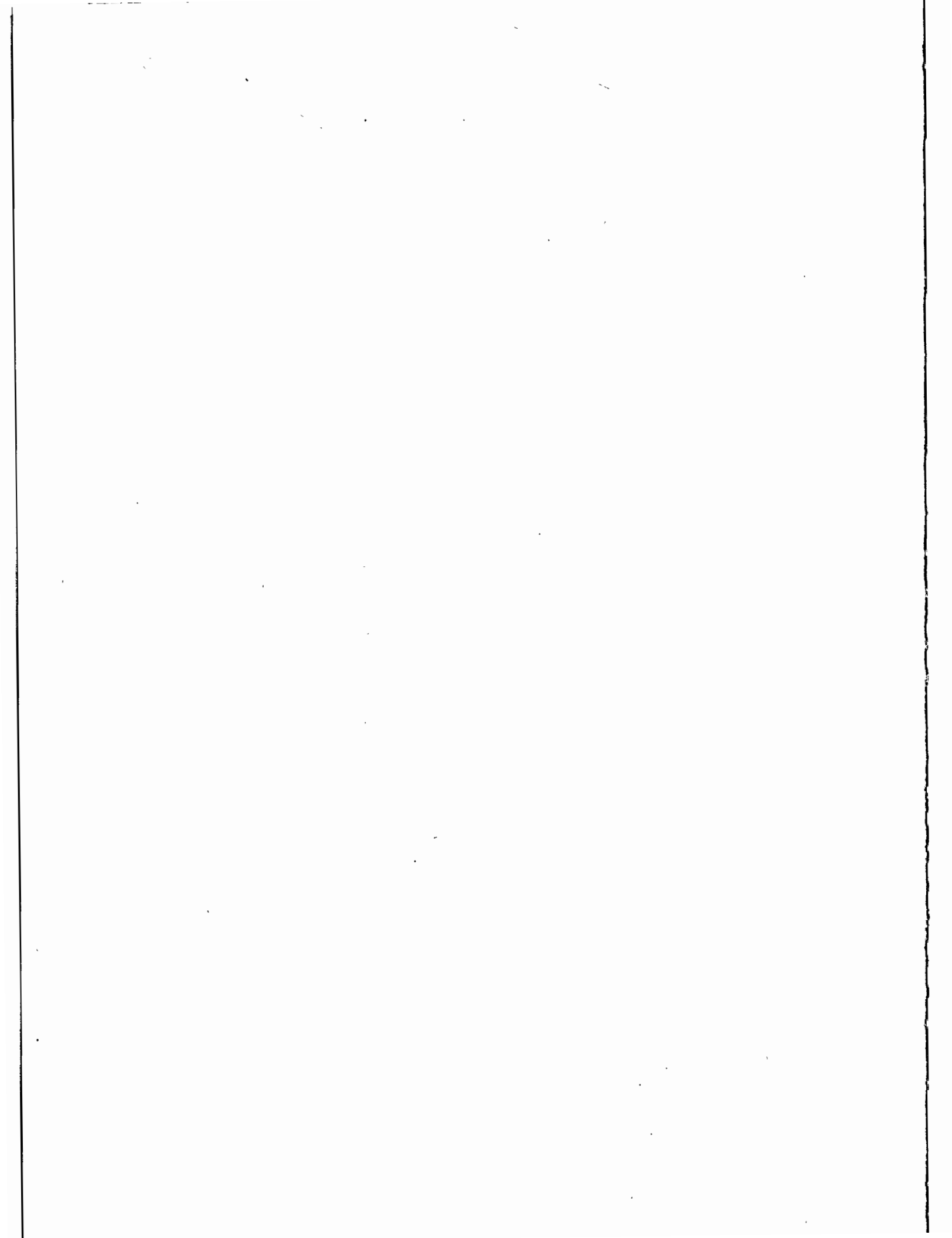
8. Acknowledgments

This paper was written during studying at the Satellite Observation Station Wettzell. The writer would like to express his hearty gratitude to Dr. R. Höpfl for often providing some references and many beneficial discussions, to Mr. W. Schlüter for his help.

References

- [1] B.I. Edelson, Dear Colleague letter
Space Science and Applications Notice, NASA, April 12, 1985
- [2] Liu Jiyu, Will Satellite Laser Ranging Measurements Be Able
to Achieve 1-cm Real Accuracy?
Second International Conference on Trends in Quantum Electro-
nics, Bucharest, September 2-6, 1985
- [3] GTE Sylvania, Proposal for Satellite Ranging system
24 May 1974
- [4] J.L. Bufton, Review of Atmospheric Correction for Laser
Ranging Data
Third International Workshop on Laser Ranging Instrumentation..
Lagonissi. May 23-27.1978
- [5] B.D. Tapley. et al. A Critical Analysis of Satellite Laser
Ranging Data
Proceedings of the Fourth International Workshop on Laser
Ranging Instrumentation, Published by the Geodetic Institute,
University of Bonn, 1982, pp. 523-567
- [6] J.W. Marini and C.W. Murray, Correction of Laser Range Tracking
Data for Atmospheric Refraction at Elevations above 10 Degrees
GSFC Report X-591-73-351, Nov. 1973
- [7] J.B. Abshire and C.S. Gordan, Atmospheric Refractivity Correc-
tions in Satellite Laser Ranging
IEEE Transactions on Geoscience and Remote Sensing September 1984
- [8] Liu Jiyu, Some Recommendations for Improving Two-color Distances
The Canadian Surveyor, Vol. 38, No. 4 Winter 1984, pp.295-298
- [9] G. Mastrocinque, Feasibility of Satellite Tracking with a Dual-
wavelength Laser Ranging System
ESA Journal, 1985, Vol. 9, pp. 273-286
- [10] M.R. Pearlman, Status of the SAO Laser Ranging Systems
CSTG Bulletin, No. 5, march 10, 1983, pp. 66-73
- [11] M.R. Pearlman, et al, The Smithsonian Astrophysical Observa-
tory Satellite Ranging Hardware
Third International Workshop on Laser Ranging Instrumentation,
Lagonissi, May 23-27, 1978
- [12] H. Puell, Subnanosecond Laser System for Satellite Ranging
Proceedings of the Fourth International Workshop on Laser
Ranging Instrumentation, published by the Geodetic Institute,
University of Bonn, 1982, pp. 277-284
- [13] J.J. Degnan, Satellite Laser Ranging: Current Status and
Future Prospects
IEEE Transactions on Geoscience and Remote Sensing,
Vol. GE-23, No.4, July, 1985, pp. 398-413
- [14] W. Koechner, Solid-state Laser Engineering
Springer-Verlag, Berlin, 1976, p. 195

- [15] J.J. Degnan, T.W. Zagwodzki, A Comparative Study of Several Transmitter Types for Precise Laser Ranging
Proceedings of the Fourth International Workshop on Laser Ranging Instrumentation, Published by the Geodetic Institute, University of Bonn, 1982, pp. 241-250
- [16] J.J. Degnan, et al, Satellite Laser Ranging Experiments with an Upgraded MOBLAS Station
The Fifth International Workshop on Laser Ranging Instrumentation held at the Royal Greenwich Observatory East Sussex, England, September 10-14, 1984
- [17] R.L. Ricklefs, P.J. Shelus, R.J. Eanes and J.R. Wiant, MLRS System Characterization
September 19, 1985
- [18] Guan Zhenhua, et al, JLJ-2 High Resolution Counter for Laser Ranging Systems, 1982 (in Chinese)
- [19] Hewlett Packard (HP), Operating and Service Manual, Computing Counter 5360A and Input Module 5365A
October 1975
- [20] Liu JiYu, Accuracy Judgement on EDM equipments (in Chinese)
Bulletin of Surveying and Mapping, No. 3, June 1983, pp. 29-35
- [21] J.F. Mangin, The Laser and the Calibration of the CERGA Lunar Ranging System
Proceedings of the Fourth International Workshop on Laser Ranging Instrumentation, Published by the Geodetic Institute, University of Bonn, 1982, pp. 313-322
- [23] E.C. Silverberg, The Feedback Calibration of the TLRS Ranging System
Proceedings of the Fourth International Workshop on Laser Ranging Instrumentation, Published by the Geodetic Institute, University of Bonn, 1982, pp. 331-337
- [24] P. Wilson, The German/DUTCH Mobile Ranging System
Proceedings of the Fourth International Workshop on Laser Ranging Instrumentation, Published by the Geodetic Institute, University of Bonn, 1982, pp. 468-483
- [25] O.J. Oaks, et al, GPS Time Transfer Receiver for the NASA Transportable Laser Ranging Network
Proceedings of the Fourth International Workshop on Laser Ranging Instrumentation, Published by the Geodetic Institute, University of Bonn, 1982, pp. 338-375
- [26] L. Carpenter, Goddard Laser Tracking Data
Third International Workshop on Laser Ranging, Lagonissi, Greece, may 23-27, 1978



SOME CURRENT ISSUES ON LASER COLLOCATIONS

M.R. Pearlman
Smithsonian Institution
Astrophysical Observatory
Cambridge, MA 02138

Telephone (617) 495 7481
Telex 921428 SATELLITE CAM

ABSTRACT

Collocation experiments are being conducted to isolate and study systematic errors in laser ranging systems. Proper use of the unique collocation configuration requires that these experiments be allowed to focus on effects that would be difficult to find in single system ground and readiness tests. This requires that (1) the systems be fully tested and field ready prior to collocation and (2) sufficient time and resources be allocated for proper test and analysis. A brief review of recent collocation requirements and experience is presented along with current issues and shortcomings.

INTRODUCTION

Laser collocations allow us to isolate and study the systematic errors in laser ranging machines. To the extent that the error sources are independent from one machine to another, systematic effects appear as offsets in short arc analyses between the collocated systems. The unique geometry of machines in close proximity permits comparative analysis without corruption from modelling errors such as atmospheric refraction, spacecraft center of mass, and spacecraft orbit. To obtain full value from the collocation, each participating system must be operated in a fully independent manner, thereby simulating conditions and performance that would be anticipated from stations operating on their own at remote locations. The more the systems have in common, the less rigorous is the test.

Even though it is not the intent, collocations have traditionally provided a full test of entire ranging operations from predictions, through hardware and procedures, to final data analysis. This is both good news and bad: A full stress test exposes all of the weak points in the system, but using the collocation configuration to find very mundane problems is a waste of very limited resources.

NATURE OF COLLOCATION RESULTS

Historically, collocations have revealed three kinds of results:

- (1) **INCIPIENT PERFORMANCE LIMITATIONS** which refer to limitations in capability imposed by the characteristics of the ranging system in its current configuration, limitations which would be difficult to find with the existing single station ground tests.
- (2) **CHARACTERIZATION EFFECTS** which refer to limitations which should have been observed and measured with single system ground tests.
- (3) **FAILURES.**

Incipient performance limitations are system shortcomings which may be very elusive and frustrating, but discovery represents experiment success; something unexpected and possibly new was discovered. In the past, effects such as wavefront variations, signal strength variations, variations with equipment temperature and azimuth dependence were discovered, and in most cases procedures were then added to the standard ground tests to include these effects.

Characterization effects are effects that we have seen before, effects for which ground based tests already exist

within the standard test procedures. Problems in this category usually arise because preliminary ground tests and engineering tests have not been properly conducted and/or analyzed.

Failures are those things that inhibit us from measuring the system performance. These are items that should have been detectable with single station preliminary testing: Failure of the equipment, improper use of operating procedures, and failure of the data processing and/or support systems.

There may be some philosophical dispute over the boundary between categories, but the basic tenet should be that a collocation is a unique event and should be allowed to focus on effects that are difficult or impossible to find with single station testing.

PREREQUISITES

To insure that we get the most value during collocation experiments, we should insist on the following prerequisites:

- Both systems should be working at a satisfactory level in terms of target acquisition, data yield, range noise, etc.
- Both systems should be working independently including: timing, software, meteorological equipment data preprocessing, etc.
- Both systems should have completed and "passed" the specified ground tests (including system characterization)
- Fully tested comparison software should be available
- A management plan with schedules, responsibilities, data flow, and anticipated system performance should have been developed.

GROUND TESTS

The ground tests and the related data analysis have been specified in detail in previous sessions of the Workshop (see Pearlman 1984) and in the Collocation Plans prepared by NASA/Bendix for measurements at GORF. These tests have included:

1. Multiple Ground Target Tests (MINICO) in which several ranging sequences are taken sequentially off of two or more ground targets at different ranges and azimuths to verify reproducibility, system linearity, and mount eccentricity model.

2. Stability tests in which ranging sequences are taken off of a single ground target for one to two hours to examine temporal stability of the system over a time period consistent with a full LAGEOS tracking sequence.
3. Wavefront tests in which a corner cube map is made to measure the laser wavefront spatial variations.
4. Signal strength tests in which extended target calibrations are taken over the full dynamic range of the ranging instrument to measure and characterize the variation in system calibration.
5. Specialized engineering tests (as necessary) including the measurement of changes in system delay with (1) PMT voltage, (2) position of return within the range gate, (3) stop channel (in multistop system), etc.

The data set for a collocation test consists of more than just simultaneous satellite ranging data. It should include the information, data and results from all of the preliminary activities, ground calibrations, and post analysis. Without this, proper interpretation of collocation results is not possible.

SATELLITE TRACKING REQUIREMENTS

The satellite data requirements for the collocation experiments conducted by NASA are based on the following:

- ° Adequate data volume and coverage to disclose systematic effects on LAGEOS
- ° Evaluation of performance on daytime tracking on LAGEOS
- ° Evaluation of performance on low orbiting satellites

Proper engineering evaluation of a laser system requires a data set sufficient not only in data volume (enough passes with simultaneous data), but also sufficient sky coverage to observe azimuth and elevation dependent errors, adequate temporal coverage to achieve the needed sky coverage and to test system reliability, and adequate operation under daytime conditions.

The requirements for satellite tracking by NASA have been specified as follows:

1. Twenty simultaneous passes on LAGEOS with:

- Data spaced over 30 minutes per pass
 - A minimum of seven two-minute overlapping normal points per pass
 - Five passes in daylight
 - Two of the passes in each sky quadrant
 - Two passes in each of the ascending and descending equatorial modes
2. Two simultaneous passes on Starlette or BE-C
- A minimum of three simultaneous normal points per pass

DATA ANALYSIS

Collocation satellite data are analyzed at several levels. The first examination is made on a single station basis and includes:

- Calibration RMS
- Calibration stability
- Pre/Post calibration shift
- Satellite data RMS
- Satellite normal point RMS
- Residual signatures to orbital solutions

At the next level, the data for the collocated systems are compared using short arc solutions to investigate effects such as:

- Mean offset
- Drift and temperal variations
- Range dependence
- Elevation and azimuth dependence
- Signal strength variations
- Diurnal variations

- Variation with system calibration
- System changes
- Temperature variations

RECENT EXPERIENCE AND ISSUES

Some of the recent collocation experiences are tabulated in Table 1. Analysis is still underway on several of the experiments, so that results since early 1985 are still preliminary. For this summary, the offset value is expressed simply as the mean difference between the systems over the full data set, paying no additional recognition to residual signatures or the actual nature of the systematic biases. As noted above, however, these signatures are a fundamental key to system performance and their close scrutiny is an essential part of any collocation evaluation. Specific experiments will be discussed by others in this session.

A tabulation of problems encountered during collocation experiments is shown in Table 2. The difficulties fall basically into two categories: (1) The ranging machines and/or their supporting systems were not ready for collocation, or (2) the machines did not stay long enough to acquire a sufficient set of data or to allow proper engineering scrutiny. We are historically behind schedule in development, construction, deployment, etc., and as such, the preliminary phases to collocation have in almost every case been compromised.

Many laser systems have participated in collocation experiments, but in most if not all cases, the collocations have been inadequate. In some cases, the machines have not really functioned. Less than half of the tests provided twenty passes of data, and even in these cases some of the passes were inadequate for proper analysis, due to insufficient data volume, insufficient coverage, and/or changes that were made during the tests that precluded test continuity. The greatest void in data acquisition, however, has probably been the lack of daylight ranging.

The maintenance of configuration control in hardware, software and procedures has been a traditional problem. In principle, the systems should be operated in a fixed, independent manner. Almost without exception, however, we have succumbed to temptation to adjust, repair, and modify. Unfortunately, there is never enough time to start the collocation test over again, and we end up with discontinuous data sets that are hard to relate.

Many problems have surfaced that relate to data processing. This, of course, becomes more prevalent as more

systems built and operated by different groups are collocated (although it has been experienced in collocations with only NASA systems). Inconsistent use of models (refraction, spacecraft center-of-mass, calibration correction, etc.) and differences in data manipulation and screening have recently required attention. One of the most notorious problems is probably that of ground surveys: to calibration targets and over the interstation vector. Ground surveys, although a routine process, must be done very carefully and analyzed properly. Surveys must be repeated on a regular basis to insure the results and to detect any local movements. More than once, ground motions or unstable calibration target structures have compromised ranging results. The ground target is in most cases the basis of our entire measurement program, yet it is often the weakest link.

Speed of data processing has been a perpetual headache. As noted earlier, analyses of experiments taken over a year ago are still underway. The lasers leave the collocation, and may take data for a year or more before we fully understand the performance characteristics. At times, even when there are indications of anomalous behavior, we do not apply the manpower and time to pursue the evidence in a timely manner. As a result, problems surface later at an even less opportune time.

Proper interpretation of the collocation results relies on the conduct of complete preliminary ground tests, analyses of this data, and timely availability of the results. This information is critical to the understanding of machine performance and may play a crucial role in proper data reduction. A recent example is system delay variation with signal strength. In those systems where the effect is pronounced, algorithms based on calibration data could have a very significant effect on satellite results. Yet, if the data is not readily available, we see serious degradation in system performance and have no opportunity to apply proper data corrections.

CONCLUSIONS

The difficulties experienced in past collocations, and improvements seen in some of the recent tests, reiterates again that collocations must be as carefully managed as any other activity making use of scarce resources. Every collocation requires a detailed plan encompassing everything from the readiness of support systems through the management of the data flow and analysis. Compromises have not served us well. The "Rush to Collocation" and the "Rush to Deploy from Collocation" have been very costly to us. In the future, every effort must be made to use collocations more effectively to study the fundamental limitations of the systems rather than merely

cleaning up the routine problems that we just did not have time to examine before.

Reference:

Pearlman, M.R., "Laser System Characterization", Proceedings of the Fifth International Workshop on Laser Ranging Instrumentation, Herstmonceux Castle, September 1984, published by Geodetic Institute, University of Bonn, Bonn, Federal Republic of Germany 1985.

RECENT COLLOCATION EXPERIENCE

| <u>DATES</u> | <u>COMPARISON</u> | <u>LOCATION</u> | <u>NO PASSES</u> | <u>OFFSET</u> |
|--------------|-----------------------------|-----------------|----------------------|---------------|
| 7/81 | MOB7- STALAS | GORF | 12 | 3-4cm |
| 9/81 - 1/82 | HOLLAS - MOB1 | HALEAKALA | 45 | <1 cm |
| 9/81 - 10/81 | MOB4 - MOB7 | GORF | 4 | 7 cm |
| 7/82 - 10/82 | MOB6 - MOB7 | GORF | 27 | 1-2 cm |
| 7/82 - 8/82 | MTLRS - TLRS1 | McDONALD | 23 | 6 cm |
| 9/82 - 11/82 | MTLRS - TLRS2 | GORF | 27 | <1 cm |
| 5/83 - 6/83 | MOB4 - MOB7 | GORF | 13 | 1 cm |
| 7/83 - 8/83 | LTRS1 - MOB8 | QUINCY | 15 | 2-3 cm |
| 10/83 | TLRS1 - MOB4 | MT. PEAK | 7 | 6 cm |
| 4/84 - 5/84 | MTLRS1 - KOOLAS | KOOTWIJK | 2 | - |
| 9/84 - 10/84 | TLRS1 - MOB8 | QUINCY | 43 | 2-3 cm |
| 11/84 | MTLRS2 - WETLAS | WETTZELL | 5 | - |
| 5/85 - 8/85 | MTLRS1 - MOB7 | GORF | 13 | 1-2 cm |
| 10/85 - 1/86 | MTLRS1 - MTLRS2 - MATLAS | MATERA | 13-36 | 1-2 cm |

TABLE 1

FAILURES

- ° SYSTEMS NOT READY
 - INADEQUATE SHAKE-OUT ON SATELLITES
 - INADEQUATE GROUND TESTING

- ° INSUFFICIENT DATA SET
 - NOT ENOUGH ACCEPTABLE PASSES
 - LIMITED SKY COVERAGE/DISTRIBUTION
 - LITTLE OR NO DAYLIGHT DATA
 - INADEQUATE TEMPORAL COVERAGE (30 DAYS)

- ° LACK OF CONFIGURATION CONTROL
 - HARDWARE
 - SOFTWARE
 - PROCEDURES

- ° LACK OF PREPARATION FOR PROCESSING
 - INCONSISTENT USE OF MODELS
 - INCONSISTENT DATA MANIPULATION
 - INCONSISTENT DATA SCREENING
 - INCORRECT SURVEY DATA
 - SLOW DATA PROCESSING

- ° LACK OF AVAILABILITY OF ENGINEERING DATA
 - GROUND TEST RESULTS

- ° SURVEY PROBLEMS
 - CALIBRATION TARGET SURVEY
 - CALIBRATION TARGET STABILITY
 - INTERSTATION VECTOR SURVEY

MANAGEMENT OF THE LASER RANGING SYSTEMS COLOCATION

A. Cenci
Telespazio S.p.A.
Via A. Bergamini, 50
00158 - Rome Italie

Telephone (39) 6 4987407
Telex 610654 TSPZROI

ABSTRACT

The colocation testing for satellite laser ranging systems provides a unique opportunity to test the ranging capabilities and to identify possible sources of systematic errors.

Being the colocation experiment strongly influenced by many unforeseeable aspects, like atmospheric conditions, systems failures, logistic problems and so on, the management of the experiment has to be carefully organized in order to reduce any other possible sources of problems as well as to optimize the operational and analysis activities.

This paper concentrates on various aspects of the colocation management, starting from the identification of the major requirements to be satisfied prior the beginning of the colocation, like site requirements, systems errors characterization, definition of tasks and responsibilities,...

The main procedures and tests to be performed during the colocation period are also discussed, with particular emphasis to the ground test procedures and supporting information data set.

Further possible sources of errors to be carefully investigated, concerning data handling and processing, are discussed too in a section dedicated to the Software Benchmarking.

Finally, a general overview of the colocation data analyses is given.

This paper refers in particular to the procedures and criteria adopted during the colocation experiment recently performed at Matera between the MTLRSI, MTLRS2 and MATLAS systems (January-March 1986).

MANAGEMENT OF THE LASER RANGING SYSTEM COLOCATION

INTRODUCTION

The laser ranging stations differ from each other in several aspects: characteristics of the laser, mount system, receiving electronics, optics, timing system, software capability, operating procedures, etc.

Any of these aspects can map into systematic errors in measurements.

The colocation testing is the only reliable method to identify laser system problems comparing two or more stations, isolating station dependent systematic errors from other major sources of errors, like atmosphere, orbit determination, station location, etc.

Being the colocation testing strongly influenced by many unpredictable aspects, like atmospheric condition, systems and logistic problems etc., the management of the experiment has to be carefully organized in order to reduce any other possible sources of problems, as well as to optimize the operational and analysis activities.

A real time supervision during the colocation period is also necessary together with a joint cooperation between all the involved groups.

This paper presents the requirements and procedures to perform the colocation testing, with particular reference to the procedures and criteria adopted during the colocation experiment performed at Matera with the MTLRS1, MTLRS2 and MATLAS systems.

Writing this paper, reference was made in particular to the standard colocation plan of the Bendix Field Engineering Corporation (ref. [2], [3]) and the 1986 Matera Colocation Plan (ref. [1]).

The report is divided into five sections: the first section summarizes the various prerequisites to be satisfied prior the beginning of the colocation.

The second section analyzes the procedures and tests to be performed during the colocation.

Section 3, is dedicated to the benchmarking of the processing software.

In section 4 an overview of the analysis procedures is given.

The last section gives a summary of the colocation reports.

An overview table is also given for each section.

1. COLOCATION PREREQUISITES

1.1. COLOCATION SCHEDULE

Particular attention has to be given to the choice of the colocation period, in relation with weather conditions and satellite visibility, in particular if second generation stations, which have only night time tracking capability, are involved.

The colocation test period must be long enough to meet the colocation data set requirements for the analysis of both short and long term biases (see sect. 2.2.). Distribution of data over at least one month is in general required.

1.2. ON SITE FACILITIES

1.2.1. Power Supply

The requirements for the electrical power are in general not critical, being at least one of the collocating stations connected to the commercial power.

In any cases, if power requirements are not largely satisfied, interactions between the systems are possible during laser firing, mainly if high energy lasers are involved. In this case, independant sources from power generators are requested.

1.2.2. Communications

The basic communication systems needed at the site are:

- telephone line: for general communication and quick-look transmission (to access MARK III data network);
- telex line: for information exchange and quick-look transmission;
- mail/carrier: express mail or carrier is necessary to maximize the full-rate data timeliness. Complete data flow tests are strongly advised before the colocation starts, in order to evaluate the real possibilities;
- on site: an internal phone line between the collocating stations should be installed in order to allow the crews to communicate each other during tracking or tests as well as for meteo measurements exchange, time comparison, emergency and so on.

1.3. COLOCATION SITE REQUIREMENTS

The main requirements for the colocation site are summarized in the following:

- re-inforced concrete slabs are required for mobile systems to accommodate for a leveled and stable support for the mounts. SLR universal NASA pads are recommended. The reference markers must be carefully isolated from the pad and extended sufficiently into the subsurface for maximum stability [4];
- the collocating stations should be positioned as close as possible, to reduce errors in local survey measurements and geometrical data analysis (60 meters or less is recommended);
- a reference marker network with a typical side length of 100 to 200 meters around the site is strongly advised;
- appropriate electrical ground network has to be installed around and under stations locations. In case of risk for excessive storm conditions, proper tie-downs are also required;
- at least three ground targets at different azimuth and distances (typically 500 to 2000 meters) should be available (corner cube reflectors and/or billboards depending on type of stations), to allow terrestrial ranging tests.

1.4. SITE SURVEY

One of the most frequently experienced source of systematic errors in colocation data analysis concerns the survey of the relative station positions and critical calibration ranges (reference markers and calibration target).

Errors on survey directly map into relative station biases, so that absolute accuracy better than 0.5 cm is required.

Accurate local survey, including pads and reference markers measurements, must be performed prior the beginning and directly after the completion of the colocation period.

Connection to the national geodetic network is also advised, although it does not impact directly the colocation experiment.

A report of the pre-survey results must be distributed to all involved analysis groups prior the first colocation data is available, as reported in sect. 5.2.

Being the survey one of the most critical pre-requisites to be satisfied for the colocation, particular attention is necessary for:

- calibration of instruments;
- measurement procedure;
- data reduction;
- error control.

Details about the above topics are given in ref. [5] and [6].

1.5. SYSTEMS CHARACTERIZATION

One of the objectives of the colocation experiment is to verify and compare the performances of the laser stations.

A complete characterization of each system is therefore required prior the colocation in terms of definition of system performance and estimation of errors budget.

With reference to the model proposed by M. Pearlman at the 5th International Workshop in Laser Ranging Instrumentation (ref. [7]), the system characterization must include at least the following items:

RANGING MACHINE ERRORS

Systematic:

- Spatial Variations (Wavefront distorsion, cube map);
- Temporal Variations (Pre-post calibration shift, long term system delay variations);
- Signal Strength Variations (unmodelled variations of system delay with signal strength);
- Calibration Path (survey, meteo - if applicable -).

Statistical noise:

- Single Shot Precision (day/night; high/low satellite);
- Calibration S.S. Precision (day/night; high/low satellite).

TIMING ERRORS

- Broadcast Monitoring (timekeeping accuracy).

MODELLING

- Data Aggregation (Normal points model accuracy, Normal Points precision/data availability);
- Atmospheric Correction (Model Accuracy, Meteo measurements accuracy).

The overall error budget should specify the relevant time period or periods for each component (pass, day, month, etc.).

The statistical means of characterizing each component must be also specified (one-sigma, peak to peak, etc.).

In order to verify the above characteristics during the colocation phase, adequate hardware and software configurations and operational procedures should be prepared prior the beginning of the experiment (see also sect. 2.6.).

1.6. MANAGEMENT AND RESPONSIBILITIES

The management of the colocation experiment needs to be organized prior the beginning of the experiment as much in detail as possible in close cooperation with all the participating groups.

All the tasks and responsibilities have to be clarified not only at high level but also at crew level which directly impacts the colocation results.

Fig. 1 shows the block diagram of the management structure which has been adopted during the Matera colocation.

The tasks performed by the various members are summarized inside the blocks.

A management on site is needed to coordinate the crews and the colocation activities.

Depending on the involved personnel and systems, different responsibilities may be attributed to the colocation manager who operates in any case in close cooperation with the stations managers under the supervision of the operational manager of the campaign.

One of the most critical areas to be handled by the colocation manager concerns the supporting information collection and exchange and the reporting.

In fact, difficulties and confusion may be experienced in colocation analysis due to missing or incomplete supporting information.

A strict control of hardware and software configurations during the colocation period is also required.

Any forced change in systems or procedures must be adequately documented.

2. COLOCATION PROCEDURES

2.1. OPERATIONAL SCHEDULING

The scheduling of the operational activities include:

- organization of the crews (shifts);
- pass scheduling;
- test scheduling;
- data and information exchange.

The definition of the acquirable passes depends on operational staff availability and organization.

Due to the particular kind of the experiment, a flexible organization is in general preferable, to reduce the effects of forced unactivity periods (due to weather, failures, etc.).

An a priori scheduling is in any case necessary together with the definition of priority criteria for both acquisition and off line activities (e.g. minimum culmination, daytime or nighttime passes, etc.) depending on forecasts and kinds of involved systems.

The requested colocation data set (see sect. 2.2.) is also considered in this context. All the requested ground test are scheduled too, following the assigned priority, as well the frequency of the data and information exchange (pass, daily, weekly, etc.).

2.2. SATELLITE RANGING

The raw satellite data set required during the colocation consists of the following:

- 1) All raw satellite data taken during the colocation period, including both simultaneous and non-simultaneous passes.
- 2) Each system should have observed a minimum of 20 LAGEOS passes with any other system spaced over a period of at least 30 days. Depending on the analysis method used the 20 passes should have either a minimum of seven consecutive overlapping two minute normal points (geometric analysis) or four consecutive two-minute normal points in three groups at the ascending, highest elevation and descending side of the pass (dynamic analysis).
- 3) these 20 passes should include a minimum of five daytime simultaneously tracked LAGEOS passes responding to the same normal point overlap criteria (if applicable).
- 4) These 20 passes must include a minimum of two simultaneously tracked LAGEOS passes in each sky quadrant and a minimum of two passes in both the ascending and descending equatorial nodes.
- 5) A minimum of two simultaneously tracked STARLETTE passes to confirm low satellite tracking capability. Each pass must contain a minimum of three 2 min normal points (if applicable).

The possibility to satisfy the above minimum data set requirements must be a priori verified in relation with the colocation schedule (ref. sect. 1.1.).

2.3. SYSTEM DELAY CALIBRATIONS

All tracking calibration data taken during the colocation must be included in the data set.

Particular attention needs to be given to the system delay variations in both short (pre-post calibration shift) and long period.

A real time analysis on this area is useful to identify system problems as well as to detect anomalous atmospheric effects along the calibration path, in case of using calibrations with external target, which directly map into systematic errors.

One interesting example is visible in fig. 2.1, where the behaviour of the calibration system delay and pre-post shift relative to the Matera colocation is shown.

Some anomalous system delay values were observed for both MATLAS and MTLRS2 systems. In the case of MATLAS, being this fact due to atmospheric effects of the external calibration path, station biases up to 10 cm have been detected on final data analysis. The jumps of the MTLRS2 system delay, due to internal system variation, did not affect on the contrary the final data, being present also during satellite ranging.

2.4. EPOCH TIMING

The philosophy which has been followed during the Matera colocation in definition of colocation procedures and criteria was to remove any possible source of a priori known errors.

Under this philosophy the system clock closure between the three systems was measured (generally on daily basis) with 100 nS accuracy and maintained to 500 nS level.

The effort to maintain time closure to less than half microsecond appears to be not fully justified being the epoch resolution in the archiving data formats actually limited to one microsecond.

In case of using Rubidium standards or in case that better time keeping accuracy be approached, comparisons made on pass-by-pass basis are necessary.

If closure within 0.5 microsecond with respect to the reference scale (USNO, BIH) is also maintained (this represents also a colocation test), both Full Rate and Quick Look data do not need in general time corrections, unless the epoch resolution be increased to accomodate the subcentimeter accuracy.

Being the colocation a unique opportunity to compare and test the entire system configuration, the comparison of different methods of synchronization is important too. In the case of Matera difference up to 0.3 microsecond between LORAN-C and GPS have been found, mainly due to the accuracy of the LORAN-C Master station offset. The storing of all timing intercomparison measurements allows also to verify and compare the system clocks stability.

A summary of timing closure informations should be included in the final colocation report.

2.5. METEOROLOGICAL DATA

Meteorological data closure between the colocating systems should be established and maintained at least to the following tolerance:

- Pressure: +0.5 mBar;
- Temperature: +5 degrees for satellite ranging,
+1 to 3 degrees C for terrestrial ranging, depending on the distance,
- Humidity: +30%.

In case of terrestrial ranging, averaging of temperature and pressure measurements taken along the target path is necessary (a variation of 1 degree in temperature introduces an error in range of about 1 mm per km).

For satellite ranging the most critical point concerns the pressure measurements.

In the case of Matera colocation, for example, a difference of about 0.8 mBar was found between the MATLAS and MTLRSI barometers, which also represents about the difference between the Bendix and IFAG standards (used to calibrate the instruments).

In order to remove any known source of relative error bias, readings from a unique pressure reference (MATLAS) were therefore used on data.

In case that a unique set of meteo instruments is used by all colocating stations, comparison between the various instruments must be also done and stored.

It is also to point out that an accuracy in the pressure readings (and relative closure) better than 0.5 mBar appears to be actually not fully significant because:

- archiving data format resolution is limited to 1 mBar;
- meteo reading are (in general) recorded only once per pass, so that changing conditions during the pass are not taken into account (variations up to 1 mB and 3 degrees have been observed during Lageos passes).

Upgradings of systems capability and data formats appear therefore necessary to accomodate subcentimeter accuracy.

A summary of the meteo closure informations should be included in the final colocation report.

2.6. GROUND TESTS

A minimum set of ground tests to be performed during the colocation period in order to evaluate system performance or to explore performance problems is described in the following.

Further investigation appear to be necessary to make the full ground test data available to all involved groups (formats and procedures need to be decided).

2.6.1. Terrestrial Targets Ranging

This test consists of a minimum of five daytime and five nighttime range series of a significant number of returns (depending on systems), over at least 3 minutes period, with the calibration data, each taken on at least three range targets at significantly different azimuth and distance.

Ranging must be done simultaneously by all the colocating systems to reduce unmodelled atmospheric effects.

The ranging conditions, e.g. return energy, should be similar to the satellite ranging.

This data can be used to confirm range bias deduced from satellite data and/or verify and compare terrestrial ranging capability.

2.6.2. Stability Test

It consists of at least two one-hour ranging on internal and/or external target to evaluate:

- range RMS stability;
- range drift;
- return energy stability.

Analysis of the pre-post calibrations data can be also used to verify the system stability ([7] , [8]).

2.6.3. Signal Strength Variation Test

It consists of ranging on internal and/or external target over the full dynamic range of the receiving system.

This is obtained performing various set of range series with a significant number of returns, changing for each set the ND optical filter in the transmitting or receiving section.

The RMS and mean variations from all set of data allow to evaluate the unmodelled variations of system delay with signal strength (arising because the performance of

devices within the systems including PMTs are amplitude and/or pulse width dependent) [7], [8].

2.6.4. Wavefront Map Test

It consists of mapping the wavefront variations by ranging on an external cube reflector several range series, at different azimuth and elevation angles (with adequate steps depending on beam divergence) in order to cover the entire laser beam.

The evaluation of the return energy variations and range variations give the map of the beam shape and the spatial wavefront distortion respectively (two tests must be done separately to remove signal strength dependence from wavefront distortion).

The measurement sets are taken in random order with return to the central reference position to check for temporal drift [7], [8].

This test is particularly important for systems with high energy laser pulses (duration over 500 ps FWHM) because the effect of spatial distortion has been experienced to be in general no more than 10% of the pulse duration.

2.6.5. PMT Test

It consists of producing a smooth systematic change in system delay as a function of PMT voltage.

This test is mandatory in case that change in PMT voltage is used to manage the received pulse to maintain the receiver system in the linear region.

2.7. QUICK LOOK DATA FLOW

The Quick-Look data are normally transmitted from the stations to the data processing centers on daily basis using telex or Mark III line.

To accommodate for a more reliable quick data analysis, the quick-look data set was expanded to 200 points per pass during the Matera collocation.

Quick Look data from all collocating stations were also collected and merged on site, after calibration corrections, in order to perform the polynomial fit analysis and a preliminary collocation data analysis (data were reformatted and processed in Telespazio, Rome; see also sect. 3.2.).

The Quick Look data flow during the Matera collocation is shown in fig. 2.2.

It has to be noted that in case of maintaining timing closure within tolerance, the quick look informations are only limited by the 0.1 nanosec. resolution in range, so that quick look analysis accuracy is expected to be comparable with that of the full-rate analysis (depending also on accuracy of the pre-post calibrations).

2.8. FULL RATE DATA FLOW

As mentioned in sect. 1.2. the timeliness of the Full Rate data flow must be optimized depending on:

- express mail/carrier availability;
- site location;
- involved pre-processing groups (number and locations);
- involved analysis centers (number and locations).

Full Rate data transmission should be in any case done at least on weekly basis.

Fig. 2.2 shows also the Full Rate data flow for the Matera colocation.

Copy of Full Rate data from MTLRS1 and MTLRS2 were also directly sent to DUT and IFAG respectively (on weekly basis) for analysis and benchmarking.

It has to be noted that several groups were involved in both pre-processing and data analysis, during the Matera colocation, so that the best timeliness for the complete full rate data flow was in general about three weeks.

The Full Rate data set and exchange procedures may also differ between the groups depending on:

- data formats (system format/standard; binary/ASCII; etc.);
- data support (9 tracks magnetic tape/Linc tape/floppy disk; etc.);
- Full Rate informations.

All the above differences may introduce difficulties in data processing and benchmarking (see sect. 3).

2.9. SUPPORTING INFORMATION

One of the major sources of confusion and delay in data analysis effort, experienced in the past colocation experiments, concerns the supporting information collection and exchange.

One of the criteria adopted during the Matera Colocation was to issue a weekly report on which the principal information to support both system performance evaluation and data analysis were summarized.

A summary of these informations, collected from each stations on daily basis, is shown in Fig. 2.3.

All tests and analysis results, not included in this form, were added as off-line activities as well as any crew comments and problem description (the Polyfit analysis section reported the results of an independent polynomial fit analysis performed on site by Telespazio using Quick Look data).

A final operational updated report, on which all the supporting information are summarized, should be issued at the end of the experiment and distributed to all participating groups (see sect. 5.).

Any additional supporting information generated on site, like tracking log, on site detailed analysis output, non-recorded test data, detailed crew comments etc., should be included in Full Rate data shipments.

3. SOFTWARE BENCHMARKING

The colocation experiment offers a unique opportunity not only to compare the performance of the hardware systems, but also to detect differences in the on site station and data control software and in the models and procedures for data preprocessing and analysis.

In our experience, a "Benchmarking" and comparison of the above software appeared as important as the system hardware comparison, in particular considering the subcentimeter accuracy being now approached in laser measurements.

3.1. SYSTEMS SOFTWARE COMPARISON

The on site software capabilities are in general dedicated to:

- system orientation;
- raw orbit propagation;
- satellite tracking;
- real time data acquisition;
- post-pass processing (raw data);
- Quick Look data generation;
- system delay calibration (raw data);
- data formatting;
- off line tests and procedures.

Although many different techniques are used, depending on hardware configurations, some common output and procedure can be verified and compared, like the following:

- Quick Look and Full Rate data formats;
- Quick Look data sampling criteria;
- Pre-Post calibrations evaluation;
- Pre-Post calibrations editing criteria;
- Raw data screening procedure;
- Full Rate data editing criteria;
- Timing and Meteo data handling;
- Modeled system delay corrections (PMT, attenuator delay).

For example, during the Matera Colocation, some differences (at centimeter level) on Quick Look system delay evaluation between MTLRS1 and MTLRS2 systems have been found, although the two system configurations were basically identical.

Different procedures and editing criteria have also been experienced concerning data screening (in both raw manual pre-screening and post fit editing).

In case that identical hardware configuration systems are involved, the interchangeability of the system software needs to be previously tested.

The same set of real or simulated data should be processed by all systems to verify and check the mentioned results and output.

In case of different systems, it may be useful to make available some software and procedures to convert data formats and maximize the compatibility between the collocating systems, to accomodate for pre-processing benchmarking and data analysis.

3.2. PRE-PROCESSING BENCHMARKING

We can divide the data pre-processing phase in the following sections (basically):

- Modelling of system delay variations;
- Pre-Post system delay calibrations;
- Timing corrections (reference to standard scales);
- Satellite time correction;
- Center of mass correction;
- Atmospheric refraction correction;
- Data re-formatting (if requested);
- Normal points generation (if requested).

The above procedures are in general not all performed by the same centers and, generally, data from different stations are processed by different centers.

To benchmark the pre-processing software, appropriate procedures must be therefore adopted each time depending on:

- systems;

- pre-processing centers;
- data formats;
- data supports;
- data availability;

and so on.

In general the philosophy should be to compare a same set of raw data after pre-processing made by different groups, looking at the pre-processed data sets in terms of:

- timing and pre-processing indicators;
- epoch differences;
- range differences;
- correction values.

Analysis can be made in terms of:

- single observation differences;
- pass-by-pass statistics (single pass average, RMS, Peak to Peak of the differences);
- global statistics (mean and RMS of the differences over all passes in data set).

The above informations may be useful to individuate the cause of eventual discrepancies (for example a constant range bias through a single pass may be attributed to differences in pre-post mean system delay evaluation).

Fig. 3 shows the two data processing flows adopted during the Matera Colocation to perform the Telespazio Analysis.

In the flow B the Full Rate data were pre-processed separately by DUT, IFAG and Bendix for MTLRS2, MTLRS1 and MATLAS respectively (part of MTLRS1 and MTLRS2 pre-processing was made by Bendix).

Data distributed by GLTN have been used for colocation analysis using GEODYN without any pre-processing option.

A independent analysis was performed using data collected directly on site (flow A in fig. 3.1) and pre-processed in terms of:

- Center of mass correction (GEODYN);
- Satellite time correction;
- Atmospheric propagation (GEODYN);
- System delay calibration.

The results of the comparisons between the two pre-processed data set in addition with a separate benchmarking performed jointly by DUT and IFAG on MTLRS1 and MTLRS2 data, pointed out some discrepancies (at centimeter level); the subsequent analysis pointed out some critical points of general interest:

- Data truncation or roundoff in the Full Rate (e.g; epochs) and Quick Look formats introduce errors of several millimeters. Sequential corrections in separate processor and/or at separate centers may worsen the problem.
- Pre-processing parameters should be carefully verified (e.g. laser wavelength).
- Data flags and applied corrections should be verified (some confusion on sign of applied corrections was experienced).
- The atmospheric refraction correction models should be periodically verified to accomodate their evaluation.
- Different screening and editing criteria may influence significantly the pre-processing (in term of pre-post system delay evaluation).

The last point is particularly important for low rate firing laser systems, for which a limited number of points from pre and post calibrations is available (at relatively high noise level).

For example, comparisons between Bendix and Telespazio pre-processing on MATLAS data showed bias differences up to 1 cm (occasionally 2 cm) on single passes (the differences averaged to zero over several passes), to be mainly attributed to different editing criteria on pre-post calibration data (ref. [10]).

A further point to be investigate concerns the normal points generation.

Due to different procedures and criteria adopted by the various centers to generate normal points (and consequently different bin widths and reference epochs), comparison can be made in general only looking at the results obtained after geometrical and/or dynamical analysis, using the same data set span from different normal point sources.

Tab. 3.1 summarizes the principal sources of preprocessing differences.

3.3. DATA ANALYSIS BENCHMARKING

Since several different groups are independently working at the analysis of data, the Matera Colocation experiment provided a unique opportunity of benchmarking the pre-processing and processing software and the method of analysis.

Besides of the global analysis approach (geometrical or dynamical) several differences in procedures and criteria have been experienced as well as consequent not negligible systematic effects on final results.

The various possible differences are summarized in tab. 3.2.

The effects on the final results caused by these different approaches are difficult to evaluate a priori, depending on data quality and quantity and on systematic effects in data distribution.

For example, differences up to 0.5 cm were found on final mean relative station biases for MATLAS using 2.5 or 3 sigma rejection criteria (up to 2 cm bias differences were found on single pass mean residuals) on Matera colocation data (ref. [10]).

About the same amount of discrepancy has been found using Full Rate data or sampled Full Rate data (every 5 seconds).

In order to accommodate the subcentimeter level accuracy, being now approached, we can therefore observe that:

- Comparison of the results from different groups appears to be fully significant only if the software used for data analysis are compared by means of a detailed benchmarking procedure.
- Aggregation of the results appear to be fully significant only in case of compatibility of all or part of the analysis approach criteria, in particular concerning data set and screening/editing procedures.
- In general, the colocation analysis (as well other data analysis) appears to be fully significant only if a detailed characterization of the adopted procedures is in addition given.

4. COLOCATION DATA ANALYSIS

4.1. ON SITE ANALYSIS

The analysis normally performed on site, having interest for colocation purpose, should include the following:

- Post pass analysis of the residuals (versus predicted orbit);
- Polynomial fit (applied to residuals and/or range);
- Data screening and editing;
- Pass statistics (duration, number of returns, sky coverage, etc.);
- Range bias determination (referred to predicted orbit);
- Time bias determination (referred to predicted orbit);
- RMS noise determination (after polynomial fitting);
- Ground test analysis (raw);
- System delay evaluation (pre-post calibration, modelling).

4.2. SATELLITE DATA ANALYSIS

Two general approaches are recognized in colocation analysis:

- Geometrical approach; basically the POLYQUICK analysis performed by Bendix (polynomial fit techniques);

- Dynamical approach; based on Orbit Determination Techniques (GEODYN, UTOPIA, etc.) including:
 - multi-short arc analysis,
 - long arc analysis,
 - long arc analysis and polynomial fit.

In both cases the following tests and relative plots can be performed:

- Mean range bias;
- Range bias drift;
- Range bias versus range;
- Range bias versus elevation;
- Range bias versus azimuth;
- Long term mean range bias stability;
- Diurnal effect;
- Range bias correlation with applied system delay.

Details on Dynamical approach analysis are given in ref. [9].

4.3. GROUND TEST ANALYSIS

Detailed ground test analysis may require additional software capabilities not available on site.

In general the analysis relative to colocation ground tests include:

- Terrestrial Ranging : similar procedures applied on satellite post-pass processing, including pre-post calibrations.
- Stability test : data binning and statistical estimation (RMS, Peak-to-Peak averaging).
- Signal strength variations : data binning and statistical estimation.
- Wavefront map test : additional software/hardware configuration is required to accommodate the beam mapping (in automatic way).

All ground test analysis should include appropriate graphics facilities like:

- targets ranging residuals (or relative differences) versus time;
- statistical ranging parameters versus time;
- statistical ranging parameters versus signal strength;
- beam map plot.

4.4. ENGINEERING ANALYSIS

Detailed data processing and additional investigation are necessary if the bias get out of the expected tolerance or problems arise.

In this case detailed system oriented engineering analysis is requested.

A detailed knowledge of the hardware/software configuration, as well as a complete access to the station logs and operational archives and procedures is necessary.

This kind of analysis may be therefore fruitfully performed only by or in close cooperation with the system operational teams and analysis centers.

Appropriate procedures should be jointly investigated each time depending on the type of problems.

5. COLOCATION REPORTS AND DOCUMENTATION

Tab. 5.1 shows a summary of the colocation reports.

This report plan has been adopted for the Matera colocation following also the past colocation experiences.

5.1. COLOCATION PLAN

A pre-colocation document, to be jointly issued by all participating groups, defines all the experiments requisites and activities, including:

- colocation prerequisites;
- colocation procedures;
- analysis procedures;
- responsibilities;
- results and reporting.

5.2. SITE SURVEY REPORT

As discussed in sect. 1.3, a technical report of the site survey should be distributed prior the beginning of the colocation and updated after its completion with the results of the post-colocation survey.

The report should include the following:

- Site description;
- Geodetic information;
- Equipment description and calibrations;
- Survey measurements procedures;
- Astronomical determinations;
- Data processing;
- Summary of results (colocation vectors and error budget);
- Pad measurements;
- Target measurements;
- Eccentricity vectors.

5.3. OPERATIONAL REPORTS

As discussed in 2.9., the weekly reports as well as the final operational report should include:

- timing information;
- meteo information;
- statistics of the satellites passes;
- on site analysis;
- ground test preliminary results;
- off line activities;
- crew commentary.

5.4. ANALYSIS REPORTS

Intermediate analysis results should be interchanged between all the involved analysis centers as soon as the first batch of data has been received and analyzed.

Results to be exchanged include:

- Pass identification;
- Station identification;
- Reference station identification;
- Number of points (accepted/rejected);
- RMS of fit;
- Estimated station relative range bias.

A brief description of analysis techniques and criteria adopted is also requested.

A final detailed individual analysis report should be issued as soon as the complete analysis and final results are available.

A final review of the results should be jointly performed by all participating groups.

5.5. FINAL REPORT

A final colocation report, including both operational (supporting information) and analysis activities is jointly issue by all participating groups.

The analysis results consist of data and data graphs which describe the performance of the colocating systems and best reflect the results of the colocation test.

This information are supplemented by comments and data provided by all participation groups.

The final report should include:

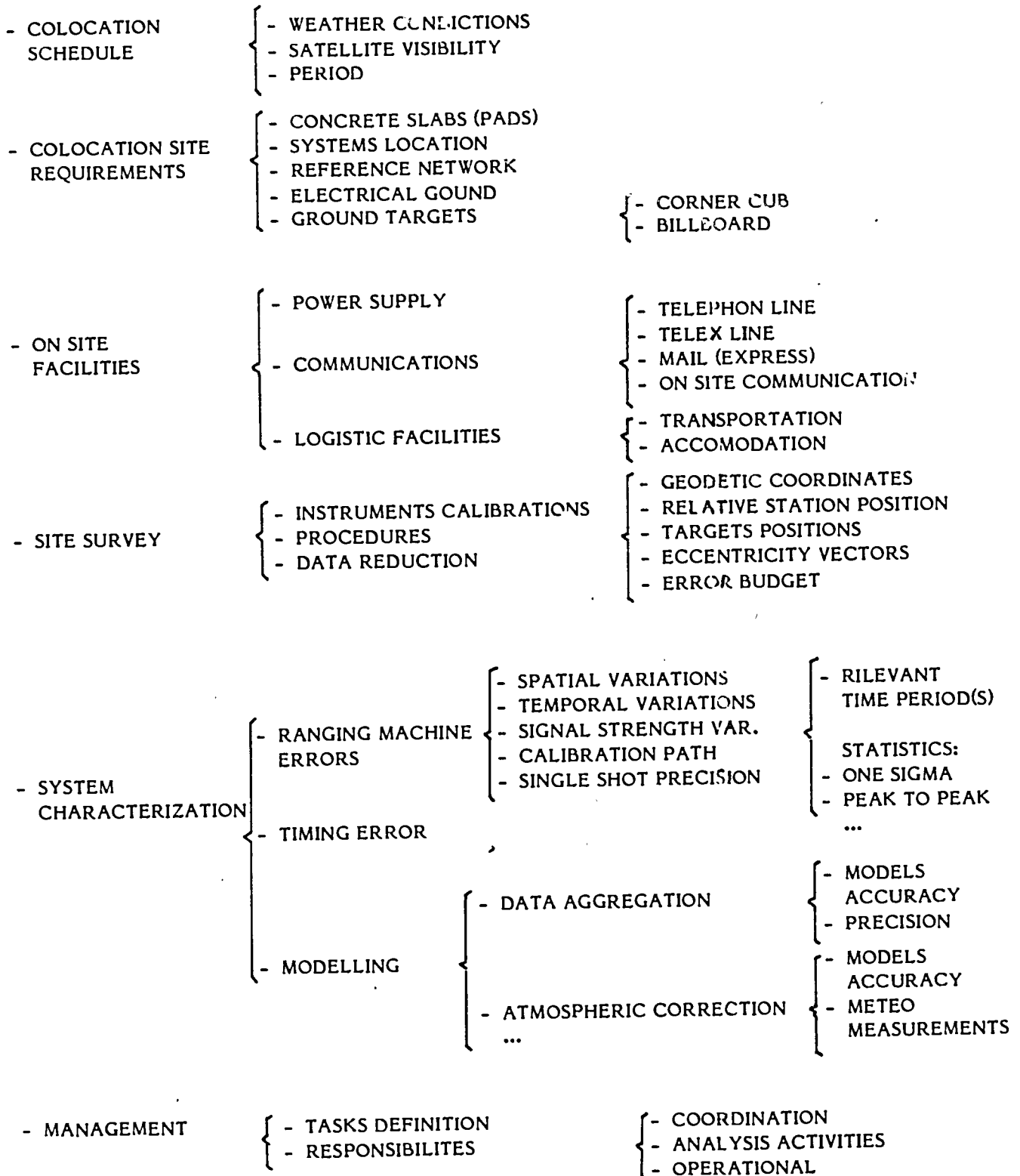
- laser systems description;
- site description;
- site survey (separate report);
- data acquisition statistic;
- description of ground tests;
- verification of epoch timing;
- verification of meteorological data;
- Quick Look data flow;
- Full Rate data flow;
- supporting information data flow;
- software benchmarking;
- analysis group reports;
- comments and conclusions.

REFERENCES

- [1] Dr. B. H. W. van Gelder
"The 1986 Matera Colocaiton Plan for MATLAS, MTLRS1 and MTLRS2"
January 1986 - Delft University of Technology (based on B.F.E.C. standard colocation analysis plan)
- [2] D. R. Edge
"Colocation Test Plan for the Laser Ranging Systems TLRS-3 and MOBLAS-7"
January 1985 - Bendix Field Engineering Corp.
- [3] Bendix Field Engineering Corp.
"MTLRS1 and MOBLAS-7 Colocation Analysis Plan"
May 1985
- [4] E. Vermaat
"Site Selection for MTLRS, Release 84.2.1"
September 1983 - Delft University of Technology
- [5] A. Cenci, D. van Loon
"Survey of the Matera Laser Station Site"
release January 1986, release May 1986 - Telespazio
- [6] D. van Loon
"On the Eccentricity Vectors for Colocation Purpose"
September 1986 - Delft University of Technology; presented at the 6th IWLRI, Juan Les Pines
- [7] M. Pearlman
"Laser System Characterization"
September 1984 - presented at the 5th IWLRI, Herstmonceux
- [8] A. Cenci
"Matera Laser System Characterization"
February 1985 - Telespazio
- [9] A. Caporali
"Colocation Data Analysis: Dynamical Approach"
September 1986 - Università di Padova; presented at the 6th IWLRI, Juan Les Pines
- [10] A. Cenci, M. Fermi
"Matera Colocation Analysis"
May 1986 (preliminary) - presented at the 2nd WEGENER/MEDLAS Conference, Dyonisos

TAB. 1

COLOCATION PREREQUISITES OVERVIEW



TAB. 2

COLOCATION PROCEDURES OVERVIEW

- OPERATIONAL SCHEDULING
 - CREW ORGANIZATION
 - PASS SCHEDULING
 - TEST SCHEDULING
 - DATA AND INFORMATION

- SATELLITE RANGING
 - RAW DATA SET
 - SIMULTANEOUS PASSES
 - SKY COVERAGE
 - SATELLITES

- SYSTEM DELAY CALIBRATIONS
 - CALIBRATION DATA SET
 - REAL TIME ANALYSIS

- EPOCH TIMING
 - TIME REFERENCES
 - LOCAL
 - REMOTE
 - TIME CLOSURE
 - GPS
 - LORAN-C
 - TV-SYNC
 - CLOCK TRIP

- METEOROLOGICAL DATA
 - METEO MEASUREMENTS
 - METEO CLOSURE

- GROUND TESTS
 - TERRESTRIAL TARGET RANGING
 - STABILITY TEST
 - SIGNAL STRENGTH VARIATIONS
 - WAVEFRONT DISTORSION
 - PMT TEST

- DATA MANAGEMENT
 - QUICK LOOK DATA FLOW
 - FULL RATE DATA FLOW
 - DATA ROUTE
 - TIMELINESS
 - FORMATS
 - SUPPORTING INFORMATION
 - WEATHER CONDITIONS
 - PASSES STATISTIC
 - POST PASS ANALYSIS
 - TARGETS RANGING
 - TIMING COMPARISON
 - OFF LINE ACTIVITIES
 - COMMENTARY
 - ...

PREPROCESSING BENCHMARKING

DATA ANALYSIS BENCHMARKING

| | | |
|------------------------------|-------------------------------------|--|
| TIMING | { reference scale satellite time | { TRUNCATION / ROUND OFF |
| SYSTEM DELAY CORRECTION | | { TRUNCATION / ROUND OFF MODELS EDITING CRITERIA |
| CENTER OF MASS CORRECTION | | |
| ATMOSPHERIC REFRACTION CORR. | | { TRUNCATION / ROUND OFF MODELS PARAMETERS : wavelength meteo data ... |
| DATA FORMATTING | | { INFORMATION FLAGS APPLIED CORRECTIONS ... |
| NORMAL POINTS GENERATION | | { TRUNCATION / ROUND OFF MODELS EDITING CRITERIA ... |

GEOMETRICAL
{ POLYQUICK }

DYNAMICAL
{ GEODYN
UTOPIA
... }

| | | |
|------------------|---|--|
| PASS ACCEPTANCE | { GLOBAL COMMON | { OVERLAPPED OBS. FULL OBSERVATIONS |
| PASS EDITING | { DURATION N° OBSERV. 2 TO 4 SIGMA REJ. (to mean range bias) ... | |
| DATA SOURCE | { QUICK-LOOK FULL-RATE | |
| DATA COMPRESSION | { NORMAL POINTS SAMPLED NONE | |
| DATA FITTING | { GLOBAL SINGLE PASS | { MULTI-STATION SINGLE-STATION |
| DATA EDITING | { GLOBAL SINGLE PASS | { 2 TO 4 SIGMA REJ. |

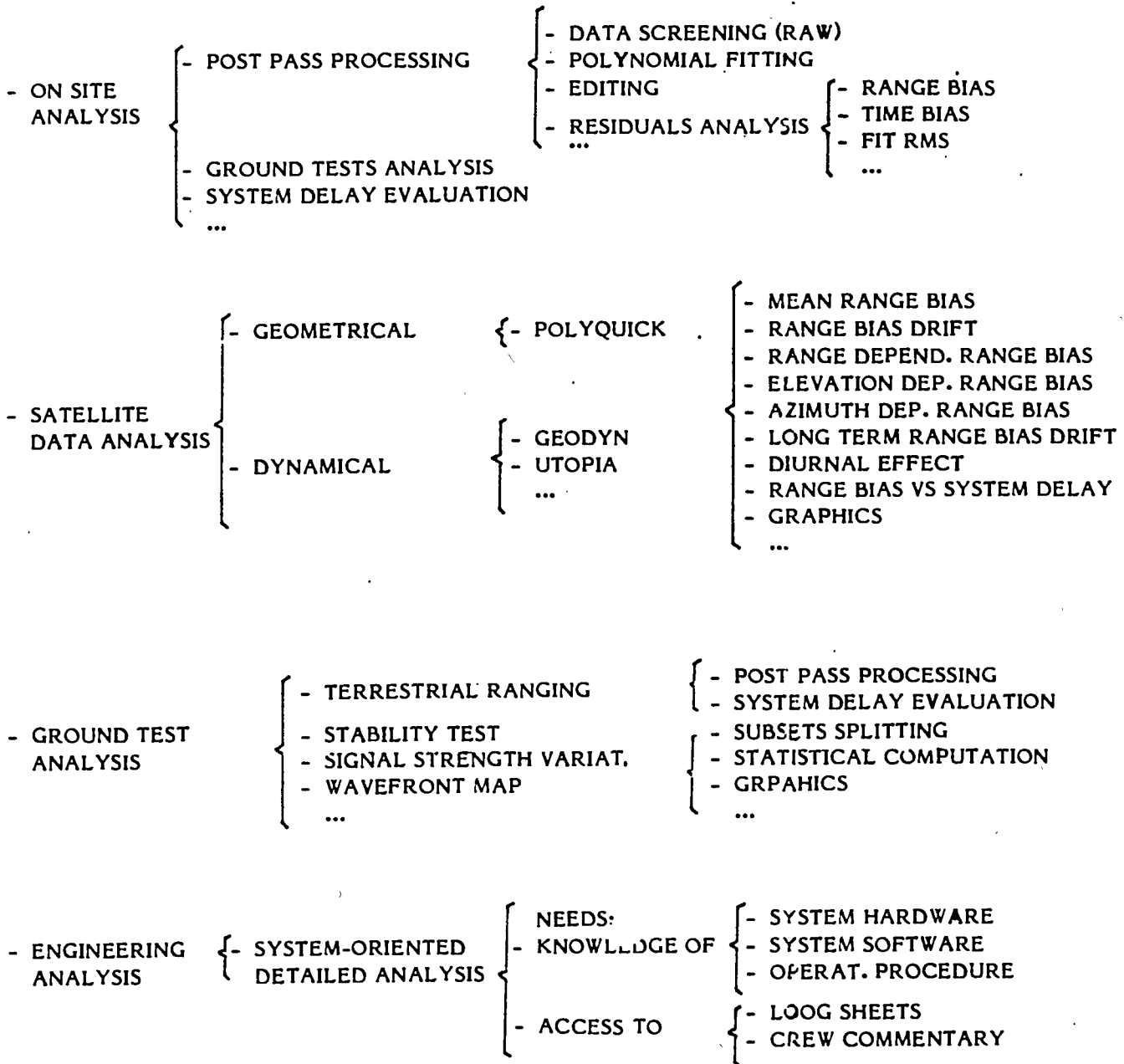
Tab. 3.1

Overview of the principal sources
of differences in Data Processing

Tab. 3.2

TAB. 4

COLOCATION DATA ANALYSIS OVERVIEW



TAB. 5

COLOCATION REPORTS SUMMARY

| <u>DOCUMENT</u> | <u>SCHEDULING</u> | <u>CONTENTS</u> | <u>DISTRIBUTION</u> |
|-------------------------|----------------------|---|--|
| - COLOCATION PLANE | BEFORE COLOCATION | COLOCATION MANAGEMENT | ALL PARTICIPATING GROUPS |
| - SITE SURVEY | BEFORE COLOCATION | SURVEY OF THE COLOCATION SITE (TO BE UPDATED AFTER POST-SURVEY) | ALL INVOLVED GROUPS |
| - DAILY OPERATIONAL | DAILY | SUPPORTING INFORM. ON SITE ANALYSIS. ... | ON SITE MANAGEMENT |
| - WEEKLY OPERATIONAL | WEEKLY | SUPPORTING INFORM. ON SITE ANALYSIS ... | ALL PRE-PROCESSING AND ANALYSIS CENTERS |
| - FINAL OPERATIONAL | N.A. | FINAL UPDATED OPERATIONAL REPORT (TO BE INCLUDED IN FINAL REPORT) | ALL INVOLVED GROUPS |
| - INTERMEDIATE ANALYSIS | AS SOON AS AVAILABLE | INTERMEDIATE ANALYSIS RESULTS | INTERCHANGED BETWEEN ALL ANALYSIS CENTER |
| - INDIVIDUAL ANALYSIS | N.A. | FINAL RESULTS FROM EACH GROUPS | COMMITTEE |
| - FINAL ANALYSIS | N.A. | FINAL AGGREGATED RESULTS (TO BE INCLUDED IN FINAL REPORT) | ALL INVOLVED GROUPS |
| - FINAL REPORT | N.A. | FINAL COLOCATION REPORT (OPERATIONAL AND ANALYSIS) PREPARED JOINTLY BY ALL COMMITTED GROUPS | SCIENTIFIC COMMUNITY |

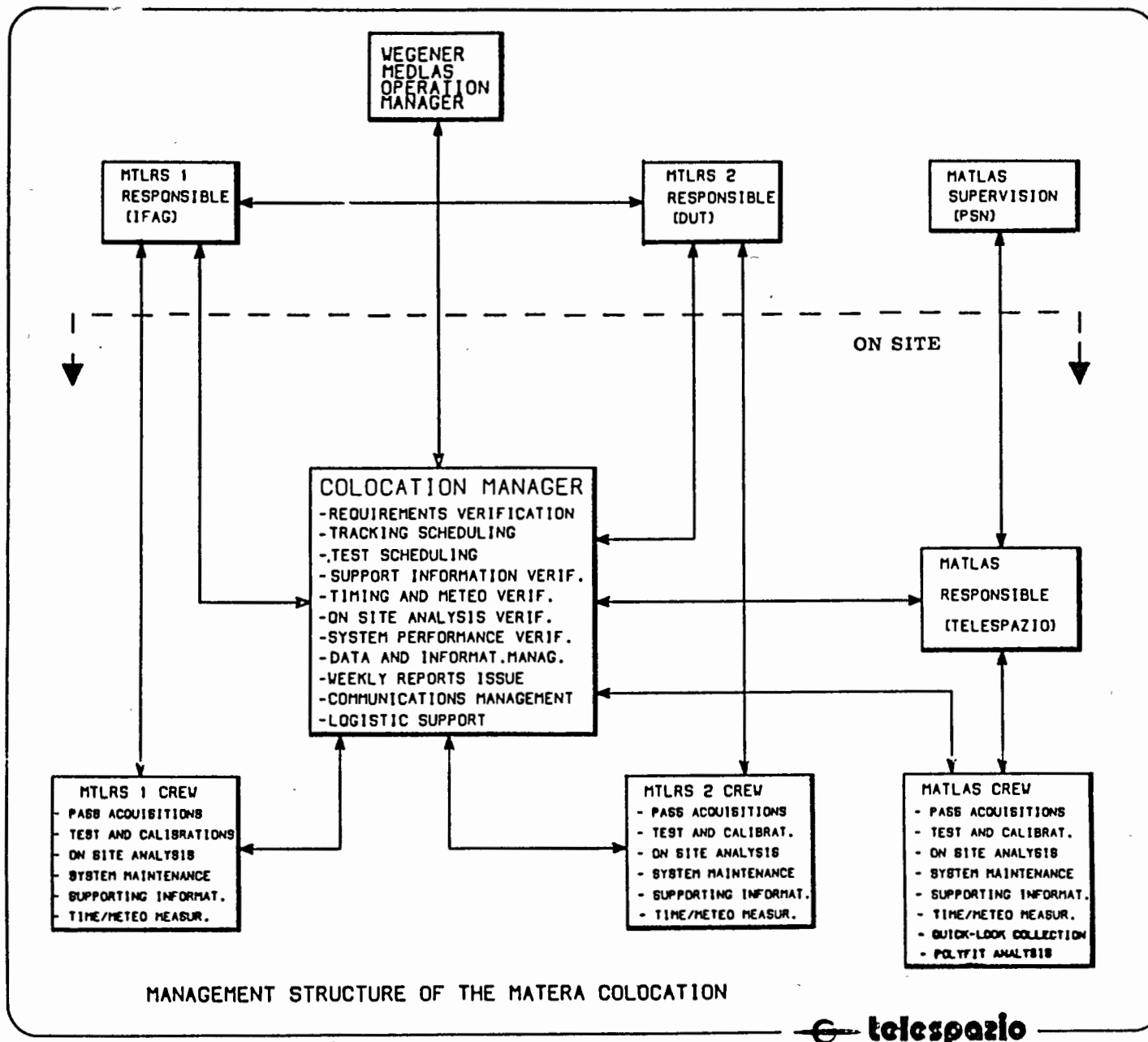


Fig. 1

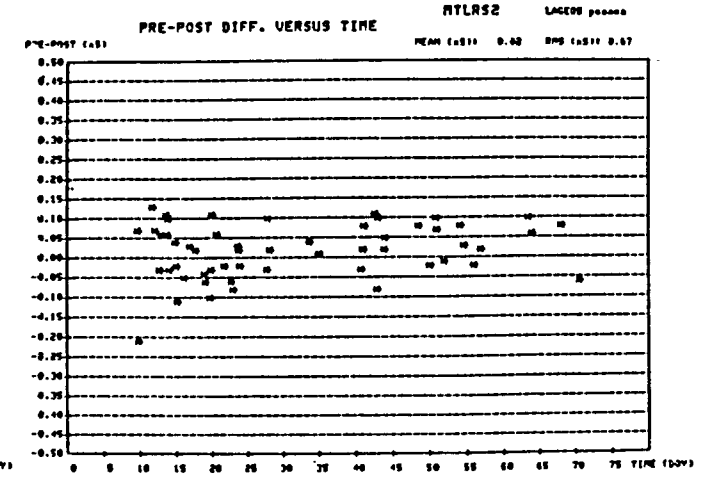
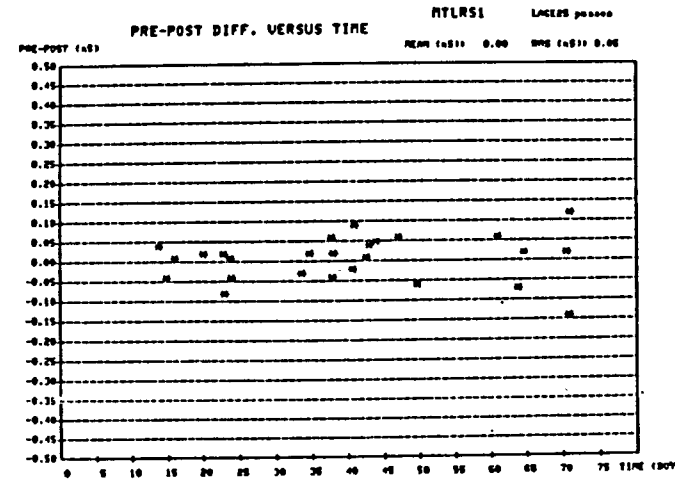
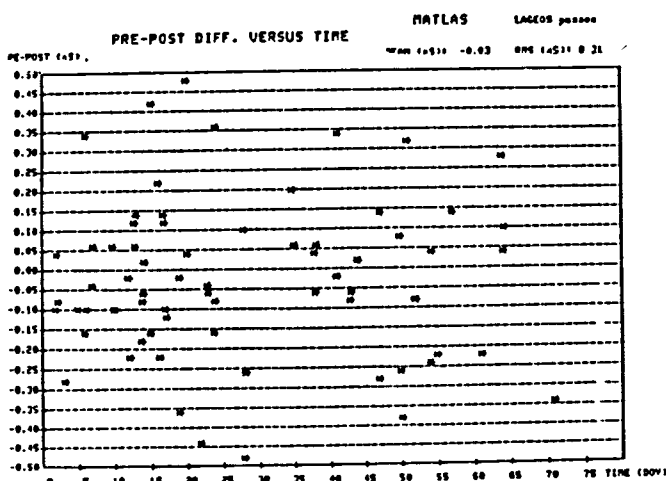
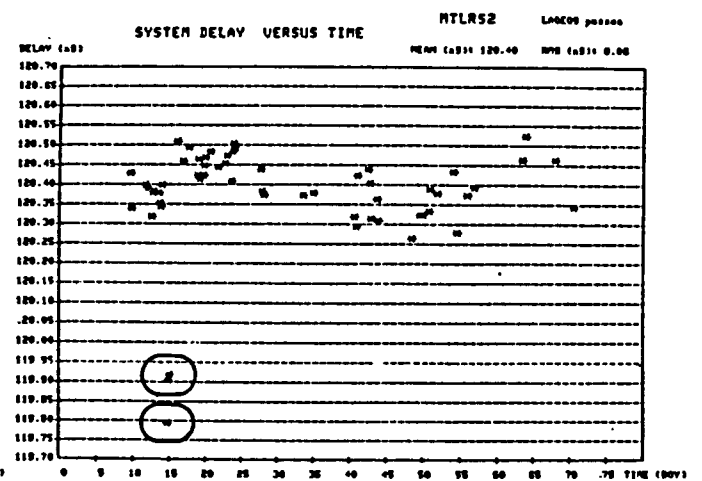
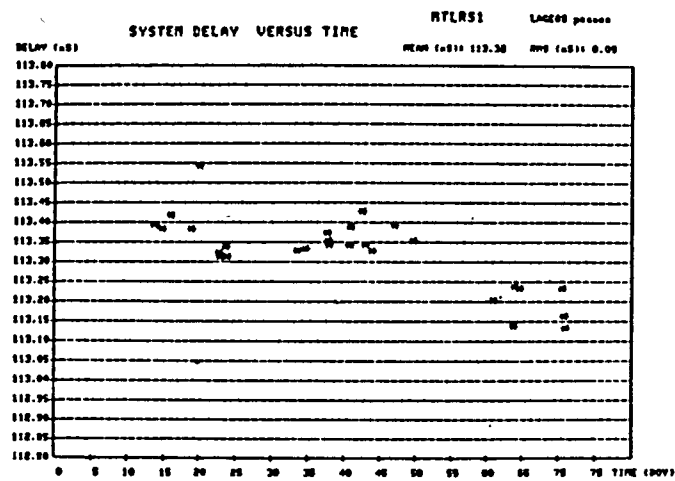
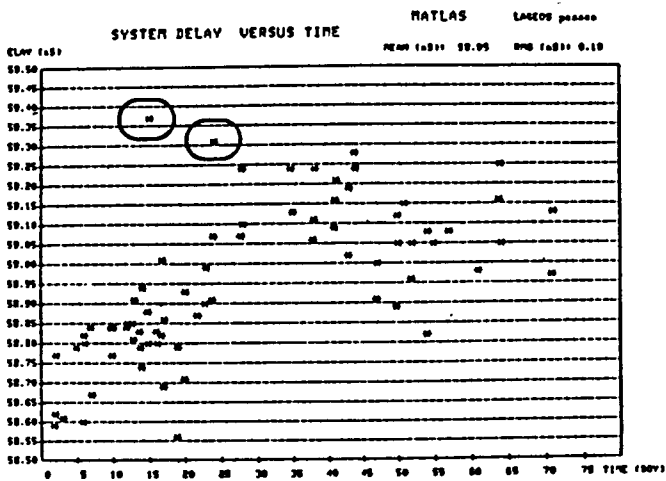


Fig. 2.1

System delay calibrations during the Matera Colocation

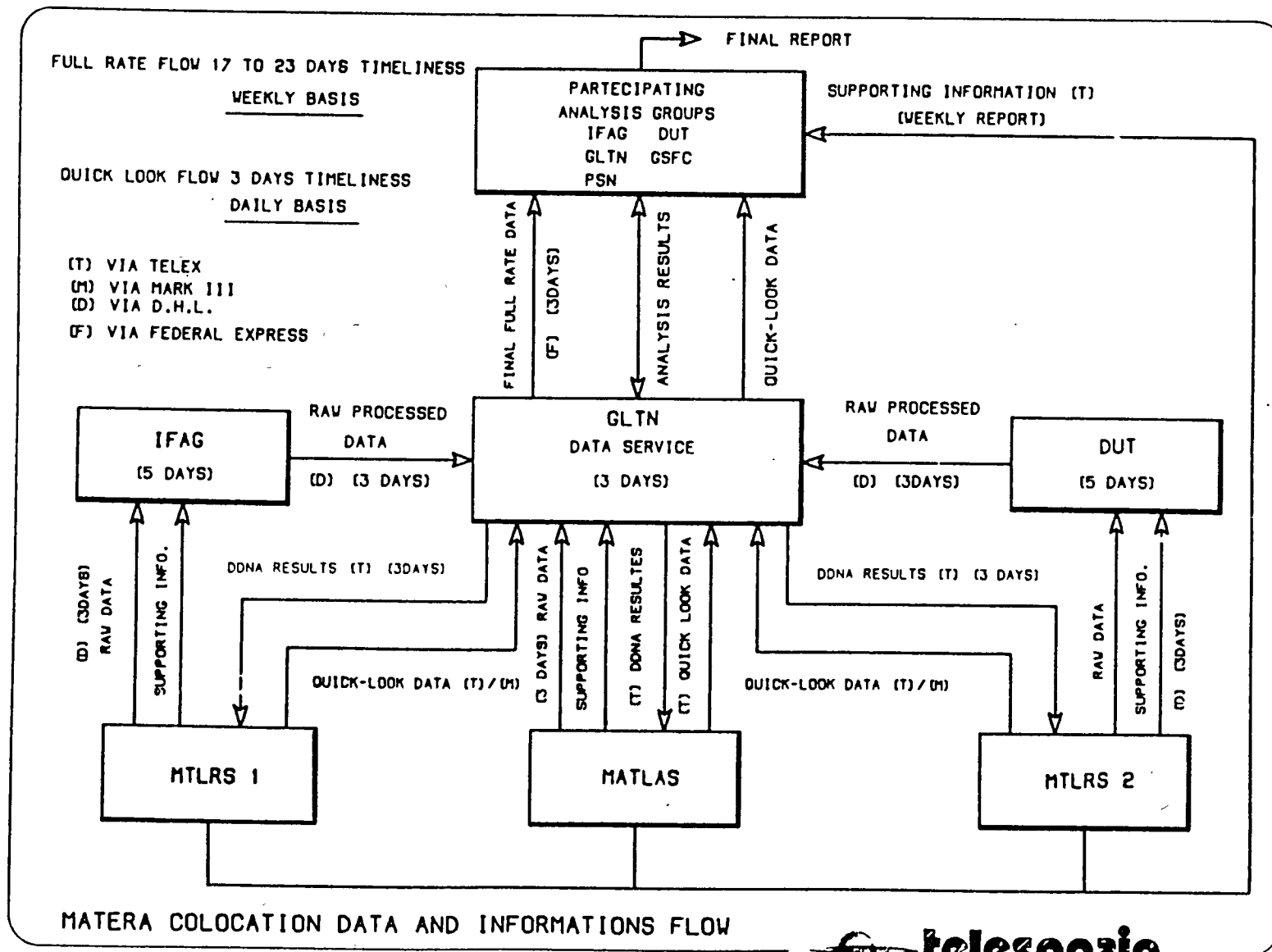


Fig. 2.2

- MATERA CO-LOCATION -

- WEEKLY REPORT FROM TO 1986 -

- WEATHER CONDITIONS -

| DAY | TEMP (DEG) | PRES (MBAR) | HUM (%) | WIND (KM/H) | CLOUD | FOG | RAIN |
|-----|---------------|----------------|------------|----------------|-------|-----|------|
|-----|---------------|----------------|------------|----------------|-------|-----|------|

STATION 7541 MTLRS2

- PASSES INFORMATION -

| PASSES | LAGEOS | STARLETTE |
|----------------------------------|--------|-----------|
| - A PRIORI ACQUIRABLE | | |
| - ACQUIRED | | |
| - NOT ACQUIRED (DUE TO WEATHER) | | |
| - NOT ACQUIRED (DUE TO PROBLEMS) | | |

- OBSERVED PASSES INFORMATION -

| STAT NAME | SAT NAM | START EPOCH YYMMDD HHMM | END HHMM | TOT OBS | VALID OBS | RANGE BIAS(m) | TIME BIAS(mS) | FIT RMS(m) |
|--------------|------------|----------------------------|-------------|------------|--------------|------------------|------------------|---------------|
|--------------|------------|----------------------------|-------------|------------|--------------|------------------|------------------|---------------|

- POLYFIT ANALYSIS -

| STAT NAME | SAT NAM | START EPOCH YYMMDD HHMM | END HHMM | TOT OBS | NO REJECTION | | 2.5 SIGMA REJECTION | |
|--------------|------------|----------------------------|-------------|------------|-----------------|---------------|------------------------|---------------|
| | | | | | VALID OBS | FIT RMS(L) | VALID OBS | FIT RMS(M) |

- TERRESTRIAL TARGETS RANGING -

| DAY/TIME | TARGET | RANGE AVER(NS) | RANGE RMS(NS) | TEMP (DEG) | PRES (MBAR) | HUM (%) | PRE (NS) | POST (NS) |
|----------|--------|-------------------|------------------|---------------|----------------|------------|-------------|--------------|
|----------|--------|-------------------|------------------|---------------|----------------|------------|-------------|--------------|

- TIMING DATA -

| DAY | TIME | UTC(MTL2)- UTC(GPS) (NSEC) SV | TIME | UTC(MTL2)- UTC(USNO) (NSEC) | TIME | UTC(MTL2)- UTC(MATL) (NSEC) |
|-----|------|-------------------------------------|------|-----------------------------------|------|-----------------------------------|
|-----|------|-------------------------------------|------|-----------------------------------|------|-----------------------------------|

- OFF LINE ACTIVITIES -

- REMARKS -

Fig. 2.3

An example of weekly Report

MATERA CO-LOCATION

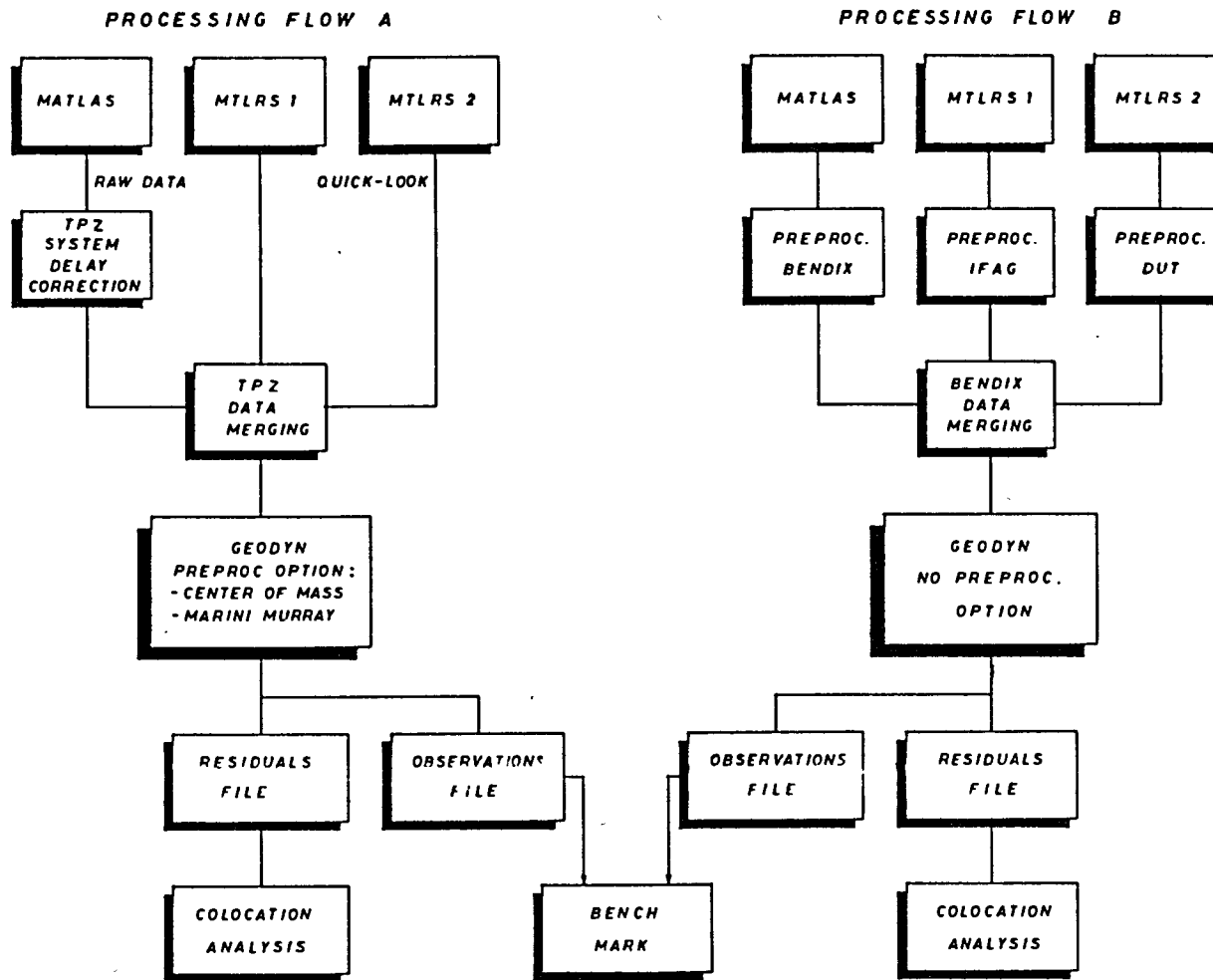


Fig. 3

An example of Analysis and Benchmark Processing

ECCENTRICITY VECTORS FOR COLOCATION PURPOSES

D.L.F. Van Loon
Delft University of Technology
Observatory for satellite Geodesy
P.O. Box 581
7300 An Apeldoorn - The Netherlands

Telephone 32 5769 341
TWX 36442 SATKO NL

ABSTRACT

Colocation testing is accepted as the only reliable method to determine systematic differences between operational laser ranging systems. To enable a direct comparison between two such systems the eccentricity vector between the reference points of the concerning instruments has to be determined. The current satellite laser ranging systems perform observations at the centimeter and even sub-centimeter level. Consequently the connecting eccentricity vector has to be determined with similar or higher accuracy.

In practice the determination passes in two steps :

- determination of the eccentricity vector between the prime markers on the respective pads, provided by a first order geodetic survey, and
- determination of the eccentricity vector between the reference point of the instrument and the prime marker, based on known instrumental parameters, eventually supplemented either with a typical instrumental establishing procedure or with other necessary geodetic measurements.

To identify systematic differences in laser ranging systems different observation techniques are applied viz : range measurements to terrestrial targets and range measurements to satellites.

Dependent on the observation technique and the analysis procedure the final eccentricity vector has to be given either in a local or in a global reference frame.

1. Introduction.

In planning of establishing a geodetic network using similar or even different types of Satellite Laser Ranging (SLA) stations, both stationary and transportable, a calibration of the concerning instruments is to be considered as necessary before going into the field.

Since third generation laser systems have a single shot precision of some centimeters, the colocation testing procedure seems to be the only reliable method to recognize systematic ranging differences between such instruments.

A direct comparison of both satellite ranging observations and terrestrial target ranging observations taken by the individual stations during simultaneous tracking offers the opportunity to evaluate laser ranging performance at the centimeter and subcentimeter level.

Different analysis methods are applied for the evaluation of colocation data, whereby the relative position of the involved instruments (the eccentricity vector) anyhow has to be determined. MERIT guidelines for geodetic survey [MERIT,83] recommend a precision better than 5 millimeter.

The determination of the eccentricity vector (fig.1.1) between the reference points of the instruments passes in practice in two separate steps:

1. between the prime markers at the respective pads (Section 3),
 2. between the reference point of the instrument and the prime marker at the pad (Section 4),
- both with their specific requirements.

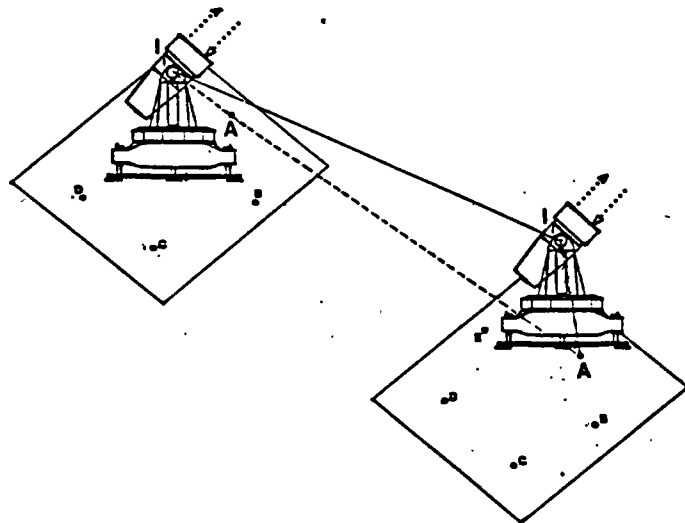
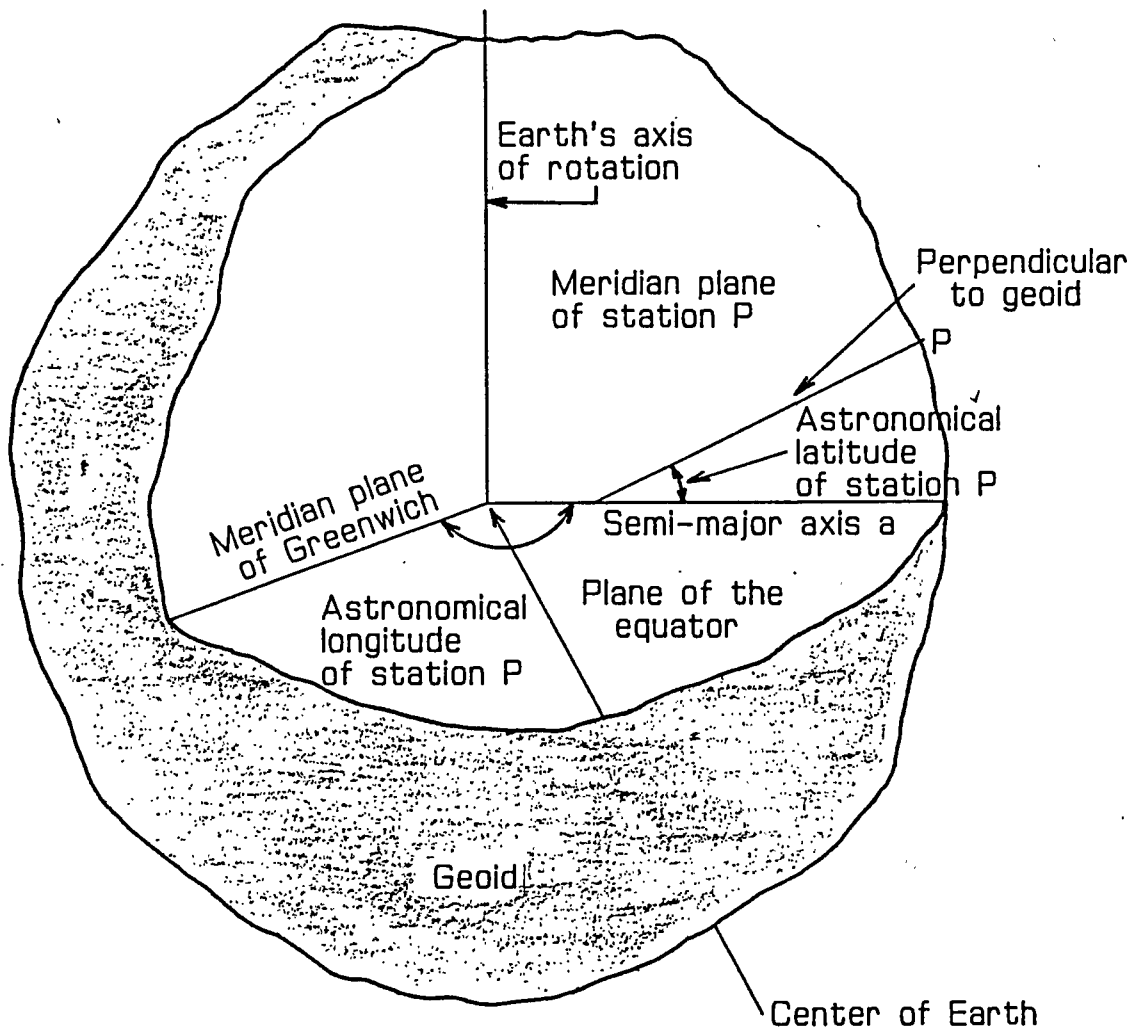


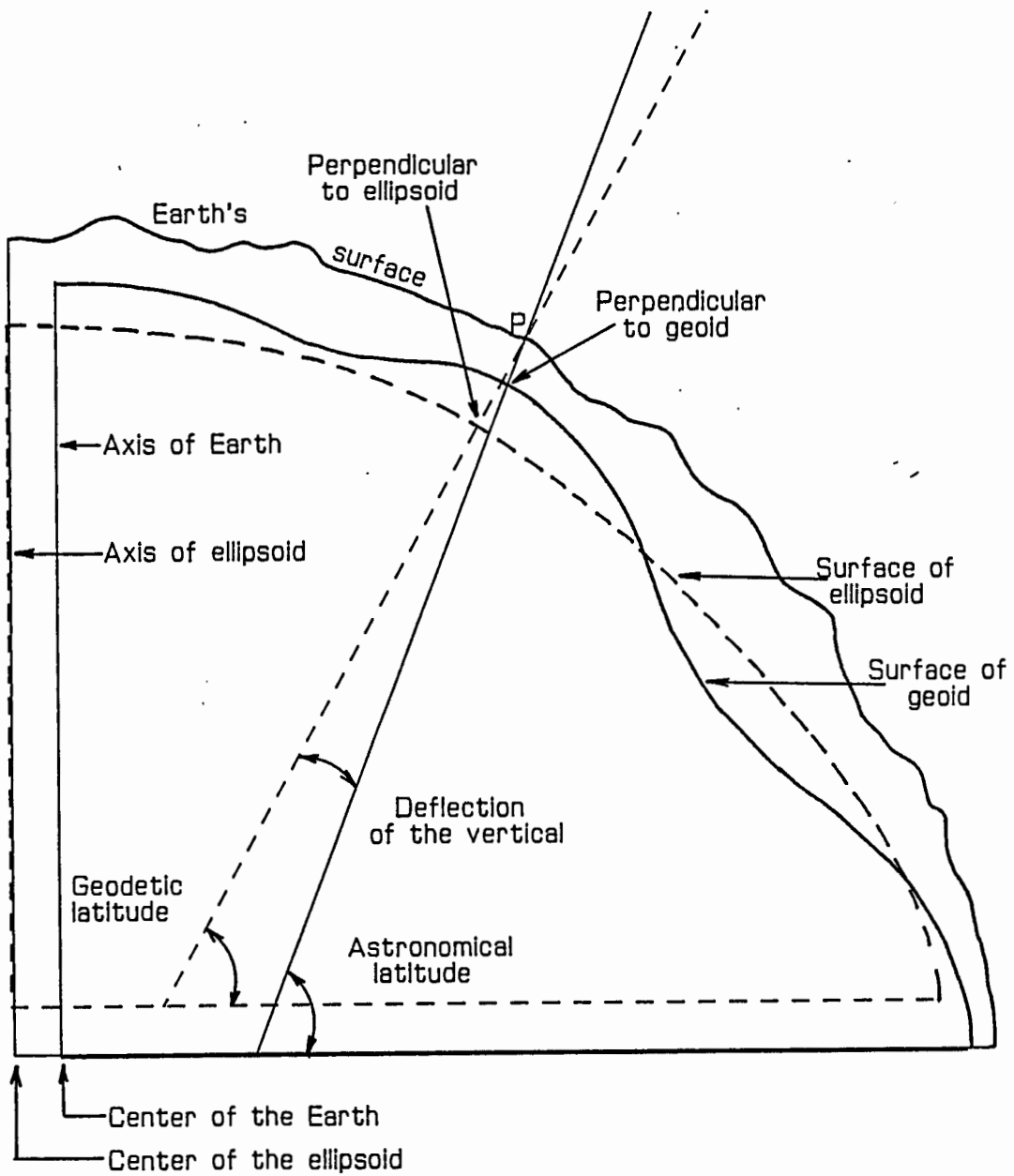
fig.1.1 Eccentricity vector between two SLA systems.

I refers to the reference point of the instrument,
while A refers to the prime marker at the pad.



ASTRONOMICAL COORDINATES

fig.2.1



DEFLECTION OF THE VERTICAL
AT STATION P

2. Reference frames.

2.1 Introduction.

Satellite ranging observations and terrestrial target ranging observations are performed by astrometric instruments, whose orientation are referred to the directions of the local plumbline and the astronomical north.

A direct comparison between the range observations emphasizes a determination of the eccentricity vector in a reference frame of an orientation, referred to the same directions.

2.2 Station coordinates.

The station position itself is on the surface of the earth defined relative to the Greenwich meridian and the equatorial plane.

As mentioned previously the observations are made with reference to the local plumbline at the station of observation P (fig.2.1 and fig.2.2).

The astronomical latitude is referred to the normal of the geoid and does not coincide exactly with the direction of the plumbline at station P and needs therefore a standard correction of

$$\Delta\phi'' = -0.000171 h \sin 2\phi \quad (2.1)$$

where ϕ is the latitude and h the geoid height at P. In general this correction can be neglected.

The longitude of station P is the angle between the meridian plane of station P and the Greenwich meridian plane.

Astronomical determinations refer to an instantaneous axis and to the equator, and by a motion of the earth relative to the axis of rotation, reduction to a common or mean position of the pole is then required.

2.3 Transformations.

Dependent on the analysis method and using either ranges to satellites or ranges to terrestrial targets, the eccentricity vector is required either in a local reference frame whose axes are referred to the local vertical and astronomical north or in a global reference frame whose axes are referred to the instantaneous pole and the Greenwich meridian.

It is to recommend to follow the MERIT Guidelines [MERIT,83] defining the offsets DX, DY, DZ in a coordinate system defined by the FK-4 Fundamental Star Catalog and referred to the pole and origin of longitude using polar coordinates and time information published by the Bureau International de l'Heure.

Transformation results into the following formulas:

$$(\underline{X}^2) = R_3(\gamma) \cdot (\underline{X}^1) \quad (2.2)$$

$$(\underline{X}^3) = R_3(-\Lambda) \cdot R_2(90 + \emptyset) \cdot (\underline{X}^2) \quad (2.3)$$

where (\underline{X}^1) is the eccentricity vector in an arbitrary local system, referred to the local vertical,

(\underline{X}^2) is the eccentricity vector in a local system oriented to the astronomical north direction and referred to the local vertical,

(\underline{X}^3) is the eccentricity vector in the global system oriented to the pole and Greenwich meridian,

γ is the rotation angle in the horizontal plane in order to orient the system with respect to the astronomical north direction,

\emptyset, Λ are respectively astronomical latitude and longitude.

3. Eccentricity vector between the prime markers.

3.1 Introduction.

Determination of the eccentricity vector between the prime markers at the respective pads has to be performed by a first order geodetic survey.

Mutual distances and 3-dimensional geometry of the collocating stations affect the accuracy to be required.

3.2 Survey equipment.

Table 3.1 summarizes geodetic survey equipment that has to be available in general. Section 2 mentioned already the rotation parameters to be determined, but also for setting-up the local network distance, angle and height difference measurements have to be made.

Besides this list is completed with information of precision, use and purpose of each individual instrument.

| <u>EQUIPMENT</u> | <u>PRECISION</u> | <u>TO USE FOR MEASUREMENTS OF</u> |
|---------------------|---|--|
| measuring tape | 20 ppm |) |
| invar tape | 2 ppm |) 1. distances |
| EDM instruments | 2 mm + 2 ppm |) |
| theodolite | 1-4 mdegrees | 2. horizontal angles 3. vertical angles |
| leveling instrument | 2 ppm | 4. height differences |
| clock and stopwatch | 0.1 sec. | 5. hourangle of sun or stars |
| <u>PURPOSE:</u> | | |
| 1.) + 2.) + 3.) | Determination of vector in an arbitrary local reference frame | |
| 4.) | To measure direct height differences | |
| 2.) + 5.) | Determination of astronomical azimuth | |
| 3.) or 4.) + 5.) | Determination of astronomical latitude and longitude | |

Table 3.1. Summary of equipment and its purpose.

3.3 Survey reconnaissance.

3.3.1 Influence of distance and vertical angle measurements on the vertical component of a local coordinate system.

The influence of distance and vertical angle measurements on the vertical component can simply be derived, assuming without correlation:

$$\sigma_H = \sqrt{HD^2 \cdot \sigma_\alpha^2 + \frac{H^2}{HD^2 + H^2} \cdot \sigma_D^2} \quad (3.1)$$

where σ_α is the precision in the vertical angle measurements,
 σ_D is the precision in the distance measurements,
 HD is the estimated horizontal distance,
 H is the estimated height difference,
 σ_H is the expected precision in the vertical component.

| HD(m) | H(m) | σ_H (mm) |
|-------|------|-----------------|
| 20 | 0-8 | 1.6 |
| 30 | 0-8 | 1.8 |
| 40 | 0-8 | 2.2 |
| 50 | 0-8 | 2.7 |
| 60 | 0-8 | 3.2 |
| 70 | 0-8 | 3.7 |

Table 3.2 Expected precision in H: (σ_H).
Assumed precisions: $\sigma_D = 3$ mm, $\sigma_\alpha = 0.003$ degr.

Table 3.2 gives an example for the Matera station and it should be noted that if a maximum tolerance of 3 mm is accepted and if the horizontal distances are larger than 50 m, it is to be preferred to measure the vertical component direct with a leveling instrument instead of calculating it from distance and vertical angle measurements.

3.3.2 Influence of astronomical observations.

An astronomical azimuth determination in order to rotate an arbitrary local system to a local system referred to the astronomical north direction, causes a maximum error in the horizontal vector components, simply expressed as

$$e = \frac{HD \cdot \sigma_A}{206.265} \quad (3.2)$$

where e is the maximum error in the horizontal components (in mm),
and $\frac{HD}{\sigma_A}$ is the horizontal distance between the stations (m),
is the estimated precision in the astronomical azimuth determination (arcsec.).

The influence of the astronomical latitude and longitude determination on the vector components can be derived from (2.1) and (2.2).

However for practical reasons it is to be preferred to ascertain a maximum tolerance in the individual vector components and then to consider the highest precision of determination of latitude and longitude to require after their successive rotations.

$$\sigma_{\phi_1}'' = \frac{e \cdot 206.265}{-\cos \lambda \cdot \cos \phi \cdot DX + \cos \lambda \cdot \sin \phi \cdot DZ} \quad (3.3)$$

$$\sigma_{\phi_2}'' = \frac{e \cdot 206.265}{-\sin \lambda \cdot \cos \phi \cdot DX + \sin \lambda \cdot \sin \phi \cdot DZ} \quad (3.4)$$

$$\sigma_{\phi_3}'' = \frac{e \cdot 206.265}{-\sin \phi \cdot DX - \cos \phi \cdot DZ} \quad (3.5)$$

$$\sigma_{\lambda_1}'' = \frac{e \cdot 206.265}{\sin \lambda \cdot \sin \phi \cdot DX + \sin \lambda \cdot \cos \phi \cdot DZ - \cos \lambda \cdot DY} \quad (3.6)$$

$$\sigma_{\lambda_2}'' = \frac{e \cdot 206.265}{-\cos \lambda \cdot \sin \phi \cdot DX + \cos \lambda \cdot \cos \phi \cdot DZ + \sin \lambda \cdot DY} \quad (3.7)$$

where $\sigma_{\phi_1}, \sigma_{\phi_2}, \sigma_{\phi_3}$ is the precision in the required latitude,
 $\sigma_{\lambda_1}, \sigma_{\lambda_2}$ is the precision in the required longitude,
 DX, DY, DZ are the coordinate differences between the stations (in m),
 e is the maximum error in the individual components of the coordinate system (in mm),
 ϕ, λ are resp. latitude and longitude.

| STATION | DX (m) | DY (m) | DZ (m) | HD (m) | e (mm) | σ_A (arcsec.) | σ_ϕ | σ_λ |
|---------|-----------|-----------|-----------|-----------|-----------|-------------------------|---------------|------------------|
| 7939 | 0 | 0 | 0 | | | | | |
| 7540 | -17.3 | -31.7 | -7.2 | 36.9 | 3 | 17 | 37 | 24 |
| | | | | | 1 | 6 | 12 | 8 |
| 7541 | -33.7 | -33.6 | -7.5 | 48.2 | 3 | 12 | 22 | 17 |
| | | | | | 1 | 4 | 7 | 5 |

Table 3.3 Requirements for the determination of the astronomical rotations at the Matera Station. Latitude = 40.6 degr. Longitude = 16.7 degr.
 DX) approximate differences in resp. east,
 DY) north and up vector components
 DZ)
 HD approximate horizontal distance
 e max. tolerance in the vector components after rotation
 σ_A) max. acceptable error in resp. the
 σ_ϕ) astronomical azimuth, latitude and
 σ_λ) longitude determination.

Table 3.3 shows a survey reconnaissance with respect to the astronomical parameters, i.c. the Matera site as an example.

If we accept a maximum error of 3 mm in the separate vector components, the determination of resp. azimuth, latitude and longitude must be performed with a precision better than 12, 17 and 22 arcseconds.

Obviously in this case we may not use the geodetic latitude and longitude as rotation parameters, because we know from geoid maps [BRENECKE et al,1983] that the deflection of the vertical (fig.2.2) at the Matera site is more than 30 arcseconds.

3.3.3 Final measurements and results.

After a thorough reconnaissance and selection of the right survey equipment and after the geodetic survey has been performed, the final results of the network, successively in an arbitrary local coordinate system, a local coordinate system oriented to astronomical north direction and a global coordinate system, have to be tested properly on the precision and reliability anyhow.

| <u>DETERMINATION OF:</u> | <u>USED EQUIPMENT</u> | <u>RMS</u> |
|--|--|------------|
| eccentricity vector in the arbitrary local reference frame | EDM and theodolite (KERN) | 3 mm |
| astronomical azimuth | KERN theodolite and clock/stopwatch | 11 arcsec. |
| astronomical latitude | MTLAS-1 and MTLAS-2 | 5 arcsec. |
| astronomical longitude | MTLAS-1 and MTLAS-2 | 5 arcsec. |

Table 3.4 Some results at the Matera site.

Table 3.4 shows the tested final results for the Matera site as an example [CENCI et al,1986].

4. Eccentricity vector between the reference point of the instrument and the prime marker.

Determination of the eccentricity vector between the reference point of the instrument and the prime marker at the pad can be performed by an establishing procedure dependent on the specific characteristics of the instrument.

The precise reference point of each instrument must be identified thoroughly e.g. the intersection of azimuth and elevation axes.

It is important that the observed ranges to both satellites and terrestrial targets are also referred to this precise reference point.

Usually the offset of an auxiliary reference point to the prime marker is determined, while the offset of the precise reference point to this auxiliary point is reconstructed from the design.

To seek for a determination procedure of the separate offsets is strongly recommended, where especially a regular calibration of the instrumental offset parameters is certainly included.

A reliable determination procedure of this eccentricity vector is applied with the MTLRS [VERMAAT et al, 1983 and VERMAAT, 1984].

Because the eccentricity vector between the reference points of the instruments is required with a precision better than 5 mm, and while in general the precision in the determination of the eccentricity vector between the prime markers will be in the order of 3 mm, consequently the precision of the eccentricity vector between the reference point of the instrument and the prime marker must be then guaranteed with a precision better than 2 mm.

5. Conclusions and recommendations.

Prior to the definitive construction of the pads at a colocation site, their relative location has to be settled on basis of geodetic requirements such as geometry, mutual distances and height differences.

The first order geodetic survey has to be performed with great care and with the proper geodetic instruments. The final results have to be tested on precision and reliability. A pre and post geodetic survey is to recommend.

A critical part of the determination of the final eccentricity vector is the determination of the offset of the precise reference point to the prime marker, that often seems to be neglected. A regular calibration, eventually verified with a geodetic survey is not abundant and to seek for a well defined determination procedure with testing possibilities on precision and reliability, is highly recommended, certainly in case of transportable systems.

References

Vermaat, E. and B.H.W. van Gelder, 1983. "On the eccentricity of MTLRS." Delft University of Technology, Reports of the Department of Geodesy, Mathematical and Physical Geodesy, No. 83.4.

Vermaat, E. "Establishing ground ties with MTLRS.", Proceedings of the fifth international workshop on laser ranging instrumentation, Herstmonceux Castle, United Kingdom, 1984 page 47.

MERIT/COTES JOINT WORKING GROUPS. "Merit campaign : connection of reference frames - implementation plan -." Bureau International de l'Heure, Paris, France, 1983.

Cenci, A. and D.L.F. van Loon, 1986. "Survey of the Matera laser station site." Telespazio S.p.A., Rome, Italy.

Schanzle, A.F., "Lectures on orbit determination and trajectory analysis." EG and G, Washington analytical services center, Inc., USA.

Mueller, I.I., 1968. "Spherical and practical astronomy as applied to geodesy." Frederick Ungar Publishing Co., New York, USA.

Brennecke, J., D. Leigemann, E. Reinhart and W. Torge, W. Weber, H.-G. Wenzel, 1983. "An european astro-gravimetric geoid.", Reihe D, heft nr. 269, Deutsche Geodaetische Kommission, Frankfurt a.M., FRG.

POLYQUICK COLLOCATION ANALYSIS

V. Husson, D. Edge
Bendix Field Engineering Corporation,
Columbia, Maryland - U.S.A. -

Telephone (301) 344 5013
TWX 197700 GLTN

ABSTRACT

POLYQUICK is a purely mathematical collocation analysis system that has been used as a key analysis tool of collocated laser data for the last five (5) years. POLYQUICK geometrically corrects the ranges from the standard system to the test system using measured or computed angles. The range error introduced in the geometric correction is dependent on the closeness of the two systems and the standard system angle accuracy. The range error is less than 1 cm if the two systems are within 60 meters of each other and if the standard system angles are accurate to 0.01 degrees

Only collocated simultaneous passes are analyzed. A least squares polynomial is fit through the standard system geometrically corrected range on a pass-by-pass basis. The polynomial generated for each pass is then used to analyze the test system data and to generate residual statistics for both stations for every simultaneous pass. Time batched normal points are created from the polynomial fit for each system for each collocated pass. These normal points are then differenced if there is an acceptable amount of data from each station in that time interval. The normal point differences then are stored for every collocated pass so that the aggregate collocation data set can be analyzed for every bias test contained in the collocation analysis plan. These bias tests have revealed systematic biases when there is an adequate number of healthy simultaneous LAGEOS passes taken over an extended period of time.

POLYQUICK COLLOCATION ANALYSIS CONCEPTS

- * MATHEMATICAL TECHNIQUES
- * SIMULTANEOUS COLLOCATION SATELLITE RANGING OBSERVATIONS
- * SATELLITE ANGLE DATA FROM ONE STATION
- * STATION SURVEY GEOMETRY
- * GEOMETRIC RANGE TRANSLATION
- * POLYNOMIAL DATA FIT TO REFERENCE STATION
- * COMPARISON OF OBSERVATION RESIDUALS
- * EVALUATION OF PASS AND AGGREGATE DATA SET STATISTICS

POLYQUICK COLLOCATION ANALYSIS SYSTEM

INPUTS

Merged Collocation
Satellite Ranging
Observations With
Supporting Angles

Survey Data For
The Collocating
Stations

PROCESS

Geometric Range Translation
Simultaneous Data Selection
Polynomial Fit
Normal Point Computation
Observations and Normal Point
Residual Computations
Comparison Statistics Computations

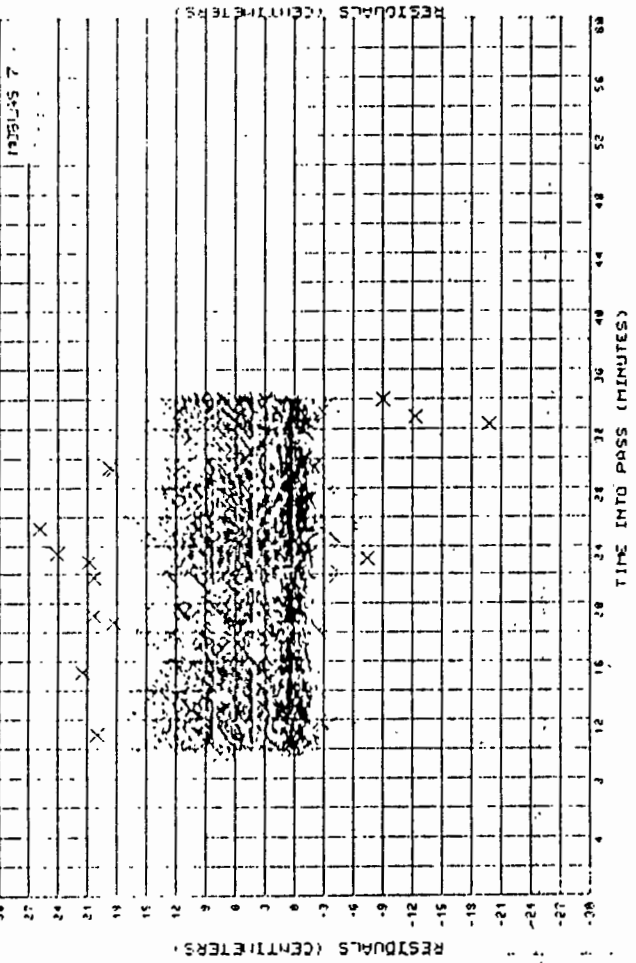
OUTPUTS

Plots
Histograms
Statistics
Data

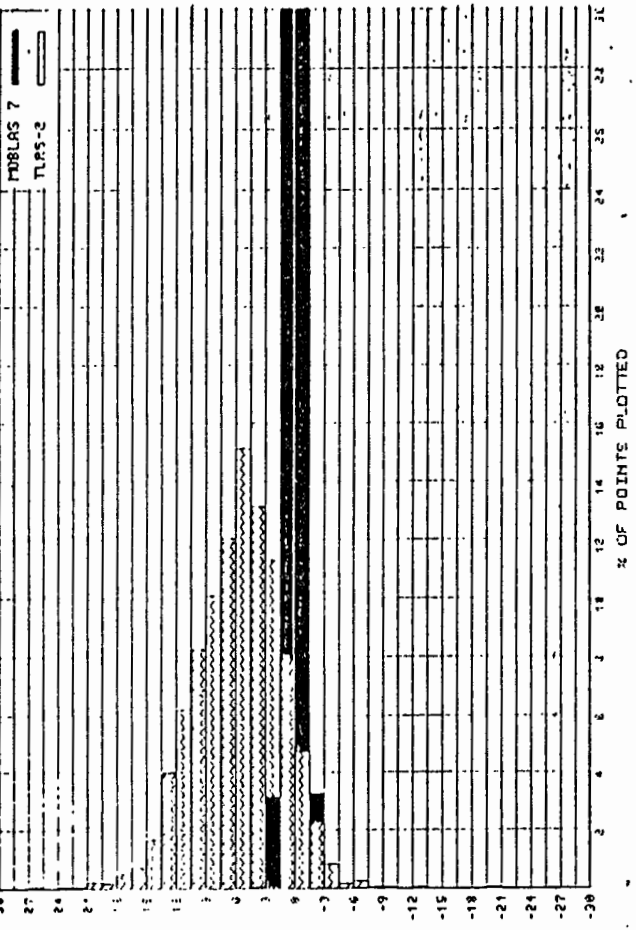
PERFORMANCE EVALUATION

Pass Analysis
Aggregate Data Set Analysis

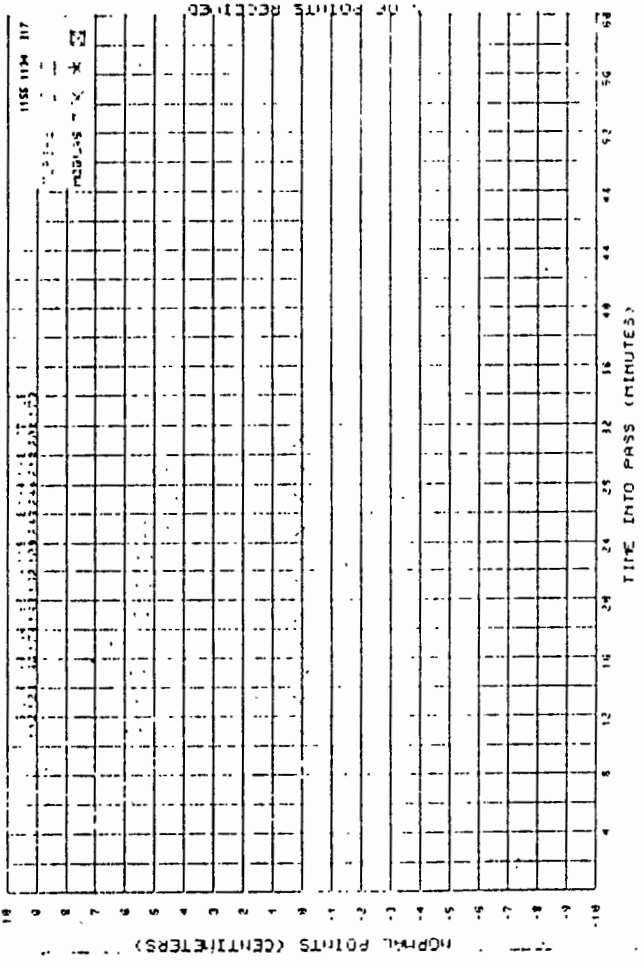
LAGEOS
8/30/88 - 9:16



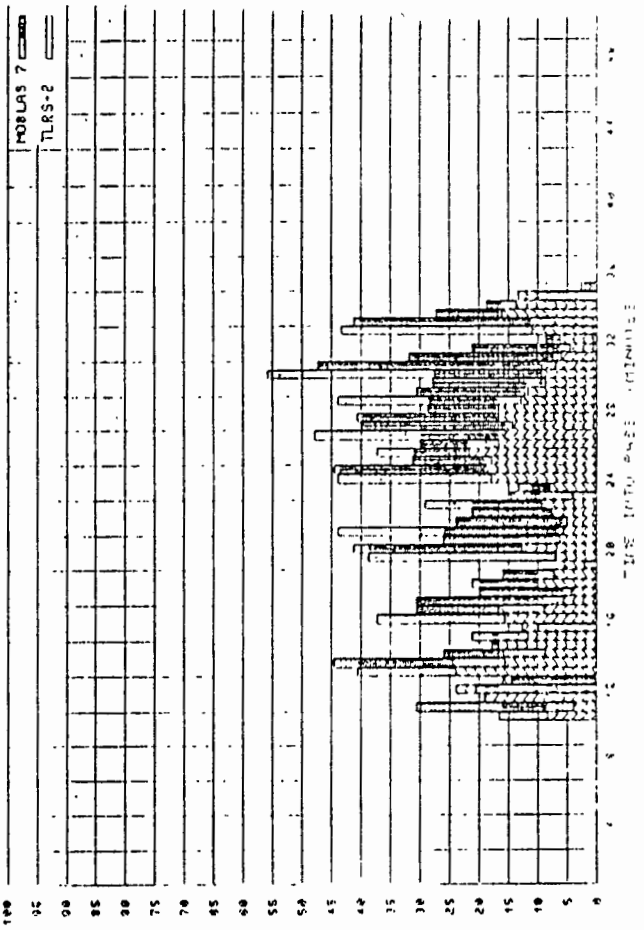
LAGEOS
8/30/88 - 9:16



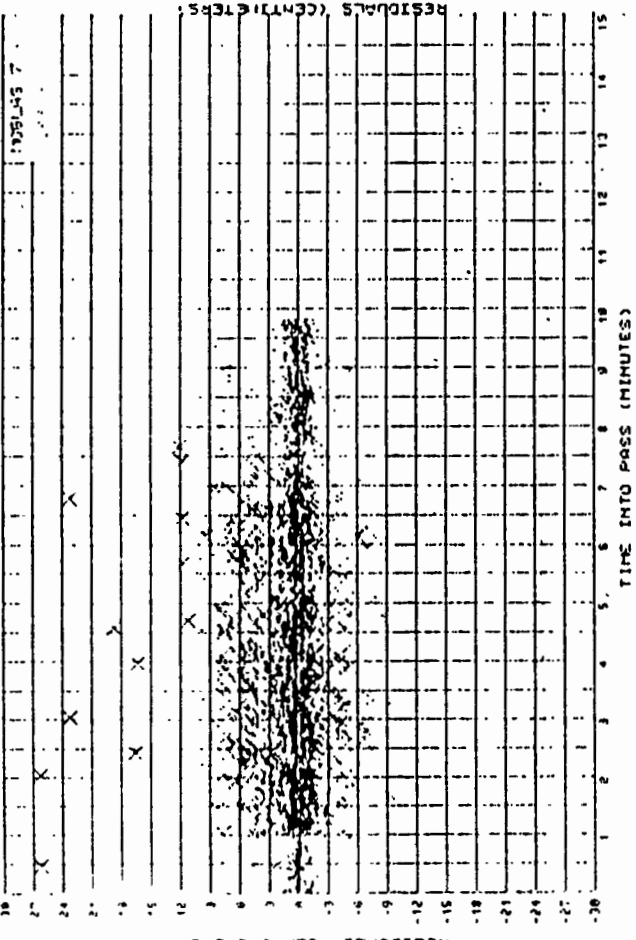
LAGEOS
8/30/88 - 9:16



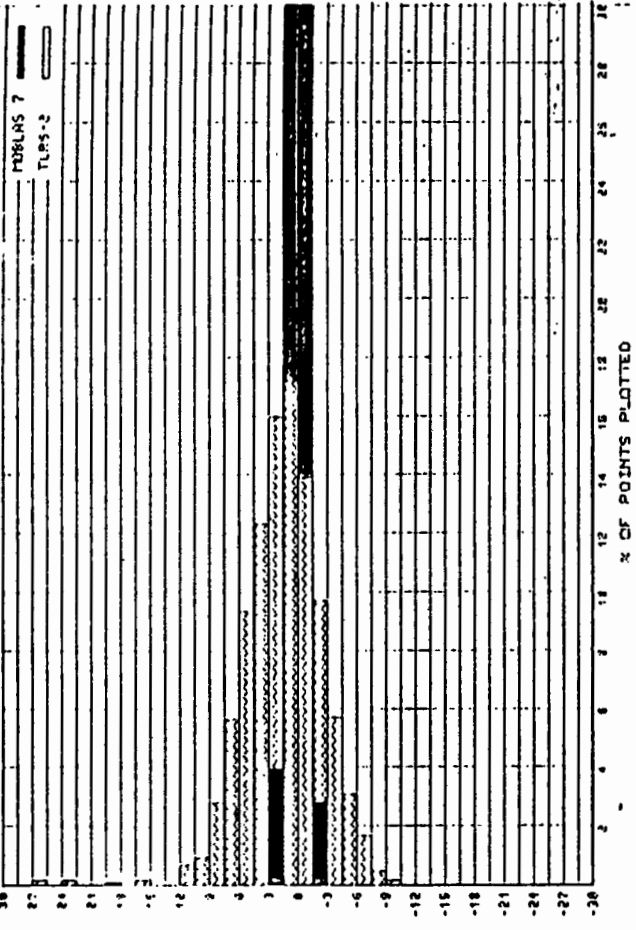
LAGEOS
8/30/88 - 9:16



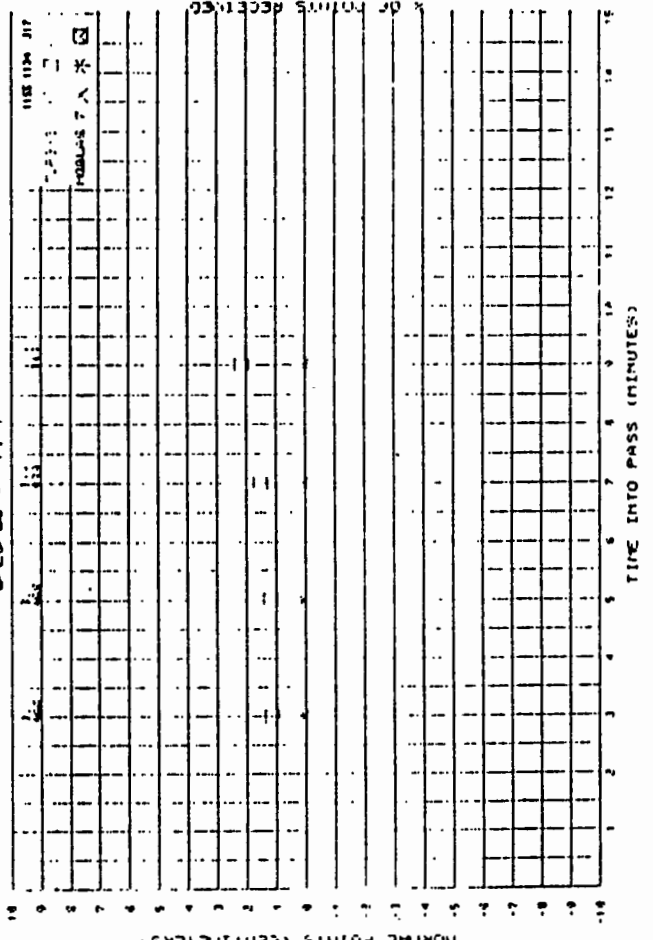
STARLETTE
8-26-88 - 7: 7



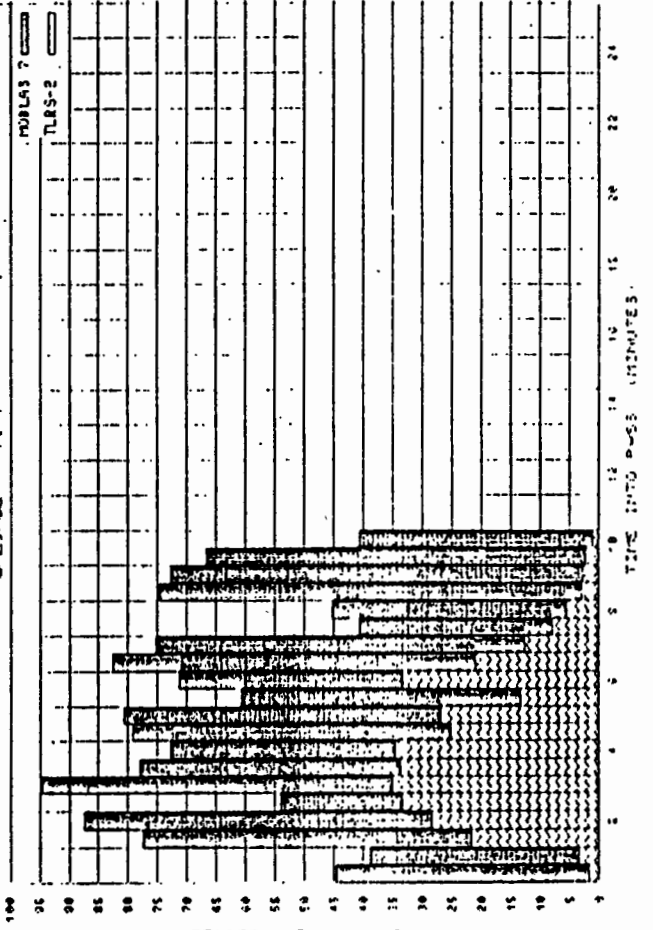
STARLETTE
8-26-88 - 7: 7



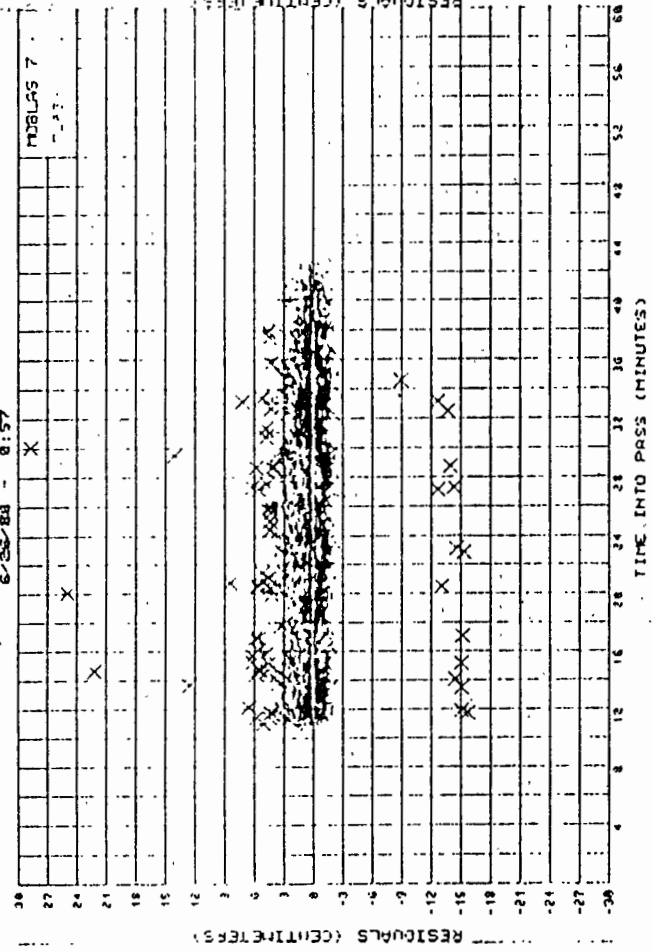
STARLETTE
8-26-88 - 7: 7



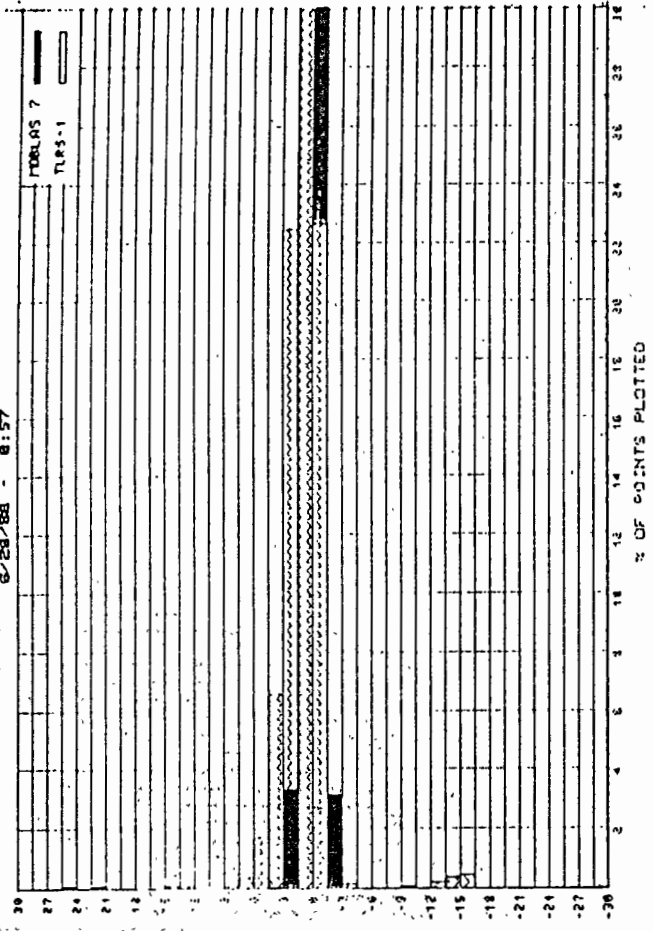
STARLETTE
8-26-88 - 7: 7



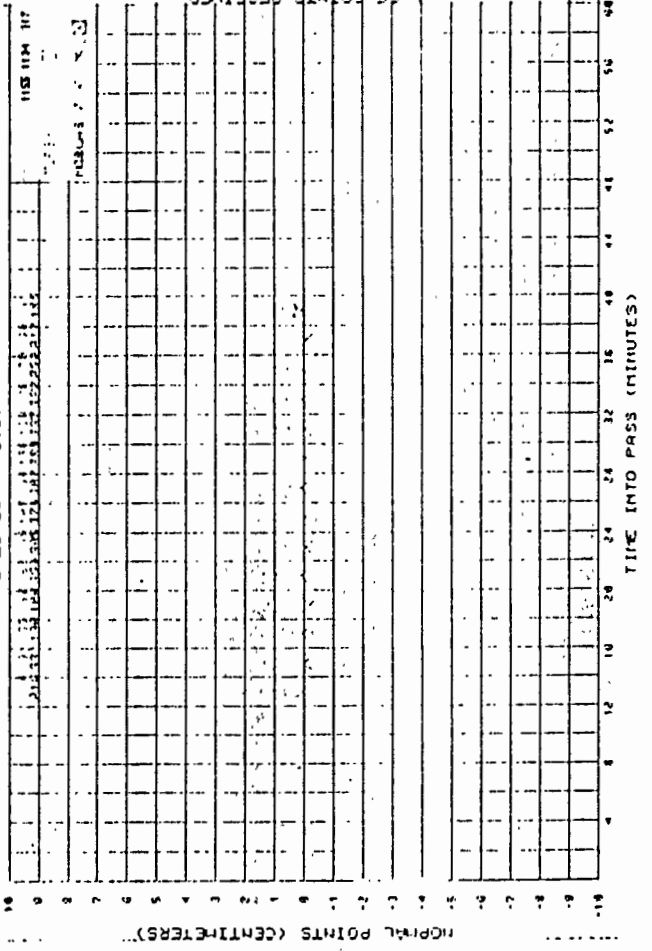
LAGEOS
6-26-86 - 0:57



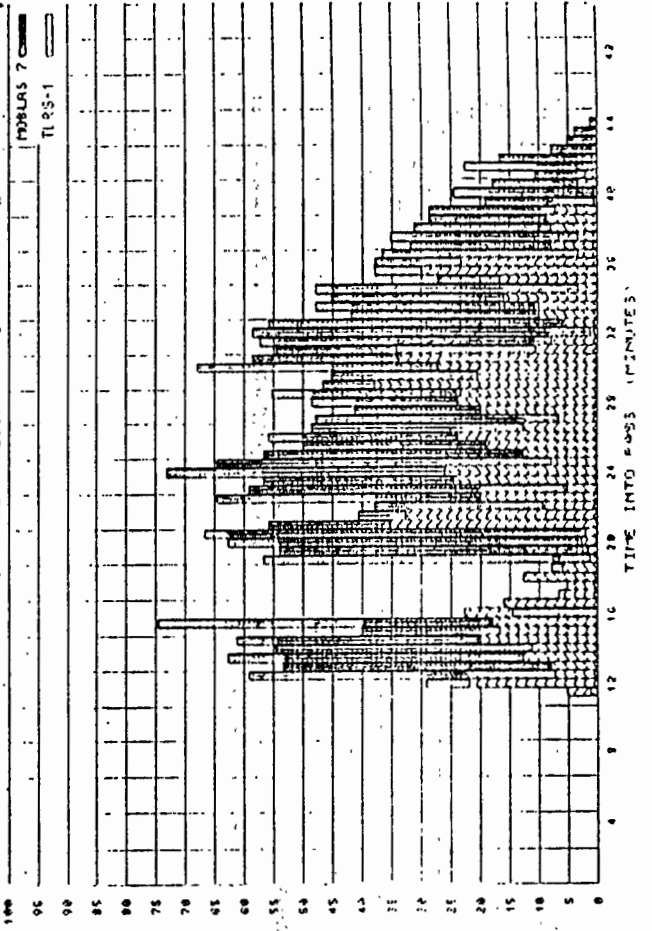
LAGEOS
6-26-86 - 0:57



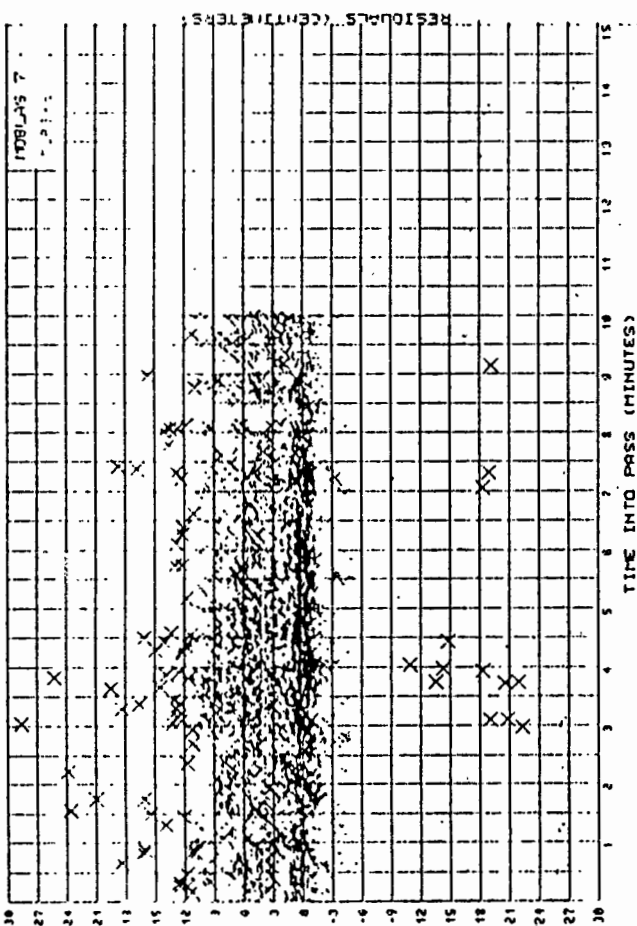
LAGEOS
6-26-86 - 0:57



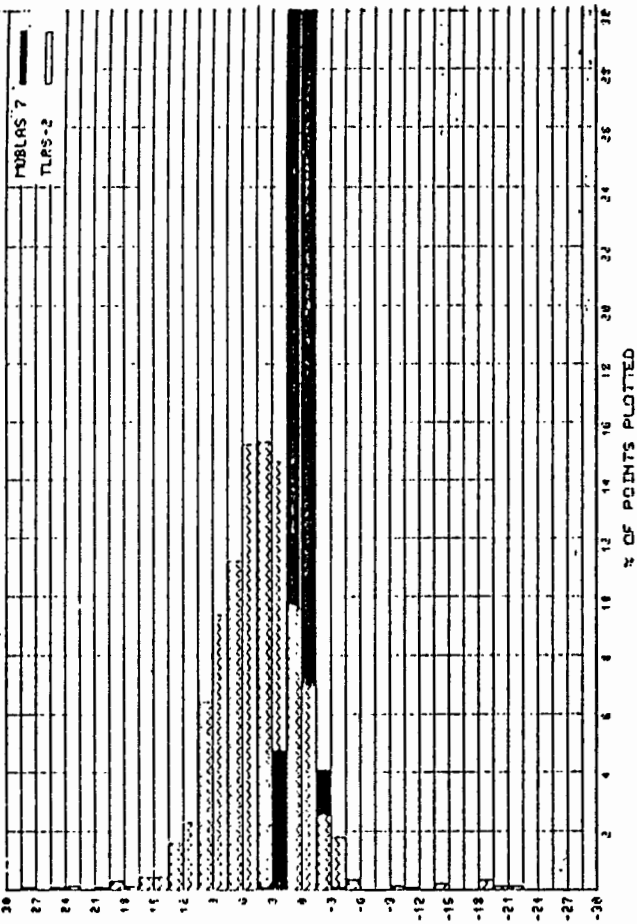
LAGEOS
6-26-86 - 0:57



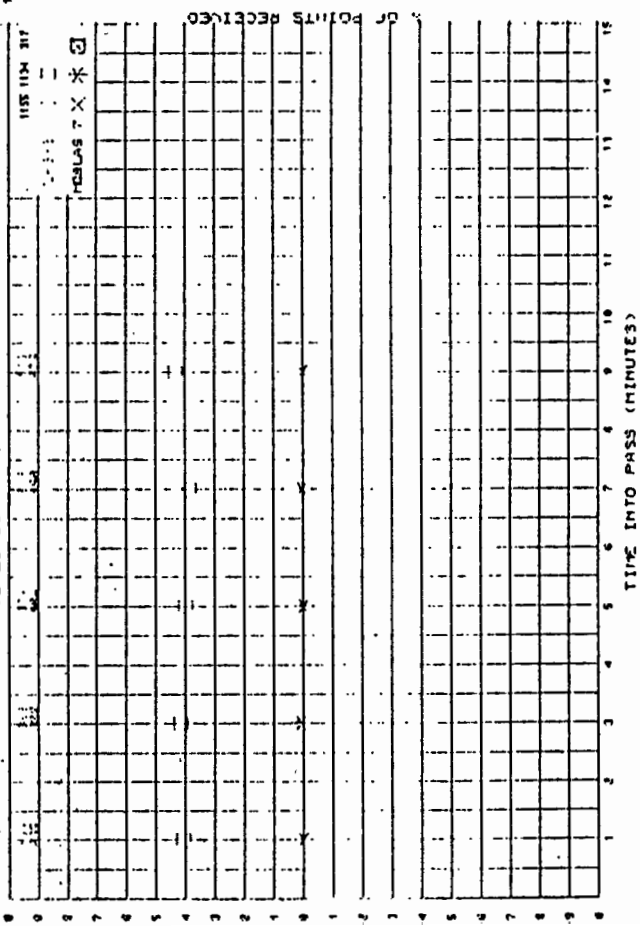
STARLETTE
8-29-88 - 8:18



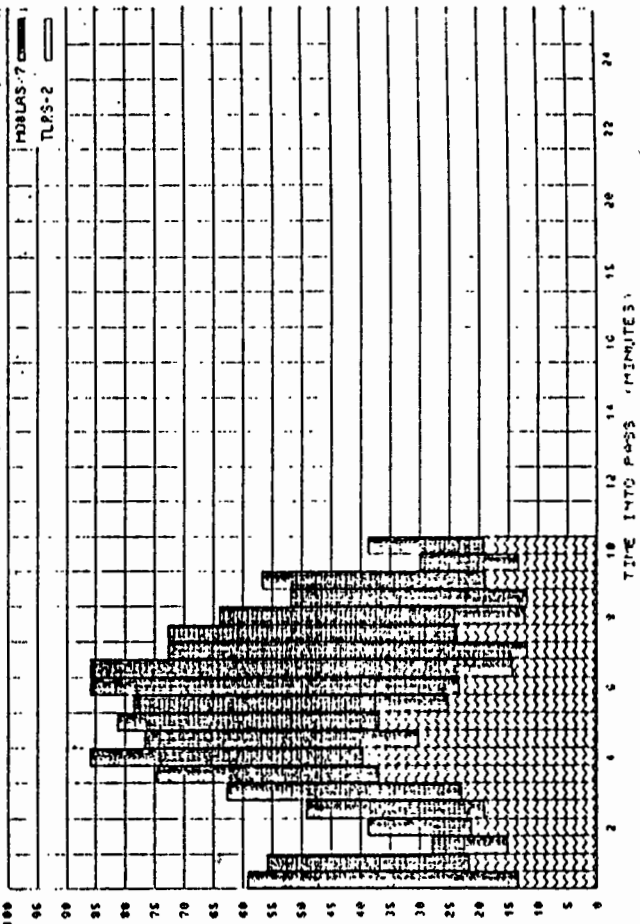
STARLETTE
8-29-88 - 8:18



STARLETTE
8-29-88 - 8:18

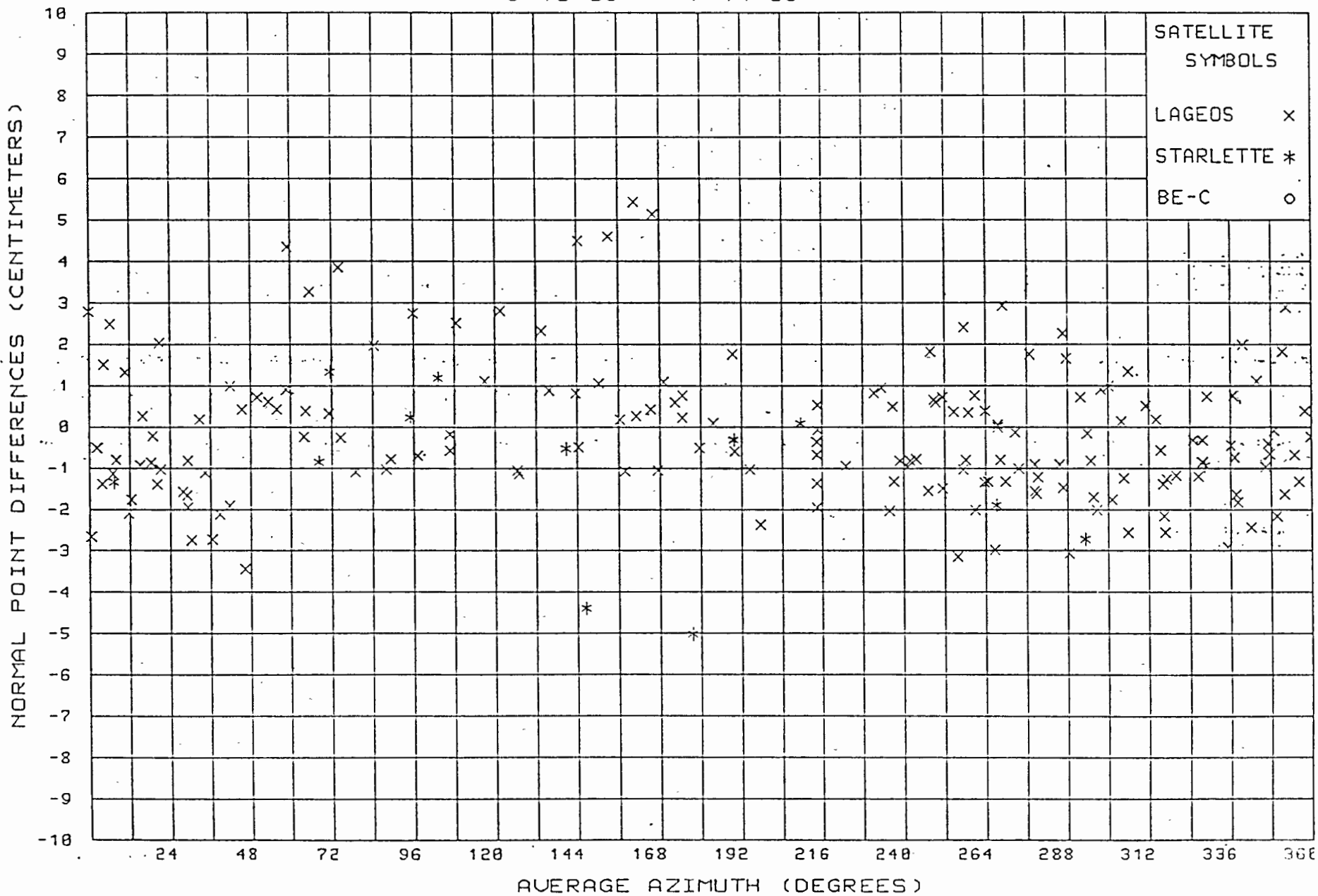


STARLETTE
8-29-88 - 8:18

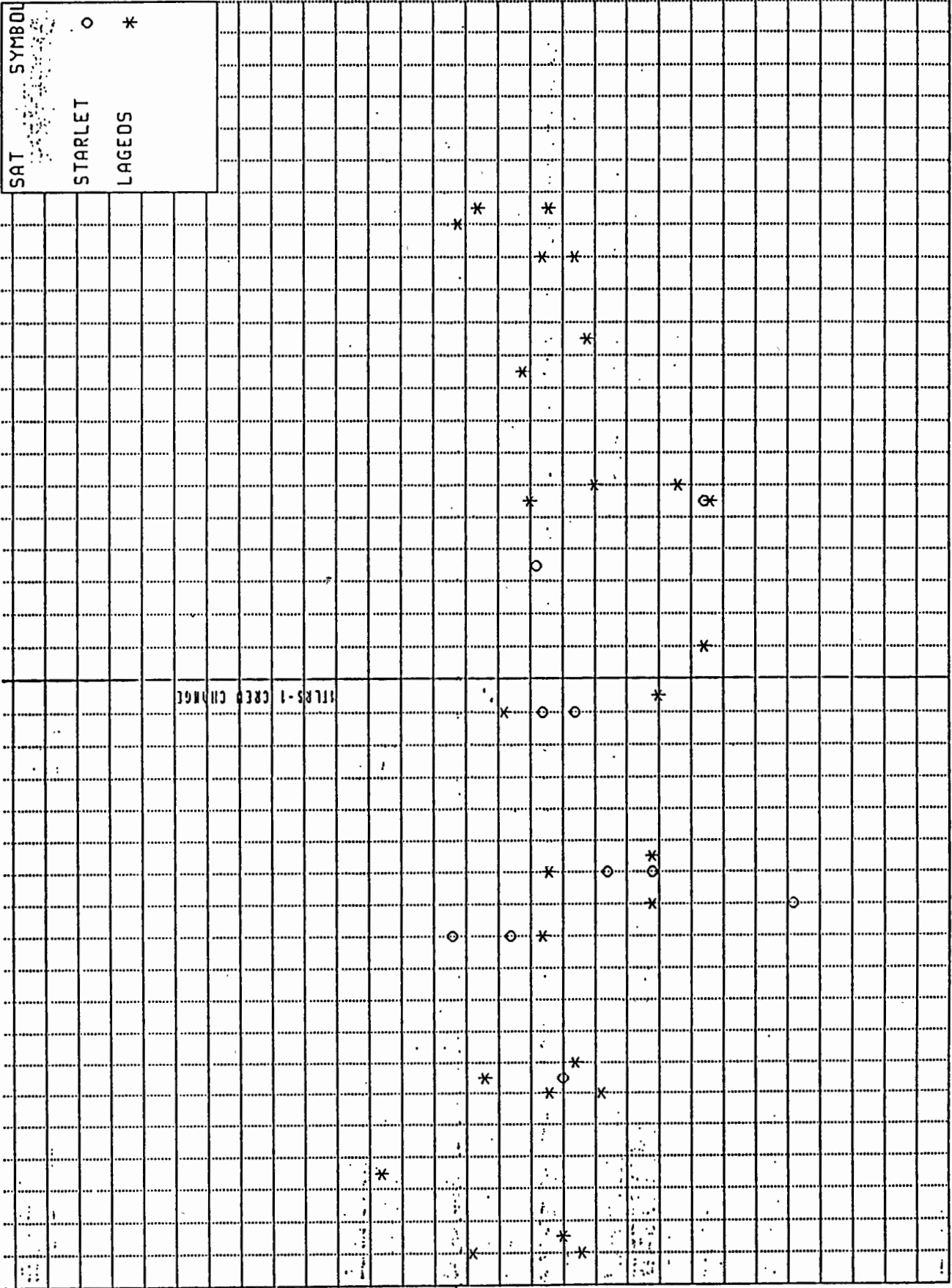


LAGEOS - STARLETTE

5/10/85 - 7/14/85



| | |
|---------|--------|
| SAT | SYMBOL |
| STARLET | ○ |
| LAGEOS | * |



RANGE BIAS VS DAY OF YEAR

DAY

MAY 10 - JULY 14 1985

Polyquick Development History

| | |
|---------|---|
| 1981 | Polyquick prototype |
| 1981-82 | GEODYN benchmarking, GEODYN output plots, early collocation support |
| 1983 | Normal point analysis added to identify sub-pass bias structure |
| 1983-84 | Enhanced fitting procedures, improved statistical techniques |
| 1984-85 | Aggregate data set analysis, special bias tests |
| 1986 | Expanded graphics, Collocation Analysis Package (CAP) developed paralleling GEODYN update changes |

EL ==> ELEVATION ANGLE FROM THE BASE STATION

AZ ==> AZIMUTH ANGLE FROM THE BASE STATION

RANGE ==> MEASURED RANGE FROM THE BASE STATION

X_s, Y_s, Z_s ==> THE X, Y, Z COMPONENTS OF THE SATELLITE FROM THE BASE STATION

X_t, Y_t, Z_t ==> THE X, Y, Z COMPONENTS OF THE TEST STATION FROM THE BASE STATION

$$\begin{aligned} X_s &= \text{RANGE} * \cos(\text{EL}) * \sin(\text{AZ}) \\ Y_s &= \text{RANGE} * \cos(\text{EL}) * \cos(\text{AZ}) \\ Z_s &= \text{RANGE} * \sin(\text{EL}) \end{aligned}$$

$$\begin{aligned} X_t &= \text{RANGE} * \cos(\text{EL}) * \sin(\text{AZ}) \\ Y_t &= \text{RANGE} * \cos(\text{EL}) * \cos(\text{AZ}) \\ Z_t &= \text{RANGE} * \sin(\text{EL}) \end{aligned}$$

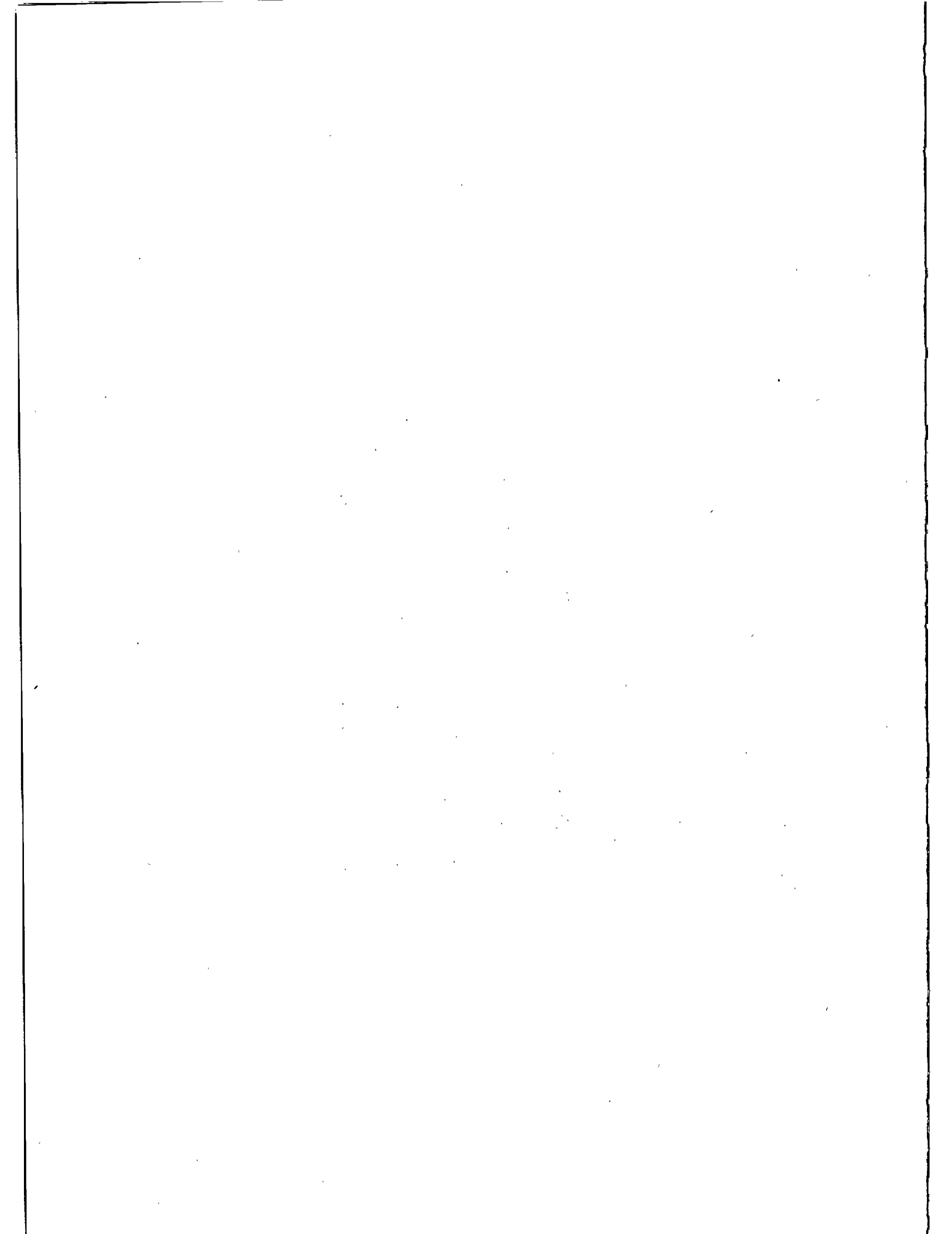
NEW RANGE =

$$\sqrt{(X_s - X_t)^2 + (Y_s - Y_t)^2 + (Z_s - Z_t)^2}$$

POLYQUICK COLLOCATION ANALYSIS SYSTEM

SUMMARY

- * ACCURATE
- * EFFICIENT
- * COMPLIMENTS ORBIT DETERMINATION TECHNIQUES
- * COMPREHENSIVE COLLOCATION ANALYSIS INFORMATION
- * MULTIPLE APPLICATIONS
- * PRIMARY TOOL FOR GLTN COLLOCATION ANALYSIS
- * SUPPORTS LASER RANGING ACCURACY IMPROVEMENTS



COLOCATION DATA ANALYSIS : DYNAMICAL APPROACH

A. Caporali
Dipartimento di Fisica Galileo Galilei
Universita di Padova
Via F. Marzolo 8
I - 35131 Padova - Italie -

Telephone (39) 49 844 278
Telex 430308 DFGGPD I

ABSTRACT

Colocation experiments of satellite laser ranging systems have proved to be much more interesting than simply a "precampaign calibration". They, in fact, permit the intrinsic precision of different ranging systems to be compared and exploited in depth. They also provide a unique source of information both to the engineer, and to the scientist.

The data analysis is the process which creates such body of information. Although virtually every group has its own technique of analysis, these can - in a broad sense - be classified within one of two different approaches : one is geometric, the other is dynamic, in the sense that a nominal ephemeris is used to filter the bulk of the curvature in the ranging data and to produce residuals.

We discuss here the basic features of the dynamic approach, in particular :

- data selection
- generation of nominal ephemeris and residuals
- criteria of editing and their impact on the results
- computation and analysis of ranging biases and calibration constants.

1. Introduction

All laser stations of the international laser tracking network differ from each other in several aspects. The characteristics of the laser oscillator, the mount, the receiving electronics, optics, timing system make each tracking station a unique instrument. And even in those cases, like the German and Dutch stations MTLRS1 and MTLRS2, where the stations are nominally identical, different procedures for calibration and satellite tracking can produce non negligible effects in the measurements.

Because any of these differences can map into systematic errors in the baseline, it is crucial for a successful campaign to dedicate sufficient time for an exhaustive calibration experiment.

This need has been recognized by NASA and the European Organizations participating in the WEGENER Consortium. In the past, colocation experiments have been done both in the United States and Europe.

From April to May, 1984 the German mobile system MTLRS1 was colocated at the Kootwijk Observatory with the fixed laser KOOLAS (Van Gelder and Blumer, 1985, Noomen, Ambrosius and Wakker, 1985). In November 1984 MTLRS1 was colocated at Wettzell with the fixed installation (Hauck and Lelgemann, 1985). In March and April 1985 MTLRS1 and 2 joined in Wettzell for a three-system colocation experiment (Hauck, van Gelder et al., 1985).

From May to July 1985 the NASA station MOB LAS7 and the German station MTLRS1 were colocated at Greenbelt, Maryland, with the objective to intercompare tracking technology and techniques of data analysis, and to transfer the Crustal Dynamics Project Laser standard to Europe (Kolenkiewicz, 1986). The data from this experiment have been analyzed by three groups, NASA, Bendix and IFAG, and their findings extensively documented (Husson 1986; Hessels et al. 1985, Kolenkiewicz et al. 1985, Hauck, Herzberger et al. 1985).

Finally, at the beginning of the Wegener MEDLAS 1986 Campaign, MTLRS1 and MTLRS2 were extensively colocated at Matera, before leaving for remote sites in the East Mediterranean Region. Table 1 summarizes these experiments and permits to appreciate how this type of experiment has evolved. A more complete list of colocation experiments is given by Pearlman (1986).

2. Dynamical Approach to the Analysis of Colocation Experiments.

2.1 Range bias, time bias and calibration constant.

It is common practice to call "range bias" and "time bias" the mean translations in space and time respectively by which the actual observed path of data differs from the path computed using a nominal ephemeris. These biases are computed by fitting the residuals r relative to predictions to a curve

$$\Delta r(t) = r_b + \dot{r}(t) t_b$$

where r_b and t_b are the range and time biases, and \dot{r} is the range rate. The time and range biases quantify how "early or late", or "off" an ephemeris is in predicting a pass over a station, and should not be confused with system biases of the ranging equipment, for which we reserve the word of "calibration constants".

If two stations are colocated, relative timing and position errors are negligible and one might expect that an ephemeris is range-and time-biased for the same amount relative to each station. This is not exactly true, as it can be seen with the following example. Given two colocated stations, compute for all passes, common and not, the range bias and time bias. Now select the range bias and time bias relative to the common passes, and note that these biases have been computed - for a given pass - using time intervals which, in general, do not exactly overlap.

Because the ephemeris is not "tailored" on a specific pass, the least squares estimated values of the range and time biases will depend on the tracked portion of the pass. Consequently, it is reasonable to expect that if two stations do not track the same portion of the pass, different estimates of range bias and time bias may result.

Only if the ephemeris happens to fit a pass with random residuals (as for multi-single pass methods, see next section) then the time bias is zero and the range bias is constant and independent of overlap.

Figures 1 and 2 have been obtained with a non tailored ephemeris for the Matera experiment (full rate data). They give the differences in range bias and time bias as a function of overlap time. They indicate that the longer the overlap, the higher is the probability that the relative range bias and time bias approaches zero.

Note that differences of several centimeters exist even for maximum overlap (45 min.). This is due to the use of unevenly spaced, full rate data, with noise of variable frequency added by the numerical differentiation of ranges to produce range-rates.

Our conclusion is that pass comparison should be safely limited to the simultaneous portion, unless one is very confident on the randomness of the residuals produced by the adopted ephemeris.

2.2 Dynamical Computations of the Calibration Constant.

The methods of analysis so far used differ in two important aspects: one is the criteria for data selection, the other is the computational technique. The Matera experiment shows an unprecedented variety of options (tab. 2). There is clearly considerable space for subjective decisions which may have non negligible impact on the final results.

The computational methods are summarized in tab. 3. They imply that there exist two basic methods of computing the relative calibration constant between two ranging systems: one is to consider the range bias as a "solve for" parameter in a multi-single pass" (see below) least squares adjustment. The other is to define the calibration constant as a mean difference - for each pass - between pairs of residuals referred to a same smooth curve (ephemeris, polynomial or both).

Concerning the first method we note, with reference to tab. 2, that by multi-single pass method it is meant a least squares fit to data of a single pass, done simultaneously for several passes. The "solve for" parameters consist of a subset of the orbital parameters chosen so that the resulting normal equations are non degenerate, and perhaps a range and time bias for each station, to accomodate for model unaccuracies. The difference in range bias is interpreted as an estimate of the calibration constant for the pass, provided the post-fit residuals are random.

Concerning the second method, the subtraction of a best fitting, smooth curve from the residuals to the predicted ephemeris removes the effect of the predicted ephemeris being not tailored on the actual data. In the Telespazio approach, the polynomial fit is done three times: first with station A residuals, and station B residuals downweighted; second, with the roles of A and B interchanged; third, residuals of A and B fitted altogether to a polynomial. The pair of time series

of residuals resulting from each fit is plotted together. The "full rate residuals" are replaced by means at common epochs, for sake of easier comparison. The three means of the polynomial residuals are finally averaged to produce, for the given pass, the estimated calibration constant.

Again the all procedure should produce random time series. It some time happens that this is not the case, due to real relative random walks of one system relative to the other, or to numerical unstabilities of the filtering procedures. Having different types of approaches available should permit to separate numerical unstabilities from system unstabilities.

Fig. 3 gives an example of residual plots obtained for the same pass by IFAG and Telespazio, during the Matera Colocation Experiment. IFAG used a "multi-single arc technique" and estimated by least squares the range bias of the ephemeris relative to each station simultaneously with an along track, radial, inclination and node correction. Telespazio instead subtracted from the orbital residuals a best fitting polynomial and computed the mean of the post-fit residual differences.

The agreement between the two methods is evident. The largest difference between the calibration constants is 1.4 cm (MATLAS-MTLRS2) and is most probably due to different criteria for data selection and editing, rather than to the computational technique.

2.3 Data Selection

The number of data present in a data set varies considerably from station to station and, for a given station, from pass to pass. Aggregating data into normal points permits a more uniform data distribution. The aggregation process is non trivial, especially if the data rate is low (e.g. Quick Look normal points, or normal points from second generation stations). A normal point made of 10 data differs from one of 11 data by 1.5 cm if the additional data point is off, relative to the mean of the other ten data points, by 15 cm (the typical noise level r.m.s. of a second generation station).

An alternate option successfully tested at Telespazio during the Matera experiment was to sample the data 1 point every 5 seconds and compare the results obtained with the full-rate data. Table 4 summarizes the results of this test.

It is interesting to note the effect of different criteria of editing of outliers: whenever MATLAS data are

used, the 3σ editing criterion in place of 2.5σ produces a shift of the calibration constant of 5mm in the negative direction.

This implies the existence of non random data aggregations, but fortunately the effect is small, especially if compared with the nominal noise level of this station.

3. Conclusion

To evaluate systematic differences between two collocated laser systems, all proposed methods of analysis are probably equally viable. It is very likely that different results, when they occur, are due to different criteria for data selection more than the computational approach itself.

Software benchmarking has proven to be a very valuable tool of comparison of procedures (A. Cenci, 1986). To separate the issue of editing from that of computational technique, a simulated data set could be generated for two collocated stations with known-but not to the analysts-relative calibration constants. No data point can be edited out. Then, the same range bias ought to be recovered by all methods of analysis. A successful benchmarking of this type between a GEODYN based algorithm and a kinematic algorithm based on POLIQUICK (Edge, 1986) has been reported by Kolenkiewickz (1986). Hopefully the same experiment is repeated for the remaining algorithms.

Whether or not this experiment is done, the evidence so far is that collocation periods of several months are very advisable, if the body of data is to be sufficiently complete.

Acknowledgment. I thank Alberto Cenci for several discussion on a first draft of the manuscript.
This work is supported by Piano Spaziale Nazionale, Consiglio Nazionale delle Ricerche.

References

- Cenci, A.: Management of the Laser Ranging Systems Colocation. Proc. of the 6th. International Workshop on Laser Ranging Instrumentation, Antibes, Sept. 22-26 1986 (this volume).
- Edge, D. : this volume.
- Hauck, H., Herzberger and P. Wilson: The Results of the Colocation Experiment MOBLAS7 - MTLRS1. IFAG Intern. Report, 1985.
- Hauck, H., van Gelder B.H.W., van Loon, D.L.F., Vermaat, E. and Blumer, B.M.H.: Co-locating MTLRS1 and MTLRS2 with the stationary Wettzell Laser Ranging System. AGU Spring Meeting, Baltimore Md: May 27-31 1985.
- Hauck, H. and Lelgemann, D.: A Comparison between MTLRS1 and the Stationary Laser System in Wettzell. Crustal Dynamics Working Meeting , NASA GSFC March 19-20 1985
- Hessel, U., Junginger, H., Etling, W., Nowak, I. : Stabilität und Winkelabhängigkeit der Kalibrations Konstante bei MTLRS1. IFAG Intern. Report, 1985.
- Husson, V.S.: MTLRS1 and MOBLAS7 Colocation Report. Bendix Field Engineering Corporation, 1986.
- Kolenkiewickz, R., Husson V.S., Dunn P.J. , Martin C.F., Poullose, S., Abresh, M.: Recent Lageos Satellite Laser Ranging Colocation Analysis. AGU Fall Meeting Dec. 12 1985, S. Francisco, Ca.
- Kolenkiewickz, R.: The MTLRS1 and MOBLAS7 Colocation. Crustal Dynamics Principal Investigator Meeting. Jet Propulsion Laboratory, March 26 1986.
- Kolenkiewickz, R.: this volume.
- Noonen, R., Ambrosius, B.A.C. and Wakker, K.F.: Results of a Colocation Experiment Between MTLRS1 and the fixed Kootwijk Laser,. Crustal Dynamics Working Meeting, NASA GSFC March 19-20 1985.
- Pearlman, M.: this volume.
- Van Gelder, B.H.W. and Blumer, B.M.H.: Co-location of KOOLAS and MTLRS1 at the Kootwijk Observatory using raw laser range data to LAGEOS. Crustal Dynamics Working Meeting, NASA GSFC March 19-20 1985.

| | Kootwijk | Wetzell | Wetzell | Gorf | Matera |
|------------------------------|--------------------------------------|--------------|--|-----------------------------------|--|
| OD | April-May '84 | November '84 | March '85 | May-July '85 | Jan-March '86 |
| TEM | M1,K | M1,W | M1,M2,W | M1,M7 | M0, M1, M2 |
| SIMULTANEOUS MEASUREMENTS | 8 | 4 | 3 M1, M2, W | 32 | 11 M0, M1, M2 |
| | | | 5 M1, W | | 24 M0, M1, |
| | | | 3 M2, W | | 39 M0, M2 |
| | | | 4 M1, M2 | | 14 M1, M2 |
| CK LOOK ALIGNMENT POINTS | X | X | X | X | (see tab.2) |
| BIAS(mm) | M1-K<-100 DUT/A M1-K:-35(+) DUT/G | M1-W 260 | M1-M2 -6 -13 W-M1/2 -1 -58 M1-M2 +15 on target | M1-M7: -5 -20 (BFEC) -3 (IFAG) | (see tab.2) |
| ANALYSIS GROUP | DUT/A DUT/G | IFAG | DUT/G IFAG | BFEC NASA GSFC IFAG | TPZ-UP IFAG UT-CSR NASA-GSFC BFEC, DUT/G |

e: M1= MTLRS1; M2=MTLRS2; K=KOOTLAS; W=WETLAS; M7=MOBLAS7; M0=MATLAS
after relative height adjustment

Table 1 Some Recent Colocation Experiments Involving European Laser Systems

| DATA SOURCE | ORBITAL FILTER RESIDUALS GENERATIONS | DATA EDITING | NORMAL POINTS | ACCEPTANCE CRITERIA | RESULTS (mm) | |
|-------------|---|--|---|----------------------------|---|--|
| UP | MO Full Rate MI, M2 QL, Full Rate | Long arc adjust- ment; polynomial fit to GEODYN residuals | tailored 2.5 and 3 sigma/single pass | 5 min. Normal residuals | Simultaneous tracking of common pass (5 min. minimum) | MO-M1 -5 MO-M2 -10 MI-M2 -5 |
| | | Multi-single pass adjustment | 3 sigma/single pass | 2 min. | Common pass | MO-M1 -7±20 MO-M2 +7±41 MO-M2 +8±10 |
| | | Single pass Polyn. with geom. correc- tions | 3 sigma/single pass | 2 min. | Simultaneous tracking of common pass | MO-M1 -38±19 MO-M2 -21±17 M1-M2 -4± 9 |
| G | | Multi-single pass adjustment | 3.5 sigma/single pass | | Common pass | MO-M1 -18±23 MO-M2 0±31 M1-M2 -20±20 |
| | | Multi-single arc adjustment | 2.7 sigma/global | 1 min. | Normal points at common epoch | MO-M1 -9± 70 MO-M2 -11±74 M1-M2 -14±33 |
| SR | | Multi-single pass adjustment polyn. fit | 3.5 sigma/single pass | 2 min. | Simultaneous tracking of common pass | MO-M1 MO-M2 TBD M1-M2 |

Figure 2: geometric and dynamic approaches to the analysis of the Matera Colocation data.

- Multi single pass techniques:

* Pass-by-pass least square estimate of a subset of orbital parameters and, for each station, of a range bias and time bias.

* Calibration constant of the pass defined as difference of range biases for that pass.

- Long arc and polynomial fit:

* "Coarse" filtering of the orbit using long arc techniques:

* Pass-by-pass "fine tuning" of long arc residuals using polynomial techniques

* Calibration constant for the pass as mean of residual differences after polynomial fit.

- Multi-arc technique:

* Ephemeris generated using normal points from global network

* Orbital residuals of normal points of colocated stations at the same epoch are differenced

* Calibration constant computed as mean of simultaneous residuals.

Table 3: Methods of computation of the calibration constant.

TELESPAZIO-University of Padova Analysis of Matera Colocation Data

STATISTICS OF RESIDUAL DIFFERENCES (cm)

DATA SET: Full rate data from Bendix MT2MAT8

| | N. of passes | FULL RATE DATA | | 1/5 SEC. SAMPLING | |
|-----------------|-----------------|-------------------|-----------------|-------------------|-----------------|
| | | 2.5 σ EDIT | 3 σ EDIT | 2.5 σ EDIT | 3 σ EDIT |
| MATLAS - MTLRSI | 17 | -0.1 \pm 2.5 | 0.3 \pm 2.7 | -0.6 \pm 2.4 | -0.3 \pm 2.8 |
| MATLAS - MTLRS2 | 36 | 0.0 \pm 1.9 | 0.5 \pm 2.0 | -0.4 \pm 2.3 | 0.2 \pm 2.3 |
| MTLRSI - MTLRS2 | 13 | -0.3 \pm 1.4 | -0.3 \pm 1.6 | 0.0 \pm 1.6 | 0.3 \pm 1.6 |

Note: Only passes with more than 5 min overlapping time and more than 30 observations are considered.

Passes on Jan. 16 01:51 and Jan. 24 23:51 are not used in MATLAS-MTLRS2 final average

Numbers after indicate the passby pass rms of the differences and are not divided by the square root of the number of passes.

Table 4: effect of different criteria of editing on final results.

Delta T-Bias vs. overlap (usec)

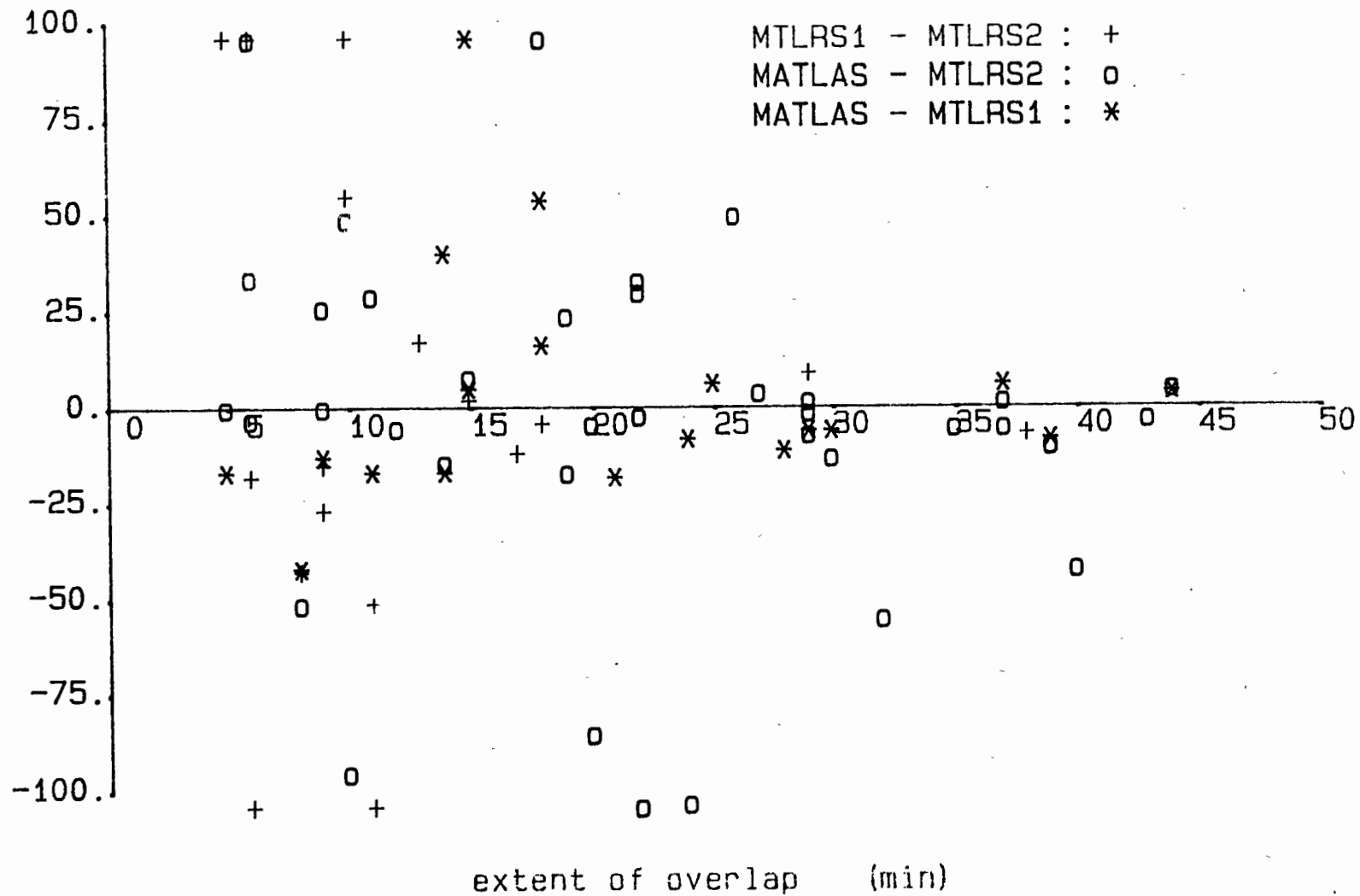


Fig. I: differences of time biases of common passes computed relative to the same reference ephemeris, as a function of interval of simultaneous tracking.

Delta R-Bias vs. overlap (mm.)

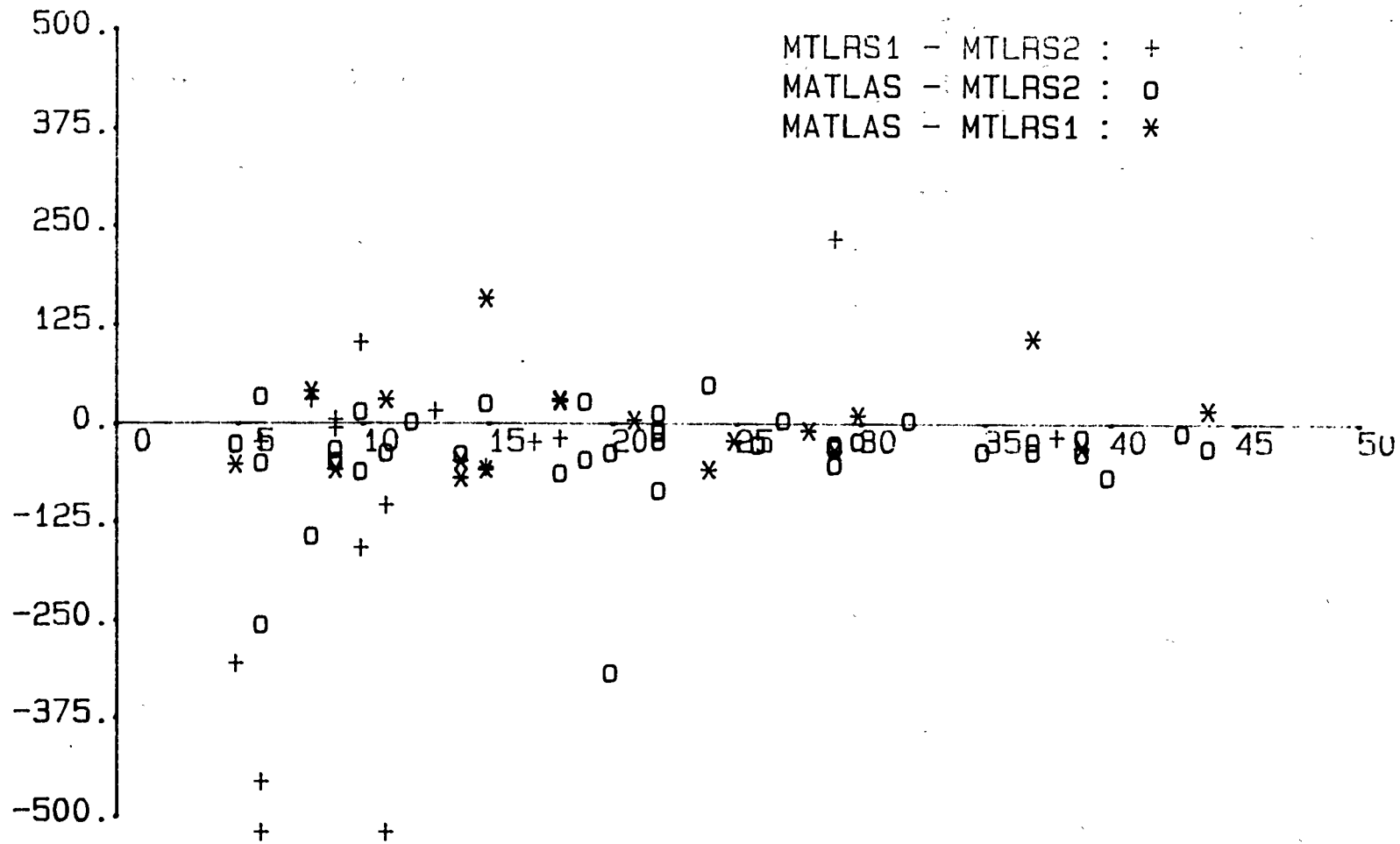


Figure 2: same as fig. I, for the range bias differences.

***** PLOT DER VERDESSUNGEN *****

EPOCHE ANFANG: 8601483842 ENDE: 8621500154
2.2.72

SCALE = 7.198 METER.
INTERVALL = 0.204 METER.

orbit residuals
of pass 8601483842
after adjusting the
orbit

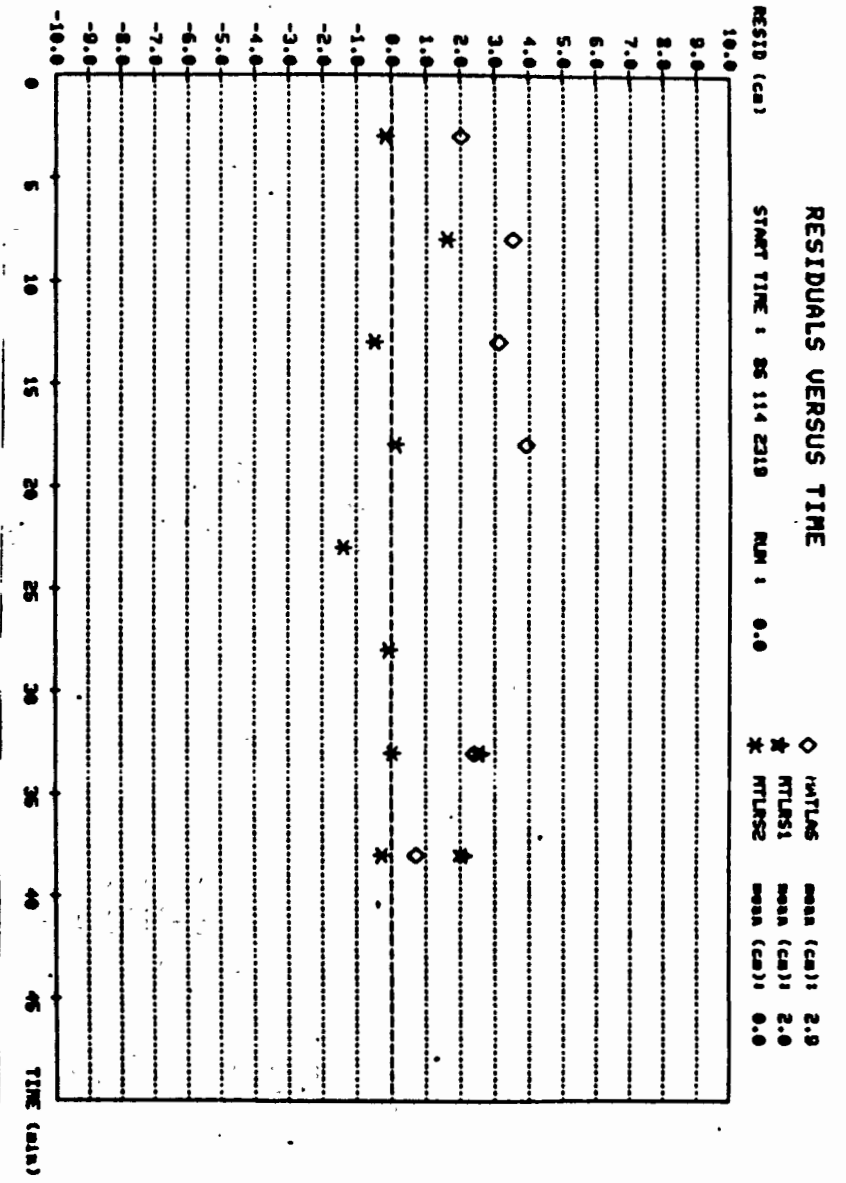
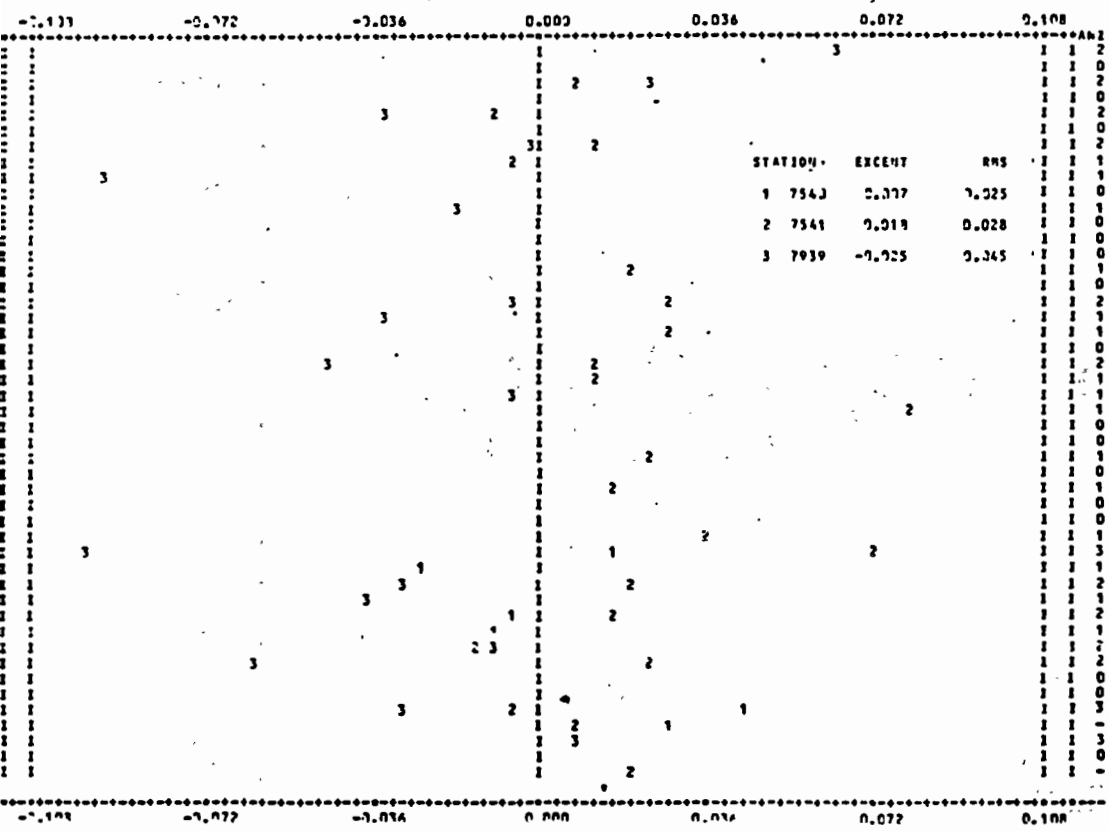


FIG.3 · Same pass analyzed by Telespazio and IFAG

GEODYN COLLOCATION ANALYSIS AND ITS COMPARISON
WITH POLYQUICK

R. Kolenkiewicz
Nasa Goddard Space Flight Center
Greenbelt, Maryland 20771 - USA -

Telephone (301) 286 5373
TWX 710828 9716

Van S. Husson
Bendix Field Engineering Corp.
Columbia, Maryland

Ch. Martin
EG&G Washington Analytical Services Center Inc.
Lanham, Maryland

S. Poulouse, M. Abresch, K. Doyle
RMS Technologies Inc.
Landover, Maryland

ABSTRACT

GEODYN is a precision orbit determination program used by NASA at Goddard Space Flight Center (GSFC) for analysis of data collected from lasers ranging to the LAGEOS satellite. This program is also used as a means of comparing satellite laser ranging systems. This process, known as collocation analysis, consists of placing two satellite laser ranging systems side by side, at a known orientation to each other, tracking the same target satellite, and comparing the range data obtained. As an aid in the analysis of these data, additional software has been developed by NASA. This software uses the GEODYN produced laser range residuals as input. An additional program developed for NASA by the Bendix Field Engineering Corporation is called POLYQUICK. This program performs collocation analysis by fitting polynomials to satellite laser ranging data. In addition to using the ranging data, POLYQUICK must also use the angular (azimuth and elevation) data obtained from one of the laser systems being compared. The advantage of the POLYQUICK over the GEODYN approach is that the analysis is independent of orbit integration and hence can be performed more rapidly. This disadvantage is that the lasers being compared must be in close proximity of each other (approximately 50 m) in order to produce accurate results. To assess the collocation software and analysis approaches, both collocation programs were utilized at GSFC for a collocation between the MTLRS-1 laser from the Federal Republic of Germany and the MOBLAS-7 laser belonging to NASA. For a typical collocation pass (6/27/85 at 04:00 hr.) containing 15 two minute overlap normal points between MTLRS-1 and MOBLAS-7, the maximum difference between GEODYN and POLYQUICK is 0.4 cm with an rms of the 15 points of 0.16 cm. For the entire pass GEODYN indicates MOBLAS-7 is measuring long relative to MTLRS-1 by 1.47 cm, and POLYQUICK indicates 1.58 cm. For a group of 13 LAGEOS passes tracked during the summer of 1985 the rms difference in pass results obtained by GEODYN and POLYQUICK amounted to 0.15 cm. Details of the GEODYN collocation analysis program and its comparison with the POLYQUICK results will be described.

INTRODUCTION

An objective of the NASA Crustal Dynamics Program is to obtain Satellite Laser Ranging (SLR) data from the Laser Geodynamics Satellite (LAGEOS). In order to achieve this goal new laser systems must be developed and compared to each other. This process of comparison is called collocation. As an aid in the analysis of these data, new computer software has been developed by NASA. This software uses laser range residuals produced by GEODYN, the precision orbit determination computer program used by NASA at GSFC. A second piece of software, called POLYQUICK, designed to do a similar task was created for NASA by the Bendix Field Engineering Corporation. Each of these programs has its place in the analysis of laser collocation data as will be described in this paper. The purpose of this paper is to compare the GEODYN analysis with the POLYQUICK analysis during a collocation.

GEODYN ANALYSIS

In order to assess the collocation software and analysis of GEODYN and POLYQUICK, both programs were used to reduce data from a recent collocation held at GSFC. The collocation selected was for the MTLRS-1 laser from the Federal Republic of Germany and the MOBLAS-7 laser belonging to NASA. This collocation was held between May and July of 1985. A typical collocation pass (6/27/85 at 04:00 hr. GMT) will be looked at in detail in order to describe the GEODYN analysis. A precision GEODYN orbit, approximately 50 minutes in duration, was fit solely through the MOBLAS-7 data with the MTLRS-1 data weighted out (not contributing) to the solution. Figure 1 shows the range residuals as a function of time for the MOBLAS-7 laser for the converged orbit. Since MOBLAS-7 is a 2.5 cm. rms system, and a three sigma editing criterion will be used, only residuals within 7.5 cm. of the orbit are used in the analysis. This amounts to using 9553 of the total 11063 points taken during this pass. Figure 2 is similar plot for the MTLRS-1 range residuals. MTLRS-1 is a 5.5 cm. rms system and a three sigma editing (16.5 cm.) is used. Therefore 3236 of the total 4423 MTLRS-1 points are retained for the analysis. The elapsed time zero in Figures 1 and 2 corresponds to 04:00 hours GMT on June 27, 1985. Beginning with this epoch time, two minute time intervals (or bins) are selected during the orbit. For each time interval the number of range residuals, the mean, the rms (sigma), and the standard deviation of the mean (sigma divided by the number of points) are computed and given the time tag for the center of the bin (the odd minute). Results for the MOBLAS-7 residuals are given in the first 5 columns of Table 1. Corresponding results for the MTLRS-1 residuals are given in columns 6 through 9. The number of points necessary in a two minute bin for each of the lasers is an option that can be set by the analyst. In this case a two minute mean point would not be considered as a part of the analysis unless it consisted of at least 300 residuals from MOBLAS-7 and 30 residuals from MTLRS-1 (indicated by an asterisk in Table 1). Differences of the means MTLRS-1 minus MOBLAS-7 (columns 7 minus 3) are given in column 10. The standard deviation of these differences is given in column 11.

For example the fifth row in Table 1 indicates an elapsed time of 9.00 minutes (04:09 hr. GMT) which corresponds to the middle of the two minute bin beginning at 04:08 and ending at 04:10 hr. GMT. There were 489 laser range residuals within ± 7.5 cm. of the computed orbit during this time period. The mean of these residuals is 0.16 cm. with an rms of 1.97 cm. which when divided by the square root of the number of points yields a standard deviation of this mean of 0.09 cm. Correspondingly there were 136 points for MTLRS-1 within ± 16.5 cm. of the orbit having a mean of -0.50 cm., an rms of 5.84 cm. and a standard deviation of 0.50 cm. The difference of the means MTLRS-1 minus MOBLAS-7 is -0.66 cm. with a standard deviation of the difference of 0.51 cm.

Figure 3 is a plot of the two minute values with associated one sigma error bars for MOBLAS-7 and MTLRS-1. These are the points in Table 1 columns 3 and 5 for MOBLAS-7 and columns 7 and 9 for MTLRS-1 which are to be considered in the solution. Note that there are 15 pairs of points sharing the same two minute bin which can be differenced.

Figure 4 is a plot of the two minute mean range differences between MTLRS-1 and MOB LAS-7. These are columns 10 and 11 of Table 1. For this set of points the weighted mean (\bar{X}), the weighted standard deviation of the mean (β) and the weighted standard deviation about the mean (ϕ), as defined below, are calculated in Table 1 and shown on Figure 4.

For a population, x_i , with uncertainties, σ_i , the weighted mean is defined as

$$\bar{X} = \frac{\sum_{i=1}^n w_i x_i}{\sum_{i=1}^n w_i}$$

where

$$w_i = \frac{1}{\sigma_i^2}$$

The weighted standard deviation of the mean, β , is given by:

$$\beta = \left[\frac{1}{\sum_{i=1}^n w_i} \right]^{\frac{1}{2}}$$

and the weighted standard deviation about the mean (absolute variance) ϕ , is:

$$\phi = \left[\frac{\sum_{i=1}^n w_i x_i^2}{\sum_{i=1}^n w_i} - \bar{X}^2 \right]^{\frac{1}{2}}$$

Figure 4 indicates the ultimate goal of the GEODYN collocation analysis for two laser systems. It indicates how well the lasers are measuring the range to the satellite and indicates the systematic trends during the pass. The results indicate that the weighted mean difference between MTLRS-1 and MOB LAS-7 is -1.47 cm. or that for this pass the MTLRS-1 is measuring short by 1.47 cm. relative to the MOB LAS-7 measurement. In addition to this bias there are systematic jumps of 1 to 2 centimeters during the measurement period. An indication of this scatter is the relatively large value of 0.84 cm. for the standard deviation about the mean. Systematic differences of this nature must be understood and corrected in order for laser systems to achieve the current goal of less than a centimeter.

GEODYN AND POLYQUICK COMPARISON

The POLYQUICK computer program (*Husson and Edge*, this issue) was used to analyze the same collocation data (6/27/85 at 04:00 hr. GMT) previously analyzed by GEODYN. Rather than using a precision orbit as its basis, POLYQUICK uses the data in the form of laser range residuals and azimuth and elevation angles together with polynomials to compare the MOBLAS-7 and MTLRS-1 laser systems. Basically this consists of transforming the laser range results from one of the collocation lasers to the second, fitting polynomials to both data sets, and taking a difference. In the POLYQUICK analysis an effort was made to use similar parameters to those used in the GEODYN analysis. This consisted of the bin size, number of points selected for each laser in the bin and common statistics. Figure 5 shows the comparison between GEODYN and POLYQUICK for the test case. The top plot is for the 15 point difference between MTLRS-1 minus MOBLAS-7 with the GEODYN results, except for the error bars repeated, and the POLYQUICK results shown for comparison. The greatest difference between any of the 15 points shown is 0.4 cm. The bottom plot is the difference (POLYQUICK minus GEODYN) where the rms difference for this pass of data is 0.16 cm. GEODYN and POLYQUICK are also in good agreement as far as the weighted mean differences for the entire pass are concerned. Where the GEODYN analysis predicts MTLRS-1 is measuring short by 1.47 cm. relative to MOBLAS-7, the POLYQUICK analysis predicts a value of 1.58 cm., or a difference of 0.11 cm. This result is just one of 13 LAGEOS passes analyzed by GEODYN and POLYQUICK during the MOBLAS-7 and MTLRS-1 collocation. The remaining results are given in Table 2. In Table 2 the date of the pass, the time of the pass, and the weighted mean difference (MTLRS-1 minus MOBLAS-7) for GEODYN and POLYQUICK as well as their differences are tabulated. The largest difference between GEODYN and POLYQUICK for a given collocation pass is 0.28 cm. and the rms difference for the 13 collocated passes is 0.15 cm. As far as the collocation between MOBLAS-7 and MTLRS-1 is concerned MTLRS-1 is measuring short relative to MOBLAS-7 by 1.80 cm. (GEODYN) or 1.76 cm. (POLYQUICK).

SUMMARY

GEODYN and POLYQUICK analyses are currently being used by NASA at GSFC for collocation analysis of satellite laser ranging systems. GEODYN uses precision orbit determination and POLYQUICK uses polynomial fits to obtain laser range residuals, from two laser systems, which can then be differenced in order to compare the ability of the systems to measure the same range distance. GEODYN requires more computer time than POLYQUICK to obtain the final result, in all other respects GEODYN is the superior method for collocation analysis. In the GEODYN analysis only ranges are required whereas POLYQUICK requires azimuth and elevation angles for its analysis. As the laser systems' accuracy increases, the polynomial approach may prove unable to achieve the precise measurements required for collocation. In addition the accuracy of the POLYQUICK results deteriorates as the distance between the collocated lasers increases, with studies indicating distances in excess of 50 meters to be prohibitive. GEODYN has the ability to dynamically solve for a relative station position (navigate) from a group of collocation passes and thus discover survey errors; this is more cumbersome to accomplish with POLYQUICK. For the current laser ranging systems undergoing collocation, the above analysis indicates that either the GEODYN or POLYQUICK approach yields comparable results. POLYQUICK should be used in conjunction with other engineering analysis on a real time basis to insure rapid turn around of the data in order to correct problems in a more timely manner.

REFERENCES

Husson, V. S., and D. R. Edge, POLYQUICK collation analysis, Sixth International Workshop on Laser Ranging Instrumentation, Antibes, France, Sept. 1986, this issue.

MOBLAS-7
LAGEOS
6/27/85 04:00

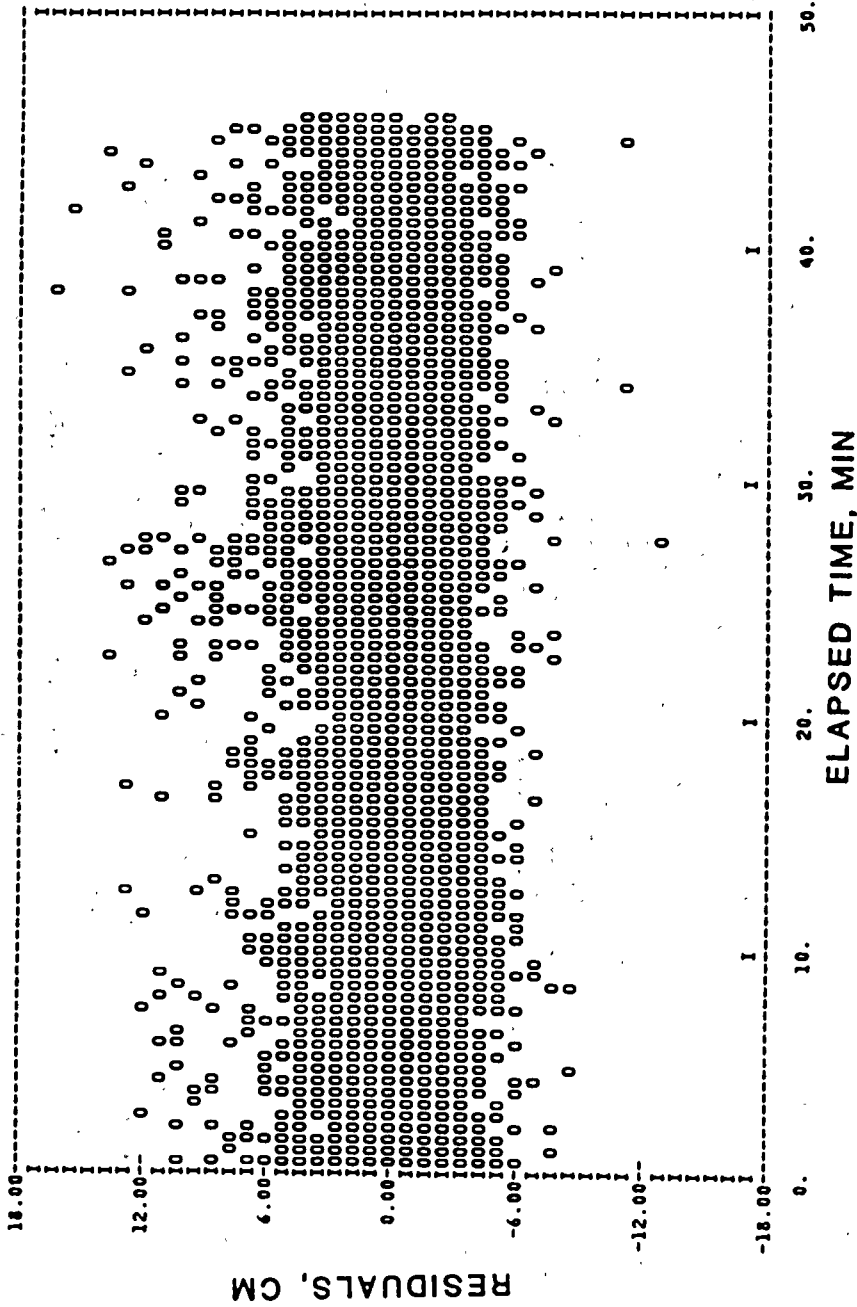


FIGURE 1 MOBLAS-7 range residuals as a function of time.

MTLRS-1
LAGEOS
6/27/86 04:00

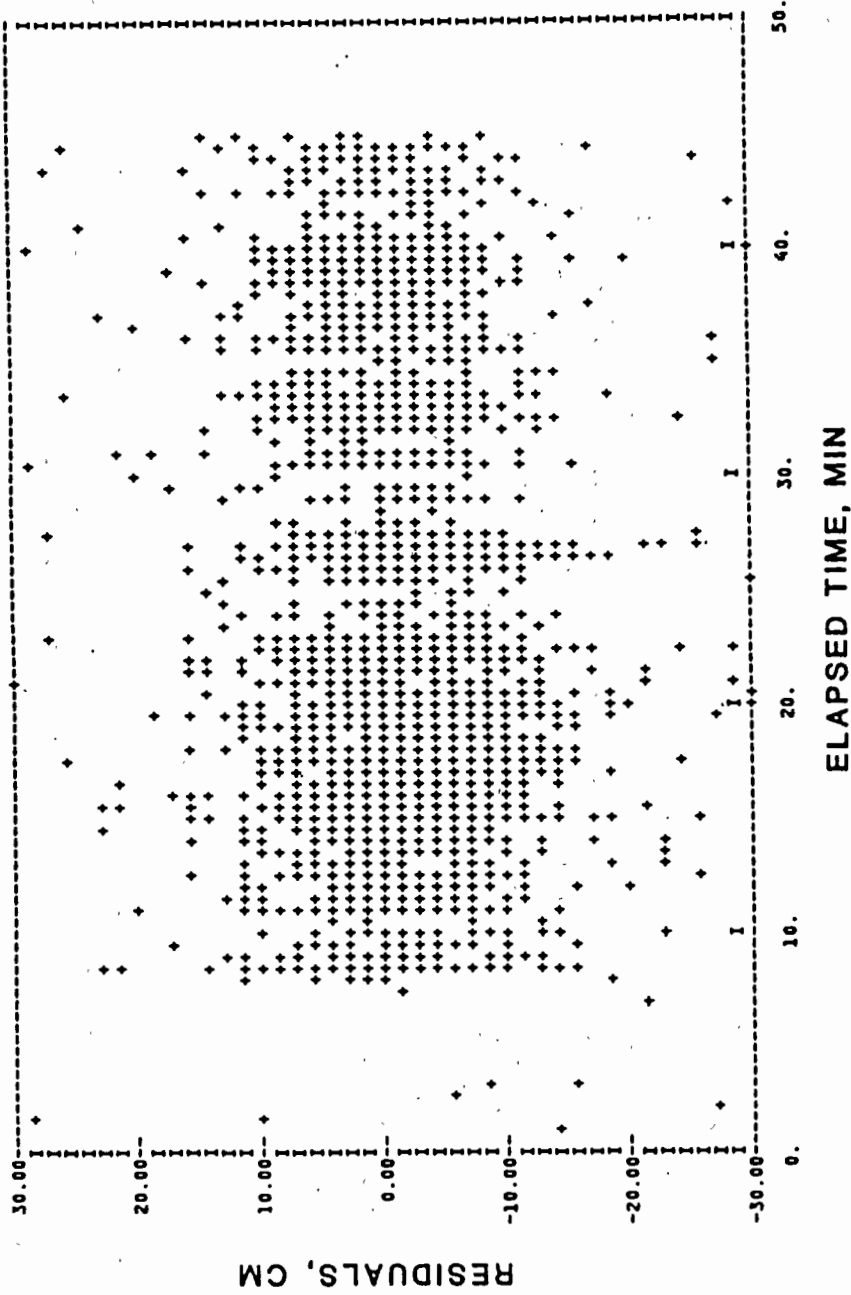


FIGURE 2 MTLRS-1 range residuals as a function of time.

LAGEOS 6/27/85 04:00

MOBLAS-7

MTLRS-1

MTLRS-1
MINUS
MOBLAS-7

| ELAPSED TIME | NO. OF POINTS | MEAN CM | SIGMA | STD. DEV. OF MEAN | NO. OF POINTS | MEAN CM | SIGMA | STD. DEV. OF MEAN | DIFF OF THE MEANS | STD. DEV. OF DIFF. |
|--------------|---------------|---------|-------|-------------------|---------------|---------|-------|-------------------|-------------------|--------------------|
| 1.00 | 258 * | -0.10* | 2.32* | 0.14* | 0 * | 0.00* | 0.00* | 0.00* | 0.00* | 0.14* |
| 3.00 | 382 | -0.11 | 2.24 | 0.11 | 0 * | 0.00* | 0.00* | 0.00* | 0.00* | 0.11* |
| 5.00 | 427 | 0.13 | 2.15 | 0.10 | 0 * | 0.00* | 0.00* | 0.00* | 0.00* | 0.10* |
| 7.00 | 502 | 0.14 | 2.00 | 0.09 | 7 * | 3.06* | 3.88* | 1.47* | 0.00* | 1.47* |
| 9.00 | 489 | 0.16 | 1.97 | 0.09 | 136 | -0.50 | 5.84 | 0.50 | -0.66 | 0.51 |
| 11.00 | 492 | 0.01 | 2.01 | 0.09 | 110 | -0.55 | 5.95 | 0.57 | -0.56 | 0.57 |
| 13.00 | 505 | -0.07 | 1.84 | 0.08 | 159 | -0.90 | 5.73 | 0.45 | -0.83 | 0.46 |
| 15.00 | 482 | -0.06 | 1.76 | 0.08 | 318 | -0.97 | 5.41 | 0.30 | -0.92 | 0.31 |
| 17.00 | 469 | 0.11 | 2.03 | 0.09 | 378 | -2.51 | 5.09 | 0.26 | -2.63 | 0.28 |
| 19.00 | 484 | -0.02 | 1.80 | 0.08 | 436 | -2.48 | 5.57 | 0.27 | -2.47 | 0.28 |
| 21.00 | 462 | -0.06 | 2.04 | 0.09 | 244 | -2.47 | 5.36 | 0.34 | -2.41 | 0.36 |
| 23.00 | 463 | -0.09 | 1.95 | 0.09 | 182 | -1.68 | 5.34 | 0.40 | -1.59 | 0.41 |
| 25.00 | 268 * | 0.26* | 2.26* | 0.14* | 91 | 0.04 | 5.32 | 0.56 | 0.00* | 0.57* |
| 27.00 | 205 * | 0.57* | 2.72* | 0.19* | 239 | -2.49 | 5.28 | 0.34 | 0.00* | 0.39* |
| 29.00 | 485 | -0.18 | 2.19 | 0.10 | 34 | -0.81 | 5.33 | 0.91 | -0.63 | 0.92 |
| 31.00 | 511 | -0.11 | 1.91 | 0.08 | 116 | -0.68 | 5.32 | 0.49 | -0.57 | 0.50 |
| 33.00 | 500 | 0.08 | 1.94 | 0.09 | 207 | -0.41 | 5.13 | 0.36 | -0.48 | 0.37 |
| 35.00 | 501 | 0.19 | 1.91 | 0.09 | 98 | -0.85 | 5.67 | 0.57 | -1.04 | 0.58 |
| 37.00 | 424 | 0.28 | 2.29 | 0.11 | 128 | -0.88 | 4.47 | 0.40 | -1.16 | 0.41 |
| 39.00 | 468 | 0.10 | 2.09 | 0.10 | 170 | -0.66 | 4.96 | 0.38 | -0.76 | 0.39 |
| 41.00 | 341 | -0.30 | 2.25 | 0.12 | 48 | -0.75 | 5.77 | 0.83 | -0.45 | 0.84 |
| 43.00 | 274 * | 0.11* | 2.55* | 0.15* | 90 | 0.13 | 5.29 | 0.56 | 0.00* | 0.58* |
| 45.00 | 161 * | 0.10* | 2.59* | 0.20* | 45 | 0.56 | 6.08 | 0.91 | 0.00* | 0.93* |

MTD. MEAN = -1.47
STD OF MEAN = 0.10
STD ABOUT MEAN = 0.84

NO. OF ITERATIONS = 4

TABLE 1 Two minute interval analysis of residuals.

LAGEOS 6/27/85 04:00

ONE SIGMA ERROR BARS

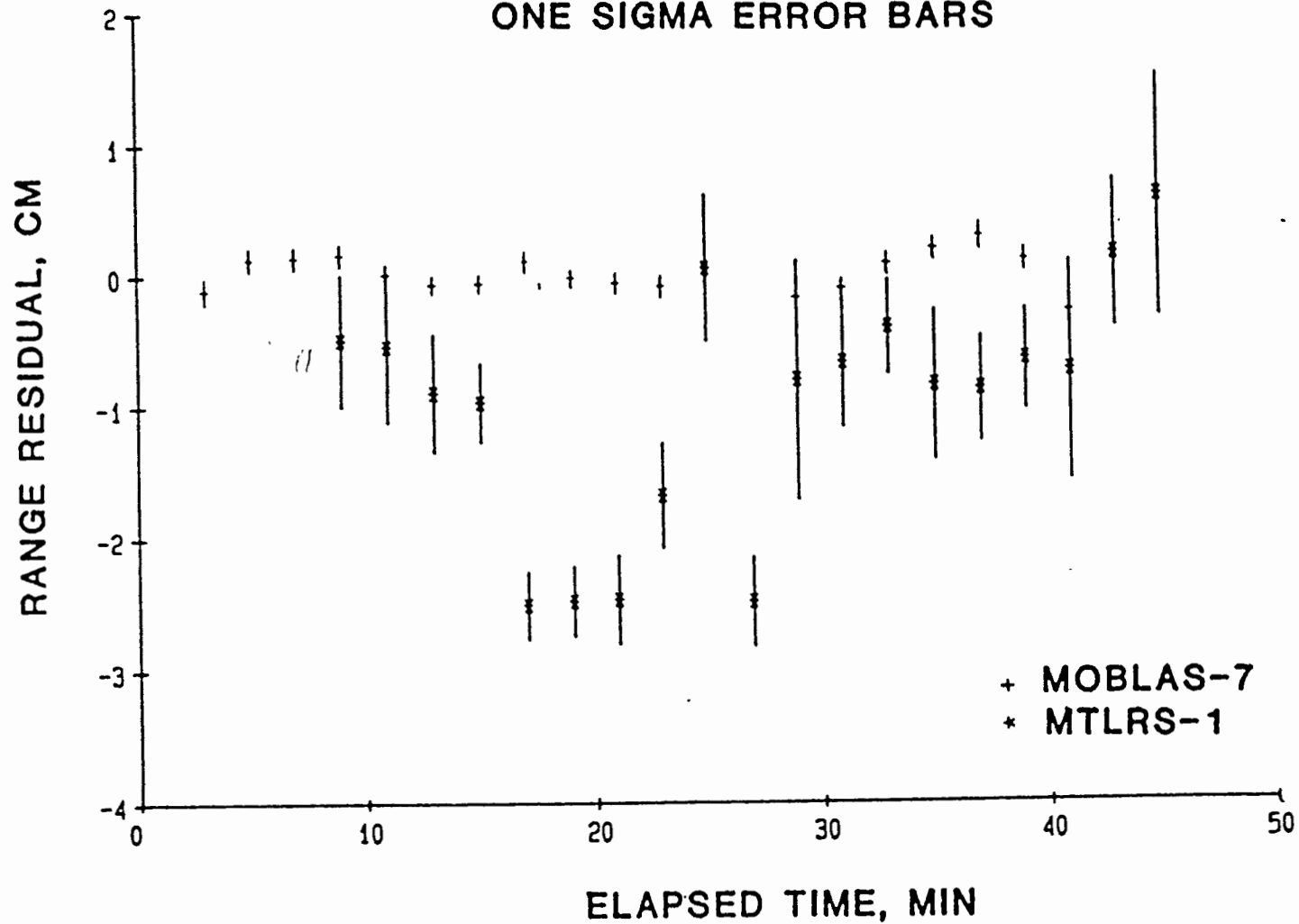


FIGURE 3 Two minute mean range residuals.

LAGEOS 6/27/85 04:00

ONE SIGMA ERROR BARS

x MTLRS-1 MINUS MOBLAS-7

$\bar{X} = -1.47, \beta = 0.10, \phi = 0.84$

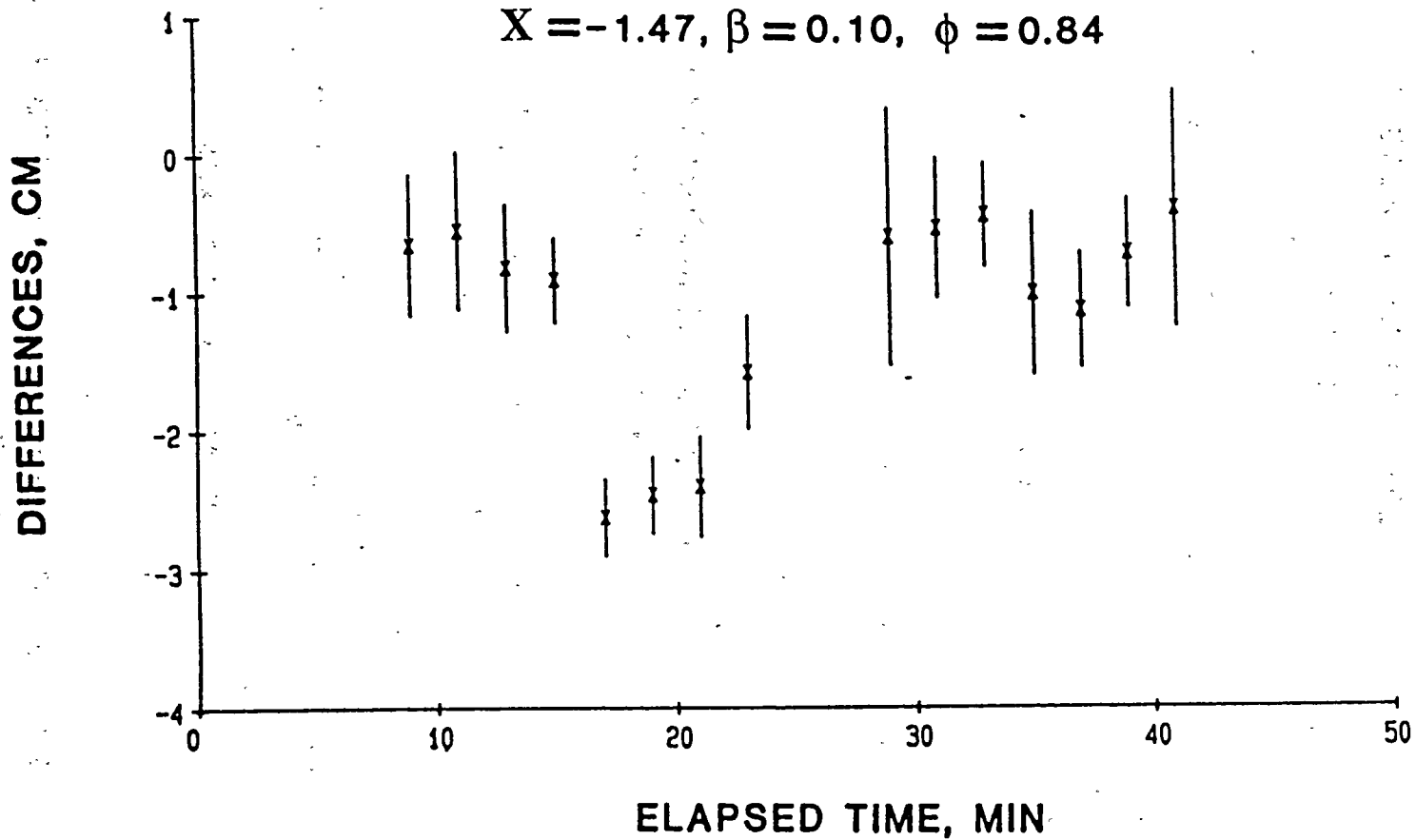


FIGURE 4. Two minute mean range residual differences.

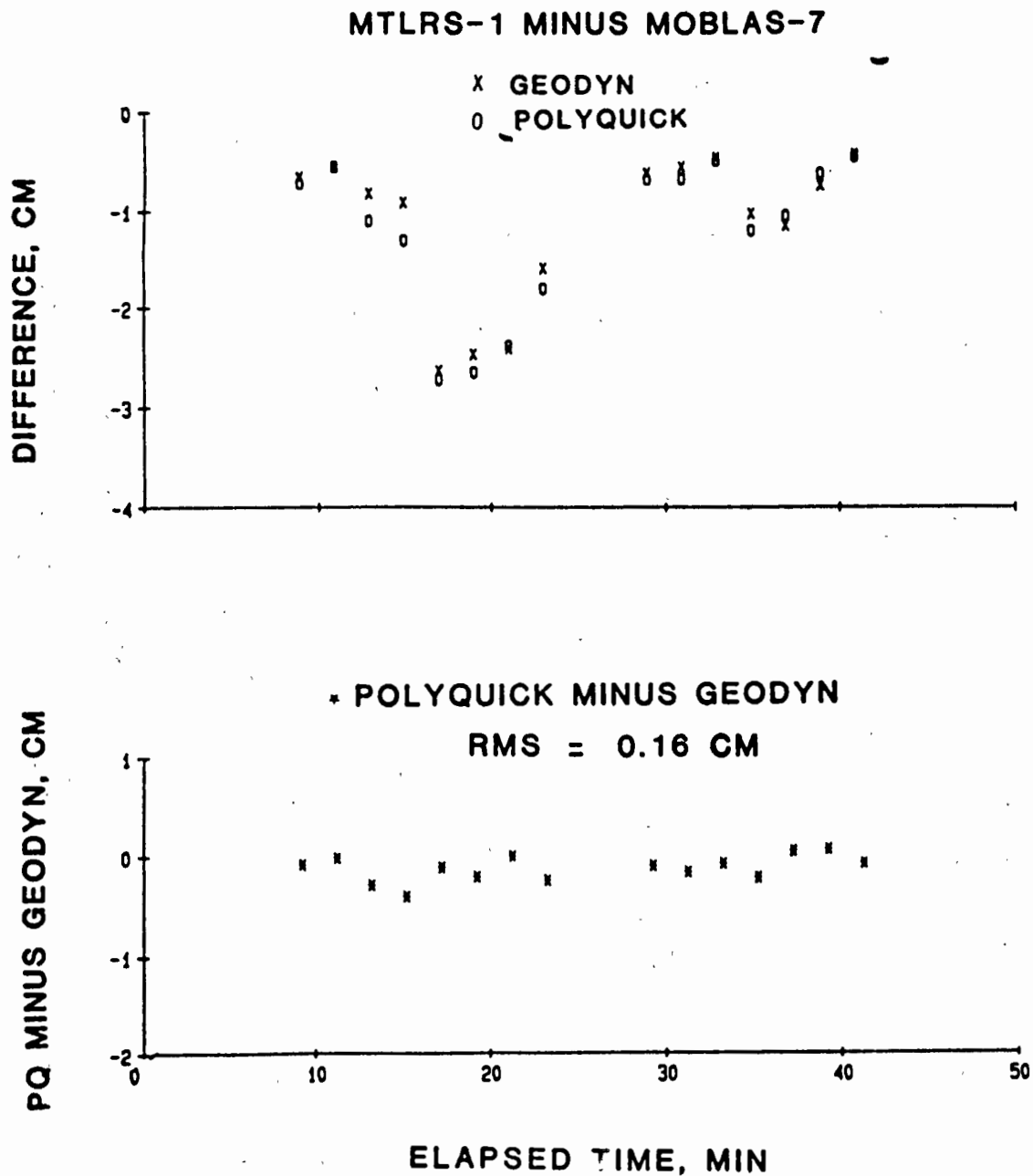


FIGURE 5 Comparison between GEODYN and POLYQUICK for LAGEOS 6/27/85.

| DATE IN 1985 | TIME, GMT | WEIGHTED MEAN DIFFERENCE MTLRS-1 MINUS MOBLAS-7, CM | | POLYQUICK MINUS GEODYN, CM |
|-----------------------|--------------|--|--------------|----------------------------------|
| | | GEODYN | POLYQUICK | |
| 5/10 | 0934 | -1.65 ± 0.20 | -1.44 ± 0.20 | 0.21 |
| 5/15 | 0612 | 1.55 ± 0.14 | 1.42 ± 0.14 | -0.13 |
| 5/20 | 0628 | -1.93 ± 0.12 | -1.96 ± 0.12 | -0.03 |
| 5/21 | 0838 | 0.05 ± 0.15 | 0.06 ± 0.15 | 0.01 |
| 5/30 | 0704 | -0.95 ± 0.10 | -0.96 ± 0.10 | -0.01 |
| 6/03 | 0848 | -1.39 ± 0.14 | -1.12 ± 0.14 | 0.27 |
| 6/14 | 0738 | -2.58 ± 0.11 | -2.60 ± 0.11 | -0.02 |
| 6/17 | 0704 | -3.76 ± 0.10 | -3.56 ± 0.10 | 0.20 |
| 6/26 | 0520 | -3.41 ± 0.18 | -3.28 ± 0.18 | 0.13 |
| 6/27 | 0400 | -1.47 ± 0.10 | -1.58 ± 0.10 | -0.11 |
| 6/27 | 0732 | -3.10 ± 0.10 | -3.08 ± 0.10 | 0.02 |
| 7/04 | 0838 | -0.66 ± 0.30 | -0.51 ± 0.30 | 0.15 |
| 7/14 | 0530 | -0.08 ± 0.20 | 0.20 ± 0.20 | 0.28 |
| WEIGHTED MEAN = -1.80 | | | -1.76 | rms = 0.15 |
| STD OF MEAN = 0.04 | | | 0.04 | |
| STD ABOUT MEAN = 1.42 | | | 1.38 | |

TABLE 2 Comparison between GEODYN and POLYQUICK for the MOBLAS-7 and MTLRS-1 collocation.

| Year | Population | Area | Population | Area |
|------|------------|-------|------------|-------|
| 1900 | 1,000 | 100 | 1,000 | 100 |
| 1905 | 1,200 | 120 | 1,200 | 120 |
| 1910 | 1,500 | 150 | 1,500 | 150 |
| 1915 | 1,800 | 180 | 1,800 | 180 |
| 1920 | 2,200 | 220 | 2,200 | 220 |
| 1925 | 2,500 | 250 | 2,500 | 250 |
| 1930 | 3,000 | 300 | 3,000 | 300 |
| 1935 | 3,500 | 350 | 3,500 | 350 |
| 1940 | 4,000 | 400 | 4,000 | 400 |
| 1945 | 4,500 | 450 | 4,500 | 450 |
| 1950 | 5,000 | 500 | 5,000 | 500 |
| 1955 | 5,500 | 550 | 5,500 | 550 |
| 1960 | 6,000 | 600 | 6,000 | 600 |
| 1965 | 6,500 | 650 | 6,500 | 650 |
| 1970 | 7,000 | 700 | 7,000 | 700 |
| 1975 | 7,500 | 750 | 7,500 | 750 |
| 1980 | 8,000 | 800 | 8,000 | 800 |
| 1985 | 8,500 | 850 | 8,500 | 850 |
| 1990 | 9,000 | 900 | 9,000 | 900 |
| 1995 | 9,500 | 950 | 9,500 | 950 |
| 2000 | 10,000 | 1,000 | 10,000 | 1,000 |

Source: U.S. Census Bureau, Statistical Abstract of the United States, 2000, Table 1-1.

REAL TIME, ON SITE EARTH ORIENTATION PARAMETER
GENERATION AT THE MLRS USING LUNAR LASER RANGING
DATA

P.J. Shelus, R.L. Ricklefs
McDonald Observatory and Department of Astronomy
University of Texas at Austin
Austin, Texas 78712-1083 - USA -

Telephone (512) 471 3339
TWX 910874 1351

ABSTRACT

For more than a year, earth rotation parameters (i.e, UT-0) have been computed on site, in real-time at the McDonald Observatory Laser Ranging Station (MLRS) using lunar observations to the Apollo 15 corner retroreflector. These parameters have then been immediately electronically transmitted, via the General Electric Company Mark III network, to the U.S. Naval Observatory for eventual use in their earth orientation prediction services. In this paper we shall briefly discuss the recent history of this endeavor, the hardware and software components which compose this system, the observational strategy which is being employed, and the results which have been obtained so far. Because of the unique nature of the lunar laser ranging data type, which allows this rather straightforward real-time, on-site earth rotation computation to be made, and because of the common software which exists at all of the lunar capable laser ranging stations, it is hoped that within a year or so all of the LLR stations will be able to provide similar services for earth orientation results.

This research is being supported by the National Aeronautics and Space Administration under Contract NAS5-29404 and Grant NAG5-754 to McDonald Observatory and the University of Texas at Austin from the Goddard Space Flight Center in Greenbelt, Maryland.

Introduction

The securing of precise Earth orientation information has long been the one of the major goals of laser ranging observations to Earth orbiting targets (see, for example, Bender et al, 1973 or Mulholland, 1980). Although much successful work has been performed at various analysis centers over the past ten years in securing these results, spurred by such international projects as EROLD and MERIT (see, for example, Langley et al, 1981 or Dickey and Williams, 1983), the presence of powerful mini- and micro-computers on-site at modern ranging stations, coupled with the long period modeling accuracies now available, make it possible for one to consider the computation of these data products in a near-real-time environment on-site at the laser ranging stations themselves. At the McDonald Observatory Laser Ranging Station (MLRS), located near Fort Davis, Texas, we have been producing such results, using lunar laser ranging observations, since early 1985. This paper describes the techniques which are being applied and the results which have so far been obtained.

Techniques

The basic equation for dynamical parameter improvement used in most lunar laser ranging analysis is the following:

$$\tau_o - \tau_c = \sum_{i=1}^n \frac{\partial \tau}{\partial \kappa_i} (\kappa_i - \kappa_c) \quad (1)$$

where τ_o and τ_c are the observed and calculated ranges (i.e., time delays), respectively, and the κ_i are parameters associated with whatever model is currently being used. Since it is convenient to deal with changes in the Earth's orientation as changes in the longitude, λ , and the latitude, ϕ , of the observing station, we can re-write equation 1 explicitly as (see, for example, Stolz and Larden, 1977 or Shelus et al, 1981):

$$\tau_o - \tau_c = \frac{\partial \tau}{\partial \lambda} (\lambda - \lambda_0) + \frac{\partial \tau}{\partial \phi} (\phi - \phi_0) + C. \quad (2)$$

For our purposes, it has been assumed that all short period terms having amplitudes of 1 cm or more, other than those dealing with the orientation of the earth, have been eliminated in the modeling and that, since we shall be averaging data over no more than a few days, all longer period terms can be assumed to be constant. We feel that this is certainly a reasonable assumption for the lunar system.

Of course, the major requirement for the production of real-time earth orientation information on-site (in addition to the capability of making the observations themselves) is the availability of a convenient and precise lunar range prediction system. The transfer of such a system to the MLRS was accomplished some two years ago when we succeeded in reproducing MIT lunar range prediction results at the 20-30 psec level. We are presently working to attain the same levels of accuracy with the JPL lunar model predictions.

The obtaining of earth orientation parameters from MLRS lunar laser ranging observations can be summarized as follows. With the completion of a lunar "run", using various interactive graphics tools, the lunar data set is statistically filtered and mathematically compressed to form a single normal point. When several such normal points have been formed within a pre-defined interval of time (usually 24-48 hours), an earth orientation solution is performed using the residual and partial derivative values appropriate to equation 2 above. At the present time, only observations to the Apollo 15 (Hadley) retroreflector are used and only a longitude, i.e., UT-0, solution is made. We consider an earth orientation reduction to be "prime" if it is obtained using data within a single lunar transit and with an hour angle spread of at least 3 hours. Under any other circumstances, the reduction is considered to be "non-prime". Results are inspected on-site for potential problems and, if they prove to be satisfactory, are placed onto the General Electric Company Mark III system for general distribution. Under normal circumstances, the total time, from the beginning of the observing sequences for a "prime" data set to Earth orientation parameter transmittal, encompasses an interval of less than 18 hours.

Results

Since February, 1985 there have been some 38 UT0 points produced at the MLRS in this real-time environment. Of these, 8 are considered "prime". Comparisons of our "quick-look" results with "full-rate" results obtained by X X Newhall at JPL (Figure 1), those obtained by the BIH (Figure 2), and those obtained by our own after-the-fact Earth orientation reduction system in Austin (Figure 3) have been quite satisfactory. For the JPL comparisons, it was necessary to convert the "standard" $UT0_R - UTC$ values to $UT0 - UTC$ by re-introducing the short period zonal tide terms (see Yoder et al, 1981). For the BIH comparisons, $UT0 - UTC$ values at McDonald Observatory were inferred from the BIH final values for x , y , and $UT1 - UTC$, interpolated to the time of the MLRS $UT0$ point..

Although our early results seem to be somewhat off the mark, as our procedures mature and our experience improves, quite a good agreement is being obtained with the more recent data. To re-iterate, and as a caveat to prospective users, it is quite important to realize that this is essentially a "quick-look" procedure. Since we deal in a real-time environment, our results can sometimes be contaminated by data which proves to be poor, under later analysis. Further, we do no fitting of the data for other parameter improvement, as is done in the regular after-the-fact, full-rate data environment. In spite of these shortcomings, we feel that our product is a good one and can serve many of the "quick-look" needs of the Earth orientation community.

As a final comment, it must be stated that the biggest difficulty with which we are being presently confronted is a severe paucity of Earth orientation results using this lunar technique. At the MLRS, the station has been working flawlessly; the data gaps are completely a product of the environment. It is hoped that most of this type of problem can be solved by a move of the MLRS from its present "saddle-site" to one at the top of a near-by mountain. On the positive side, in our processing of lunar laser ranging data from the Haleakala site, we are attempting to apply the self-same MLRS data reduction techniques to compute Earth orientation parameters from Hawaii data. In addition, we are also interested in the sharing of this software with other stations, which have equipment that is capable of making similar types of reductions on-site, and are encouraging them to undertake similar "quick-look" types of analyses to obtain additional earth orientation results.

Acknowledgements

The authors cannot too strongly acknowledge and thank Robert W. King at MIT for his invaluable aid in the implementation of the MIT lunar range prediction package at the MLRS.

Additional computer equipment, which provides the capability of simultaneous data gathering and data reduction at the MLRS, has been secured, in part, through funding provided by Dennis D. McCarthy of the U. S. Naval Observatory. Many thanks also go to Nelson Zarate, who produced large parts of the original version of the Earth orientation analysis routines, and to Janice Storm, who runs the present software system so productively at the MLRS. Finally, we acknowledge that this research is being supported at McDonald Observatory and the University of Texas at Austin by National Aeronautics and Space Administration Contract NAS5-29404 and Grant NAG5-754 out of Goddard Space Flight Center, Technical Officers Mr. Robert L. Appler and Dr. Gilbert D. Mead, respectively.

References

- Bender, P.L., Currie, D.G., Dicke, R.H., Eckhardt, D.H., Faller, J.E., Kaula, W.M., Mulholland, J.D., Plotkin, H.H., Poultney, S.K., Silverberg, E.C., Wilkinson, D.T., Williams, J.G., and Alley, C.O. 1973, "The Lunar Laser Ranging Experiment", *Science*, **182**, 229-238.
- Dickey, J.O. and Williams, J.G. 1983, "Earth Rotation from Lunar Laser Ranging", *Astron. Astrophys. Suppl. Ser.*, **54**, 519-540.
- Langley, R.B., King, R.W., and Shapiro, I.I. 1981, "Earth Rotation from Lunar Laser Ranging", *J. Geophys. Res.*, **86**, 11913-11918.
- Mulholland, J.D. 1980, "Scientific Achievement from Ten Years of Lunar Laser Ranging", *Rev. of Geophy. and Sp. Phys.*, **18**, 549-564.
- Shelus, P.J., Zarate, N.R., and Eanes, R.J. 1981, "Earth Rotation from a Simultaneous Reduction of LLR and LAGEOS Laser Ranging Data", *Proceedings of the 63rd Coll. of the IAU*, O. Calame, ed., D. Reidel, 31-40.
- Stolz, A. and Larden, D. 1977, "Accuracy Obtainable for Universal Time and Polar Motion During the EROLD Campaign", *Scientific Applications of Lunar Laser Ranging*, J.D. Mulholland, ed., D. Reidel, 37-50.
- Yoder, C.F., Williams, J.G., Parke, M.E., and Dickey, J.O. 1981, "Short Period Tidal Variations of Earth Rotation", *Ann. des Geophy.*, **37**, 213.

Figure 1. MLRS Earth Orientation Parameters

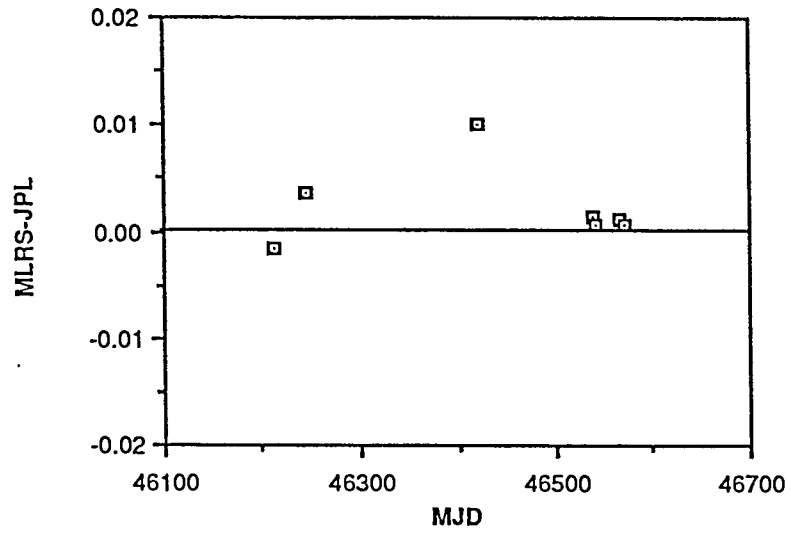


Figure 2. MLRS Earth Orientation Parameters

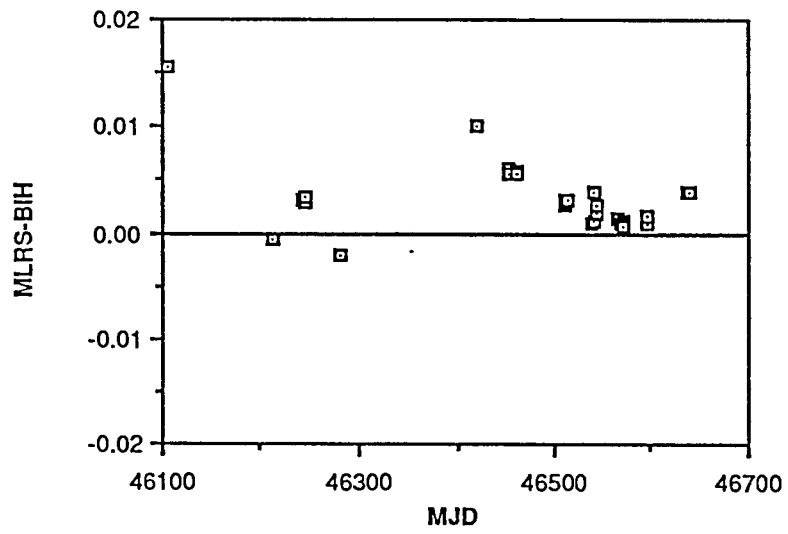
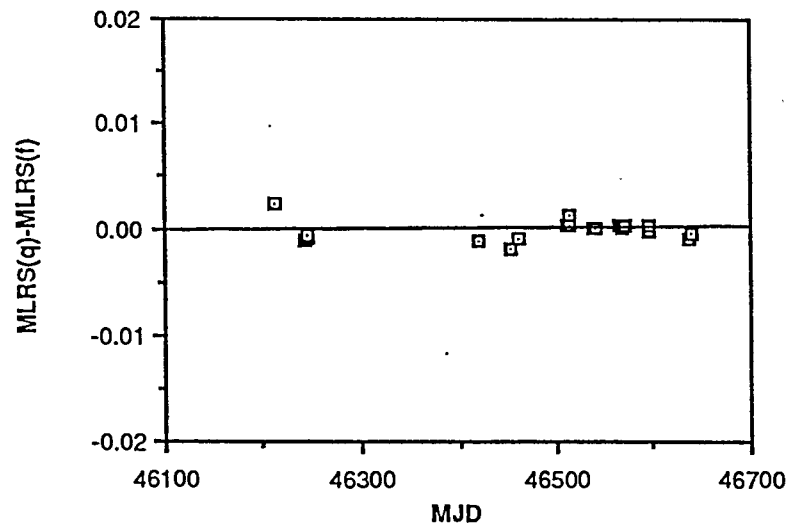
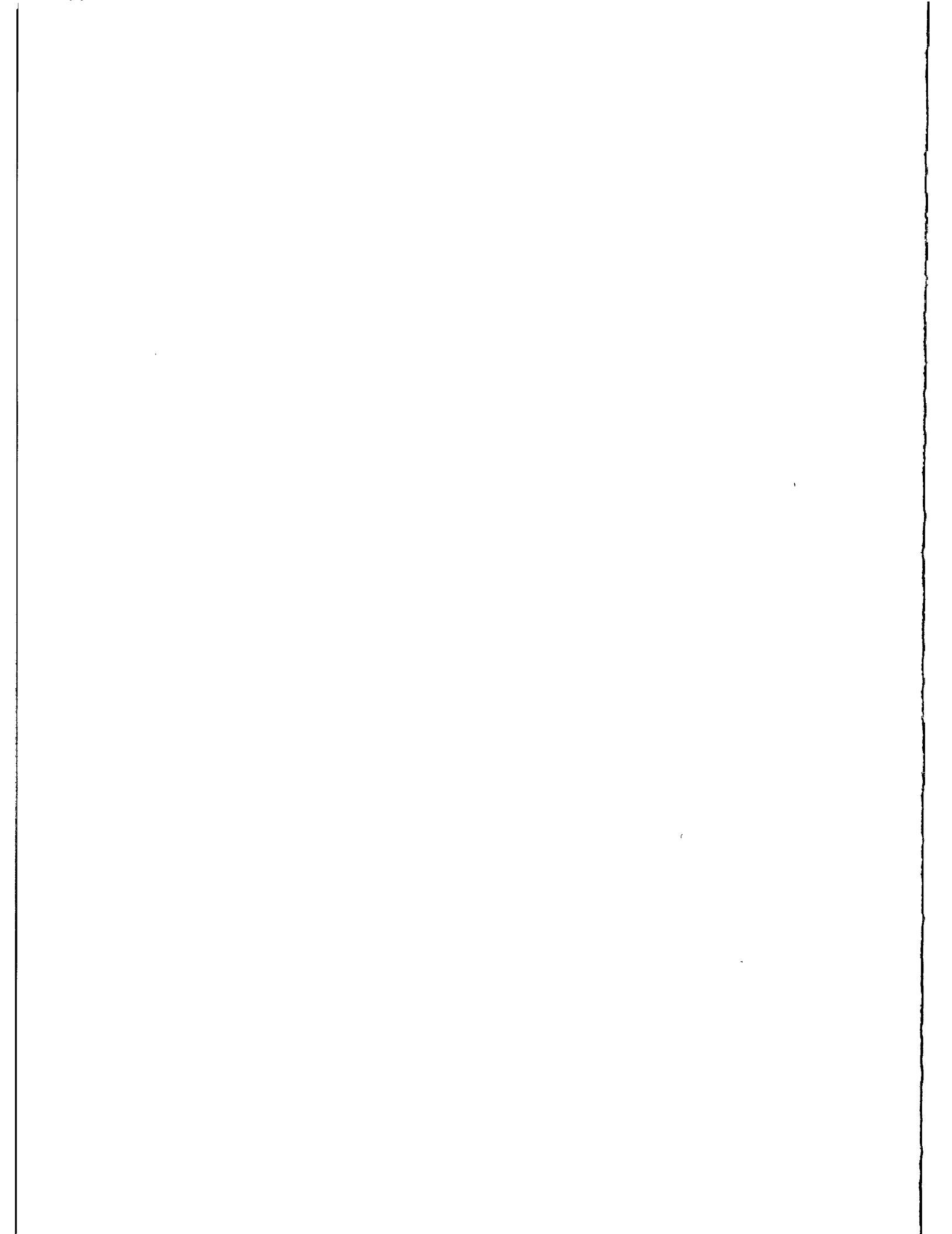


Figure 3. MLRS Earth Orientation Parameters





A NOTE ON THE USE OF THE CSR LAGEOS EPHEMERIDES

G.M. Appleby, A.T. Sinclair
Royal Greenwich Observatory
Herstmonceux Castle
Hailsham
East Sussex BN27 1RP - England -

Telephone (0323) 833171
Telex 87451

ABSTRACT

Using the predicted state vectors of the satellite LAGEOS supplied by the Center for Space Research, Texas University, to form local predictions, the UK Satellite Laser Ranging System at the Royal Greenwich Observatory routinely obtains very precise range observations of the satellite both during the day and at night. This note describes our method of improving extrapolated quantities implicit in the predictions, such that remaining prediction errors are of the order of only 5m in range. We further obtain approximate values of UT1-UTC during periods when several passes have been observed within a short time interval.

A NOTE ON THE USE OF THE CSR LAGEOS EPHEMERIDES

G.M. Appleby and A.T. Sinclair
Royal Greenwich Observatory
Herstmonceux Castle
Hailsham
East Sussex BN27 1RP
England

Telephone (0323) 833171
Telex 87451

Summary. Using the predicted state vectors of the satellite LAGEOS supplied by the Center for Space Research, Texas University, to form local predictions, the UK Satellite Laser Ranging System at the Royal Greenwich Observatory routinely obtains very precise range observations of the satellite, both during the day and at night. This note describes our method of improving extrapolated quantities implicit in the predictions, such that remaining prediction errors are of the order of only 5m in range. We further obtain approximate values of UT1-UTC during periods when several passes have been observed within a short time interval.

1. Introduction

The principal target for the SLR operations being carried out at the Royal Greenwich Observatory, Herstmonceux, is the Laser Geodynamic Satellite, LAGEOS. In order to predict accurately the position of the satellite at any time we depend upon the set of daily state vectors supplied by the Center for Space Research at Texas University (CSR). These vectors are used as starting values for an integration of the satellite's equations of motion to yield its expected position at any given time. The integration uses a simplified force model, and so the optimum accuracy of the integration over 1 day would be a few metres. However, as the orbit is predicted ahead for many months, the real errors are considerably greater. The principal errors are an along-track displacement of the satellite, and an error due to the assumed value of UT1-UTC. This note describes our use of these predictions with particular reference to the determination of the along-track error from our range measurements and the correction of the assumed values of UT1-UTC implicit in the starting values, in order to improve the accuracy of the predictions to about 5 metres. We further derive some near-realtime values of UT1-UTC from our range measurements.

2. The accuracy of the CSR predictions

The CSR predictions for Lageos are issued for up to 18 months ahead, so inevitably they have increasing errors towards the end of their span. The major source of error is the uncertain drag-like acceleration affecting Lageos, which leads to an along-track positional error. This acceleration is generally modelled very well by CSR, the remaining error being only 600 m in along-track position (equivalent to a time bias of 100 ms) at the end of ephemeris 19. This would cause a maximum effect at the start or end of a pass on the two-way range of 500 m or 1700 ns. Such an error would cause serious problems for day-time ranging with a narrow range gate, but fortunately the time bias varies slowly, and the current value can be determined as part of the pre-processing of the range data obtained in each Lageos pass (Appleby and Sinclair, 1985). The time bias is determined as a correction to the orbital mean anomaly of the satellite, and this is converted to a time bias by dividing by the mean motion.

The second most significant source of error in the CSR predictions is caused by errors in the extrapolated values of UT1 used by CSR in referring their predictions to the Greenwich meridian. The coordinate system of the CSR state vectors is nominally the true equator of date and the Greenwich meridian, but as is shown in Figure 1, the CSR x-axis will differ from the Greenwich meridian by $1.00273 \Delta UT1$, where $\Delta UT1$ is the error in the extrapolated value of UT1, and where we are measuring angles in time units. The typical magnitude of the error $\Delta UT1$ is about 100 ms, which was the value half-way through ephemeris 19. The simplest way to use the CSR predictions is to ignore this error, and treat the predictions as if they were referred to the Greenwich meridian. For a north-south pass of Lageos this had little effect on range, but for an east-west pass it changes the two-way range at the start or end of a pass by 80 m or 260 ns.

The variation of range through an east-west pass caused by an error in UT1(extrap) is very similar to that caused by a time bias, such that an error of 100 ms in UT1 (extrap) has virtually the same effect on range for an east-west pass as a time bias of 15 ms. Hence if the effect of the error in UT1(extrap) is not corrected in the predictions, the value of the time bias determined from east-west passes will be corrupted by the order of 15 ms, while from north-south passes the correct value of the time bias will be obtained.

For a ranging system using a narrow range gate of the order of 100 ns, and particularly during day-time ranging, this variation of the value determined for the time bias according to the pass direction is very inconvenient, since the typical error in time bias of 15 ms can cause two-way range residuals for a subsequent pass of 80 m or 260 ns. Hence at RGO the error in UT1(extrap) is corrected during the computation of predictions.

Further it is expected that this unpredictable error in UT1(extrap) may well be the dominant effect in future Lageos ephemerides, as the model representing the drag forces on the satellite inevitably improves. We comment in passing that the velocities given in the CSR state vectors are, for historical reasons, referred to the reference frame rotating with the Earth, and have to be converted to an inertial frame before performing the numerical integration. This is done in the CSR program IRVINT. It is also carried out in the equivalent RGO program ORBIT, which uses a reference frame defined by the true equator of date and X axis which is displaced from the mean equinox of date by $1.00273 \Delta UT1$. This reference

frame error has negligible effect on the calculation of the forces acting on the satellite, and hence in the derived predicted position. For subsequent calculation of topocentric position, the satellite coordinates are again referred to the CSR reference frame.

3. Application of corrections to UT1(extrap)

In order to minimise the pass-dependent effect on the determination of the time bias we need a close approximation to the error of UT1(extrap) to be used in computing predictions. The extrapolated values of UT1-UTC used by the CSR to generate the predictions are available in a file along with the state vectors on the magnetic tapes distributed by CSR. Thus for a given pass we compute

$$\Delta UT1 = (UT1-UTC)_{CSR} - (UT1-UTC)_{BIH}$$

where we have obtained $(UT1-UTC)_{BIH}$ by short extrapolation from the most recent values of the BIH rapid service. We then reduce the longitude of the station by $1.00273 \Delta UT1$ (in time measure), thus effectively removing the small rotation about the z-axis between the satellite and terrestrial reference systems. This will improve the accuracy of the predictions, and a solution for or time-bias will be free from corruption by $\Delta UT1$, regardless of orientation of the pass. With the removal of the reference system error in this way, and using recently-determined values of the time bias, we find we can predict the range to the satellite to an accuracy of about 5m, or 30ns in 2-way time-of-flight. The plot shown as Figure 2 gives the derived time bias values for the duration of CSR ephemeris 19. The small scatter of values about the fitted smooth curve shows the effectiveness of the above method. The small size of the time bias, even near the end of the ephemeris, shows how well the CSR drag model has predicted the accelerations experienced by Lageos.

4. Estimation of UT1-UTC from the observations

Based on the above analysis it is clear that any small errors in our short-term extrapolation of $(UT1-UTC)_{BIH}$ should become apparent as small differences in the determined value of the time bias according to pass direction. In particular if we observe several passes in a day, we may use the N-S or S-N passes to derive a current, uncorrupted, value for the time bias. This value may then be assumed when reducing an E-W pass and the observations used to derive a correction to our assumed value of UT1-UTC.

In practice we use the observed ranges from 2 or more passes in a given day in a simultaneous solution for time bias, correction to our assumed $(UT1-UTC)$ and correction to the geodetic latitude of the SLR instrument. The latitude correction allows for small errors in our short-term extrapolated values of the coordinates of the pole. Strictly we should only determine UT0-UTC from one observing station, but we find that our extrapolation of the coordinates of the pole from the rapid service results are usually in error by no more than ± 0.005 in x_p and y_p . Then for the coordinates of Herstmonceux ($\lambda \approx 0^\circ$, $\phi \approx 51^\circ$),

$$\begin{aligned} \delta UT1 &= 0.005 \tan \phi \\ &= 0.4 \text{ms} \end{aligned}$$

is the corruption to UT1-UTC due to the error in the extrapolated x_p and y_p . This error is within the probable error of the derived values of $(UT1-UTC)$ by our approximate method. The results of some determinations of

UT1-UTC are given in Figure 3, where the values are compared to the raw UT1-UTC results taken from BIH Circular D.

5. Conclusion.

We have described our use of the University of Texas Lageos ephemerides to generate predictions in order to obtain laser range measurements. We have shown that given the best available estimated values of UT1-UTC we can effectively remove the errors in the extrapolated values of UT1-UTC implicit in the satellite reference system. We can then use our range measurements to derive uncorrupted estimates of orbital along track error which can be used to improve subsequent predictions such that the prediction errors are less than 5 metres. We further find that we can obtain approximate values of UT1-UTC from our observations on days when several passes of Lageos have been observed, the accuracy of these estimates depending upon how well the long-term behaviour of the node of the orbit has been modelled in the CSR ephemerides.

Reference: Appleby, G.M. and Sinclair, A.T. 1985.
SLR Technical Note No.5.
Data Processing and Preliminary Analysis Software for the UK
Satellite Laser Ranging Facility.

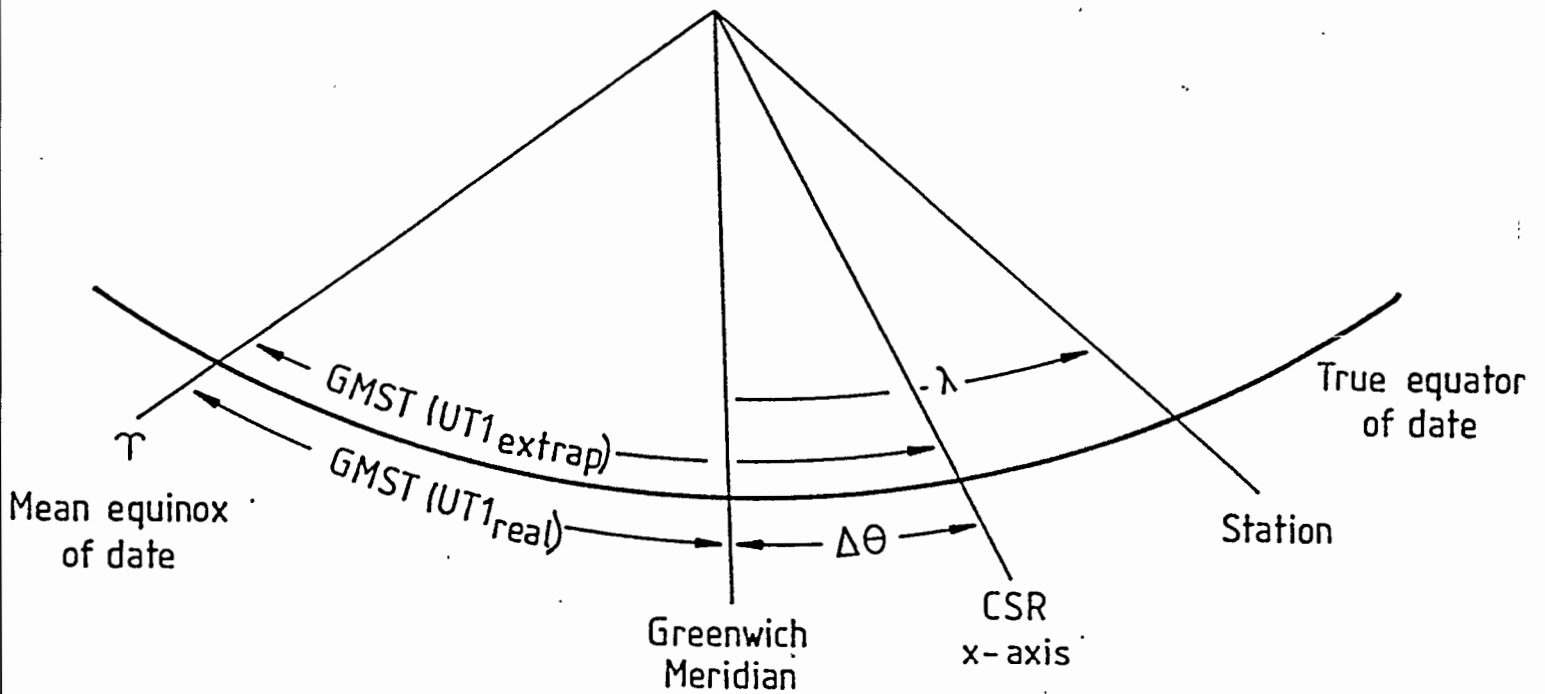


Figure 1. The location of the CSR x-axis relative to the Greenwich Meridian.

$$\Delta\theta = 1.00273 \cdot \Delta UT1 \quad (\text{in time units}),$$

where $\Delta UT1 = UT1(\text{extrap}) - UT1(\text{real})$.

The longitude of a station should be reduced by $\Delta\theta$ in order to refer it to the CSR x-axis.

REAL TIME UT0 DETERMINATION AT CERGA LLR STATION

Ch. Veillet, D. Feraudy, J. Pham-Van
CERGA
Avenue Copernic
06130 Grasse - France -

Telephone 93 36 58 49
Telex 470865 F

ABSTRACT

UT0 determinations based on single night LLR data are presented. They use Pole coordinate predictions from BIH. Comparisons are made with final values by CERGA and JPL. The available software can be used at the end of an observing session in order to allow close real-time UT determination.

1/ Introduction

A great advantage of the LLR technique is to be able to provide a quite accurate UT0 value in close real time, for instance at the end of an observing night. In fact, the three Earth Rotation parameters can be determined from LLR if various stations give data at the same time. Unfortunately, such a situation occurs rarely and only single station (CERGA) UT0 determinations will be presented here.

2/ CERGA data and UT0 determination

Table 1 shows the number of UT0 determinations made in 1985 with the LLR data from the various stations, together with the corresponding number of nights and the mean standard deviation. A UT0 value can be obtained from data on a single lunar reflector and a single night as long as the hour angle coverage is large enough. As the CERGA station is able to range more than one reflector on a single night, there are more UT0 values than observing nights for this site.

| Stations | UT values | nights | msd (ms) |
|---------------|-----------|--------|----------|
| McDonald 2.7m | 12 | 12 | .6 |
| MLRS | 6 | 5 | .3 |
| Haleakala | 29 | 28 | .3 |
| CERGA | 118 | 67 | .7 |

Table 1 - Statistics on UT determinations from LLR for 1985

3/ Single night process

Three examples are shown using two different nights and two reflectors. The first night is one of the longest never obtained at CERGA. It covers more than 10 hours. Fig 1 shows the residuals (observed-calculated) determined on the station computer from the prediction software (based on DE121/LLB13 JPL ephemeris) and the predicted ERP from BIH. These residuals are fitted in order to extract the UT information. The found value for $UT0 - UTC$ is given on the figure and compared with CERGA and JPL a *posteriori* determinations using Circular D BIH Pole coordinates. For such a night on Appolo XV, the error on $UT0 - UTC$ is small, mainly due to the very long hour angle coverage. Even with a few data, as on Fig. 2 (Lunakhod 2 on the same night), this error is small for the same reason.

As the last observing session (Fig. 3) is much shorter, the uncertainty on $UT0 - UTC$ is much larger. However, the "real-time" value is very close to the final one. The error on UT due to the fact that "real-time" determinations are made with predicted Pole coordinates is small: X and Y are easy to predict with a quite good accuracy.

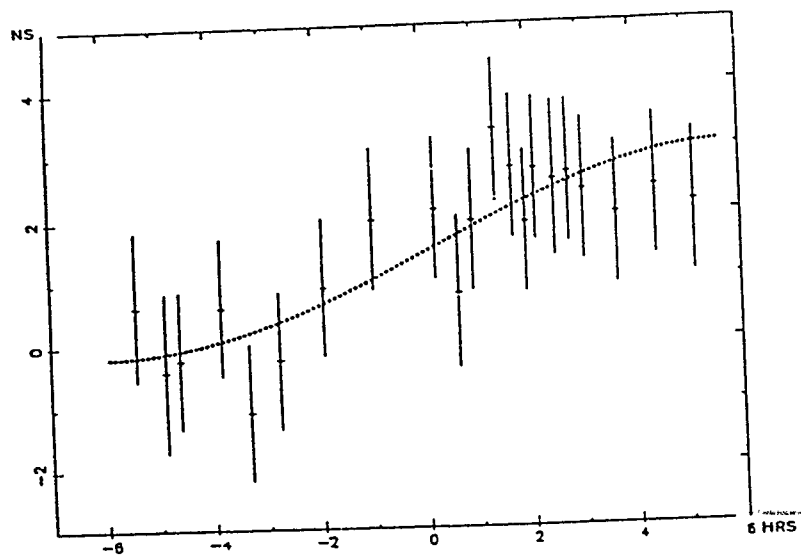
4/ Conclusion

The software used for these "real-time" UT determinations is available at the station and can be run at the end of an observing session. The agreement between them and the "final" values is quite good and shows that LLR "real time" UT can significantly contribute to accurate short term UT predictions.

CERGA + BIH prediction
 UTOR - UTC = .53166

CERGA + Cir. D
 UTOR - UTC = .53176 (16)

JPL + Cir. D
 UTOR - UTC = .53198 (14)



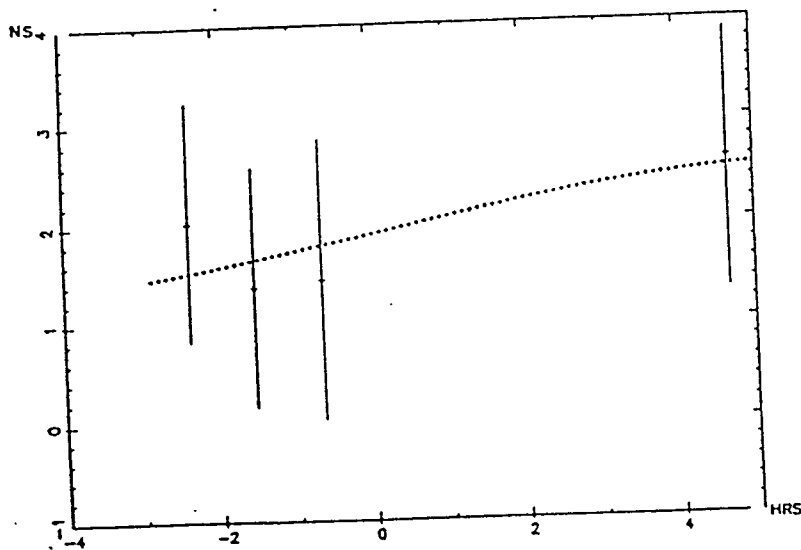
CERGA - Apollo XV - 6/Sep/1985

Fig. 1 - Residuals of range measurements (+) over one night relative to hour angle.
 Dashed curve shows the fit used for UT determination

CERGA + BIH prediction
 UTOR - UTC = .53183

CERGA + Cir. D
 UTOR - UTC = .53132 (43)

JPL + Cir. D
 UTOR - UTC = .53154 (41)



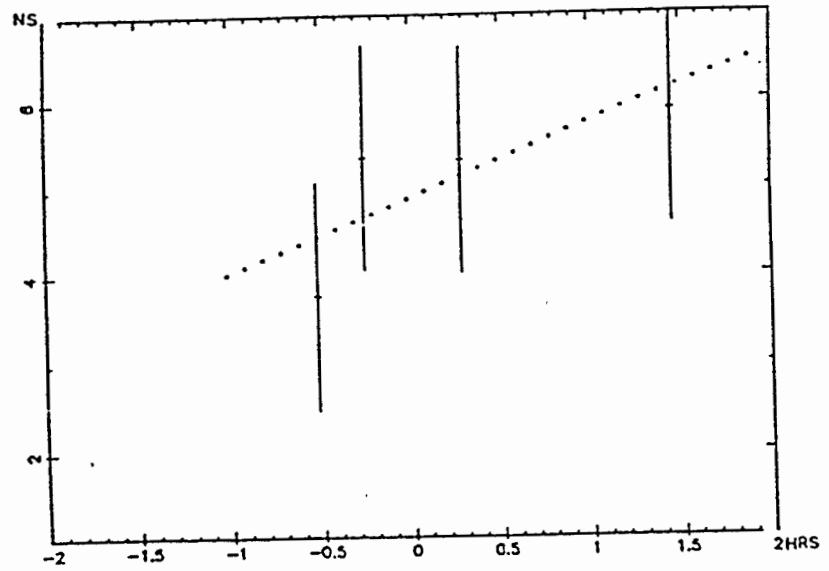
CERGA - Lunakhod 2 - 6/Sep/1985

Fig. 2 - Residuals of range measurements (+) over one night relative to hour angle.
 Dashed curve shows the fit used for UT determination

CERGA + BIH prediction
 UTOR - UTC = .54075

 CERGA + Cir. D
 UTOR - UTC = .54060 (133)

 JPL + Cir. D
 UTOR - UTC = .54117 (125)



CERGA - Apollo XV - 28/Aug/1985

Fig. 3 - Residuals of range measurements (+) over one night relative to hour angle.
 Dashed curve shows the fit used for UT determination

Derived UT1-UTC compared with BIH raw values

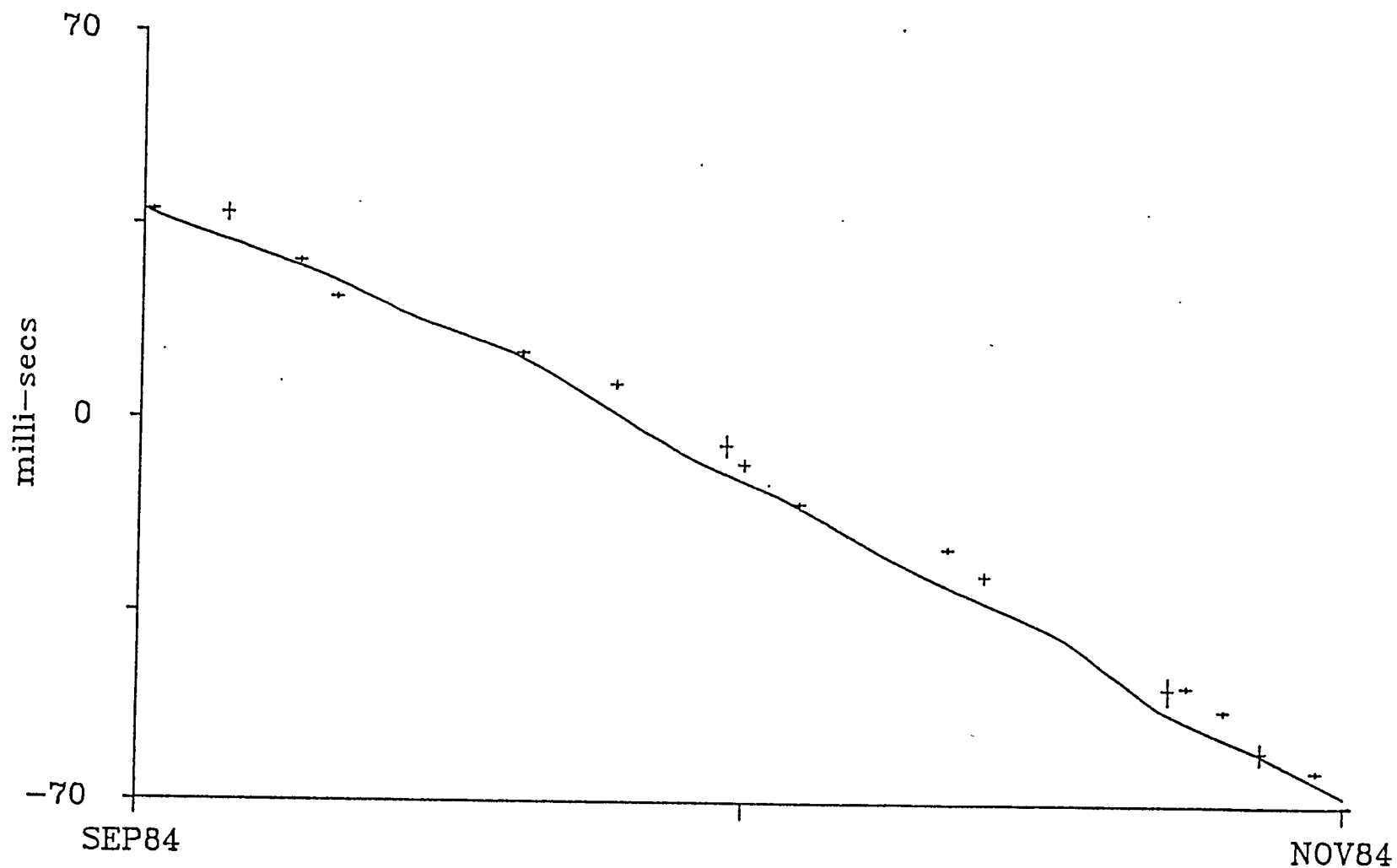


Figure 3. Values of UT1-UTC derived by combining Lageos range observations from 2 or more passes on a given day. The values are shown with 1-sigma error bars, and the full line has been drawn through 5-day raw values of UT1-UTC taken from BIH Circular D.

Observed Time Bias (ms)

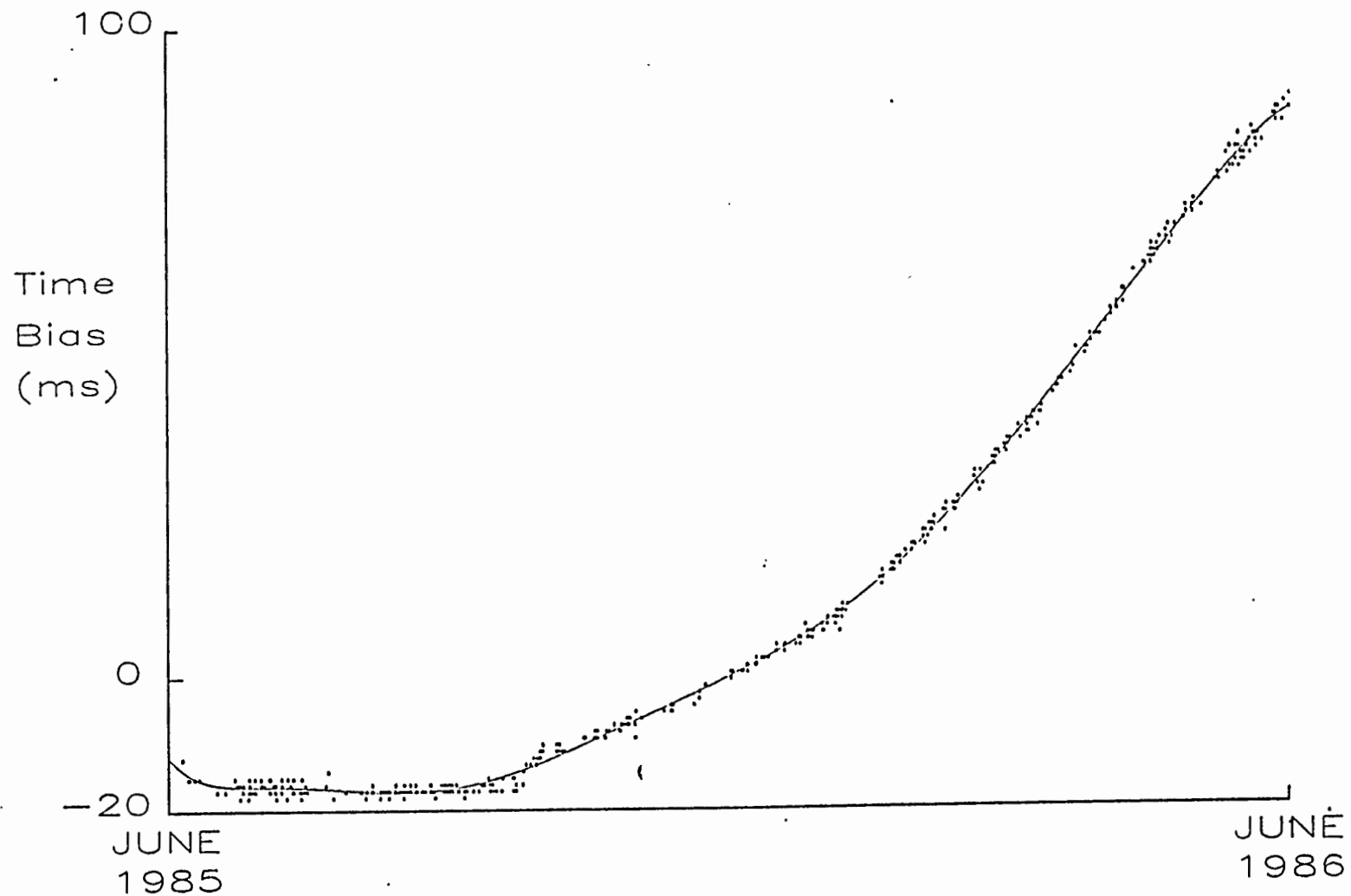


Figure 2. Determinations of Lageos orbital time bias.

Each point gives the time bias value in milliseconds as derived from observations of a single pass. The formal standard errors of the determinations are about 0.1ms. The full line shows a fitted high order polynomial.

A SIMPLE SOFTWARE SCHEDULING TOOL FOR EFFICIENT OBSERVING
OPERATIONS AT A LUNAR/LAGEOS LASER RANGING STATION

P.J. Shelus
McDonald Observatory and Department of Astronomy
University of Texas at Austin
Austin, Texas 78712-1083 - USA -

Telephone (512) 471 3339
TWX 9108741351

ABSTRACT

Once a laser ranging station has crossed the threshold from implementation and development to routine observing, one of the major problems of station operation (aside from preventive maintenance, repairs and upgrades) concerns the efficient scheduling of observing manpower, especially when several different targets are to be regularly observed. This paper describes a simple yet powerful tool which we have developed over the years to aid us in efficient observing crew scheduling for a mix of lunar and LAGEOS operations at the McDonald Laser Ranging Station (MLRS), which is located near Fort Davis, Texas. With a single glance, one can scan the graphical output from this software tool to see lunar and LAGEOS observational opportunities at the MLRS with such items as the visibility times of the moon and LAGEOS, the rising and setting times of the sun, moon, and LAGEOS, the maximum elevation and duration of all visible LAGEOS passes, as well as the lunar phase, age, maximum elevation, and declination during lunar visibility. With this graphical information at one's fingertips, it is then a simple procedure to manually schedule observing crews to take maximum advantage of mutual target visibilities and/or to accommodate whatever station and personnel constraints may be active. This tool has been created using Microsoft_r FORTRAN and is presently running on an Apple_r Macintoshtm computer. Only very slight revisions would need to be made to accommodate the specific locations of other ranging stations and, since the compiler used is a full implementation of FORTRAN 77, few (if any) changes would need to be made for transporting the code to other computers.

This research is being supported by the National Aeronautics and Space Administration under Contract NAS5-29404 to McDonald Observatory and the University of Texas at Austin from the Goddard Space Flight Center in Greenbelt, Maryland.

Introduction

The uses of laser ranging data in the astronomical and geodynamical sciences is now well established. In order to take maximum advantage of whatever resources are available to these scientific endeavors, it is imperative that all possible efficiencies be brought to bear in all phases of data gathering, reduction, and analysis. In a part-time project over the past several years we have put together and implemented a very simple software tool at McDonald Observatory which allows us to manually schedule our observing crews with a minimum of effort while preserving the opportunity for full man-power utilization and maximum target coverage. Our initial task had been made somewhat more difficult due to our responsibilities to both the lunar and the LAGEOS user communities.

On first glance, as one examines the output of this software tool, one might be tempted to comment that the exercise has been a trivial one since the results obtained are so well known and so readily available from so many sources. And we are quick to agree, except for the fact that it is not only the results of the computations which are important, it is also the ease and the convenience with which those computations can be performed and the manner in which those results can be presented. Our purpose was to bring together, in a single, easy to understand graphical display, many of the relevant parameters of solar, lunar, and LAGEOS visibility at the location of a particular laser ranging facility, thereby allowing for the simple and efficient scheduling of observing operations.

Program Description

The nucleus of this software tool is a LAGEOS visibility package which had been assembled by Richard J. Eanes, of the Department of Aerospace Engineering and Center for Space Research at the University of Texas at Austin, to be run on a CDC Cyber computer in simple batch mode. Using nominal elements for the orbit of LAGEOS, such parameters as rise and set times, rise and set point angles, and maximum elevation angles were produced for any input station location and range of dates. With the later inclusion of general mathematical expansions for the orbits of the sun and the moon, also produced were the positions of both the sun and the moon at LAGEOS rise and set times as well as at the time of maximum LAGEOS elevation. The results of these computations could be presented in columnar form on a standard line-printer.

The additions to this program, which were provided by the present author, were several-fold. The logic of the program was altered to compute approximate solar and lunar rise and set times in addition to those of LAGEOS. Added to the program were algorithms to provide the approximate lunar age, phase, and declination at maximum lunar elevation, as well as a day-of-the-week algorithm. The changes which were most extensive (and the most helpful, however) were those which dealt with the printed output. Finally, the entire program was modified to be run, in interactive mode, on a personal, desk-top micro-computer (an Apple® Macintosh™). As a bonus, and specific to the Macintosh™ environment, is the ability to create special symbols for the standard printer output (especially useful for providing lunar phase information) and the ability to use other standard Macintosh™ software, like Microsoft® Word and MacDraw™, for greater readability and to actually manually incorporate scheduling information in the final output.

Output Products

Figure 1 gives a sample of actual program results. The standard output text file shown has been processed by Microsoft® Word to provide for font selection, page alignment, and the

setting of margins and page breaks. Program output is generally printed using an Apple LaserWriter, but excellent results are obtained using any Macintosh™ compatible dot-matrix printer. In the example, for the ten day interval, September 1-10, 1986, one sees complete time-lines which illustrate the visibility of the sun, the moon, and LAGEOS at the MLRS, together with other information vital for crew scheduling.

The very top line on the page gives the month and the year, followed by three lines delineating three appropriate time scales, i.e., Central Daylight Time, Universal Time, and Central Standard Time. Each daily time line is identified by the day-of-the-week, i.e., S, M, T, W, T, F, S and the calendar day-of-the-month at the extreme left. Hour marks are given by vertical bars, "|", and tick marks delineate 12-minute intervals. A sun symbol, "☉", appears when the sun is above the horizon as seen from the MLRS. Just above the sun-line is the moon-line. A changing lunar symbol, denoting the moon's phase (new, "☾"; waxing crescent, "☾"; 1st quarter, "☽"; waxing gibbous, "☾"; full, "☉"; waning gibbous, "☾"; 3rd quarter, "☾"; waning crescent, "☾"), appears when the moon is above 20° elevation as seen from the MLRS. The approximate lunar declination and age at maximum lunar elevation appear at the extreme right end of the moon-line. The LAGEOS time-line is just below the sun-line with a LAGEOS symbol, "☾", appearing when LAGEOS is above 20° elevation as seen from the MLRS. The two digit number, appearing just to the right of each set of LAGEOS symbols, denotes the approximate maximum elevation at MLRS for that particular LAGEOS pass.

Figure 2 illustrates the results which were obtained by manually inserting scheduling information onto the basic time-lines, using the commercial software product MacDraw™ (a simple and convenient process). Scheduling for this particular illustration has assumed a two-crew operation; one to follow the moon, the other to follow LAGEOS. Each crew takes the other target to be a target of opportunity, when applicable. The large open rectangles represent the suggested lunar crew coverage; the small open rectangles (within the large open rectangles) represent the LAGEOS passes which should be accessible to the lunar crew as a target of opportunity. The large filled rectangles represent the suggested LAGEOS crew coverage. It is especially important to again note that the scheduling part of this software tool is not automatic; it is accomplished manually by a human scheduler after the software tool has done its work in producing the various time-lines.

Conclusions

Although simple in concept (but a little tougher in the original implementation) this software tool now proves to be invaluable to us for the quick and easy scheduling of MLRS laser ranging operations. Listing 1 depicts the actual FORTRAN code now in use. This code can be made available in Apple® Macintosh™ 3 1/2-inch disk format; upon request, for individuals who might wish to implement it on their own systems. Note that station coordinates and local time modifications would need to be made in order to incorporate the system at other installations.

Without too much difficulty the code for this tool can be modified to run with almost any FORTRAN-capable system. As proof of this fact, we have already ported this code (with only very minor changes) for running on an IBM® PC/AT™ (see Figure 3 for sample output). Although this version does not have access to the special lunar phase characters which are available with the Apple® Macintosh™ version, nor is it as yet amenable to the convenient manual insertion of specific crew scheduling information via a MacDraw type of software interface, the output is quite satisfactory and eminently useful. The output shown in Figure 3 was printed on an Apple Laser Writer after the original test file was ported to a VAX 11/780. Very satisfactory results are also obtained by using a standard dot-matrix printer. This IBM®

PC/AT™ version should also be available, on request, to interested users in appropriate machine-readable form in the very near future.

Acknowledgements

I cannot too strongly acknowledge and thank Richard J. Eanes of the University of Texas Department of Aerospace Engineering and Center for Space Research and the work which he had performed on the original LAGEOS visibility package. Many thanks also go to Jerry Wiant, Randy Ricklefs, Windy Williams, and Robert Gonzalez (all associated with MLRS laser ranging operations at McDonald Observatory) for all of their inputs, which have made this tool so much more valuable to our operations. This research is being supported at McDonald Observatory and the University of Texas at Austin by National Aeronautics and Space Administration Contract NAS5-29404 out of Goddard Space Flight Center, Robert L. Appler, Technical Officer.

Sep 1986

| CST | 1 | 2 | 3 | 4 | 5 | 6 | 7 | 8 | 9 | 10 | 11 | N | 1 | 2 | 3 | 4 | 5 | 6 | 7 | 8 | 9 | 10 | 11 | M | 1 | |
|-----|----|---|---|---|----|----|----|----|----|----|----|----|----|----|----|----|----|----|---|---|---|----|----|----|---|--------|
| UT | 6 | 7 | 8 | 9 | 10 | 11 | 12 | 13 | 14 | 15 | 16 | 17 | 18 | 19 | 20 | 21 | 22 | 23 | 0 | 1 | 2 | 3 | 4 | 5 | 6 | UT |
| CST | M | 1 | 2 | 3 | 4 | 5 | 6 | 7 | 8 | 9 | 10 | 11 | N | 1 | 2 | 3 | 4 | 5 | 6 | 7 | 8 | 9 | 10 | 11 | M | 1 |
| M | 1 | | | | | | | | | | | | | | | | | | | | | | | | | 23/27 |
| | | | | | | | | | | | | | | | | | | | | | | | | | | |
| T | 2 | | | | | | | | | | | | | | | | | | | | | | | | | 19/28 |
| W | 3 | | | | | | | | | | | | | | | | | | | | | | | | | 13/29 |
| T | 4 | | | | | | | | | | | | | | | | | | | | | | | | | 7/ 1 |
| F | 5 | | | | | | | | | | | | | | | | | | | | | | | | | 1/ 1 |
| S | 6 | | | | | | | | | | | | | | | | | | | | | | | | | -5/ 2 |
| S | 7 | | | | | | | | | | | | | | | | | | | | | | | | | -11/ 3 |
| M | 8 | | | | | | | | | | | | | | | | | | | | | | | | | -17/ 4 |
| T | 9 | | | | | | | | | | | | | | | | | | | | | | | | | -22/ 6 |
| W | 10 | | | | | | | | | | | | | | | | | | | | | | | | | -26/ 7 |

Figure 1. Standard Output (via Microsoft Word).

Sep 1986

| CST | 1 | 2 | 3 | 4 | 5 | 6 | 7 | 8 | 9 | 10 | 11 | N | 1 | 2 | 3 | 4 | 5 | 6 | 7 | 8 | 9 | 10 | 11 | M | 1 | |
|-----|----|---|---|---|----|----|----|----|----|----|----|----|----|----|----|----|----|----|---|---|---|----|----|----|---|--------|
| UT | 6 | 7 | 8 | 9 | 10 | 11 | 12 | 13 | 14 | 15 | 16 | 17 | 18 | 19 | 20 | 21 | 22 | 23 | 0 | 1 | 2 | 3 | 4 | 5 | 6 | UT |
| CST | M | 1 | 2 | 3 | 4 | 5 | 6 | 7 | 8 | 9 | 10 | 11 | N | 1 | 2 | 3 | 4 | 5 | 6 | 7 | 8 | 9 | 10 | 11 | M | 1 |
| M | 1 | | | | | | | | | | | | | | | | | | | | | | | | | 23/27 |
| | | | | | | | | | | | | | | | | | | | | | | | | | | |
| T | 2 | | | | | | | | | | | | | | | | | | | | | | | | | 19/28 |
| W | 3 | | | | | | | | | | | | | | | | | | | | | | | | | 13/29 |
| T | 4 | | | | | | | | | | | | | | | | | | | | | | | | | 7/ 1 |
| F | 5 | | | | | | | | | | | | | | | | | | | | | | | | | 1/ 1 |
| S | 6 | | | | | | | | | | | | | | | | | | | | | | | | | -5/ 2 |
| S | 7 | | | | | | | | | | | | | | | | | | | | | | | | | -11/ 3 |
| M | 8 | | | | | | | | | | | | | | | | | | | | | | | | | -17/ 4 |
| T | 9 | | | | | | | | | | | | | | | | | | | | | | | | | -22/ 6 |
| W | 10 | | | | | | | | | | | | | | | | | | | | | | | | | -26/ 7 |

Figure 2. Manually Amended Output (via MacDraw).


```

PROGRAM PASFRE
C
C...PROGRAM TO PREDICT THE TIMES OF SATELLITE PASSES AND THE
C LOCATION OF THE SUN AND MOON DURING THE PASSES
C
C...PROGRAMMED BY: RICHARD JAMES, CENTER FOR SPACE RESEARCH,
C DEPT. OF AEROSPACE ENG. AND ENG. MECHANICS,
C UNIVERSITY OF TEXAS AT AUSTIN
C
C...VERSION OF 13 JUN 83
C
C...Amended by Peter J. Shelus to MacFortran Capability for MLRS crew
C scheduling.
C...April, 1985
C

```

```

DOUBLE PRECISION JD, JDP
DOUBLE PRECISION XMJD, XMJDF, XMJD1, XMJD2, DO, D
REAL LUN, LUNMAG, LUNAE, LUNEL, LUNRBO, LUNST, LUNLON,
1 LUNLAT
logical deprin1, deprin2
real sunup1, sunup2, lunup1, lunup2, lagup1, lagup2
integer dayid
character*1 idow, moonsym, axel(2), idays(7)
character*4 sun, sun, lag, up, dn
character lunin(121), sunin(121), lagin(122)
DATA idays /'M', 'T', 'F', 'S', 'S', 'M', 'T'/
DATA deprin1/.FALSE./, deprin2/.FALSE./
DATA sun/'moon'/, sun/'sun' /, lag/'lago' /, up/'up' /, dn/'down'/
DIMENSION LUN(3), STALUN(3)
DIMENSION SUN(3), SAT(3)
DIMENSION STASAT(3), STASUN(3), STA(2), IMDY1(5), IMDY2(5)
DIMENSION IMDY3(5), IMDY4(5), IMDY5(5)
DATA ELAST /-99999./, NPT /0/
DATA TRASS /0/
DATA DTMIN /12./, XMJDF /46247.25/
DATA ELMIN /20./
DATA SUNLIM /5./
DATA RE /6378137./, FINV /298.255/
C...McDonald Observatory, Fort Davis, Texas
DATA STAE, STALON, STALAT /1963.344, 255.984083795, 20.676976609/
DATA STA(1) /0./
DATA IMAX / 9999999999999 /, DAYMAX / 10. /
DATA RAD /0.0174532925199433/
DATA DEG /57.295779513082 /
DATA PI /3.14159265358979/
DATA TMOPI /6.2831853071796/
DATA CLITE /299792458./
C
C...SATELLITE EPHEMERIS
DATA DO /2442905.5/
C XMO, XMI ARE EPICYCLIC VALUES RATES (DEG/DAY) FOR TRUE OF DATE NODE
C XLO, XLI ARE FOR ANG OF LATITUDE (PERT+MEAN)
C XMO, XMI ARE FOR TRUE OF DATE PERIAPSE
C XMO, XMI ARE FOR MEAN ANOMALY
C NOTE: PERIODIC PERTURBATIONS ON PERIAPSE AND MEAN ANOMALY CAN
C BE SEVERAL DEGREES, BUT IN ANG OF LATITUDE THEY ARE AROUND
C TENTHS OF DEGREES.
C...JD=2442905.5
DATA XMO, XMI / 29.5672, 0.34256/
DATA XLO, XLI /223.195, 2298.9763/
DATA XMO, XMI /259.235, -0.2126/
DATA XMO, XMI /223.860, 2299.1889/
DATA XINCL /109.845/
DATA ECC / 0.0046 /
DATA ASAT /12.2726/
C

```

```

C-----
C This is a temporary 'read & write' test patch!
C
OPEN (UNIT=2, FILE='CALENDAR')
REWIND 2
11 call covers (jmo, jmo, iyr, XMJDF, DAYMAX, deprin2)
if (deprin2) then
OPEN (UNIT=3, FILE='EAMES.OUT')
REWIND 3
endif
dayid=1
hymoon=0.0
maxelct=3
DTDAY = DTMIN/1440.
CALL SHADMO
C
C...CONVERT ANGLES TO RADIANS
XMO = XMO*PI/180
XMI = XMI*PI/180
XLO = XLO*PI/180
XLI = XLI*PI/180
XMO = XMO*PI/180
XMI = XMI*PI/180
XINCL = XINCL*PI/180
COSI = COS(XINCL)
SINI = SIN(XINCL)
CLTST = COS(STALAT*PI/180)
SLTST = SIN(STALAT*PI/180)
CLNST = COS(STALON*PI/180)
SLNST = SIN(STALON*PI/180)
IF (STA(1).NE.0.) GO TO 5
FLAT = 1./FINV
ESQUAR = FLAT*(2.-FLAT)
XMS = RE/SQRT(1.-ESQUAR*SLTST**2)
XNFB = XMS + STAE
STA(1) = XNFB*CLTST*CLNST
STA(2) = XNFB*CLTST*SLNST
STA(3) = (XNFB-ESQUAR*XMS)*SLTST
5 CONTINUE
C
C...DATE LOOP
call time (itzero)
I = 0
10 I = I + 1
IF (I.GT.IMAX) GO TO 20
C...DATES BY SEARCH AT DTMIN (MINUTES) SPACING FROM XMJDF
DELDAY = (I-1)*DTDAY
IF (DELDAY.GT. DAYMAX) GO TO 20
XMJD = XMJDF + DBLE(DELDAY)
C
C...COMPUTE TOPOCENTRIC SATELLITE AND SUN VECTORS
JD = XMJD + 2400000.500
D = JD - DO
C
C...GREENWICH HOUR ANGLE, OR SIDEREAL TIME AT 0 DEG LONG.
TRETAG = RAOC(JD, TRETAD)
COSTE = COS(TRETAG)
SINTB = SIN(TRETAG)
C
C...SATELLITE COORDS IN TRUE OF DATE SYSTEM
XM = XMO + XMI*D
XL = XLO + XLI*D

```

```

XM = AMOD(XM, TMOPI)
XL = AMOD(XL, TMOPI)
XM = AMOD(XM, TMOPI)
IF (XM.LT.0.) XM = XM + TMOPI
IF (XL.LT.0.) XL = XL + TMOPI
IF (XM.LT.0.) XM = XM + TMOPI
XL = XL + 2.*ECC*SIN(XM)
COSM = COS(XM)
SINM = SIN(XM)
SLAM = SIN(XL)
CLAM = COS(XL)
SATMAG = (1. - ECC*COS(XM))*ASAT
SAT(1) = (COSM*CLAM - SINM*COSI*SLAM)*SATMAG
SAT(2) = (SINM*CLAM + COSM*COSI*SLAM)*SATMAG
SAT(3) = (SINI*SLAM)*SATMAG
C
C...ROTATE ABOUT X AXIS TO GET (PSUEDO)BODY FIXED POSITION
CALL XROT(SAT, COSTE, SINTB)
C
C...GET TOPOCENTRIC SATELLITE POSITION
CALL TOPO(SAT, STA, STASAT, CLTST, SLTST, CLNST, SLNST, SATAT, SATEL,
1 SATRO)
c IF (SATEL.LT.ELMIN) GO TO 10
SATRO = (2.*SATRO/CLITE)*1000.
C
C...GET SATELLITE LATITUDE, LONGITUDE, AND HEIGHT
CALL GTRAK (SAT, SATMAG, RE, ESQUAR, SATST, SATLON, SATLAT)
C
C...GET THE SOLAR AND LUNAR POSITION VECTORS IN THE MEAN OF DATE
C EQUATOR AND EQUINOX SYSTEM.
CALL SUNLUN (JD, SUN, LUN)
SUNMAG = SQRT(SUN(1)**2 + SUN(2)**2 + SUN(3)**2)
LUNMAG = SQRT(LUN(1)**2 + LUN(2)**2 + LUN(3)**2)
C
C...ROTATE ABOUT X TO GET SUN AND MOON IN (PSUEDO)BODY FIXED SYSTEM
C...REMEMBER THIS PROGRAM NEGLECTS NUTATION AND POLAR MOTION
CALL XROT(SUN, COSTE, SINTB)
CALL XROT(LUN, COSTE, SINTB)
C
C...GET SUB-SUN POINT ON THE EARTH
CALL GTRAK (SUN, SUNMAG, RE, ESQUAR, SUNST, SUNLON, SUNLAT)
CALL GTRAK (LUN, LUNMAG, RE, ESQUAR, LUNST, LUNLON, LUNLAT)
C
C...GET TOPOCENTRIC SUN AND MOON COORDINATES
CALL TOPO(SUN, STA, STASUN, CLTST, SLTST, CLNST, SLNST, SUNAE, SUNEL,
1 SUNRBO)
CALL TOPO(LUN, STA, STALUN, CLTST, SLTST, CLNST, SLNST, LUNAE, LUNEL,
1 LUNRBO)
AGELUN = (LUNLON-SUNLON)*29.330539/360.
IF (AGELUN.LT. 0.) AGELUN = AGELUN + 29.330539
IF (AGELUN<-1.845659.AND.AGELUN>-27.684880) moonsym=' '
IF (AGELUN<-1.845659.AND.AGELUN<-5.536976) moonsym=' '
IF (AGELUN<-5.536976.AND.AGELUN<9.228293) moonsym=' '
IF (AGELUN<9.228293.AND.AGELUN<12.919611) moonsym=' '
IF (AGELUN<12.919611.AND.AGELUN<16.610928) moonsym=' '
IF (AGELUN<16.610928.AND.AGELUN<20.302248) moonsym=' '
IF (AGELUN<20.302248.AND.AGELUN<23.993563) moonsym=' '
IF (AGELUN<23.993563.AND.AGELUN<27.684880) moonsym='g'
if (LUNEL>hymoon) then
declun=ASIN(LUN(3)/LUNMAG)*DEG
lunde=INT(declun+0.5)
hymoon=LUNEL
AGELUN = (LUNLON-SUNLON)*29.330539/360.
IF (AGELUN.LT. 0.) AGELUN = AGELUN + 29.330539
lunage=INT(AGELUN+0.5)
endif
c...Monitor rising and setting times of all three objects*****
c...Initialize parameters if this the first time through:
if (I=1) then
lunup2=LUNEL
sunup2=SUNEL
lagup2=SATEL
write(9,1001) LUNEL, SUNEL, SATEL
lunlin(1)=' '
lagin(1)=' '
sunlin(1)=' '
if (LUNEL>ELMIN) lunlin(1)=moonsym
if (SATEL>ELMIN) lagin(1)='0'
1001 format('LUNEL=',F10.5,'; SUNEL=',F10.5,'; SATEL=',F10.5)
call prepape(jmo, iyr)
else
c...Come here for second time and later returns:
lunup1=lunup2
lunup2=LUNEL
sunup1=sunup2
sunup2=SUNEL
lagup1=lagup2
lagup2=SATEL
if (lunup1<ELMIN.AND.lunup2>ELMIN) write(9,9) I, XMJD, sun, up
if (sunup1<ELMIN.AND.sunup2>ELMIN) write(9,9) I, XMJD, sun, dn
if (sunup1>0.0.AND.sunup2<0.0) write(9,9) I, XMJD, sun, dn
if (lagup1<ELMIN.AND.lagup2>ELMIN) write(9,9) I, XMJD, lag, up
if (lagup1>ELMIN.AND.lagup2<ELMIN) then
write(9,9) I, XMJD, lag, dn
maxelag=IFIX(ELMAX*0.5)
call convert(maxelag, axel)
maxelct=1
endif
9 format('I = ',16,'; XMJD = ',F15.5,'; ',A4,' is ',A4,'.')
k=mod(I,120)
if (k>1) then
lunlin(k)=' '
if (maxelct>2) lagin(k)=' '
sunlin(k)=' '
if (LUNEL>ELMIN) lunlin(k)=moonsym
if (SATEL>ELMIN.AND.maxelct>2) lagin(k)='0'
if (maxelct=1) then
lagin(k)=axel(1)
lagin(k+1)=axel(2)
endif
if (SUNEL>0.0) sunlin(k)='0'
if (mod(k,3)=1) sunlin(k)='|'
elseif (k=0) then
lunlin(120)=' '
if (maxelct>2) lagin(120)=' '
sunlin(120)=' '
if (LUNEL>ELMIN) lunlin(120)=moonsym
if (SATEL>ELMIN.AND.maxelct>2) lagin(120)='0'
if (maxelct=1) then
lagin(120)=axel(1)
lagin(121)=axel(2)
endif
if (SUNEL>0.0) sunlin(120)='0'
if (mod(k,3)=1) sunlin(120)='|'
elseif (k=1) then
lunlin(121)=' '
if (maxelct>2) lagin(121)=' '
sunlin(121)=' '
if (LUNEL>ELMIN) lunlin(121)=moonsym
if (SATEL>ELMIN.AND.maxelct>2) lagin(121)='0'

```

```

laglin(121)=max(1)
laglin(122)=max(2)
else
laglin(122)=-
endif
if(SUNEL>0.0) sunlin(121)='0'
if(mod(k,5)-1) sunlin(121)='1'
write(2,106) lunlin, lundec, lunage
write(2,108) ldown, dayid, sunlin
write(2,109) laglin
write(2,107)
106 format(5x,121a1,14,'/',12)
107 format(' ')
108 format(a1,13,1x,121a1)
109 format(5x,122a1)
call prtym(itzero,dayid,DAYMAX)
hyscom=0.0
if (dayid=0.0R.dayid=20) then
call postage
call prepage(jmo,lyr)
endif
if (dayid=1st(DAYMAX)) then
call postage
endif
ldown=days(mod(idint(XMJD),7)+1)
dayid=dayid+1
lunlin(1)=' '
laglin(1)=' '
sunlin(1)=' '
if(LUNEL>ELMIN) lunlin(1)=moonsyn
if(SATEL>ELMIN) laglin(1)='0'
if(SUNEL>0.0) sunlin(1)='0'
if(mod(k,5)-1) sunlin(1)='1'
endif
maxelct=maxelct+1
endif
if (SATEL.LT.ELMIN) GO TO 10
C.....
if(deprin) then
c2345678912345678921234567893123456789412345678951234567896123456789712
C...First de=bug print (20 April)
WRITE(9,1)I,DELDAY,SATEL, XMJD,SUNEL,JD,LUNEL,D,THETAG
1 FORMAT('I',16,2X,'DELDAY=',F15.5,' SATEL=',F15.5/
2 15X,'XMJD ',F15.5,' SUNEL=',F15.5/
3 15X,'JD ',F15.5,' LUNEL=',F15.5/
4 15X,'D ',F15.5,' THETAG=',F15.5)
C READ(9,2)CINPOT
2 FORMAT(F10.5)
C...End of first de=bug print (20 April)
endif
C.....
C...CHECK FOR A NEW PASS
IF (ABS(D-DLAST)=1440. .LT. 30.) GO TO 15
IF (NPT.EQ.0) GO TO 30
C
C...PASS COMPLETED, PRINT SUMMARY.
IPASS = IPASS + 1
SUNELA = SUNELA/NPT
AMJDP = AMJDP/NPT
UTP = AMJDP - AINT(AMJDP)
SOLTA = UTP*24. + STALON/15.
SOLTA = ANCD(SOLTA,24.1)
PTIME = (XMJD2-XMJD1)*1440.
IMAXEL = ELMAX + 0.5
if(deprin) then
JDP = DBLE(XMJD1) + 2400000.500
CALL KALDAY(JDP,IMDY1,XSEC1,MONTE1)
JDP = DBLE(XMJD2) + 2400000.500
CALL KALDAY(JDP,IMDY2,XSEC2,MONTE2)
C WRITE(9,320) IPASS, AMJDP, IMDY1(3)-1900, IMDY1(1), IMDY1(2),
C 1 IMDY1(4), IMDY1(5), IMDY2(4), IMDY2(5), PTIME, NPT,
C 2 SUNELA, SOLTA
C 320 FORMAT (/1X,'PASS ',I4,F12.4,2X,3I2,1X,2I2,1X,2I2,F6.2,14,
C 2F10.3)
write(3,310) IMDY1(3)-1900, MONTE1, IMDY1(2), IMDY1(4), IMDY1(5),
1 IMDY2(4), IMDY2(5), AMJDP
C WRITE(1,340) IMDY1(3), IMDY1(1), IMDY1(2), IMDY1(4), IMDY1(5),
C 1 IMDY2(4), IMDY2(5), IMAXEL
C 340 FORMAT (1X,14,1X,13,1X,13,1X,13,1X,13,1X,13,1X,13)
310 FORMAT (/1X,'PASS OF ',12,1X,A3,1X,12,' BEGIN ',12,13,
1 ' END ',12,13,4X,' MID-MJD ',F12.4)
write(3,315) A11, ELL, A12, ELL
315 FORMAT (3X,'SATELLITE AT AND EL AT RISE = ',2F7.2,3X,
1 ' SET = ',2F7.2)
write(3,316) BALUN1, BALUN2, ACELUN
316 FORMAT (3X,'LUNAR HOUR ANGLE AT RISE AND SET = ',2F7.2,
1 2X,' LUNAR AGE = ',F7.2,' DAYS')
write(3,317) SUNELA, SOLTA
317 FORMAT (3X,'SUN ELEVATION = ',F10.3,3X,' LOCAL MEAN ',
1 ' TIME = ',F10.3,' HOURS')
JDP = DBLE(TEMAX) + 2400000.500
CALL KALDAY(JDP,IMDY3,XSEC3,MONTE3)
write(3,600) IMDY3(4), IMDY3(5), ELMAX
600 FORMAT (3X,'TIME OF MAX EL (2E HM) = ',12,13,3X,
1 ' MAX EL = ',F6.2,' DEG')
IF (DLIT2.LT.0.) GO TO 30
JDP = DBLE(DLIT1) + 2400000.500
CALL KALDAY(JDP,IMDY4,XSEC4,MONTE4)
JDP = DBLE(DLIT2) + 2400000.500
CALL KALDAY(JDP,IMDY5,XSEC5,MONTE5)
write(3,601) IMDY4(4), IMDY4(5), IMDY5(4), IMDY5(5)
601 FORMAT (3X,'SATELLITE IS SUNLIT FROM ',12,13,' TO ',
1 12,13)
IF (DBURN.GE.0.) write(3,602)
602 FORMAT (3X,'SATELLITE TOO CLOSE TO SUN AT SOME POINT IN THE',
1 ' PASS',/)
endif
C
C...BEGIN A NEW PASS
30 CONTINUE
NPT = 0
AMJDP = 0
SUNELA = 0.
XMJD1 = XMJD
A11 = SATEL
E11 = SATEL
C BALUN1 = (STALON-LUNLON)/14.492
BALUN1 = (STALON-LUNLON)/15.
IF (BALUN1.LT.-12.) BALUN1 = BALUN1 + 24.
IF (BALUN1.GT.12.) BALUN1 = BALUN1 - 24.
C
C...GET AGE OF MOON AT PASS START.
ACELUN = (LUNLON-SUNLON)*29.530539/360.
IF (ACELUN.LT.0.) ACELUN = ACELUN + 29.530539
ELMAX = 90.
DLIT1 = 999999.
DLIT2 = -999999.
DBURN = -999999.
C
C...NOT A NEW PASS
15 DLAST = D

```

```

A12 = SATEL
E12 = SATEL
C BALUN2 = (STALON-LUNLON)/14.492
BALUN2 = (STALON-LUNLON)/15.
IF (BALUN2.LT.-12.) BALUN2 = BALUN2 + 24.
IF (BALUN2.GT.12.) BALUN2 = BALUN2 - 24.
NPT = NPT + 1
FJD = SNGL(JD)
SUNELA = SUNELA + SUNEL
AMJDP = AMJDP + XMJD
C
C...GET MAX ELEVATION POINT
IF (SATEL.GT.ELMAX) ELMAX = SATEL
IF (SATEL.EQ.ELMAX) TEMAX = XMJD
C
C...SUN AND SATELLITE GEOMETRY
CALL SBADOM(SAT,SATMAC,SUN,SUNMAC,SEFRAC,RSUN,RSUN1,RSUN2)
SATSUM = ACOS(STASAT(1)*STASUN(1) + STASAT(2)*STASUN(2)
1 + STASAT(3)*STASUN(3))*DEG
C
C...FIND INTERVAL DURING WHICH SATELLITE IS SUNLIT
IF (SEFRAC.LT.0.) GO TO 16
IF (XMJD.LT.DLIT1) DLIT1 = XMJD
IF (XMJD.GT.DLIT2) DLIT2 = XMJD
16 CONTINUE
C
C...IS SATELLITE TOO CLOSE TO THE SUN
IF (SATSUM.LT.SUNLIM) DBURN = XMJD
C
C...RECYCLE
GO TO 10
C
C 20 CONTINUE
write(9,101)
101 format('This session is over. However your job is not totally'//
1 'done. The print file now must be properly formatted using'//
2 'WORD. Once you have file CALENDAR in WORD, do the following:'//
3 ' 1. choose WIDE in the PAGE SETUP section under FILE;'//
4 ' 2. change all the MARGINS to 0.5 (except for GUTTER);'//
5 ' 3. under FORMAT, choose the 9-point COURIER font;'//
6 ' 4. insert page breaks (SHIFT-ENTER) at the 10 and'//
7 ' 20 day calendar lines during each month and at the'//
8 ' end of each month.'//
9 'That's all there is. Press RETURN and then open WORD to begin'//
10 'the re-formatting process.'//
11 'If you asked for a LAGEOS summary print-out, you'll find it'//
12 'in the file named "LANES.OUT"')
accept lyr
END
subroutine cheknd(answer)
character*1 answer
write(9,101)
1 type(9,102)
101 format('Do you need a LAGEOS summary print-out'//
1 ' (Answer "Y" or "N")')
102 format(' Enter your choice here (followed by a RETURN)--->')
103 format('You typed a ',A1/
1 'I expected Y or N. Try again')
accept answer
if(answer='Y'.OR.answer='y'.OR.answer='N'.OR.answer='n')return
write(9,103)answer
go to 1
end
subroutine cnvrt(i,c)
character*1 c(2)
if (i>9 .AND. i<100) then
i1=i/10
i2=i-10
c(1)=CHAR(i1+48)
c(2)=CHAR(i2+48)
else
c(1)=' '
c(2)=' '
write(9,101)
101 format('Call to CNVRT with out of range Argument, i =',I6,')')
endif
return
end
subroutine prtym(itzero,lday,DAYMAX)
call time(41)
ihrl=int(it/3600.)
ian1=int((it-ihrl*3600.)/60+0.5)
elapsd=REAL(it-itzero)/60.0
togo=elapsd/REAL(lday)*(DAYMAX-REAL(lday))
finished=REAL(it)+togo*60.
ihrl=int(finished/3600.)
ian2=int((finished-ihrl*3600.)/60+0.5)
write(9,101)lday,elapsd,togo,ihrl,ian1,ihrl,ian2
101 format('Computations for day ',I2,' have just been completed.'//
1 'Elapsed time : ',F5.1,' minutes.'//
2 'Est.time to go: ',F5.1,' minutes.'//
3 'Time right now: ',I2,'.',I2//
4 'Est.comp.time : ',I2,'.',I2)
return
end
SUBROUTINE SUNLON (TJD, XS, XM)
C
C...GET MEAN OF DATE EQUATOR AND EQUINOX SOLAR AND LUNAR POSITION
C VECTORS FROM BROWNS LUNAR THEORY
C
DOUBLE PRECISION TJD
DIMENSION XS(3), XM(3), ARG(5)
DATA LUNPRE /2/
C
CALL DIANA (TJD, LUNPRE, XM, ARG)
C
C...GET SOLAR ORBIT ELEMENTS
AUS = 1.496E11
ECS = 0.01673104 - 0.1144422E-8*(TJD-2415020.000)
XIS = 0.
CAPOMS = 0.
PERIS = ARG(5)
XMS = ARG(2) - ARG(5)
C
C...CONVERT ORBIT ELEMENTS TO POSITION VECTOR
CALL KEP (AUS, ECS, XIS, PERIS, CAPOMS, XMS, XS)
C
C...ROTATE ECLIPTIC ELEMENTS INTO EQUATORIAL SYSTEM
CALL ECLEQ (XS, TJD)
CALL ECLEQ (XM, TJD)
C
RETURN
END
subroutine convers(imo,jmo,lyr,xmjdf,daymax,deprin2)
double precision xmjdf
character*1 jmo
character*1 answer
logical leap,deprin2
write(9,101)
type(9,102)
accept imo
write(9,103)

```

```

accept iyr
C...Check if "long Zanes-type print-out" is desired
call chetend(answer)
if(answer='Y'.OR.answer='y') deprin2=TRUE.
write(9,105)
101 format('MRS Observing Crew Scheduling Calendar Program'///
1 'Enter the month for which a calendar is desired.'//
2 '(1-Jan, 2-Feb, 3-Mar, ..., 12-Dec) /
3 '(Complete your entry by pressing RETURN)')
102 format('Your choice-->' )
103 format('///
1 'Enter the year for which the calendar is desired.'//
2 '(A 4-digit number is desired, i.e., 1984, 1985, etc)'/
3 '(Complete your entry by pressing RETURN)')
104 format('Your choice-->' )
105 format('///Thank you!///
1'This should take about 30 minutes. Go and have a cup of coffee!')
SELECT CASE (imo)
case (1) jmo='Jan'
case (2) jmo='Feb'
case (3) jmo='Mar'
case (4) jmo='Apr'
case (5) jmo='May'
case (6) jmo='Jun'
case (7) jmo='Jul'
case (8) jmo='Aug'
case (9) jmo='Sep'
case (10) jmo='Oct'
case (11) jmo='Nov'
case (12) jmo='Dec'
END SELECT
leap=.FALSE.
if(mod(iyr,4)=0.AND.mod(iyr,100)NE.0)leap=.TRUE.
if(imo=2.AND.leap)then
daymax=29
elseif(imo=4.AND.NOT.leap)then
daymax=28
elseif(imo=4.OR.imo=6.OR.imo=9.OR.imo=11)then
daymax=30
else
daymax=31
endif
xjdf=367*iyr-7*(iyr+(imo+9)/12)/4-3*((iyr+(imo-9)/7)/100+1)/4
+275*imo/9+1+1721029-2400000.75
write(9,201)xjdf
201 format('///XJDFF =',F9.2)
return
subroutine prepape(jmo,yjr)
character*3 jmo
integer yjr
C...Prepare and print 'month and year' header, then skip a line.
write(2,101)jmo,yjr
write(2,102)
101 format('M, J, A, S, O, N, D')
102 format(' ')
C...Print CDT, UT, and CST lines, then skip a line.
call cdline
call utline
call cstline
write(2,103)
C...Return to call routine
return
end
subroutine postape
C...Print CST, UT, and CDT lines.
call cdline
call utline
call cstline
return
C...Return to call routine
return
end
subroutine cdline
C...Prepare and print 'CDT' line
type(2,103)
do 10 i=2,11
10 type(2,104)i
type(2,105)
do 20 i=1,11
20 type(2,104)i
write(2,106)
103 format(' CDT 1')
104 format(' N')
105 format(' M 1 CDT')
return
end
subroutine utline
C...Prepare and print 'UT' line
type(2,103)
do 10 i=7,23
10 type(2,104)i
do 20 i=4,6
20 type(2,104)i
write(2,105)
103 format(' UT 6')
104 format(' 15')
105 format(' UT')
return
end
subroutine cstline
C...Prepare and print 'CST' line
type(2,103)
do 10 i=1,11
10 type(2,104)i
type(2,105)
do 20 i=1,11
20 type(2,104)i
write(2,106)
103 format(' CST M')
104 format(' 15')
105 format(' N')
106 format(' M CST')
return
end
SUBROUTINE DIANA( DATE, EXACT, XE, ANGLE )
C...COMPUTES GEOCENTRIC COORDINATES OF THE MOON BY ILL
C LUNAR THEORY
C...PRECISION= 2. SEC. OF ARC IN LONGITUDE (WHEN EXACT=4)
C 1. SEC. OF ARC IN LATITUDE (WHEN EXACT=4)

```

```

C...INPUT PARAMETERS
C DATE JULIAN DAY IN EPOCHERIS TIME (DOUBLE PRECISION)
C EXACT INTEGER NUMBER -1,2,3,4 FOR PRECISION
C 4 WILL BE THE MOST ACCURATE
C...OUTPUT PARAMETER
C XE THE POSITION OF THE MOON WITH RESPECT TO ECLIPTIC SYSTEM
DOUBLE PRECISION DATE
DIMENSION XE(3), ANGLE(5), IX(4), X(61), IY(4), Y(48),
$ IX(4,20), X(20), IX(10), IX(4,10), IX(13), IX(4,13), SERX(61),
$ SERX(48), SERN(10), SERG(13), SERI(3), NG(4), NX(4), NY(4),
$ NX(4), NN(4), ADD(3)
INTEGER SERX, SERX, SERI, SERN, SERG, EXACT
DATA RAD /0.0174532925199433/
DATA PI /3.1415926535897/
DATA TMOP1 /6.2831853071796/
DATA SECRAD /4.8481368110945E-6/
DATA AE /6378137./
C...SUPPLY DATE (JULIAN DATE+DECIMAL OF THE DAY) AND EXACT (1 TO 4)
DATA NX/6,21,39,61/, NY/4,13,23,48/, NZ/1,4,10,30/,
$ NN/3,7,10,10/, NG/0,0,2,13/
DATA SERX/78,3,25,15,53,26,32,6,16,40,21,32,54,103,109,
$ 9,70,27,41,14,59,64,39,24,2,71,84,110,78,58,47,77,46,
$ 90,108,32,34,187,60,31,79,85,95,96,116,5,149,17,124,118,
$ 193,129,125,72,83,89,135,69,102,150/
DATA SERI/410,412,398,423,408,481,460,425,456,458,479,397,579,
$ 563,434,414,427,438,456,494,457,436,469,421,400,409,477,
$ 518,509,483,370,511,406,464,544,413,399,444,411,581,516,
$ 432,513,548,549,492,424,550/
DATA SERN/787,789,792,793,795,791,796,790,788,794/
DATA SERG/669,721,737,678,700,717,641,709,642,723,650,
$ 633,733/
DATA SERX/808,809,803,823,807,816,831,836,820,830,893,
$ 859,810,815,825,814,824,822,802,835,837,834,871,860,
$ 849,846,865,842,888,832/
DATA IX/1,0,0,0, 1,0,0,-2, 0,0,0,2, 2,0,0,0, 0,+1,0,0,
$ 0,0,2,0, 2,0,0,-2, 1,1,0,-2, 1,0,0,2, 0,1,0,-2, 1,-1,
$ 0,0,0,0,1, 1,1,0,0, 0,0,2,-2, 1,0,2,0, 1,0,-2,0,
$ 1,0,0,-4, 3,0,0,0, 2,0,0,-2, -1,1,0,-2, 0,1,0,2, 1,0,0,-1,
$ 0,1,0,1,1, -1,0,2, 2,0,0,2, 0,0,0,4, 3,0,0,-2, 2,-1,0,0,
$ 1,0,-2,-2, 2,1,0,-2, 1,0,0,1, 0,2,0,-2, 2,1,0,0, 0,2,0,0,
$ 1,2,0,-2, 1,0,-2,2, 0,0,2,2, 1,1,0,-4, 2,0,2,0, 1,0,0,-3,
$ 1,1,0,2, 2,1,0,-4, 2,-1,0,-2, 1,-2,0,0, 1,-2,0,-2, 0,1,
$ 2,-2, 2,1,0,0, 0,1,0,-4, 2,0,0,-1, 0,1,-2,2,
$ 2,0,-2,0, 1,1,0,2, 2,0,0,-2, 3,0,0,-4, 2,-1,0,2, 1,2,0,0,
$ 1,-1,0,-1, 3,0,0,2, 1,0,2,2, 4,0,0,-2/
DATA IY/1,0,0,0, 1,0,0,-2, 0,0,0,2, 2,0,0,0, 1,0,0,2,
$ 1,1,0,-2, 0,1,0,-2, 2,0,0,-2, -1,1,0,0, 0,1,0,0, 1,1,
$ 0,0,0,0,1, -1,0,2,0, 0,0,2,-2, 3,0,0,0, 1,0,0,-4,
$ 2,0,0,4, 2,1,0,2, -1,0,2, -1,1,0,2, 0,1,0,1, 3,0,
$ 0,-2, 0,2,0,0, 2,0,0,0, 0,0,0,4, 1,0,0,1, 1,1,0,2,
$ 2,-1,0,0, 2,1,0,0, 1,1,0,-4, 1,0,2,-2, 2,1,0,-2, 1,0,
$ 0,4, 0,1,0,-4, 1,2,0,-2, 1,0,0,-3, 0,0,0,3, 4,0,0,0,
$ 1,0,0,-1, -1,0,2,-2, 2,-1,0,2, 3,0,0,2, 2,1,0,-4, -1,
$ 2,0,2, -1,2,0,0, -1,1,0,4, 2,0,0,-1, -1,2,0,-3/
DATA IZ/1,0,0,0, 1,0,0,-2, 0,0,0,2, 2,0,0,0, 1,0,0,2,
$ 1,1,0,-2, 1,1,0,0, -2, 1,1,0,0, 0,0,0,1, 1,1,0,0, 1,0,
$ -2,0, 3,0,0,0, 1,0,0,-4, 0,1,0,0, 2,0,0,-4, 0,1,0,2,
$ 2,0,0,-2, 2,0,0,2, 0,0,0,4, 1,-1,0,2, 1,-1,0,-2, 0,1,
$ 0,1, 2,-1,0,0, 3,0,0,-2, 1,0,0,1, 0,0,2,-2, 2,1,0,0,
$ 0,2,0,-2, 1,0,2,-2, 1,1,0,-4/
DATA JX/1,0,1,1, 1,0,1,-2, -1,0,1,-2, -2,0,1,0, 0,1,1,
$ -2, -1,0,1,0, 0,-1,1,-2, 1,0,1,-4, 0,0,1,-4, -2,0,1,2/
DATA JY/2,0,0,-2, 1,1,0,-2, -1,1,0,-2, 3,0,0,0, 0,1,0,0,
$ 1,1,0,2, 0,0,0,1, 0,2,0,-2, 0,0,0,2, 1,1,0,-4, 1,0,0,4,
$ 1,0,0,1, -1,1,0,2/
DATA X/2263.6, -4386.5, 2369.9, 769.0, -668.1, -411.6,
$ -211.6, 147.0, 192.0, -163.1, 147.7, -125.2, -109.7,
$ -55.2, -45.1, 39.3, -38.4, 36.1, -30.8, 28.3, -24.4,
$ 18.6, 18.0, 14.6, 14.4, 13.9, -13.2, 9.7, 9.4, -8.6,
$ -8.5, -8.1, -7.6, -7.3, -7.4, -6.4, -5.7, -4.4, -4.0,
$ 3.2, -2.9, -2.7, -2.5, 2.6, 2.5, -2.1, 2.0, 1.9, -1.8,
$ 1.8, -1.4, -1.3, 1.3, 1.2, -1.1, 1.2, -1.1, -1.1, 1.0,
$ -1.0, -0.5/
DATA Y/22609., -4578.1, 2373.4, 768., 192.7, -182.4, -165.,
$ -152.5, -138.8, -127.0, -115.2, -112.8, -85.1, -52.1,
$ 50.6, -38.6, -34.1, -31.7, -25.1, -23.6, 17.9, -16.4,
$ 16.6, 14.78, 14.06, -13.51, -11.75, 11.67, -10.56, -9.66,
$ -9.52, -7.58, 6.89, -6.46, 6.4, -4.01, 3.60, 3.59,
$ 3.37, 3.32, 2.96, -2.34, -2.40, -2.32, -2.27, 2.01, -1.82/
DATA Z/186.5, 34.3, 28.2, 10.2, 3.1, 1.9, 1.3, 1.2, -1.0,
$ -0.9, -0.71, 0.62, 0.60, -0.40, 0.37, -0.30, -0.30, 0.28,
$ 0.26, 0.23, -0.23, 0.15, 0.13, -0.12, -0.11, -0.11, -0.10,
$ 0.09, -0.08, 0.07/
DATA EM/-526.0, 44.3, -30.6, -24.6, -22.6, 20.6, 11.0,
$ -6.0, -3.3, -2.0/
DATA EG/5.7, 2.1, -1.5, -1.3, -1.3, 0.8, -0.7, -0.7, 0.6,
$ -0.5, -0.4, 0.4, -0.4/
IF (EXACT.LT.1) GO TO 20
IF (EXACT.GT.4) GO TO 30
NX=NX (EXACT)
NY=NY (EXACT)
NZ=NZ (EXACT)
IX=IX (EXACT)
IY=IY (EXACT)
IZ=IZ (EXACT)
D=DATE-2415020.00
DD=0/1.E4
DD2=DD*DD
DD3=DD*DD
ANGLE(1)=-270.434164E0+13.1763965268E0*D-.0000850E0*DD2
$ +.00000039E0*DD3
ANGLE(2)=-279.696678E0+.9856473354E0*D+.00002267E0*DD2
$ +.00000000E0*DD3
ANGLE(3)=-334.329356E0+1.114040802E0*D-.00077392E0*DD2
$ -.00000026E0*DD3
ANGLE(4)=-239.183275E0-.0529539222E0*D+.0001557E0*DD2
$ +.00000000E0*DD3
ANGLE(5)=-281.220844E0+.0000470684E0*D+.0000339E0*DD2
$ +.00000007E0*DD3
C ANGLE1 IS MEAN LONGITUDE OF MOON AT EPOCH
C ANGLE2 IS MEAN LONGITUDE OF SUN AT EPOCH
C ANGLE3 IS LONGITUDE OF LUNAR PERIGEE AT EPOCH
C ANGLE4 IS LONGITUDE OF ASCENDING NODE AT EPOCH
C ANGLE5 IS LONGITUDE OF SOLAR PERIGEE AT EPOCH
DO 1 I=1,5
J=ANGLE(I)/360.E0
I=ANGLE(I)-360.*J)*RAD
IF (ANGLE(1).LT.0.0) ANGLE(1)=ANGLE(1)+2.*PI
ADD(1)=-2.*PI*(1.422222E0+.0000153622E0*D)
ADD(2)=-2.*PI*(.48298132E0-.000147269147E0*D+43.E-16*D*D)
ADD(3)=-2.*PI*(.33732431E0-.000010104982E0*D+191.E-16*D*D)
EEL=ANGLE(1)+SECRAD*(14.27*SIN(ADD(3))+7.26*SIN
$ (ANGLE(4))+.84*SIN(ADD(1)))
C THE 1.9 ARCS/SEC TERM ON ANODE (BELOW) IS COMPUTE WITH
C APPROXIMATE ARGUMENT
ANCOE=ANGLE(4)+SECRAD*(96.*SIN(ANGLE(4))+(15.6+1.9)
$ *SIN(ADD(2)))
C MOON=ANGLE(3)+SECRAD*(-2.10*SIN(ADD(1)))-2.08*SIN
$ (ANODE)+.84*SIN(ADD(2)))
EL=EL-CMOON
ELP=ANGLE(2)-ANGLE(5)
F=EL-ANCOE
DEE=EEL-ANGLE(2)
IF (EL.LT.0.0) EL=EL+TMOP1

```

```

IF(F.LT.0.0) F=F+TWOFI
IF(DEL.LT.0.0) DEE=DEE+TWOFI
CLONG=EEL
S=F
PAR=3422.7*SECRAD
DO 11 K=1,MX
CLONG=CLONG+X(K)*SECRAD*SIN(IX(1,K)*EL+IX(2,K)*ELP
+IX(3,K)*F+IX(4,K)*DEE)
IF(CLONG.GE.TWOFI) CLONG=CLONG-TWOFI
IF(CLONG.LT.0.0) CLONG=CLONG+TWOFI
DO 12 K=1,MY
S=S+Y(K)*SECRAD*SIN(IY(1,K)*EL+IY(2,K)*ELP
+IY(3,K)*F+IY(4,K)*DEE)
SCREM=(1.-.4664E-3*COS(ANODE)-.754E-4*COS
(ANODE+4.82))*SIN(S)
BETA=(18519.7E0*SCREM-6.2*SIN(3.*S))*SECRAD
DO 13 K=1,MS
FAR=FAR+Z(K)*SECRAD*COS(IZ(1,K)*EL+IZ(2,K)*ELP
+IZ(3,K)*F+IZ(4,K)*DEE)
DO 14 K=1,MW
BETA=BETA+WH(K)*SECRAD*SIN(IN(1,K)*EL+IN(2,K)*ELP
+IN(3,K)*F+IN(4,K)*DEE)
GIC=0
DO 15 K=1,MG
GOC=EG(K)*COS(IG(1,K)*EL+IG(2,K)*ELP+IG(3,K)*F
+IG(4,K)*DEE)
GIC=GIC+GOC
GIC=CLONG+GIC
CONTINUE
BETA=BETA+GIC*SIN(S)
C...COMPUTE THE LUNAR COORDINATES WITH RESPECT TO MEAN
C OF DATE SYSTEM
R=AE/SIN(PAR)
CI=COS(CLONG)
SI=SIN(CLONG)
CD=COS(BETA)
SD=SIN(BETA)
XE(1)=R*CD*CI
XE(2)=R*CD*SI
XE(3)=R*SD
RETURN
20 WRITE(9,25) EXACT
25 FORMAT(IX,'PRECISION INDICATOR, EXACT, NOT IN RANGE AT
$ POINT',I5)
GO TO 40
30 WRITE(9,35) EXACT
35 FORMAT(IX,'PRECISION INDICATOR, EXACT, OUT OF RANGE AT
$ POINT',I5)
40 CLONG=0.0
BETA=0.0
PAR=0.0
RETURN
C... END DIANA
END
SUBROUTINE ECLEQ (X,TJD)

```

```

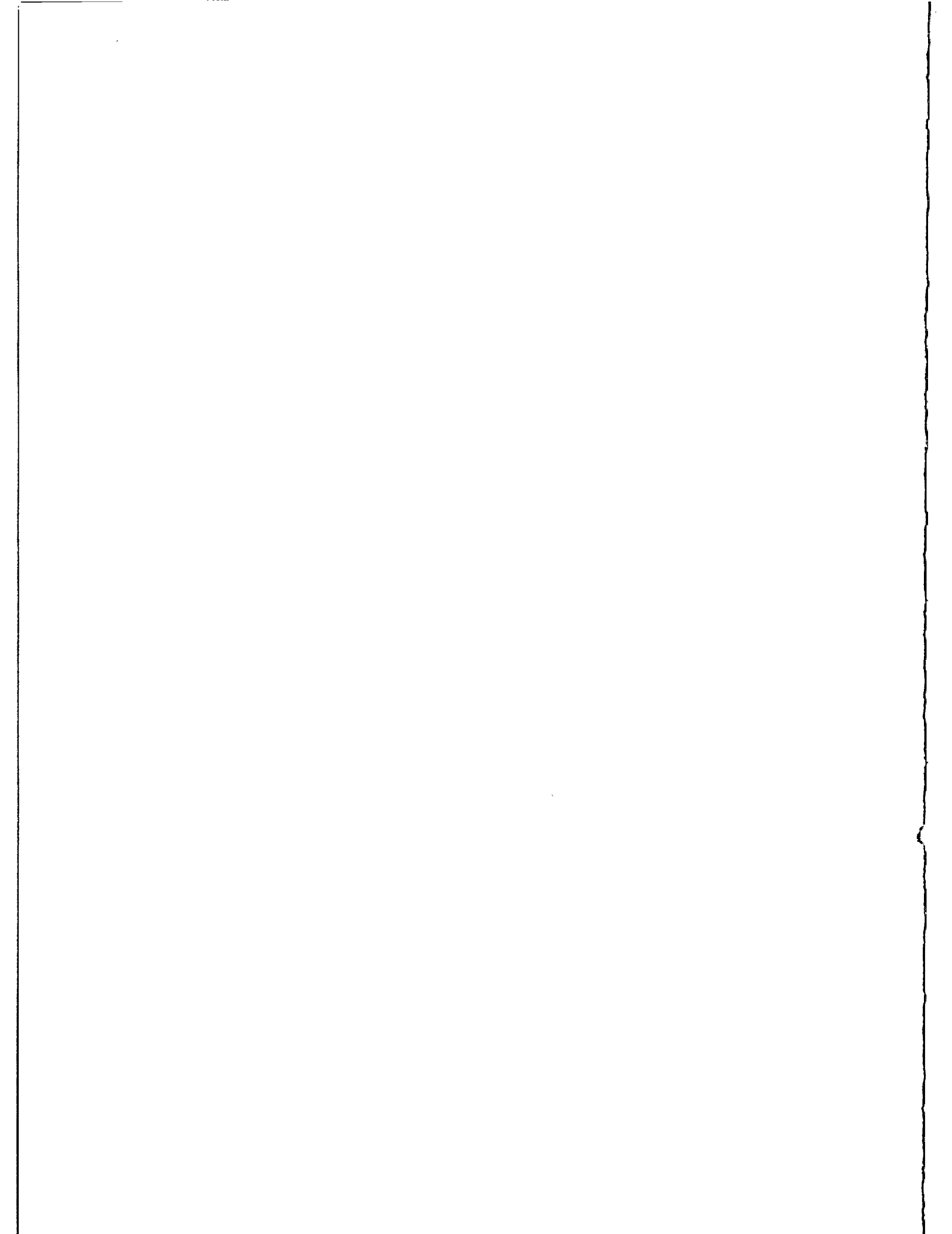
C...VERSION #10727
C...AUTHOR: BRIAN CUTBERTSON, U.T. ASTRONOMY/AEROSPACE
C...PURPOSE: TO ROTATE ECLIPTIC CARTESIAN COORDINATES INTO MEAN
EQUATORIAL COORDINATES USED FOR IRV INTEGRATIONS.
C...
C... DOUBLE PRECISION TJD
C... DIMENSION X(3)
C...
C... POLYNOMIAL COEFFICIENTS FOR MEAN OBLIQUITY DIVIDED BY 362525*N:
DATA EP0, EP1 /4.0931975520273E-1, 6.2179594501235E-9 /
DATA EP2, EP3 /2.1441068744107E-17, 1.8008716772507E-22 /
C...
C... JULIAN DAYS ELAPSED SINCE 1900 JAN 0 DAYS 12 HOURS:
T1900 = TJD - 2415020.000
T19002 = T1900 + T19001
T19003 = T1900 + T19002
C...
C... COMPUTE MEAN OBLIQUITY:
EFSM = EP0 - EP1*T19001 - EP2*T19002 + EP3*T19003
SEM = SIN (EFSM)
CEM = COS (EFSM)
C...
C... ROTATE FROM ECLIPTIC PLANE TO MEAN EQUATORIAL PLANE:
X2 = X(2)*CEM - X(3)*SEM
X(3) = X(2)*SEM + X(3)*CEM
X(2) = X2
C...
C... DONE:
RETURN
END
SUBROUTINE KEP (A, EC, I, OMEG, CAOMEG, M, X)
C... COMPUTES THE POSITION FROM THE ORBITAL ELEMENTS
C... INPUT PARAMETERS:
OMG THE GRAVITATIONAL PARAMETER
A THE SEMI-MAJOR
EC THE ECCENTRICITY
I THE INCLINATION
OMEG THE ARGUMENT OF PERIGEE
CAOMEG THE LONGITUDE OF THE ASCENDING NODE
M THE MEAN ANOMALY
C... NOTE: ALL ANGLES SHOULD BE INPUT IN RADIANs
C... OUTPUT PARAMETERS:
X THE POSITION VECTOR
DIMENSION P(3), X(3)
REAL I,M
DATA TOL/1.E-06/
C... COMPUTE THE SEMI-MINOR AXIS
E2=EC**2.E0
EDIFF=1.0E0-E2
B=A*SQRT(EDIFF)
C... SOLVE KEPLERS EQUATION
E=0
1 SE=SIN(E)
E=M+EC*SE
SE=SIN(E)
CHECK=E-EC*SE-M
IF (ABS(CHECK).GT.TOL) GO TO 1
C... COMPUTE THE MAGNITUDE OF POSITION VECTOR
CE=COS(E)
R=A*(1.0E0-EC*CE)
C... COMPUTE THE TRUE ANOMALY
SF=B*SE/R
CF=A*(CE-EC)/R
F=ATAN2(SF,CF)
C... COMPUTE THE SINE AND COSINE OF THE ARGUMENT OF
PERIGEE +THE TRUE ANOMALY
OMEGA=OMEG+F
CTR=COS(OMEGA)
STR=SIN(OMEGA)

```

```

CI=COS(I)
SI=SIN(I)
C... COMPUTE THE SINE AND COSINE OF THE LONGITUDE
C OF THE MOON
COM=COS(CAOMEG)
SOM=SIN(CAOMEG)
C... COMPUTE THE POSITION VECTOR
P(1)=-COM*CTR-SOM*STR*CI
P(2)=-SOM*CTR+COM*STR*CI
P(3)=-STR*SI
X(1)=P(1)*R
X(2)=P(2)*R
X(3)=P(3)*R
RETURN
C... END KEP
END
SUBROUTINE RROT (X, C, S)
DIMENSION X(3)
T1 = X(1)*C + X(2)*S
X(2) = -X(1)*S + X(2)*C
X(1) = T1
RETURN
END
SUBROUTINE GTRAK (SAT, RSAT, RE, ESQUAR, SATST, SATLON, SATLAT)
DIMENSION SAT(3)
DATA DEG /57.29577 95130 82/
SATLAT = ASIN(SAT(3)/RSAT)
SATLON = ATAN2(SAT(2), SAT(1))
SATHT = RSAT - RE
SATLAT = SATLAT*DEG
SATLON = SATLON*DEG
IF (SATLON.LT.0.) SATLON = SATLON + 360.
RETURN
END
SUBROUTINE TOPO (SAT, STA, STASAT, CLAT, SLAT, CLON, SLON, AZI, ELE,
RBO)
DIMENSION SAT(3), STA(3), STASAT(3), T(3)
DATA DEG /57.29577 95130 82/
DO 10 I=1,3
10 STASAT(I) = SAT(I) - STA(I)
T(1) = -STASAT(1)*SLON + STASAT(2)*CLON
T(2) = -STASAT(1)*SLAT*CLON - STASAT(2)*SLAT*SLON + STASAT(3)*CLAT
T(3) = STASAT(1)*CLAT*CLON + STASAT(2)*CLAT*SLON + STASAT(3)*SLAT
RBO = SQRT(T(1)**2 + T(2)**2 + T(3)**2)
DO 20 I=1,3
20 STASAT(I) = T(I)/RBO
ELE = ASIN(STASAT(3))
AZI = ATAN2(STASAT(1), STASAT(2))
ELE = ELE*DEG
AZI = AZI*DEG
IF (AZI.LT.0.) AZI = AZI + 360.
RETURN
END
SUBROUTINE KALDAY (JD, IPTIMES, XSEC, MONTH)
C... PROGRAMMED BY JAMES D. MCHILLAN - UNIV. OF TEXAS - 7/23/1973,
C... MODIFIED BY RICHARD EAMES, UT AUSTIN, 26 MARCH 1977
C...
C... PURPOSE: TO COMPUTE THE CALENDAR DAY FROM THE JULIAN DATE (JD)
C...
C... INPUT FORMAL PARAMETERS: (ANGLES ARE IN RADIANs)
JD THE JULIAN DATE IN DOUBLE PRECISION
C...
C... OUTPUT FORMAL PARAMETERS
IPTIMES AN INTEGER ARRAY CONTAINING THE MONTH, DAY OF MONTH,
YEAR, HOUR, AND MINUTE IN THAT ORDER
XSEC SECONDS (FLOATING POINT)
MONTHS THREE CHARACTER COLLERITH (38) NAME OF THE MONTH
C...
C... DOUBLE PRECISION JD
C... DIMENSION IPTIMES(5), MONTHS(12)
C...
C... DATA MONTHS /31JAN, 31FEB, 31MAR, 31APR, 31MAY, 31JUN,
31JUL, 31AUG, 31SEP, 31OCT, 31NOV, 31DEC /
MONTHS(1)='JAN'
MONTHS(2)='FEB'
MONTHS(3)='MAR'
MONTHS(4)='APR'
MONTHS(5)='MAY'
MONTHS(6)='JUN'
MONTHS(7)='JUL'
MONTHS(8)='AUG'
MONTHS(9)='SEP'
MONTHS(10)='OCT'
MONTHS(11)='NOV'
MONTHS(12)='DEC'
C...
C... COMPUTE THE HOUR, MINUTE, AND SECOND.
JDINT = JD
XTIME = AMOD (SINGL(JD-JDINT)*24.0+12.0,24.0)
IPTIMES(4) = XTIME
XTIME = (XTIME-IPTIMES(4)) * 60.0
IPTIMES(5) = XTIME
XSEC = (XTIME-IPTIMES(5)) * 60.0
C...
C... COMPUTE THE YEAR, MONTH, AND DAY.
IF (IPTIMES(4).LT.12) JDINT = JDINT + 1
LX = JDINT + 68569
NX = 4 * LX / 146097
LX = LX - (146097*NX+3)/4
IPTIMES(3) = 4000 + (LX+1) / 1461001
LX = LX - 1461*IPTIMES(3)/4 + 31
IPTIMES(1) = 80 * LX / 2447
IPTIMES(2) = LX - 2447*IPTIMES(1)/80
LX = IPTIMES(1) / 11
IPTIMES(1) = IPTIMES(1) + 2 - 12*LX
IPTIMES(3) = 100*(NX-49) + IPTIMES(3) + LX
C...
C... SET THE NAME OF THE MONTH
LX = IPTIMES(1)
MONTH = MONTHS(LX)
C...
C... RETURN
END
SUBROUTINE SHADOW (X, R1, RSOL, RSOL1, FRAC, RSUN, RSUM1, RSUM2)
C...
C... PURPOSE: DETERMINE AMOUNT OF SHADOWING USING A CYLINDRICAL OR
CONICAL SHADOW MODEL
C...
C... CODED BY: J RIES - UNIVERSITY OF TEXAS - FEB 1980
C...
C... REFERENCE: D. BAILEY; SOLAR RADIATION PRESSURE CALCULATIONS IN THE
CLODTH PROGRAM; WOLF RESEARCH AND DEVELOPMENT CORP.
C...
C... INPUT FORMAL PARAMETERS:
X THE SATELLITE POSITION IN 1950.0 NON-ROTATING COORDINATES
R1 MAGNITUDE OF X
RSOL POSITION OF THE SUN IN 1950.0 NON-ROTATING COORDINATES
RSOL1 MAGNITUDE OF RSOL

```

A NEODYMIUM YAG ACTIVE MIRROR FOR THE
AMPLIFICATION OF MODE-LOCKED LASER PULSES

S.R. Bowman, L.M. Ding, C.O. Alley
F.M. Yang, J. Fogleman
Department of Physics and Astronomy
University of Maryland
College Park, MD 20742 - USA -

Telephone (301) 454 3405

ABSTRACT

We report the development of the first Neodymium YAG active mirror amplifier. This device has advantages over other high average power amplifier geometries when the laser output energy is limited by the peak power damage threshold.

Our research objective is to increase the quantity and quality of data acquired from lunar laser ranging. This requires a combination of single shot laser energy, average power, and pulse duration that was unavailable in previous solid state laser designs. We have therefore conducted research on a new Nd:YAG amplifier configuration that should allow the production of one Joule, 50 picosecond pulses at an average power of 10 to 20 Watts.

Our active mirror configuration is best described by Figures (1) and (2). Three one inch diameter beam footprints lie along the 4 inch crystal length. The crystal thickness is 14 millimeters and the back surface reflections make this an inherently double-pass device. External mirrors transfer the beam from one footprint to the next.

The advantages of this amplifier geometry are three fold. Firstly, with the mirror geometry, large apertures are possible with the presently available crystals of Nd:YAG. Large apertures are essential to avoid damage and beam distortions that occur at high peak intensities and Nd:YAG is still the best solid state material for high average powers. Our mirror dimensions were chosen to make optimum use of a 4 inch diameter boule. Secondly, thermal birefringence and thermal focusing are eliminated by having the laser propagate parallel to the thermal gradients in the mirror.¹ Areas near the mirror's edges where the gradients are nonuniform can be simply avoided. The Nd:YAG active mirror amplifier should have crystal stress fracture limited average power capability without restriction to linear laser polarization. Lastly, the large open faces of the mirror geometry allow for several optically isolated gain paths through the same amplifier. This permits multipass gains of 40 dB for a single device.

Several areas critical to the success of the Nd:YAG active mirror have been investigated. The most important of these is the durability of the dielectric coating on the mirror's back face. This coating must reflect the normally incident high intensity laser without damage and transmit the flashlamp pump band over wide angles. It is exposed to the cooling water and is stressed by the heated YAG substrate. Immersion and laser exposure tests at 1 GW/cm^2 were conducted on samples of commercially supplied coatings. Back surface coatings for the mirror were selected that showed no laser or deterioration after a ten day immersion test. Another area critical to this design is the question of distortions from back surface flatness errors.² This design is very sensitive to such errors because of the high index of refraction of YAG and because of the requirement for multipass operation. Static beam distortions were reduced to below $1/15$ wave per reflection through the use of compensation polishing on the front face. Dynamic surface distortions as well as gain variations across the beam depend linearly on the nonuniformity of the flashlamp pump intensity. Great care was taken with the pumping cavity in order to obtain less than a 2% RMS variation in the pumping spatial distribution. Other distortion mechanisms such as crystal mounting and coolant back pressure were measured and found not to be a serious problem. At the time of this writing thermal distortion, laser gain, and beam quality measurements are in progress.

1. J.A. Abate, "Flashlamp-induced thermal distortions in active-mirror Nd:glass laser amplifier," Wavefront Distortions in Power Optics SPIE (1981) 293, 114.

2. J.A. Abate, et al., "Active mirror: a large-aperture medium-repetition rate Nd:glass amplifier," Appl. Optics (1981) 20, 351.

Active Mirror Amplifier Concept

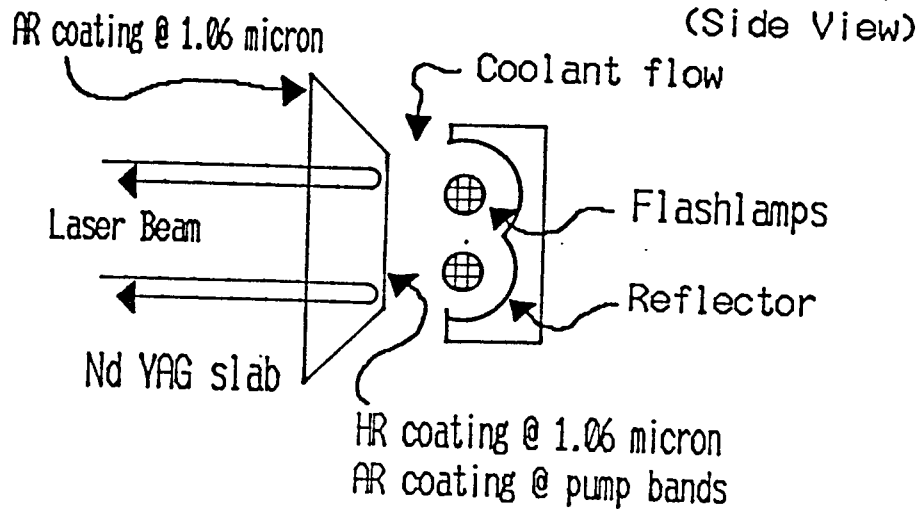


Figure 1

Active Mirror Amplifier Concept

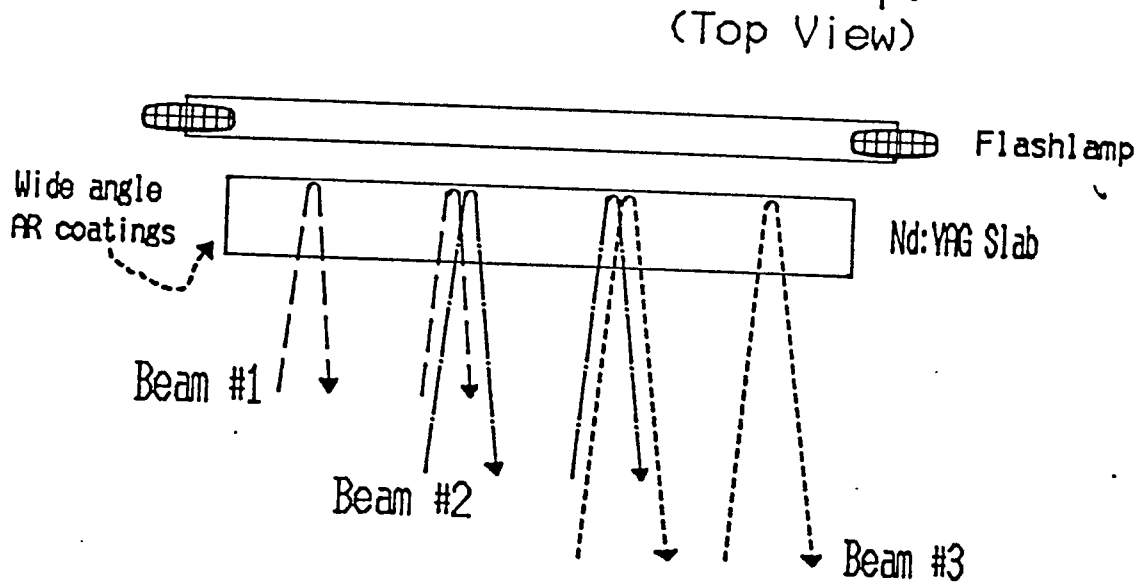
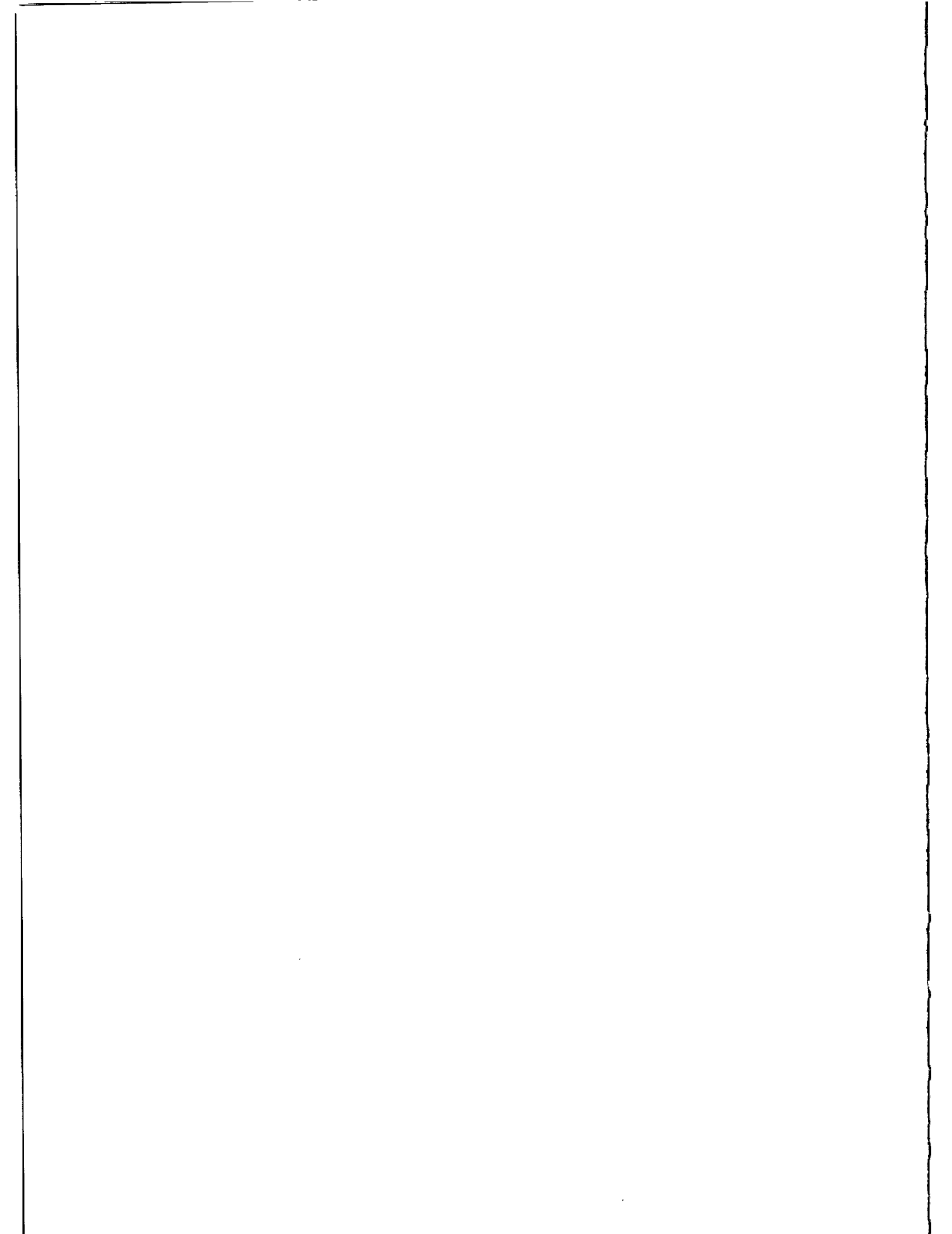


Figure 2



JAPANESE GEODETIC SATELLITE "AJISAI" LAUNCHED IN AUGUST 1986

M. Sasaki
Hydrographic Department of Japan
3-1, Tsukiji 5-Chome, Cho-ku
Tokyo, 104 - Japan -

Telephone (03) 541 3811
Telex 2522452 HDJODC J

ABSTRACT

The Japanese Experimental Geodetic Satellite "AJISAI" with functions for laser ranging and photographing from the ground was launched on August 12, 1986. The tracking observation of AJISAI has been made after the launch by laser ranging and photographing techniques under international cooperation. According to a simulation the range accuracy of one to two centimeters level is attainable by applying edge detection method with narrow laser pulse. A construction of a marine geodetic controls around Japan is to be made by the Hydrographic Department of Japan using the AJISAI satellite and a transportable laser ranging station.

JAPANESE GEODETIC SATELLITE "AJISAI" LAUNCHED IN AUGUST 1986

M. Sasaki
Hydrographic Department of Japan
3-1, Tsukiji 5-chome, Chuo-ku
Tokyo, 104 Japan

Telephone (03) 541 3811
Telex 2522452 HDJODC J

ABSTRACT

The Japanese Experimental Geodetic Satellite "AJISAI" with functions for laser ranging and photographing from the ground was launched on August 12, 1986. The tracking observation of AJISAI has been made after the launch by laser ranging and photographing techniques under international cooperation. According to a simulation the range accuracy of one to two centimeters level is attainable by applying edge detection method with narrow laser pulse. A construction of a marine geodetic controls around Japan is to be made by the Hydrographic Department of Japan using this AJISAI satellite and a transportable laser ranging station.

1. INTRODUCTION

The Japanese Experimental Geodetic Satellite (EGS) was launched at the Tanegashima Space Center by using the first H-I rocket of the National Space Development Agency (NASDA) of Japan on August, 1986 and the satellite was named "AJISAI" which means "HYDRANGEA" of flower in Japanese. The original mission of this satellite was to determine the location of isolated islands, to adjust the triangulation network and to know the relation between the Japanese Geodetic Coordinate System (Tokyo Datum) and those of other parts of the world.

The original design in early 1970s was a balloon of 10 meters diameter for both photographing and laser ranging. The design of the satellite was changed to a rigid type to avoid the air drag and the unreliability at the expansion of balloon to space later. The flight model of the satellite was completed by NASDA and launched. The specifications and observation project of "AJISAI" are presented here.

2. FUNCTIONS AND SPECIFICATION OF "AJISAI"

The function of the satellite "AJISAI" are (1) to reflect input laser light back toward the incident direction by Corner Cube Reflectors (CCRs) and (2) to reflect solar light to the ground by solar reflecting mirrors.

The body of the satellite is hollow sphere made of glassfiber-reinforced

plastics. The surface of the body is covered with CCRs and solar light reflectors (Fig. 1). Twelve pieces of unit CCRs form a set of Laser Reflector (LR) and 120 sets of the LR are distributed on the surface almost uniformly. The effective area for laser light reflection within the full prospect angle of 30 degrees from the center of the satellite is 91.2 cm². The remainder part of the surface is covered with 318 pieces of solar reflectors. The reflectors are mirrors with the radii of the curvature from 8.4 to 8.7 m. The base of the mirror is made of an alloy of aluminum and the surface is coated by an oxide silicon for protection from flaring and diminution of quality. The reflective efficiency of the mirror is 0.85. The diameter of "AJISAI" is 2.15 m and its total weight is 685.2 kg.



Fig. 1 Japanese Geodetic Satellite "AJISAI".

"AJISAI" was given a spinning of 40 rpm before detachment from the rocket. The spin axis was set in parallel to the earth rotation axis and almost every observers on the ground in the dark can observe the flashing light of reflection from the solar reflectors of "AJISAI" in repetition rate of 2 pps if the satellite is exposed to the solar light. The flashing duration is about 5 msec and the brightness of the reflective light is from 1.5 to 4.0 star magnitude as shown as followings:

The intensity of the reflected light from a mirror sphere through atmosphere is given by

$$I = \gamma I_s \frac{a^2}{4r^2} T$$

and the brightness expressed in star magnitude is

$$m = -2.5 \log I$$

where I_s : intensity of input light, γ : reflectivity of a sphere, a : radius of a sphere, r : range from observer to a sphere, T : transparency of atmosphere. The magnitude of the brightness is estimated by using some values of specifications and atmosphere as

I_s : ($m_s = -2.5 \log I_s = -26.8$: star magnitude of the sun), γ : 0.85, a : 8.5 m, T : $\exp(-k \sec z)$ for a model transparency of atmosphere, z : zenith distance, k : atmospheric condition (0.3 : good, 0.4 : medium, 0.5 : not good). The results are shown in Table I.

The flash can be taken in a photo with a number of fixed stars by using a camera on an equatorial mount and the direction of the satellite from the observer can be measured referring the star

Table I Brightness of "AJISAI" expressed in star magnitude

| elevation | range | transparency | | |
|-----------|-------|-----------------|-------------------|---------------------|
| | | k=0.3 (good) | k=0.4 (medium) | k=0.5 (not good) |
| deg | km | mag | mag | mag |
| 90 | 1500 | 1.44 | 1.55 | 1.65 |
| 80 | 1519 | 1.47 | 1.58 | 1.69 |
| 70 | 1577 | 1.56 | 1.71 | 1.80 |
| 60 | 1680 | 1.73 | 1.86 | 1.98 |
| 50 | 1841 | 1.98 | 2.12 | 2.26 |
| 40 | 2080 | 2.32 | 2.50 | 2.67 |
| 30 | 2428 | 2.81 | 3.03 | 3.24 |
| 20 | 2931 | 3.52 | 3.84 | 4.15 |

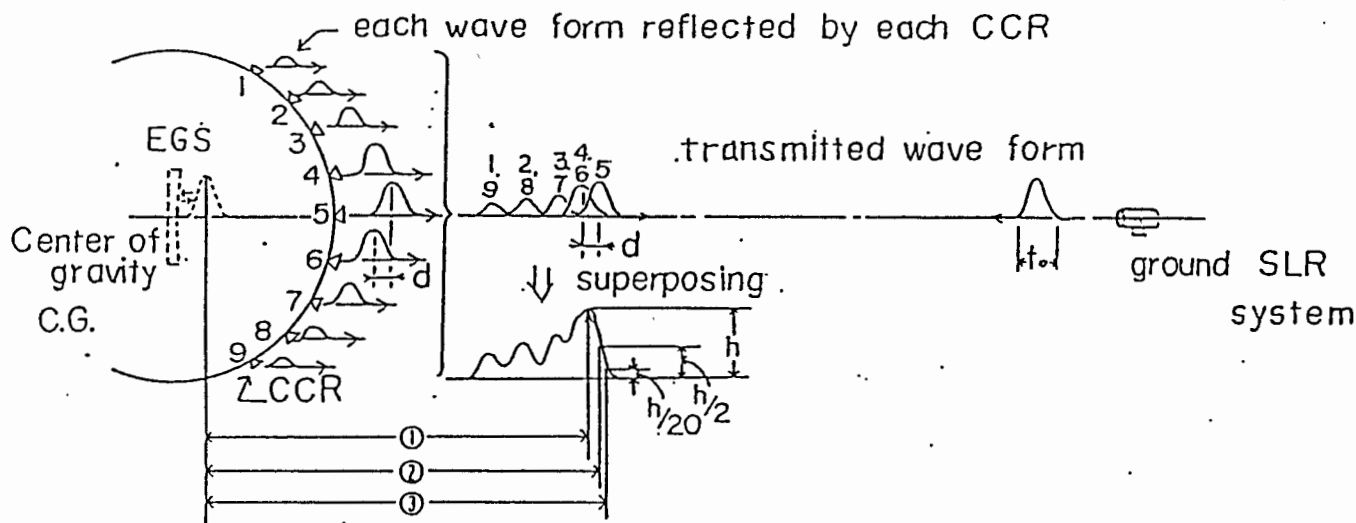


Fig. 2 Concept of simulation to know wave form of return pulse and range bias. Range bias for (1) first peak position, (2) half height position and (3) rising position.

coordinate system.

For the estimation of the ranging accuracy of "AJISAI", a simulation has been conducted by NASDA. The concept of the simulation is given in Fig. 2. In this simulation no atmospheric fluctuation effect is considered. A kind of the full width at half-maximum (FWHM) of 78 psec (200 psec for total width within three times of the standard deviation of a Gaussian shape) are used. The incident direction of 60 in number are selected geometrically in 30 degrees step from -60 degrees to +60 degrees for latitude and in 30 degrees step for longitude around the spin axis. The resultant change of position (half distance) of the first peak, rising position of half height of the highest peak and rising position of 1/20 height of highest peak are shown in Table II. The mean value of the position of the first peak and its root mean square (RMS) are :

$$1013.3 \pm 11.3 \text{ mm.}$$

The reflection patterns for the three typical cases are given in Fig. 3. The results of the simulation above indicate that the range accuracy to "AJISAI" attains 1 to 2 cm level when a high precision Satellite Laser Ranging (SLR) system with a narrow-pulse-laser-transmitter and with multi-photoelectron-detection or front-edge-detection method. The most of Lageos capable SLR systems can be attainable to the front edge detection of return laser light from "AJISAI" since the lower orbit than Lageos (5900 km) gives much stronger return energy of laser light.

The launch of "AJISAI" was made successfully at 20^h 45^m on August 12, 1986 (UT) and the tracking observations by NASDA, JHD (Hydrographic Department of Japan) and other supporting organizations including the National Aeronautics and Space Administration (NASA) of the United States has been continued. The determined orbit is circular with the inclination of 50.0 degrees and altitude from the ground is 1500 km high.

Table II Change of range bias for reflective pulse from "AJISAI"

| pulse width | measuring position | range bias | |
|-------------|--------------------|---------------|---------------|
| | | maximum mm | minimum mm |
| 200 ps | first peak | 1026 | 984 |
| | half height | 1031 | 1011 |
| | rising | 1037 | 1031 |
| 300 ps | first peak | 1026 | 984 |
| | half height | 1034 | 1019 |
| | rising | 1043 | 1035 |

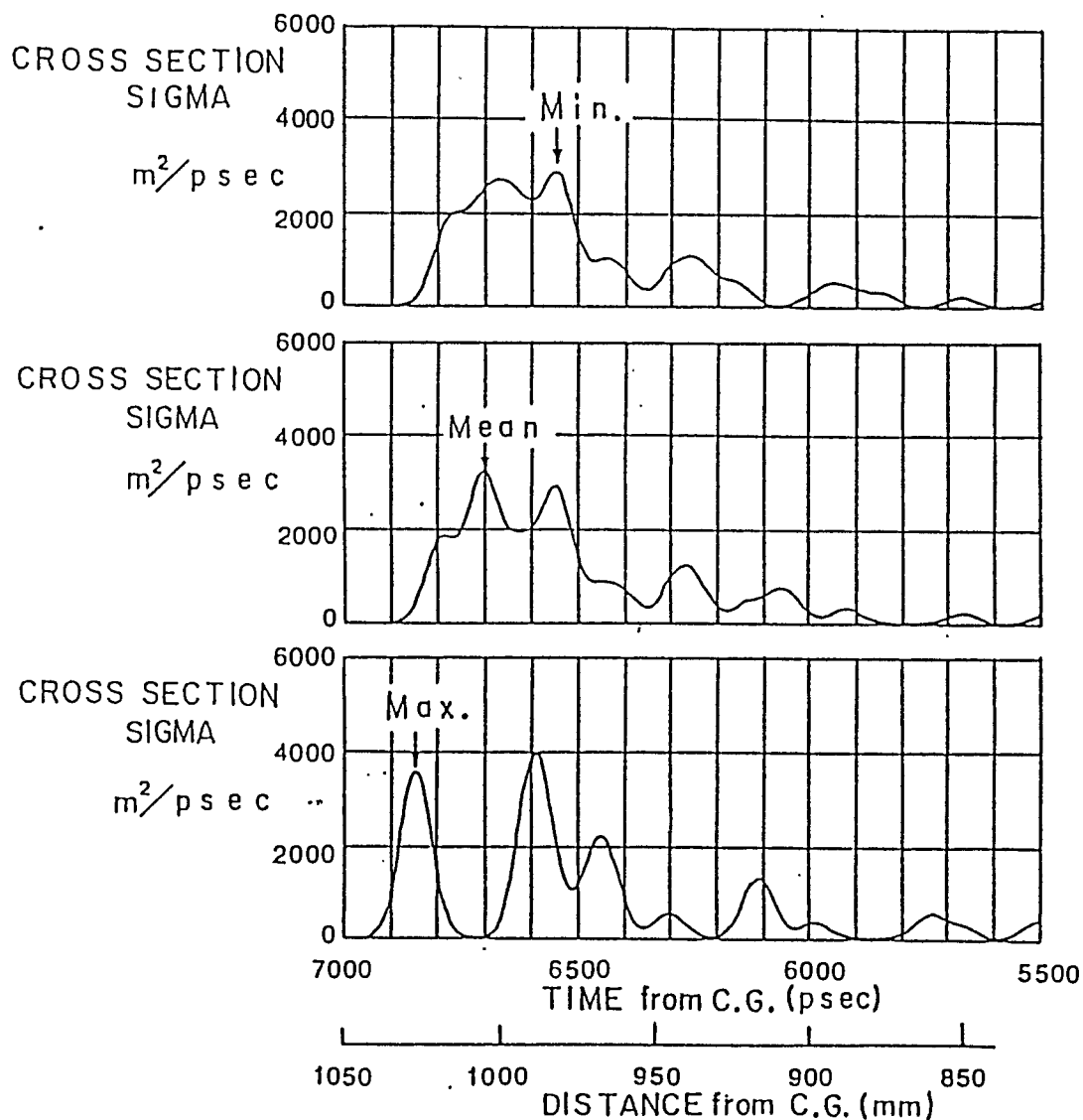


Fig. 3 Examples of laser reflection pattern. For the cases of the first peak position of the minimum-, mean- and maximum-range bias.

3. COMPARISON OF ORBITAL STABILITY WITH OTHER GEODETIC SATELLITES

"AJISAI" satellite is a fully passive satellite for use of both laser ranging and photo direction observation. For the laser ranging there are two passive sphere satellites of Lageos and Starlette. The diameter, weight and orbital height for both satellites are 0.60 m, 411 kg, 5900 km and 0.24 m, 47 km, 900 km respectively. There were three balloon satellites in 1960s.

To realize the stable orbit against air drag and radiation pressure effects, large mass/cross-section-area (M/A) ratio is preferable. M/A ratio is an index to indicate the stability of radiation pressure and $1/\rho M/A$ is an index for air drag stability in the atmospheric density of ρ . The M/A ratio for the satellite. The values of M/A ratio and $1/\rho M/A$ for AJISAI and sphere laser satellites are shown in Table III for comparison.

The air drag effect is more sensitive for orbital stability of the geodetic satellite than radiation pressure. Concerning that higher orbit of satellite is preferable to avoid effect of uncertainty of geopotential, the stability of the orbit of AJISAI seems a little better than or at least almost the same as that of Starlette.

In addition to the availability to geometrical use and dynamical use of AJISAI for geodetic purpose, one more remarkable subject is that the precise determination of orbit of AJISAI in long period improves the accuracy of coefficients of the geopotential.

Table III Comparison of AJISAI with other rigid laser satellite

| | mean altitude | M/A mass/area | $1/\rho M/A$ mass/air-density·area |
|-----------|---------------|--------------------|---------------------------------------|
| | km | kg/m ² | x 10 ⁴ m |
| AJISAI | 1500 | 148 | 2.6 |
| Starlette | 900 | 816 | 1.9 |
| Lageos | 5900 | 1140 | 370 |

4. METHOD OF OBSERVATION

There are several methods in geodetic use of this "AJISAI" satellite. One is fully geometrical method by using simultaneous observations of distance and direction at some stations. Namely, two kinds of observations are made at a base station (known position or given position) and temporary stations (unknown positions, e.g. isolated islands). The position of the satellite is given by distance and direction observation from the known position and unknown positions are determined from the position of the satellite by similar distance and direction observations at these points. A SLR system and a Satellite Camera are also necessary at a temporary station in this method. The location of an unknown position is given by only one set of observation in principle.

The other geometrical method is to use several SLR systems simultaneously in a region of a few thousands kilometers. The range correction of this satellite is well determined as shown in a simulation above and simultaneous precision ranging can determine baselines in a centimeter level.

The dynamical method is also useful to determine the location of SLR stations based on a geocentric coordinate and other geophysical parameters as geopotential coefficients, air drag effect and tidal effects. For each method or combined methods it is effective to hit laser beam well on this satellite because of its brightness.

JHD is under preparation of a SLR system and satellite camera at fixed base station (Simosato Hydrographic Observatory) and a transportable SLR station and satellite camera for temporary stations of which geodetic position should be combined with the base station. For these equipments, another report is presented in this laser workshop. By using these equipments, marine geodetic controls are to be expanded by JHD around Japan to combine isolated islands with the Tokyo Datum.

5. SUPPORTING OBSERVATIONS FOR "AJISAI" AND INTERNATIONAL COOPERATION

The observation of "AJISAI" by using the SLR systems at the Simosato Hydrographic Observatory has been made from just after the launch. 25,300 ranges of 27 passes were obtained at the observatory in August 1986. The preliminary range accuracy for them, 7~8 cm level, seems a little better than those of other geodetic satellite, 9~10 cm level, within early stage after the launch. The supporting observations of Japanese domestic organizations were made. The SLR data and pointing information were transferred to the Tsukuba Space Center of NASDA and the Satellite Geodesy Office in the Headquarters of JHD through a microcomputer network (PC-VAN). The orbital elements have been created continuously at those places and distributed to domestic observation sites.

JHD has an agreement for cooperation of SLR observation and its data exchange with NASA. The Goddard Laser Tracking Network of NASA also started the supporting observation for "AJISAI" from just after the launch and distributes their own orbital elements of AJISAI to cooperative SLR stations. Observation data and results of research work of AJISAI will be exchanged between JHD and NASA.

Other international SLR stations in England, Switzerland and so on also tracking AJISAI and more wider cooperation with France, China, West Germany, Australia and Austria is expected. For these international cooperation for AJISAI observation JHD with NASA will play a role of data distribution center. The work on collection of SLR and photograph data, determination of orbit, distribution of orbital elements, data file management and data analysis has started in JHD.

REFERENCES

- Ganeko, Y., K. Komaki and H. Hashimoto, "On the geodetic satellite GS-1", in Proc. Sympo. on Space Techniques in Positional Astronomy, A. Tsuchiya, Ed. Tsukuba, pp.12-18, 1983 (in Japanese).
- Hashimoto, H. and K. Saito, "Development of the Experimental Geodetic Payload", in Proc. 17th Sympo. for engineering results in NASDA, 1985 (in Japanese).
- Sasaki, M., "Optimum orbit of the Geodetic Satellite GS-1", Rep. Hydrogr. Researches, JHD, no.14, pp.131-144, 1979 (in Japanese).
- Sasaki, M., "Observation Project of Japanese Geodetic Satellite GS-1", in Proc. Sympo. on Application on Space Techniques to Astronomy and Geophysics, H. Kinoshita, I. Murata and K. Nakajima, Ed. Tokyo, pp.27-31, 1986.
- Sasaki, M. and H. Hashimoto, "Launch and Observation Program of the Experimental Geodetic Satellite of Japan", IEEE Transactions on Geoscience and Remote Sensing, to be published.
- Sasaki, M. and Y. Suzaki, "Satellite Ranging System at the Simosato Hydrographic Observatory and the Transportable System", in this issue.

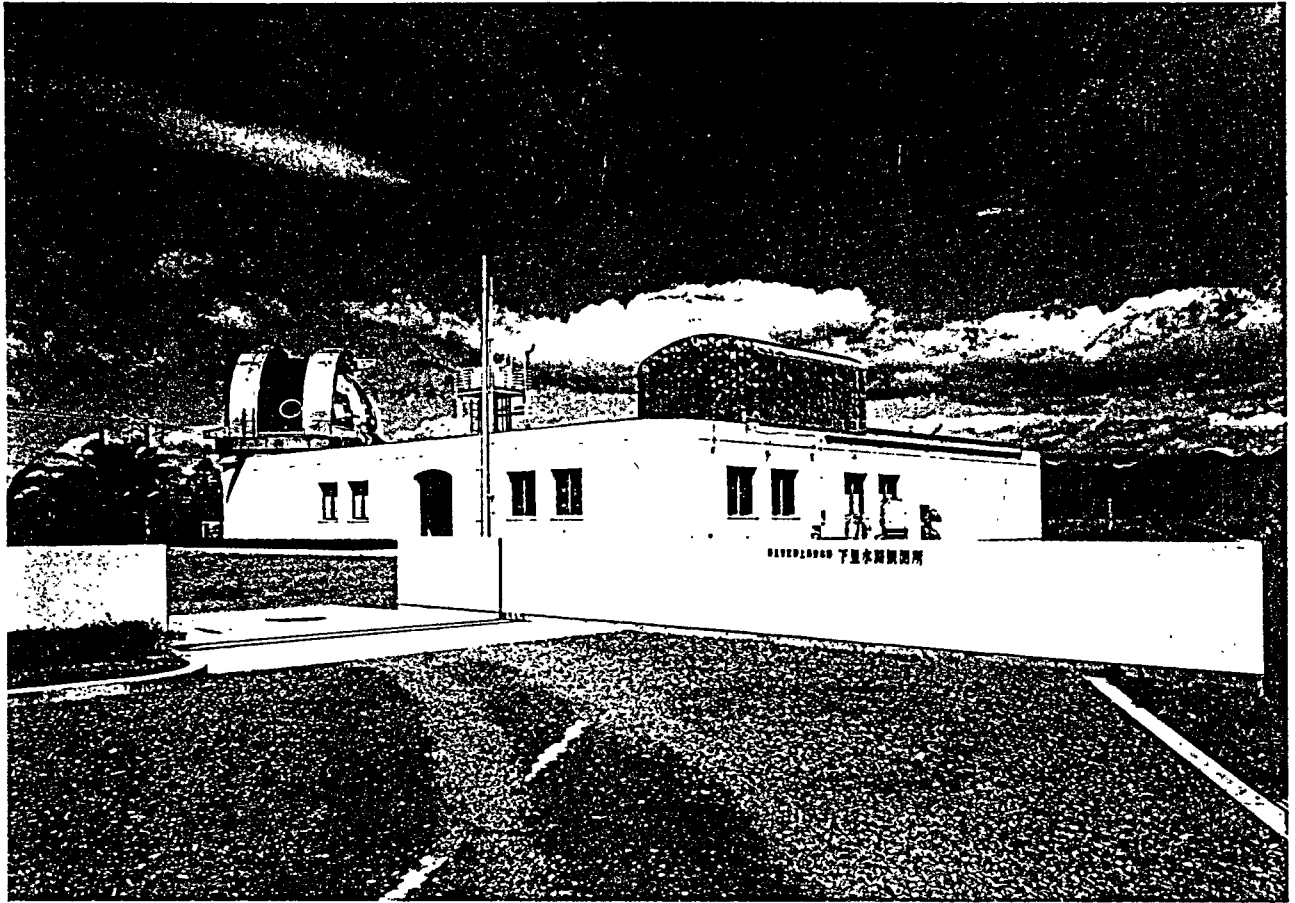


Fig. 1 External View of the Simosato Hydrographic Observatory

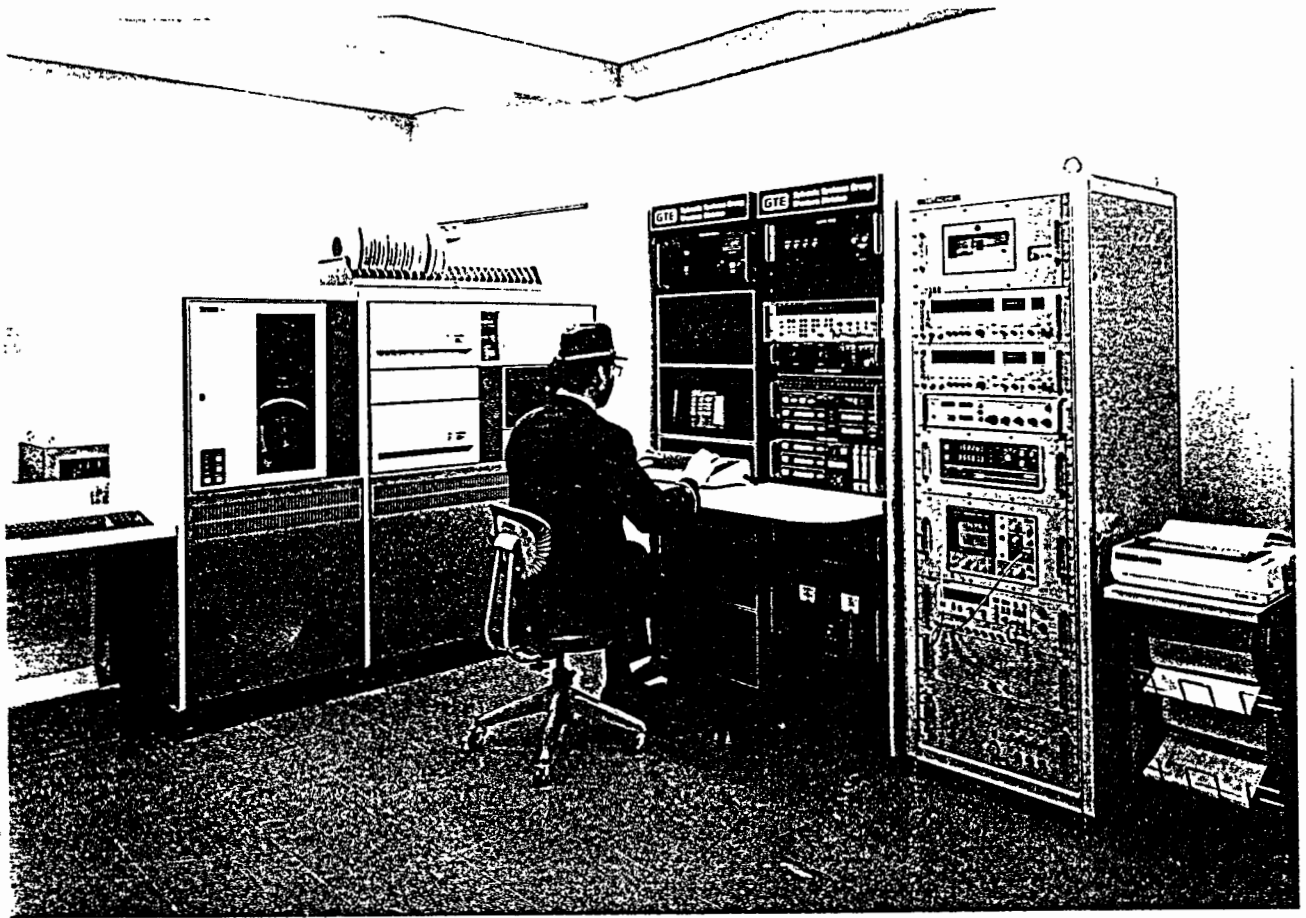


Fig. 2 Electronics

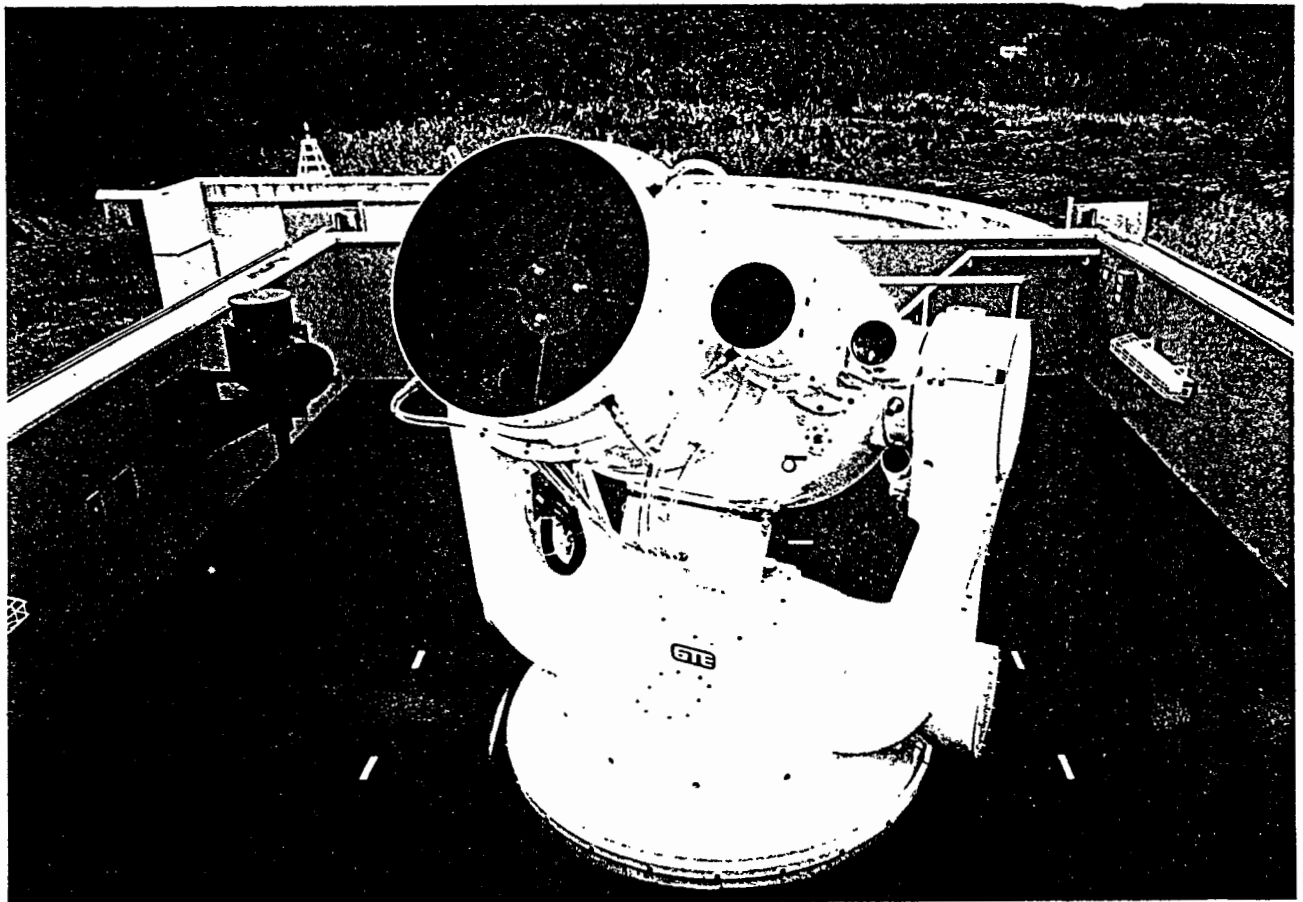


Fig. 3 Optics / Mount

***** SATELLITE TRACKING REPORT *****
 Station : 793E (SIMOSATO)
 (-3822.38448km, 3699.36735km, 3507.57235km)
 (6371.73470km, 135.9370deg, 33.5777deg)
 Satellite : S602101
 Used ORBITAL : 1986.08.14 0:00:00 (UT)
 Pass starts : 1986.08.13 17:43:00 (UT)
 Atmosphere : Sky/Shadow code 1
 Humidity 99.0%
 Temperature 23.2deg
 Pressure 1007.1mmHg
 System control : Leveling angle 0.0061deg(CDS(AZ- 93.0600deg))
 Collimation angle -0.0046deg
 Encoder offset (160.1600deg, 4.5500deg)
 Telescope sag 0.0000deg
 Refraction factor 0.9610
 Laser firing 250msec
 pre Range offset 7.1msec
 post Range offset 7.3msec

Produced by T.Yamasuchi (Phone 045-803-7253)

RHS of Br = 0.079(m) Number of Br = 1501

| UT | -2m | -150cm | -1m | -50cm | 0 | 50cm | 1m |
|----------|-----|--------|-----|-------|---|------|----|
| 17:43:10 | : | : | : | : | : | : | : |
| 17:43:20 | : | : | : | : | : | : | : |
| 17:43:30 | : | : | : | : | : | : | : |
| 17:43:40 | : | : | : | : | : | : | : |
| 17:43:50 | : | : | : | : | : | : | : |
| 17:44:00 | : | : | : | : | : | : | : |
| 17:44:10 | : | : | : | : | : | : | : |
| 17:44:20 | : | : | : | : | : | : | : |
| 17:44:30 | : | : | : | : | : | : | : |
| 17:44:40 | : | : | : | : | : | : | : |
| 17:44:50 | : | : | : | : | : | : | : |
| 17:45:00 | : | : | : | : | : | : | : |
| 17:45:10 | : | : | : | : | : | : | : |
| 17:45:20 | : | : | : | : | : | : | : |
| 17:45:30 | : | : | : | : | : | : | : |
| 17:45:40 | : | : | : | : | : | : | : |
| 17:45:50 | : | : | : | : | : | : | : |
| 17:46:00 | : | : | : | : | : | : | : |
| 17:46:10 | : | : | : | : | : | : | : |
| 17:46:20 | : | : | : | : | : | : | : |
| 17:46:30 | : | : | : | : | : | : | : |
| 17:46:40 | : | : | : | : | : | : | : |
| 17:46:50 | : | : | : | : | : | : | : |
| 17:47:00 | : | : | : | : | : | : | : |
| 17:47:10 | : | : | : | : | : | : | : |
| 17:47:20 | : | : | : | : | : | : | : |
| 17:47:30 | : | : | : | : | : | : | : |
| 17:47:40 | : | : | : | : | : | : | : |
| 17:47:50 | : | : | : | : | : | : | : |
| 17:48:00 | : | : | : | : | : | : | : |
| 17:48:10 | : | : | : | : | : | : | : |
| 17:48:20 | : | : | : | : | : | : | : |
| 17:48:30 | : | : | : | : | : | : | : |
| 17:48:40 | : | : | : | : | : | : | : |
| 17:48:50 | : | : | : | : | : | : | : |
| 17:49:00 | : | : | : | : | : | : | : |
| 17:49:10 | : | : | : | : | : | : | : |
| 17:49:20 | : | : | : | : | : | : | : |
| 17:49:30 | : | : | : | : | : | : | : |
| 17:49:40 | : | : | : | : | : | : | : |
| 17:49:50 | : | : | : | : | : | : | : |
| 17:50:00 | : | : | : | : | : | : | : |
| 17:50:10 | : | : | : | : | : | : | : |
| 17:50:20 | : | : | : | : | : | : | : |
| 17:50:30 | : | : | : | : | : | : | : |
| 17:50:40 | : | : | : | : | : | : | : |
| 17:50:50 | : | : | : | : | : | : | : |
| 17:51:00 | : | : | : | : | : | : | : |
| 17:51:10 | : | : | : | : | : | : | : |
| 17:51:20 | : | : | : | : | : | : | : |
| 17:51:30 | : | : | : | : | : | : | : |
| 17:51:40 | : | : | : | : | : | : | : |
| 17:51:50 | : | : | : | : | : | : | : |
| 17:52:00 | : | : | : | : | : | : | : |
| 17:52:10 | : | : | : | : | : | : | : |
| 17:52:20 | : | : | : | : | : | : | : |
| 17:52:30 | : | : | : | : | : | : | : |
| 17:52:40 | : | : | : | : | : | : | : |
| 17:52:50 | : | : | : | : | : | : | : |
| 17:53:00 | : | : | : | : | : | : | : |
| 17:53:10 | : | : | : | : | : | : | : |
| 17:53:20 | : | : | : | : | : | : | : |
| 17:53:30 | : | : | : | : | : | : | : |
| 17:53:40 | : | : | : | : | : | : | : |

1 17:43:13.283765 0 18.91581012 330.5359 21.6536 -0.00129217 0.155

Fig. 4 "AJISAI" Ranging Data Obtained at Simosato

Table 3 Major Specifications of the HTLRS

| | |
|-----------------------|-------------------|
| receiver diameter | 35cm |
| laser : output energy | 50mJ |
| pulse width | 200ps |
| repetition rate | 5 - 10pps |
| range resolution | 20ps |
| range accuracy | 5cm/shot |
| transportation | air transportable |

THE PROPOSAL OF
STRICTLY SIMULTANEOUS SATELLITE LASER RANGING

F.M. Yang
Department of Physics and Astronomy
University of Maryland
College Park, MD 20742 - USA -

Telephone (301) 454 3405
Telex 908787

ABSTRACT

A proposal of synchronized laser ranging to artificial satellites from different stations is presented in this paper. In this operational mode, the laser firing epoch at each station should be strictly controlled by computers so that all laser pulses transmitted from different stations arrive at a satellite at certain moments (such as seconds, or tenths of second) with a minimum time uncertainty. (20 microseconds can be easily obtained for present passive mode-locked lasers).

All full-rate range data attained in this mode can be analysed by dynamic technique as usual. Besides, based on the 3-D multilateration method (1), a strictly geometric solution without polynomial smoothing and complex interpolation may be achieved, and 5 mm accuracy baselines between laser stations could be obtained in near future.

I Introduction

The range accuracy of satellite laser ranging systems has greatly improved in recent years. A few 1 cm accuracy systems (for single measurement) are now operational [2][3][4]. For removing systematic errors, millimeter level real time calibration technique are now in common use at most stations. Streak-camera-based two color satellite laser ranging systems have been under development, and appear capable of measuring the atmospheric delay with an accuracy of 5 mm or better [5].

The analysis of SLR data is now dominated by dynamic method and a great deal of scientific results in geodesy and geodynamics have been achieved in the recent 10 years. But one realizes that there still are some difficulties in the dynamic technique because of complex perturbation factors influencing on orbits of satellites, so some results derived from the same LAGEOS data by different analysis groups are quite different, such as in the intercomparison of 22 baseline lengths determined by SLR and VLBI respectively [6][7]. The authors of [7] found a scale difference of 1.9×10^{-8} , but no difference was found in [6]. It was also shown in Fig.13 of [8] that a few measured baseline values seem suspicious. The errors in the best gravity model we now have will affect baseline estimate with 2 cm uncertainty. In the mentioned comparison of baseline length determinations [6], the uncertainty of baselines from SLR (dynamic method) is 2-4 cm, a little worse than those from VLBI (1-3 cm). However, the fact is that a few SLR systems have already had the capability of 1 cm single shot accuracy. Could one use the geometric simultaneous ranging technique proposed by some investigators over 10 years ago to exploit this high range accuracy and to obtain ground baselines with the same or better accuracy? If one could, the future results would be a very important check to the SLR dynamic method. Although there are many difficulties for simultaneous observations, a large number of updated SLR stations have existed in some regions, especially in Europe and North America, and the reliability of these SLR systems has been greatly improved, so the possibility of successful simultaneous observations are much improved.

II Method and Purposes

In previous geometric solution tests, such as [9], only quasi-simultaneous observations were used which required complex smoothing and interpolation. This could lead to additional errors which could not be ignored in the processing of 1 cm accuracy data.

For SLR stations using 10 Hz laser systems, the arriving time differences of laser pulses from different sites to LAGEOS would be about 50 msec, equal to maximum range differences of about 200 meters. Even for those stations which can synchronize the transmit pulses from different systems to a certain time standard (e.g. UTC USNO), the arriving time epoch of laser pulses from different stations will still be different by up to 10-15 msec owing to variations of relative positions of the satellite and stations. This corresponds to range differences of about 40-60 meters. Due to high frequency perturbation factors, it is not easy to interpolate these quasi-simultaneous observations (40-200 meters range differences) to the 1 mm level accuracy which seems necessary for processing 1 cm accuracy data.

The routine predictions of one way flight time from stations to LAGEOS have been made as good as $0.5 \mu\text{sec}$. During this time uncertainty, the maximum radial motions of LAGEOS relative to stations is only 2 mm. So, if the laser firing epoch at each participating station can be strictly controlled, the epoch of pulses arriving at the satellite from different stations will be the same with this same time uncertainty. For active Q-switch and mode-locked laser systems, firing epoch can be controlled within 100 nsec, but for those mode-locked systems having passive devices (such as dye cell), firing epoch can be controlled to about $20 \mu\text{sec}$, which means only 80 mm maximum variation of slant ranges of LAGEOS. Based on the accurate timing of transmitted pulses and returned signals, and the routine predictions of range rates of LAGEOS, the measured ranges could be easily interpolated to the same time to 1 mm accuracy. In this way, a strictly geometric solution, which includes accurate baselines and 3-D relative coordinates of LAGEOS and stations, can be accessible.

These results can contribute towards the following topics:

- 1) Comparison of SLR dynamic solutions and VLBI baselines results;
- 2) Control of geodetic network and monitoring of tectonic plate motions and deformations, and assessment of earthquake hazards. Especially, the high temporal resolution of this method may be very useful to obtain the variations of baselines;
- 3) Verification of real accuracy of distant laser ranging technique;
- 4) Assist in accurate determination of UT1. By means of determined three-dimensional station coordinates and LAGEOS space positions at different epochs, the directions of the satellite relative to this station network at those epochs with $0.0005''$ ($1 \text{ cm} / 6000 \text{ KM}$) accuracy can be calculated. If the space directions of two baselines in the network can be determined at some epoch by co-location observations with VLBI or LLR technique at the three relevant stations, then the directions to LAGEOS relative to the inertia reference frame at those epochs can be figured out with the same accuracy, so, the technique could help dynamic methods improve the determination of UT1.

III Technical requirements

1) It is necessary to have 6 or more stations which can range to LAGEOS with 1 cm accuracy participating in the observation in order to obtain stable solutions^{[1][10]};

Fig.1 is the geometry of simultaneous LAGEOS laser ranging. Table 1 is the estimate of co-observable time of LAGEOS at different baselines. Assuming the lowest elevation for LAGEOS ranging is 20° , two stations which are separated by 6000 KM can have 10 or more minutes of common visibility. For $P_1 P_3$ baseline (4450 KM), when the elevation of LAGEOS at station P_1 is 20° , the satellite may be at the zenith of station P_3 at the same time.

2) In order to ensure a sequence of 4 or more stations simultaneous strikes, the percentage of LAGEOS returns at most stations must be about 30% (Table 2). This requires multi-photoelectron receiver and nighttime ranging. For example,

if there are 6 participating stations, 5 Hz repetition lasers, 20% percentage of returns for each station, and 10 minutes co-observation period, giving 3000 transmitted pulses. Then from Table 2, the total number of 4 and more stations simultaneous ranges will be 78 (3000×0.026). If the percentage increases to 30% for these same stations, the total number of simultaneous ranges will be 420.

3) The laser firing epoch at all stations must be strictly controlled by computers, so that laser pulses coming from all stations strike LAGEOS simultaneously with an uncertainty of less than 20 μ sec. This operation mode will be different from the current mode and the fire intervals will no longer be exactly constant at each station. For 10 Hz repetition laser systems, we have,

$$\begin{aligned} \text{Firing commands} &= i/10 \text{ seconds} - (1/2) * \text{Predicting flight time} \\ &\quad - \text{Delay time of firing circuit} \\ &\quad (i = 1, 2, 3, \dots, n) . \end{aligned}$$

Before ranging, the delay time of each laser firing system must be input into computer as a parameter.

It should be pointed out that this laser operational mode will be adopted in the LASSO experiment with millisecond level uncertainties in firing times.

4) The clocks at each station must be synchronized to 0.3 μ sec (1.2 mm range uncertainty) with respect to a master clock. It can be achieved via Loran-C, TV and portable clocks.

IV Estimate of baseline accuracy

JPL's P.R.Escobal and K.M.Ong had made a lot of numerical simulations for baseline solutions with simultaneous laser ranging. Their conclusion was " the method of multilateration can determine the relative three-dimensional solution coordinates with an accuracy that is limited only by the hardware measurement system. If a highly accurate laser ranging system (1 cm accuracy) is used, then accuracies in the 1 cm range can be expected." [10].

In fact, Ong and Escobal employed only a total of 100 trajectory points from a few passes of two different altitude satellites in the simulations. If more stations join in the strictly simultaneous laser ranging and accumulate numbers of passes, especially from two LAGEOS-like satellites, better results of baselines will be obtained, for example, if 10-20 passes with more strikes can be used to the reduction, it will be reasonable to achieve 5 mm baseline accuracy.

The following accuracy of baselines can be expected:

1 cm ---- Temporal solution (a few passes from different satellites in several hours);

0.5 cm ---- Average solution (over dozen passes in several days).

I would like to thank Prof.C.O.Alley and J.Rayner for helpful discussions.

References

1. P.R.Escobal, H.F.Fliegell, R.M.Muller, K.M.Ong, O.H.vos Roos and M.S.Shumate: 3-D Multilateration: A Precision Geodetic Measurement System, JPL Quarterly Technical Review, Vol.2, No.3, (1972).
2. J.J.Degnan, Satellite Laser Ranging: Current Status and Future Prospects, IEEE Trans. on Geoscience and Remote Sensing, Vol.GE-23, No.4, p.398 (1985).
3. T.Varghese, Recent MOBILAS Upgrades, this proceedings.
4. B.Greene, Recent Development at Orroral, this proceedings.
5. J.B.Abshire and S.Gardner, Atmospheric Refractivity Corrections in Satellite Laser Ranging, IEEE Trans. on Geoscience and Remote Sensing, Vol.GE-23, No.4, p.414 (1985).
6. R.Kolenkiewicz, J.Ryan, and M.H.Torrence, A Comparison Between LAGEOS and Very Long Baseline Interferometry Determined Baseline Lengths, J.G.R., Vol.90, No.B11, p.9265 (1985).
7. B.D.Tapley, B.E.Schutz, and R.J.Eanes, Station Coordinates, Baselines, and Earth Rotation From LAGEOS Laser Ranging: 1976-1984, J.G.R., *ibid*, p.9235 (1985).
8. D.C.Christodoulidis, D.E.Smith, R.Kolenkiewicz, S.M.Klosko, M.H.Torrence, and P.J.Dunn, Observing Tectonic Plate Motions and Deformations From Satellite Laser Ranging, *ibid*, p.9249 (1985).
9. E.C.Pavlis, On the Geodetic Applications of Simultaneous Range Differences to LAGEOS, *ibid*, p.9431 (1985).
10. K.M.Ong and P.R.Escobal, Multilateration: A Nondegenerate Method of Obtaining Station Coordinates and Satellite Ephemerides, J. of Astronautical Sciences, Vol.XXI, No.5&6, p.206 (1974).

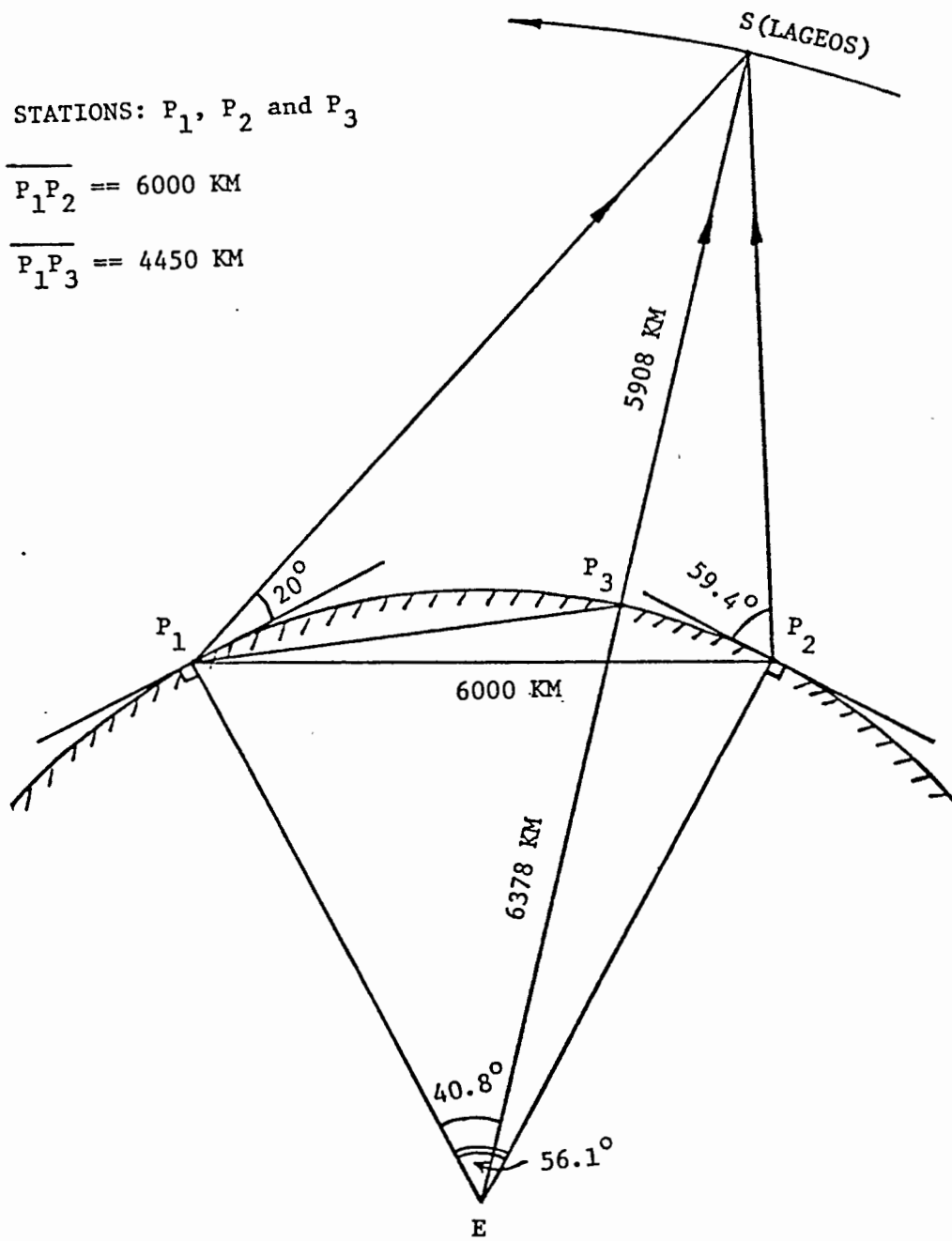


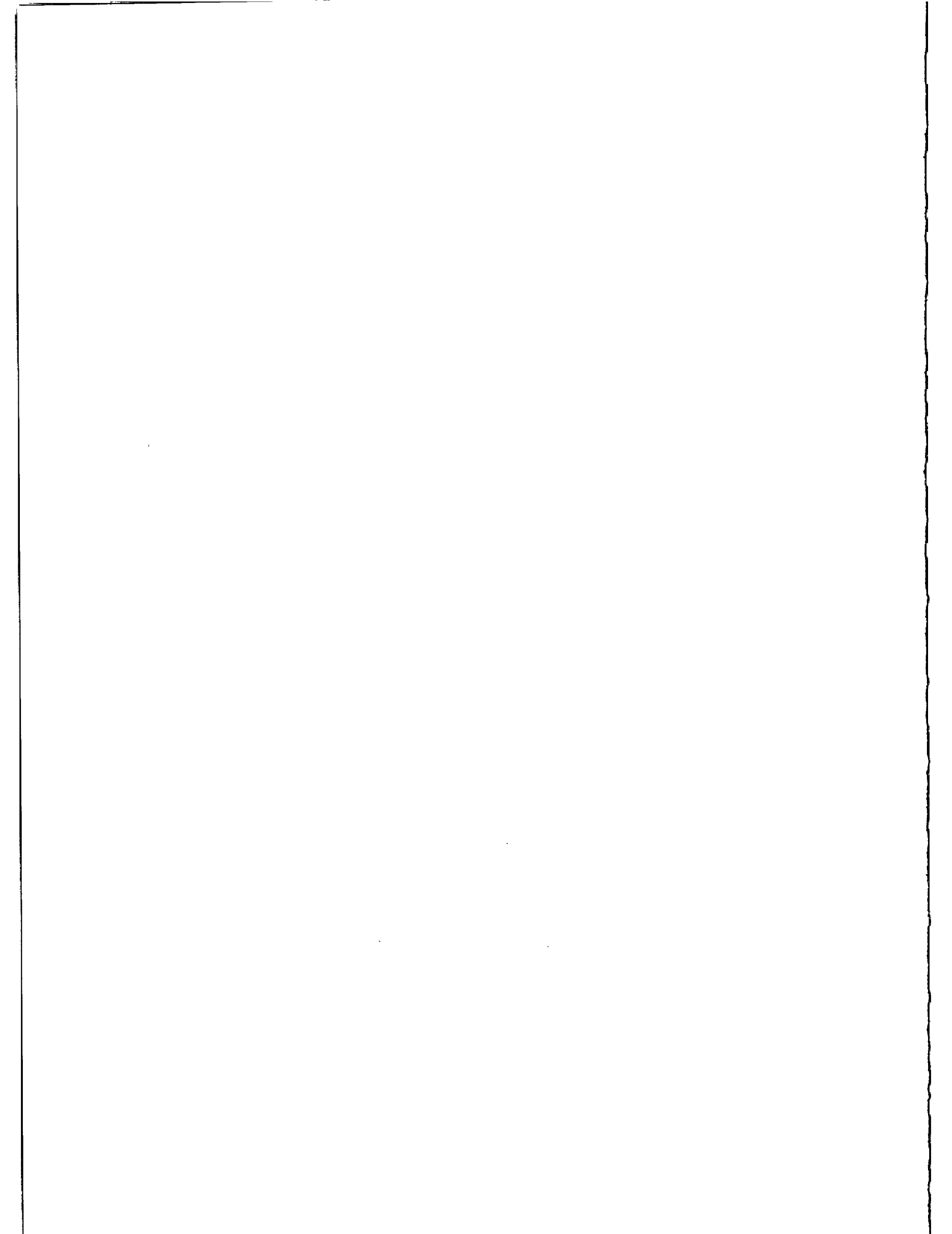
Fig.1 Geometry of Simultaneous Laser Ranging

Table 1
 Estimate of Co-observable Time of LAGEOS
 at Different Baselines

| Lengths of Baselines | 4450 KM | 6000 KM |
|--|------------|------------|
| Co-observable Lengths of Arc with respect to Earth's Center (Elevation: 20° above) | 40.8° | 25.5° |
| Estimate Co-observable Time (Minutes, Elevation > 20°) | 20-30 min. | 10-16 min. |

Table 2
 The Probability of at least 4 Stations Simultaneous Ranging
 in the Cases of Different Number of the Participating Stations

| Assuming Percentage of Returns at Each Stations | Participating Station Numbers | | | | |
|---|-------------------------------|------|------|------|------|
| | 4 | 5 | 6 | 7 | 8 |
| 0.2 | .0016 | .008 | .026 | .063 | .132 |
| 0.3 | .008 | .04 | .14 | .34 | .73 |
| 0.4 | .026 | .14 | .45 | 1 | 1 |
| 0.5 | .062 | .34 | 1 | 1 | 1 |
| 0.6 | .130 | .73 | 1 | 1 | 1 |



STREAK CAMERA BASED LASER RADAR RECEIVER
ITS PERFORMANCE AND LIMITATIONS

I. Prochazka, K. Hamal
Czech Technical University
Faculty of Nuclear Science and Physical Eng.
Brehova 7, 115 19 Prague - Czechoslovakia -

Telephone 848840
TWX 121254 FJFI C

ABSTRACT

The expected streak camera based satellite laser radar receiver performance is discussed. The effects of receiver diameter/field of view, the spatial/temporal relation are described. The noise sources in the receiver were analysed. The low signal - down to a single photoelectron - temporal properties of the C979 Hamamatsu camera and the trigger delay variations were tested.

The streak is one of the candidates for the detector of the laser ranging system with subcentimeter accuracy. To get the subcentimeter ranging accuracy, the two color ranging technique is unavoidable to model the atmosphere on the basis of two colour differential time delay. To achieve the 1mm absolute ranging accuracy, this time delay must be measured with the accuracy about 0.7psec /1/. The streak camera commercially available (August 1986) have the 2 picoseconds temporal resolution. Several two colour ground target ranging experiments using streak cameras have been described /2,3,4,.../. Although, these experiment gave promising results, the application of the streak camera for the satellite laser ranging system introduces some new problems : see WG2. Streak camera simplified scheme is on WG3 together with the signal level calculation /5/.

Receiver field of view limit

For camera top performance , the light spot size on the photocathode must not be wider than 30 μm . This fact restricts substantially the field of view achievable. Assuming the maximal ratio $f/D > 1$ of the receiver optics, the fields of view for different receiver diameters are tabulated on WG4.

Temporal/angular relation

The streak tube is sensitive to a position within the photocathode, where the photons are absorbed. Assuming the streak speed, the tube magnification and the streak velocity at the screen, the streak velocity at the photocathode was calculated (see WG5) for N895 and N1357 tubes. On the same picture there is a table of temporal/angular sensitivity of the streak camera based receivers with different input optics diameter. For example, let us suppose the receiver system of 1 meter diameter equipped with the "10psec" streak tube N895. If the direction of the signal detected is deviated at 2 arcsec from the expected direction , the induced timing bias will approach 2.4 picosecond.

Noise sources and low signal response

The main noise sources are listed on WG6, the possibilities of noise reduction are included. As only a very small area of the photocathode is involved , its noise contribution is negligible compared to other sources. The SIT TV camera noise contribution may be reduced by cooling, its signal to noise ratio may be increased by the persistence integration over the consequent 6-15TV frames. The A/D conversion noise contribution may be reduced by cooling, as well, by proper shielding from RF interference and by proper signal processing.

The streak camera C979 low signal performance was tested at the following set up : see fig.2 on WG7. The 12psec pulse from frequency doubled Nd YAP was reflected by the $R=4\%/85\%$ etalon 130psec and detected by the streak camera. Thus a pair of 12psec pulses spaced at 130 psec arrived at the photocathode, the second pulse 21 times stronger. The strong pulse response was used as a reference, the low pulse response was investigated. The data were transferred from the streak to the HP1000 computer for storing and

off-line processing. A new, in house built preprocessor/interface board for the Hamamatsu Temporal Analyser C1098, which permits both direction communication, recording rate up to 5 Hz, 1-15 persistence integration has been used. The original Hamamatsu algorithm for the persistence integration/calibration was found to introduce highly correlated noise on the single PE level, that is why a new algorithm was developed and applied /6/. To reduce the dark noise, the whole streak camera system was cooled down to +5 deg Centigrade. The record of the doubled pulse is on fig. 3 (strong signal response). To ephase the first pulse, the streak is slightly saturated and the 1:21 ratio is affected. To measure the low signal response, the laser output was attenuated, for each signal strength the series of 500 records was recorded. Using the strong signal response as a reference, the data were overlapped. The actual signal strength was determined in two ways: measuring the laser output power and applying the calibrated ND filters and by signal strength table supplied by the manufacturer. The agreement of both values was within a factor of 3, the second method was giving more stable results and was used later.

The plot of 300 shots out of 500 overlap with a mean signal strength 3 PE and 0.7 PE per shot entering the MCP is on fig.4 and 5. The signal of 3 PE and 0.7 PE on the MCP input corresponds to about 100 and 20 photons on the photocathode input. Obviously, at the signal strength of 3PE and lower, the pulse response is spread, the "dual peak" pulse shape appears and is reproducible. The 24 pseconds contribution is unexplained.

Trigger delay

The trigger delay is the time between the electrical pulse is applied and the streak sweep start. This time is about 10 nsec at the fastest sweep 0.5 nsec/screen. Due to the sweep electrical circuit construction, the delay is drifting in a range up to 1 nanosecond. On fig. 6 there is a plot of the trigger delay drift within 3 hours after ON. The temperature dependence of this effect was tested and found of order lower. No stabilisation of the effect was found within 5 hours after camera ON.

Literature

- 1/ J.J.Degnan, Satellite laser ranging, current status and future prospects, IEEE, Geoscience and remote sensing, Vol. GE-23, No.4
- 2/ J.B.Abshire, J.F.McGarry, H.E.Rowe, J.J.Degnan, Streak camera based laser ranging receiver development proceedings of the 5th IWLRI, Herstmonceux, England, 1984
- 3/ K.Hamal, I.Prochazka, J.Gaignebet, Two wavelength picosecond ranging of ground target, in /2/
- 4/ J.Gaignebet, J.L.Hatat, K.Hamal, I.Prochazka, H.Jelinkova, Two wavelength ranging on ground target using Nd YAG 2HG+Raman in this proceedings
- 5/ Picosecond Steak Camera and its Applications, Picoseconds Vol.14, June 1983, published by Hamamatsu Corp. Japan
- 6/ P.Valach, MS Thesses, FJFI CVUT, Prague, 1986

| Goals of using streak camera as a LR receiver | | Problem areas of streak camera SLR application | | | | | | | | | | | | | | | | |
|---|--------|--|--|--|--|------|-------|---------------------|--------|--------|---------------|-------|-------|----------------|--------|--------|--|--|
| <p>GOALS :</p> <ul style="list-style-type: none"> - subcentimeter ranging accuracy by picosecond laser ranging - atmospheric correction determination by means of two colour ranging and dispersion measurement. <p>Streak camera performance</p> <table border="1"> <thead> <tr> <th></th> <th colspan="2">tube</th> </tr> <tr> <th></th> <th>N895</th> <th>M1357</th> </tr> </thead> <tbody> <tr> <td>temporal resolution</td> <td>18psec</td> <td>2 psec</td> </tr> <tr> <td>dynamic range</td> <td>> 200</td> <td>> 100</td> </tr> <tr> <td>trigger jitter</td> <td>18psec</td> <td>5 psec</td> </tr> </tbody> </table> | | | tube | | | N895 | M1357 | temporal resolution | 18psec | 2 psec | dynamic range | > 200 | > 100 | trigger jitter | 18psec | 5 psec | <p>Problem areas :</p> <ul style="list-style-type: none"> - receiver aperture/field of view echo signal propagation direction - noise sources - low signal response - trigger delay variations | |
| | tube | | | | | | | | | | | | | | | | | |
| | N895 | M1357 | | | | | | | | | | | | | | | | |
| temporal resolution | 18psec | 2 psec | | | | | | | | | | | | | | | | |
| dynamic range | > 200 | > 100 | | | | | | | | | | | | | | | | |
| trigger jitter | 18psec | 5 psec | | | | | | | | | | | | | | | | |
| K.Hanal, I.Prochazka Streak Camera Based LR Receiver Its Performance and .. | | 1 | K.Hanal, I.Prochazka Streak Camera Based LR Receiver Its Performance and .. | | | | | | | | | | | | | | | |
| | | | 2 | | | | | | | | | | | | | | | |

| Streak camera signal/data flow | | Receiver field of view limit | | | | | | | | | | | | | | | | | | | | | | | | | | | | | |
|---|---------------|------------------------------|--|----|------------|--|--|-----|------|------|--|-----|------|--------------------|--|----|------|------------------------------|--|--|-----------|--|--|-------------------|---------------|----------|----------|---------|----------|-----------|-----------|
| <p>Hananatsu streak camera scheme</p> <pre> graph LR Photocat[Photocat.] --> Screen[Screen] Screen --> SIT[SIT TV readout] SIT --> AD[A/D] AD --> TV[TV monitor] AD --- SP[Signal processing] </pre> <p>Signal levels</p> <table border="1"> <tbody> <tr> <td>Photocathode</td> <td>(S - 20)</td> <td>IN</td> <td>30 Photons</td> </tr> <tr> <td></td> <td></td> <td>OUT</td> <td>3 PE</td> </tr> <tr> <td>Mesh</td> <td></td> <td>OUT</td> <td>1 PE</td> </tr> <tr> <td>Microchannel plate</td> <td></td> <td>IN</td> <td>1 PE</td> </tr> <tr> <td>A/D (settings G4, MCP4, P15)</td> <td></td> <td></td> <td>3.5 count</td> </tr> </tbody> </table> <p>Tab. 1</p> | | Photocathode | (S - 20) | IN | 30 Photons | | | OUT | 3 PE | Mesh | | OUT | 1 PE | Microchannel plate | | IN | 1 PE | A/D (settings G4, MCP4, P15) | | | 3.5 count | <p>Receiver field of view limit</p> <ul style="list-style-type: none"> - light spot size on photocathode 38 μmeters - assuming the receiver f/D > 1 <p>The maximum receiver field of view</p> <table border="1"> <thead> <tr> <th>receiver diameter</th> <th>field of view</th> </tr> </thead> <tbody> <tr> <td>2 meters</td> <td>3 arcsec</td> </tr> <tr> <td>1 meter</td> <td>6 arcsec</td> </tr> <tr> <td>0.5 meter</td> <td>12 arcsec</td> </tr> </tbody> </table> | | receiver diameter | field of view | 2 meters | 3 arcsec | 1 meter | 6 arcsec | 0.5 meter | 12 arcsec |
| Photocathode | (S - 20) | IN | 30 Photons | | | | | | | | | | | | | | | | | | | | | | | | | | | | |
| | | OUT | 3 PE | | | | | | | | | | | | | | | | | | | | | | | | | | | | |
| Mesh | | OUT | 1 PE | | | | | | | | | | | | | | | | | | | | | | | | | | | | |
| Microchannel plate | | IN | 1 PE | | | | | | | | | | | | | | | | | | | | | | | | | | | | |
| A/D (settings G4, MCP4, P15) | | | 3.5 count | | | | | | | | | | | | | | | | | | | | | | | | | | | | |
| receiver diameter | field of view | | | | | | | | | | | | | | | | | | | | | | | | | | | | | | |
| 2 meters | 3 arcsec | | | | | | | | | | | | | | | | | | | | | | | | | | | | | | |
| 1 meter | 6 arcsec | | | | | | | | | | | | | | | | | | | | | | | | | | | | | | |
| 0.5 meter | 12 arcsec | | | | | | | | | | | | | | | | | | | | | | | | | | | | | | |
| I.Prochazka, K.Hanal Streak Camera Based LR Receiver Its Performance and .. | | 3 | I.Prochazka, K.Hanal Streak Camera Based LR Receiver Its Performance and .. | | | | | | | | | | | | | | | | | | | | | | | | | | | | |
| | | | 4 | | | | | | | | | | | | | | | | | | | | | | | | | | | | |

| Temporal / angular relation | | |
|-------------------------------------|-----------|----------|
| Streak tube | N895 | N1357 |
| | 18 ps | 2 ps |
| streak velocity at the screen | 67 ps/mm | 25 ps/mm |
| tube magnification | 3.5 | 1.3 |
| streak velocity at the photocathode | 235 ps/mm | 33 ps/mm |

| receiver diameter | temporal/angular sensitivity psec/arcsec | |
|-------------------|--|-------|
| | N895 | N1357 |
| 2 meters | 2.35 | 0.32 |
| 1 meter | 1.18 | 0.16 |
| 0.5 meter | 0.59 | 0.08 |

| Noise sources | | |
|-----------------|--------------|--------------------------------------|
| Noise source | contribution | reduction possibility |
| photocathode | low | cooling |
| MCP intensifier | high | gating, cooling |
| SIT TV camera | medium | persist. intg., cooling |
| A/D conversion | medium | persist. integration data processing |

I. Prochazka, K. Hanal
Streak Camera Based LR Receiver Its Performance and .. 5

I. Prochazka, K. Hanal
Streak Camera Based LR Receiver Its Performance and .. 6

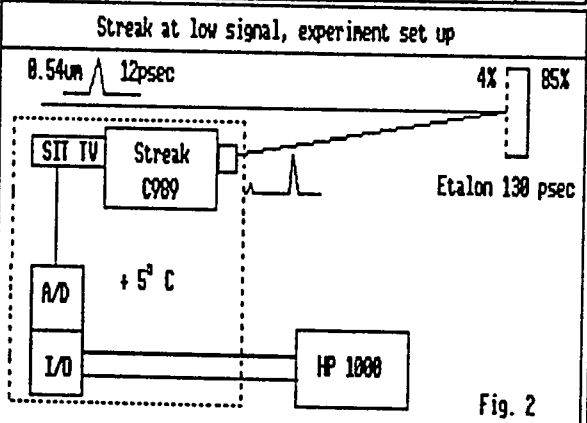


Fig. 2

- cooling to +5° C
- no MCP gating available
- inhouse built preprocessor/interface
 - * recording/transfer rate up to 5 pps
 - * 1-15 persistence integrations
 - * new calibration/integration algorithm
- streak records overlap

I. Prochazka, K. Hanal
Streak Camera Based LR Receiver Its Performance and .. 7

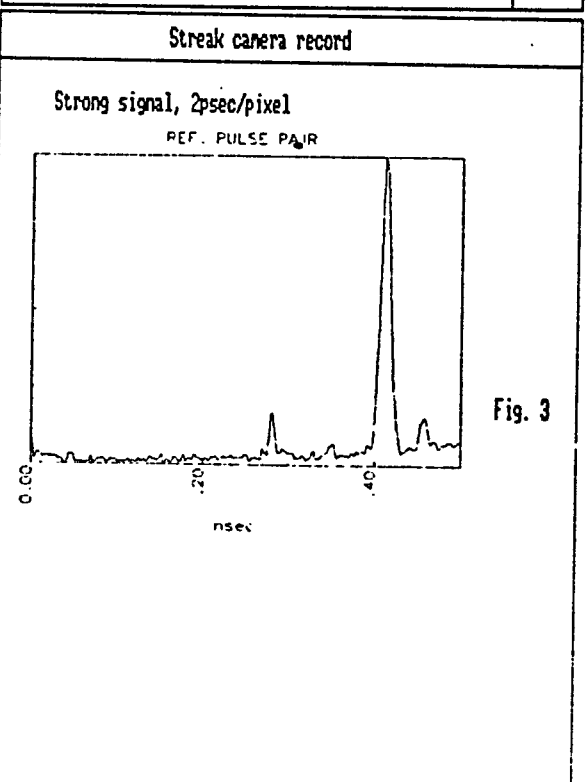

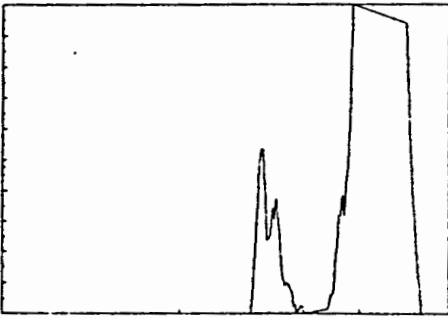
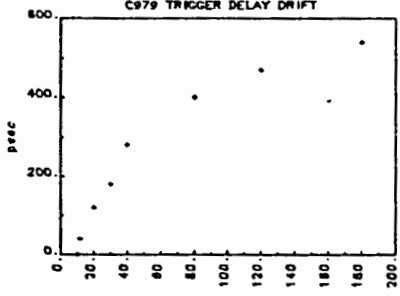


Fig. 3

I. Prochazka, K. Hanal
Streak Camera Based LR Receiver Its Performance and .. 8

| | | | | | | | | | | | |
|--|--|----------------------|---------|---------------------------------------|---------|--|---------|----------------------------|---------|---|---------|
| <p style="text-align: center;">Streak low signal response, 300 records overlap</p> <p style="text-align: center;">3 PE entering MCP, approx. 100 Photons on photocathode</p>  <p style="text-align: right;">500psec/ screen</p> <p style="text-align: right;">Fig. 4</p> <p style="text-align: center;">0.7 PE entering MCP, approx. 20 Photons on photocathode</p>  <p style="text-align: right;">500psec/ screen</p> <p style="text-align: right;">Fig. 5</p> | <p style="text-align: center;">Low signal pulse spread</p> <table border="0" style="width: 100%;"> <tr> <td>driving pulse length</td> <td style="text-align: right;">12 psec</td> </tr> <tr> <td>streak strong signal response+overlap</td> <td style="text-align: right;">16 psec</td> </tr> <tr> <td>sweep nonlinearity contribution (unmodelled)</td> <td style="text-align: right;">11 psec</td> </tr> <tr> <td>streak low signal response</td> <td style="text-align: right;">31 psec</td> </tr> <tr> <td>unexplained $\sqrt{31^2 - 16^2 - 11^2}$</td> <td style="text-align: right;">24 psec</td> </tr> </table> <p style="text-align: right;">Table 3</p> <p>* dual peak pulse shape for signal strength < 3PE is reproducible</p> | driving pulse length | 12 psec | streak strong signal response+overlap | 16 psec | sweep nonlinearity contribution (unmodelled) | 11 psec | streak low signal response | 31 psec | unexplained $\sqrt{31^2 - 16^2 - 11^2}$ | 24 psec |
| driving pulse length | 12 psec | | | | | | | | | | |
| streak strong signal response+overlap | 16 psec | | | | | | | | | | |
| sweep nonlinearity contribution (unmodelled) | 11 psec | | | | | | | | | | |
| streak low signal response | 31 psec | | | | | | | | | | |
| unexplained $\sqrt{31^2 - 16^2 - 11^2}$ | 24 psec | | | | | | | | | | |
| <p>I.Prochazka, K.Hanal Streak Camera Based LR Receiver Its Performance and ..</p> | <p>K.Hanal, I.Prochazka Streak Camera Based LR Receiver Its Performance and ..</p> | | | | | | | | | | |
| <p style="text-align: center;">Trigger delay variations</p>  <p style="text-align: right;">Fig. 6</p> <ul style="list-style-type: none"> - the saturation was not found within 3 hours, - the temperature changes +5 C to +35 C have low impact on the trend - the effect complicates the streak camera application in the automated laser radar system | <p style="text-align: center;">Conclusion</p> <ol style="list-style-type: none"> 1. The temporal resolution of 10/2 (0.4)psec and dynan. ratio 200/100 are attractive for two color laser ranging applications. 2. The "FOV" limitation and the angular/temporal sensitivity are serious problems affecting the system design and its limitations. 3. The use of streak camera at extremely low light levels has been demonstrated for conventional 10psec tube. (Using the new Hamamatsu ps tube+2MCP, the 1PE detection should be possible as a standard technique) 4. The trigger delay time/temperature variations complicate the automation of TV time delay measurements and makes the application of streak camera as a vernier to a ranging counter very difficult | | | | | | | | | | |
| <p>K.Hanal, I.Prochazka Streak Camera Based LR Receiver Its Performance and ..</p> | <p>K.Hanal, I.Prochazka Streak Camera Based LR Receiver Its Performance and ..</p> | | | | | | | | | | |

TWO WAVELENGTH RANGING ON GROUND TARGET
USING ND:YAG 2HG + RAMAN.0.68 μ M PULSES

J. Gaignebet, F. Baumont, J.L. Hatat
C.E.R.G.A.
Avenue Nicolas Copernic
06130 - Grasse - France -

Telephone 93 36 58 49
Telex 470865 F

K. Hamal, H. Jelinkova, I. Prochazka
Czech Technical University
Faculty of Nuclear Science and Physical Eng.
Brehova 7, 115 19 Prague - Czechoslovakia -

Telephone (1) 848840
Telex 121254FJFI C

ABSTRACT

A two color ranging experiment is described here. The system is designed with the following goals.

- Ground to Ground measurements with a precision at 10^{-7} for distances ranging from 50 km to 300 km
- Ground to satellite ranging with an accuracy of 5 mm (shot to shot basis)
- Possibility to develop a space borne system around the ideas tested on the ground.

0.68 μ m, the upper one to the stimulating 2HG (0.53 μ m). The streak sweep is 4psec/pixel in the dual window mode.

Signal processing results

A mirror mounted upside down led to a temporal/spatial structure with double pulse. This degradation was emplied by the Raman Cell (threshold and staturation effect) and gave us serious difficulties on the processing and application of correlation algorithms.

Thus we think that the results are not very significant and that the experiment must be reimplemented to give true figures.

Literature

- 1/ Picosecond Streak Camera and its applications, Picoseconds, Voll4, June 1983, published by Hamamatsu Corp. Japan
- 2/ P.Valach, Diploma Work, FJFI CVUT, Prague, 1986
- 3/ I.Procházka Start detector for the mode locked train laser radar in this proceedings
- 4/ Y.Tarasov, Laser physics Moscow, 1983
- 5/ I.Procházka, K.Hamal, Streak camera as a LR reseceiver, its performance and limitations in this proceedings
- 6/ K.Hamal, H.Jelinkova, Stable saturable dye for 1.06 μ m in this proceedings

Laser transmitter for 1.06/0.68/0.53 μm

The optical scheme is on fig 1. The oscillator is formed by 100%/5m/concave mirror in the contact with 2mm flowing dye cell and a wedged plate (M1). The design of the cell ensures optimum laminar dye flow. The cell is filled with the saturable dye ML51/6/. The YAG rod 3x50mm 2deg/2deg is Quantel pumping head (OSC). The iris diameter 1.6mm ensures the single mode operation. The front mirror (M2) is a quartz plate 0.025mm thick. Quartz plates (P1,P2) are at the Brewster angle to optimize the polarisation of the output beam for the pulse slicer (SL). The telescope (T) 1:2 matches the beam for the double pass amplifier (G/AMPL/O/M6). The NdYAG rod 7x114 is in Quantel head. The output beam passes the second harmonic generator (SHG), the +1meter focusing lens (L) and enters the Raman hydrogen cell (RAM).

Assuming the purpose - two wavelength ranging in the field conditions - the attention has been focused to the shortest pulse available from the compact set up. The output pulse length from the oscillator/ampl./2HG was 14psec. The pumping energy was varied from the threshold up to 2.3 times above it. No change in the output pulse duration has been observed. The output pulse length at 0.68 μm from the Raman cell was measured 14psec (fig.2), assuming the camera resolution 10psec, the deconvoluted value is 10psec. The Raman cell output was acceptably stable. The 0.68 μm output is collinear with the 0.53 μm input/output and therefore no angle compensation is required.

Two wavelength ranging experimental set up

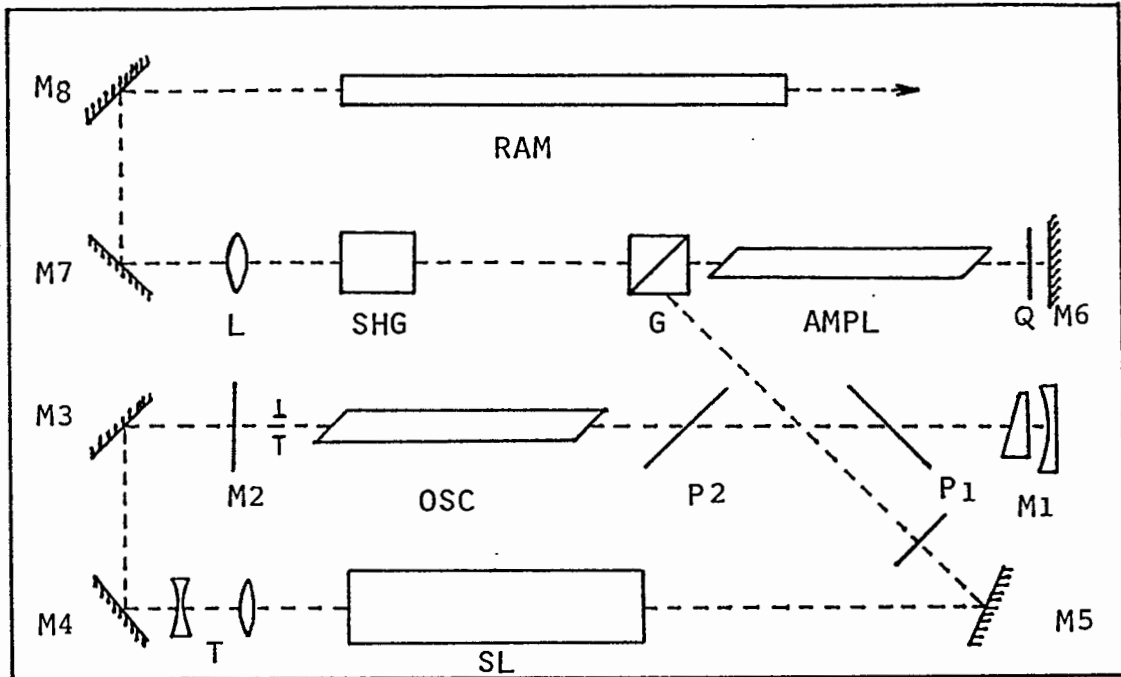
The block scheme of a two wavelength picosecond ranging experiment is on fig 3. The laser output is directed to a corner cube placed at the distance 2m or 110meters for an calibration (indoor) and outdoor passes respectively. A small fraction of the transmitted pulse is picked up and fed to the semiconductor switch /2/ to start the ranging counter and /after an appropriate delay/ the streak camera. The reflected light pulse is passing an optical delay of 20 nsec, ND filters and a dispersion prism. The additional cylindrical lens optics and a streak slit are projecting the input light on two spots on the streak tube photocathode. The Hamamatsu C979 /1/ Temporal disperser system was used. The streak image is monitored by the SIT TV camera and digitized in the Temporal analyser Hamamatsu C1098. Using an in house built preprocessor/interface board in the Temporal analyzer /3/ the digitised data are on line transferred to a computer system HP1000 for display, storing and off line processing. The recording speed exceeds 5 frames/second. The readout system permits to process two windows of one streak image simultaneously. This way, both pulses at different wavelength are recorded at the same time and the trigger jitter contribution to the time delay measurement is suppressed.

The "sweep monitor" camera output signal stops the ranging counter, thus the camera trigger jitter is not involved in the resulting error budget.

Streak camera ranging data

The typical streak record of the TW ranging at 0.53/0.68 μm is on fig.4 . The lower trace corresponds to the Raman down shift

Laser scheme



| | |
|--------|-----------------------------------|
| M1-M8 | ... mirrors |
| L | ... positive lens $f = 1m$ |
| RAM | ... Raman cell |
| SHG | ... second harmonic generator |
| G | ... Glan Thompson polariser |
| AMPL | ... double pass amplifier rod |
| Q | ... quarter wave plate |
| I | ... diaphragm |
| OSC | ... oscillator rod |
| P1, P2 | ... quartz Brewster angles plates |
| T | ... beam expanding telescope |
| SL | ... slicer |

Fig. 1

Raman cell output temporal/spatial structure

Simultaneous 0.68/0.53um record, indoor pass

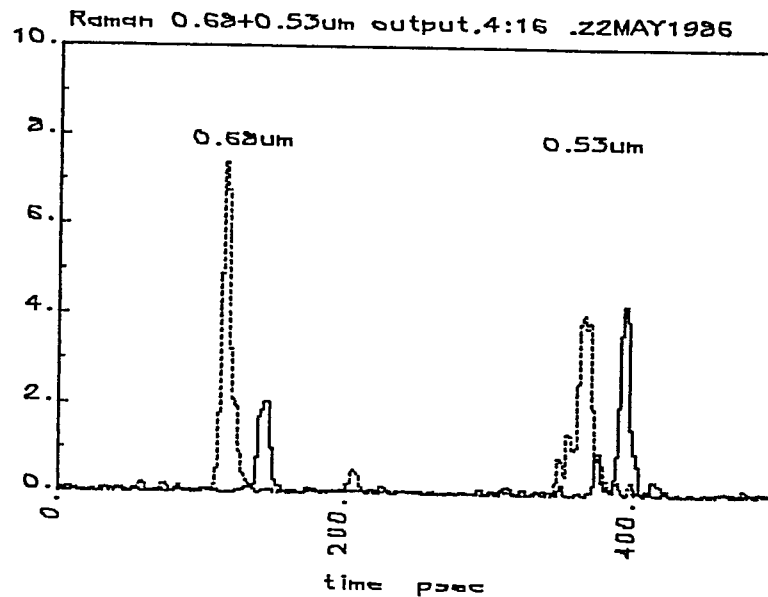
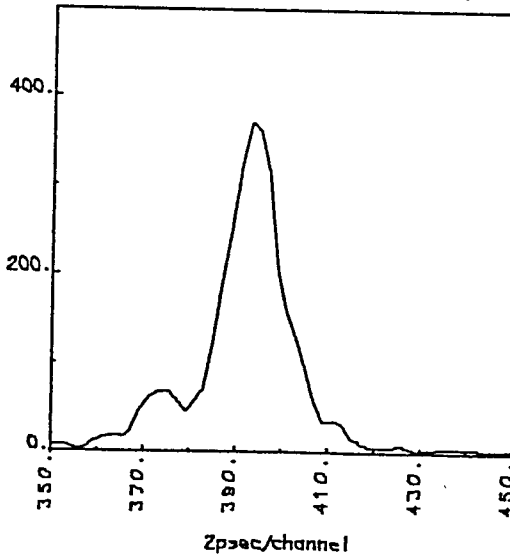


Fig. 6

2HG signal overlap

indoor

Raman TW ranging, indoor, 0.53um overlap



outdoor

Raman TW ranging, 0.53um outdoor overlap

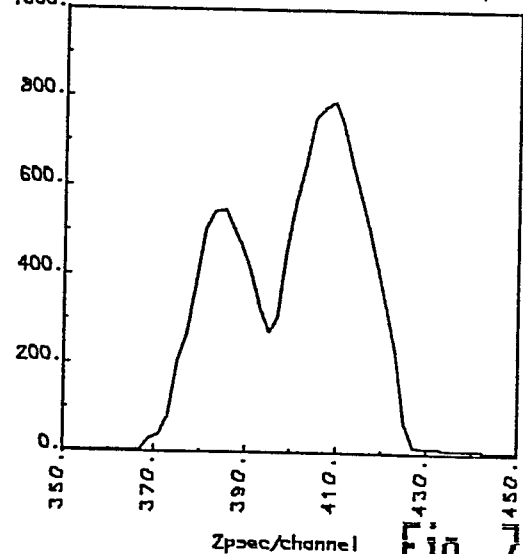
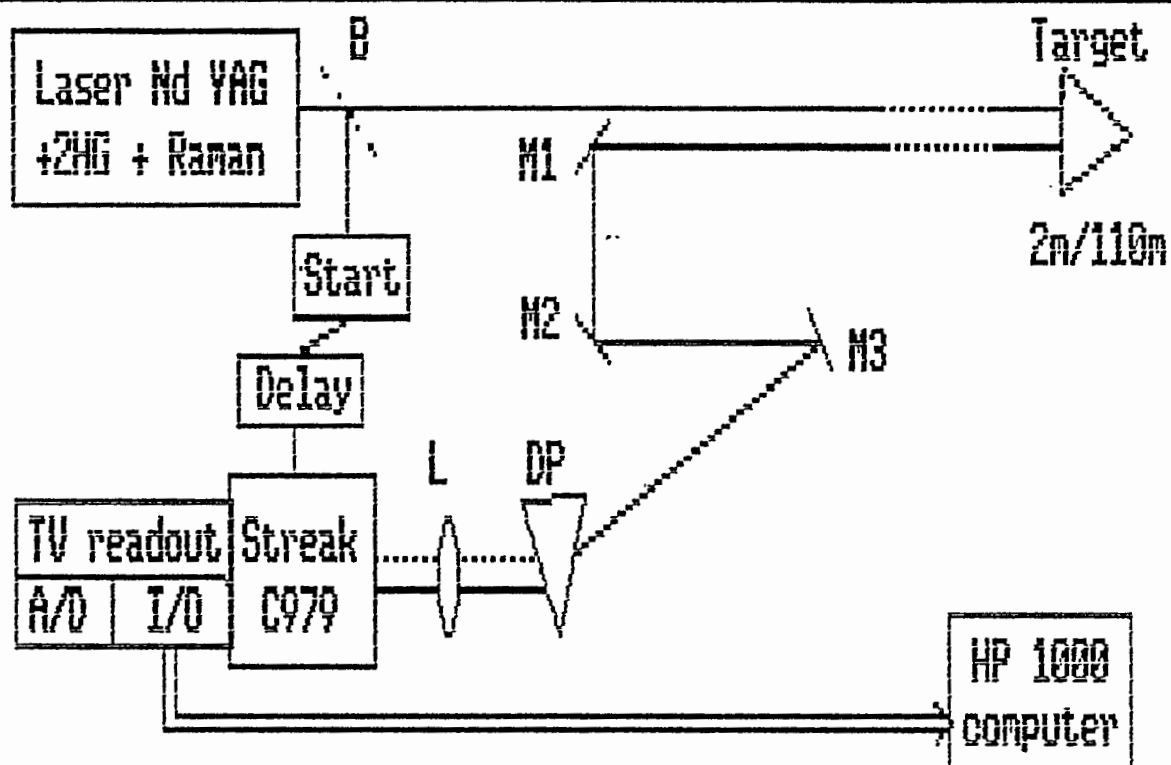


Fig. 7, 8

J. Gaignebet, J. L. Hatat, K. Hamal, I. Prochazka, H. Jelinekova
Two Wavelength Ranging on Ground Target Using Raman...

Two wavelength ranging block scheme



B ... beam splitter

Start ... triggering semiconductor switch

M1, M2, M3. mirrors forming the optical delay 20 nsec

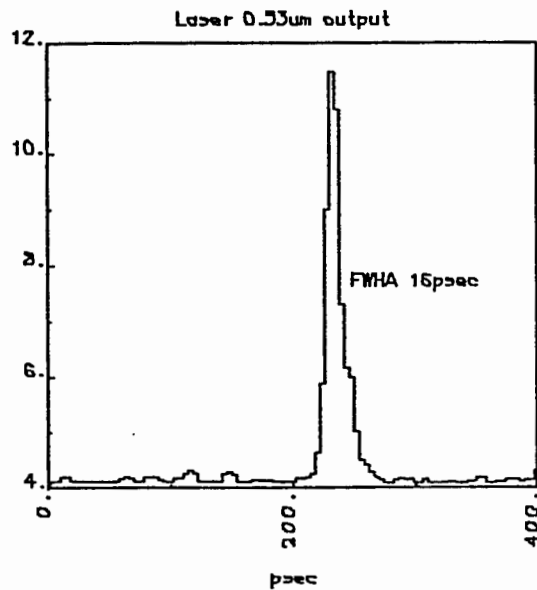
A/D ... part of Hamamatsu Temporal Analyser

I/O ... inhouse built preprocessor/interface

L ... focusing lens

DP ... dispersion prism

Laser output pulses

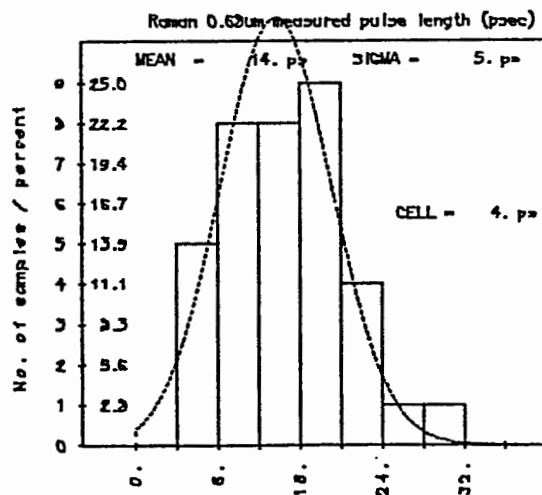


0.53 μm 2HG Nd YAG

FWHA mean : 17 psec

deconvoluted : 14 psec

Fig. 2



0.68 μm Raman

FWHA mean : 14 psec

deconvoluted: 10 psec

Fig. 3

Two wavelength ranging streak records

Indoor pass

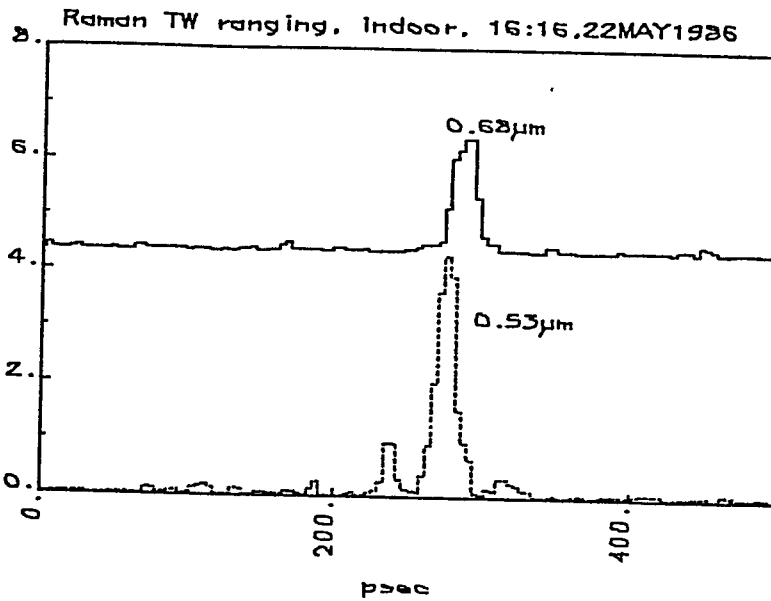
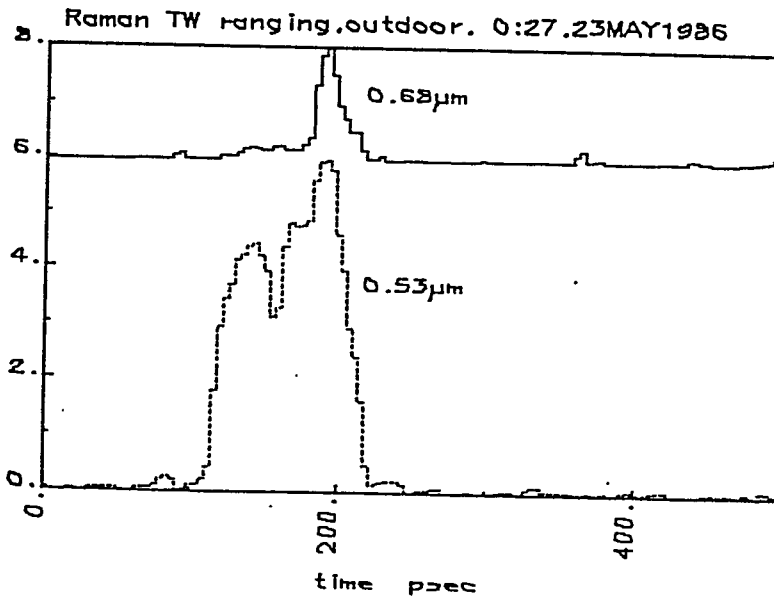
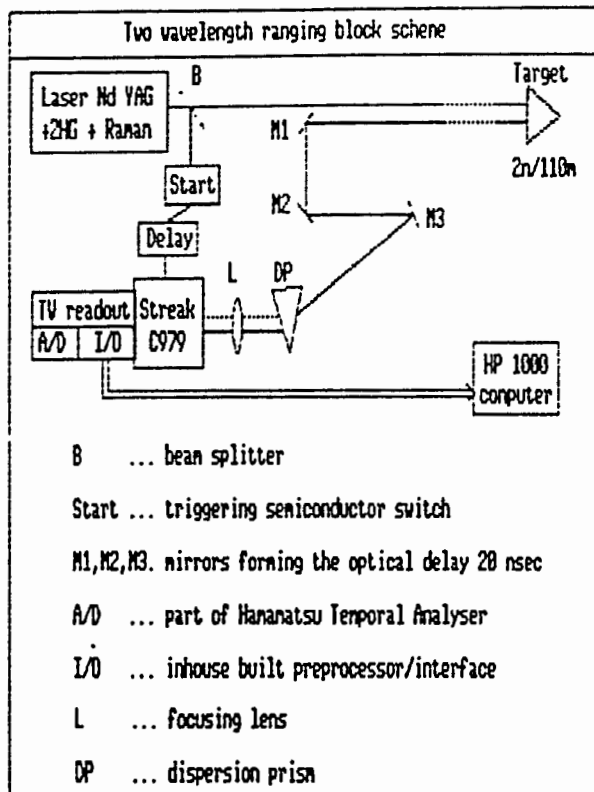


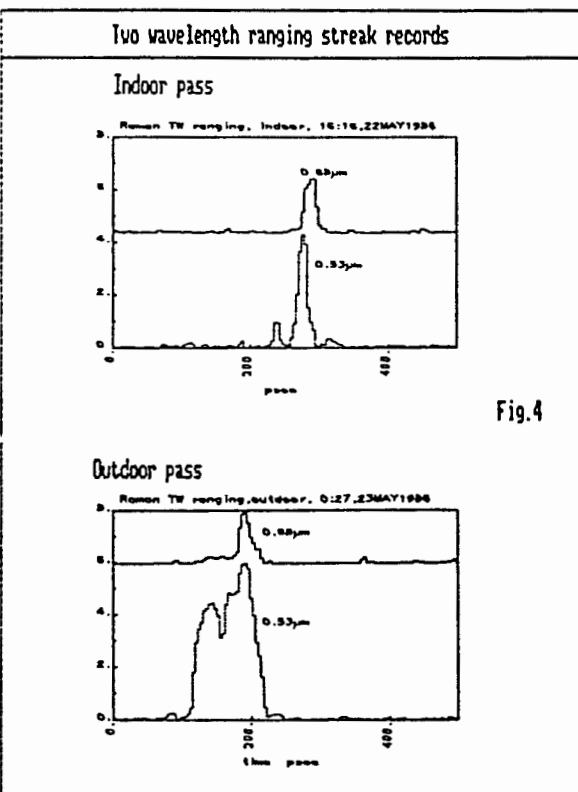
Fig.4

Outdoor pass

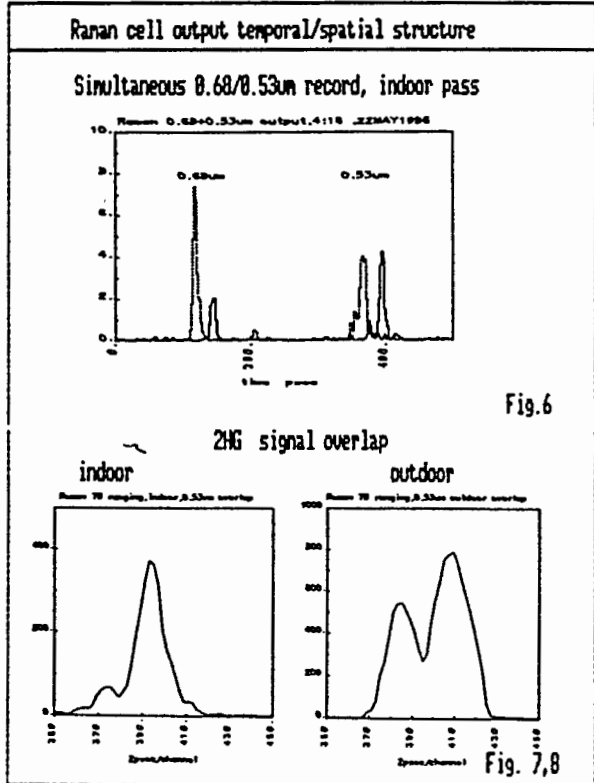




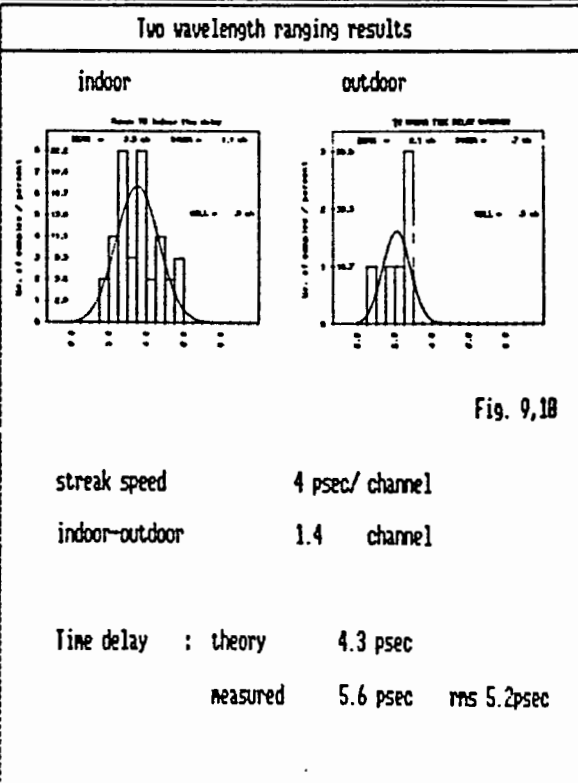
J. Gaignebet, J. L. Hatat, K. Hanal, I. Prochazka, H. Jelinkova
 Two Wavelength Ranging on Ground Target Using Raman... 4



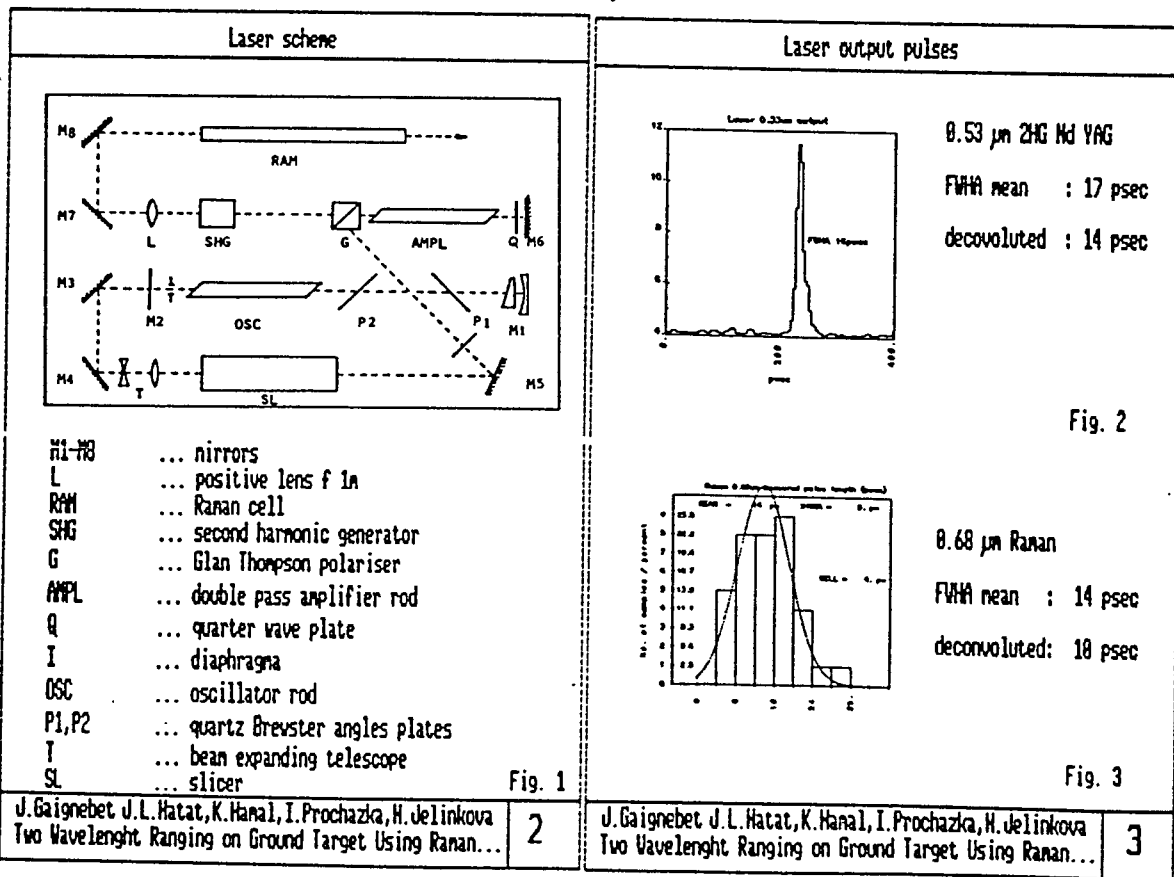
J. Gaignebet, J. L. Hatat, K. Hanal, I. Prochazka, H. Jelinkova
 Two Wavelength Ranging on Ground Target Using Raman... 5

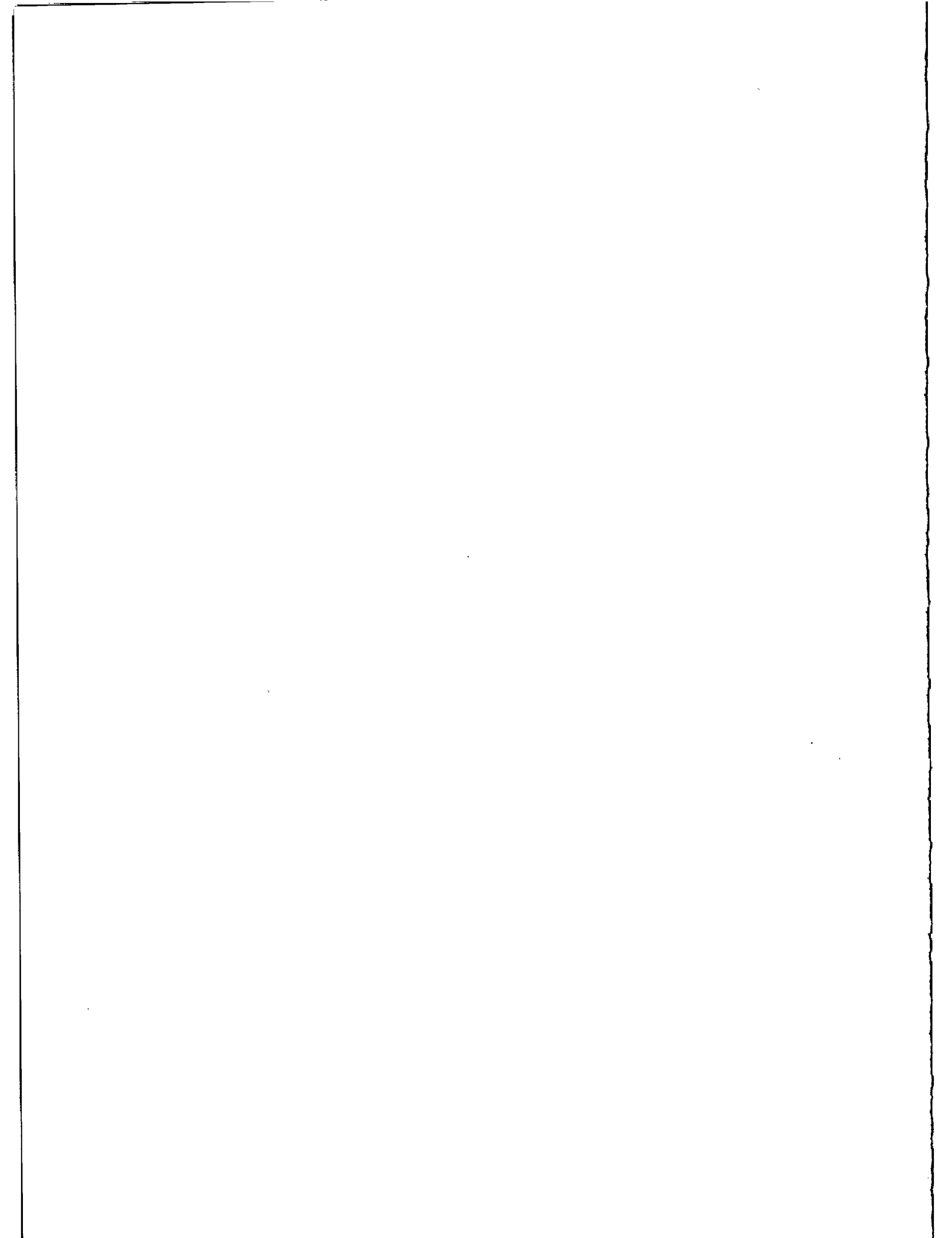


J. Gaignebet, J. L. Hatat, K. Hanal, I. Prochazka, H. Jelinkova
 Two Wavelength Ranging on Ground Target Using Raman... 6



J. Gaignebet, J. L. Hatat, K. Hanal, I. Prochazka, H. Jelinkova
 Two Wavelength Ranging on Ground Target Using Raman... 7





PICOSECOND LASER RANGING USING PHOTODIODE

I. Prochazka, K. Hamal
Czech Technical University
Faculty of Nuclear Science and Physical Eng.
Brehova 7, 115 19 Prague - Czechoslovakia -

Telephone 848840
TWX 121254 FJFI C

ABSTRACT

The two wavelength (1.06 μm and 0.53 μm) laser ranging experiments using photodiode is described. The ultimate jitter limits for different type of photodiodes was measured at the signal strength $1.E4$ to $1.E5$ photons. The jitter limit of 10 psec for TW time delay measurements was found for the in house built HP S5 diode biased 0.1V below break. The minimal signal strength 10,000 photons at 0.53 μm was detected. The jitter of 15 psec rms for two wavelength time delay measurement was achieved.

INTERKOSMOS SATELLITE LASER RADAR NETWORK

PICOSECOND LASER RANGING USING PHOTODIODE

I. Prochazka, K. Hanal

Czech Technical University
Faculty of Nuclear Science and Physical Engineering
Brehova 7, 115 19 Prague, Czechoslovakia

I. Prochazka, K. Hanal
Picosecond Laser Ranging Using Photodiode

0

Goals of picosecond laser ranging using photodiode

GOALS :

- subcentimeter laser ranging
- two colour ranging using single photodiode at high signal strength levels
- measurements :
 - * ultimate jitter limit for photodiode based laser radar receiver
 - * ultimate signal strength for 1.06um and 0.53um ranging

I. Prochazka, K. Hanal
Picosecond Laser Ranging Using Photodiode

1

INTERKOSMOS SATELLITE LASER RADAR NETWORK

Experimental set up

Example of Tranzient record

I. Prochazka, K. Hanal
Picosecond Laser Ranging Using Photodiode

2

Tranzient data processing

Tranzient data processing

Smoothering, sweep nonlinearity compensation

Pulse position determination:

- Mean of pulse half amplitude leading/trailing edge
- * minimal amplitude 1 div (10mV)
- * jitter 13 - 8 psec 1 - 8 div ampl.
- * time walk (20 psec
- * simple and fast

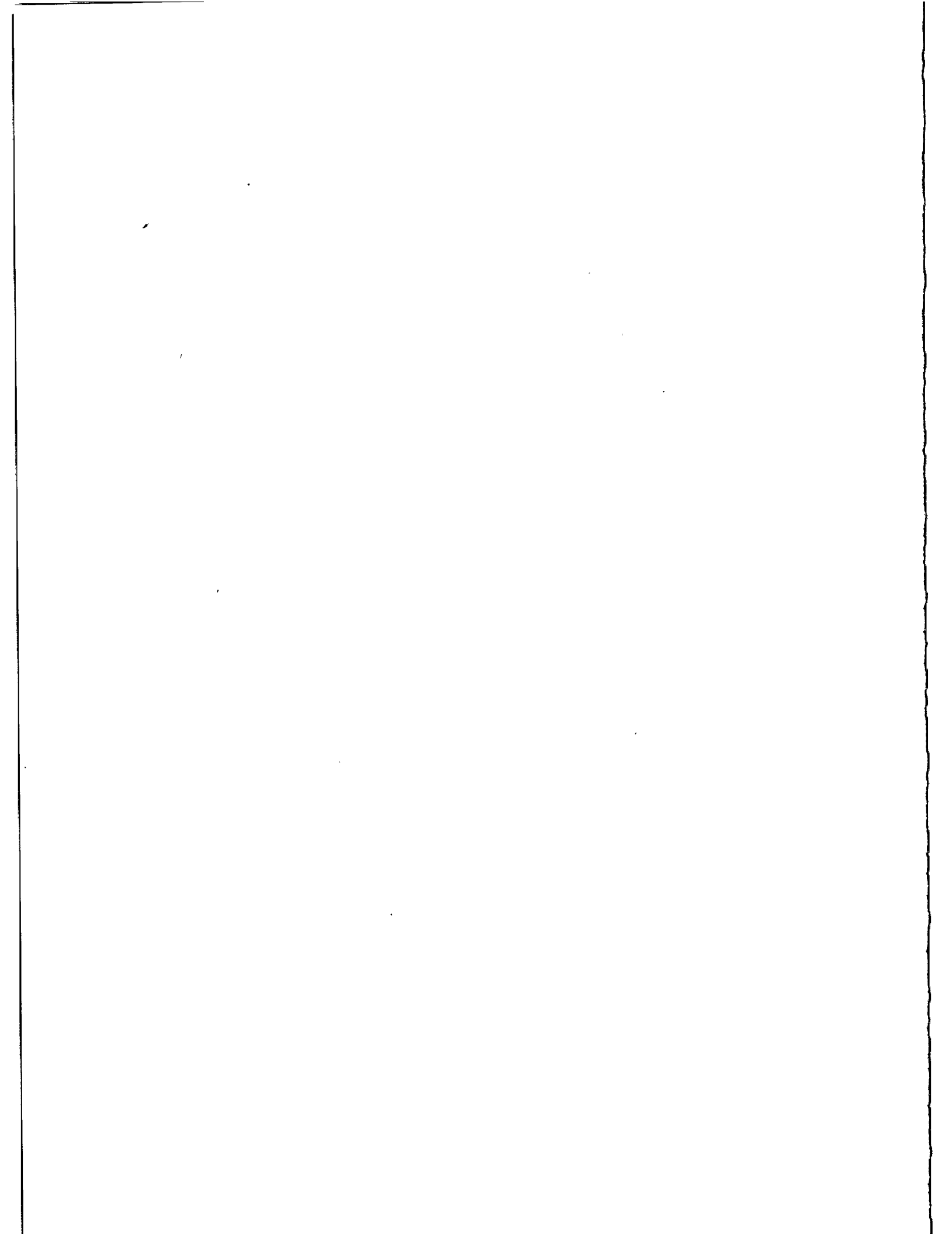
Pulses separation determination:

Correlation algorithm

- * min. amplitude 0.2 div
- * jitter 18 - 6 psec 0.2 - 8 div
- * time walk 100 psec 0.2 - 8 div
- software compensation is required
- * time consuming

I. Prochazka, K. Hanal
Picosecond Laser Ranging Using Photodiode

3



MULTIPLE WAVELENGTH LASER RANGING

B.A. Greene
Division of National Mapping
P.O. Box 31
Belconnen ACT 2616 - Australia -

Telephone (6162) 525095
Telex AA62230

T.A. Herring
Harvard/Smithsonian Center for Astrophysics
60 Garden Street
Cambridge MA 02138 - USA -

Telephone (617) 4959279
Telex 921418

ABSTRACT

The establishment of sub-centimeter accuracy satellite-laser ranging (SLR) systems may require such systems to operate at more than one wavelength in order to ensure that range corrections made to compensate atmospheric dispersion are themselves accurate. Analytic expressions to be applied to the observed dual (or multiple) color ranges are derived with particular emphasis on their application in an operational environment. Full consideration is given to the design needs for sub-centimeter accuracy systems, resulting in system design parameters for operational multiple wavelength SLR stations. Progress on the design and construction of such a system is reported.

1. INTRODUCTION

The refractive index of the earth's atmosphere depends on the wavelength of the signal transmitted through it. At optical wavelengths, this dispersion of the atmosphere should be sufficiently large that two ranges to a body measured with different wavelengths could be used to estimate the contribution of atmospheric refraction to each of the ranges. Since the signals at each of the wavelengths will be affected differently by the atmosphere, the difference in the ranges should be related to the total contribution of the atmospheric refraction at each of the wavelengths. The applications of the such techniques to satellite-laser ranging (SLR) have been discussed by Bender and Owens, 1965; Owens, 1967; Abshire and Gardner, 1985.

In this paper we examine the dual-color correction in detail. In particular we consider the effects of the approximations made in deriving the standard refractive index formulas, the contribution of water vapor, and the effects of ray bending. We also examine the equipment needed for the dual-color correction to make a significant improvement in the accuracy of satellite laser ranging.

2. THEORY OF THE DUAL-COLOR CORRECTION

The oneway range to a satellite measured with a signal which is affected by the earth's atmosphere is approximately given by (here we neglect the effects of the motion of the satellite relative to the transmitting station)

$$R_o = \int_{atm} n_g(s) ds \quad (1)$$

where \int_{atm} is the integration along the path followed by the signal, and $n_g(s)$ is the group refractive index at each point s along the path. Ideally, we would like to estimate the contribution of the atmospheric refraction to the integral given in equation (1) so that we could estimate the geometric part of the range, R_g , given by

$$R_g = \int_{vac} ds \quad (2)$$

where \int_{vac} is the integration along the straight line path between the transmitter and the satellite. We will define the contribution of atmospheric refraction, R_a , to the observed range to be $R_o - R_g$. R_a will be wavelength dependent (see e.g., Owens, 1967) because of the wavelength dependence of both n_g and the integration path in equation (1). If we can write equation (1) in the form

$$R_{oj} = R_g + F(\lambda_j)G_a(P, T, e, \dots) \quad (3)$$

where the subscript j denotes a specific wavelength, F is a function only of wavelength λ_j , and G_a is only a function of atmospheric parameters such as pressure, P ; temperature, T ; and water vapor partial pressure, e ; then we could obtain estimates

of R_g from measurements of R_o at two wavelengths. Measurements R_{o1} and R_{o2} made at wavelengths λ_1 and λ_2 can be combined using

$$\hat{R}_g = \frac{F(\lambda_2)R_{o1}}{F(\lambda_2) - F(\lambda_1)} - \frac{F(\lambda_1)R_{o2}}{F(\lambda_2) - F(\lambda_1)} \quad (4)$$

to obtain an estimate of the geometric range. \hat{R}_g will differ from R_g due to measurement errors in R_{o1} and R_{o2} , and due to equation (3) not fully representing the effects of the atmospheric contribution to the observed range.

To assess the likely improvement of using equation (4) instead of relying on other means to calibrate R_a , we will examine the effects of the approximations made in manipulating equations (1) and (2) into the form of equation (3), and the effects of noise in the measurements R_{o1} and R_{o2} on \hat{R}_g . We commence our discussion by examining the group refractivity of a mixture of gases (such as those in the earth's atmosphere). The group refractivity is derived from the phase refractivity, n_p , which for non-polar gases, is given approximately by the Lorenz-Lorentz equation (Bottcher, 1952)

$$\frac{n_p^2 - 1}{n_p^2 + 2} = \sum_i \mathcal{R}_i(\lambda)\rho_i \quad (5)$$

in which \mathcal{R}_i is the specific refraction and ρ_i is the partial density of the i th component of the mixture. The specific refraction is derived from a measurement of $\frac{n_p^2 - 1}{n_p^2 + 2}$ for a single constituent of the mixture at a specific value of ρ_i and λ . From equation (5) we see that the determination of n_p reduces to determining the function $\mathcal{R}_i(\lambda)$ and the determination of ρ_i for any atmospheric conditions. For our study we take the formulas of Owens (1967) for $\mathcal{R}_i(\lambda)$ and ρ_i for dry, CO₂ free air; water vapor; and CO₂. These formulas and their ranges of validity are summarized in Table 1.

To derive an equation of the form of equation (3) we need to make some assumptions (which we will evaluate the effects of later in this paper). The first approximation we need to make will allow us to convert equation (5) from its non-linear form to a linear one. If we expand the left hand side of equation (5), assuming n_p is close to 1, then the equation reduces to

$$2(n_p - 1)/3 - (n_p - 1)^2/9 = \sum_i \mathcal{R}_i(\lambda)\rho_i. \quad (6)$$

If the second order term is neglected, then we may express the phase refractivity of each constituent, n_{pi} , in the mixture as a function only of the $\mathcal{R}_i(\lambda)$ and ρ_i for that constituent *i.e.*,

$$2(n_{pi} - 1)/3 = \mathcal{R}_i(\lambda)\rho_i. \quad (7)$$

Owens (1967) derived a simplified set of refractivity formulas based on the expansion given in equation (7). In this linearized form, refractivity formulas can be given for each constituent of the atmospheric mixture separately. However, since the mixing ratios of many of these constituents remain constant through out the atmosphere, many of them can be grouped together.

Table 1. Equations for atmospheric refractive index (compiled from Owens, 1967)

Dry air, CO₂ free air

$$((\mathcal{R}_o)_1 - 1) \times 10^8 = 8340.78 + \frac{2405640.}{(130 - \sigma^2)} + \frac{15994.}{(38.9 - \sigma^2)}$$

$$\rho_1 = 348.328 \frac{P_1}{T} \left[1 + P_s (57.90 \times 10^{-8} - \frac{9.3250 \times 10^{-4}}{T} + \frac{0.25844}{T^2}) \right]$$

$$(\rho_o)_1 = \rho_1 (P = 1013.25 \text{ mb}, T = 288.16 \text{ K})$$

Range of validity: 2303–20,586 Å; 240 K < T < 330 K; 0 < P < 4 atm.

Water vapor

$$((\mathcal{R}_o)_2 - 1) \times 10^8 = 295.235 + 2.6422\sigma^2 - 0.03138\sigma^4 + 0.004028\sigma^6$$

$$\rho_2 = 216.582 \frac{e}{T} \left[1 + e \left[1 + 3.7 \times 10^{-4} \left[-2.37321 \times 10^{-3} + \frac{2.23366}{T} - \frac{710.792}{T^2} + \frac{7.75141 \times 10^4}{T^3} \right] \right] \right]$$

$$(\rho_o)_2 = \rho_2 (P = 13.33 \text{ mb}, T = 293.16)$$

Range of validity: 3611–6440 Å; 250 K < T < 320 K; 0 < P < 100 mb.

Carbon dioxide

$$((\mathcal{R}_o)_3 - 1) \times 10^8 = 22822.1 + 117.8\sigma^2 + \frac{2406030.}{(130 - \sigma^2)} + \frac{15997.}{(38.9 - \sigma^2)}$$

$$\rho_3 = 829.37 \frac{P_3}{T}$$

$$(\rho_o)_3 = \rho_3 (P = 1013.25 \text{ mb}, T = 288.16 \text{ K})$$

Range of validity: 2379–6010 Å; 240 K < T < 330 K; 0 < P < 17 mb.

P_1 is partial pressure of dry air (mbar),
 e is partial pressure of water vapor (mbar),
 P_3 is partial pressure of CO₂ (mbar),
 T is temperature (K),
 σ is $\frac{1}{\lambda}$ (μm^{-1}).

In Table 2 we give Owens formulas for the group and phase refractivities for dry air with 0.03 % CO₂ (standard air), and for water vapor. The form of the refractivities is

$$n_{gi}(\lambda) = f(\lambda)D_i \quad (8)$$

where $f(\lambda)$ depends only on λ , and D is independent of λ . Substituting equation (8) into the definition of R_a , we obtain

$$R_a(\lambda) = \int_{atm} (1 + \sum_i f_i(\lambda)D_i) ds - \int_{vac} ds. \quad (9)$$

If we assume that $\int_{atm} = \int_{vac}$ then equation (9) reduces to

$$R_a(\lambda) = \sum_i f_i(\lambda) \int_{vac} D_i ds \quad (10)$$

where we show the integration path to be through vacuum to emphasize that we have assumed that the integration along the atmospheric path and the vacuum path are the same in order to obtain equation (10).

For the Owen's simplified formulas i takes on two values, one for standard air and one for water vapor. We may now write an equation for R_{oj} almost in the form of equation (3), *vis.*

$$R_{oj} = R_g + f_d(\lambda_j) \int_{vac} D_d ds + f_w(\lambda_j) \int_{vac} D_w ds \quad (11)$$

where we show explicitly the terms for standard air with a subscript d and those for water vapor with a subscript w . If the water vapor terms are neglected in equation (11) then $f_d(\lambda_j)$ corresponds to $F_d(\lambda_j)$ in equation (3), and $\int_{vac} D_d ds$ corresponds to $G(P, T, E, \dots)$. $f_d(\lambda_j)$ then becomes the frequency dependent function we should use in computing the dual color correction.

3. ACCURACY OF THE DUAL-COLOR CORRECTION

The usefulness of the dual color correction will depend on two factors: the effects of noise in the range measurements, and the effects of the approximations we have made in deriving equation (11). The effects of noise can be simply computed by evaluating the coefficients in equation (4) for pairs of wavelengths commonly used in satellite laser ranging. In Table 3, we give the coefficients of the linear combinations for four laser wavelengths. Even for largest separation of wavelengths ($\lambda = 1.064$ and $0.355 \mu\text{m}$), the dual color estimate of the range will 11 times noisier than in individual range measurements at the two wavelengths (assuming equal range error for the two wavelengths). Also, any biases in the range measurements will also be amplified by a similar amount.

In addition to the noise in the dual color system, we need to examine the effects of the assumptions we have made in deriving the correction formulas. We

Table 2. Simplified equations for atmospheric refractive index (compiled from Owens, 1967)

Dry air with 0.03 % CO₂ (Standard air)

$$(n_p - 1) \times 10^8 = \left[2371.34 + \frac{683939.7}{(130 - \sigma^2)} + \frac{4547.3}{(38.9 - \sigma^2)} \right] D_s$$

$$(n_g - 1) \times 10^8 = \left[2371.34 + \frac{683939.7(130 + \sigma^2)}{(130 - \sigma^2)^2} + \frac{4547.3(38.9 + \sigma^2)}{(38.9 - \sigma^2)^2} \right] D_s$$

$$D_s = \frac{P_s}{T} \left[1 + P_s(57.90 \times 10^{-8} - \frac{9.3250 \times 10^{-4}}{T} + \frac{0.25844}{T^2}) \right]$$

Water vapor

$$(n_p - 1) \times 10^8 = [6487.31 + 58.058\sigma^2 - 0.71150\sigma^4 + 0.08851\sigma^6] D_w$$

$$(n_g - 1) \times 10^8 = [6487.31 + 174.174\sigma^2 - 3.55750\sigma^4 + 0.61957\sigma^6] D_w$$

$$D_w = \frac{e}{T} \left[1 + e \left[1 + 3.7 \times 10^{-4} \times \left[-2.37321 \times 10^{-3} + \frac{2.23366}{T} - \frac{710.792}{T^2} + \frac{7.75141 \times 10^4}{T^3} \right] \right] \right]$$

investigated these effects by ray tracing through model atmospheres and computing the dual-color correction from the ranges computed in the ray trace. In the ray trace model, the full Lorenz-Lorentz equation for the refractivity of the mixture was used. Thus, we were able to assess the effects of all of the assumptions we had made. The summary of the results obtained from the ray tracing are given in Table 4.

The two largest sources of error in Table 4 arise from the presence of water vapor, and the effects of the bending of the ray as the signal propagates through the atmosphere. These two effects affect the dual color correction because their wavelength dependence is different from that for standard air. The wavelength dependence of water vapor is given in Tables 2 and 3. The contribution of water vapor to the error was almost independent of the choice of wavelength pairs. However, this result should be treated cautiously because only one the wavelengths we examined was within the range of validity of the refractive index formulas for water vapor. The errors due to water vapor could be reduced by removing the water-vapor contribution to the observed ranges before the dual color correction was computed. However, the dual-color correction would then be influenced by errors in modeling the distribution of water vapor in the atmosphere. As a general rule, the error in the dual-color correction will be approximately 50-100% larger than the error in computing the water vapor contribution to the ranges.

Table 3. Refractive index dispersion and dual color combinations

| <u>Dispersion functions, $f(\lambda)$</u> | | | | |
|--|-------------------|--|--|--------------|
| λ | | $f_d(\lambda)$ | $f_w(\lambda)$ | |
| (μm) | | | | |
| 1.064 | | 7866.06 | 6638.81* | |
| 0.694 | | 8028.77 | 6839.15* | |
| 0.532 | | 8235.85 | 7085.63 | |
| 0.355 | | 8925.00 | 7954.92* | |
| <u>Dual color combination</u> | | | | |
| λ_1 | λ_2 | $\frac{f_d(\lambda_2)}{f_d(\lambda_2)-f_d(\lambda_1)}$ | $\frac{f_d(\lambda_1)}{f_d(\lambda_2)-f_d(\lambda_1)}$ | Noise ratio† |
| (μm) | (μm) | | | |
| 1.064 | 0.694 | 49.34 | 48.34 | 69.0 |
| 1.064 | 0.532 | 22.27 | 21.27 | 30.8 |
| 1.064 | 0.355 | 8.43 | 7.43 | 11.2 |
| 0.694 | 0.532 | 39.77 | 38.77 | 55.5 |
| 0.694 | 0.355 | 9.96 | 8.96 | 13.4 |
| 0.532 | 0.355 | 12.95 | 11.95 | 17.6 |

* These wavelengths fall outside the range of validity of the water vapor refractive index formula

† The noise ratio is computed assuming that the ranges at the two wavelengths are measured with the same standard deviation. The noise ratio gives the ratio the standard deviations of the dual-color-corrected range to the standard deviation of the range measurements.

In the case of bending, the error in the dual-color correction arises because the bending contribution to the range depends on both the group- and phase-refractivities. The error due to bending is approximately equal to the difference in the range along the curved path followed by the ray and the straight line path. Again, this error can be reduced by either by correcting the observed ranges for the effects of bending, or by developing elevation-angle dependent coefficients for combining the ranges at the two wavelengths. Each of these approaches would introduce a dependence in the dual-color correction on the model of the atmosphere used to compute the bending. For observations made with elevation angles greater than 20°, the effects of errors in the bending correction should be small.

There are several other cautions which should be issued concerning dual-color corrections. For laser systems with very short pulses (5-10 ps), the bandwidth of the pulses will be large (6-3 Å). If the pulse shape in the wavelength domain is very irregular, then the effective wavelength to be used in computing the coefficients

Table 4. Errors in dual-color ranging

| Source | Error at Z=0° (mm) | Error at Z=70° (mm) | Comments |
|----------------------------|-----------------------|------------------------|---|
| Use of simplified formulas | < 0.3 | < 1 | λ 1.064, 0.355 μm P= 1013.25-900 mbar T= 293 - 273 K |
| %CO ₂ | < 0.01 | < 0.03 | for 0.03 % changes |
| water vapor | \approx 6 | \approx 17 | 20 mbar H ₂ O for all λ pairs |
| bending | 0 | \leq 4 | all conditions |
| wavelength | 0.3 | 1 | for 1 Å change in λ |

for the dual-color correction may not be the wavelength of the laser itself. The sensitivity of the dual-color corrections to wavelength changes is given in Table 4. A few millimeters of error could be introduced by such effects. Also, the most accurate refractivity formulas should be used in any computation of the corrections. As an example, if the standard IUGG refractivity formulas are used to compute the coefficients for the dual-color correction, then errors of several centimeters can be introduced into the corrected ranges.

The dual-color correction will amplify any noise in the range measurements, generally by at least an order of magnitude. To achieve 1 centimeter dual-color ranges, the ranges at the two wavelengths will need to be measured with sub-millimeter accuracy.

4. SYSTEM DESIGN CONSIDERATIONS

There is no known technique for determining the true flight time difference to 0.5 mm (3 ps) on a single shot. This level of precision can be approached by averaging. The two principal techniques available are:

- average range differences (ARD), and
- difference average ranges (DAR).

These two techniques have fundamentally different observables, and different noise ratios. The average range difference (ARD) method utilizes direct observations of range difference, which are averaged to produce the required precision. The second technique (DAR) simply measures the actual ranges at two or more wavelengths with high precision, and determines the range difference by subtraction of normal points for range at a given epoch. Because subtraction of two observables is involved, the noise ratio is around 1.4 times worse than for the ARD method.

To achieve 1 cm range corrections using ranging wavelengths which are within the range of validity of the formulas used, a range difference error of less than 0.5 mm, or 3 ps is required.

The principal characteristics of state-of-the-art ARD and DAR systems designed to produce this precision for ranging to LAGEOS are given in Table 5. The ARD system utilizes a combination of MCP PMT and streak camera to yield 45 ps single shot uncertainty in range difference. Thus 225 observations are required to produce 3 ps uncertainties in range difference. A drawback of the ARD technique is that range returns at both wavelengths are required, from the same shot, to produce an observation. Thus if the probabilities of obtaining range measurements at wavelengths λ_1 and λ_2 are n_1 and n_2 respectively, then the probability of obtaining these events simultaneously is $n_1 n_2$. In practice, because of the requirement to split the signal to a range detector (PMT) and a range difference detector (streak camera) the probability is even lower. The measurement frequency will be around 1 Hz for a system which could produce range measurements in each color individually at 4 Hz from a 10 Hz laser system. Thus it takes such a system 225 seconds to determine range difference to 3 ps.

Table 5. Characteristics of ARD and DAR systems.

| | Average Range Difference (ARD) | Difference Average Range (RAD) |
|--------------------------------|-----------------------------------|-----------------------------------|
| Required observation precision | 3 ps | 2 ps |
| Single observation precision | 45 ps | 50 ps |
| No. of observations required | 225 | 625 |
| Observation frequency | 1 Hz | 4 Hz |
| Time required | 225 sec | 156 sec |
| Error tolerance | good | poor |
| Complexity | poor | good |
| Data modeling | poor | good |
| Calibrations | poor | good |
| Automation | poor | good |

The DAR system requires many more measures to obtain the same result. This is because single shot observation error is slightly larger, and the precision ultimately required is 1.4 times smaller (2 ps). However, this system accumulates range at 4 Hz (same power as the ARD system above) and thus can obtain the range difference required in 156 seconds.

It can be seen that the systems are comparable in performance. Both currently would require 3-4 minutes to obtain a single measure of the range difference suitable for atmospheric correction. This elapsed time is approaching the time density of normal point observations of range data, and would be satisfactory for elevation angles above 20°, and all except the lowest satellites.

There are major differences between the two techniques in some area which may ultimately decide which, if any, finds its way into the operational domain. Points to be considered in this context are:

- tolerance of systematic errors,
- system complexity,
- capability for further modeling of data,
- ease and rigor of calibration, and
- automation.

The ARD technique tolerates systematic errors in the actual range measurement (as opposed to the range difference) and order of magnitude higher (20 ps) than the DAR technique. Since it is extremely difficult to construct a ranging system with less than 2 ps systematic error in the range measurement (excluding atmosphere), this may be a telling factor.

System complexity considerations favor the DAR technique, as ARD requires a state-of-the-art streak camera and considerably more optics. A wider analysis of the probable applications of dual-color ranging suggest that a major application will be in mobile SLR systems. This is because errors or biases (in laser ranging products) due to errors in atmospheric correction will tend to integrate towards zero over time. Most of this error is thought to arise from azimuthal assymetry in the atmosphere, which, for most locations, should be random with respect to time. For a fixed station, it is likely (although not proven) that the resultant error in the laser ranging products will be small compared to their uncertainty. However, for a mobile station, this consideration may require lengthy site stays (many weeks to months) just to ensure that these errors are "randomized", when the time required on site to obtain sufficient tracking data may be only a few days. Thus a dual-color capability could enhance mobile SLR productivity by a considerable amount. The complexity of currently viable ARD designs is not compatible with mobile operations.

The DAR technique has another slight advantage in the area of satellite (target) modeling. The individual color range data can be analyzed to extract the satellite target depth by Fourier/deconvolution techniques. The higher density of data available, as well as good satellite models, facilitate this. The ARD technique has observables doubly convoluted with the satellite target depth function, making extraction of the desired observable more difficult.

Calibration of DAR systems is straightforward. Techniques exist (Greene, 1986a; 1986b) to rigorously calibrate ranging systems to 0.1 mm. The DAR system is essentially only two perfectly colocated ranging systems operating at different colors: calibration of ARD systems can use the same techniques. ARD systems cannot yet be satisfactorily calibrated, and it remains to be seen whether some errors associated with streak cameras can be satisfactorily modeled (Prochazka and Hamal, 1986).

Finally, automation will be a major factor in the future evolution of dual-color systems. While it may be feasible to automate ARD systems with steak cameras, DAR systems now exist which are fully automated. This automation

process required several years of development on systems considerably less complex than ARD systems.

5. LASER DESIGN CONSIDERATIONS

The selection of operating wavelength, pulse energy, pulse width, and pulse repetition frequency are all facilitated by the foregoing considerations.

The choice of wavelength should be made from within the validity range of the formulas used. This limits operating wavelengths to the spectrum from 2300 Å – 20,000 Å and sets a lower bound on the noise ratio which is achievable.

The choice of laser pulse widths is also restricted. Any technique for dual-color ranging presently requires very high SNR to achieve good results. For example, neither of the techniques discussed above can achieve the single shot precision quoted in Table 5 unless a large (>100 photons/color) signal is received at the receiver.

However, SNR is almost directly proportional to the square of the pulse width for pulses from 5 ps to 100 ps. This is because, as the pulse width is reduced, the filter bandwidth must be increased, admitting more noise. At the same time, less energy can be transmitted because of the energy density limitations in the laser and the optics. Data volume, upon which both ARD and DAR depend, is also proportional to laser pulse energy. Thus there is a clear case for using longer rather than shorter laser pulses, within this domain (5–100 ps), with currently available laser and optics technology (*e.g.* 5 GW/cm² coating limits).

The uncertainty in determining the power spectrum of the laser for pulse widths below 30 picoseconds, and the consequent errors in dual-color range corrections, are a final encouragement to select a pulse width in the upper half of the range considered.

6. EXPERIMENTAL RESULTS

With the sole exception of its poor tolerance for systematic error, the DAR technique seems superior for practical implementation. The possibility of ranging in two more colors with a systematic error of 2 ps in each has been explored on the Natmap Laser Ranging System (NLRS). During 1986 it was progressively enhanced to the point where one-color ranging could be executed with less than 2 ps systematic error for ranging operations not exceeding 20 minutes duration (Greene, 1986a). It now remains to replicate parts of this system to allow multiple wavelength operations, and the experimental determination of atmospheric range correction.

CONCLUSIONS

We have examined the dual-color correction to determine if such a technique will yield improved range accuracy by calibrating the contribution of atmospheric refraction to satellite range measurements. Our analysis indicates that sub-millimeter accuracy in the range measurements will be required to achieve one centimeter accuracy in the dual-color ranges. There are also systematic effects in the correction,

due mainly to water vapor and ray-bending which may in the future limit the accuracy of the dual-color ranges. For ranges made at 20° elevation angle, these systematic effects could introduce errors of ≈ 2 centimeters in the dual-color range. These errors could be reduced by modeling the water vapor and bending contributions to the ranges.

Acknowledgements

This work was supported in part by the U.S. Air Force Geophysics Laboratory, contract F-19628-86-K-0025; NASA grant NAG5-538; and NSF grant EAR-83-06380.

References

- Abshire, J.B., and C.S. Gardner, *IEEE Trans Geoscience and Remote Sensing*, GE-23, 414-425, 1985.
- Bender, P.L. and J.C. Owens, *J. Geophys. Res.*, 70, 2461, 1965.
- Böttcher, C.J.F. *Theory of Electric Polarization*, Elsevier Publ. Co. Amsterdam, 1952.
- Greene, B.A., "Calibration of sub-millimeter precision satellite laser ranging system", *6 th International Workshop on Laser Ranging Instrumentation*, Antibes, France, 1986a.
- Greene, B.A., "Calibration of sub-picosecond timing systems", *6 th International Workshop on Laser Ranging Instrumentation*, Antibes, France, 1986b.
- Owens, J.C., *Appl. Opt.*, 6, 51-58, 1967.
- Prochazka, I., and K. Hamal, "Streak camera based laser radar receiver: its performance and limitations", *6 th International Workshop on Laser Ranging Instrumentation*, Antibes, France, 1986

PROBLEMS INDUCED BY MULTICOLOUR TELEMETRY
ON LASER RETROREFLECTOR DEVELOPMENT

F. Guerin, G. Cerutti-Maori
AEROSPATIALE
100 Boulevard du Midi
06322 Cannes La Bocca Cedex - France -

Telephone (33) 92 92 71 27
Telex 470902 F

ABSTRACT

Aerospatiale's concept of retröreflectors coated with silver -
Aerospatiale experience over 20 years - is optimized for laser
wavelengths in the range 500-800 nm.

Further investigation is needed to adapt the thermal and optical
concept for use in a spectral range extended to ultraviolet (380 nm).

1 - History

AEROSPATIALE (AS) experience in laser retroreflectors started in 1965 for D1-C satellite. For more than 10 years, AS developed laser retroreflector arrays designed for use with Ruby Lasers ($\lambda = 694 \text{ nm}$) : PEOPLE, D2-B, TL2, STARLETTE.

In 1978, the laser retroreflector array designed for LASSO experiment was specified for two lasers : Ruby $\lambda = 694 \text{ nm}$ and doubled Neodyme $\lambda = 532 \text{ nm}$.

Following the evolution of laser technology, the laser ranging users are interested by multicolour laser ranging, for instance Alexandrite lasers ($\lambda = 760 \text{ nm}$, $\lambda = 380 \text{ nm}$).

Today, the ERS-1 laser retroreflector array is specified for $\lambda = 694 \text{ nm}$ and 532 nm and will be used with the 2 wavelengths of Alexandrite laser.

2 - AEROSPATIALE's concept

AS has been using cube corners made of high homogeneity synthetic silica (Heraeus Suprasil) in order to achieve a very high optical transmission and a good insensitivity to space radiations.

The entrance pupil can be an hexagone (D1-C, PEOPLE, D2-B), a triangle (TL2) or a circle (STARLETTE, LASSO, ERS-1).

Low thermal conductance fixations to the frame were developed in each case.

The silica trihedron rear faces are coated with protected silver.

The angular tolerances on the 90° trihedron are optimized for the mission (velocity aberration) and the thermal gradients inside the cube corner's material.

3 - Laser retroreflector to station link budget

According to Fournet's formula (Reference n° = 1), the number of photons received back in the ground station after 2 ways travel in the atmosphere is :

$$N_{\text{photons}} = K \frac{T_a \frac{2}{\cos Z}}{D^4} R \sum_{\text{C.C.}} F(G_i, \rho)$$

Z = zenith angle of the satellite from the laser station

T_a = atmosphere transmission

R = corner cube reflection coefficient

ρ = velocity aberration

G_i = apparent corner cube area

D = distance from ground station to satellite.

The first term is a function of satellite to station geometry.

The second term is dependent only on the laser retroreflector array.

Hence, the optimization of the link budget will be achieved by optimization of the product of the two. Very severe specifications on the laser retroreflector array will not compensate for very faint return signals caused by large zenith angles.

The reflection coefficient is the ratio of the retroreflected energy to the incident energy.

The last expression is the sum of the individual corner cube's efficiencies considered as light sources incoherent to each other. The efficiency informs about the distribution of light in the cube corner's diffraction pattern.

4 - Thermal environment

The distribution of light inside the diffraction pattern is a function of :

- pupil's diameter
- dihedral angular offsets
- laser wavelength
- thermal state of the cube corner

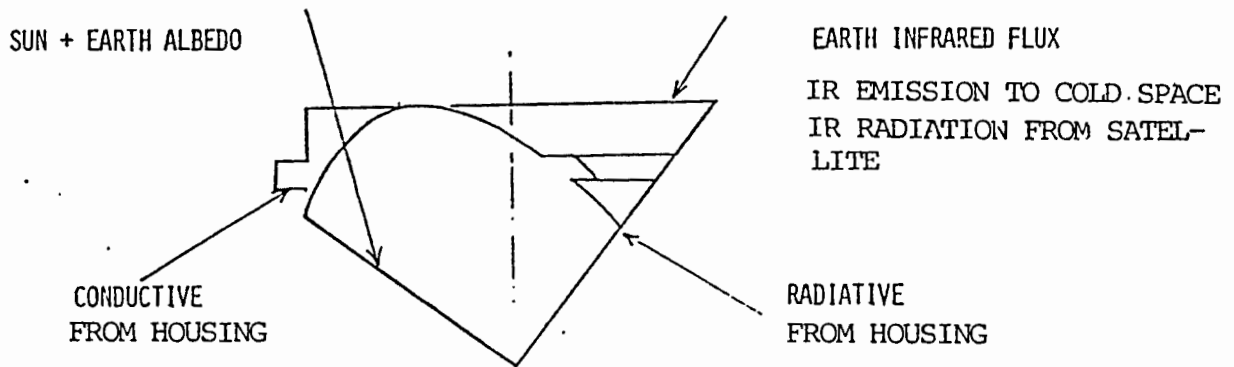


Fig. 1 : Thermal inputs

The thermal inputs on the corner cubes are :

- radiative :
 - . the solar and earth albedo fluxes, in the visible range, mainly absorbed by the silvered faces,
 - . the thermal infrared flux from the Earth and the satellite, the radiation to cold space,
 - . radiative exchanges between the housings and the silvered faces of the corner cubes,
- conductive : between the housing and the "ears" of the corner cube.

Because the silica is a bad heat conductor, thermal gradients appear in the corner cube's material and distort the diffraction pattern. In orbit, the cube corners are rarely in thermal equilibrium because their thermal environment is changing (see fig. 6).

In the case of a spinned satellite, the laser retroreflector successively views Sun, Earth, deep space.

In the case of a low orbit satellite like ERS-1, the laser retroreflector views permanently Earth with 3 phases :

- Solar flux with high incidence,
- Earth albedo flux from sunlit Earth,
- Thermal infrared flux from Earth.

AS developed a software taking into account the thermal gradients inside the real cube corner in the computation of the diffraction pattern (see fig. 1 bis).

5 - Velocity aberration

Velocity aberration represents the small angular shift between the incident and retroreflector beams caused by the relative motion of the satellite in relation to the ground station (fig. 2) for :

- Lunar laser ranging $0,7 \leq \rho \leq 1,4$ arcseconds
- Geostationary orbit $3,5 \leq \rho \leq 4,2$ arcseconds
- Low orbit (ERS-1) $5,2 \leq \rho \leq 10,5$ arcseconds

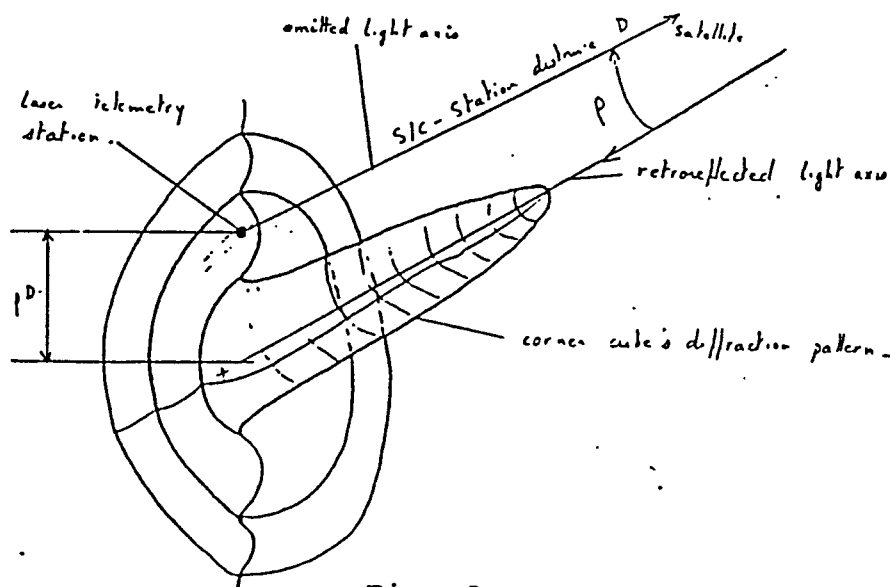
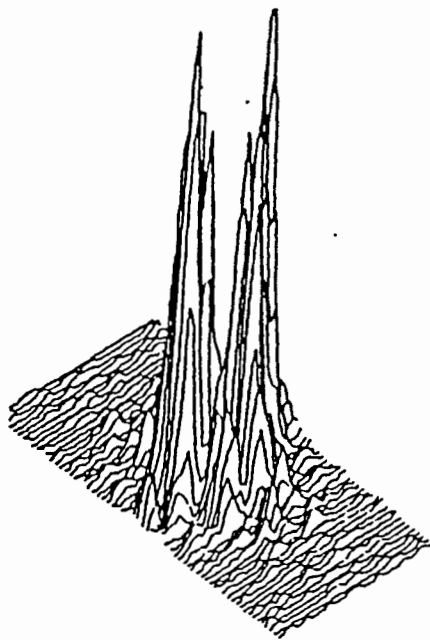
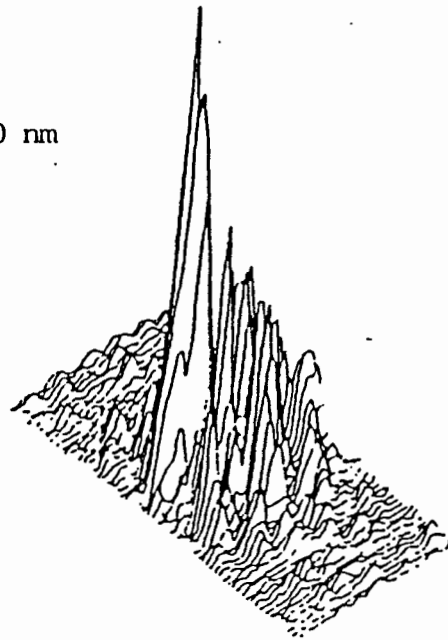


Fig. 2

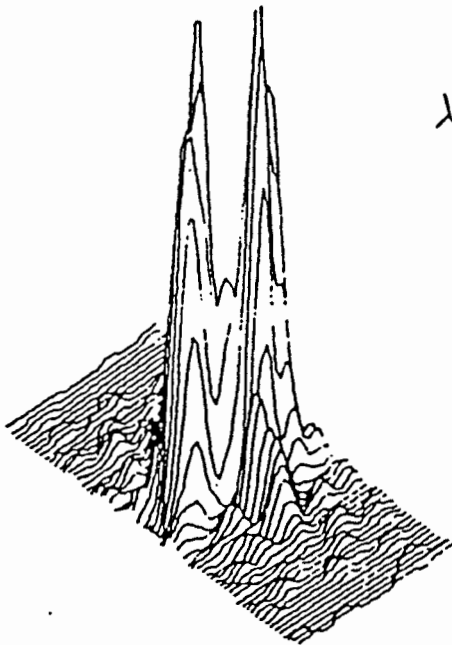


$\lambda = 380 \text{ nm}$

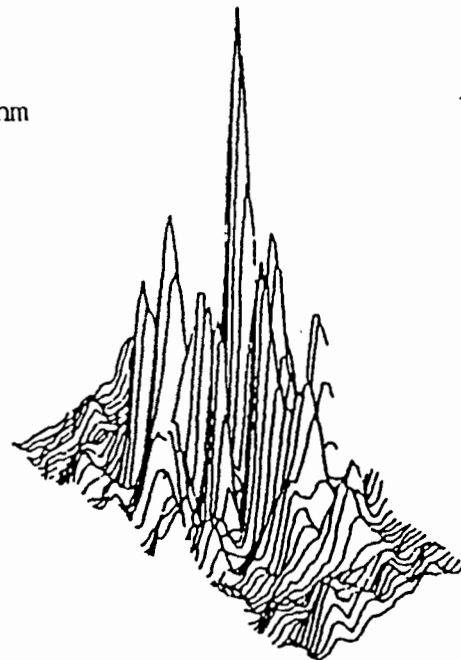


Thermal equilibrium

Thermal gradients



$\lambda = 633 \text{ nm}$



Thermal equilibrium

Thermal gradients

Fig. 1 bis : Computed diffraction patterns for a real cube corner (diameter \varnothing 33 mm) - Scale 64 x 32 arcseconds

6 - Corner cube's efficiency

The efficiency represents the mean value of the retroreflected flux at an angular distance ρ from the center of the diffraction pattern :

$$F(G_i) = 3.05 \times 10^{-10} \frac{S_{cc}}{\Omega_\rho} \frac{E_\rho}{E}$$

E = total retroreflected flux

E_ρ = retroreflected flux in an angular ring, radius ρ

S_{cc} = surface area of the corner cube's pupil (cm^2)

Ω_ρ = solid angle of the ring ρ viewed from the cube corner (sr)

Efficiency depends on :

- corner cubes' geometry (diameter, dihedral angular offsets),
- velocity aberration ρ
- beam incidence angle i (Fig. 3),
- laser wavelength,
- thermal state of the corner cube.

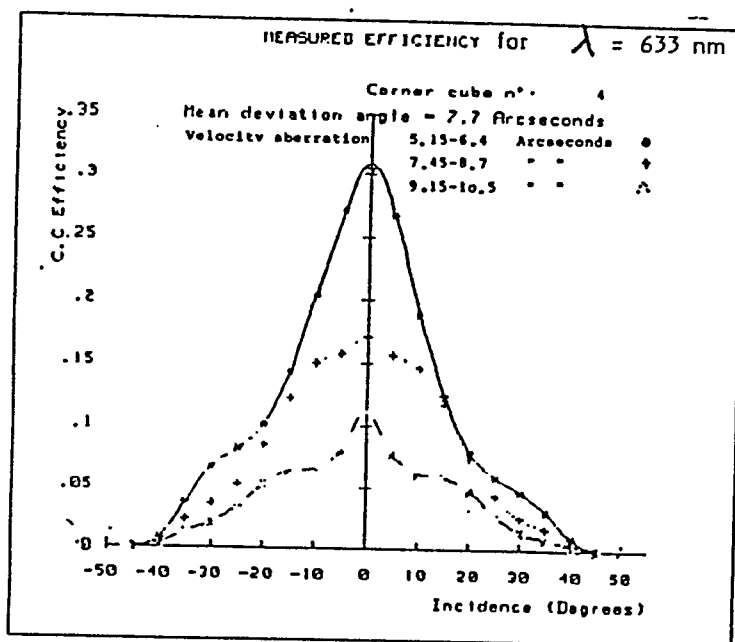


Fig. 3 : Example of ERS-1 Laser Retroreflector

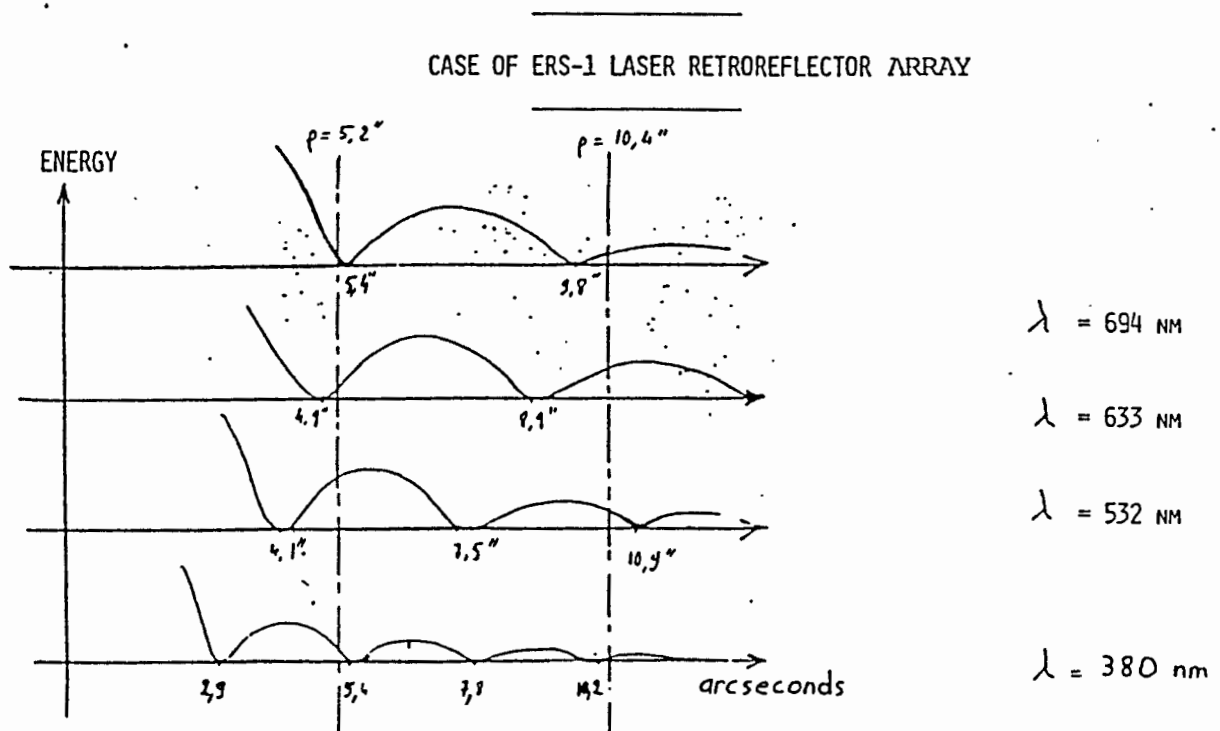
7 - Efficiency is highly dependent on wavelength

In the case of a perfect cube corner (perfect 90° trihedron), the diffraction pattern is nearly an Airy disk : it varies with wavelength (fig. 4).

When λ varies from 694 nm to 380 nm, the velocity aberration range for ERS-1 [5.2 ; 10.4 arcseconds] passes from the first bright ring to the 2nd and 3rd bright rings.

For the real cube corners, the diffraction patterns are very different from Airy disk if the dihedral angle offsets are larger than 3 arcseconds (typically). The aim of the retro-reflectors designer is to obtain less energy in the central peak, no dark rings, energy spread on pattern a little larger than the velocity aberration rings. Similarly, the diffraction pattern -hence efficiency- changes very much when λ varies from $\lambda = 694$ nm to 380 nm.

Fig. 4 : AIRY DISK AS A FUNCTION OF WAVELENGTH



8 - Reflection coefficient decreases in the blue-UV region

The reflectivity of silver decreases very rapidly when λ becomes smaller than 0.4 μm . Fig. 5 shows the corner cubes' reflection coefficient R as a function of wavelength.

R is slightly above specification for $\lambda = 400 \text{ nm}$.

On the other hand, the atmospheric transmission is lower for wavelength 400 nm than for wavelengths 500-700 nm.

Hence, the link budget -ground station to satellite- decreases rapidly when wavelength becomes smaller than 400 nm.

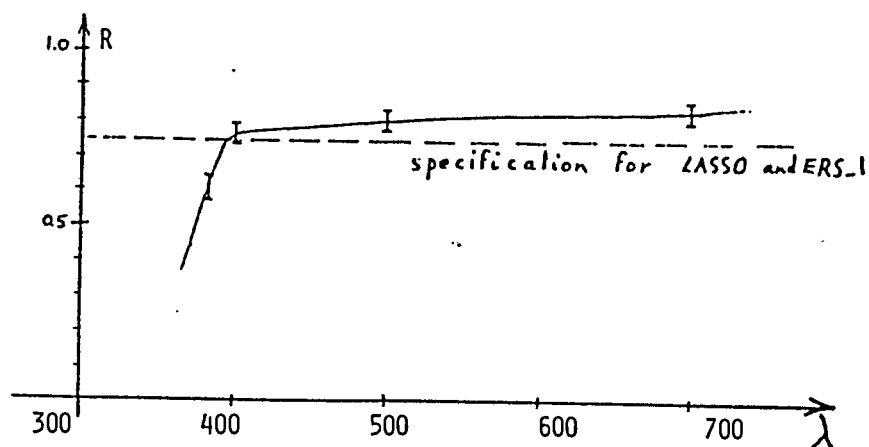


Fig. 5 : Reflection coefficient versus wavelength

For use with 380 nm lasers, a coating with higher UV reflectivity will be investigated -Al for example-. Solar absorptance α_s being 0.12 for Al and 0.05 for Ag, the thermal behaviour of the cube corners will be different. Higher thermal gradients will appear with Al coated cube corners : the thermo-optical concept needs to be adapted.

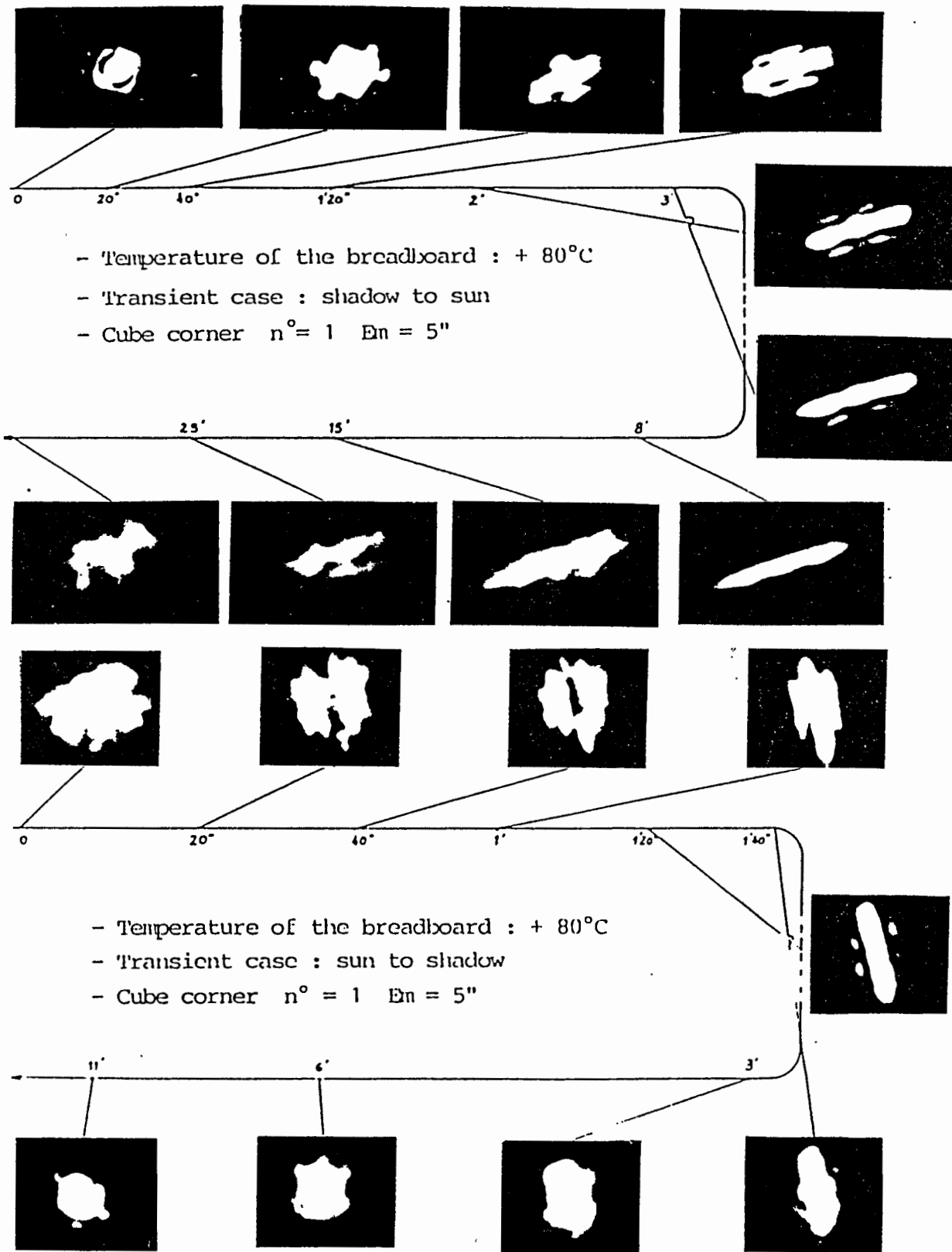


Fig. 6 : Evolution of the C.C. diffraction pattern with thermal environment : Results of Starlette thermoptical tests

9 - Conclusion

The concept of retroreflectors coated with silver is optimized (reflectivity/thermal behaviour) for laser wavelengths in the range 500-800 nm.

A larger spectral range -up to ultraviolet wavelengths- needs further investigation in order to optimize the optical and thermal behaviour of the laser retroreflector array. In 1984, AS was contracted for the design of ERS-1 laser retroreflector array : the test results will be known in a few months.

References :

1. Bulletin du Groupe de Recherches en Géodésie Spatiale n° 1, juin 1971 : Techniques Laser en Géodésie Spatiale.

LASER RANGING INSTRUMENTATION

6th INTERNATIONAL WORKSHOP

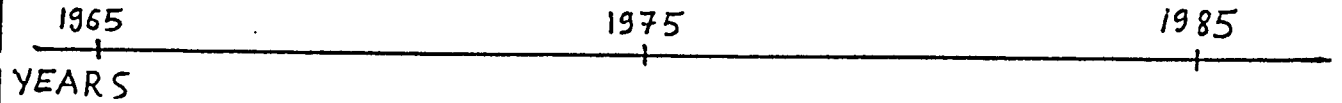
PROBLEMS INDUCED BY MULTICOLOUR TELEMETRY
ON LASER RETROREFLECTOR DEVELOPMENT

BY G. CERUTTI-MAORI - F. GUERIN, ETABLISSEMENT DE CANNES

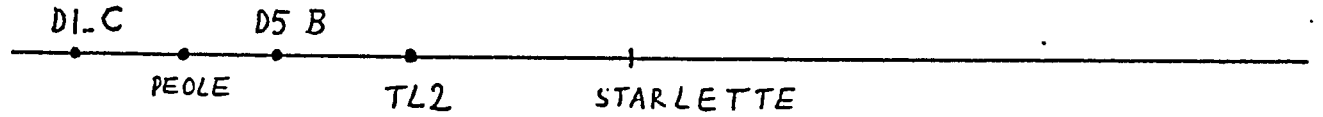


HISTORY

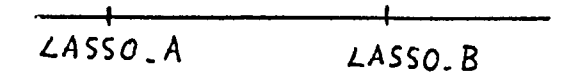
TYPE OF LASER.



RUBY



RUBY + DOUBLED NEODYME



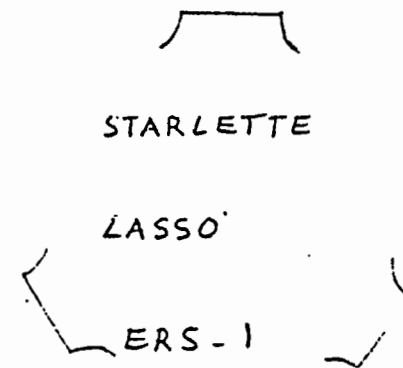
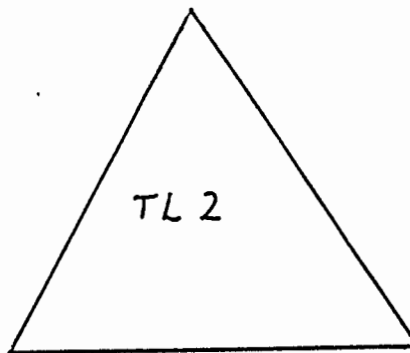
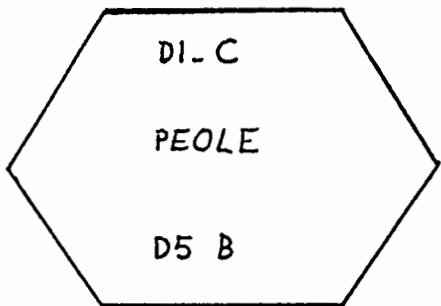
RUBY + DOUBLED NEODYME +
ALEXANDRITE (760 nm + 380 nm)





AEROSPATIALE LASER REFLECTOR

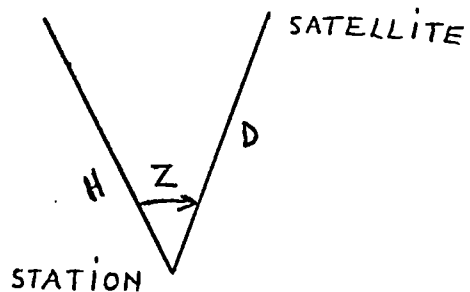
- CUBE CORNER
- HIGH HOMOGENEITY SYNTHETIC SILICA (HERAEUS SUPRASIL)
- ENTRANCE PUPIL



- LOW CONDUCTANCE FIXATION
- REFLECTIVE FACES COATED WITH SILVER PROTECTED BY INCONEL.



LASER RETROREFLECTOR TO STATION LINK BUDGET



NUMBER OF PHOTONS RECEIVED BACK AT GROUND STATION : FOURNET'S FORMULA

$$N_{\text{photons}} = K \underbrace{\frac{T_a \frac{2}{\cos Z}}{D^4}}_{\text{S/C STATION GEOMETRY}} \underbrace{R \sum_{\text{c.c.}} f(G_i; \rho)}_{\text{L.R.}}$$

T_a : ATMOSPHERIC TRANSMISSION

R : c.c. REFLECTION COEFFICIENT

ρ : VELOCITY ABERRATION

G_i : APPARENT c.c. AREA

LINK BUDGET OPTIMIZATION ⇒ OPTIMIZATION OF $\frac{T_a \frac{2}{\cos Z}}{D^4} R \sum_{\text{c.c.}} f(G_i)$



aerospatiale

LASER RETROREFLECTOR EFFICIENCY

DEFINITION

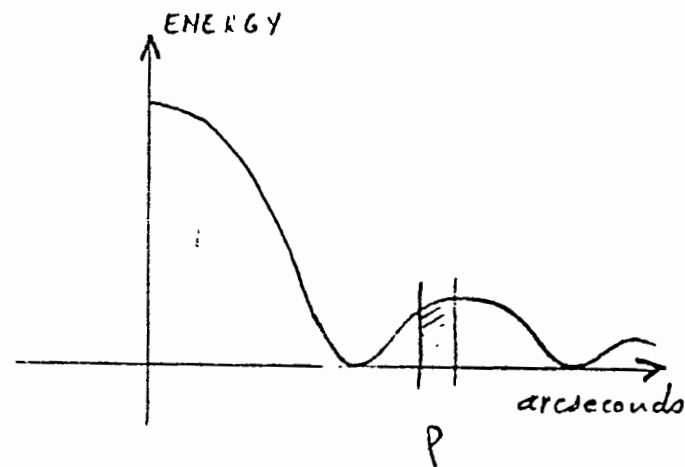
E_p = RETROREFLECTED ENERGY HAVING A CERTAIN
VELOCITY ABERRATION

E = TOTAL RETROREFLECTED ENERGY

$$F(G_i) = K \frac{E_p}{E}$$

DEPENDS ON :

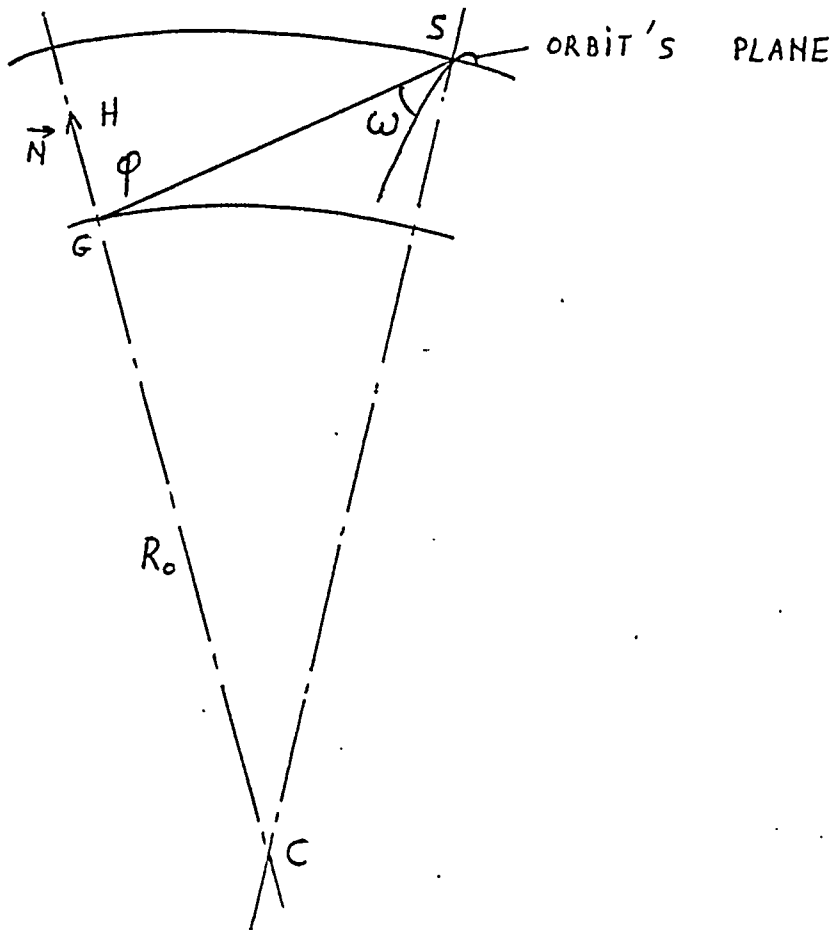
- VELOCITY ABERRATION ρ
- INCIDENCE
- WAVELENGTH
- c.c. DIAMETER
- c.c. DEVIATION ANGLES
- THERMAL ENVIRONMENT





VELOCITY ABERRATION

SMALL ANGULAR SHIFT (ρ) BETWEEN INCIDENT AND RETROREFLECTED LASER BEAMS, DUE TO THE RELATIVE MOTION OF SATELLITE/STATION



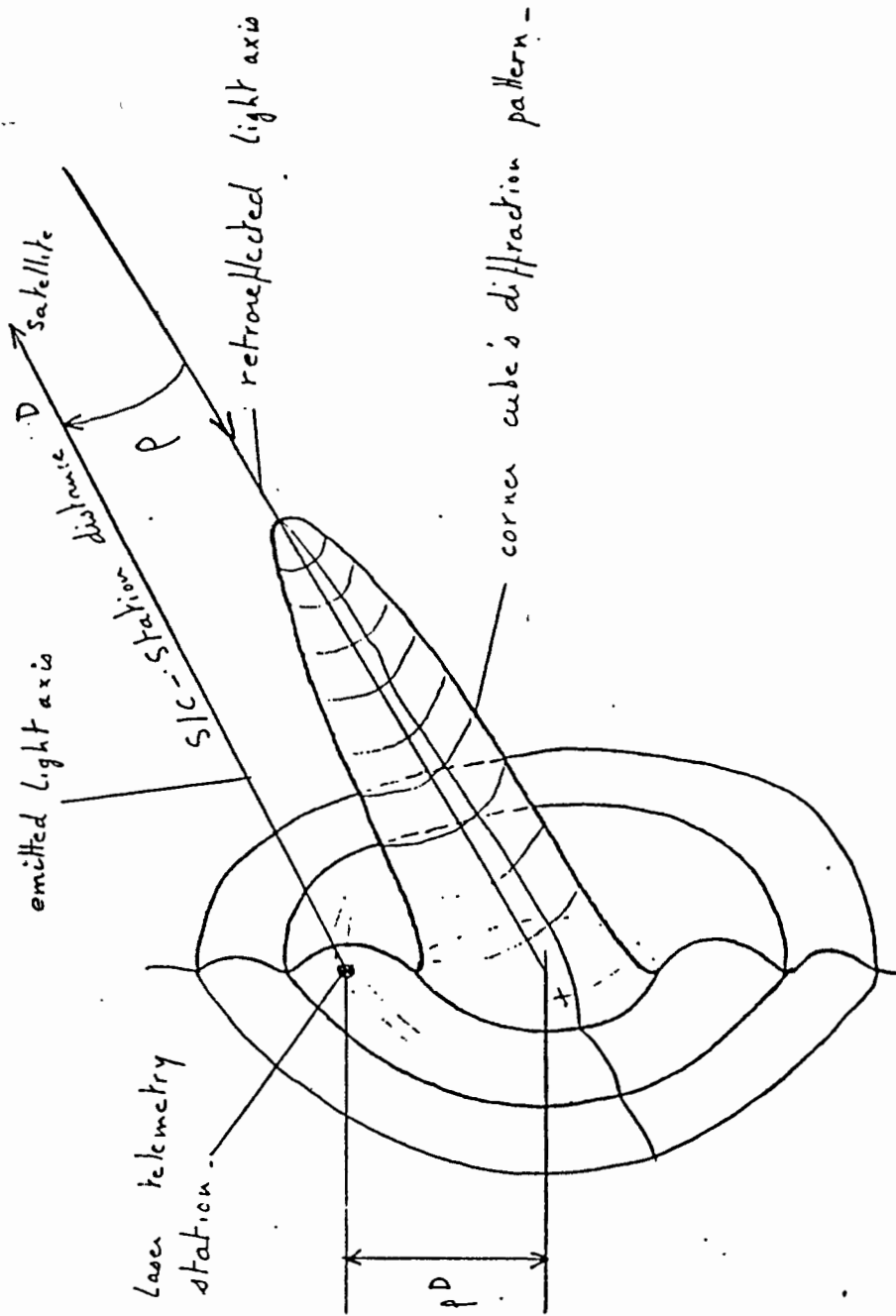
: ANGLE BETWEEN ORBIT'S PLANE AND PLANE CONTAINING G, \vec{N}, S

$$\sin \rho \approx \rho = \frac{2v}{c} \sqrt{1 - \frac{R_0}{R_0 + H} \sin^2 \varphi \cos^2 \omega}$$

FOR LASER RETROREFLECTOR :

- ON MOON $0,7'' \leq \rho \leq 1,4''$
- ON GEOSTATIONARY ORBIT (LASSO) $3,5'' \leq \rho \leq 4,2''$
- ON LOW ORBIT (ERS-1) $5,2'' \leq \rho \leq 10,5''$

INFLUENCE OF VELOCITY ABERRATION ON EFFICIENCY



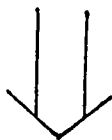


INFLUENCE OF INCIDENCE

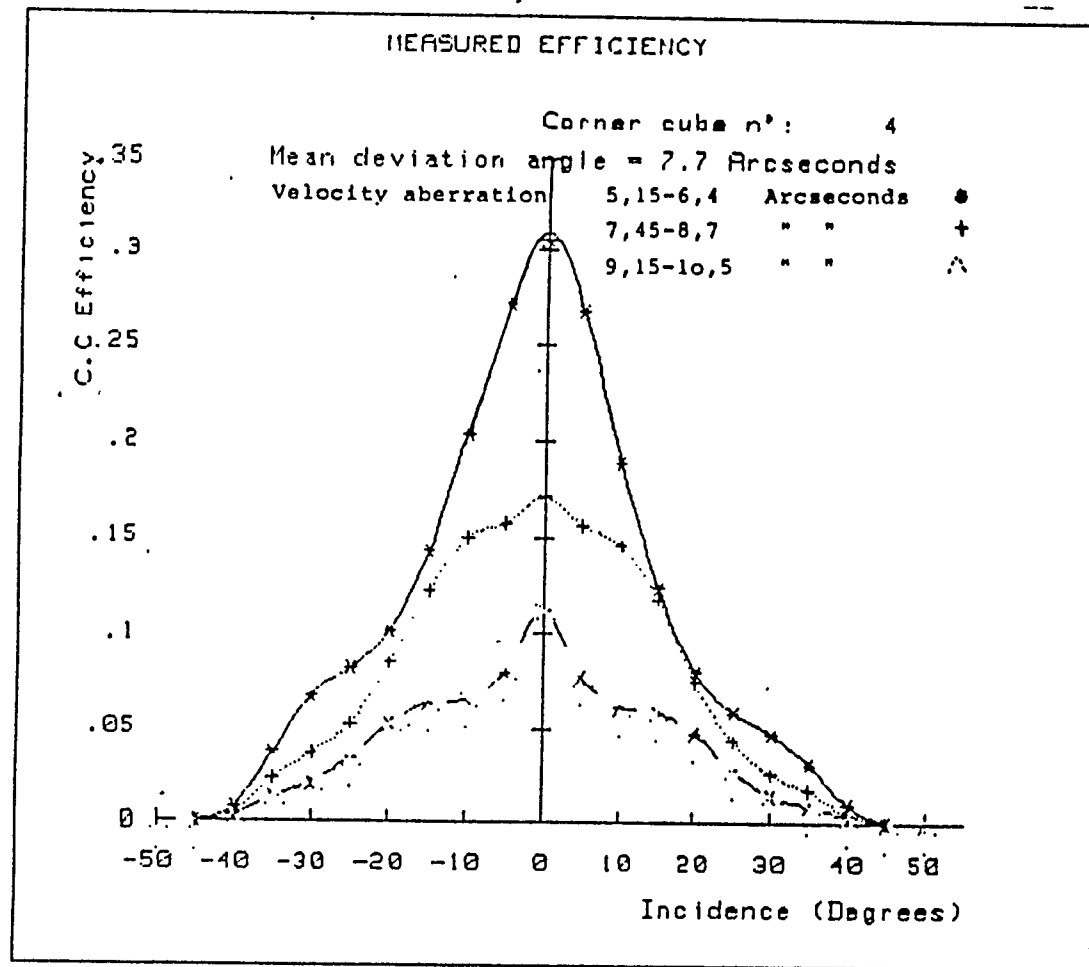
VARIATION OF PUPIL



VARIATION OF RETROREFLECTED ENERGY



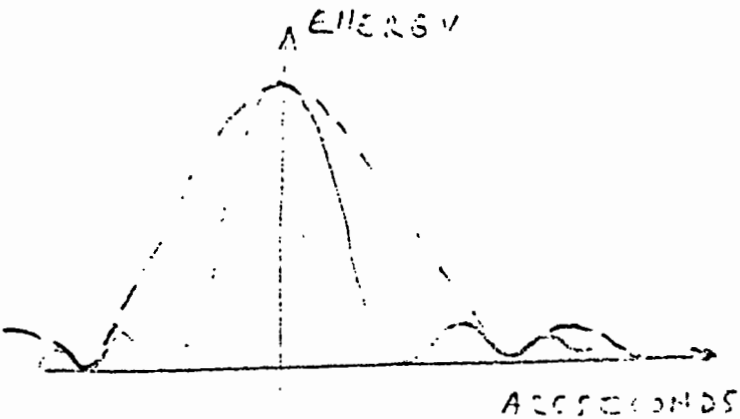
IMPACT ON LASER RETROREFLECTOR GEOMETRY



EXAMPLE OF ERS-1 LASER RETROREFLECTOR



INFLUENCE OF WAVELENGTH AND CUBE CORNER DIAMETER



DIFFRACTION PATTERN (AIRY DISK) IS A FUNCTION OF

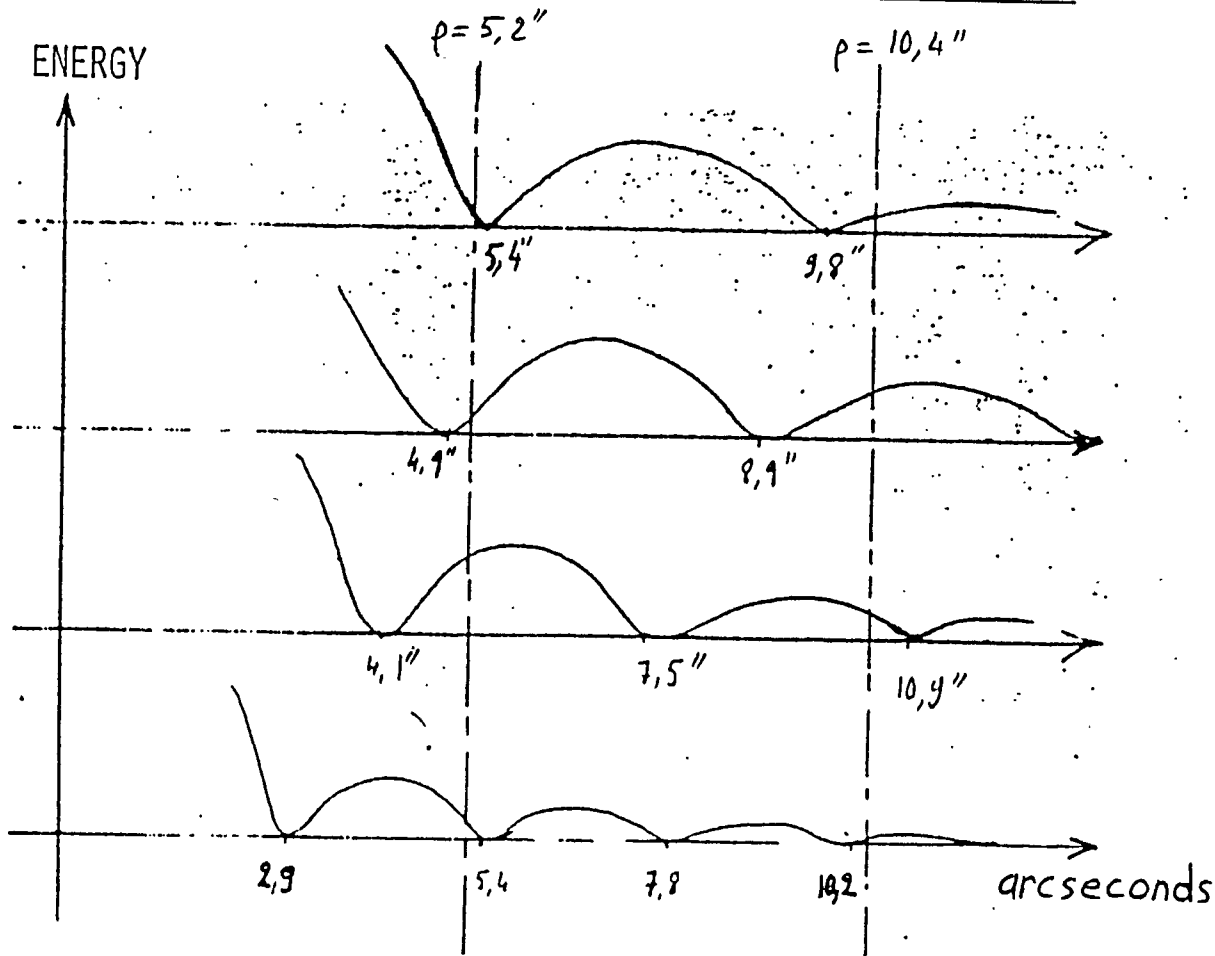
$$\lambda/a$$

FOR THE REAL CUBE CORNER, DIFFRACTION PATTERN IS A FUNCTION OF :

- DEVIATION ANGLES
- WAVELENGTH
- THERMAL ENVIRONMENT

AIRY DISK AS A FUNCTION OF WAVELENGTH

CASE OF ERS-1 LASER RETROREFLECTOR



$\lambda = 694 \text{ nm}$

$\lambda = 633 \text{ nm}$

$\lambda = 532 \text{ nm}$

$\lambda = 380 \text{ nm}$

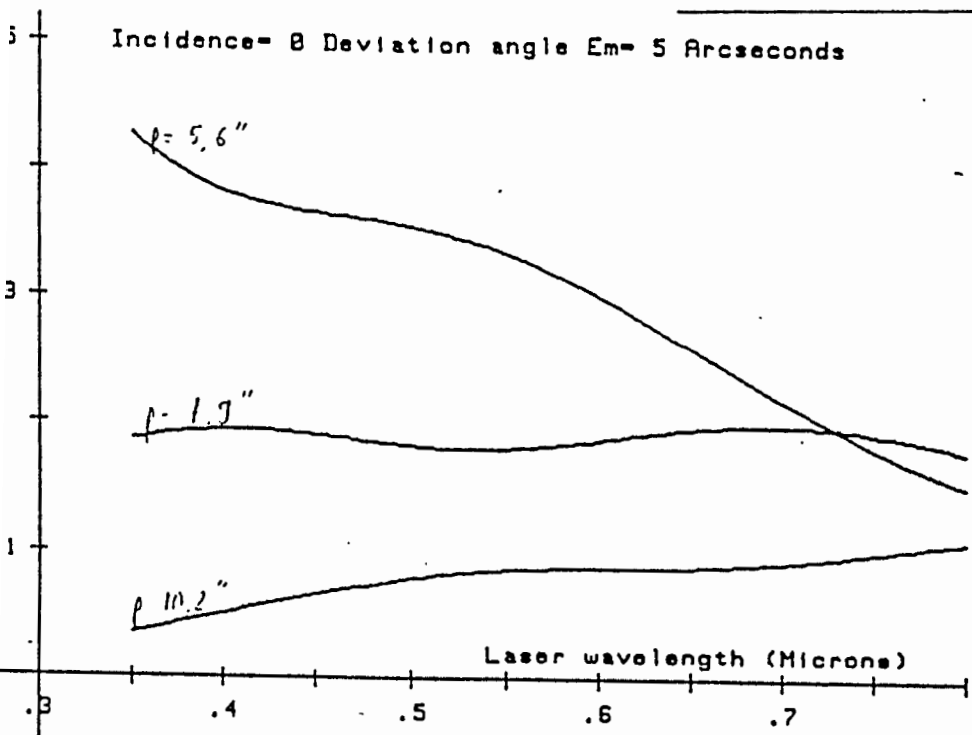
WHEN WAVELENGTH VARIES FROM $\lambda = 694 \text{ nm}$ TO $\lambda = 380 \text{ nm}$, THE VELOCITY ABERRATION RANGE VARIES FROM 1ST BRIGHT RING TO 2ND AND 3RD BRIGHT RINGS.



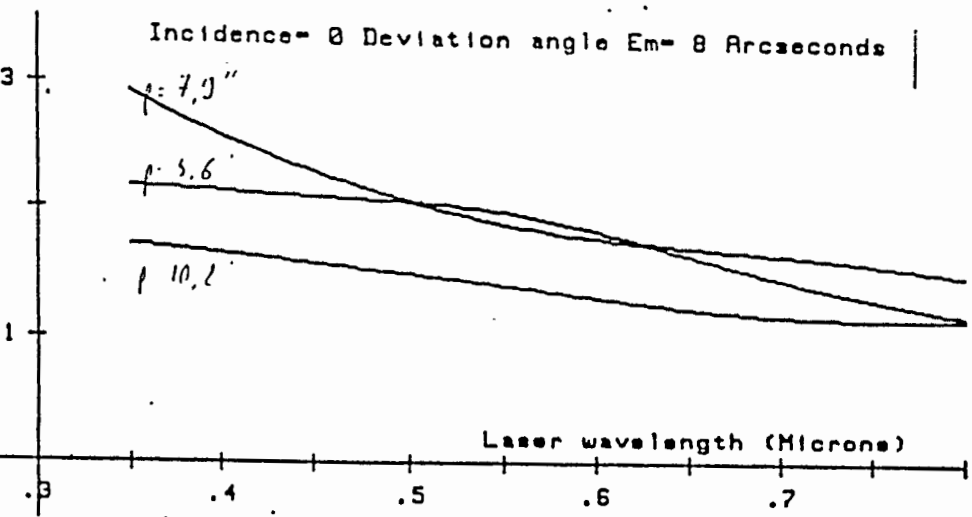
EFFICIENCY AS A FUNCTION OF WAVELENGTH

APPLICATION OF FOURNET'S FORMULA

Incidence = θ Deviation angle $E_m = 5$ Arcseconds



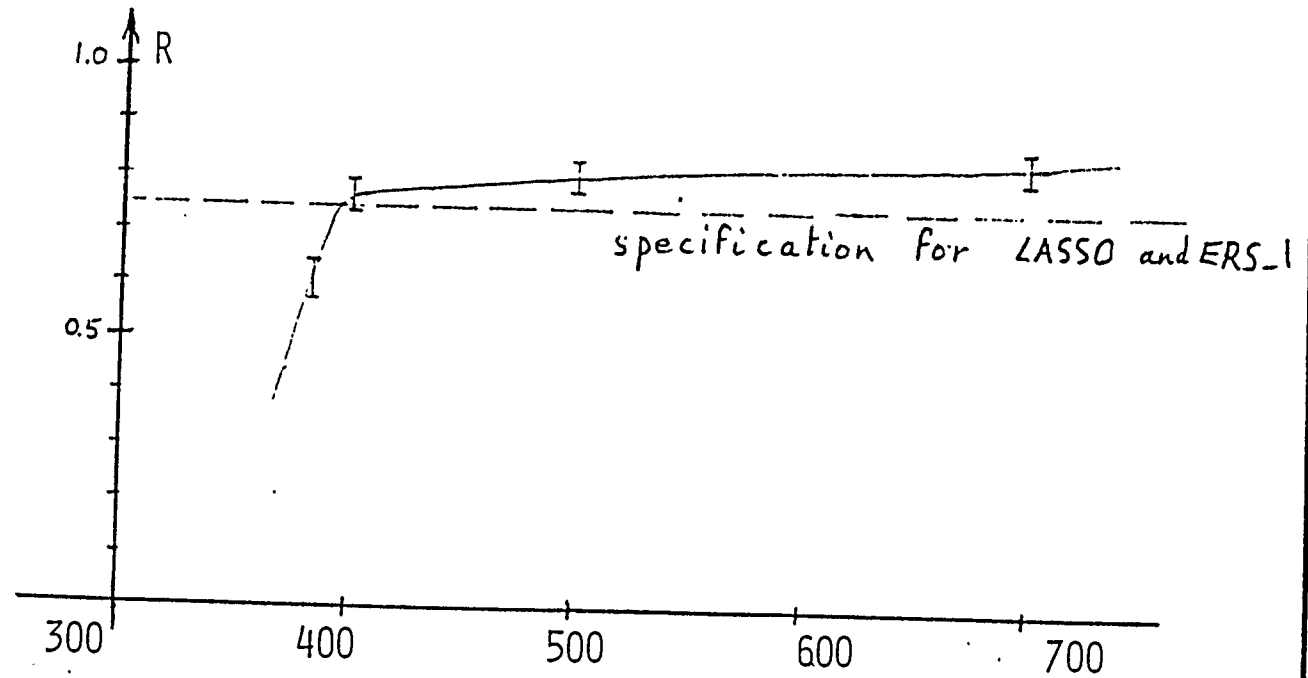
Incidence = θ Deviation angle $E_m = 8$ Arcseconds



INFLUENCE OF WAVELENGTH

R = CUBE CORNER REFLEXION
COEFFICIENT

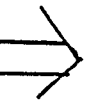
$$= \frac{\text{RETROREFLECTED FLUX}}{\text{INCIDENT FLUX}}$$



FOR $\lambda < 0,4 \mu\text{m}$

R IS LOW

ATMOSPHERIC TRANSMISSION IS LOW



LOW LINK BUDGET



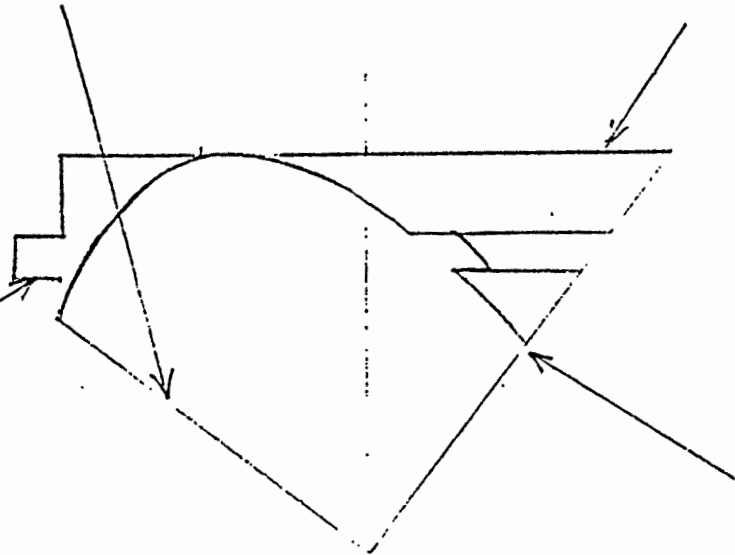
INFLUENCE OF THERMAL ENVIRONMENT

SUN + EARTH ALBEDO

EARTH INFRARED FLUX

CONDUCTIVE

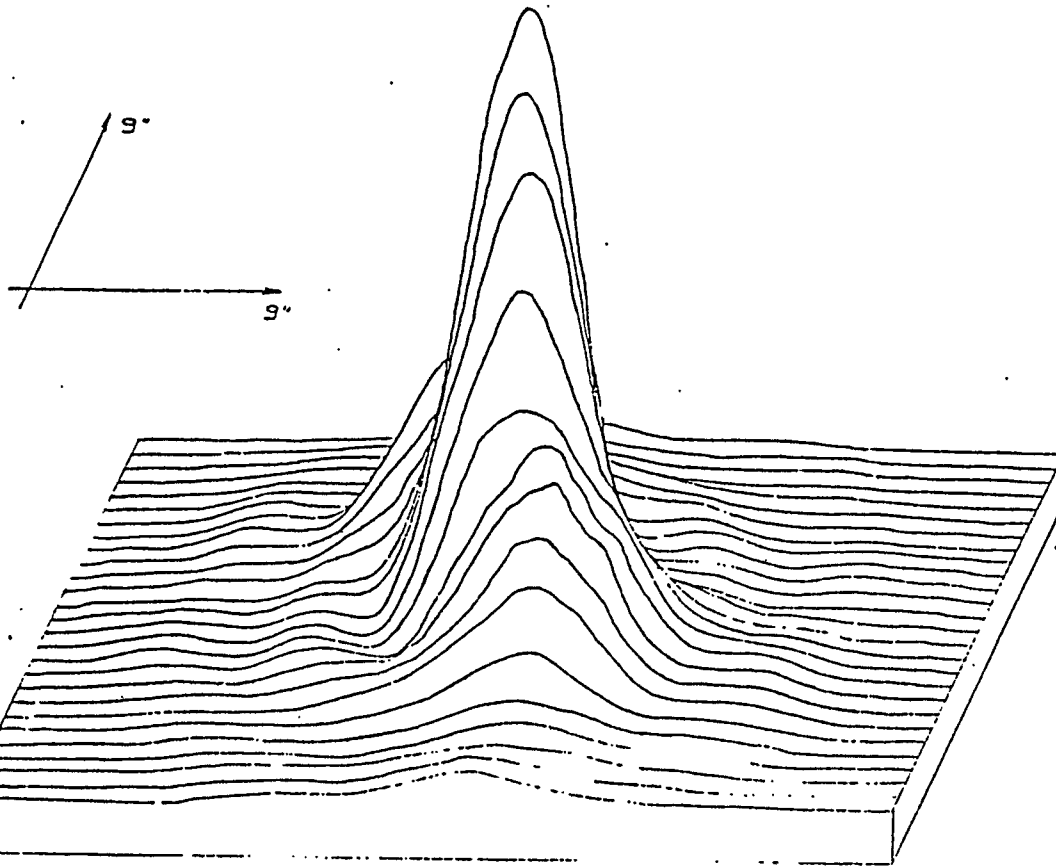
RADIATIVE





RESULTS FROM STARLETTE THERMOPTICAL TEST

CUBE CORNER WITH $E_M = 8''$



SHADOW CASE

FRAME TEMPERATURE : 20°C

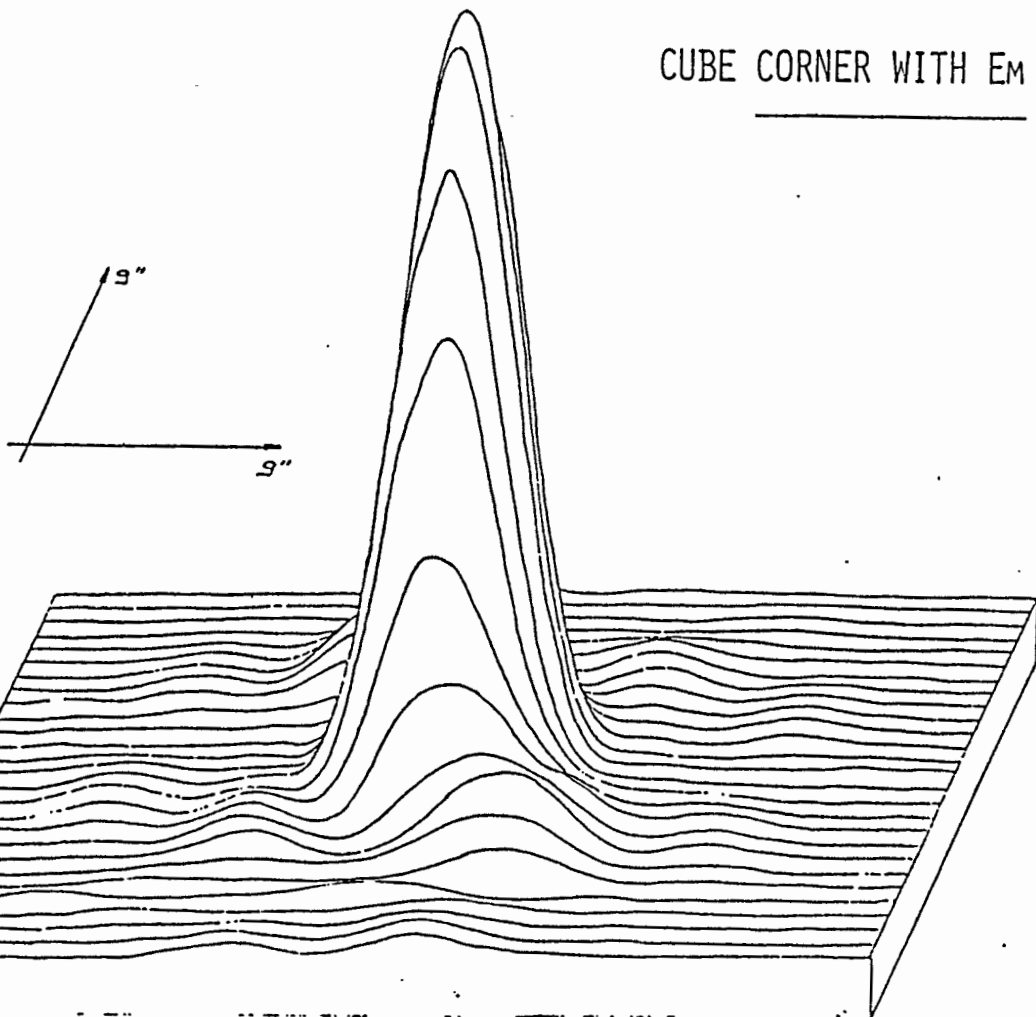
CUBE CORNER TEMPERATURE : 10°C

EFFICIENCY = 0.27 FOR $p = 5''$
= 0.06 FOR $p = 9''$



RESULTS FROM STARLETTE THERMOPTICAL TEST

CUBE CORNER WITH $E_M = 8''$



SHADOW CASE

FRAME TEMPERATURE : 80°C

CUBE CORNER TEMPERATURE : 60°C

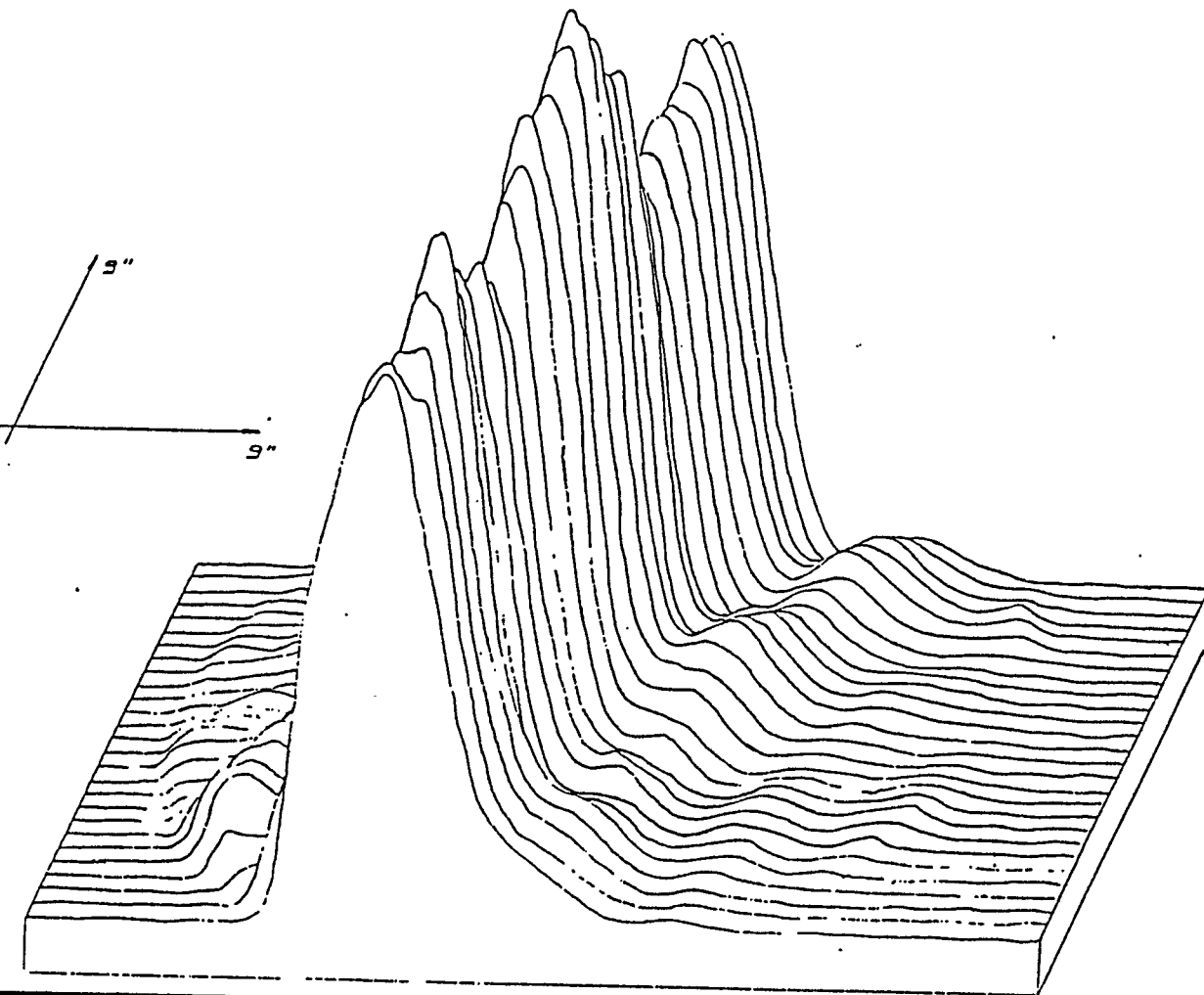
EFFICIENCY = 0,12 FOR $\rho = 5''$

= 0,04 FOR $\rho = 9''$

RESULTS FROM STARLETTE THERMOPTICAL TEST

CUBE CORNER WITH $E_M = 8''$

SUN CASE

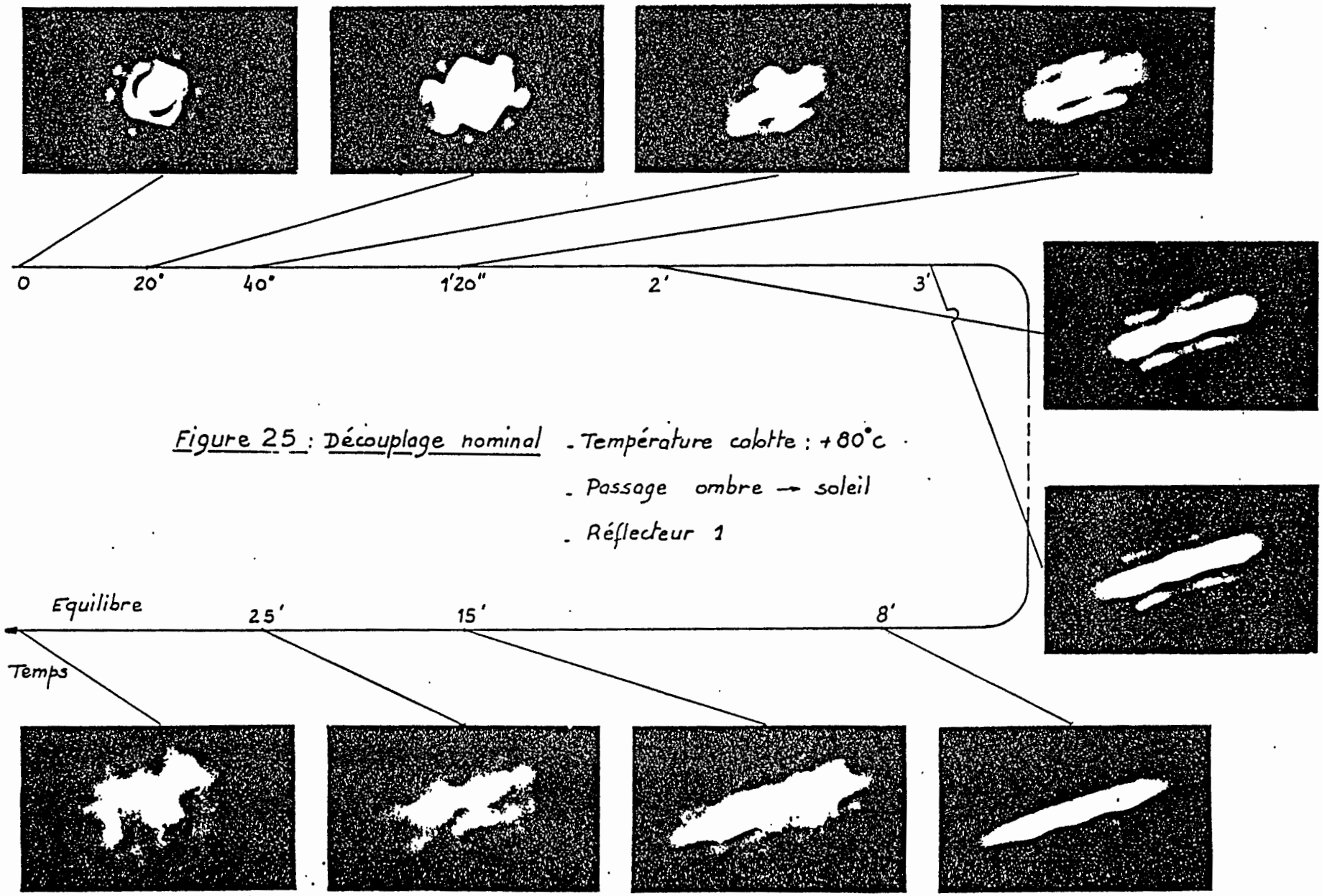


FRAME TEMPERATURE : $19^{\circ} C$

CUBE CORNER TEMPERATURE : $20^{\circ} C$

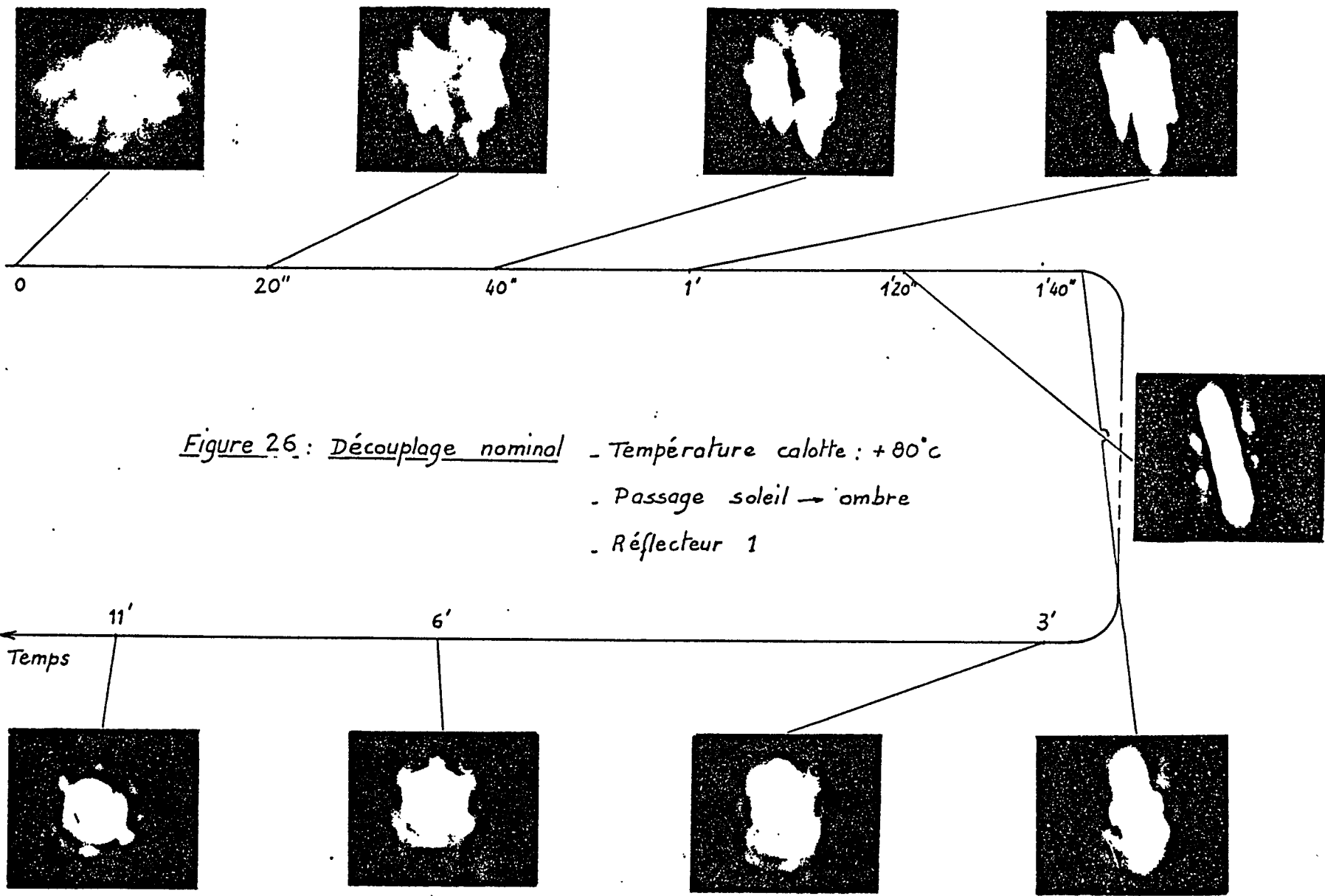
EFFICIENCY = 0,11 FOR $P = 5''$
= 0,09 FOR $P = 9''$

RESULTS OF STARLETTE THERMOPTICAL TEST



EVOLUTION OF DIFFRACTION PATTERN / THERMAL ENVIRONMENT

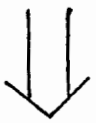
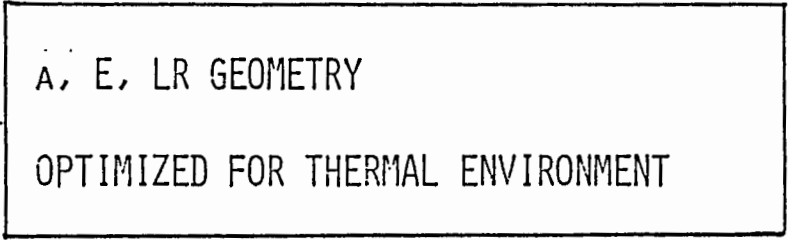
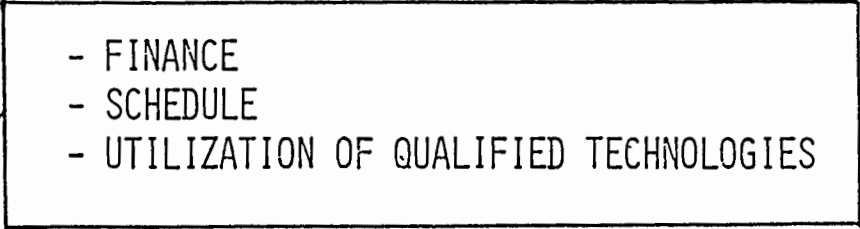
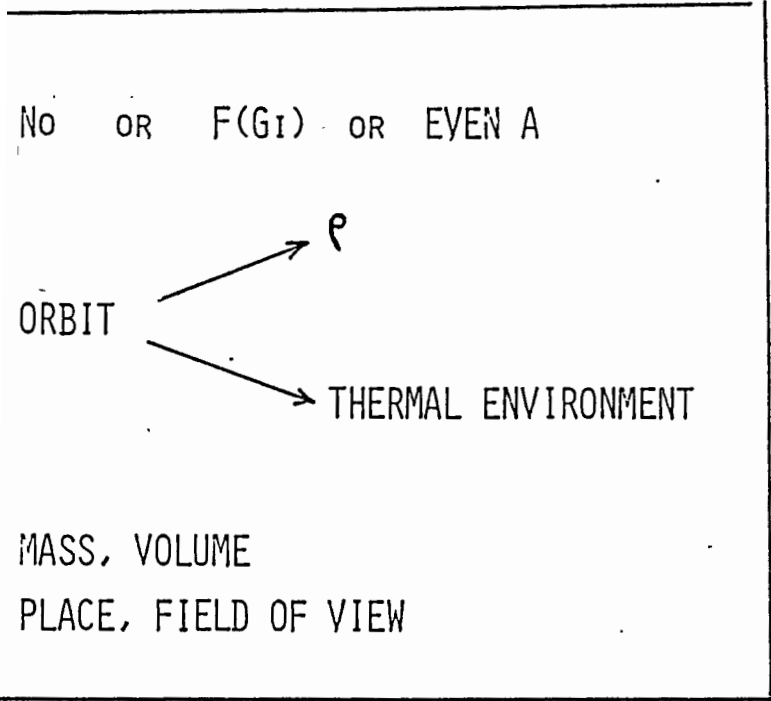
RESULTS OF STARLETTE THERMOPTICAL TEST



CONCLUSION

IMPOSED

LIMITATIONS



MULTICOLOR LASER TELEMETRY HAS A DIRECT IMPACT ON LASER RETROREFLECTOR CONCEPT

THE LASER RETROREFLECTOR FOR ERS-1 IS UNDER DEVELOPMENT AT AEROSPATIALE/CANNES.

SPECIAL STUDY GROUP ON LUNAR LASER RANGING

Report prepared by
Ch. Veillet
CERGA
Av. Copernic
06130 GRASSE

C. Alley (Maryland) - B. Greene (Orroal) - S. Bowman (Maryland) - J.F. Mangin (CERGA) - X
X Newhall (JPL) - J. Pham-Van (CERGA) - J. Rayner (Maryland) - P. Shelus (Mc Donald) - W.
Schlüter (Wetzzel) - C. Steggarda (Maryland) - J.M. Torre (CERGA) - T. Varghese (Bendix) - C.
Veillet (CERGA) - M. White (Maui) - J. Wiant (Mc Donald)

1/ LLR observing strategy - needed accuracy

All stations are working at first on Appolo XV and don't try generally any other reflector before having returns from that target. The largest hour angle coverage should be obtained for Earth rotation parameter determination, and as many reflectors as possible on the same time for libration studies. Thus the best strategy finally adopted (in good observing conditions) is to focus on two reflectors (Apollo XV and another) in order to have at the end of the observing session two long series of data for ERP, and to range the other targets more sporadically if time is available. The second ERP target should change from night to night for libration purposes. Lunakhod 1 has been once more mentionned. The fruitless systematic search for returns from this target made a few years ago at the Mc Donald 2.7-m reflector seems to prevent any station with smaller receiving area from loosing time with new attempts.

A two centimeters accuracy for Lunar normal points seems achievable in a near future, and is important at least for a complete ERP determination including not only UT0, but also the Pole coordinates. A MCP detector at Maui could be one of the means to reach this accuracy very soon. This implementation is strongly supported by the Lunar community.

2/ Normal point format

A new format defined by R. Ricklefs after many exchanges with stations and users, has been presented to CSTG and COSPAR last July. It is decided to overlap both the old and the new format for three months from January through March 1987. A report presenting the new format will be sent to all stations and users before the end of the year. During the overlap period it is possible that minor changes could be accommodated if that is necessary.

It is also planned to have a format for ERP transmission. It will be studied starting from the JPL format.

3/ Rapid data exchanges

C. Veillet suggests that exchanges of normal points or ERP determinations could be done rapidly on a regular basis. BIH is looking for ERP data on Thursday morning. Thus the data could be put on Mark 3 on Tuesday night to give one day for analyzing and transmitting ERP results to BIH and the other interested centers. As Maui will be able very soon to process the Lunar returns and to build normal points at the station, it is planned to try such a quick data transmission at the beginning of 1987.

4/ LLR capability at Orroral

B. Greene presents the Lunar situation at Orroral. GPS work made busy a large part of the team for the last year, and the development of good capabilities for SLR took most of the time. Upgrades seem necessary for increasing the return rate (actually one per minute), among which a larger laser energy (400 or 500 mJ per pulse) should be the most efficient.

5/ LLR at Wettzel

Two contracts for a LLR/SLR station have been signed recently, one for the instrument (75 cm reflector, Zeiss), and the other one for hardware and software (EOS, B. Greene). The delivery is planned for 21 months after contract signature.

6/ MLRS site

P. Shelus presents objective comparative measurements of the seeing made at the present MLRS location and at Flat Top by echosond. They show clearly that Flat Top is always better, and most often much better than the actual site. It is now time to prepare schedule and finance proposals for an eventual move of MLRS. Such a move is wished by all the participants. More on this matter will be discussed during the CDP meeting at GSFC in October.

7/ Miscellaneous remarks

P. Shelus mentions that the astronomical community needs very accurate UT1 values in real time for absolute pointing on very sophisticated telescopes.

S. Bowman presents a study on the efficiency of the reflectors as a function of numerous parameters (libration, illumination, etc ...).

Mount modelling and absolute pointing are discussed. Some pointing differences between stars and the Moon are mentionned for both Orroral and Maryland stations. This problem will be examined by an exchange of lunar position predicions between CERGA and MLRS.

FIRST LUNAR RANGING RESULTS FROM THE
UNIVERSITY OF MARYLAND RESEARCH STATION AT THE
1.2 METER TELESCOPE OF THE GODDARD SPACE FLIGHT CENTER

C.O. Alley, S.R. Bowman, J.D. Rayner,
C.A. Steggerda and J.A. Fogleman
Department of Physics and Astronomy
University of Maryland
College Park, Maryland 20742

Telephone: (301) 454-3405
Telex: 90 87 87 PHY UN MD CORK

B.C. Wang
Yunnan Observatory, Academia Sinica
Kunming, People's Republic of China

Telephone: 71347
Telex: 64040 YUOBS CN

F.M. Yang
Shanghai Observatory, Academia Sinica
Shanghai, People's Republic of China

Telephone: 386191
Telex: 33164 SHAO CN

ABSTRACT

The first lunar laser ranging returns with our new laser and detection system attached to the 1.2 meter telescope at the Goddard Optical Research Facility were recorded on August 26, 1986 from the Apollo 15 Laser Ranging Retro-Reflector (LR³) at Hadley Rille. Eleven photons were detected over a five minute interval with a firing rate of 10 Hertz. The energy per shot was about 130 millijoules, the pulse duration was 100 picoseconds, and the event timer resolution was 50 picoseconds. The standard deviation of the range was 2.5 cm, corresponding closely to the predicted spread from the calculated libration tilt of the Apollo 15 LR³ of ± 3.5 cm. The standard deviation of the mean was 0.75 cm. We believe this to be the "tightest" lunar range data point ever measured.

INTRODUCTION

The first detection of light quanta reflected from the Moon with our research station at the 1.2 meter telescope located at the Goddard Optical Research Facility of the U.S. National Aeronautics and Space Administration was achieved on August 26, 1987 at 08:44 UT. The target was the Apollo 15 Laser Ranging Retro-Reflector at Hadley Rille. Eleven returns were recorded from 3000 shots fired at 10 Hertz for a period of five minutes. The pulse duration was 100 picoseconds and the energy per pulse was about 130 millijoules.

The new laser system has been under development for several years (S.R. Bowman et al, 1982; 1985), and was first tested with LAGEOS ranging in 1984. Some details of the system are discussed in other papers at this Workshop:

"The Use of Geiger Mode Avalanche PhotoDiodes for Precise Laser Ranging at Very Low Light Levels: An Experimental Evaluation"

by S. R. Bowman, Y. H. Shih, and C. O. Alley

"Zero Range Real Time Calibration"

by J.D. Rayner, S.R. Bowman, C.O. Alley and F. M. Yang

"Analysis and Performance of a Passive Polarization Coupling Switch for Lunar Laser Ranging"

by S. R. Bowman, J. D. Rayner, and C. O. Alley.

A complete description of the new system is contained in the Maryland Ph.D. Dissertation of S.R. Bowman, "The Design, Construction and Testing of a High Precision Lunar Laser Ranging Station," April, 1986.

Telescope and Coupling Optics

The 1.2 meter telescope is shown in a cut-away view in Figure 1. It was used by our group in 1978 with a 0.5 millijoule per pulse, 10 Hz, frequency doubled Nd:YAG laser to achieve the first single-photon ranging to artificial satellites (reported at the Third International Workshop on Laser Ranging Instrumentation in Lagonisi, 1978). The 45° bending mirror can be placed in different azimuthal positions, allowing as many as eight different experiments to be accommodated at the telescope. Part of the Maryland equipment is shown in Figure 2, coupled by the passive polarization switch to one of the ports.

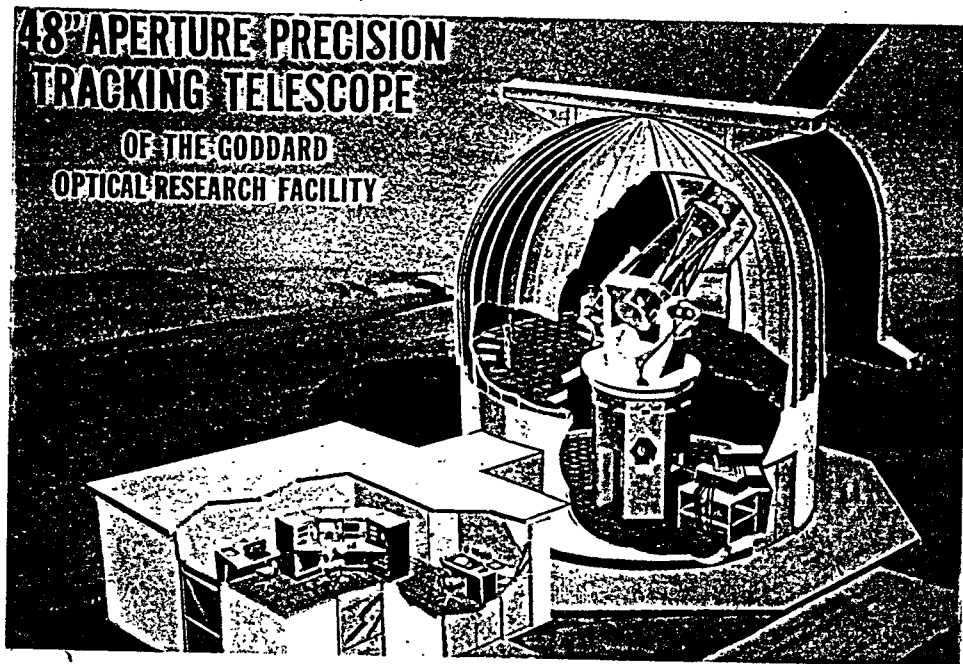


Figure 1

The telescope is computer controlled with 22 bit resolution optical encoders on the elevation and azimuth axes. Using a mount model calibrated by pointing to stars in known directions, absolute pointing is possible at a level of two or three seconds of arc. However the accuracy tends to degrade rapidly as temperature conditions change even during an observing run. Some limited success with absolute pointing to the lunar reflectors has been achieved, but will not be discussed here.

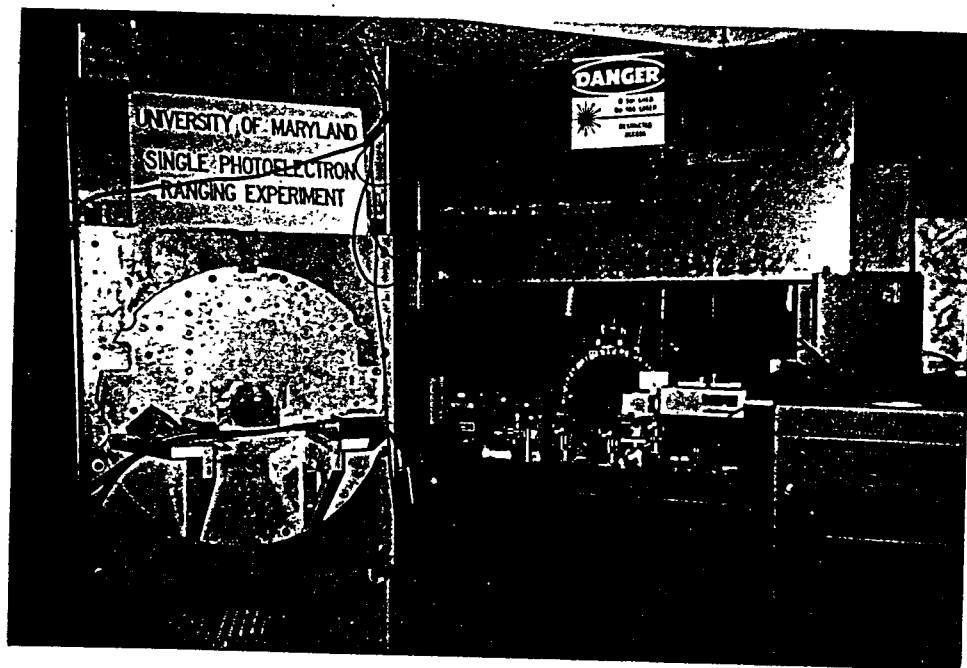


Figure 2

New Laser

The frequency-doubled, Nd:YAG laser, which uses spatial filters and re-imaging optics to minimize damage from the high peak power densities, was designed expressly for lunar ranging and has operated successfully with 350 millijoules output in a green pulse of 100 ps duration at 10 Hz. However the probability of damage is too large at this energy level. In the measurements reported here the output was limited to about 130 millijoules per pulse.

An active mirror slab geometry Nd:YAG laser has been designed and constructed to allow more energy at high repetition rates. It has not yet been added to the ranging system. This laser is discussed in another paper at this workshop:

"An Active Mirror Geometry Laser Amplifier
for High Average Power Laser Ranging"
by S. R. Bowman, L. M. Ding, and C. O. Alley

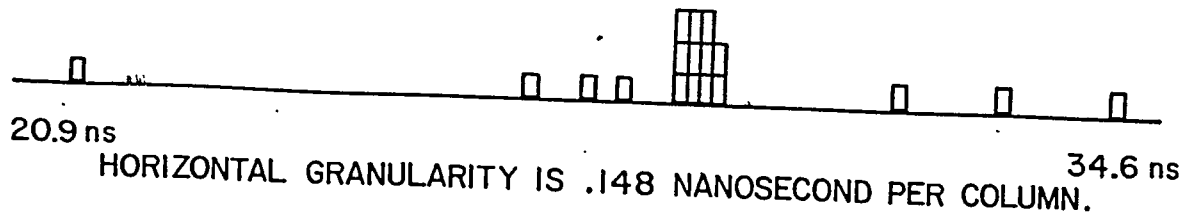
Geiger Mode Avalanche Photo-Detector

Following a suggestion at the Fifth Laser Ranging Instrumentation Workshop (B. Hyde, 1985), this type of detector was studied by us and used successfully in the new lunar laser ranging system. High quantum efficiency for single photon detection (20-30%), fast response, and large output voltage (5 volts) are among its desirable features. Details are given in the workshop paper by Bowman et al, referenced in the Introduction.

Timing and Calibration

The Maryland Event Timer, improved to 50 picosecond resolution (Steggerda, 1985), was used. The real time zero range calibration which is made possible by the large output voltage of the avalanche photo-detector is discussed by Rayner et al in the paper at this workshop referenced in the Introduction.

The zero range calibration for the measurement reported here is 103.5 ± 0.05 ns for the round trip range time.



ROUND TRIP RESIDUALS FROM THE JPL ANALYSIS OF THE
RETURNS OF AUG. 26, 1986 (COURTESY OF X X NEWHALL)

Figure 3

Data

Figure 3 shows the histogram produced at the Jet Propulsion Laboratory during the analysis of the round trip times of the detected light quanta. Eleven returns are displayed in four contiguous bins 0.148 ns wide. The other entries in the histogram represent the background noise just before fourth quarter. The spatial filter was set at 5 arcseconds, the spectral filter width was 1.5 Angstroms, and the range gate was opened 300 ns before the prediction.

Mean = 29.24 ns

Standard Deviation = 0.166 ns

Standard Deviation of the Mean = 0.05 ns

For the one-way range, these times give

Standard Deviation = 2.5 cm

Standard Deviation of the Mean = 0.75 cm.

It is interesting to note that the expected front to back spread from the libration tilt of the Apollo 15 LR³ on August 26, 1986 was 7 cm, or ± 3.5 cm. This is in reasonable agreement with the measured spread.

We believe this set of returns, although small in number of photons, to be the "tightest" in terms of spread yet achieved in lunar ranging.

Acknowledgments

It is a pleasure to acknowledge important contributions to this work by W. L. Cao, M. Z. Zhang and N. H. Wang of the Shanghai Institute of Optics and Fine Mechanics during their visits to the University of Maryland. We also thank our

colleagues D. G. Currie and J. D. Mullendore of the University of Maryland for many valuable contributions during the early days of this research. We are indebted to many people associated with the Goddard Space Flight Center: to John Degnan for his early technical contributions to this work and for his continuing expert interest; to Mike Figzmaurice for allowing the use of the 48 inch telescope; to Jan McGarry, Arnie Abbott, and Dick Chabot for technical support of the telescope; and to Tom Zagwowski for sharing the LAGEOS ranging experience at the telescope. We thank also our friends at the Jet Propulsion Laboratory, Jim Williams, Jean Dickey, and Skip Newhall for their invaluable help in identifying initial mistakes in the station coordinates and for the computer analysis of the measured data.

We acknowledge with gratitude not only the financial support of the U.S. Naval Observatory which has made this research possible, but also the strong technical contributions and interest of members of its Time Services Department.

References

S. R. Bowman, W. L. Cao, J. J. Degnan, C. O. Alley, M. Z. Zhang, and C. L. Steggerda, "The New University of Maryland Laser," Fourth International Workshop on Laser Ranging Instrumentation, Austin, Texas, edited by Peter Wilson by the Geodetic Institute, University of Bonn, 1982.

S. R. Bowman, C. O. Alley, J. T. Degnan, W. L. Cao, M. Z. Zhang, and N. H. Wang, "New Laser Developments towards a Centimeter Accuracy Lunar Ranging System," Fifth International Workshop on Laser Ranging Instrumentation, Herstmonceux Castle, England, edited by Jean Gaignebet of the by Groupe de Recherches de Geodesie Spatiale, Grasse, 1985.

B. Hyde, "Further Thoughts on a Minimal Transmitter for Laser Ranging", Fifth International Workshop on Laser Ranging Instrumentation, Herstmonceux Castle, England, Groupe de Recherches de Geodesie Spatiale, Grasse, 1985.

C. A. Steggerda, "Current Developments in Event Timers at the University of Maryland," Fifth International Workshop on Laser Ranging Instrumentation, Herstmonceux Castle, England, Groupe de Recherches de Geodesie Spatiale, Grasse, 1985.